Deciphering pathological heterogeneity in familial Alzheimer's disease

By

Nanet Willumsen

Thesis submitted for the degree of Doctor of Philosophy at University College London

Declaration

I, Nanet Willumsen confirm that the work presented in this thesis is my own. Where information has been derived from other sources, I confirm that this has been indicated in the thesis.

N.Willumsen

Acknowledgements

Firstly I would like to thank Alzheimer's Research UK for the funding which enabled this research to take place. None of this research would be possible without the donated brain tissue and therefore I am grateful to those who donated.

I have been guided through this PhD by my three supervisors, Dr Tammaryn Lashley, Dr Natalie Ryan and Dr Selina Wray. Each of you has provided advice and support in your own unique ways and I know I am fortunate to have had all your individual contributions throughout this process. This has not only included technical advice, but personal support too. Your excitement and interest in your fields of research has been encouraging and your personal accomplishments inspiring.

Throughout my PhD I have worked with many people. I would especially like to thank those who have made large contributions throughout my project. Firstly I want to thank Dr Christina Toomey, who is invaluable in the QSBB for her knowledge and assistance. I would also like to thank Dr Charlie Arber for all his help and suggestions with my iPSC work. Part of the iPSC reprogramming was jointly conducted with Christopher Lovejoy and I am glad to have worked with him. During my time I have also made great friends who have been there throughout and I am happy we got to share part of our PhD journeys together and it would not have been the same without Dr Lauren Gittings and Melissa Wren. There are many others in the Wray lab and QSBB brain bank who have played important roles so I would like to extend my thanks to all those I cannot name in this space, including Dr Aoife Kiely.

I would like to thank my family for their support during this process. Lastly I would like to thank my partner Myles Vincent for his continual belief in me and encouragement throughout the last few years. Together we have had to forgo a lot during this PhD and I can't wait for us to make up lost time once this is over!

Abstract

Introduction: Alzheimer's disease (AD) is the most common neurodegenerative dementia and its cause is unknown. In rare cases AD can be caused by mutations in the *PSEN1*, *PSEN2* or *APP* gene and this form of AD is termed familial Alzheimer's disease (FAD). While the genetic cause is determined, there is considerable heterogeneity in terms of clinical presentation and pathological appearance at post-mortem. Previously it has been suggested pathological features of FAD may influence clinical features. It has also been suggested that FAD mutations may influence both pathological and clinical features. Common features of AD may also play a role in FAD, such as microglial activation and the influence of genetic modifiers of disease, such as *APOE*. The aims of this thesis were to investigate the associations of Aβ pathology (including CAA) and microglial load to age at onset and disease duration. Investigate histological profiles of Aβ pathologies (including CAA) and microglial load and the associations between these pathologies in genetic causes of FAD and *APOE* genotypes. Observe the contribution of specific Aβ peptide species to the histological profiles of Aβ pathology, and the association of these peptide with FAD and *APOE* genotypes. Generate and differentiate FAD patient derived iPSC to neuronal cultures to assess the association of FAD mutation with Aβ peptide profiles and PSEN1 maturity in a neuronal model of FAD. We hypothesise that histological features and Aβ peptide profiles will segregate with FAD mutation location, while microglial phenotype will associate with specific Aβ pathologies. Additionally, we predict the Aβ profiles observed in FAD cell lines will reflect histological profiles of Aβ aggregation.

Materials and Methods: Nissl staining was performed on the frontal cortex of 20 FAD cases from the Queen Square Brain Bank (QSBB) (*PSEN1* mutation carriers n=16, 10 pre-codon 200, 6 post-codon 200 and *APP* mutation carriers n=4). Cortical layers were delineated and serial sections immunohistochemically stained with antibodies against Aβ, Iba1, CD68 and CR3/43 and a subset were also stained for Tau. Aβ plaque type, load (% area stained), proportion of Aβ positive cerebral amyloid angiopathy (CAA), and microglial load were analysed per cortical layer. Additionally, in frontal and occipital cortex tissue from the 20 QSBB cases and an additional 21 FAD cases from the Institute of Psychiatry,

Psychology and Neuroscience (combined total n=41, *PSEN1* mutation carriers n=31, 20 pre-codon 200, 11 post-codon 200 and *APP* mutation carriers n=10) the proportion and severity of cortical and leptomeningeal CAA were investigated via vessel counts. In the temporal and occipital cortex of the 20 QSBB cases, IHC with Aβ isoform specific antibodies was conducted to investigate genetic contribution to isoform specific pathology. Finally, 5 induced pluripotent stem cell (iPSC) lines from FAD patients were generated. Four FAD lines and two control lines were differentiated into cortical neurons to investigate Aβ isoform production via ELISA and PSEN1 protein levels and maturity were assessed.

Results: Clinical features in this FAD cohort were influenced by both FAD mutation and *APOE* status. Pathological Aβ deposits showed variability across cortical layers, and specific features were more associated with distinct mutations. Microglial phenotype did not differ by FAD mutation group or *APOE* status however associations with Aβ pathologies were observed. CAA differed between mutations groups, while *APOE4* genotype had a non-significant effect of CAA pathology in FAD. Analysis of Aβ production from FAD iPSC derived cortical neurons showed that Aβ production differed not only compared to control cell lines but compared to other independent *PSEN1* mutations. This could be the result of changes to PSEN1 maturation.

Conclusions: It was shown that there is pathological heterogeneity in FAD of which some aspects associate with specific FAD mutation subgroup. For instance, greater Aβ and CWP frequency in the lower layers in the *PSEN1* post-codon 200 group as well as greater proportion and severity of CAA. Correlations between plaques, CAA and microglia indicate contribution of clearance mechanisms to histological features observed in FAD, which can differ by mutation group. Specifically, CD68 was generally associated with greater CAA and reduced Aβ pathology. In the cellular models, specific FAD mutations, particularly those post-codon 200, affect Aβ peptide ratios, which associates with observed pathological heterogeneity and suggests that differences in the aggregation and clearance of these peptides modifies the histological appearance of Aβ pathology. Combined with the observed effect of *APOE* genotype on disease duration, peptide profiles and CAA severity, this may contribute to the differences in clinical aspects of FAD.

Impact statement

This thesis has investigated heterogeneity in FAD by investigating many features of the disease. Some of the key findings observed from the provided clinical and genetic data include the confirmation of mutation effects on age at onset and disease duration, and the discovery of the association of *APOE*4 on disease duration in this FAD cohort. The increased knowledge available about the specific effects of genetics on disease course would have a beneficial impact on those with FAD who seek to know more about the disease. This would be available to those with FAD through information disseminated to them via clinicians involved in their care or through support networks.

Histologically we have shown specific associations between pathologies which suggests shared molecular links. We have also shown the associations of genetics with these pathologies. This will be beneficial in the research community as it highlights regions for further investigations. These further investigations will be of importance as many of these features have been shown to be related to genetic factors and/or have an impact on disease presentation or disease course. In the future, greater understanding of molecular mechanisms will help improve treatment approaches. A manuscript which is in preparation containing some of the findings from this thesis will enable the dissemination, enabling the research community to access these findings.

The cell analysis has revealed mutation specific effects on Aβ production and PSEN1 maturity. From the lines produced there has been one publication so far (Charles Arber *et al.*, 2019a) which has expanded the knowledge of the field to researchers. This knowledge will influence future research into FAD as the specific impact of these mutations on disease mechanisms will be explored. Importantly this will be possible to models beyond iPSC, widening the breadth of research in this area. Any future publications with the extended data would continue to contribute to this.

Finally, throughout this thesis there have been multiple presentations of the data at a range of scientific conferences, including posters and oral presentations. These include Alzheimer's Research UK conference 2018, Alzheimer's

Association International Conference, 2018 and 2019, British Neuropathological Society Conference 2018, Institute of Neurology/Institut du Cerveau et de la Moelle épinière 2018 and the International Cerebral Amyloid Angiopathy Conference 2018. Scientific discussions arisen from these events with peers has increased dissemination of these results and gathered interest for research into FAD and its disease mechanisms. These abstracts are also readily available online.

Table of Contents

Table of tables

Table of figures

Publications

Published:

Familial Alzheimer's disease patient-derived neurons reveal distinct mutation-specific effects on amyloid beta.

Arber C, Toombs J, Lovejoy C, Ryan NS, Paterson RW, Willumsen N, Gkanatsiou E, Portelius E, Blennow K, Heslegrave A, Schott JM, Hardy J, Lashley T, Fox NC, Zetterberg H, Wray S.

Mol Psychiatry. 2019 Apr 12. doi: 10.1038/s41380-019-0410-8.

In preparation:

Familial Alzheimer's disease mutations in *PSEN1* accelerate human stem cell neurogenesis.

Charles Arber, Christopher C Lovejoy, Nanet Willumsen, Argyro Alatza, Jacqueline Casey, Georgie Lines, Caoimhe Kerins, Anika Muller, Henrik Zetterberg, John Hardy, Natalie S Ryan, Nick C Fox, Tammaryn Lashley and Selina Wray

Variability in the type and layer distribution of cortical Aβ pathology in familial Alzheimer's disease.

Nanet Willumsen, Teresa Poole, Jennifer M Nicholas, Nick C Fox, Natalie S Ryan, Tammaryn Lashley.

Chapter 1

Introduction

1 Introduction

1.1 Alzheimer's disease and familial Alzheimer's disease

Alzheimer's disease (AD) is the most common form of dementia, with dementia estimated to have affected 47 million people worldwide in 2015, with numbers set to increase (M. Prince *et al.*, 2013; World Health Organization, 2015). The cause of sporadic AD (sAD) is unknown, although there are well established genetic risk factors such as carrying at least one *Apolipoprotein E4* (*APOE4)* allele or Triggering receptor expressed on myeloid cells 2 (*TREM2)* single nucleotide polymorphisms (Corder *et al.*, 1993; Guerreiro *et al.*, 2013; Thorlakur Jonsson *et al.*, 2013; Poirier *et al.*, 1993; Saunders *et al.*, 1993). Mutations in the *Amyloid precursor protein (APP*) promoter region may also increase AD risk (Brouwers *et al.*, 2006). Additionally, sex is another AD risk factor with females more at risk than males (Hebert *et al.*, 2013), however the precise mechanisms underlying this risk are unclear (Ferretti *et al.*, 2018). AD remains a clinico-pathologically diagnosed disease. By definition, AD brains show an accumulation of pathological misfolded proteins into amyloid beta (Aβ) plaques and neurofibrillary tangles (NFTs) containing tau and an inflammatory response in the form of activated microglia (H. Braak & Braak, 1991; Dá Mesquita *et al.*, 2016; Hyman *et al.*, 2012; Dietmar R. Thal *et al.*, 2002).

Familial Alzheimer's disease (FAD) is similar to sAD with many shared clinical and pathological features such as memory decline and accumulation of misfolded tau and Aβ proteins. However, FAD is caused by autosomal dominant mutations in the *Presenilin 1* (*PSEN1), PSEN2* or *APP* genes and by rare *APP* duplications (Goate *et al.*, 1991; Kasuga *et al.*, 2009; Rovelet-Lecrux *et al.*, 2006; Scheuner *et al.*, 1996; Sherrington *et al.*, 1996; Sleegers *et al.*, 2006). *APP* lies on chromosome 21 and individuals with Down syndrome (DS), due to trisomy of chromosome 21, invariably develop amyloid plaques and NFTs at autopsy if they live until middle age (J. Hardy & Allsop, 1991; Prasher *et al.*, 2008; Wiseman *et al.*, 2018). In FAD, although symptoms tend to begin at a younger age compared to sAD, disease duration generally appears to be similar (Bateman *et al.*, 2011; Godbolt *et al.*, 2004; Ryman *et al.*, 2014).

Both sAD and FAD are neurodegenerative conditions for which there are currently no disease-modifying therapies, although there are reports of an

amyloid modifying treatment slowing disease progression in clinical trials (Sevigny *et al.*, 2016). Available symptomatic treatments have limited effects (Casey *et al.*, 2010) and there have been many failed clinical trials (Doody *et al.*, 2013; Egan *et al.*, 2018; Vandenberghe *et al.*, 2016). As FAD is caused by genetic mutations, its origin is known and can be studied to understand the pathomechanisms of disease. Due to their similarity, understanding FAD may also contribute to understanding sAD and has the potential to improve knowledge and options for the development of future AD treatments.

1.2 Clinical aspects of FAD

Clinically, patients with FAD typically present with early amnestic symptoms (Storandt *et al.*, 2014), although atypical cognitive symptoms and additional neurological features are also seen (Bateman *et al.*, 2011; Joshi *et al.*, 2012; Ryan *et al.*, 2016). The age at symptom onset can be variable but typically ranges between 30-60 years, with significant proportions of the variance in age at onset accounted for by mutation type and family history (Bateman *et al.*, 2011; Gómez-Tortosa *et al.*, 2010; Ryan *et al.*, 2016; Ryman *et al.*, 2014). *PSEN2* mutation carriers typically have later ages at onset than *PSEN1* and *APP* mutation carriers while *PSEN1* mutation carriers generally have earlier onset than *APP* mutation carriers. Disease duration may also be longer in *PSEN2* carriers (Lippa *et al.*, 2000; Marín-Muñoz *et al.*, 2016; Ryman *et al.*, 2014; Shea *et al.*, 2016). Interestingly, there may be possible disease onset modifiers in *PSEN2* mutation carriers, with genome analysis linking various loci to age at onset, including a region in chromosome 17, near the gene for Nicastrin, a component of γ-secretase (Marchani *et al.*, 2010; Wijsman *et al.*, 2005). In a meta-analysis of age at onset and disease duration, polynomial regression revealed an inverted U-shaped relationship, with shorter disease durations in those with particularly early or late onset (Ryman *et al.*, 2014; Shea *et al.*, 2016).

Within *PSEN1* mutation carriers, clinical presentation may be influenced by mutation location. *PSEN1* mutations prior to codon 200 have been associated with an earlier age at onset compared to those with mutations post-codon 200 (Lippa *et al.*, 2000; Shea *et al.*, 2016). Motor symptoms have also been shown to be more frequent in *PSEN1* post-codon 200 cases (Ryan *et al.*, 2015a; Vöglein *et al.*, 2019).

Other factors that are relevant in sAD may also affect FAD onset and progression, although they are less understood. For example, females have a higher risk of dementia compared to males and in FAD males have been shown to have a non-significant later age at onset compared to females in a meta-analysis (Ryman *et al.*, 2014). However, in sAD it has also been suggested that differences in presentation between males and females may lead to altered interpretation of onset and even diagnosis, leading to perceived sex differences, and it is possible these issues could exist in FAD (Liesinger *et al.*, 2018). *APOE* genotype may also play a role on features of FAD, however its exact effect is not known and will be discussed in chapter: 1.14. Further to this, the interaction of these risk modifiers may also be important. For example, associations between sex and AD may be mediated by other factors, including *APOE* (Altmann *et al.*, 2014; Breitner *et al.*, 1999).

1.3 **Aβ pathology in Alzheimer's disease**

Neuropathologically, sAD is characterised by an accumulation of pathogenic misfolded proteins into extracellular Aβ plaques and intracellular tau forming neurofibrillary tangles, with an inflammatory reaction (Dá Mesquita *et al.*, 2016). In FAD the same pathological features are found, although it has been proposed that Aβ accumulation may be higher (Cairns *et al.*, 2015). Amyloid plaques are considered one of the classic neuropathological hallmarks of AD and this observed accumulation of Aβ, along with the finding that *APP* mutations cause FAD, lead to the amyloid cascade hypothesis (JA Hardy & Higgins, 1992). The pre-aggregate oligomeric forms of Aβ peptides that are also present in AD are thought to be the main toxic species of Aβ causing cell death (Deshpande *et al.*, 2006; Kutoku *et al.*, 2015). This may be particularly true at early stages of AD, prior to plaque development. Some have proposed that the development of plaques is initially a protective mechanism; providing a sink for these toxic oligomeric Aβ peptides (Treusch *et al.*, 2009). This is a debated hypothesis, but eventually the disruption caused by large aggregates is thought likely to negatively impact upon cellular functioning and health (Adlard & Vickers, 2002).

There are multiple Aβ peptides of differing lengths which are found in AD and these slight changes in length can have impactful effects on the nature of the peptide. The most common Aβ peptides investigated pathologically using current

methods are Aβ40, 42, 43 and pyroglutamated Aβ, a toxic post translationally modified form of Aβ (Harigaya *et al.*, 2000; Portelius *et al.*, 2015; Russo *et al.*, 2002; Saido *et al.*, 1995). Other Aβ peptides do exist but are less frequently detected using current techniques and so have been studied to a lesser degree. Revealing the full structure of the Aβ peptide has not been easy, and is complicated by its environmental conditions. Whether the Aβ domain is associated with γ-secretase, free in the extracellular matrix, present as a monomer, oligomer or in a fibrillar form gives rise to structural differences. Aβ can exist with either predominant alpha helical structures or beta-sheets and is able to transition between alpha helical and beta sheets (M. Yang & Teplow, 2008). Importantly, the C-terminal end is likely to influence aggregation propensity, with hydrophobic residues stabilising and shifting the state to more beta sheet-formation (Zeenat *et al.*, 2014). The C-terminal end is where differences in peptide length occur.

Assemblies of monomers as oligomers may exist as different species which can affect the toxicity of the oligomers (Ahmed *et al.*, 2019). Aβ fibrils contain β-sheets, which lead to β-pleated sheet aggregates (Benzinger *et al.*, 1998). Protein sequence can influence the organization of the β-pleated sheets and overall fibrillary formation (Balbach *et al.*, 2000). A recent study has finally provided the structure of Aβ fibrils, derived from human AD brains (Kollmer *et al.*, 2019). The fibrils were formed of right-handed twists of beta sheets connected together by hydrophobic residues. Three main forms were observed accounting for 75% of the fibrils present, highlighting structural heterogeneity within Aβ fibrils. Importantly, this work uncovered differences between human derived fibrils and those obtained by other methods, supporting the need for studies to be biologically relevant to human AD.

Aβ42

Aβ42 is the most commonly observed peptide using immunohistochemical techniques on human AD brain tissue. There is reduced Aβ42 seen in AD CSF (Blennow et al., 2010) due to increased cortical Aβ42 deposition in AD, indicating this peptide is pathogenic. Increased Aβ42 in FAD compared to sAD brain tissue has also been observed (Lemere *et al.*, 1996). Aβ42 is a hydrophobic peptide and consequently, prone to aggregation and is believed to be the most

aggregation prone isoform (Jarrett *et al.*, 1993). In SY5Y cell culture models using synthetic Aβ peptides, Aβ42 has been shown to aggregate into oligomers faster than Aβ40 and Aβ43. This increased aggregation potential not only provides seeds for further enhanced aggregation but the faster generation of oligomeric species is also likely to be detrimental, as oligomers have been shown to be the most toxic species (Fu *et al.*, 2017). As it was readily observable and measurable, a lot of focus was initially placed on studying Aβ42. However, other isoforms are also likely to be important in AD and as techniques advance, previously undetectable forms can now be investigated.

Aβ40

Aβ40 is the most abundant Aβ peptide observed in human CSF including in AD patients (Fukuyama *et al.*, 2000; Mehta *et al.*, 2000), and in human cell lines (Asami-Odaka *et al.*, 1995; Turner *et al.*, 1996). Aβ40 is two amino acids shorter than Aβ42 and resulting in a less aggregation prone form. This consequently enables Aβ40 to be more readily cleared than Aβ42 and is likely the reason Aβ40 is less frequently deposited in the cortex as plaques. However, Aβ40 is frequently found within vessel walls as cerebral amyloid angiopathy (CAA), indicating that it is able to aggregate and cause pathology. Additionally, oligomeric species of Aβ40 may have toxic effects on cellular health (Hayashi *et al.*, 2009; Jana *et al.*, 2016; Sarkar *et al.*, 2014).

Aβ43

Compared to Aβ42, Aβ43 has an additional threonine at position 43 of the C-terminus. This has been show to help its nucleation and aggregation potential *in vitro* using synthetic peptides (Conicella & Fawzi, 2014). Importantly, similar observations have been made *in vitro* in a Drosophila transgenic model, with a high ability of Aβ43 to aggregate observed, and it was concluded this may trigger aggregation of the Aβ40 peptide, highlighting how it can affect pathology in multiple ways (Burnouf *et al.*, 2015). While Aβ43 has typically been less studied, recent research has highlighted Aβ43 may be particularly important in FAD. For example, it was shown that Aβ43 was raised in iPSC derived cortical neurons from *PSEN1* R278I mutation cell lines (Charles Arber *et al.*, 2019a). This was also observed in a knock in mouse model expressing the PSEN1 R278I mutation,

along with accelerated plaque pathology including pronounced Aβ43 deposition in plaque cores (Saito *et al.*, 2011b).

1.4 **Tau pathology in Alzheimer's disease**

Tau is a microtubule binding protein encoded by the *microtubule associated tau protein (MAPT*) gene (Andreadis *et al.*, 1992). Tau contains either three or four repeats of a microtubule binding domain (termed 3R/4R tau) which is important for its function as a microtubule stabilising protein (Cleveland *et al.*, 1977a, 1977b; G. Lee *et al.*, 1989). Tau pathology is also seen in AD, with tau present in intracellular tangles known as neurofibrillary tangles (NFTs), made up of hyperphosphorlyated 3R and 4R tau peptides (Grundke-Iqbal *et al.*, 1986). However tau pathology is not specific to AD as it is seen in many other neurodegenerative diseases (D. W. Dickson *et al.*, 2010; Kouri *et al.*, 2011). Mutations in the *MAPT* gene coding for tau cause familial Frontotemporal dementia (FTD), however no mutations in *MAPT* have so far been linked to AD (Rizzu *et al.*, 1999; Rosso *et al.*, 2003; Rosso *et al.*, 2001). In FAD, tau accumulation is seen as a secondary pathology, with Aβ considered the primary cause of disease. Analysis of brain scanning and CSF data has indicated tau deposits in brains of those with sAD after Aβ deposition begins to occur and this has lead to a hypothesis whereby Aβ pathology precedes tau pathology (Jack Jr *et al.*, 2010). In FAD, plasma Aβ biomarker readouts of Aβ pathology are altered in FAD E280GA mutation carrying children compared to non-carriers (Quiroz *et al.*, 2015). Similar observations are also seen with higher Aβ42 concentrations in CSF and plasma in E280A mutation carrying young adults compared to controls (Reiman *et al.*, 2012). In FAD mutation carriers participating in the multi-centre Dominantly Inherited Alzheimer Network (DIAN) study, CSF Aβ42 is reduced 10-20 years before expected age at onset in association with amyloid deposition on amyloid imaging also seen around this time (Fagan *et al.*, 2014). Recent longitudinal biomarker analysis has confirmed Aβ pathology as the earliest preclinical feature in FAD (G. Wang *et al.*, 2019). This shows how there is a sequence of events which occur after Aβ pathology begins, although the precise mechanisms for how Aβ leads to tau pathology are still unclear. Despite this, tau on Positron-emission tomography (PET) imaging does correlate with cognitive decline in AD (Ossenkoppele *et al.*, 2016) and FAD after alterations in amyloid (Gordon *et al.*, 2019).

A three tiered pathological grading system has been established for the neuropathological confirmation of AD, which combines the results from Thal phasing (Aβ plaque location), Braak and Braak staging (NFTs) and Consortium to Establish a Registry for Alzheimer's Disease (CERAD) scoring (frequency of neuritic plaques) (Hyman *et al.*, 2012). Thal phasing scores Aβ plaques, from 0 to 5, based on their presence, starting in the neocortex, allocortex, basal ganglia and finally cerebellum (Dietmar R. Thal *et al.*, 2002). Braak and Braak staging scores tau, from I to VI, based on the presence of NFTs throughout the proposed regions of chronological tau spread, beginning in the transentorhinal cortex, spreading to limbic regions and finally spreading to the isocortical regions (H. Braak & Braak, 1991; Nagy *et al.*, 1998). CERAD scoring assesses the frequency of neuritic plaques, with higher frequency given higher scores (Mirra *et al.*, 1991). The semi-quantitative grading guide is shown in Figure 1-1. Using this system the pathology grade given is assessed by frequency of plaques within a given field. Combining these grading systems generates a score for amyloid plaques (A), tau positive NFT's (B) and neuritic plaques (C), creating the 'ABC' score, graded 0-3 for each category, determining the likelihood of sAD with 'A3B3C3' definite Alzheimer's, as shown in Table 1-1, from Montine *et al.* (2012). The grading systems are also used to neuropathologically confirm FAD pathology.

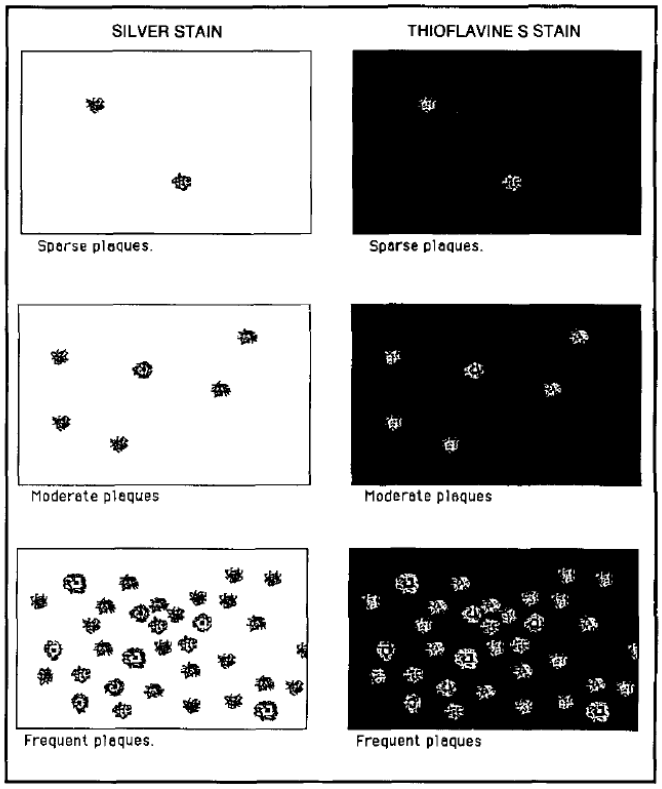

Figure 1-1 CERAD scoring guide.

Cartoon example of scoring level (Sparse, moderate, frequent) for senile plaques in 100X microscopic field. Image taken from Mirra et al. (1991).

"A"	Thal Phase for Aβ plaques	"B"	Braak and Braak NFT stage	"C"	CERAD neuritic plaque score
0	0	0	None	0	None
1	1 or 2	1	I or II	1	Sparse
2	3	2	III or IV	2	Moderate
3	4 or 5	3	V or VI	3	Frequent

AD neuropathologic change		B[a]		
A[b]	C[c]	0 or 1	2	3
0	0	Not[d]	Not[d]	Not[d]
1	0 or 1	Low	Low	Low[e]
	2 or 3[f]	Low	Intermediate	Intermediate[e]
2	Any C	Low[g]	Intermediate	Intermediate[e]
3	0 or 1	Low[g]	Intermediate	Intermediate[e]
	2 or 3	Low[g]	Intermediate	High

Table 1-1 ABC score for AD neuropathologic change.

"A" refers to suggested modified Thal staging of Aβ (Dietmar R. Thal *et al.*, 2002). "B" refers to suggested modified Braak and Braak staging of NFT (Heiko Braak *et al.*, 2006; H. Braak & Braak, 1991). "C" refers to CERAD scoring system of neuritic plaque scoring (Mirra *et al.*, 1991). Scores are then combined to generate the ABC score with grades from 0 to 3. Table adapted from Hyman *et al.* (2012); Montine *et al.* (2012).

1.5 Genetics of familial Alzheimer's disease

FAD can be caused by autosomal dominantly inherited mutations in one of three genes, *APP, PSEN1* and *PSEN2* and by *APP* duplications. These mutations are thought to show almost 100% penetrance, although incomplete penetrance has rarely been observed (Thordardottir *et al.*, 2018). A rare *APP* variant (A673T) has also been reported in healthy Icelandic elderly controls that appears to be protective against the development of AD. This mutation leads to impaired β-secretase processing of APP, leading to a reduction in the production of Aβ *in vitro* (T. Jonsson *et al.*, 2012). Interestingly, a different substitution at the same site, the *APP* A673V variant, only appears to cause disease in the homozygous state and has been identified in an Italian family with an autosomal recessive pattern of inheritance (Di Fede *et al.*, 2009). Novel FAD mutations are still being discovered (Giau *et al.*, 2018; Guven *et al.*, 2019) and recently a patient with an early and aggressive form of FAD has been described who is homozygous for the *PSEN1* A431E mutation (Parker *et al.*, 2019). *PSEN1* mutations are the most common and currently there are over 300 known *PSEN1* mutations, 48 known *PSEN2* mutations and 59 known *APP* mutations, although not all are clearly pathogenic (Alzforum mutation database). *APP* duplications can also lead to FAD, with Aβ plaque pathology and prominent CAA (Cabrejo *et al.*, 2006; Rovelet-Lecrux *et al.*, 2006). The phenotype of AD associated with *APP* duplications can be heterogeneous, even within a single family (Guyant-Marechal *et al.*, 2008). However, there is a particularly high incidence of seizures in *APP* duplication carriers (higher than in *APP* or *PSEN1* mutation carriers), and some also suffer intracerebral haemorrhage (McNaughton *et al.*, 2012; Zarea *et al.*, 2016). There are also *APP* mutations within the Aβ coding domain which cause severe CAA and recurrent intracerebral haemorrhage (Ryan & Rossor, 2010), discussed in 1.10 and 1.11.

1.6 **Amyloid precursor protein (APP)**

The *APP* gene encodes the amyloid precursor protein (APP). The physiological function of APP is unknown however is it likely involved in synaptic processes and maintenance (Leyssen *et al.*, 2005; Priller *et al.*, 2006; Z. Wang *et al.*, 2009), with early transgenic mice studies showing a protective effect of human APP against neurodegeneration (Mucke *et al.*, 1994). APP is a transmembrane precursor protein which undergoes processing into fragments via two related pathways. In the non-amyloidogenic pathway, APP is cleaved by α-secretase, releasing the extracellular soluble APPα fragment and preventing the formation of the Aβ peptide (Esch *et al.*, 1990; Lammich *et al.*, 1999). The remaining membrane bound C83 fragment is then cleaved by the γ-secretase complex releasing an extracellular P3 domain and the APP intracellular C domain (AICD).

The function of APP is unknown although it may be beneficial to neuronal health in conditions of neuronal damage in vitro and enhances cell proliferation in vivo (M. P. Demars *et al.*, 2011; Thornton *et al.*, 2006). The function of P3 is also unknown, however it may be neurotoxic and may promote inflammatory responses (Nhan *et al.*, 2015). The function of the AICD is still debated but it appears to have many functions, including nuclear signalling and transcriptional regulation (Bukhari *et al.*, 2017). These molecules related to the amyloid cascade are beginning to be investigated more as alterations in the levels of these proteins many have consequences on cellular health.

In the amylodogeneic pathway, APP is cleaved by β-secretase (BACE1) releasing the sAPPβ fragment (Vassar *et al.*, 1999). There is little known about this fragment. The remaining membrane bound C99 fragment then undergoes an initial endopeptidase cleavage releasing the AICD. The remaining Aβ peptide is then sequentially cleaved by carboxypeptidase-like cleavages by the γ-secretase complex. This produces Aβ peptides of varying length, between 38-43 amino acids, which are released from the membrane into the extracellular space (Qi-Takahara *et al.*, 2005).

APP is known to be a single pass transmembrane protein (Gralle *et al.*, 2002). On the intracellular C-terminal side is a short cytoplasmic tail. Crystal structure of the N-terminal side indicates that juxtaposed to the membrane is an unstructured domain followed by multiple conserved domains which form folding regions,

involved in protein interactions (Dulubova *et al.*, 2004; Rossjohn *et al.*, 1999; Y. Wang & Ha, 2004).

1.7 **Presenilin 1 (PSEN1) and Presenilin 2 (PSEN2) proteins**

PSEN1/2 code for the homologous multi-transmembrane proteins Presenilin 1 and Presenilin 2 (PSEN1/PSEN2), which form part of the four component γ-secretase complex along with Nicastrin, APh1 and PEN2, reviewed in De Strooper (2003). The assembly of the γ-secretase complex is suggested to occur on an initial APh1-nicastrin scaffold, which PSEN1 binds to (St George-Hyslop & Fraser, 2012). This likely occurs in the secretory organelles on its transport to the cell surface (Kaether *et al.*, 2002). Collectively, the γ-secretase complex is believed to compose of 20 transmembrane (TM) regions contributed to by the four components mentioned. Within the TM region, PSEN1 is centrally located, with its amino-terminal fragment (NTF) packing against PEN2 and its carboxyl-terminal fragment (CTF) interacting with APh-1, which is associated with Nicastrin, whose extracellular domain directly binds Pen-2 (Bai *et al.*, 2015; Sun *et al.*, 2015). At the plasma membrane PSEN1 is able to interact with its substrates such as APP.

PSEN1/2 is believed to contain the catalytic subunit of γ-secretase within TM domains 6 and 7 at two conserved aspartate residues, with other regions important for protein binding and substrate stabilisation (Brunkan & Goate, 2005; De Strooper *et al.*, 2012; De Strooper *et al.*, 1998; Y. M. Li *et al.*, 2000; Wolfe *et al.*, 1999). PSEN1/2 has two main catalytic functions, an initial epsilon cleavage activity and secondary carboxypeptidase cleavage activity.

Catalysis of APP, a major PSEN1 substrate, occurs via initial epsilon cleavage producing the AICD and a membrane bound Aβ peptide cleaved at residue 48 or residue 49 (Kakuda *et al.*, 2006). Following this, the peptide undergoes successive carboxypeptidase cleavage at every ~3rd residue, followed by release (Takami *et al.*, 2009). The selection of epsilon cleavage at 48 or 49 determines the Aβ peptides that can be produced via two separate production pathways, as shown in Figure 1-2.

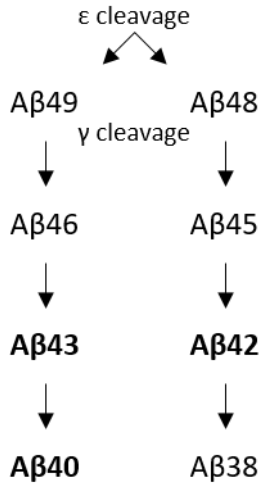

Figure 1-2 Aβ cleavage by

Episilon (ε) cleavage at 48/49 determines the downstream Aβ peptides that can be produced by successive γ-secretase cleavages. Aβ49>46>43>40 and Aβ48>45>42>38. Indicated in bold are Aβ43, 40 and 42, commonly investigated Aβ peptides.

Conformational states of PSEN1 are believed to relate to substrate binding and retention time and likely substrate cleavage processing due to accessibility to PSEN1 active sites (Somavarapu & Kepp, 2017). Indeed, conformational changes can lead to altered Aβ peptide production (Tominaga *et al.*, 2016). Besides cleaving APP, γ-secretase also cleaves other substrates such as Notch and these may be important in FAD pathogenesis (Chávez-Gutiérrez *et al.*, 2012; Szaruga *et al.*, 2015).

Using immunolabelling in adult human brain tissue, PSEN1 was shown to be widely distributed in cortical and subcortical regions, with claims that the distribution and levels of PSEN2 and PSEN1 immunolabeling were similar between sporadic AD and control brains. PSEN1 was particularly prominent within large pyramidal neurons in cortical layers 2, 3 and 5 in 12 control brains. Generally in the sporadic AD brain, PSEN1 and PSEN2 levels were not altered in pyramidal neurons of layers 3 and 5, layers which have dense Aβ pathology. When comparing controls with sAD and FAD cases, similar distribution was seen across all groups, except in one *PSEN1* M139I mutation case (Mathews *et al.*, 2000). Concerning the precise cellular locations, a study in mouse brain has shown that PSEN1 is distributed through the neuroaxis, mainly within neurons and throughout axon processes (Siman & Salidas, 2004). These data show that PSEN1 expression does not differ between FAD mutation carriers or healthy

controls, implying its function is relevant in disease rather than that genetic mutations lead to differences in levels of transcription.

1.8 *PSEN1* mutations on PSEN1 activity in familial Alzheimer's disease

Within *PSEN1,* mutations are found throughout the protein coding region and it is emerging that specific mutation locations may affect disease pathophysiology and phenotype (Bentahir *et al.*, 2006; O. Nelson *et al.*, 2010; Ryan *et al.*, 2016). It was originally assumed that FAD mutations would work by increasing Aβ levels, however evidence suggests there are different ways in which mutations cause disease, and this is influenced by the mutation location.

One way in which mutations can effect PSEN1 is via the endopeptidase activity (Bentahir *et al.*, 2006; Capell *et al.*, 2000). Mutations which effect the endopeptidase activity could affect Aβ levels and which pathway of Aβ production is selected, leading to altered ratio of the peptides within those pathways (Chávez-Gutiérrez *et al.*, 2012).

Many *PSEN1* mutations lead to FAD by decreasing the carboxypeptidase activity. FAD mutations that severely compromise γ-secretase activity affect residues that map near the proposed active site (Bai *et al.*, 2015; Sun *et al.*, 2017). The effect of compromised carboxypeptidase activity results in release of longer Aβ peptides which are more prone to aggregation (Chávez-Gutiérrez *et al.*, 2012; Scheuner *et al.*, 1996; Szaruga *et al.*, 2015) This in turn leads to more oligomeric Aβ and greater extracellular deposition (Dennis J. Selkoe, 1997).

PSEN1 exists as an immature protein which requires endoproteolysis to become mature PSEN1, consisting of the PSEN1 N-terminal fragment (NTF) and C-terminal fragment (CTF) (Thinakaran *et al.*, 1996). Mutations near the endoproteolysis site are proposed to inhibit the cleavage that converts the immature form into the mature product (Steiner *et al.*, 1999). This can then lead to altered processivity by the enzyme (Quintero-Monzon *et al.*, 2011). Interestingly, even within the immature PSEN1, the catalytic pore is still able to be formed (Takeo *et al.*, 2012), which suggests that γ-secretase activity can still occur, although it is likely reduced, possibly explaining altered Aβ peptide production in mutations near this location.

Mutations not within the catalytic domain can likely affect the protein structure/stability and this may also impact upon interactions with substrate and modulators, which will contribute to disease (Bai *et al.*, 2015; Somavarapu & Kepp, 2016; Sun *et al.*, 2017).

1.9 Effect of *APP* mutations on APP processing in familial Alzheimer's disease

The mutations in *APP* may lead to FAD by interfering with APP processing, which appears to alter Aβ ratios (Szaruga *et al.*, 2017). In particular, mutations in APP can destabilise the enzyme-substrate complex reducing sequential cleavage, leading to the premature release of longer, more aggregation prone, Aβ peptides. The mutations within *APP* could affect the interaction with the PSEN1 catalytic domain and lead to release of longer peptides from γ-secretase prematurely and increasing Aβ42:40 ratios, while mutations near the α-secretase site may influence α or β secretase cleavage of APP, increasing the ratio of β secretase amyloidogenic selection (De Jonghe *et al.*, 2001; Herl *et al.*, 2009).

As mentioned, *APP* mutations can lead to increased Aβ42:40 ratios and this can be by increased relative Aβ42 production, as well as decreased relative Aβ40 production (Murrell et al., 2000, Hsu et al., 2018). These altered ratios can cause disease even when total levels of Aβ are lowered (Ancolio et al., 1999), highlighting the importance of the balance between Aβ peptides.

1.10 Cerebral amyloid angiopathy

CAA is caused by deposition of Aβ within cerebral vessels leading to weakening and damage to the vessels and impaired perivascular drainage, reviewed in Bell and Zlokovic (2009); Carare *et al.* (2013); Revesz *et al.* (2003). CAA can be seen through the cortex including the frontal and temporal regions however there appears to be a predisposition towards the occipital cortex, with higher CAA frequently observed in this region (J. Attems, 2005; Johannes Attems *et al.*, 2005; Lopez & Claassen, 1991; Vinters & Gilbert, 1983). CAA is a common feature in AD, with reports of around 76% prevalence in AD brains at autopsy, although like amyloid plaques, it can also be seen in patients without dementia (Johannes Attems *et al.*, 2005; Vinters & Gilbert, 1983). CAA is a common pathological feature seen in FAD, while additional associated pathologies such as

microbleeds and white matter hyperintensities may be seen on neuroimaging in some individuals with FAD (Ryan *et al.*, 2012; Ryan *et al.*, 2015a). Down syndrome-AD (DSAD) individuals also have prominent CAA, which appears to be more extensive than in sAD (Carmona-Iragui *et al.*, 2017; Helman *et al.*, 2019).

Artery walls are comprised of three layers. The innermost layer, the tunica intima, is made up of endothelial cells surrounded by an inner basement membrane. The tunica media is the middle layer, primarily comprised of smooth muscle cells. The outer layer, the tunica externa, contains the outer basement membrane (Cipolla, 2009). It was thought deposition of primarily Aβ40 and Aβ42 in arteries developed in the outer basement membrane, gradually developing and being present in the vicinity of smooth muscle cells, reviewed in Revesz *et al.* (2003); Dietmar Rudolf Thal *et al.* (2008). More recent evidence however, suggests it may develop in the basement membrane of the tunica media (Keable *et al.*, 2016). CAA is commonly graded by assessing the degree of Aβ deposition and health of the vessel, ranging from no deposition, through mild, moderate to severe (Vonsattel *et al.*, 1991).

1.11 Cerebral amyloid angiopathy in familial and sporadic Alzheimer's disease

Hereditary cerebral haemorrhage with amyloidosis (HCHWA) is a form of CAA, which is caused by the autosomal dominantly inherited mutation *APP* E693Q, also known as the Dutch mutation. HCHWA presents with haemorrhagic stroke between the ages of 39-76 years (average age 50 years), and patients generally go on to develop dementia. Pathologically, there is severe amyloid deposition in the vasculature and diffuse plaques are present, but neurofibrillary tangles are absent (Timmers *et al.*, 1990). This mutation is associated with altered APP processing increasing relative levels of Aβ and N-terminally truncated Aβ, accelerated Aβ aggregation *in vitro* and increasing fibril formation (Fernandez-Madrid *et al.*, 1991; Levy *et al.*, 2006; Van Broeckhoven *et al.*, 1990). There are other hereditary forms of CAA caused by *APP* mutations which lie within the APP Aβ domain, just distal to the α-secretase cleavage, such as the E693K (Italian) which lead to reduced Aβ42:Aβ40 ratio due to decreased Aβ42, with no alteration in Aβ40 levels (Bugiani *et al.*, 2010). There is also an *APP* L705V mutation which

presents with severe CAA and haemorrhages but no parenchymal Aβ or NFT's (Obici *et al.*, 2005).

Interestingly, alternative mutations at the E693 site, lead to different clinical phenotypes and neuropathological features. The Arctic (E693G) mutation causes dementia, with no signs of stroke or vascular lesions detected upon imaging in mutation carriers. Pathologically, there is predominant Aβ40 with a high fibrillisation propensity, neuritic plaques and NFT's, in addition to CAA (Kamino *et al.*, 1992; Nilsberth *et al.*, 2001). This highlights the importance of the specific mutations even at the same location which can lead to distinct pathological and clinical phenotypes, although CAA pathology is prominent in all these intradomain APP mutations. Other nearby FAD-causing *APP* mutations include the D693deletion mutation, which display very low Pittsburgh compound (PiB) - PET amyloid on neuroimaging. Surprisingly the ratio of Aβ42:Aβ40 was unchanged in this variant and overall both Aβ42 and Aβ40 levels were decreased. With decreased Aβ levels it would be expected that reduced risk of AD may be seen, however, this mutation leads to an increased resistance to degradation of the Aβ peptide, and potentially increased oligomerisation, leading to prolonged toxic effects of the oligomers (Tomiyama *et al.*, 2008). Mutations can cause both CAA as well as plaque pathology, such as the *APP* D694N (Iowa) mutation which displays intense Aβ40 plaque pathology (Grabowski *et al.*, 2001). It is important to know the likelihood of CAA within a given mutation as this may influence response to amyloid modifying therapies. CAA related pathologies increase with amyloid-modifying therapeutics, with an exacerbation of CAA and haemorrhage a potential consequence (Nicolll *et al.*, 2003; Sakai *et al.*, 2014; R. A. Sperling *et al.*, 2011; Zotova *et al.*, 2013b).

As mentioned above, some FAD cases are particularly associated with CAA and neuroimaging features of CAA appear to be more common in FAD than sAD (Carmona-Iragui *et al.*, 2017). Certain FAD mutations have been associated with more severe CAA, particularly those *APP* mutations within the Aβ coding domain (Ryan & Rossor, 2010). Differences may also exist between *PSEN1* mutation carriers with mutations post-codon 200 reported to cause more severe CAA pathology than pre-codon 200 mutations (David M. A. Mann *et al.*, 2001). Case

reports do however show that there is large variation in CAA presence between individuals so other factors may also play a role.

Understanding the impact of CAA is important as it may, possibly in conjunction with parenchymal Aβ pathology, be associated with cognitive decline (Boyle *et al.*, 2015; Vidoni *et al.*, 2016). Furthermore, as mentioned previously, CAA may transiently increase following amyloid modifying therapy (Nicoll *et al.*, 2006; Nicolll *et al.*, 2003). Due to this effect, it is particularly important to understand CAA in FAD as amyloid-modifying therapies continue to be explored in clinical trials for FAD mutation carriers.

1.12 **Aβ clearance**

Although Aβ build up is a hallmark of sAD and FAD, a number of Aβ clearance mechanisms exist. The understanding of Aβ clearance mechanisms is continually developing and although currently there are multiple known ways of clearance, more recently described methods are being explored. The precise mechanisms of some of these pathways, and the importance of their roles as major contributors to Aβ clearance are unknown (M. K. Rasmussen *et al.*, 2018; Tarasoff-Conway *et al.*, 2015).

Cellular uptake

Aβ can be internalised and degraded and internalised and shunted across cells within cells of the CNS, with key cells involved in these clearance pathway have been reviewed by others, including astrocytes (Ries & Sastre, 2016) perivascular macrophages (Bell & Zlokovic, 2009; Lai & McLaurin, 2012) and microglia (Doens & Fernández, 2014; Paresce *et al.*, 1996; Ries & Sastre, 2016). These cells can express several receptors involved in the recognition of Aβ or Aβ bound substrates and the subsequent internal degradation can occur via multiple routes which are beyond the scope of this thesis, but are discussed elsewhere, see Tarasoff-Conway *et al.* (2015). An important microglial receptor involved in Aβ internalisation and clearance is TREM2, whose risk SNPs are implicated in AD (Guerreiro *et al.*, 2013; Thorlakur Jonsson *et al.*, 2013; Lill *et al.*, 2015). While cellular uptake is a clearance mechanism of Aβ, it is possible that eventual dysregulation in cellular processes due to increased toxic Aβ can occur (Tarasoff-Conway *et al.*, 2015).

Cells also express receptors which are involved in the transport of ligands through cells. From analysis in mouse models and human cell models, an important mechanism for Aβ clearance across the BBB is via low-density lipoprotein receptors (LDLR) such as LDLR-related protein 1 (LRP1) dependant mechanisms which can mediate Aβ clearance across the BBB, with LRP1 being present in smooth muscle cells (Deane *et al.*, 2004; Kanekiyo *et al.*, 2012; Shibata *et al.*, 2000). Importantly, the AD linked APOE protein has been shown to influence Aβ clearance via LDL receptors, with APOE bound Aβ binding the very-low-density-lipoprotein (VLDL) receptor, where rate of clearance is impacted by APOE isoform in the order APOE2>APOE3>APOE4 (Deane *et al.*, 2008). APOE may also be important in clearance of Aβ via mediation by ATP-binding cassette transporters (ABC transporters) such as ABCA1. From review of the literature, it is thought that this mechanism is via promotion of APOE lipidation, which is important for Aβ-APOE interactions and clearance (Elali & Rivest, 2013). Again, *APOE* isoform specific effects appear to negatively attune the clearance capabilities, reviewed in Tarasoff-Conway *et al.* (2015). For example, compared to *APP/PS1ΔE9/ApoE3*$^{+/+}$*/Abca1*$^{-/+}$ mice, *APP/PS1ΔE9/ApoE4*$^{+/+}$*/Abca1*$^{-/+}$ mice exhibited greater Aβ deposition and microdialysis results showed reduced Aβ clearance (Fitz *et al.*, 2012). The authors postulated this was as a result of decreased Abca1 due to heterozygosity causing reduced lipidation which had a negative impact in the *APOE*4 genotype carriers. These data suggest that reduction in clearance via the BBB, especially in an APOE4 dependant manner, could lead to build up of Aβ and development of CAA.

Enzymatic degradation

One method of Aβ breakdown is through degradation enzymes located intracellularly and/or within the extracellular space, such as insulin degrading enzyme (IDE), angiotensin-converting enzyme-2 (ACE-2), and neprilysin (NEP) which have been shown effective in animal and cell models (Hama *et al.*, 2001; S. Liu *et al.*, 2014; Qiu *et al.*, 1998). As reviewed by (Miners *et al.*, 2011), it appears that enzymatic degradation of Aβ is more efficient on the monomeric soluble forms and aids in reducing Aβ into less neurotoxic forms which are easier to clear. However as they discuss, it is possible that some degradation pathways can lead to production of peptides with an altered formation that can increase the neurotoxic and aggregation propensity of the peptide. There is also a concern

that breakdown of fibrillary species may lead to release of oligomeric species, which may result in more cellular harm (Qiu *et al.*, 1998).

IDE is a protease that was found to be responsible for Aβ degradation, in addition to insulin cleaving capabilities (Qiu *et al.*, 1998), and it has been shown to contribute to the regulation of the degradation of Aβ and insulin *in vivo* (Farris *et al.*, 2003). A meta-analysis of human studies investigating IDE revealed IDE protein levels were reduced in AD patients compared to controls, although activity and mRNA levels showed variable results (H. Zhang *et al.*, 2018). Genomic investigations have highlighted the possible association of genomic variation within or near the IDE locus with AD (J. A. Prince *et al.*, 2003), implicating IDE clearance in sAD development.

ACE-2 cleavage occurs between Asp^{7}-Ser^{8} (Hu *et al.*, 2001) creating short n-terminal peptides and n-terminally truncated Aβ which appears to reduce the aggregation and deposition of Aβ. ACE-2 protein expression has been observed histologically in the endothelial and smooth muscle cells of the brain (Hamming *et al.*, 2004), suggesting enzymatic degradation of Aβ may occur at the vascular region. A reduction in ACE-2 activity has been observed in human post mortem brain tissue, and inversely correlated to levels of Aβ and tau pathology, with ACE-2 also significantly reduced in *APOE*4 carriers (Kehoe *et al.*, 2016).

NEP is a membrane protein with an endopeptidase activity that is mainly expressed in neurons but can also be active in astrocytes and microglia and is implicated in AD, reviewed in Grimm *et al.* (2013). It has been observed in multiple models that NEP is involved in Aβ clearance, and NEP inhibition is associated with increased Aβ deposits in a rat model (Iwata *et al.*, 2000) while increased NEP is associated with reduced deposition in a transgenic mouse models (Leissring *et al.*, 2003; Marr *et al.*, 2003). Reduced NEP mRNA, protein and activity levels have been observed in AD brain tissue compared to controls (S. Wang *et al.*, 2010) supporting the importance of clearance mechanisms in the AD. In concordance with this, loss of NEP function was shown to not only increase Aβ deposition but lead to CAA development in a mouse model (Farris *et al.*, 2007). Furthermore, analysis of human CSF revealed higher NEP levels were associated with reduce CSF Aβ42, while reduced NEP associated with greater neurodegeneration indicated by CSF tau levels (Grimmer *et al.*, 2019).

IPAD

Important mechanisms in relation to CAA are those that involve cerebral vasculature and the blood brain barrier (BBB), reviewed in Bell and Zlokovic (2009). This includes the mentioned receptor mediated transport across the BBB and importantly, perivascular drainage, which involves transport of interstitial fluid (ISF) containing Aβ along the basement membrane of capillaries and arteries, leading up to the leptomeninges (Preston *et al.*, 2003; Weller *et al.*, 1998). This has been called the intramural periarterial drainage (IPAD) pathway and allows the removal of solutes from the ISF.

CAA development via the IPAD pathway is an important method of clearance likely to contribute to CAA development. In the IPAD pathway, ISF flows along the extracellular spaces of the blood vessel cells such as the basement membrane (Carare *et al.*, 2008), leading to eventual drainage to lymphatic systems. The ISF contains solutes and waste for clearance and includes Aβ. Aβ drainage via this route can lead to build-up of Aβ, although the clearance mechanism which aids this clearance route is still uncertain (Diem *et al.*, 2017) but is likely powered by smooth muscle vasomotion (Aldea *et al.*, 2019). APOE isoforms are also likely to affect clearance efficiency by this mechanism, with APOE4/Aβ complexes displaying weaker attachment to laminin of the basement membrane compared to APOE3/Aβ, which will results in less efficient clearance of APOE4/Aβ complexes along the IPAD pathway (Zekonyte *et al.*, 2016). Reduced efficiency will allow opportunity for aggregation and deposition to occur.

One benefit of studying CAA in FAD is the reduction in comorbidities associated with age that are present in patients with sAD, which may also impair clearance routes. However, it is important to acknowledge the possibility that long term effects of mutations in *APP* and *PSEN1* may have had other impacts which could have implications for BBB integrity, influencing patho-mechanisms in non Aβ related ways. One such way could be through the PSEN1 substrate Notch (Geling *et al.*, 2002; Yu *et al.*, 2000), which is involved in the development and health of blood vessels (Gridley, 2007).

1.13 **APOE**

APOE is a 299 amino acid length lipoprotein (Rall Jr *et al.*, 1982) and reviewed in R. W. Mahley *et al.* (1984) with a receptor binding region and a lipid ligand binding region. Single nucleotide polymorphisms (SNPs) within the *APOE* gene leading to different amino acids at residues 112 and 158 produce the different isoforms of APOE: ε2, ε3 and ε4 (Rall Jr *et al.*, 1982; Weisgraber *et al.*, 1981). *APOE4* is the ancestral allele, although *APOE*3 is the most common, with *APOE*2 the least common (Fullerton *et al.*, 2000). In mice, APOE is highly expressed in the brain and mainly produced by astrocytes and microglia, although neurons and other cell types can also produce APOE (Xu *et al.*, 2006; Ye Zhang *et al.*, 2014).

APOE is involved in lipid metabolism, with a main function in transportation of lipids including cholesterol, reviewed in R. Mahley (1988). With this role, APOE has been associated with cardiovascular health as well as AD (Willer *et al.*, 2008). These two disorders can be interrelated, with cardiovascular health also associated with AD (G. Liu *et al.*, 2014). In addition to cardiovascular and sAD risk, APOE4 is associated with cerebrovascular risk, such as increased risk for ischemic stroke (Wei *et al.*, 2017). The SNPs which encode the various isoforms cause amino acid substitutions which lead to differences in isoform structure, stability and binding, thus APOE4 is found to be less stable, enabling greater aggregation propensity, and have an altered structure increasing its binding to certain molecules, including receptors (Morrow *et al.*, 2000; Zhong & Weisgraber, 2009).

As mentioned in 1.12, APOE is involved in Aβ clearance and this is via interaction with membrane protein receptors of the LDLR family (David M. Holtzman *et al.*, 2012). LDLR receptors have been shown to be expressed in neurons, glia and the blood brain barrier (Q. W. Fan *et al.*, 2001; Ye Zhang *et al.*, 2014). This ubiquitous expression indicates the importance of the function of these receptors and their signalling pathways.

1.14 ***APOE* genotype in Alzheimer's Disease**

Certain APOE isoforms are specifically associated with AD. The *APOE* gene has long been associated with risk for AD, with different allelic contributions determining the level of risk (Allen D. Roses, 1996; Corder *et al.*, 1993). The risk

of AD is increased as the allelic number of *APOE*4 increases, while *APOE*2 has been shown to have a protective role, associated with a later symptom onset in sAD (Chartier-Hariln *et al.*, 1994; Corder *et al.*, 1993).

Specifically in FAD, in a systematic review and meta-analysis it was found that the *APOE* genotype had no effect on age at onset (Forleo *et al.*, 1997; Ryman *et al.*, 2014). However, *APOE*4 was associated with younger onset in a single large Colombian kindred harbouring the *PSEN1* E280A mutation (Pastor *et al.*, 2003) while later, the *APOE*2 allele was found to delay onset while *APOE4* did not modify onset in *PSEN1* E280A mutation carriers (Vélez et al., 2016). *APOE*4 genotype has also shown to influence younger onset in *PSEN2* mutation carriers (Wijsman *et al.*, 2005), and *APP* V717I mutation carriers (Sorbi *et al.*, 1995).

Studies into the effect of *APOE* on disease duration in AD have yielded varying findings. In a meta-analysis of up to 1700 cases, it was shown to have no effect (Allan & Ebmeier, 2011). However in a separate study of AD patients, a trend towards increased disease duration in *APOE4* carriers was observed (Masullo *et al.*, 1998) and increased survival of *APOE4* carriers was found in another study of AD patients (Basun *et al.*, 1995). Little is known about the effect of *APOE* genotype on disease duration in FAD, but as APOE plays such a key role in AD in general, it seems important to explore its relationship to disease in FAD.

Evidence of an interaction between *APOE* genotype and *PSEN1* mutation has been investigated in carriers of the potentially risk modifying, but not FAD causing, *PSEN1* E318G mutation. Benitez *et al.* (2013) found that the *APOE*4 genotype was associated with AD in these mutation carriers. However, a subsequent study of 3420 individuals found no significant association of *PSEN1* E318G mutation and AD, regardless of *APOE* genotype (Hippen et al., 2016). Moreover, a study of two Brazilian cohorts, including 53 individuals with a familial history of AD and 120 with sporadic AD, concluded that the E318G variant increases AD risk, independently of *APOE*4 status (Abdala *et al.*, 2017).

1.15 **Interaction of APOE with Aβ**

APOE can bind Aβ and this has been shown in post-mortem human brain samples, whereby increased binding was present in *APOE*4 carriers (Mouchard *et al.*, 2019). Binding of Aβ by APOE through multiple bonds can accentuate the

aggregation of Aβ, particularly with APOE4 (Garai *et al.*, 2014; Ghosh *et al.*, 2018). Several studies have reported that there are human APOE isoform-dependent differences in Aβ deposition in mice, with greater deposition in the order: APOE4>APOE3>APOE2 (Bales *et al.*, 2009; Castellano *et al.*, 2011; Youmans *et al.*, 2012). In humans, *APOE*4 genotype associated differences have also been observed, with neuropathological studies suggesting that *APOE*4 allele dosage is associated with a number of pathological features in AD including increased intraneuronal Aβ, increased Aβ oligomerisation, and extracellular deposition in the brain (Christensen *et al.*, 2010; Hashimoto *et al.*, 2012; Kumar *et al.*, 2015; Schmechel *et al.*, 1993). While increased extracellular Aβ has been found in the human brain, the precise type of deposit may also be influenced, with *APOE*4 associating with the severity of CAA deposition but not with the amount of parenchymal Aβ (Chalmers *et al.*, 2003). These preferences may be due to a mixture of structural effects of APOE and Aβ isoforms, and the APOE clearance methods.

1.16 ***APOE*** **and cerebral amyloid angiopathy**

While CAA is a common feature of sAD and FAD, it is also influenced by *APOE* genotype in these conditions, which could be responsible for some of the variability observed. As mentioned previously, APOE is directly involved in Aβ clearance, with isoform specific efficiency. These differences at the molecular level are linked to pathological differences in Aβ pathology. In particular, the *APOE4* genotype is linked to CAA, with a meta-analysis indicating *APOE4* as a risk variant while *APOE2* may result in less CAA (Rannikmäe *et al.*, 2014; Rannikmäe *et al.*, 2013). Post mortem analysis in 93 sAD patients revealed a significant association of CAA pathology with the *APOE*4 genotype, with increasing *APOE*4 allele number associated with increasing severity of CAA (N. Sakae *et al.*, 2019).

However, the role of *APOE* genotype in CAA is not clear cut, as carriers of the *APOE2* allele have been found to have more severe CAA than those with the *APOE*3/3 genotype, despite the *APOE2* allele conferring lower risk for AD (P. T. Nelson *et al.*, 2013). In another study, it was found that AD patients who were *APOE*2 carriers had worse small vessel disease, as indicated by increased white matter hyperintensities, and this was associated with worse cognitive

performance in non-memory domains (Groot *et al.*, 2018). Although in a separate imaging study, which also included amyloid imaging with PiB, a protective effect of *APOE*2 on amyloid accumulation was suggested in patients with subcortical vascular mild cognitive impairment (MCI) (Y. J. Kim *et al.*, 2017). A Meta-analysis found *APOE*2 to be associated with certain markers of cerebrovascular disease (Schilling *et al.*, 2013), which may contribute to the association between *APOE*2 and CAA. As with the uncertainties in sAD, the role of *APOE* genotype in FAD is unclear although one study suggests the *APOE4* genotype does not influence neuroimaging features of CAA in FAD (Carmona-Iragui *et al.*, 2017). Yet an association between *APOE4* and more severe CAA at post mortem has been noted in a small number of FAD cases (Ryan *et al.*, 2015a).

1.17 **Microglia**

Microglia are the immune cells of the brain, initially derived from but separate to the peripheral macrophages. They have a varied range of functions such as clearance of debris, reaction to infection and neuronal damage, and have a role in signalling. Microglia are constantly surveying their local environment and maintaining it, playing a large role in homeostatic maintenance (Nimmerjahn *et al.*, 2005). During homeostatic surveying states, they do not necessarily have high expression of cytokines (Morris & Esiri, 1998), however under certain conditions they can become reactive and move to sites of insult/injury and provide support. This change in state leads to morphological and chemokine expression changes (Nagayach *et al.*, 2016). They were originally classified into two states – resting or activated, with the activated state existing in either an ‘M1’ inflammatory or ‘M2’ anti-inflammatory state. The M2 state was later subdivided into ‘M2A’ and ‘M2b’ (Boche *et al.*, 2013; Tang & Le, 2016).

The M1 and M2 states of microglia are associated with release of specific cytokines and cultured human microglia have been shown to produce these cytokines in response to stimulation (De Groot *et al.*, 2001). Cytokines are extracellular molecules which are used as signalling factors. In the M1 state, microglia release cytokines which lead to a pro-inflammatory response in the surrounding environment, examples of such cytokines are TNFα and interleukin 1β (Bamberger *et al.*, 2003; Combs *et al.*, 2001). In the M2 state, microglia release cytokines such as interleukin 4 and interleukin 10, which are associated

with an anti-inflammatory state, with these factors upregulating responses involved in tissue repair (Colton, 2009). Released cytokines are able to stimulate microglia, neurons and astrocytes, highlighting the range of impact these cells can have in the brain. Other methods by which microglia stimulate responses is by expression of MHC class II receptors, which are antigen presenting receptors which lead to stimulation of receptor cells, reviewed in Schetters *et al.* (2018).

These states are not however static and microglia, like macrophages of the periphery, can likely shift between these states, adapting to the needs of their local environment (Stout *et al.*, 2005). The ability of microglia to react to stimuli and change phenotypically, and their ability to revert back highlights how microglia represent a continuum rather than defined M1 and M2 states (Rezaie & Male, 2002). The changes can be short or long term with a pro-inflammatory or anti-inflammatory phenotype. This also highlights how study of microglia and microglia in diseases such as AD can be challenging. As AD changes over time and microglia can modify their response, the phenotype of studied microglia may only be relevant to the situation in which the study was conducted. Additionally, the restricted classification of microglial subtypes is a reductionist approach and it is important to recognise that microglia may express a range of different markers and cytokines that do not necessarily always co-segregate. Microglial phenotypes may therefore be better considered as a non-linear spectrum.

1.18 **Microglial subtypes**

Despite the concerns above, microglia are studied within these ‘M1/M2’ classifications. Particular markers have been associated with the different microglia activation classes and these are routinely used in immunohistochemical studies within both animal and human tissue and have been used extensively in research on AD (Hopperton *et al.*, 2017).

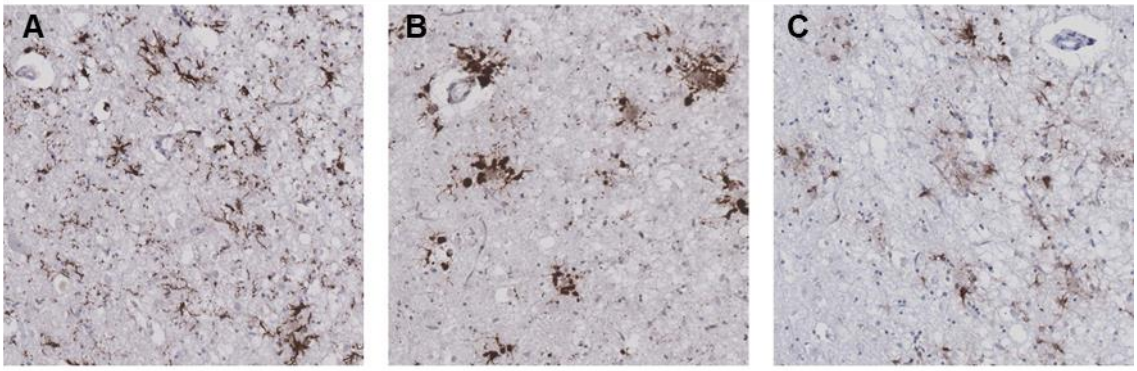

Figure 1-3 Representative images of microglia morphology.

A: Iba1 positive microglia with ramified processes. B: CD68 positive microglia with rounded morphology. C: CR3/43 positive microglia with shortened processes. Human frontal cortex, original images taken at 20x magnification.

Iba1

Ionized calcium-binding adaptor molecule 1 (Iba1) is a 17kDa protein involved in calcium binding and is encoded within the major histocompatibility domain (Imai *et al.*, 1996). Iba1 has been shown to specifically identify microglia via immunohistochemistry and its expression is increased upon activation of microglia (Ito *et al.*, 1998). Iba1 colocalises with F-actin and binds F-actin, indicating its function in membrane ruffling and phagocytosis (Ohsawa *et al.*, 2000; Y. Sasaki *et al.*, 2001). As Iba1 is thought to be expressed in most microglia it is often used as a global marker of surveying microglia (Boche *et al.*, 2013). Morphologically Iba1 positive microglia display highly ramified processes (Figure 1-3 A).

CD68

Cluster of Differentiation 68 (CD68) is a transmembrane protein and is a marker of phagocytosis due to its lysosomal location and is used to identify phagocytic microglia (Holness & Simmons, 1993; Pulford *et al.*, 1989). Expression of CD68 is commonly associated with an anti-inflammatory phenotype, active in clearing up debris (Boche *et al.*, 2013; Ulvestad *et al.*, 1994). However there is concern that CD68 can stain non-resident microglia in a pathologic brain, so caution needs to be applied when analysing CD68 data (Matsumoto *et al.*, 2007). Phagocytic microglia typically displaying a rounded morphology (Figure 1-3 B).

CR3/43

CR3/43 identifies microglia which are presenting major histocompatibility complex class II (MHC class II) molecules encoded by HLA DR+DP+DQ. CR3/43 is specifically localised to the plasma membrane of microglial cells (McGeer *et al.*, 1988; Styren *et al.*, 1990). These antigen presenting microglia are typically considered pro-inflammatory in AD (D. W. Dickson *et al.*, 1993; McGeer *et al.*, 1993). A typical CR3/43 morphology is shown in Figure 1-3 C.

1.19 **Microglia in familial and sporadic Alzheimer's disease**

Neuroinflammation is associated with many neurodegenerative diseases. Importantly, recent genetic studies show that inflammation and microglial related genes are linked to AD risk (Villegas-Llerena *et al.*, 2016), suggesting they have an important role in AD. There are multiple factors which can stimulate microglia in neurodegeneration, but importantly for AD, Aβ can act as an immune activator, reviewed in (C. Y. D. Lee & Landreth, 2010). In response to Aβ, microglia have been shown to release TNFα and interleukin 1β which are pro-inflammatory cytokines (Bamberger *et al.*, 2003; Combs *et al.*, 2001). Oligomeric Aβ has been shown to produce a stronger M1 response in microglia, suggesting microglial reactivity may be damaging in AD (Michelucci *et al.*, 2009). Contrastingly, microglia have also been associated with Aβ clearance so may have beneficial effects in AD (Koenigsknecht & Landreth, 2004; Mandrekar *et al.*, 2009; Paresce *et al.*, 1996). With further reports of conflicting results on microglial phenotypes in AD, there is still uncertainty regarding the exact role of microglia in AD and whether they are protective or pathogenic (Hansen *et al.*, 2018; Hopperton *et al.*, 2017). The role may even vary over the disease course.

In life, microglial response has been studied with PET imaging studies using ligands against Translocator Protein (TSPO), a mitochondrial protein highly expressed in microglia and upregulated in activated microglia, although also associated with astrocytes (Anholt *et al.*, 1986; Veiga *et al.*, 2007). Z. Fan *et al.* (2017) found that in patients with MCI, an increased microglial activation compared to controls decreased over time, with a concurrent increase in fibrillary Aβ. In AD patients, compared to controls, there was a gradual increase over time in microglial activation. These findings highlight the variable nature of the microglia response over the disease course. In a study by Parbo *et al.* (2017), it

was shown via PET imaging, that in the majority of MCI patients with Aβ load there was microglial activation and this cortical distribution overlapped that of the Aβ distribution. As MCI patients can go on to develop AD, it would be interesting to see in the future which of these cases go on to develop AD and the pattern of subsequent microglial activation in these patients. However there are studies which do not show involvement of microglia in amnestic MCI (aMCI), using PET ligands (Knezevic *et al.*, 2018). This was, however, a small study of only eleven aMCI cases and fourteen controls. Again, lack of microglial involvement was found in another PET study (Kadir *et al.*, 2011), although this was in AD patients and so the difference in disease stage may be the cause for discrepancy in results. Pathological analysis supports the concept that microglia are implicated in neurodegenerative disease, with the number, health and density of microglia proposed to vary between different neurodegenerative diseases, including AD (Bachstetter *et al.*, 2015), with discrete differences seen between dementias suggesting microglia can associate with disease presentation (Taipa *et al.*, 2017). Increased fractional area of immunoreactive microglia in possible AD compared to controls, suggests that microglia are involved early in AD, as suggested by the PET imaging studies (Vehmas *et al.*, 2003).

In human post-mortem tissue, microglial and glial response are shown to be increased in AD patients compared to controls (Taipa *et al.*, 2018) and, similar to neuroimaging findings, the involvement of microglia with AD pathology may increase over time (Serrano-Pozo *et al.*, 2016) suggesting an ongoing active role in the disease pathogenesis. In FAD, microglial response has also been noted at post mortem and different inflammatory phenotypes may be linked to mutation (Ryan *et al.*, 2015a). However, there is a lack of detailed research in larger FAD cohorts into the role of microglia and inflammation in these patients. Understanding how microglial involvement associates with disease pathology and outcome may be of importance.

As increased microglial activation is associated with AD compared to controls, it has also been observed that microglial pathology at post mortem is associated with cognitive outcomes in AD (Minett *et al.*, 2016). Specifically, it was shown that Iba1 was negatively associated with dementia whilst CD68, MSR-A and CD64 were positively associated. Importantly, in those without dementia, cognitive function was associated with microglial expression, with a positive association

with Iba1 and negative with CD68 and this remained true in those with AD pathology. This study highlights the potential role of microglia in pre-symptomatic stages. It is necessary to further investigate these associations to understand and potentially consider avenues for enhancing microglial function, if increasing evidence suggested this may be beneficial to the disease course.

A recent systematic review of articles comparing microglial activation markers in AD compared to controls has shown that specific markers of activated microglia were more associated with disease, including CD68 and CR3/43, rather than pan markers of microglia, such as Iba1 (Hopperton *et al.*, 2017). This highlights the importance of the state of the microglia, rather than just abundance, to disease. Knowing what states are present in FAD patients may help to understand the contribution they may be playing within disease. It is important to note, however, that meta-analyses may be affected by perturbations in results caused by differences in methodologies of the individual articles. However, a recent study has also shown that mean microglial density did not distinguish between AD and non-AD controls. Although, when assessing density of staged microglia stained with CR3/43, with stages reflective of activation stage, significant differences could be observed between AD and non-AD controls, specifically within cortical regions such as mid-frontal and inferior temporal. This study was also able to confirm that the proportion of activated microglia relative to total microglial density was discriminative of AD compared to controls (Felsky *et al.*, 2019).

It is important to remember that microglial activity has been shown to change over time during the disease course, and thus their protective and or damaging phenotypes could alter over time. It was hypothesised that Aβ clearance becomes less efficient as the disease progresses (Paresce *et al.*, 1997). Recently, a study which used PET over disease progression in mice expressing mutant APP-SL70 protein, reportedly found a saturation of microglial response relative to continued amyloidosis (Blume *et al.*, 2018). Whilst this does not confirm a direct link between increased Aβ and microglia, or explain what specific changes are occurring in response to Aβ, it does indicate that microglial response over time becomes less efficient. If microglia are indeed initially protective then understanding how to maintain this protective phenotype may help in the search to find novel treatments for AD.

1.20 **APOE and microglia**

Assessing the interaction of microglia in FAD with other AD associated risk genes, such as *APOE,* is important as *APOE* genotype has been seen to associate with differing microglial pathology. Results from *App* transgenic mice studies have indicated that this is via APOE dependant mechanisms on microglial response to Aβ pathology (Huynh *et al.*, 2017). Analysing this relationship may provide further information on the importance of interplay between different genes and the disease, especially in FAD where known causative genetic mutations are responsible for the disease. In human brain tissue, the *APOE*2 allele was significantly associated with expression of many commonly used markers of microglial state in AD, for example the *ε2* allele was associated with Iba1 and MSR-A expression, while *ε4* was associated with the expression of CD68, HLA-DR and CD64, markers associated with a reactive phenotype in AD (Minett *et al.*, 2016). With greater astrocytic pathology in AD *APOE*4 carriers having also been found (Alafuzoff *et al.*, 1999). A link between APOE, microglia and pathology may be due to Aβ degradation. APOE facilitates the degradation of Aβ by microglia, again in an APOE isoform dependant manner, with APOE4 being less efficient at promoting Aβ degradation (Jiang *et al.*, 2008) and reviewed in C. Y. D. Lee and Landreth (2010). This is likely due to APOE's role in cholesterol transport (Egensperger *et al.*, 1998; C. Y. D. Lee *et al.*, 2012). And greater microglial activation has been noted in sAD cases with *APOE*4 genotype (Egensperger *et al.*, 1998), and greater microglial reactivity around plaques in mice expressing the human APOE4 isoform compared to those expressing the human APOE3 isoform (Rodriguez *et al.*, 2014).

1.21 **Cortical Layers**

The mammalian cortex develops through a sequential series of progenitors cells producing neurons that generate the cortex. The neocortex is comprised of 6 layers, although the calcarine fissure of the occipital cortex is further sub divided and cortical limbic structures comprise 3 layers (Noctor *et al.*, 2004). Excitatory neurons of the cortical layers are generated in the order 1>6>5>4>3>2 as they radiate from the ventricular surface to the pial surface. Development from progenitors requires expression of proneural genes and pathways, down regulation of proliferative genes, cell cycle exit and terminal neuronal

differentiation (Guillemot *et al.*, 2006). Neurons derive from cells that originate from the neuroepithelium. Neurons which make up cortical layers have their own distinct morphologies, projection routes and neurotransmitter expression. Although, each layer also consists of multiple neuronal types in addition to glia. GABAergic inhibitory neurons derive from the ventral telencephalon and migrate into the developing cortex (Fisher *et al.*, 1988; Ma *et al.*, 2013).

Neocortex			Calcarine fissure
Layer	Neuronal composition	Connections	Layer
Pial surface			
I (1) Molecular layer	Cajal-Retzius	Thalamic input Neuronal fibres and terminations	I (1)
II (2) External granular layer	densely packed stellate	Intrahemispheric cortico-cortico outputs	II (2)
III (3) Pyramidal layer	Large pyramidal neurons	Intra/inter hemispheric cortico-cortico projections	III (3)
IV (4) Inner granular layer	Small densely packed stellate Basket	Thalamic input Output to layers 2/3 Intra-layer connections	IVA (4a) IVB (4b) IVC (4c)
V (5) Ganglionic layer	Large pyramidal	Cortico-striatal output and spinal cord Upper layer cortical input	V (5)
VI (6) Multiform layer	Small polymorphic	Cortico-Thalamic input/output	VI (6)
White matter			

Table 1-2 The structure of the cerebral cortex.

The connectivity within the cortex is complex, however studies have enabled the development of a simplified cascade of the excitatory connections in the cortex, with reviews (Gerfen *et al.*, 2016; Kubo & Nakajima, 2003) piecing these studies and pathways together, see Table 1-2. After receiving sensory input, messages are projected from the thalamus, terminating on layer IV neurons. From there, messages are projected to the upper layers II/III neurons, which then project to other cortical regions. Lower layers V/VI receive cortical input and layer V projects to subcortical centres while layer VI projects back to thalamic regions. The calcarine region of the occipital cortex also has 6 layers but layer IV is further subdivided, with the difference in composition a reflection of its function as the primary visual centre (Gerfen *et al.*, 2016; Kubo & Nakajima, 2003). All together the connectivity allows the appropriate behavioural modulation in response to stimuli. Genetic defects and extrinsic factors leading to disruption of cortical layer

development and these connectivity pathways, cause neurodevelopmental disorders with epilepsies (Cugola *et al.*, 2016; Spalice *et al.*, 2009). As pathology potentially afflicts specific layers more profoundly than others, this may lead to specific phenotypic disturbances due to disrupted pathways, as has been previously suggested (Armstrong, 2012). Therefore, it is possible that similar connections begin to be disrupted in FAD as are seen in these neurodevelopmental disorders. In fact, a study in a 5xFAD mouse model noted cross laminar circuitry dysfunction in the AD mouse (Crook *et al.*, 1998).

1.22 Models of Alzheimer's and familial Alzheimer's disease

Limitations exist with using human post mortem tissue from FAD patients to study the disease, notably that pathology has reached end-stage and we cannot monitor processes as they occur, or perturb the system to assess downstream effects. Understanding early mechanisms too will be vital to understanding and targeting pathogenic processes with therapeutics. Therefore, there is a need for a model which enable these different questions to be investigated to better understand the biological processes.

Animal models

Although not within the scope of this project, it is important to note that multiple animal models for FAD exists, although these have failed to capture pathology and neurodegeneration fully (reviewed in Drummond and Wisniewski (2017)). Although similar, wild type (WT) mouse *App* differs to human *APP* (De Strooper *et al.*, 1991) and as mice do not inherently develop AD, transgenic mice have to be used. There are multiple mouse models which use FAD mutations, in particular, the 5xFAD model is popular. This transgene model contains five human FAD mutations to bring on an early AD pathology phenotype; *APP* KM670/671NL, *APP* I716V, *APP* V717I, *PSEN1* M146L and *PSEN1* L286V; and presents Aβ deposition and gliosis although tau pathology is lacking (Oakley *et al.*, 2006). However, this genetic makeup is not representative of that seen in the natural history of FAD (Jankowsky & Zheng, 2017). Many transgenic mouse models use promoter driven over expression to induce pathological phenotypes. This forcing of disease is not reflective of the natural disease aetiology, especially in the case of sAD. Additionally, models often fail to recapitulate all aspects of

disease, with plaques, tangles and neurodegeneration not present in a single system, as well as clinical aspects (reviewed in Drummond and Wisniewski (2017)) making it hard to know whether the observed processes are relevant or even present in AD. Other mice models use *Apoe* genotype variants for modelling AD, however the APOE protein is not the same in mice as in humans, with murine APOE resembling human APOE3 due to differences in amino acid residues which affects intra and inter molecular binding of APOE (Dong & Weisgraber, 1996; Raffaï *et al.*, 2001). Even when expressing humanised APOE protein there are likely to be inconsistencies in disease mechanism between Apoe/*APOE* models and sAD and FAD patients (Jankowsky & Zheng, 2017), indeed there are even differences in effect on Aβ pathology by human/mouse APOE in the same model (Liao *et al.*, 2015). Induced pluripotent stem cells (iPSC) are an alternative model which are more physiologically relevant.

iPSC

Induced pluripotent stem cells (iPSC) are an alternative model which are physiologically relevant. The generation of iPSC from patient fibroblasts taken directly from sAD or FAD patients provide an alternative in vitro model of physiological relevance. Fibroblasts are converted to iPSC using specific transcription factors (Oct3/4, Sox2, Klf4, and c-Myc) to induce a pluripotent state (Takahashi *et al.*, 2007) that is indistinguishable from human embryonic stem cells (Mallon *et al.*, 2014). The resulting iPSC can be differentiated into a wide range of lineages, including neurons, astrocytes and microglia, discussed in Penney *et al.* (2019). By using specific molecules in a regimented time line, the extrinsic signalling factors in normal brain development are recapitulated and neurons of varying lineages can be generated. A common method to generate cortical neurons involves dual SMAD inhibition to create glutamatergic cortical neurons which involves the inhibition of Bone morphogenetic protein (BMP) and transforming growth factor-β (TGFβ) signalling. Inhibition of the SMAD family signalling cascade, important for cell regulation and growth, leads to a neural ectoderm fate capable of neurogenesis (Chambers *et al.*, 2009; D. S. Kim *et al.*, 2010; Shi *et al.*, 2012b). This method reliably generates cortical neurons (Shi *et al.*, 2012b), mimicking the temporal sequence of events that occurs during corticogenesis in the developing brain, reviewed in McConnell (1995). As previously discussed, neurogenesis leads to production of neurons that resemble

the order of neurogenesis which leads to the 6 cortical layers (6>5>4>3>2) followed by astrocyte generation. Corticogenesis takes around 100 days, and because of this developmental order, neurons are typically grown in culture to day 100, where representative neurons of all cortical layers are present. As Aβ pathology starts in the cortex in human, analysing this cell type is particularly relevant to modelling FAD. In fact, iPSC models have been shown to react to modulators of PSEN1, with an influence Aβ ratios, results of which were not observed using other cell types or animal models (Q. Liu *et al.*, 2014). This highlights the importance of this model in research.

One of the major benefits of patient derived iPSCs is that they have the same genetic background as the patient, although this is potentially problematic in itself; unknown genetic modulators may exist in different patients. Additionally there is concern for retention of epigenetic modifications of the original cell type during reprogramming which may influence downstream differentiation (Polo *et al.*, 2010), however it has been shown that different donor cells from the same individual are remarkably similar despite their different origin (Kyttälä *et al.*, 2016). However, this issue is not necessarily resolved in other cell models but is slightly controlled for in isogenic lines.

In addition to this popular method, alternative techniques exist which act to decrease the time taken to generate neurons in as little as 5 days, with approaches including over expression of neurogenin-2 (NGN2) or temporal application of a cocktail of small molecule inhibitors which promotes neurogenic fates (Qi *et al.*, 2017; Yingsha Zhang *et al.*, 2013), and new methods are still emerging (Y. Xue *et al.*, 2019). Additionally, generation of cerebral organoids from iPSC is an expanding field. Here cultures are grown in 3D rather than as adherent 2D cells, which is believed to be more representative of the environmental conditions experienced in vivo. The protocols for these methods were originally established and shown to display disease pathology by Lancaster and Knoblich (2014); Lancaster *et al.* (2013) However, an issue with organoids is their heterogeneous nature, although different methods are becoming available to influence the cellular components of the organoids. The benefits and pitfalls of organoids are discussed (C. Arber *et al.*, 2017; Pașca, 2018). While iPSC neurons cannot develop the classical hallmarks of extracellular Aβ plaques and

tangles, they can be used to model early molecular and intracellular changes associated with disease.

Stem cell models of FAD

Human embryonic cell models with overexpressed transgenic *PSEN1* mutations were developed as a method to study FAD mutations. Findings from these lines recapitulate the observation of altered Aβ processing across mutations, indicating they are a useful model (Honda *et al.*, 2016). Recently, there has been an increase in the generation of FAD cell lines derived from patient fibroblasts, including iPSC from DS patients (Armijo *et al.*, 2017; Dashinimaev *et al.*, 2017; Hibaoui *et al.*, 2014; Israel *et al.*, 2012; Moore *et al.*, 2015; Mou *et al.*, 2012; Muratore *et al.*, 2014; Minna Oksanen *et al.*, 2018; Sproul *et al.*, 2014; Vallejo-Diez *et al.*, 2019; Yagi *et al.*, 2011). Comprehensive libraries of FAD patient fibroblasts have also been generated (Karch *et al.*, 2018; Wray *et al.*, 2012). The development of these models indicates the direction of future research in AD, with FAD iPSCs a central tool.

Pathology in AD iPSC

As iPSC neuronal models of sAD/FAD are used to investigate AD, it is important that they recapitulate aspects of disease. Aβ is the major pathological hallmark of sAD, and so Aβ alterations are frequently investigated in these models. In one of the earliest studies, increased Aβ40 was observed in both *APP* duplication and sAD derived lines (Israel *et al.*, 2012). Aβ alterations have even been shown in *APOE* sAD models, with aberrations in *APOE*4 genotype cell line organoids compared to *APOE*3, with Clustered Regularly Interspaced Short Palindromic Repeats (CRISPR) technology rescuing the *APOE4* phenotype by changing it to *APOE*3 (Y.-T. Lin *et al.*, 2018). In an FAD line with the *PSEN1* E120K, increases in both intracellular and extracellular Aβ levels were observed (L. Li *et al.*, 2018). Alterations in absolute levels as well as ratios were also observed in FAD *PSEN1* A246E lines compared to controls (Mahairaki *et al.*, 2014). Mutations specific effects on Aβ can also be observed, with a study showing that the *APP* E693Δ deletion line shows intracellular Aβ accumulation, a feature observed pathologically in a mouse model with this mutation, despite no evidence of plaque pathology (Kondo *et al.*, 2013; Tomiyama *et al.*, 2010).

While alterations in Aβ production and intracellular deposition can be observed, it is less easy to investigate extracellular plaque pathology in 2D iPSC models. The frequent removal and replacement of fresh media removes Aβ from the extracellular environment. Additionally, the extracellular environment lacks extracellular matrix, supplying no scaffold for aggregate entrapment. 3D and organoid based models do however enable the investigation of plaque pathology. As this is a newer methodology there is little literature available, however, Aβ plaque like aggregates have been shown in some 3D models which have used FAD, DS and sAD lines, and these aggregates were not been observed in the non-AD control lines (Gonzalez *et al.*, 2018; Raja *et al.*, 2016). However evidence of Aβ plaques were not observed in our iPSC *APP* mutation organoid culture (Charles Arber *et al.*, 2019a).

Tau pathology is a histological feature in AD brains and has been noted in iPSC models. Increases in tau phosphorylation has been observed in different AD models, including sAD, *APP* duplication and FAD lines (Israel *et al.*, 2012; Ochalek *et al.*, 2017). Increased total tau in addition to phosphorylated tau has also been observed (Muratore *et al.*, 2014), and importantly this was downstream of Aβ alterations. In the previously mentioned Raja *et al.* (2016) et al paper, intracellular Aβ aggregates also occurred at an earlier time point to changes in phosphorylated tau levels in the FAD lines compared to controls in 3D models. Interestingly, slight differences in extent of Aβ or tau pathology due to mutation were observed. In the Y.-T. Lin *et al.* (2018) study, the *APOE*4 line also had increased tau hyper phosphorylation compared to the *APOE*3 lines. DS models from iPSC also recapitulate AD pathology with Aβ and tau alterations (Shi *et al.*, 2012a). Although interestingly, correction of the extra copy of *APP* does not reverse all pathologies, which suggests non-Aβ pathways of toxicity also exist (Ovchinnikov *et al.*, 2018). These results show that multiple facets of AD can be replicated in these models.

While iPSC models have been able to produce AD models of cortical neurons, certain populations may be more susceptible to induced cell death (Duan *et al.*, 2014). Both sAD and FAD neurons derived from patient iPSC were shown to have increased apoptosis during co culture with murine derived activated microglia (Balez *et al.*, 2016). With DS models also showing increased apoptosis under induced apoptotic conditions (Ovchinnikov *et al.*, 2018). While these

increases in apoptosis are under induction, this still highlights the vulnerability of the neurons, and is relatable to the environment in AD brains where multiple pathologies and toxicities are present.

While Aβ and tau are major hallmarks, dysfunction in other cellular processes also occur in AD. In sAD iPSC, alterations in mitochondrial function were noted, and interestingly these were not correlated to Aβ or tau (Birnbaum *et al.*, 2018). Mitochondrial dysfunction has also been shown in *APP* and *PSEN1* mutation cell lines (L. Li *et al.*, 2018; L. Li *et al.*, 2019). As mitochondrial function is known to be relevant in many neurodegenerative diseases (M. T. Lin & Beal, 2006), the results highlight the complexity of AD but also the benefit of iPSC to investigate mechanisms. The role of cholesterol esters has also been investigated in sAD iPSC, with results showing cholesterol esters independently affect Aβ and tau via different mechanism (van der Kant *et al.*, 2019). The involvement of cholesterol is particularly interesting considering the previously mentioned role of APOE4 in cholesterol homeostasis. Premature neuronal differentiation was also noted in FAD *PSEN1* iPSC lines and was speculated to be involved in wnt-notch pathways, with notch being a known substrate for PSEN1 (J. Yang *et al.*, 2017). This pathway may be of importance as reduced neurogenesis has been observed in FAD mutation mice (M. Demars *et al.*, 2010). Using isogenic iPSC with *APP* and *PSEN1* mutations, it has been shown that mutation lines have altered transcriptional expression including endocytosis related genes, and this was complemented by changes in early endosomes, and an accumulation of APP CTF (Kwart *et al.*, 2019). These findings highlight the understudied role of intracellular CTF of APP, and how this model is ideal for analysis of this pathology. As discussed by Penney *et al.* (2019) The role of FAD mutations in other cortical cell types are being to be explored with the development of FAD mutation carrying iPSC derived microglia and astrocytes.

1.23 **Main aims**

Chapter 3

To determine the association of specific Aβ pathologies (Cored, cotton wool and diffuse plaques and occurrence CAA) with clinical factors (age

at onset and disease duration) and assess if they are associated with causative FAD mutation or *APOE* genotype.

To determine if there are specific Aβ pathologies or distribution patterns across the cortical layers and if these different Aβ pathologies have specific associations with each other, that are distinct in genetic causes of FAD.

Chapter 4

To determine if microglial pathology associates with clinical data (age at onset and disease duration), differs between FAD mutation and *APOE* genotypes, and assess if microglial load correlates with Aβ pathology in FAD mutation groups.

Chapter 5

Section 1

Use a detailed classification of Aβ+ve CAA from IHC analysis to determine if the proportion and severity of CAA associates with Aβ plaque type and load in genetic causes of FAD in the QSBB cohort.

Section 2

Use a detailed classification of Aβ+ve CAA from IHC analysis to determine if the proportion and severity of CAA associates with microglial load in genetic causes of FAD in the QSBB cohort.

Section 3

Investigate associations between sex, mutation and *APOE* genotype with clinical aspects of FAD (age at onset and disease duration) in the extended cohort.

Asses the extended cohort to determine if the proportion and severity of CAA associates with clinical aspects of FAD (age at onset and disease duration) and if the proportion and severity of CAA differs between FAD mutation and *APOE* genotypes.

Chapter 6

To describe the observed contribution of specific Aβ peptides to specific Aβ plaque types (Cored, CWP, diffuse) and CAA via IHC analysis and qualitatively assess if the observed contribution of specific Aβ peptides to pathological deposits differs by genetic cause of FAD and/or by *APO*E genotype in the temporal and occipital cortices.

Chapter 7

To generate a range of FAD mutation containing stem lines by reprogramming patient derived fibroblasts, including the E280G mutation, allowing neuronal differentiation and analysis of mutation specific effects on Aβ peptide profiles and PSEN1 maturity.

Chapter 2

Materials and Methods

2 Materials and Methods

2.1 Statement of work conducted

Clinical data for the QSBB and IOPPN FAD cases (Age at onset, disease duration and majority of *APOE* genotypes) were provided in case data made available to me. Cell lines *PSEN1* Y115H, *PSEN1* R2781 and *APP* V717I were jointly reprogrammed by myself and PhD student Christopher Lovejoy. The *PSEN1* E280G lines were made independently by myself. DNA used for *APOE* genotyping from cell lines *PSEN1* Y115H, *PSEN1* R2781 and *APP* V717I were extracted using the Trizol™ method by Dr Charlie Arber. The R278I.CA protein lysate sample used as a positive control for western blot positive was provided by Dr Charlie Arber. All brain tissue analysis was conducted blinded to FAD mutation, *APOE* genotype and sex. Cell work was conducted aware of FAD mutation, however all lines were treated with the same conditions.

2.2 Cortical Tissue

2.2.1 *Case collection*

Brain samples were obtained from the Queen Square Brain Bank (QSBB) for Neurological Disorders, University College London, United Kingdom and the Institute of Psychiatry, Psychology and Neuroscience (IOPPN), King's College London, United Kingdom. All brain tissue used in this study had been donated by individuals with symptomatic FAD due to mutations within the *PSEN1* or *APP* gene. The protocols used for brain donation and ethical approval for this study were approved by a London Research Ethics Committee and tissue is stored for research under a license from the Human Tissue Authority. The standard diagnostic criteria for the neuropathological diagnosis of AD were used in all cases (H. Braak & Braak, 1991; Hyman *et al.*, 2012; Dietmar R. Thal *et al.*, 2002). Patients had undergone genetic testing during life to confirm presence of a mutation linked to FAD. All case demographics are shown in Table 2-1. Initially, pathological analysis was conducted on tissue from all FAD cases held at the QSBB (20 cases). This will be referred to as the QSBB cohort. In order to study a larger number of subjects, tissue was also requested from all FAD cases from families that had been clinically investigated at the DRC who had previously

undergone brain donation to IOPPN brain bank (21 cases), the combination of QSBB and IOPPN will be referred to as the extended cohort.

Case	Sex	Age at onset	Disease duration (yrs)	Mutation	*APOE*	Braak Tau	Thal Phase	CERAD	PM delay (hrs/mins)	Brain bank
1	F	42	9.7	*APP* V715A	-	6	5	Frequent	45:00	IOPPN
2	M	40	19.0	*APP* V717I	33	6	5	Frequent	15:00	IOPPN
3	F	59	12.8	*APP* V717I	33	6	5	Frequent	3:30	IOPPN
4	F	47	14.6	*APP* V717I	33	6	5	Frequent	23:00	IOPPN
5	F	53	6.5	*APP* V717I	33	6	5	Frequent	-	QSBB
6	F	56	12.6	*APP* V717I	34	6	At least 4	Frequent	10:00	IOPPN
7	F	50	6.5	*APP* V717I	33	6	5	Frequent	16:25	IOPPN
8	M	56	10.1	*APP* V717I	33	6	5	Frequent	68:05	QSBB
9	M	49	13.0	*APP* V717I	44	6	5	Frequent	32:10	QSBB
10	F	51	8.7	*APP* V717L	33	6	5	Frequent	89:42	QSBB
11	M	39	12	*PSEN1* Intron4	33	6	5	Frequent	36:00	IOPPN
12	F	35	5	*PSEN1* Intron4	33	6	5	Frequent	-	IOPPN
13	M	36	6	*PSEN1* Intron4	33	6	5	Frequent	6:00	IOPPN
14	F	36	5.0	*PSEN1* Intron4	33	6	5	Frequent	64:15	QSBB
15	F	35	16.9	*PSEN1* Intron4	44	6	5	Frequent	32:30	QSBB
16	F	39	8.1	*PSEN1* Intron4	33	6	5	Frequent	-	QSBB
17	M	42	9	*PSEN1* Intron4	33	6	5	Frequent	43:10	QSBB
18	F	34	10	*PSEN1* Y115C	34	6	5	Frequent	14:50	IOPPN
19	M	35	9	*PSEN1* E120K	-	6	5	Frequent	-	IOPPN
20	F	37	4	*PSEN1* E120K	33	6	5	Frequent	57:00	IOPPN
21	F	31	6	*PSEN1* E120K	33	6	5	Frequent	24:15	QSBB

22	M	59	11	*PSEN1* S132A	34	6	5	Frequent	161:15	QSBB
23	M	36	6	*PSEN1* M139V	34	6	5	Frequent	-	IOPPN
24	F	41	8.9	*PSEN1* M139V	33	6	5	Frequent	-	QSBB
25	F	53	8	*PSEN1* I143F	33	6	5	Frequent	-	IOPPN
26	M	48	6	*PSEN1* M146I	23	6	5	Frequent	115:35	QSBB
27	F	36	13	*PSEN1* L153V	34	6	5	Frequent	47:00	IOPPN
28	M	43	9	*PSEN1* delta 167	44	At least 5 *	5	Frequent	-	IOPPN
29	F	40	13.6	*PSEN1* E148D	-	6	5	Frequent	153:30	QSBB
30	F	45	13	*PSEN1* E148D	34	6	5	Frequent	63:25	QSBB
31	F	48	11	*PSEN1* I202F	44	6	5	Frequent	26:15	QSBB
32	M	44	9.3	*PSEN1* L235V	33	6	5	Frequent	72:00	IOPPN
33	M	47	11	*PSEN1* L250S	33	6	5	Frequent	32:20	QSBB
34	M	51	17	*PSEN1* R269H	44	6	5	Frequent	30:00	IOPPN
35	F	46	19	*PSEN1* R278I	34	6	5	Frequent	31:55	QSBB
36	M	54	12	*PSEN1* R278I	23	6	5	Frequent	77:45	QSBB
37	M	44	9	*PSEN1* E280G	33	6	5	Frequent	-	IOPPN
38	F	47	18	*PSEN1* E280G	34	6	5	Frequent	22:00	IOPPN
39	F	42	11	*PSEN1* E280G	34	6	5	Frequent	11:00	QSBB
40	M	42	5	*PSEN1* A434T & T291A	33	5	5	Frequent	43:50	QSBB
41	M	44	5	*PSEN1* P436S	33	6	5	Frequent	7:00	IOPPN
Average		44.47	10.52							

Table 2-1. Summary of cases.

PM: post mortem. No *APOE* genotype available for cases 1, 19 and 29. *Occipital cortex missing preventing complete grading.

2.3 Histological staining and immunohistochemistry (IHC)

2.3.1 *Tissue Preparation*

Donated brain tissue had been previously embedded in paraffin according to QSBB standard protocols, see Table 2-2. 7µm thick serial sections of formalin fixed paraffin embedded (FFPE) tissue were cut from the frontal and occipital cortices. Slides were dried at 37˚c before overnight (O/N) baking at 60˚c prior to staining. The second frontal gyrus was used for pathological analysis of Aβ and microglia in the QSBB cohort. The second frontal gyrus and the occipital cortex were used for CAA analysis in the extended pathology cohort. The temporal cortex and occipital cortex were used for Aβ isoform specific analysis in the QSBB cohort.

Step	Reagent	Time
1	70% alcohol	6.00 hrs
2 & 3	90% alcohol	2 x 6.00 hrs
4 to 7	Absolute alcohol	4 x 6.00 hrs
8 & 9	Chloroform	2 x 6.00 hrs
10 to 12	Wax	3 x 6.00 hrs

Table 2-2 Standard protocol paraffin embedding of tissue.

2.3.2 *Cresyl Violet/Nissl staining*

For Cresyl violet staining of Nissl substance, a 0.1% Cresyl violet (acetate) (83860.120, Prolabo) solution was made and filtered (1202 320, Whatman). Cresyl violet was brought to 60˚c prior to use. Tissue sections were deparaffinised in xylene and rehydrated in 100%, 90%, and 70% industrial methylated spirit (IMS) for 5 mins each, followed by a brief distilled water (ddH_20) wash. 10% acetic acid (final concentration 0.05%) was added to the warm Cresyl violet solution to which slides were incubated at 60˚c for 3mins. Sections were removed, briefly washed in ddH_20, dehydrated through 70%, 90%, and 100% IMS until there was clear a background with strong cellular morphology, cleared in xylene and mounted with DPX (ThermoFisher Scientific).

2.3.3 *Immunohistochemistry*

Serial tissue sections adjacent to Cresyl violet stained sections were deparaffinised in xylene and rehydrated in 100% and 90% IMS for 5mins each and blocked for endogenous peroxidase activity in 0.3% H_20_2 in methanol for 10mins (23615.261, VWR), followed by appropriate pre-treatment (Table 2-3). All slides were pressure cooked in citrate buffer for 10mins then blocked in 10% milk/1X Tris-buffered saline with Tween™ 20 detergent (TBS-T; 28360, ThermoFisher Scientific) for 30mins at room temperature (RT). Primary antibodies (Table 2-3), were diluted in TBS-T, applied to slides and incubated as required. Sections were washed in TBS-T and the secondary antibody was applied for 30mins RT. Sections were rinsed with TBS-T followed by incubation with VECTASTAIN® EliteABC Kit PK-6100 (Vector Laboratories Ltd). Slides were washed in TBS-T and colour was developed with di-aminobenzidine (DAB)/TBST-T/H_2O_2 (DAB, Sigma). Sections were rinsed and counter stained with Mayer's Haematoxylin (1g haematoxylin, 50g potassium or aluminium alum, 0.2g sodium iodate, 50g chloral hydrate) for 40s, room temperature (RT), followed by a brief H_20 wash and incubation in warm H_20 for 5mins. Sections were dehydrated through 70%, 90% and 100% IMS for 5mins each and cleared in xylene for at least 40mins and mounted with DPX (DPX, ThermoFisher Scientific). Nissl and IHC stained slides were scanned at 40x magnification using the Leica slide scanner SCN400 producing digitized images.

Aβ M0872 was used for total Aβ as it is well established within the lab, has shown specific binding in IHC and has been used in multiple publications. Aβ40, Aβ42, and Aβ43 peptide specific antibodies were selected based on provider certification of specificity and use in published literature.

IBA1, CD68, CR3/43 and AT8 were used as they are well established within the lab, have shown specific binding in IHC and have been used in multiple publications. Secondary antibodies used have also shown consistent, specific results in the lab and published data.

Antibody	Company #	Species	Clonality	Pre-treatment	Dilution	Conditions
Aβ	DAKO M0872	Mouse	mAb	FA + PC	1:100	4˚c O/N
CD68	DAKO M0876	Mouse	mAb	PC	1:100	1hr RT
Iba1	WAKO 019-19741	Rabbit	pAb	PC	1:1000	1hr RT
CR3-43	DAKO M0775	Mouse	mAb	PC	1:150	1hr RT
AT8	Thermo MN1020	Mouse	mAb	PC	1:600	1hr RT
Aβ40	Merk AB5074P	Rabbit	pAb	FA + PC	1:100	4˚c O/N
Aβ42	BioLegend 805509	Mouse	mAb	FA + PC	1:500	4˚c O/N
Aβ43	BioLegend 805607	Mouse	mAb	FA + PC	1:500	4˚c O/N
Swine anti-rabbit	DAKO E0353		polyclonal	-	1:200	30min RT
Rabbit anti-mouse	DAKO E0354		polyclonal	-	1:200	30min RT

Table 2-3 Antibody conditions.

FA: formic acid. PC: pressure cooker. #: product number.

2.3.4 *Thioflavin-S Staining*

FFPE sections were dewaxed in xylene, rehydrated in ethanol (100%, 95%, 70%, 50%) and stained in aqueous 1.0% thioflavin-S (T1892-25g, Sigma) solution for 7 mins. They were then differentiated in 70% ethanol for 5mins and left to wash overnight in PBS before cover slipping in aqueous mountant (DPX). Sections were viewed under a fluorescent microscope Leica DM5500 B (Leica microsystems, Wetzlar, Germany).

2.4 Image analysis

2.4.1 *Tissue section selection*

Digitised slides were viewed in Aperio ImageScope (Aperio ImageScope, Leica). The ruler tool was used to mark a ~6mm line along the length of tissue opposite the ‘localisation notch’ created during brain dissection. A rectangle region of ~6mm length and varying depth, depending on grey matter depth, was extracted. The same region was extracted for all stains on the sequential sections. Nissl

stained slides were extracted creating a 40x magnification region for layer delineation. IHC slides were extracted at 50% to create a 20x magnification region for analysis. The region encompassed all six cortical layers from the pial surface to below the edge of the white matter.

2.4.2 *Layer delineation*

In Adobe® Photoshop® software (Adobe® Photoshop® CC 2017, Adobe Systems Incorporated) digitized Nissl sections where used to delineate the 6 cortical layers in the second frontal gyrus. The 'create layer' tool was used to place a transparent overlay, over the original image. Using the free-hand pen tool, laminae and grey matter/white matter boundaries were marked on the overlay. Laminae delineation was judged by cell type and composition using reference to multiple guides (Kolb et al., 2007; Triarhou, 2013; Wells, 1983). Serial stained sections were opened in Adobe® Photoshop®, and the overlay placed over them. Due to different angling on slides during tissue preparation, rotational adjustments were made by hand to align the overlay. Using visual landmarks and Mayers heamotoxylin stain, which highlighted cells as a guide, the overlay was superimposed, matching laminae boundaries. The serial sections were saved with the overlay visible (Figure 2-1).

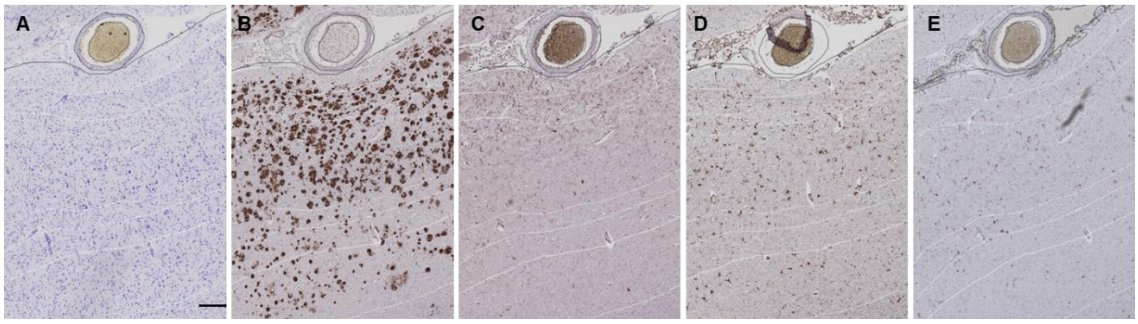

Figure 2-1 Representative serial sections showing layer superimposition.
Staining and IHC showing A: Nissl stain, B: Aβ, C: Iba1, D: CD68 and E: CR3/43 in serial sections from an individual case. Faint white lines depict cortical layer boundaries. Scale bar represents 200µm, 2x magnification objective.

2.4.3 *Areal fraction analysis*

All IHC stained sections with laminar overlay depicting cortical layer boundaries were analysed per cortical layer for percentage area stained (referred to as load). Images were opened in Image J (Schneider *et al.*, 2012) and using the region of

interest (ROI) macro, individual cortical layers were selected one at a time. Within each cortical layer, Python (Python 3.6.0, Python Software Foundation) was used to randomly generate 15 coordinates for 100 x 100 pixel regions of interest. At 20x magnification this was equivalent to 50μm^2 regions. Bland-Altman plots and linear regression were utilised to determine the number of squares required for reproducible results (Figure 9-1, Table 9-1). 15 squares were generated for each layer. The percentage area stained by DAB for each square was analysed by a threshold analysis method, using a pre-defined macro (developed by Dr Yau Lim, Kings College London) in ImageJ. A unique threshold was set to pick up the DAB staining for each antibody with the same threshold applied to all cases. If a particular case/image needed slight adjustment to the threshold, this was conducted and results included in the analysis. An average was generated from the 15 squares.

2.5 Pathological assessment

Pathological assessment was assessed for intra and inter-rater reliability. Good consistency and agreement was found (Table 9-2, Table 9-3)

2.5.1 *Aβ plaque type assessment*

In Adobe® Photoshop®, semi-quantitative quantitation of Aβ positive pathology in each cortical layer was performed based on Consortium to Establish a Registry for Alzheimer's Disease recommendations (CERAD) (Mirra *et al.*, 1991). Evaluation was conducted blinded to mutation or clinical information. Frequency scores were based on the CERAD scale of 0-3 (none, sparse, moderate and frequent) however, tissue was assessed by individual cortical layers at 20x magnification within the region of analysis to generate scores for each layer for each plaque type (diffuse, cored and cotton wool plaques (CWPs)) and for cortical CAA (For representative images see Figure 2-2 I-L). Individual layer scores were combined generating 'total CERAD scores' used in analysis. Leptomeningeal CAA present above the pial surface and subpial Aβ pathology present only in cortical layer 1 was similarly assessed on a 0-3 scale in their respective regions.

Cored plaques were defined as those with a dense core of Aβ surrounded by a 'halo' of Aβ. Diffuse plaques were a range of sizes consisting of Aβ which could be present as a range of deposits, with varying density and size. CWPs (cotton

wool plaques) are a specific type of plaque, which can be highlighted with serial sections stained for a number of markers (Figure 2-3). CWPs are easily identifiable using hematoxylin and eosin as the plaque displaces adjacent structures (A). Aβ IHC shows that they are positive for Aβ, with a circular morphology and defined edges (B). IHC with AT8 tau antibody, which recognises phosphorylated tau at serine 202 and threonine 205, also reveals the distinctive CWP morphology with slightly more intense staining within the CWPs (C). Thioflavin staining indicates a lack of fibrillar amyloid within the cotton wool plaques (D), whilst fibrillar amyloid can be identified in other plaques such as cored plaques and within blood vessel walls (E).

2.5.2 *Assessing the proportion and severity of cortical and leptomeningeal CAA*

Aβ positive cortical and leptomeningeal CAA pathology was determined from Aβ IHC sections using a 4 tier system to grade severity (Vonsattel *et al.*, 1991). The classifications were unaffected, mild, moderate and severe (0-3, respectively), see Figure 2-2 A-H for representative images. Only vessels cut cross-sectionally showing the full circumference of the vessel wall were counted. No distinction between types of vessels was made.

The proportion and severity of CAA was assessed in 100 cortical vessels and up to 100 leptomeningeal vessels. In the frontal cortex vessels were counted in and around the area where CERAD analysis was conducted. In the occipital cortex, cortical CAA vessel counts were conducted in the calcarine region. In the leptomeninges, frontal cortex vessels were counted from the edge of the tissue by the localisation notch. In the Occipital cortex vessels were counted along and around the calcarine region.

The proportion of CAA was calculated as a percentage by dividing the number of vessels with CAA by the total number of vessels counted and multiplying by 100. The severity of CAA was calculated by dividing the number of vessels at each grade (0/1/2/3) by the total number of vessels counted and multiplying by 100.

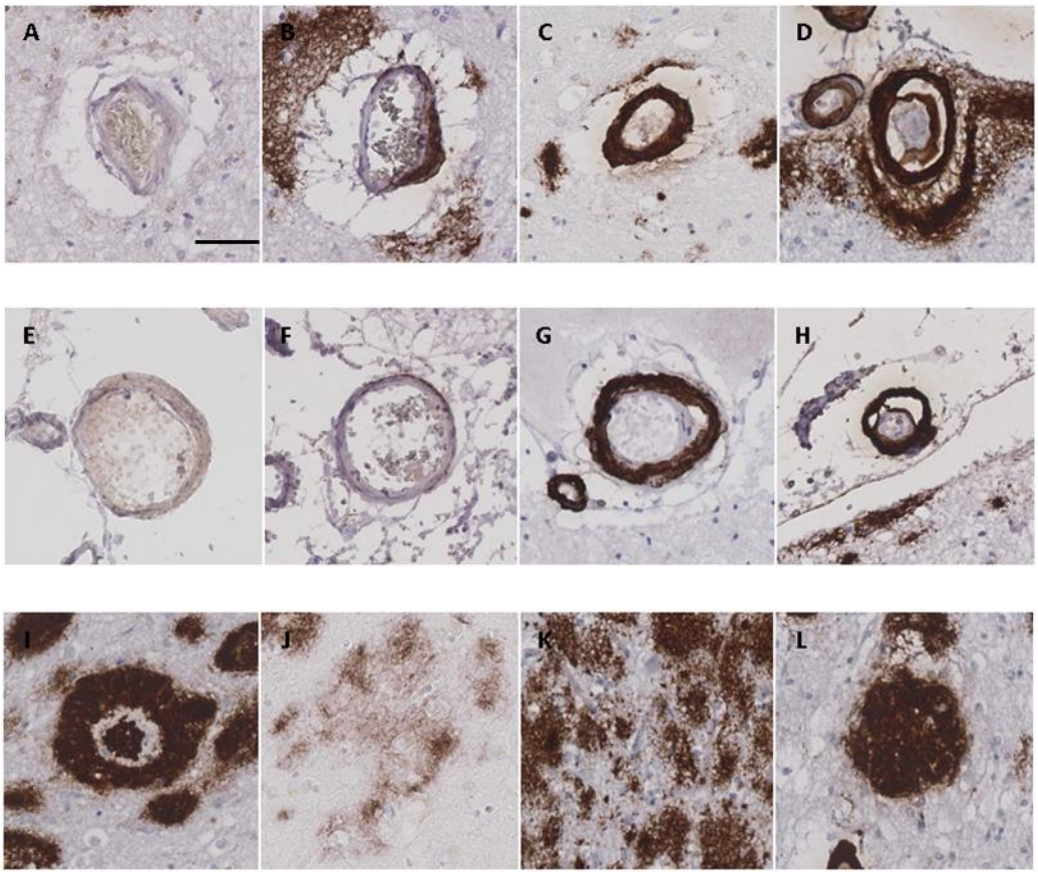

Figure 2-2 Representative examples of CAA and plaque type classifications.
From left to right: unaffected, mild, moderate, and severe CAA seen in the cortex (A-D) and leptomeninges (E-H). Representative examples of plaque type: cored (I), diffuse (J, K) and cotton wool (L). Scale bar = 50µm, 20x objective.

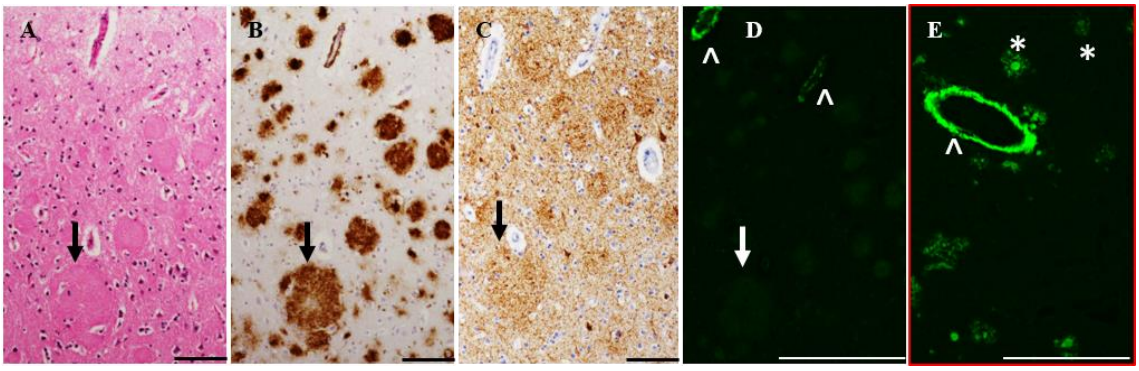

Figure 2-3 Serial sections from frontal cortex of an FAD case showing cotton wool plaques (CWP) (A-D).

A) Haematoxylin and Eosin stain shows disruption of extracellular matrix around CWP. B) Aβ positive CWPs. C) Tau staining shows light positivity in CWPs D) Thioflavin positive fluorescence staining shows minimal positivity of CWPs, with noticeable staining of blood vessels (^). Arrows (Black, A-C, white D) highlight a large CWP seen in all sections, although other CWPs are visible. E) A non-serial section of occipital cortex from the same

FAD case showing thioflavin positive staining with strong positivity of cored plaques (*) and a noticeable blood vessel (^). Black scale bar = 100µm White scale bar = 246.8µm.

2.6 Cell culture

Fibroblasts were obtained from skin biopsies taken from five individuals carrying FAD mutations. All participants gave informed consent and the study was approved by the joint research ethics committee of the National Hospital for Neurology and Neurosurgery and the Institute of Neurology. The procedure for generation and characterization of fibroblast lines has been previously described (Wray *et al.*, 2012). Seeded fibroblasts were maintained in fibroblast media (Table 2-5 Fibroblast media.) in T75 flasks (156499, Thermo Scientific) until passaging for reprogramming (2.6.1 Reprogramming). Cell cultures were carried out in class 2 hoods in sterile conditions. All cells were maintained at 37˚c, 5% CO_2.

2.6.1 *Reprogramming*

Patient derived fibroblasts were plated in to T75 flasks and grown to confluency. Fibroblasts were used at passage (P) 3 or below for nucleofection by electroporation. When confluent, fibroblasts were detached from T75's with trypsin for 5mins at 37˚c, 5% CO_2. Fibroblast media was added to the T75 and gently pipetted to guarantee lifting of fibroblasts from the flask. Cells were placed in to a 15ml falcon and centrifuged at $200g_{(av)}$ for 3mins to pellet cells. Cells were re-suspended in 100µl nucleofection solution (PBP2-00675, Lonza), containing episomal DNA coding for Oct4, Klf4, Sox2 and c-myc proteins, transferred to an Amaxa Nucleofector 2b cuvette (Lonza AAB 1001) and electroporated using the program setup: NHDF, human, neonate. Electroporated cells were removed from the cuvette with an Amaxa pipette and plated in two wells of a geltrex (1:100, DMEM/F12) (A1413302, Life Technologies) coated 6-well plate (10119831, Fisher Scientific). Electroporated cultures were maintained in fibroblast media which was changed every three days.

Six days after electroporation, cells were lifted with 1X trypsin (15090-046, Gibco) for 5 mins at 37˚c, 5% CO_2. Trypsin was removed and cells were re-suspended in fibroblast media. Suspended cells were plated on to either geltrex coated feeder free or geltrex coated mouse embryonic fibroblast CF-1 (MEF) feeder layer coated (ATCC® SCRC-1040™) 10cm dishes (172958, Nunc). For feeder cell

cultures, MEF's were plated on day 5 in to a 10cm dish at approx. 0.8 X 10^4 cells/cm2. On day 8 after electroporation, fibroblast feeder-free cultures were switched to Essential-8 stem cell media (Table 2-6) and media changed daily. For feeder cultures, media was switched to human embryonic stem cell media (HES) (Table 2-7) and changed daily. By day 20-25 iPSC colonies begin to emerge, see Figure 2-4.

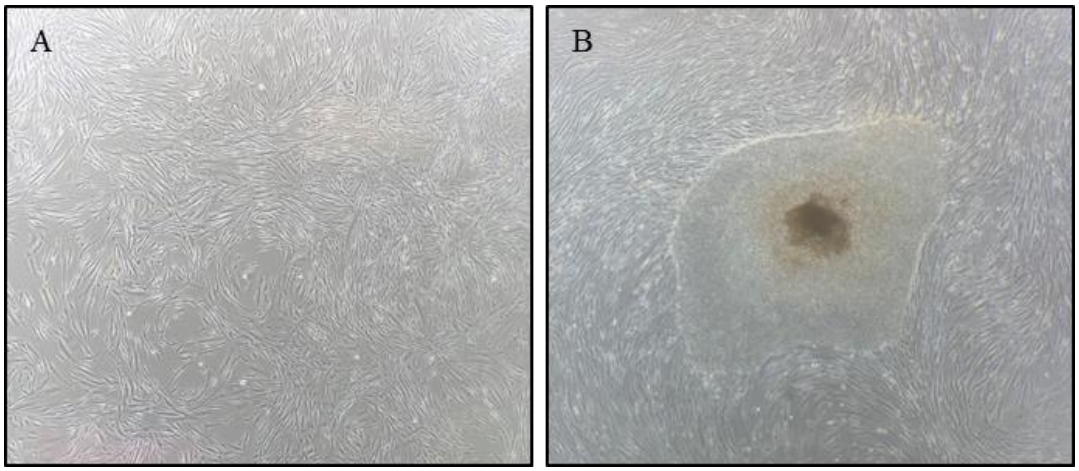

Figure 2-4 Representative images of fibroblast reprogramming.
A) Fibroblasts post day 8 before colony development, and B) Stem cell colony at day 25 surrounded by fibroblasts. No scale bar as photos taken on a camera phone aimed down a microscope eyepiece.

2.6.2 *iPSC colony selection and expansion*

Colonies with an iPSC morphology were picked using a pipette tip and replated in to one well of a geltrex coated 24-well plate. In order to expand iPSC, lines were passaged every 5-7 days using 0.5mM Ethylenediaminetetraacetic acid (EDTA) for 5mins (15575-038, Invitrogen). iPSC morphology was defined as a colony of densely packed cells with a high nucleus to density ratio, smooth edge of the colony with no evidence of cellular migration. Morphology was analysed visually on a brightfield microscope (Olympus CKX41).

2.6.3 *Culture of iPSC*

iPSCs were maintained on geltrex coated 6-well plates (10119831, Fisher Scientific). iPCS media was changed daily, and cells were split when colonies were large but not touching other nearby colonies. iPSC were split using 0.5mM EDTA for 5 mins, on to geltrex coated six well plates at a ratio of 1:6.

Mutation	Line name	Sex	D.O.B.	Biopsy date	Age at onset	Status at biopsy	Generated for this thesis?
-	A1	F	-	*20-24	-	-	No
-	RB101	M	-	*45-49	-	-	No
APP V717I		F	1970	15.12.14	-	Asymptomatic	Yes^
PSEN1 Y115H		M	1971	22.11.10	34	Affected	Yes^
PSEN1 M146I	M146I	M	1974		33	Affected	No
PSEN1 R278I	R278I	M	1950	15.11.10	58	Affected	Yes^
PSEN1 E280G	E280G.A	M	1966	15.09.15	38	Affected	Yes
PSEN1 E280G	E280G.B	M	1968	10.03.14	41	Affected	Yes

Table 2-4 Stem cell lines used in this thesis.

*Approximate age provided by the EBISC website from which the two lines were obtained.

^Generated in collaboration with Christopher Lovejoy and Dr Charlie Arber.

2.6.4 *Cryopreservation of Stem Cells*

iPSCs were pre-incubated for 1hr with 5µM Y-27632 ATP-competitive inhibitor of Rho-associated protein kinase (Y2 ROCK inhibitor) (SCM075, Sigma). Cells were lifted with EDTA for 5mins, 37ºC, 5%CO_2, EDTA was aspirated and cells were re-suspended in E8 media + 10% DMSO (D2650, Sigma), placed into 2ml cryovials (CLS430488, Corning) and frozen at -80˚c in Nalgene® Mr. Frosty (C1562, Sigma). For long term storage cells were transferred to liquid nitrogen.

2.6.5 *Cortical Neuron induction*

Stem cell colonies from 5 wells of a 6-well plate were passaged with EDTA and pooled into 1 well on a 6-well plate. Once cells reached 100% confluency (within 48hrs), media was switched to neural induction media (Table 2-8) and media replaced daily. On day 12 of neural induction, media was replaced and cells were gently dissociated from the plate as a sheet using a cell scraper (541070, Greiner Bio-One International) and plated in neural induction media on geltrex coated

plates at a ratio of 1:3. The following day media was switched to neural maintenance media (Table 2-8).

2.6.6 *Cortical neuron maintenance*

Neuronal rosettes were fed every 48hr with neural maintenance media. Once confluent, rosettes were passaged using Dispase (50 U/ML) (17105041, Gibco) at 37˚c, 5% CO_2 for 15 to 30 mins. Once the clumps of cells had lifted, they were transferred into 15ml falcon tubes containing 10ml Dulbecco's phosphate-buffered saline (DPBS) (14190-326, ThermoFisher Scientific) and washed three times with DPBS to remove residual Dispase. Cells were re-suspended in neural maintenance media and were gently pipetted to break the larger clumps before replating into 12-well pates (10098870, Fisher Scientific) pre-coated O/N at 37˚c, 5% CO_2 with laminin (1:50, DPBS) (L2020, Sigma). Cells were split at a ratio of one 6 well to three 12 wells. Media was changed every 2-3 days. This procedure was repeated around day 20 to further expand the precursors. Once substantial neurogenesis could be observed (around day 27-31), cells were split at a ratio of ~1:2 using Accutase to generate single cell cultures (A11105-01, Gibco). Accutase was added to the cells and they were incubated at 37ºc, 5% CO_2 for 5-10mins (500µl per well on 12-well plate). Once lifted, cells were centrifuged at 180$g_{(av)}$ for 3 mins, media was aspirated and cells were re-suspended in N2B27 and plated on 12-well laminin coated plates (1:100, DPBS).

Neurons were split for the final time at day 35-38, at a ratio of ~1:2/3 using Accutase as described and were plated on to pre-coated poly-L-ornithine (4hrs 37ºc, 5% CO_2) (P4957, Sigma) and laminin (O/N, 37ºc, 5% CO_2) (1:100, DPBS) coated 12 well plates, or on to poly-L-ornithine and laminin coated coverslips in 12 well plates. Cells were maintained with half media change every 3-4 days.

2.6.7 *Conditioned cell media collection*

Conditioned media was collected from iPSC derived cortical neurons. On day 98, cells underwent half media change (neural maintenance media). On day 100, half the conditioned media was collected and replaced with fresh media. Conditioned media was centrifuged at 2000$g_{(av)}$, 5 mins RT. Media was aliquoted in 1ml volumes in low binding screw cap tubes (72.694.406, Sarstedt) and immediately stored at -80˚c.

2.6.8 *Media compositions*

Reagent	Volume (ml)	Final concentration	Reference
DMEM/F-12, GlutaMAX	450	-	10565018 – Gibco
Fetal Bovine Serum	50	10%	10500064 – Gibco
Pen Strep	2.5	Penicillin = 25U/mL Streptomycin = 25µg/mL	15070-063 – Gibco

Table 2-5 Fibroblast media.

Reagent	Volume (ml)	Final concentration	Reference
Essential 8	490	-	A1A517001 – Gibco
Essential 8 supplement	10	1X	A1A517001 – Gibco

Table 2-6 Stem cell media

Reagent	Volume (ml)	Final concentration	Reference
DMEM/F12, Glutamax	40 ml	-	10565018 – Gibco
Knock out serum	10 ml	20%	10828028 – Gibco
L-glutamine	0.5	2Mm	25030024 – Gibco
Non-essential amino acids	0.5	1X	11140050 – Gibco
Pen strep	0.5	Penicillin = 50 U/ML, Streptomyocin = 50µg/ml	15070-063 – Gibco
2-Mercaptoethanol	0.05	50µM	31350-010 - ThermoFisher Scientific
Fibroblast Growth Factor-basic	0.01	20ng/ml	100-18B – Peprotech

Table 2-7 Human embryonic stem cell media.

Reagent	Volume (ml)	Final concentration	Reference
Neurobasal media	242.25	-	12348017 – Gibco
DMEM/F-12, GlutaMAX	242.25	-	10565018 – Gibco
N2 supplement	2.5	.5X	17502048 – Gibco
B27 supplement	5	.5X	17504044 – Gibco
Pen Strep	2.5	Penicilin = 25U/ml Streptomycin = 25µ/ml	15070063 – Gibco
L-Glutamine	2.5	1mM	25030024 - ThermoFisher Scientific
Non-Essential Amino Acids	2.5	.5X	11140050 – Gibco
β-mercaptoethanol	0.5	50µM	31350010 - ThermoFisher Scientific
Insulin	0.125	.00025µg/ml	19278 – Sigma
For neural induction media add:			
Dorsomorphine	50µl	1µM	3039 - R&D Systems
SB431542	500µl	10µM	1614 - R&D Systems

Table 2-8 Neural maintenance media.

2.7 Molecular biology

2.7.1 *DNA extraction from cortical tissue*

100ug of cerebellar tissue (frozen cortical if cerebellum not available) was placed on wet ice in a 1.5ml tube. 50w/v extraction buffer (NaCl 0.1M (S-9625, Sigma), Trizma Base 20mM (T-1503, Sigma), EDTA disodium 25mM (E-5134, Sigma), SDS 0.5% (L-4390, Sigma) in ddH_20, autoclaved before use) was added. Tissue was homogenised (TissueRuptor, Qiagen) and extraction buffer was added up to a volume of 60v/v. Proteinase-K (1mg/ml) was added and samples mixed by inversion followed by incubation at 55˚c O/N with occasional vortexing. 1:1:1 Phenol, chloroform, isoamyl alcohol (15593-031, Invitrogen) was added to the samples and briefly vortexed. Samples were centrifuged at 12,000 rpm for 4 mins. The aqueous layer was removed and placed in a clean 1.5ml tube, the remainder was discarded according to hazardous waste protocols. To the new tubes 10v/v 3M NaAC at pH 5.5 was added and briefly mixed. 100% ethanol was added to a volume of 1.5ml and mixed by inversion. Samples were incubated at -20˚c for 1hr to precipitate DNA. Samples were spun at 12,000rpm, 4˚c for 20 mins, after which the aqueous layer was discarded. 75% ethanol was added and incubated at 4˚c

for 30 mins. Samples were spun at 12,000rpm for 5 mins, ethanol was removed and tubes left open to air dry for 30 mins, RT. DNA was re-suspended in TE solution (10m mM Tris-hcl pH 8.0, 1 mM EDTA in ddH_20) and measured for DNA concentration on a spectrometer (Eppendorf Biospectrometer® fluorescence, Eppendorf).

2.7.2 *DNA extraction from cell cultures*

To harvest DNA from cell lines the TRIzol™ (15596026, Invitrogen) protocol was used. Media was aspirated from confluent cells in one well of a 6 well plate and 1ml TRIzol™ was added and pipetted multiple times to dissociate and homogenize cells and the suspension placed in to an Eppendorf on dry ice and stored at -80˚c until use. Frozen samples were thawed on ice then left at RT for 5mins. 200µl Chloroform (22711.290, VWR) was added, samples vigorously shaken then incubated for 3 mins followed by centrifugation at 12,000$g_{(av)}$, 4˚c for 15 mins. Aqueous RNA phase was extracted and stored at -80˚c. To the DNA containing interphase, 300µl 100% ethanol was added and samples shaken, incubated for 3 mins and centrifuged at 2000$g_{(av)}$, 4˚c for 5 mins. The protein containing supernatant was removed and stored at -80˚c. Pelleted DNA was resuspended in 1ml sodium citrate in 10% ethanol, pH 8.5 and incubated for 30mins with regular inversion followed by centrifugation at 2000$g_{(av)}$, 4˚c for 5 mins. Supernatant was discarded and the sodium citrate step was repeated. After discarding supernatant, the pellet was resuspended in 1.5ml 75% ethanol and incubated for 20 mins with regular inversion followed by centrifugation at 2000$g_{(av)}$, 4^{o}c for 5 mins. Supernatant was discarded and pellet air dried for 10 mins before resuspension in 300µL 8mM NAOH, followed by centrifugation at 12,000$g_{(av)}$, 4˚c for 10 mins. The DNA containing supernatant was stored at -20^{o}c.

2.7.3 *APOE Genotyping*

DNA was analysed for *APOE* genotyping. DNA was PCR amplified (TC-Plus, TECHNE) using a GC rich Taq polymerase PCR kit (20123, Qiagen) and primers specific to the *APOE* gene, as previously described (Emi *et al.*, 1988). Primer sequence:

F (F4): 5’ ACAGAATTCGCCCCGGCCTGGTACAC 3’
R (F6): 5’ TAAGCTTGGCACGGCTGTCCAAGG 3’

PCR cycle:

x1	Hot lid	105˚c	2mins
x1	Initial denaturation	94˚c	5mins
x30	Denaturation	94˚c	30secs
	Annealing	60˚c	30secs
	Elongation	72˚c	30secs
x1	Final elongation	72˚c	5mins

Amplified DNA underwent restriction enzyme digestion with HhaI (R6441, Promega) and was visualised on a 5% agarose gel composed of 2% agarose (A9539, Sigma) and 3% high resolution agarose (50091, Lonza) with 1X GelRed^{tm} (BT41003, Biotium) under UV light (MniBis Pro, DNR). *APOE* genotype was determined by bands present at specific molecular weight compared to a DNA ladder of known molecular weight (SM1313, Thermo) (Hixson & Vernier, 1990) and in comparison to known positive controls.

2.7.4 *PSEN1 Genotyping*

To confirm FAD mutations were present in the E280G cell lines, DNA was amplified by PCR using primers for *PSEN1* exon 8 which contains the SNP residue at 280bp of the amplicon. Primer sequence:

F: 5’ TCCTCCCTACCACCCATTTAC 3’
R: 5’ GGAGTTCCAGGAATGCTGTG 3’

PCR cycle:

x1	Hot lid	105˚c	2mins
x1	Initial denaturation	94˚c	5mins
x30	Denaturation	94˚c	30secs
	Annealing	65˚c	30secs
	Elongation	72˚c	30secs
x1	Final elongation	72˚c	5mins

The amplified PCR product was cleaned up using ExoSAP-IT^{TM} (78201.1.ML, ThermoFisher Scientific) to remove primers and PCR reagents. Purified sequences were sent to Source Bioscience (https://www.sourcebioscience.com) for sequencing. Sequence reads were viewed in SnapGene® 4.3.2 and presence of correct nucleotide at the mutation location was confirmed.

2.7.5 *TREM2 Genotyping*

TREM2 sequencing was done in the E280G cell lines as one of the patients had been found to carry a variant during life*. TREM2* Primers were designed for sequencing *TREM2* exon 2 which contains multiple SNP's with potential implication in AD. Primers were designed using NCBI primer blast (www.ncbi.nlm.nih.gov) using the NCBI sequence ref 'NC_000006.12 Homo sapiens chromosome 6, GRCh38.p12 Primary Assembly'. Amendments were made to output primer sequences to reduce non-specific binding, and retested on NCBI primer blast until no non-specific sequences were found. In-Silico PCR was run on UCSC Genome Browser (genome.ucsc.edu) using the current assembly (Dec. 2013 (GRCh38/hg38)), with *TREM2* the only in-silico amplification result with an expected length of 385bp. Primers were supplied by Sigma-Aldrich (Sigma® Life Science) with the sequence as follows:

F: 5' AATGAATGTCTCCTCCCCAGAGCTGTCC 3'
R: 5' CACTGCCCACTCACCTGCCAGCACCT 3'

TREM2 primers were tested via PCR (Veriti™, 4375305, Applied Biosystems™) on human brain DNA, with a range of annealing temperatures (63˚c, 65˚c, 67˚c, 70˚c) tested for optimisation, with 65˚c selected as optimal (Figure 2-5). Amplified DNA was visualised under UV on a 1% agarose gel. *TREM2* genotyping was conducted on DNA from stem cell lines E280G.A and E280G.B.

Optimal PCR cycle:

x1	Hot lid	105˚c	2mins
x1	Initial denaturation	94˚c	5mins
x30	Denaturation	94˚c	30secs
	Annealing	65˚c	30secs
	Elongation	72˚c	30secs
x1	Final elongation	72˚c	7mins

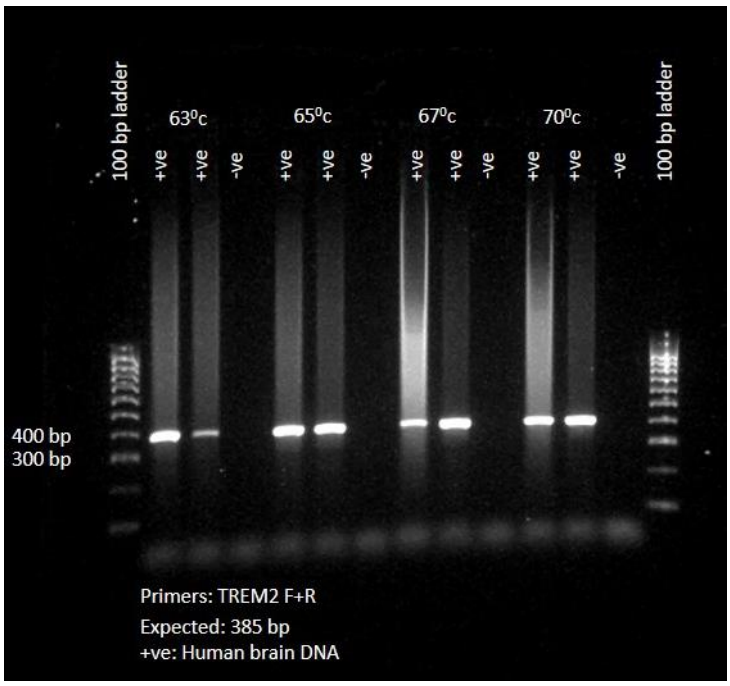

Figure 2-5 T*REM2* primer optimisation on human brain DNA.

2.7.6 *Protein extraction from brain homogenate*

Tissue was homogenised in protein lysis buffer composed of:

50mM tris HCL, 175mM BaCL, protease inhibitor (11836170001, Roche), phosphatase inhibitor (04906837001, Roche) and 1% triton-X (X100, Sigma) in dH_2O.

Frozen cortical tissue samples were weighed and ice cold 5X w/v protein lysis buffer was added. Sample and buffer was transferred in to a dounce and homogenised and resulting homogenate pipetted into an Eppendorf. Homogenates were centrifuged at 1000 *x g* (3500rpm), 4^0c, for 5 mins. Supernatant containing soluble protein was removed, aliquoted and stored at -80^0c.

2.7.7 *Protein and RNA collection from cell samples*

Cells which had been used for conditioned media collection were detached using Dispase for 20 mins at 37ºc, 5% CO_2. Detached cells were placed in to Eppendorfs and spun at $200g_{(av)}$, RT, for 1min to pellet cells and supernatant aspirated. For protein collection, the pellet was resuspended in ~200µl radioimmunoprecipitation assay buffer (RIPA) buffer containing phosphatase and

protease inhibitors. Samples were homogenised, spun at 4ºc and stored at -80˚c. For RNA collection, the pellet was resuspended and dissociated in Trizol (500µl per 1 well on 12 well plate), placed immediately on dry ice then stored at -80˚c.

2.7.8 *Protein concentration determination*

Protein concentration of cell and brain homogenate samples were determined using the Bio-Rad *DC*™ Protein Assay.

20µl of reagent S (5000115, Bio-Rad) was added to 1ml reagent A (5000113, Bio-Rad). A 1:1 standard curve from 4mg/ml to 0.125mg/ml with a blank at 0mg/ml was generated by diluting bovine serum albumin (BSA) in either RIPA buffer (for cells) or protein lysis buffer (for brain). In triplicate, 5µl of standard and sample lysate were added to individual wells. 25µl of reagent A+S was added to each well followed by 200µl reagent B (5000114, Bio-Rad). The plate was shook at 700rpm for 1 min and left to develop for 15 mins, RT. Absorbance at 750nm was read on the Spark™ 10m plate reader (Tecan). Protein concentration was determined from the standard curve of the standards using the equation x=(y-m)/b.

2.7.9 *Western blot*

30µg of protein with 1X NuPage™ LDS sample buffer (NP0007, ThermoFisher Scientific) and 1X NuPAGE™ reducing agent (NP0004, ThermoFisher Scientific) was denatured at 70˚c for 10 mins followed by brief centrifugation. 25µl of protein was loaded in to a 10% Bis-Tris gel (NP0301BOX, ThermoFisher Scientific) in MES SDS running buffer and run at 150 volts for 1hr 30 mins on ice. Protein was transferred on to nitrocellulose membrane at 30 volts for 1hr on ice. Membrane was blocked in 5% BSA/0.1%Phosphate-buffered saline-tween (PBS-tween: PBS; 18912-014, Gibco. Tween; P1379-100ML, Sigma) for 30 mins, RT. Primary antibody rat anti-PSEN1 N-term (1:500, MAB1563, Millipore) was incubated in 5% BSA O/N at 4ºc. Membrane was washed x3 with 0.1% PBS-tween and incubated in goat anti-rat secondary antibody (1:10,000, A21096, Alexa Fluor®), for 1hr, RT, protected from light. Membrane was washed with 0.1% PBS-tween and x2 PBS before imaging on an Odyssey Fc (Li-cor). Membrane was then incubated for 1hr, RT, with mouse anti-β-actin (1:1000, Sigma) as a loading control. Membrane was washed x3 with 0.1% PBS-tween and incubated in

donkey anti-mouse secondary antibody (1:10,000, 926-68071, Li-cor) for 1hr, RT, protected from light. Membrane was washed with 0.1% PBS-tween and x1 with PBS before imaging on an Odyssey Fc (Li-cor).

2.7.10 *ELISA analysis of Aβ isoforms in conditioned cell media*

Enzyme-linked immune-sorbent assay (ELISA) for Aβ isoforms was conducted using D100 neuron conditioned cell media.

Protocol for: Amyloid beta1-43 Solid phase sandwhich ELISA (27710, IBL)

Samples were brought to room temperature and reagents were prepared to working concentrations. Calibrators were prepared according to manufacturer guidelines generating a 1:1 dilution series of known concentration of Aβ43 from 150pg/ml to 2.34pg/ml with a blank at 0pg/ml. 100µl of calibrator, control and samples were added to individual wells in duplicate, shaken at 700rpm for 1 min and left to incubate at 4^0c O/N. Wells were washed x7 with wash buffer followed by incubation with 1X enzyme conjugate solution for 1hr, 4^0c. The plate was washed x9 with wash buffer followed by addition of 100µl TMB solution for 30 mins, RT, protected from light. 100µl stop solution was then added and the plate was read immediately at 450nm, with a reference of 650nm (FLUOstar Omega Microplate Reader, BMG Labtech).

Protocol for: V-PLEX Aβ Peptide Panel 1 (6E10) Kit (1 Plate) (K15200E, Mesoscale Discovery).

Samples were brought to room temperature and reagents were prepared to working concentrations. Calibrators were prepared by diluting 10µl of each detection antibody (Aβ38, Aβ40, Aβ42) in 370µl Diluent 35. Samples were diluted 1:1 in diluent 35 generating 7 calibrators and a blank at 0pg/ml. Aβ38 range; 14100 - 3.44pg/ml: Aβ40 range; 15200 - 3.71pg/ml: Aβ42 range; 2360 - 0.576pg/ml. ELISA plate was blocked with 150µl of Diluent 35 and incubated for 1hr, RT, 700rpm followed by x3 wash with wash solution. Next, 25µl of detection antibody was added to each well and 25µl of calibrators/sample/control were added to individual wells, in duplicate and incubated for 2hr, RT, 700rpm. The plate was washed x3 with wash solution. 150µl of 2X read buffer was added and plate was immediately read (MESO QuickPlex SQ 120, MSD).

To analyse Aβ levels between lines, results were converted into ratios. Ratios are considered a more accurate way to analyse and compare Aβ isoform levels than absolute levels (Hansson *et al.*, 2019). Ratios also negate the effect of cell density variation, which would affect comparisons between absolute levels.

2.7.11 *RNA extraction*

Aqueous RNA phase from neuronal cell cultures (obtained by the method described in 2.7.2) underwent RNA extraction. All steps except centrifugation were conducted in a fume hood and filter tips were used (TipOne®, StarLab). To the aqueous phase, 0.5ml 100% isopropanol (437423R, VWR) was added per 1ml trizol used and left to incubate on ice for 10 mins at 4ºc followed by centrifugation at 12,000$g_{(av)}$, 4^0c, for 45 mins. Following centrifugation, the supernatant was discarded and the remaining pellet washed with 1ml 75% ethanol per 1ml trizol used. The sample was mixed by repeat inversion and centrifuged at 7500$g_{(av)}$, 4^0c, for 5 mins. The resulting supernatant was discarded and pellet left to air dry for 10 mins, at RT. The RNA pellet was resuspended by pipetting in 20µl nuclease free H_20.

From the 20µl RNA suspension, 1µl was diluted 1:10 and concentration and purity analysed on the NanoDrop ND 1000 (ThermoFisher). The concentration, A260/A280 ratio and A260/A230 ratio were measured (Table 9-4).

2.7.12 *Complementary DNA (cDNA) synthesis*

The SuperScript IV Reverse Transcription Kit (18091050, ThermoFisher) was used for cDNA synthesis following maufacturers protocol. cDNA synthesis was conducted in a 96well plate and incubations were completed in the PCR machine. For each sample 500ng RNA was combined with 1ul of 50uM random hexamers, 1µl 10mM dNTP mix and nuclease free H_20 to a volume of 13µl and incubated at 65^0c for 5mins followed by incubation on ice for at least 1min. To each sample a premade solution containing 4µl 5X SSIV Buffer, 1µl 100 mM DTT, 1µl RNaseOUT recombinant RNase Inhibitor (40U/µl) and 1µl SuperScript IV Reverse Transcriptase (200U/µl) was added. The plate was briefly mixed and centrifuged. The plate was then incubated at 23^0c for 10mins, immediately

followed by incubation at 55^0c for 10 mins and the reaction was inactivated at 80^0c for 10 mins. cDNA was stored at -80^0c.

2.7.13 *Quantitative PCR (qPCR)*

Preparation for qPCR was conducted on ice and each sample was run in triplicate on the same plate, with one individual induction run per plate analysed. Initially, 2µl of the cDNA was diluted in 18µl H_20 to make a working solution. For each reaction, 10µl 2X Power SYBR™ Green PCR Master Mix, (4368708, ThermoFisher), 7.8 µl nuclease free H_20 and 0.1µl of 100µM forward and reverse primer were mixed and pipetted into a 96 well plate, avoiding the outer wells. For each sample, 2µl of the working solution cDNA was added to the Power SYBR™ Green PCR Master Mix in the 96well plate. The plate was briefly mixed and centrifuged and qPCR run on the Mx3000P qPCR system (Aligent) using the Sybrgreen with dissociation curve program. The dissociation curve was inspected to check for one peak, indicating the production of one product.

x1	Initial denaturation	95°c	10mins
x40	Denaturation	95°c	30secs
	Annealing	60°c	1min
	Elongation	72°c	1min
Dissociation curve x1		95°c	1mins
		55°c	30secs
		95°c	30secs

Primers used for qPCR had been designed to span exon-exon junctions so that only cDNA transcribed from mRNA would be amplified. Primer sequences were designed by Dr Charlie Arber (*PSEN1*) and by Dr Roberto Simone (60S ribosomal protein L18a (RPL18a)). RPL18a was used as a housekeeping gene. Primer sequence for qPCR:

PSEN1 F: CAATACTGTACGTAGCCAGA

PSEN1 R: AATGGGGTATAGATTAGCTG

RPL18a F: CCCACAACATGTACCGGGAA

RPL18a R: TCTTGGAGTCGTGGAACTGC

The cycle threshold (Ct) values generated from the qPCR of *PSEN1* and *RLPI18* were used to generate results expressed as fold change. In Microsoft Excel 2016, for each gene, Ct values of the triplicate repeats were used to generate the mean average. Delta Ct values were calculated by subtracting the mean *RLI18* Ct from the mean *PSEN1* Ct for each cell line. To normalise to control (RB101), the RB101 Delta Ct was subtracted from the Delta Ct for each line, generating the Delta Delta Ct value which was converted to fold change using the equation: fold change = 2^(-Delta Delta Ct). Fold change values were used for statistical analysis.

2.7.14 *Immunocytochemistry (ICC)*

Coverslips were washed with DPBS and fixed for 15-20 mins in 4% PFA, RT. PFA was removed and coverslips gently washed 2 times with excess 1X PBS. Coverslips were either stored in PBS at 4˚c or used immediately for ICC.

Coverslips were blocked for 20 mins in 5% BSA/.3% PBS-triton. Block was removed and primary antibodies in 5% BSA/.3% PBS-triton (T8787, Sigma) were added for 2hrs RT or 4˚c O/N. The primary antibodies used in this study were: mouse anti-Stage-specific embryonic antigen 4 (SSEA4) (1:300, 330402, Biolegend), rabbit anti-octamer-binding transcription factor 4 (Oct4) (1:400, SC-8628, Santa Cruz), mouse anti-BRN2 (1:50, SC-393324, Santa Cruz), rabbit anti-T-Box Brain Transcription Factor 1 (TBR1) (1:300, AB31940, Abcam), mouse anti-class III beta-tubulin (TUJ1) (801201, Biolegend) and rabbit anti-TUJ1 (802001, Biolegend). Primary antibody was removed and followed by x3 5 min wash with 1XPBS-triton at RT. Secondary antibody in 5% BSA/.3% PBS-triton was added and incubated for 1hr at RT in the dark. The fluorescent secondary antibodies used in this study were as follows: 488 Donkey anti-Goat (1:5000, A11055, Alexa Fluor®), 488 Donkey anti-Rabbit(1:5000, A21206, Alexa Fluor®), 594 Donkey anti-Mouse (1:5000, A21203, Alexa Fluor®) and 594 Donkey anti-Rabbit (1:5000, A21207, Alexa Fluor®). Cells were then rinsed once with PBS-triton and incubated with DAPI (1:5000, D1306, Invitrogen) for 10 mins at RT protected from light. Cells were rinsed once with PBS-triton followed by 1X PBS. Coverslips were rinsed with .3% PBS-triton followed by 1X PBS, mounted on to slides with fluorescence mounting medium (1:500, S3023, DAKO) and stored at

4˚c protected from light and imaged on a Leica DM5500 B microscope using Leica Application suite X software (Leica microsystems, Wetzlar, Germany).

2.8 **Statistics**

2.8.1 *Pathological data analysis*

Analysis of the neuropathological data was performed for all cases and assessed as a whole cohort, by mutation sub-groups and by *APOE* status.

In the QSBB cohort (n=20), mutation sub-groups are *PSEN1* cases with mutations pre-codon 200 (n=10) and post-codon 200 (n=6), and *APP* (n=4*)* mutation cases. In the extended cohort (n=41), mutation sub-groups are *PSEN1* cases with mutations pre-codon 200 (n=20) and post-codon 200 (n=11), and *APP* (n=10*)* mutation cases.

To group by *APOE* status, cases were separated into those without an ε4 allele e.g. ε2/3 and ε3/3, and those with at least one ε4 allele e.g. ε3/4 and ε4/4. In the QSBB cohort, *APOE4* non-carriers n=12 and *APOE4* carriers n=7. In the extended cohort, *APOE4* non-carriers n=24 and *APOE4* carriers n=14, additionally *APOE* was further grouped by *APOE* genotype ε2/3 (n=2), ε3/3 (n=22), ε3/4 (n=9) and ε4/4 (n=5) allele carriers in the extended cohort

Statistical analyses were carried out using StataIC 15 (StataCorp. 2017. *Stata Statistical Software: Release 15*. College Station, TX: StataCorp LLC), GraphPad Prism version 8.00 for Windows (GraphPad Software, La Jolla California USA, www.graphpad.com) or IBM SPSS Statistics for Windows, version 25.0 (IBM Corp., Armonk, N.Y., USA).

Testing reliability and normality

Intra-class correlation coefficient analysis was conducted using SPSS (Table 9-2, Table 9-3). Bland Altman plots were generated on Excel (Figure 9-1), while the complementary linear regression was conducted on Graphpad Prism (Table 9-1). Histograms for visual inspection of normality were generated on SPSS. QQ plots for visual inspection of normality were generated on Stata.

Nominal data

To test that there were no significant over representations of the defined mutation sub-groups, *APOE* status or sexes within those groups, the data was analysed by Fisher's exact (StataIC 15).

Linear regression

When possible, linear regression was used to assess associations between the data. Adjustments made for explanatory variables such as mutation sub-group, *APOE* status, sex and age at onset have been indicated within the results. Addition of multiple other variables such as age at onset, disease duration or PM delay have not been included as increasing the number of explanatory variables within a small cohort can prevent observation of important associations All linear regressions were conducted on StataIC 15.

Correlation analysis

Correlation analyses were conducted using Kendall's tau-b. This approach was used for all data types (ordinal and continuous) to retain consistency across analyses.

Group comparisons

Comparisons between two groups were conducted using exact Mann-Whitney-Wilcoxon rank sum (StataIC 15). Comparisons between three or more independent groups were conducted using Kruskal-Wallis with Dunn's post hoc test for multiple comparisons applied where appropriate. Comparisons between three or more groups where data was classified as repeated measures were analysed using Friedman ANOVA (StataIC 15).

Graphs

Graphs representing data analysis were produced on Graphpad Prism.

Significance

A probability value of less than $p<0.05$ was considered significant, with post hoc multiple comparison test adjusting the significant level appropriately for the analysis conducted.

2.8.2 *Cell data analysis*

Cell data was checked for normality using QQ plots. Cell data was assessed using One-way ANOVA with a probability value of less than $p<0.05$ considered significant. When ANOVA analysis reached statistical significance, Tukey's post hoc test was used, adjusting the significant level appropriately for the analysis conducted. All cell data statistics were conducted on GraphPad Prism.

Chapter 3

Aβ pathology in FAD

3 Aβ pathology in FAD

3.1 Abstract

Introduction: Alzheimer's disease is the most common cause of dementia and in a small minority of cases is familial, due to autosomal dominant mutations in the *PSEN1*, *PSEN2* or *APP* genes. Considerable phenotypic and pathological heterogeneity may be observed in FAD (Maarouf *et al.*, 2008; Ryan *et al.*, 2016), with previous work suggesting that causative gene and mutation position may both influence the clinical and pathological features (D. M. A. Mann *et al.*, 2001a; Ryan *et al.*, 2015a). Here we investigate the pathological distribution and plaque type of Aβ and CAA pathology throughout the six cortical layers of FAD cases to determine any common patterns between different mutation cases.

Material and Methods: Frontal cortex of 20 FAD cases with mutations in *APP* (n=4) or *PSEN1* (n=16, 10 located pre-codon 200 and 6 post-codon 200) were analysed and *APOE* status was available for most cases. Sequential sections were stained immunohistochemically for Aβ and Nissl to determine the cortical layers. Specific plaque pathologies were semi-quantitatively graded and Aβ load (% area stained) was determined to assess the amount of Aβ present in each cortical layer. Associations between pathologies, clinical and genetic data were analysed.

Results: We found age at onset to be associated with genetic mutation and sex in this FAD cohort, with a younger onset in *PSEN1* mutations pre-codon 200 compared to *APP* mutations only (p=0.02) after adjusting for gender and *APOE4* status, and in females compared to males (p=0.02) after adjusting for mutation sub-group and *APOE4* status. Possession of an *APOE*4 allele was associated with increased disease duration (p=0.002) but not with age at onset (p=0.23), after adjusting for mutation sub-group and gender. The spread of Aβ pathology across the six cortical layers differed in the different mutation carriers and even varied between cases with the same mutations. In all groups, average Aβ load was highest in layer 3 while the *PSEN1* post-codon 200 group had higher Aβ load in lower cortical layers, with a small number of this group having increased cotton wool plaque pathology in lower layers. Cotton wool plaque frequency was

positively associated with severity of CAA in the whole cohort and *PSEN1* post-codon 200 group.

Conclusions: Determining the differences in the spread of Aβ pathology between the different mutation cases in relation to *APOE* status and clinical symptoms may provide us with a biological relevance of why certain cortical layers are affected and others spared from underlying pathology.

3.2 **Introduction**

3.2.1 *Aβ plaque types*

Aβ deposits exist in multiple distinct forms and these have been classified into specific plaque types. Common plaques observed are the cored plaques and diffuse plaques in addition to the less frequently observed CWPs. Cored plaques consist of a dense circular centre composed of Aβ, surrounded by a ring or 'halo of Aβ. While diffuse plaques exists in a range of varying size without a central core. CWPs were first described as large distinct eosinophilic structures. In hematoxylin-eosin–stained sections they were readily distinguishable, with a lack of neuritic pathology shown by Bielschowsk staining, and lacking a dense core upon immunohistochemistry (IHC) with Aβ antibodies and minimal reactivity with Thioflavin S (Crook *et al.*, 1998; Verkkoniemi *et al.*, 2000)

The areas around cored plaques are shown to associate with dystrophic dendrites (Adlard & Vickers, 2002), and cored plaques are often associated with Thioflavin-S positive tau pathology (T. C. Dickson & Vickers, 2001), implicating them as a particularly toxic plaque formation. Cored plaques are also thought to associate with inflammatory reactivity (Nagele *et al.*, 2004). It has also been proposed that cored plaques originate from intracellular Aβ deposit rather than extracellular deposits (D'Andrea & Nagele, 2010). Uncertainty around plaques highlight the importance of further study.

The major component of diffuse plaques is generally Aβ42. They are frequent and seen in almost all cases of AD. They are not associated with immunoreactivity (D'Andrea *et al.*, 2004). However, they are not likely to be innocent bystanders, as when only diffuse Aβ pathology is present, tau pathology

can also be present. This relationship has not been found to be associated with *APOE* genotype (Abner *et al.*, 2018).

Using IHC, CWPs have been shown to be composed mainly of Aβ42, with minimal reactivity to Aβ40 antibodies (Uchihara *et al.*, 2003; Verkkoniemi *et al.*, 2001; Yokota *et al.*, 2011). Indeed, the aetiology of CWPs has been proposed as a consequence of high rates of Aβ42 production, which has been observed in some mutations which displayed CWPs (Dumanchin *et al.*, 2006; Houlden *et al.*, 2000). This indicates that pathological features may be linked to Aβ production: a feature affected by FAD mutations.

Although the aetiology of the different plaques remain unknown, the influence of Aβ isoform and of structural arrangement of Aβ oligomers and fibrils is likely to influence morphological features (C. Xue *et al.*, 2019). Another theory is that plaques mature over time, from a diffuse form to a cored plaque. It was noted that there was a higher proportion of cored plaques in older individuals (Maat-Schieman *et al.*, 2000) and others predict that diffuse plaques gradually mature in to cored plaques over time due to the nature of the composition of the plaque (Michno *et al.*, 2019). However, a lack of significant differences in the number of cored plaques in early AD compared to late AD has been observed. If plaques graduated from diffuse into cored plaques over time, a higher proportion of cored plaques in late stage AD would be expected (T. C. Dickson & Vickers, 2001).

3.2.2 *Distribution of Aβ pathology across cortical layers*

Aβ pathology in sAD and FAD may not be evenly distributed or randomly distributed in the cortex and a few studies have investigated this. In both sAD and FAD, a consistent maximal density of Aβ pathology has been found in the largest cortical layer, layer 3. Densities in other layers was seen to vary. In some of these studies, these differences between layers were significant, however others did not find significant differences, noting distribution to be random (Colle *et al.*, 2000; Dèlaere *et al.*, 1989; Duyckaerts *et al.*, 1986; Kalimo *et al.*, 2013; Pearson *et al.*, 1985; Rogers & Morrison, 1985). The lack of agreement between these different studies is likely to be due to different methods used. A range of techniques for visualising plaques were employed, such as IHC, Bodians protargol, Von Braunmuhl, thioflavin S and Bielschowsky staining, which will not all highlight the

same plaques equally. Additionally, the method of determining plaque density varied with use of plaque number, or percentage area coverage or other estimations. Furthermore, in some experiments cortical layers were not strictly defined and cortical layers were also sometimes grouped for comparison, e.g. upper compared to lower layers. However, the consistent finding of layer 3 across all studies, even with these varying research methods, implies an important role of this layer in AD pathology.

A study examining a group of 20 AD patients, including four cases with FAD mutations, reported that Aβ density across the cortex did not appear to markedly differ between cases, although the cortical layers were not specifically delineated (Armstrong, 2015). Such small numbers of FAD cases may not reflect differences that may be present in a larger cohort with a wider variety of mutations. It will be important to investigate this as not only do mutations have independent effects on Aβ pathology, there may also be mutation specific effects through mechanisms downstream of PSEN1/APP interactions with other proteins. One thing that can be taken from the study is that there were no clear differences between sAD and FAD, which implies a common mechanism.

Interestingly, in a report on three subjects from the same family with the *PSEN1* P264L mutation, pathological differences between same mutation carriers were found. Regional differences in pathology were observed and it was noted that these coincided with the clinical phenotype. Associations were detected between neocortical/thalamic involvement and psychiatric symptoms, striatal/amygdaloid involvement and Parkinsonism, brainstem involvement and spastic paraparesis (Martikainen *et al.*, 2010). While no firm conclusions can be drawn from this report of a small number of cases, it highlights the interesting heterogeneity of FAD Aβ pathology and how that may be linked to disease phenotype. Uncovering these associations may help understand the underlying mechanisms. Furthermore, it was also noted that the male *APOE*3/4 carrier in this study had a profound laminar specific Aβ pattern that was consistent across the frontal, temporal and parietal cortices, which was absent from the *APOE*3/3 carries (1 Male, 1 Female) except in the parietal cortex of the male. This highlights the need to investigate laminar distributions of Aβ pathology with the layers well-defined, in a variety of FAD mutations.

Despite these laminar patterns of Aβ distribution being highlighted in multiple studies, the reason for the differences between cortical layers is unknown. The fact that differences in regional distribution were potentially associated with the clinical phenotype supports the question of whether laminar distribution patterns could also have this association.

3.2.3 *Distribution of Aβ plaque types across cortical layers*

As well as the differences in plaque distribution across the cortical layer, the type of plaques observed also differ. In a small FAD cohort, CWPs were found mostly in upper layers (Shepherd *et al.*, 2005). In a sAD cohort, cored plaques were particularly noted in layer 5 of the superior frontal gyrus (T. C. Dickson & Vickers, 2001) while in another study they were more numerous in layer 2 and three (Delaère *et al.*, 1991), and this same study also found diffuse plaques more numerous in layers 2,3 and 5. In FAD cases with *PSEN1* mutations, a division of pathological phenotypes was noted, with cases showing either type 1 or type 2 pathology (David M. A. Mann *et al.*, 2001). This study was conducted using the Aβ42(43) antibody which recognises both Aβ42 and Aβ43. Type 1 Aβ42(43) IHC was characterised by greater plaque density in cortical layers 2 and upper 3 compared to layers 5 and 6. Diffuse plaques predominated in upper layers while cored plaques were more frequent in layer 6. Cored plaques were also more frequent at the depths of the cortical sulci. Subpial deposits were infrequent. Aβ40 IHC showed mild to moderate small cored or compacted deposits spread evenly along laminae, usually in layers 2 and 3, with notable plaques at the depths of the cortical sulci. Some subpial deposition was present. Type 2 Aβ42(43) IHC was characterised by larger plaques, which could be centered around CAA. Aβ40 IHC showed weak diffuse staining but large clustered cored plaques centred around CAA. Within the cases included in this study the *PSEN1* pre-codon 200 cases tended to have type 1 pathology while the post-codon 200 cases tended to have type 2 pathology.

3.2.4 *Clinical associations with Aβ plaques*

As plaques are seen to be neurotoxic, different plaque types may be linked to different clinical features. This may be due to their composition, or other factors that differ in relation to plaque type. Different studies looking at human brain

tissue have found a variety of findings. A larger plaque size has been positively associated with age at onset, independent of disease duration or *APOE* status (Serrano-Pozo *et al.*, 2012). Neuritic plaques have been found to be associated with cognitive measures while diffuse plaques were not (Alberto Serrano-Pozo *et al.*, 2013). In a separate study, neuritic plaques were associated with a range of cognitive dysfunctions (Malek-Ahmadi *et al.*, 2016). In opposition, diffuse plaques have been seen in cognitively normal elderly people with no association with cognitive measures, suggesting they are not necessarily related to clinical phenotype (Knopman *et al.*, 2003). However in a different study, diffuse plaques were said to coincide with early cognitive changes in AD (Wolf *et al.*, 1999). Plaque type alone may not be purely responsible, as the actual conformation of Aβ variants has been shown to segregate with distinct AD subtypes (J. Rasmussen *et al.*, 2017). Greater research in relevant human tissue on plaques and phenotype and genetic information may help decipher the relevance of these plaques to clinical disease.

Clinically, CWPs have been frequently observed in patients with spastic paraparesis and other motor symptoms (Brooks *et al.*, 2003; Karlstrom *et al.*, 2008; S. Zhang *et al.*, 2015). These observations are particularly associated with certain mutations, such as *PSEN1* exon 9 deletions (D. M. A. Mann *et al.*, 2001b; Steiner *et al.*, 2001). Interestingly, they may be more common in *PSEN1* mutations which lie post-codon 200 such as the previously mentioned *PSEN1* exon 9 deletion, *PSEN1* G217R/P2646L/L435F mutations and others (Crook *et al.*, 1998; Heilig *et al.*, 2010; Martikainen *et al.*, 2010; Niwa *et al.*, 2013; Norton *et al.*, 2009; M. J. Smith *et al.*, 2001). Despite this, CWPs have also sometimes been observed in patients with *PSEN1* mutations pre-codon 200 and have been observed in patients who did not display spastic paraparesis (Shrimpton *et al.*, 2007; Sutovsky *et al.*, 2018). Additionally, CWPs can rarely be found in SAD patients (Le *et al.*, 2001; Yokota *et al.*, 2011). Interestingly, variations in the presence of CWPs or lack thereof has been observed in same mutation carriers, leading some authors to speculate that CWPs are not linked to FAD mutation but rather to another modifier (Rogaeva *et al.*, 2003). These various observations warrant further investigation to decipher the pathological cause and consequence of these distinct plaques.

3.2.5 *Pathological differences between FAD mutation carriers*

As mentioned, there are clinical differences between FAD mutations. This has been seen to also extend into pathological differences. Differences have been seen between *PSEN1* mutation carriers sub-divided into those with mutations pre-codon 200 and those post-codon 200. Those with mutations post-codon 200 were seen to have a higher prevalence and severity of CAA and they were found to have significantly higher Braak scores (Ringman *et al.*, 2016). In a separate large cohort study, similar results were found (David M. A. Mann *et al.*, 2001). *PSEN1* post-codon 200 cases appeared to have greater Aβ40 pathology than those pre-codon 200, while there was no difference in Aβ42(43), although variability across all mutations was considerable. The increased severity of CAA seen in the post-codon 200 cases may be related to the increased Aβ40 pathology, as this is prone to accumulate in vessels. In a small cohort study, which used 10 of the FAD cases described and used in the project within this thesis, it was shown that the pre-codon 200 group had worse axonal health, assessed pathologically with markers for density and integrity (Ryan *et al.*, 2015a). However, these differences were regionally limited and not widespread. The proportion of vessels affected by CAA was numerically higher in the post-codon 200 group, although this was not significant. It was also noted that there was consistently higher CAA severity in the FAD cases carrying the *APOE4* allele, although case numbers were limited. In such a small cohort it may be difficult to detect group differences, so further study is warranted and has motivated the project described in this thesis.

3.2.6 *Aims*

Aβ pathology and the heterogeneity therein may be associated with different mutations and/or clinical features. The heterogeneity of Aβ can be manifested in the types of plaques or their distributions and these differences may reflect underlying molecular mechanisms. By analysing the Aβ pathology in FAD tissue, associations can be explored, developing understanding of pathogenic mechanisms. For the QSBB FAD cohort the aims are:

1. To determine the contribution of mutation, sex and *APOE* genotype on clinical factors (age at onset and disease duration).

2. To determine if Aβ plaque type, Aβ load or occurrence of CAA is associated with age at onset or disease duration in the QSBB FAD cohort.

3. To determine if there are differences in Aβ plaque type or pattern of distribution across the cortical layers, Aβ load or occurrence of CAA in genetic causes of FAD.

4. To determine if the *APOE* genotype modulates Aβ plaque type, pattern of distribution across the cortical layers, Aβ load or occurrence of CAA in FAD.

5. To determine if there are specific associations between the different types of Aβ pathology, and if these associations are observed in the FAD mutations specific sub groups.

3.2.7 *Materials and Methods*

As discussed in chapter: 2 - 2.5.2, this project utilises IHC and image analysis methods. In brief, serial sections of frontal cortex from 20 QSBB FAD cases were cut and stained with Nissl and an anti-Aβ antibody. A consistent region of the second frontal gyrus was analysed semi-quantitatively (CERAD scores) and quantitatively (Aβ load). CERAD scores were given for each individual cortical layer and a total CERAD score across all layers was generated. Aβ load was measured for each individual cortical layer and an average Aβ load across all layers generated. Statistical analysis were conducted testing associations between clinical genetic and pathological data (Chapter: 2.8.1).

3.3 **Results**

Subject details are summarised in Table 3-1. The 20 FAD cases used in this chapter are all from the QSBB and will be referred to as the QSBB cohort. The individuals in this study included: 16 subjects with *PSEN1* mutations, of which 10 were located pre-codon 200 (Four intron4, one E120K, one S132A, one M139V, one M146I and two E184D) and six were located post-codon 200 (one I202F, one L250S, two R278I, one E280G and one double mutation A434T & T291A), and four subjects with *APP* mutations (one V717L and three V717I).

3.3.1 *Neuropathological Summary*

All cases reached end stage AD with a score of A3B3C3 according to the current diagnostic criteria, indicating frequent neuritic plaques, neurofibrillary pathology spread to the occipital cortex reaching Braak and Braak stage 6 (except case 16 who scored 5) and Aβ pathology in the cerebellum reaching Thal stage 5. Neuropathological assessment was conducted by clinical neuropathologists.

Case	Sex	Age at onset	Disease duration	Mutation	*APOE*	Braak Tau	Thal phase	CERAD
1	F	36	5	PSEN1 Intron4	3/3	6	5	Frequent
2	F	35	16.9	PSEN1 Intron4	4/4	6	5	Frequent
3	F	39	8.1	PSEN1 Intron4	3/3	6	5	Frequent
4	M	42	9	PSEN1 Intron4	3/3	6	5	Frequent
5	F	31	6	PSEN1 E120K	3/3	6	5	Frequent
6	M	59	11	PSEN1 S132A	3/4	6	5	Frequent
7	F	41	8.9	PSEN1 M139V	3/3	6	5	Frequent
8	M	40	6	PSEN1 M146I	2/3	6	5	Frequent
9	F	48	13.6	PSEN1 E184D	-	6	5	Frequent
10	F	45	13	PSEN1 E184D	3/4	6	5	Frequent
11	F	48	11	PSEN1 I202F	4/4	6	5	Frequent
12	M	47	11	PSEN1L250S	3/3	6	5	Frequent
13	F	46	19	PSEN1 R278I	3/4	6	5	Frequent
14	M	54	12	PSEN1 R278I	2/3	6	5	Frequent
15	F	42	11	PSEN1 E280G	3/4	6	5	Frequent
16	M	42	5	PSEN1 A434T & T291A	3/3	5	5	Frequent
17	F	51	8.7	APP V717L	3/3	6	5	Frequent
18	M	56	10.1	APP V717I	3/3	6	5	Frequent
19	F	50	6.5	APP V717I	3/3	6	5	Frequent
20	M	49	13	APP V717I	4/4	6	5	Frequent
Mean	8M:12F	45.05	10.24					

	Whole cohort N=20	*PSEN1* pre-codon 200 N=10	*PSEN1* post-codon 200 N=6	*APP* N=4	P-value*
APOE (% *APOE4* carrier**)	37	33	50	25	0.70
Sex (% Female)	60	70	50	50	0.60

Table 3-1 Study participants.

F = Female, M = Male. PMD = Post Mortem Delay. No APOE data for case 9 as DNA was not available. *Fisher exact test. **N=19 as *PSEN1* pre-codon 200 case 9 had no *APOE* genotype data available.

3.3.2 *Clinical and genetic comparisons*

There were no statistically significant differences between the *APP* and the two *PSEN1* mutation sub-groups for sex or *APOE4* status (Fisher's exact, Table 3-1).

Age at onset and disease duration were compared by mutation sub-group, sex and *APOE4* status. Consistent with previous studies, observed mean age at onset was lower in the *PSEN1* pre-codon 200 group (41.6 years) than the *PSEN1* post-codon 200 group (46.5 years) and *APP* group (51.5 years) (Figure 3-1 A). After adjusting for sex and *APOE4* status, there was some evidence (global F test p=0.06) of an association between age at onset and mutation sub-group, with mean age at onset an estimated 8.8 years older (95% CI: 1.5, 16.1; p=0.02) for *APP* mutation carriers compared with *PSEN1* pre-codon 200 carriers. Adjusted differences in age at onset were not statistically significantly different for *APP* mutation carriers compared to *PSEN1* post-codon 200 carriers (5.9 years older; 95% CI: 2.0 younger, 13.8 older; p=0.13) or for *PSEN1* post-codon 200 carriers compared with *PSEN1* pre-codon 200 carriers (2.9 years older; 95% CI: 3.6 younger, 9.4 older; p=0.35).

In the cohort as a whole, females had a lower observed mean age at onset than males (42.0 years vs 49.6 years) (Figure 3-1 C). After adjusting for mutation sub-group and *APOE4* status, mean age at onset was an estimated 7.3 years younger (95% CI: 13.1, 1.4) for females compared with males (F test p=0.02). After adjusting for mutation sub-group and sex, mean age at onset was an estimated 3.5 years older (95% CI: 2.5 younger, 9.5 older) for individuals with the *APOE4* allele compared with those without but this was not statistically significant (F test p=0.23) (Figure 3-1 F).

Observed mean disease duration differed between mutation sub-groups (*PSEN1* pre-codon 200 (9.8 years), *PSEN1* post-codon 200 (11.5 years); and *APP* (9.6 years)) but these differences were not statistically significant (global F test p=0.73) after adjusting for sex and *APOE4* status (Figure 3-1 B). There was no evidence (F test p=0.89) of an association between disease duration and sex after adjusting for mutation sub-group and *APOE4* status, with mean disease duration an estimated 0.20 years shorter (95% CI: 3.2 shorter, 2.8 longer) for females compared with males (Figure 3-1 D). However, there was strong

evidence of an association (F test p=0.002) between disease duration and *APOE4* status, after adjusting for mutation sub-group and sex, with mean disease duration an estimated 5.4 years longer (95% CI: 2.4, 8.5) for individuals with the *APOE4* allele, compared with those without (Figure 3-1 E).

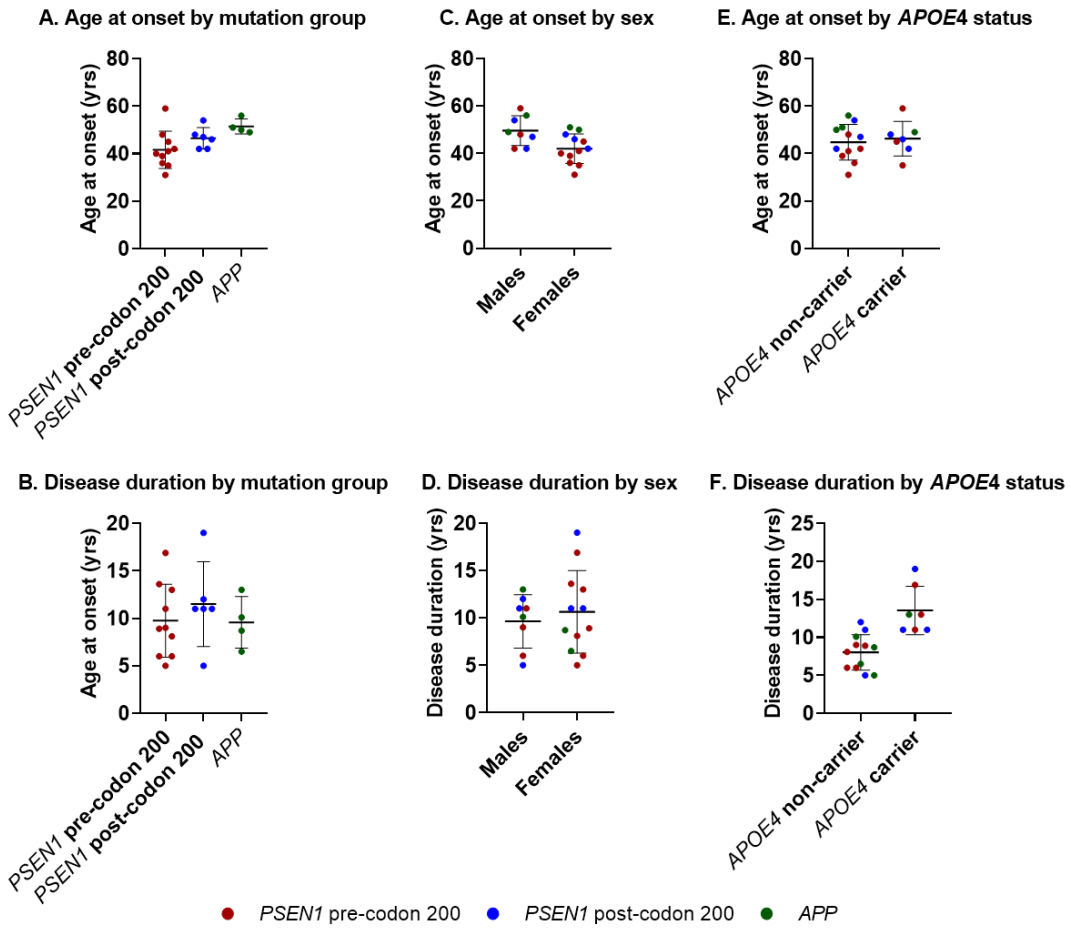

Figure 3-1 Graphs depicting age at onset and disease duration.

Age at onset (A) and disease duration (B) by mutation group. Age at onset (C) and disease duration (D) by sex. Age at onset (E) and disease duration (F) by *APOE*4 status. Error bars represent mean and standard deviation (SD).

3.3.3 *CERAD Aβ pathology scores*

As described in the methods, frontal cortex tissue sections from the QSBB cohort were immunohistochemically stained for Aβ. Representative images of these sections are shown in Figure 3-2.

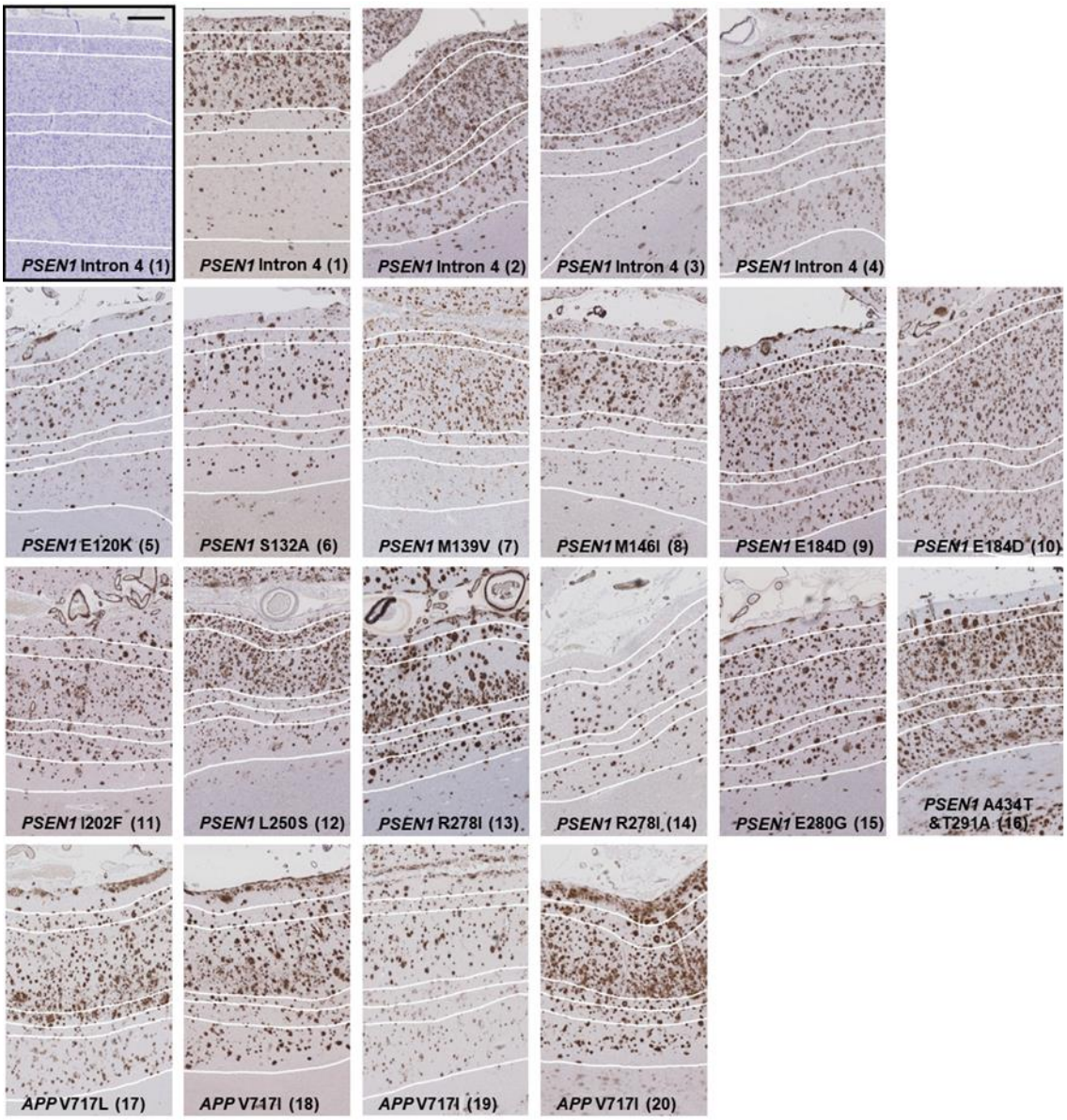

Figure 3-2 Representative images of Aβ immunohistochemically stained frontal cortex of each individual case within the mutation sub-groups.

PSEN1 pre-codon 200 (10 cases), *PSEN1* post-codon 200 (6 cases) and *APP* (4 cases). One Nissl stained PSEN1 Intron4 mutation tissue section is shown (black box) to highlight how the layers were defined based on cellular morphology and applied to the serial Aβ section. The 6 cortical layers are defined by white lines, with layer 1 at the pial surface and layer 6 adjacent to the white matter. Black scale bar = 500µm. Numbers in brackets refer to case number. From these sections, CERAD pathology scores were generated and are presented in Table 3-2.

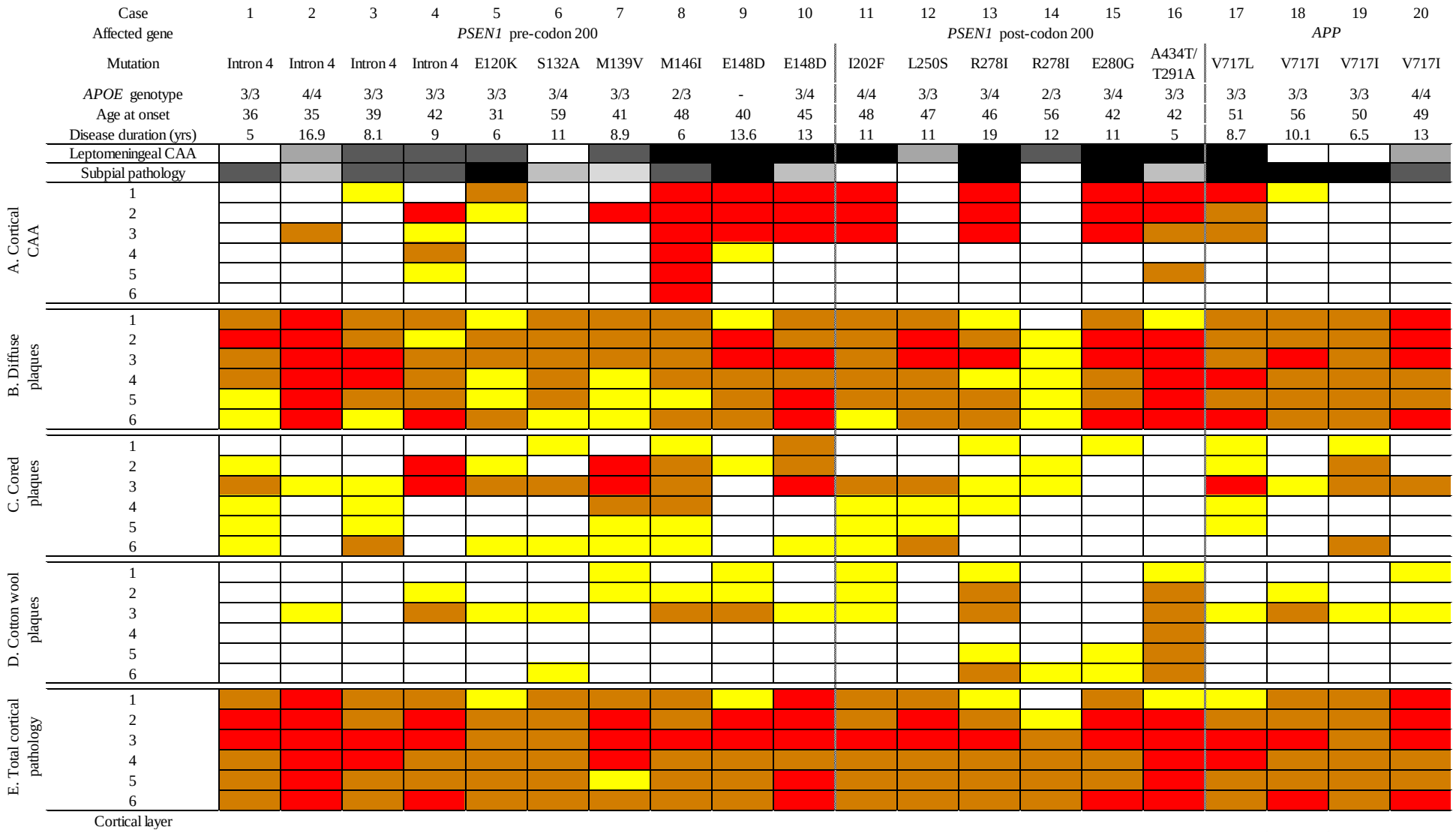
Case
Affected gene
PSEN1 pre-codon 200
PSEN1 post-codon 200
APP
Mutation
Intron 4
Intron 4
Intron 4
Intron 4
E120K
S132A
M139V
M146I
E148D
E148D
I202F
L250S
R278I
R278I
E280G
A434T/ T291A
V717L
V717I
V717I
V717I
APOE genotype
3/3
4/4
3/3
3/3
3/3
3/4
3/3
2/3
-
3/4
4/4
3/3
3/4
2/3
3/4
3/3
3/3
3/3
3/3
4/4
Age at onset
36
35
39
42
31
59
41
48
40
45
48
47
46
56
42
42
51
56
50
49
Disease duration (yrs)
5
16.9
8.1
9
6
11
8.9
6
13.6
13
11
11
19
12
11
5
8.7
10.1
6.5
13
Leptomeningeal CAA
Subpial pathology
A. Cortical CAA
B. Diffuse plaques
C. Cored plaques
D. Cotton wool plaques
E. Total cortical pathology
1
2
3
4
5
6
Cortical layer

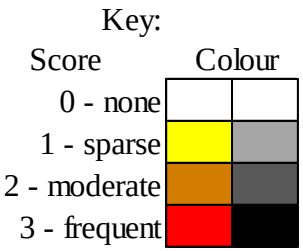

Table 3-2 Tables showing modified CERAD score of Aβ pathology type per cortical layer by individual case.

Leptomeningeal and subpial pathology varies between cases, with presence of one not indicative of the other. (A) CAA pathology scores highlight a predominance of CAA in a subset of cases, with an upper layer predisposition. (B) Diffuse type plaques are seen throughout all cases to varying degrees between cases and within individual cases. (C&D) Cored and Cotton wool plaque pathology scores show that there is variation in presentation between cases, and within the same cases. (E) Total cortical pathology score shows that not all cases have the same level of plaque deposition. Dashed lines divide the subgroups, *PSEN1* pre-codon 200, *PSEN1* post-codon 200 and *APP*.

3.3.3.1 *Associations with clinical data*

Frequency of the total CERAD Aβ pathology types (representative images shown in Figure 2-2) were analysed in relation to age at onset and disease duration. In the whole cohort, regression analyses adjusted for *APOE4* status assessing associations between age at onset and the CERAD Aβ pathology scores found a mixture of positive (Cored plaques, CWP) and negative (Leptomeinigeal CAA, subpial pathology, Cortical CAA, diffuse plaque and total cortical pathology) associations. A trend for negative association was found with disease duration. However, none of the adjusted associations were statistically significant, with small effect sizes and large CI's (p-values ranged from p=0.09 to p=1.00) (Figure 3-3).

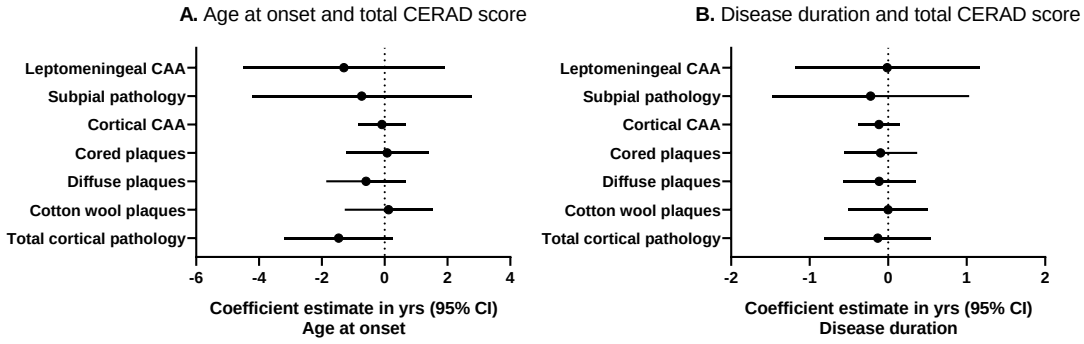

Figure 3-3 Linear regression adjusted for *APOE4* for CERAD and clinical data.

Linear regression adjusted for *APOE4* status showing the association between total CERAD Aβ pathology scores and age at onset (A) and disease duration (B). Coefficient estimates and 95% confidence intervals for the whole cohort are represented for each CERAD pathology. The coefficients are the estimated difference in the outcome (age at onset or disease duration) for one unit increase in the explanatory variable (CERAD pathology score).

3.3.3.2 *Associations by mutation sub-groups*

Microscopically, large heterogeneity in the appearance of Aβ pathology was evident throughout the cortical layers of the FAD cases, Figure 3-2 and Table 3-2 show the CERAD scores for each case, giving the leptomeningeal CAA and subpial Aβ pathology, cortical CAA and plaque types in each cortical layer and the overall levels of Aβ plaque deposition. Observed leptomeningeal CAA and subpial Aβ pathology differed markedly between cases, being either absent, sparse, moderate or frequent (Table 3-2). Based on visual inspection of the Aβ distribution throughout the cortical layers, variations were observed between

carriers of the same mutation. For example, one *PSEN1* R278I mutation case (case 13) contained more Aβ pathology compared with the other *PSEN1* R278I case (case 14); interestingly case 13 had the genotype *APOE*3/4 compared to case 14 which is *APOE*2/3. Additionally, differences within the pattern and distribution of plaques across the layers could be seen between these two cases, with case 13 having larger and greater plaque deposition particularly in layer 3, and greater cortical CAA and subpial deposition (Figure 3-2 Table 3-2). However, similarities in layer deposition could be seen within carriers with the same mutation, such as the *PSEN1* E148D carriers, with dense deposition across all layers (cases 9 and 10) (Figure 3-2). Similarly, distinct distribution patterns could be seen between different cases, with *APP* V717L case 17 and V717I cases 18 and 20 showing frequent subpial Aβ deposition and distinct plaque gradient from the upper to the lower of layer 3 (Figure 3-2). In contrast, *PSEN1* E120K and S132A (cases 5 and 6) appear to have a more uniform distribution across layer 3 (Figure 3-2). Most cases showed the highest amount of Aβ staining within cortical layer 3, while the amount in the lower layers varied e.g. *PSEN1* M139V (case 7) has very little lower layer deposition compared to the dense lower layer deposition seen in *PSEN1* A434T & T291A (case 16) (Figure 3-2, Table 3-2).

Visually the *PSEN1* pre-codon 200 and *APP* groups were noticeably more likely to have subpial pathology (presence in 100% of cases) than the *PSEN1* post-codon 200 group (presence in 50% of cases). However, comparing each total CERAD score in turn formally between the three mutation sub-groups, there were no statistically significant differences (leptomeningeal CAA p=0.17, cortical CAA p=0.41, subpial p=0.10, cored p=0.27, diffuse p=0.46, CWP p=0.62 and total cortical pathology p=0.87, global test Kruskal-Wallis). None of the CERAD Aβ pathologies differed by *APOE4* status (exact Mann-Whitney-Wilcoxon rank sum).

3.3.3.3 *Correlations between CERAD Aβ pathology scores*

In the whole cohort, the CERAD frequency of leptomeningeal CAA was correlated with total cortical CAA (correlation coefficient τ_b=0.73 p=0.0001, Kendall' tau-b). When the sub-groups were assessed separately there was a consistent positive correlation (Figure 3-4 A-D) that remained strong in the two *PSEN1* sub-groups. A trend for positive correlation between both total CERAD cortical and leptomeningeal CAA with total CWP score was seen across all groups except the

small *APP* group. Specifically, in the whole cohort, cortical and leptomeningeal CAA scores were both positively correlated to total CWP scores (τ_b=0.49 p=0.008 and τ_b=0.37 p=0.05, respectively) and in the sub-group analyses there was a particularly strong correlation in the *PSEN1* post-codon 200 group for cortical CAA (τ_b=0.86) and leptomeningeal CAA (τ_b=0.78). In contrast, there was an observed trend for negative correlations between total cored plaque score and other Aβ pathologies (Subpial pathology, diffuse plaques, CWPs) and this was particularly evident in the *PSEN1* post-codon 200 group, although there is some variation across groups (Figure 3-4 A-D).

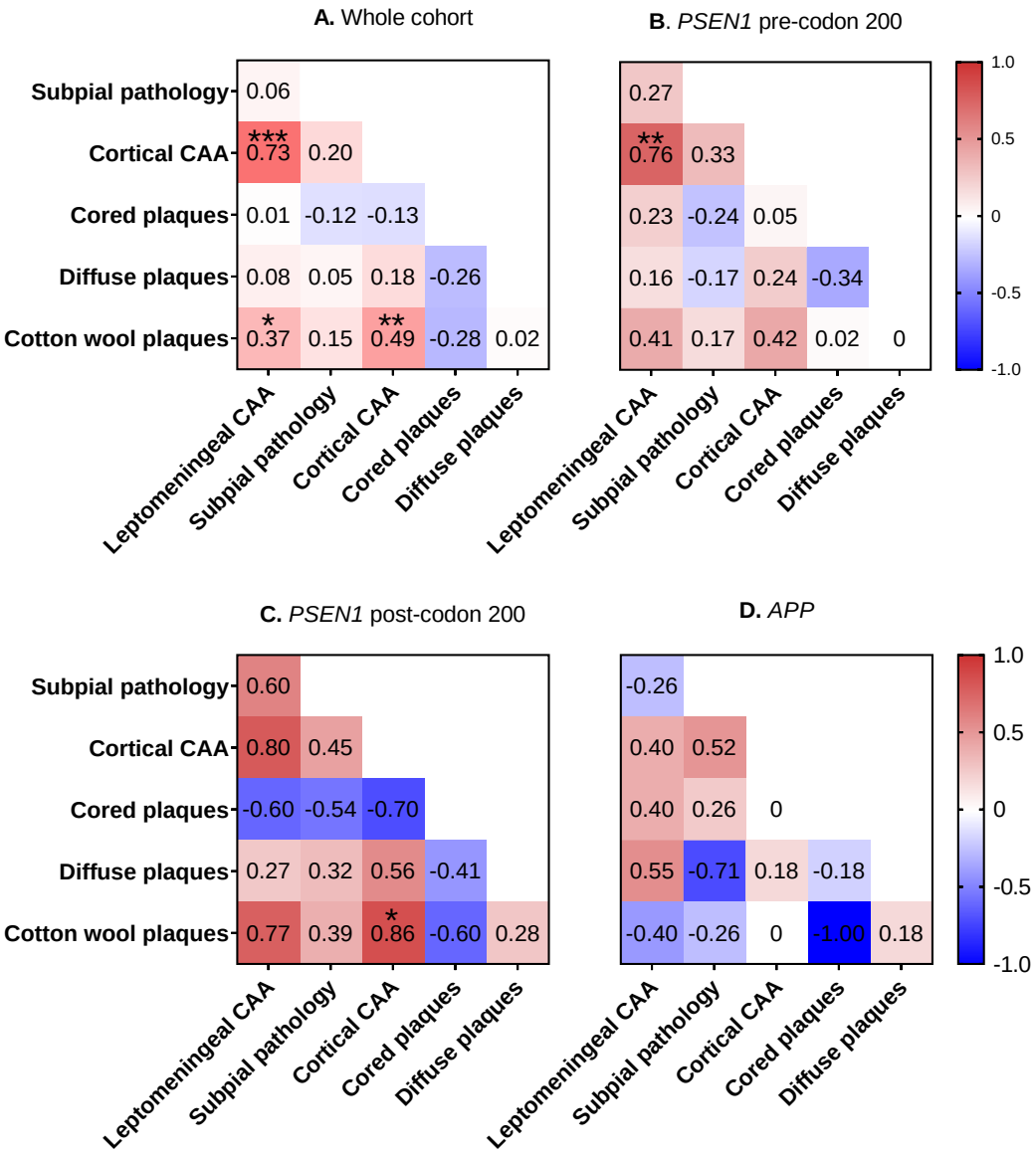

Figure 3-4 Correlation between total CERAD pathologies.

Heat maps showing the relationship between the total modified CERAD scores: A) Whole cohort, B) *PSEN1* pre-codon 200, C) *PSEN1* post-codon 200, D) *APP*. τ_b values for Kendall's tau-b correlation coefficients are shown. Asterisks represent significant correlations *p<0.05 **p<0.01 ***p<0.001. Red = positive correlation. Blue = negative correlation.

3.3.3.4 *Differences across cortical layers*

As reported above, no evidence was found of total CERAD Aβ pathology scores differing between the sub-groups. However, when comparing individual cortical layer CERAD scores (0 to 3) between sub-groups, some differences were found in CWPs in layers 5 and 6 (global test p=0.02 and p=0.02, Kruskal Wallis). Specifically, in layer 5 the *PSEN1* post-codon 200 group had higher CWP

frequency (0.67 ± 0.82) compared to the *PSEN1* pre-codon 200 group (0.00 ± 0.00) (p=0.01, Dunn's test) and the *APP* group (0.00 ± 0.0) (p=0.04). This pattern was also seen in layer 6, with the *PSEN1* post-codon 200 group again having a higher frequency of CWPs (1.0 ± 0.89) than the *PSEN*1 pre-codon 200 (0.1 ± 0.32) (p=0.01, Dunn's test) and *APP* group (0.0 ± 0.0) (p=0.02, Dunn's test) (individual layer scores shown in Table 3-2). There was, however, layer 5 and 6 variability particularly within the *PSEN1* post-codon 200 sub-group (See Appendix: Figure 9-2), so with a larger cohort it would be interesting to investigate whether differences are driven by specific individual mutations. No differences for other plaque types were found. There were also no patterns of differences at the cortical layer level in total CERAD Aβ pathology scores between *APOE*4 carriers and non-carriers.

3.3.4 *Aβ load in the cortical tissue*

3.3.4.1 Associations with clinical data

For the whole cohort, associations between mean Aβ load (measured as a percentage area stained) across the six cortical layers and age at onset and disease duration were assessed, adjusted for *APOE*4 status (Figure 3-5). Mean Aβ load was not statistically significantly associated with age at onset although a consistent negative association was found for mean Aβ load and Aβ load for individual cortical layers. Mean Aβ load was non-significantly positively associated with disease duration, and this trend was seen for most cortical layers, with evidence for an association found (F test p=0.0003) for layer 6 Aβ load and disease duration (β: 0.21 additional year of duration for each percentage point increase in Aβ load; 95% CI: 0.004, 0.41; p=0.05).

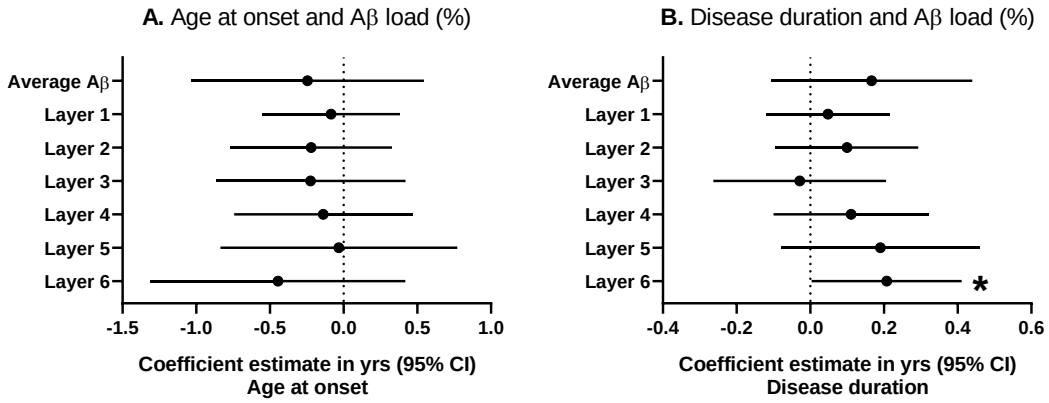

Figure 3-5 Linear regression adjusted for *APOE4* status for Aβ and clinical data.

Linear regression adjusted for *APOE4* status showing the association between Aβ load and age at onset (A) and disease duration (B). Coefficient estimates and 95% confidence intervals for the whole cohort are represented, for the mean Aβ load and for each cortical layer. The coefficients are the estimated difference in the outcome (age at onset or disease duration) for a one percentage point increase in the explanatory variable. *p=0.05.

3.3.4.1 *Comparison between FAD mutation sub-groups and APOE genotypes*

When mean Aβ load was compared between mutation sub-groups, the *PSEN1* post-codon 200 group had the highest observed mean load, followed by the *APP* group, whilst the *PSEN1* pre-codon 200 group had the lowest (12.7% ± 6.4, 8.3% ± 3.8, 11% ± 5.5, respectively), although there was no statistically significant difference between the groups (p=0.26 Kruskal-Wallis). Mean Aβ load was observed to be higher in *APOE4* carriers than non-carriers (13.1% ± 5.9, 8.5% ± 4.3 respectively), although with only weak evidence (p=0.08, exact Mann-Whitney-Wilcoxon rank sum), most likely due to the small sample size.

3.3.4.2 *Correlations with CERAD Aβ pathology scores*

Associations between Aβ load and the frequency of the different CERAD Aβ pathologies were investigated. Leptomeningeal CAA, subpial Aβ and cortical CAA did not significantly correlate with Aβ load. When the three different plaque types were examined separately, there was a clear trend of a negative correlation between cored plaque score and Aβ load, both for the whole cohort and for all sub-groups (

Figure 3-6), and this was statistically significant for the whole cohort (τ_b=-0.37, p=0.03 Kendall's tau-b). This contrasted with the consistently positive correlations seen between diffuse plaque score and Aβ load, and between CWP score and Aβ load; these associations were statistically significant for diffuse plaques in the whole cohort (p=0.001) (Figure 3-6).

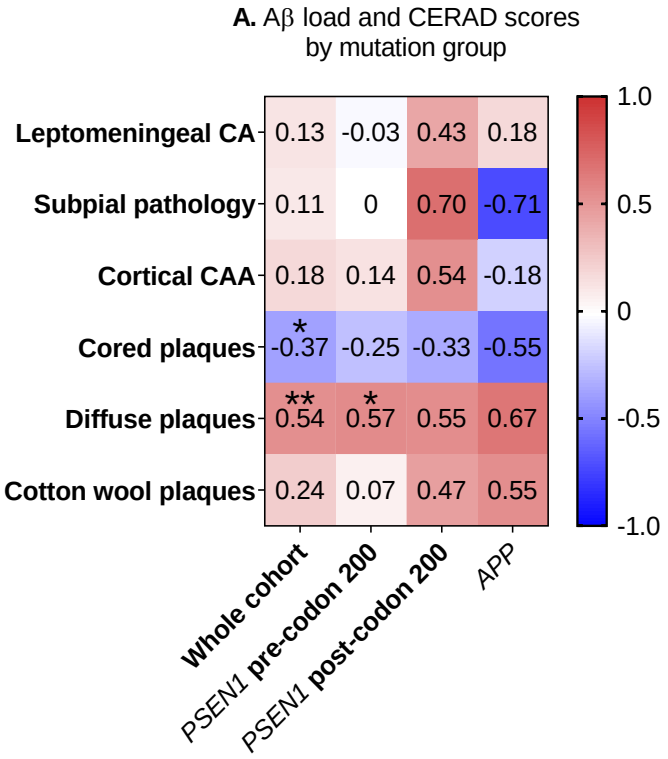

Figure 3-6 Correlations between Aβ load and total CERAD scores.

τb values for Kendall's tau-b correlation coefficients are shown for the whole cohort and mutation sub-groups. Asterisks represent significant correlations *p<0.05 **p<0.01. Red = positive correlation. Blue = negative correlation.

3.3.4.3 *Differences across cortical layers*

Visual inspection of the cases revealed that Aβ deposition was not evenly distributed across the cortical layers (See Figure 3-2) In the whole cohort and within each mutation sub-group, observed mean Aβ load was consistently numerically highest in layer 3 of the frontal cortex (whole cohort 14.57% ± 6.33; *PSEN1* pre-codon 200 12.64% ± 6.12; *PSEN1* post-codon 200 15.99% ± 6.88; *APP* 17.24% ± 6.07).

It was assessed whether Aβ load differed between the different layers. There was evidence that this was the case for the whole cohort (p<0.0001, Friedman

ANOVA), with the highest load being observed in upper layers 2 and 3, a pattern that was also seen across the three sub-groups (Figure 3-7). The Aβ load of each individual layer was compared between the mutation sub-groups, adjusted for *APOE4* status**.** Evidence was found (global test p=0.007) that Aβ load in layer 5 differed between sub-groups, with mean Aβ load higher in *PSEN1* post-codon 200 group compared to both the *PSEN1* pre-codon 200 group (7.16 percentage points higher; 95% CI: 2.9, 11.41; p=0.003) and the *APP* group (6.91 percentage points higher; 95% CI: 1.68, 12.15; p=0.01), after adjusting for *APOE4* status. There was weaker evidence (global test p=0.06) for differences in Aβ load in layer 4, with *PSEN1* post-codon 200 cases again having higher load than the *PSEN1* pre-codon 200 group (7.99 percentage points higher; 95% CI: 1.51, 14.46; p=0.02). These data suggest that mutation location may be associated with the distribution of pathology across some cortical layers, but larger sub-group sizes would be needed to investigate this further. See Figure 3-7 for the graph depicting average Aβ load across layers for the QSBB cohort and mutation sub-groups.

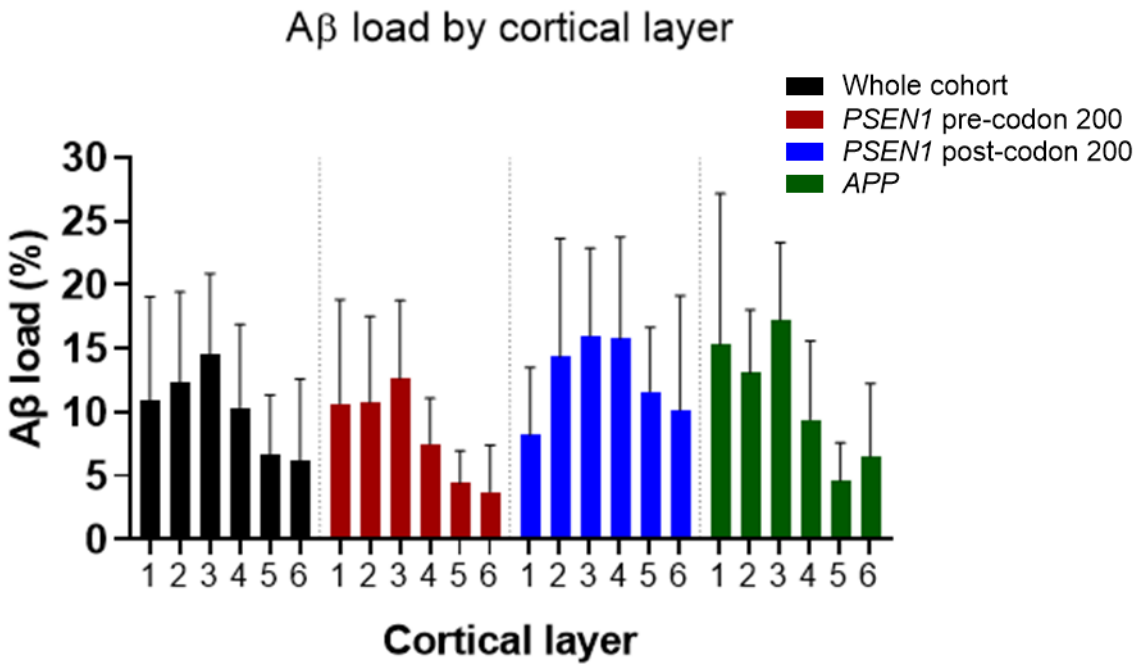

Figure 3-7 Mean Aβ load (%) per cortical layer.

Mean Aβ load per cortical layer for the whole cohort and individual mutation groups. Error bars represent SD.

3.3.5 *Aβ pathology and tau load*

As tau is an important aspect of pathology in AD and FAD we assessed tau pathology in a small subset of cases. Tau load was measured in the same way as Aβ load (2.4) in 6 cases from the QSBB cohort (cases 1,4,13-16). The average tau load was correlated with clinical data and Aβ pathologies using Kendall's tau-b.

Tau load did not significantly correlate with age at onset (τ_b=-0.3, p=0.42) or disease duration (τ_b=-0.07, p=0.85) (Figure 3-8 A). Tau load did not significantly correlate with CERAD scores: Leptomeningeal CAA τ_b=0.08 p=0.84, Subpial pathology τ_b=0.65 p=0.08, cortical CAA τ_b=0.14 p=0.7, Cored plaques τ_b=0.28 p=0.44, diffuse plaques τ_b=0.07 p=0.85, CWPs τ_b=0.14 p=0.7, total cortical pathology τ_b=0.14 p=0.7, see Figure 3-8 B. Tau load did not significantly correlate with Aβ load (τ_b=-0.07, p=0.85, Figure 3-8 C). As there were no significant associations, and strength of correlations were generally weak, no further cases were investigated.

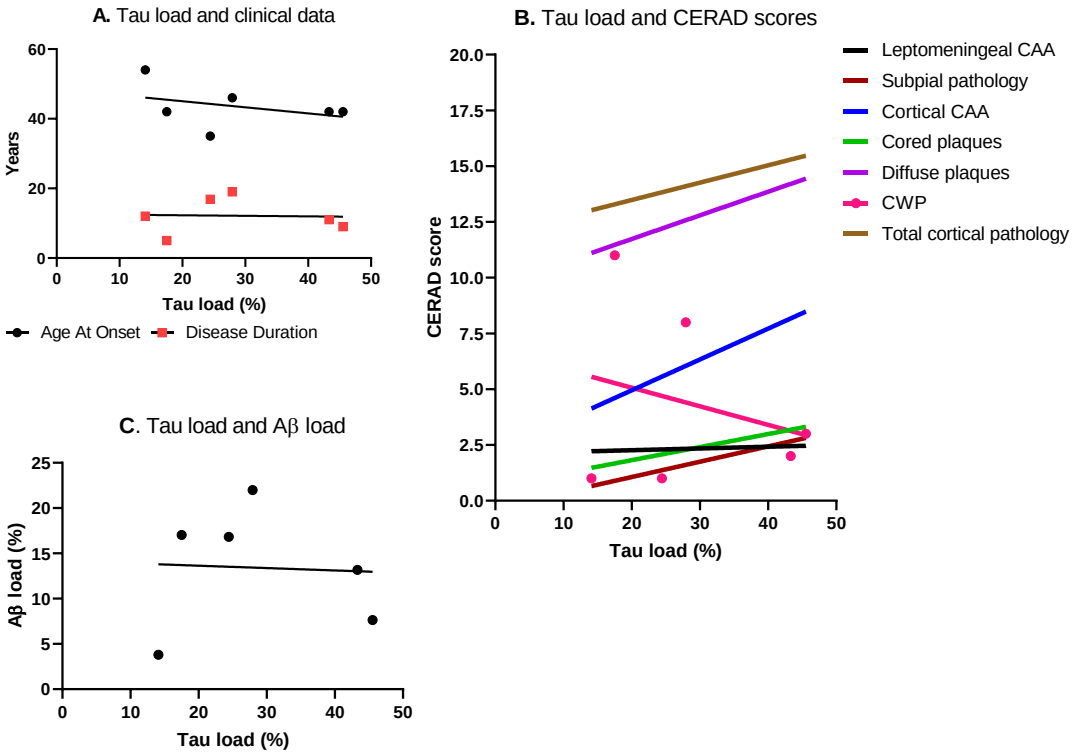

Figure 3-8 Tau load correlations.

A: Clinical data. B: CERAD scores. C: Aβ load, pink dots represent total CWP score. All graphs are Kendall's tau-b correlation and lines represent direction of relationship fitted by linear regression.

3.4 **Chapter discussion**

	Main findings
Clinical and demographic	FAD mutation and sex were associated with age at onset. *APOE* genotype was associated with disease duration.
Type and distribution of Aβ pathology	Observationally, Aβ pathology type and distribution could differ across cortical layers and between different and same mutation carriers.
Association between CERAD scores and Aβ load, with clinical data	CERAD pathology scores had no signification association with age at onset or disease duration. Aβ load did not associate with age at onset, but lower layer load associated with longer disease duration.
Correlation between CERAD scores	General positive correlation between leptomeningeal and cortical CAA and both CWPs and subpial pathology (except in the *APP* group). A trend for negative correlation between cored plaques and both diffuse and CWPs.
Correlation between CERAD scores and Aβ load	Leptomeningeal and cortical CAA and subpial pathology generally positively correlated with Aβ load Cored plaques negatively associated with Aβ load. Diffuse plaques and CWPs positively associated with Aβ load.
Cortical layer differences	There was a pattern for higher Aβ load in upper layers compared to lower layers. CWP pathology and Aβ load was higher in the lower layers of the *PSEN1* post-codon 200 group

In this study we investigated associations between genotype, clinical data and pathological data in a small FAD cohort. A key finding was that possession of an *APOE4* allele was associated with longer disease duration, after adjusting for mutation sub-group and sex. In addition, sex was associated with age at onset in

this cohort, with females having a younger age at onset after adjusting for mutation sub-group and *APOE4* status. Our pathological analysis did not demonstrate evidence of significant differences in the type, frequency or layer distribution of Aβ pathology between *APOE4* carriers and non-carriers, raising the question of whether the differences we observed in age at onset and disease duration may be mediated by mechanisms beyond Aβ. Our pathological analysis did however highlight positive associations between frequency of CWPs and both cortical and leptomeningeal CAA (total CERAD CAA scores). Furthermore, presence of CWPs was observed to be higher in lower cortical layers in some *PSEN1* post-codon 200 cases, which may relate to observed clinical and pathological differences in FAD patients with mutations located post-codon 200.

In line with previous findings, our data show that mutation type and its location is associated with age at onset in FAD (Chapter: 3.3.2). Specifically, *PSEN1* mutations pre-codon 200 had a significantly earlier age at onset than *APP* mutation carriers, which may indicate that the mutation location has a particularly important role in *PSEN1* function. It was seen that many of our *PSEN1* pre-codon 200 cases with earliest ages at onset had mutations within the region coding for the transmembrane (TM) TM1-TM2 loop. This domain is involved in dimerisation of *PSEN1/PSEN2*, substrate entry and contributes to γ-secretase processivity (Cervantes *et al.*, 2001; Cervantes *et al.*, 2004; Sun *et al.*, 2015). Deletion of this TM1/2 region results in decreased γ-secretase, abnormal APP processing and trafficking and inefficient presenilase endoproteolysis (Annaert *et al.*, 2001). Mutations in this region could therefore be associated with a particularly aggressive early onset phenotype.

In our cohort, females had an earlier age at onset than males after adjusting for mutation sub-group and *APOE4* status (Chapter: 3.3.2). Previous FAD studies which have included some of the cases within this study have shown a trend for younger age at onset in females (Ryman *et al.*, 2014). Our findings highlight the importance of considering and investigating potential sex differences in disease manifestation and progression in FAD and the mechanisms that may be driving such differences. This is an area of growing interest in AD research (Ferretti *et al.*, 2018), which could be informed by the insights gained from the study of FAD, where patients are typically young and lack the co-morbidities that can confound studies of older individuals with dementia. It is important to note that in the QSBB

cohort, females had a non-significant higher proportion of *PSEN1* pre-codon 200 mutation carriers which contribute to the younger age at onset. Further study of a larger cohort is needed to assess the role of sex in FAD in more detail.

Similar to other findings in FAD studies, *APOE4* status in our cohort did not affect age at onset (Forleo *et al.*, 1997; Ryman *et al.*, 2014). However, we found that possession of at least one ε4 allele was associated with longer disease duration (Chapter: 3.3.2). The effect of *APOE4* genotype on disease duration in FAD is not well known and in sporadic AD its effect is uncertain. In a meta-analysis of 1,700 cases, it was shown to have no effect, however in two studies of AD patients, a trend towards increased disease duration in *APOE4* carriers was observed and, separately, increased survival of *APOE4* carriers was found (Allan & Ebmeier, 2011; Basun *et al.*, 1995; Masullo *et al.*, 1998). Differences between studies may be linked to mixed populations of participants affected by factors such as age and sex, which may mask results as these factors have been shown to differentially influence the effect of *APOE* on clinical symptoms (Dal Forno *et al.*, 2002; De Luca *et al.*, 2016). Our finding indicates that *APOE4* is associated with disease duration in FAD and, in line with other studies, suggests *APOE4* may have a disease prolonging role in AD that should be explored further.

Although differing Aβ distribution between cases was evident microscopically, Aβ load was consistently higher in layer three amongst all groups (Chapter: 3.3.3.4 and 3.3.4.3), as found in previous studies of sAD and FAD (Armstrong, 2015; Duyckaerts *et al.*, 1986; Pearson *et al.*, 1985; Rogers & Morrison, 1985). This consistent feature of high pathology in layer 3 implies a common mechanism in sporadic and familial AD although the reason for this vulnerability to Aβ deposition is not known. Various hypotheses suggest an increased vulnerability to AD pathomechanisms of certain neuronal populations, such as specific subsets of pyramidal cells, neurons with complex dendritic morphologies and specific neuronal circuits (Capetillo-Zarate *et al.*, 2006; Delatour *et al.*, 2004; Hof & Morrison, 1991; Hof *et al.*, 1990). In particular, there is some evidence that cortical-cortical connections, predominant in layer 3, may be particularly vulnerable (Delatour *et al.*, 2004). Interestingly, it has been shown in murine models that layer 5-6 neurons are less susceptible to Aβ toxicity than layer 3 neurons indicating that there may be some intrinsic factor involved (Romito-DiGiacomo *et al.*, 2007). This is particularly interesting as lower layers were seen

to display lower Aβ pathology in this cohort. Despite all groups sharing layer 3 as the site of highest Aβ deposition, there were differences between the groups in that the post-codon 200 group had higher Aβ deposition in the lower cortical layers than the other groups. Extrinsic factors may also influence vulnerability and pathology, for instance, upper layer astrocytes have been shown to be enriched for APOE expression (Bayraktar *et al.*, 2018).

In the post-codon 200 group, not only was there greater Aβ deposition in the lower layers but there was also greater CWP frequency in these layers (Chapter: 3.3.3.4 and 3.3.4.3). CWP pathology has often been seen in kindreds and individual cases with *PSEN1* mutations post-codon 200, such as the *PSEN1* exon 9 deletion, G217R, P2646L and L435F mutations (Crook *et al.*, 1998; Heilig *et al.*, 2010; Martikainen *et al.*, 2010; Norton *et al.*, 2009; M. J. Smith *et al.*, 2001). This suggests mutations post-codon 200 support the development of CWP's, however they can be found in cases with *PSEN1* pre-codon 200 mutations (Sutovsky *et al.*, 2018). Understanding the aetiology of CWP's will be important due to their association with clinical phenotypes such as spastic paraparesis and other motor symptoms (Brooks *et al.*, 2003; Karlstrom *et al.*, 2008; S. Zhang *et al.*, 2015). Higher rates of motor symptoms are observed in *PSEN1* post-codon 200 cases (Dintchov Traykov *et al.*, 2009; Gómez-Tortosa *et al.*, 2010; Raman *et al.*, 2007; Ryan *et al.*, 2016), supporting a link between the clinical phenotype and cotton wool pathology. The increased frequency of CWPs in lower layers, especially layer 5, that we observed in our *PSEN1* post-codon 200 mutation cohort is perhaps consistent with this clinicopathological association as cortical layer 5 contains projections to the striatum, which is involved in motor control (Gerfen *et al.*, 2016). While the evidence suggests a link, firm conclusions cannot be drawn as CWPs can exist without spastic paraparesis and CWPs can be found in sporadic AD, albeit infrequently (Le *et al.*, 2001; Shrimpton *et al.*, 2007). Further investigation of the localisation of CWPs and their relationship with spastic paraparesis, particularly in *PSEN1* post-codon 200 cases, may provide more detail on how these observations may be linked.

In the whole cohort, total CERAD pathological Aβ plaques were not significantly associated with age at onset or disease duration (Chapter: 3.3.3.1). Similarly, Aβ load was not significantly associated with age at onset, although there was a general negative trend (Chapter: 3.3.4.1), but large variance reduces confidence

in this assumption. Aβ load in layer 6 was positively associated with disease duration and this trend was consistent for the remaining layers (Chapter: 3.3.4.1). However, for all these associations, effect sizes were small with some large CI's, suggesting little confidence in the association, and larger numbers would be needed to gain a more informative result. The trend could however suggest the association with duration becomes more apparent in the lower layers. This could indicate a temporal deposition of Aβ with upper layers, especially layer 3, depositing Aβ earlier and lower layers later. Previous post-mortem analysis has shown that increased spread of senile plaque pathology occurs over time in AD, and Aβ load in certain cortical regions correlates with disease duration (Armstrong, 2014; Cupidi *et al.*, 2010). Although these studies do not refer to cortical layer deposition, they support the concept of a time dependant spread in pathology.

Analysis of CAA revealed no significant correlations with Aβ load (Chapter: 3.3.4.2), however positive correlations between CAA and CWPs were found in the full cohort and in the *PSEN1* post-codon 200 group separately using CERAD measures (Chapter: 3.3.3.3). Previously, CWPs have been observed in FAD cases with severe CAA (Niwa *et al.*, 2013) and CWPs in FAD have been found to correlate with white matter hyperintensities on MRI, which are a potential imaging marker of CAA (Ryan *et al.*, 2015a). However, the precise link between these pathologies is unclear and interestingly CAA is predominantly composed of Aβ40 (Tian *et al.*, 2004) while CWPs are composed mainly of Aβ42 (Miravalle *et al.*, 2005; Shrimpton *et al.*, 2007; Steiner *et al.*, 2001; Verkkoniemi *et al.*, 2001), although Aβ40 can be present (D. M. A. Mann *et al.*, 2001b). Despite this, our findings relating to CWPs and CAA, especially in reference to *PSEN1* post-codon 200 mutations, support a pathological link.

Tau is an important pathology in AD, and in conjunction with Aβ, CSF levels provide prognostic value (Fagan *et al.*, 2014). Our results have shown that in this pathological cohort, tau load did not associate with age at onset or disease duration (Chapter: 3.3.5). While this was only analysed in a small subset of cases, the correlation coefficient was especially low. This study involves end stage tissue which may mask any association, as imaging studies in patients reveal tau alterations and associations early in disease. Pathologically, tau load and measures of Aβ and Aβ positive types of pathology did not significantly correlate

in this cohort (Chapter: 3.3.5). As the assessment has been conducted at end stage, there may be a ceiling effect, where the levels of both are so high that no correlation can be seen. It is still under debate how Aβ leads to tau pathology but it is likely that once tau pathology begins, its spread and further increase may be independent of Aβ. Recent research in FTLD has suggested tau pathology may be associated with *APOE* genotype, independent of Aβ and so it may be important to consider this association (Koriath *et al.*, 2019). Within this subset influence of *APOE* genotype could not be tested due to small numbers, but would be interesting to assess in future large cohorts. This will be especially important as it has been shown that restriction of tau pathology, in the presence of Aβ pathology, can delay onset of AD in FAD E280A mutation carriers, in a potentially *APOE* dependant manner (Arboleda-Velasquez *et al.*, 2019). Although again this is a single patient report and so needs further investigations to support the findings.

All FAD cases in this cohort had been neuropathologically diagnosed with end stage severe AD. Despite this, a more detailed investigation of the type and layer distribution of amyloid pathology highlighted differences between cases, with mutation location associated with certain clinical and pathological features. Broad pathological categorizations may mask more detailed mutation-specific effects on pathogenic processes. Investigating these differences could provide better knowledge of the mechanisms of pathology and be an important tool for better understanding heterogeneity in AD. Despite distinct pathology patterns between mutation sub-groups, differences in pathology were also noted between cases with the same mutation indicating that other factors may influence pathology and clinical features in addition to the causative FAD mutation. *APOE4* genotype may be an important factor and associated with disease duration. Additionally, sex differences in age at onset were observed, with a younger age at onset in females, although larger studies will be needed to confirm this finding. Further investigation of the role of these factors in FAD may provide insights into how they are involved in the mechanisms underlying AD in general.

Chapter 4

Microglial response in FAD

4 Microglial response in FAD

4.1 Abstract

Introduction: Microglia are known to play a role in AD. In FAD, the contribution of microglia to pathological and clinical phenotype is less understood, however, inflammatory responses have been observed in relation to clinical trials (Boche *et al.*, 2010; R. A. Sperling *et al.*, 2011; Zotova *et al.*, 2013a). Here we investigate the pathological distribution of microglia throughout the six cortical layers of FAD cases and associations with Aβ pathology to determine any common patterns, phenotypic associations and explore variability between different mutation cases.

Methods: Sections from the frontal cortex of 20 FAD cases with mutations in *APP* (n=4) or *PSEN1* (n=16, 10 located pre-codon 200 and 6 post-codon 200) were analysed. Sequential sections were stained immunohistochemically for Iba1, CD68 and CR3/43, Aβ and Nissl were used for cortical layer determination. Microglial load was assessed in relation to clinical data, genetic mutation and *APOE* status. Associations between microglial markers and Aβ pathology were assessed.

Results: Microglia displayed uneven distribution across the cortex, with trends for greater microglial load in upper layers, similar to Aβ distribution. In the whole cohort, CD68 was negatively correlated with average Aβ load, with the association significantly negative in layer 3 but in contrast, significantly positive in layer 6. Microglial markers showed plaque specific associations with Iba1 and cored plaques negatively correlated in the QSBB cohort and CD68 and CWPs positive correlated in the *PSEN1* post-codon 200 group. Microglial markers did not differ between mutation groups and although trends were observed across groups, were not significantly correlated to clinical data, accept between CR3/43 and age at onset in the QSBB cohort.

Conclusions: The results suggest that microglial distribution is uneven across the cortex and this pattern is similar to Aβ distribution. We also reveal that there may be associations with microglial phenotype and specific Aβ pathologies. Additionally, trends in correlation between the microglial markers and clinical data suggest microglial response may associate with clinical course. Microglia therefore may significantly affect FAD.

4.2 Introduction

4.2.1 *Microglia and layers*

Aβ has been shown to have a variable distribution across cortical layers. As microglia are believed to be associated with Aβ pathology, there may be a relationship between these pathologies within the cortex in AD. In rodent studies it has been shown that Iba1+ microglia are largely homogenous throughout the cortical layers in the uninjured brain, highlighting a homogenous distribution in a non-pathological state (Kongsui *et al.*, 2014). However, in a disease state, changes in microglial location have been observed. Using IHC in patient brain tissue, Sheng *et al.* (1998) found that not only were IL-1A +ve microglia numbers significantly greater in AD than in controls, but the cortical laminar distribution had highest numbers seen in layers 3 to 5, which is where greatest Aβ deposition is frequently observed, as discussed in chapter 3.2.2. Additionally in the study, cortical laminar distribution of IL-1A +ve microglia in AD cases correlated with cortical laminar distribution of APP immunoreactive neuritic plaques, indicating an association. Interestingly, the cortical laminar distribution of IL-1A +ve microglia in controls also correlated with the neuritic plaque pathology seen in AD cases. The authors suggested these findings could indicate a role for microglia in driving location of plaque development. A further study from the same author found microglial expression of IL-1A positively correlated with neuritic plaque distribution in separate cortical regions, highlighting the widespread association between microglia and AD pathology in the diseased brain (Sheng *et al.*, 1995). Another IHC study in human brain tissue found that the numerical density of HLA-DR immunoreactive microglia in the middle temporal gyrus of five late stage AD patients was significantly higher than in controls, as was the mean cross-sectional area. Additionally, numerical density of these microglia was greater in the outer three cortical laminae in both AD and controls (Carpenter *et al.*, 1993). Again, as the distribution pattern was also seen in controls, it lead the authors to hypothesise that HLA-DR microglia may be involved in plaque development. While there are studies highlighting the relationship between microglia, Aβ and layers in AD, there is also research conflicting with this view. Roe *et al.* (1996) concluded that microglial distribution was not linked to neuritic plaques within the hippocampus in AD, and that microglial distribution was largely variable within cases.

Evidence for differences in brain regional microglial pathology in genetically different causes of FTLD have also been shown. Differences in the distribution of Iba1 +ve microglia in the middle frontal gyrus were found in cases with frontotemporal lobar degeneration (FTLD) associated with progranululin mutations but not FTLD cases associated with pathogenic *C9ORF72* repeat expansions. This difference was not found in the other regions, indicating not only layer specific but region specific differences, as well as potential genetic contributions (Nobutaka Sakae *et al.*, 2019).

While microglia distribution has been investigated in relation to plaque location in AD, there is little study into the natural distribution of microglia and the changes in distribution over time in relation to degeneration. Indeed it is now becoming apparent that understanding the natural heterogeneity and disease specific heterogeneity is important, particularly when considering avenues for therapeutic intervention (Silvin & Ginhoux, 2018). If the homeostatic nature in health is not fully understood then it will be hard to speculate how this should be modified for therapeutic benefit.

4.2.2 *Microglia and Aβ*

In AD, microglia are heavily linked to Aβ pathology. The presence of Aβ receptors on microglia (Doens & Fernández, 2014; Zhao *et al.*, 2018) suggests that the microglial response in AD is related to Aβ pathology. Interestingly, the microglia expressed receptor TREM2, which is an AD associated risk gene, has been shown to bind Aβ in vitro using synthetic Aβ peptides, and in a cellular model, TREM2-deficiency resulted in significantly reduced Aβ degradation (Zhao *et al.*, 2018). Furthermore, Aβ aggregates have been shown to be internalised by murine microglia via receptor mediated mechanisms (Paresce et al., 1996). IHC on both mouse and human tissue has also shown Aβ particles within microglia (Keren-Shaul *et al.*, 2017). Mechanisms for Aβ internalisation include lysosomal pathways, autophagy and the ubiquitin proteasome system, reviewed in Zuroff *et al.* (2017). Collectively, this implies that microglia aid in the clear up of toxic proteins in AD. This has been supported by findings in a singly transgenic APP Tg2576 mouse model, where after treatment with an anti-Aβ antibody, microglial activation was associated with facilitating Aβ plaque removal (Donna M. Wilcock *et al.*, 2004). Upon neuropathological examination, immunization in humans has

also shown plaque reduction (Jäkel *et al.*, 2019; Nicolll *et al.*, 2003) and this has been associated with inflammatory responses (Boche *et al.*, 2010; Ferrer *et al.*, 2004) and microglial markers (Nicoll *et al.*, 2006; Nicolll *et al.*, 2003).

The important role of microglia and the immune response in AD is highlighted by the consistent findings of microglial related genes in GWAS studies on AD, for example *TREM2* (Jansen *et al.*, 2019; Lill *et al.*, 2015), and other microglial specific genes which intersect with AD pathology, such as ATP-binding cassette transporter A7 (ABCA7) and complement receptor type 1 (CR1), reviewed in Villegas-Llerena *et al.* (2016). The connection is further emphasised *in vivo* by successful modulation of pathology and cognitive disturbances in mice models of AD treated with immunomodulatory agents, reviewed in (Martinez & Peplow, 2019). It will be important to understand these relationships in the human brain more deeply if effective treatments are to be developed.

IHC and silver staining of human AD hippocampus in cases with and without dentate gyrus plaque pathology revealed microglia were more frequent in the areas with most numerous plaques in AD plaque positive cases. A subtype of microglia labelled with ferritin were less common in plaque free regions. In the AD plaque positive cases, microglial distribution was similar in plaque positive and negative regions compared to controls and plaque negative cases where the distribution was more uniform. This implies a change in microglial in conjunction with plaque pathology, although microglial distribution was not a significant predictor of plaque location, and there was large variability in microglial and plaque pathology between cases. This left the authors to hypothesise that other factors, such as synaptic degradation, may influence microglial distribution. This is not an unreasonable link to make, and has some supporting evidence. Hong *et al.* (2016) investigated microglial distribution in mice and although they did not find significant relations, it was noted that there was some specific microglial location patterns, supporting our question of the relevance of microglial location to pathology. Additionally we will be assessing microglial pathology by analysing density and Aβ density, rather than location predictors which may provide new findings in our regions of study. In transgenic mice models expressing mutated humanised APP/PSEN1, crossed with microglia deficient mice, amyloid plaque formation and maintenance was not dependent on the presence of microglia (Grathwohl et al., 2009). This was observed in two different mice models, one

which usually displays an aggressive pathology while the other typically has a slower development with presence of dense cored and diffuse plaques and CAA. However, there was a slight (15%) reduction in diffuse plaques in the single *APP* mutation mice. Whilst this is an interesting study contradicting the theory of microglia influencing Aβ pathology, findings from mouse models of AD should be interpreted with caution. The complexities of human AD are not fully recapitulated in these models, and many more human studies have found some notable microglial involvement.

D'Andrea *et al.* (2001), used triple IHC in hippocampus and entorhinal cortex of AD brain and observed three populations of Aβ plaques related to inflammation. This lead to the hypothesis that plaques without microglia were recently formed, followed by a recruitment of inflammatory microglia and finally astrocyte involvement. Of course, as this was IHC, exact time frame of activity cannot be certain.

4.2.3 *Microglia and plaque type*

As discussed above, microglia are associated with Aβ plaques. An early review of the literature highlighted that Aβ plaques and microglial load were shown to frequently correlate (Sheng *et al.*, 1998). As there are multiple forms of Aβ plaques, it is reasonable to question if there is a specific relationship between plaque type and microglial phenotype. Especially as plaque types and microglial phenotype have both separately been shown to have specific clinical associations. It has also more recently been shown that the location and number of microglia differed between different AD subtypes, indicating that microglia can differ depending on pathology, and pathology can differ depending on AD (Boon *et al.*, 2018). An early study using human hippocampal tissue found that compact deposits stained with Bielschowsky and thioflavine S were associated with (HLA)-DR-positive reactive microglia, however, diffuse plaques were not always associated (Itagaki *et al.*, 1989). Similarly, another study using human cerebellar tissue from AD cases found that HLA-DR+ve microglia were associated with plaques, however the morphology of the microglia differed depending on the plaque type, with a more ‘activated’ morphology found in areas with compact reticular amyloid deposits (Mattiace *et al.*, 1990). A. Sasaki *et al.* (1997) also found a lack of association between diffuse plaques and CR3/43 +ve microglia,

and found no association with subpial Aβ deposits. More recently it was shown that dense core plaques were associated with HLA-DR expressing microglia, while diffuse plaques were not specifically associated with microglia (Hendrickx *et al.*, 2017). While this shows specific associations, it also highlighted the importance different microglia markers for the study of microglia pathology in AD. With these studies indicating a link, more in depth analysis of plaque type and microglial phenotype could provide more information on the immunogenic nature of plaques.

CAA is another pathology and microglial phenotype and CAA pathology may also be associated. (Zabel *et al.*, 2013) showed that certain Aβ ligands associated with clearance, that are expressed in microglia, were present at higher concentrations in AD + CAA cases compared to AD only cases, in tissue enriched for vessels, and there were greater complex of Aβ with these ligands in AD + CAA cases. The involvement of CAA and microglial pathology will be discussed further in chapter: 5.2.3.

4.2.4 *Aims*

Microglial pathology and the heterogeneity therein may be associated with different mutations and/or clinical features. Additionally, microglial pathology may associate with Aβ pathology, and this may be plaque type specific. Potential associations may highlight disease pathways connecting the various pathologies seen in sAD and FAD. To address this, the aims for the QSBB FAD cohort aims are:

1. To determine if microglial load or pattern of distribution across the cortical layers differs between genetic causes of FAD.

2. To determine if microglial load correlates with Aβ plaque type.

3. To determine genetic causes of FAD, sex or *APOE* genotype modulate differences in microglial load.

4. To determine if microglial load correlates with age at onset or disease duration.

5. To determine if microglial load associated with Aβ load.

4.2.5 *Material and methods*

The methodology for this chapter has been described in chapter: 2 - 2.4.3. In brief, sections serial to those generated for chapter: 3.3 underwent IHC with antibodies against Iba1, CD68 and CR3/43. Generally, Iba1 is considered a pan marker for surveying microglia, staining homeostatic microglia, CD68 is a marker of phagocytic microglia typically associated with an anti-inflammatory state, and CR3/43 is a marker of antigen presenting microglia typically associated with a pro inflammatory state (see 1.18 Microglial subtypes). The % area stained with each antibody for each cortical layer was quantitatively assessed generating the layer specific microglial load and an average microglial load for each antibody. The load was statistically analysed in relation to clinical, genetic and histological data for microglial load and Aβ pathologies generated in chapter: 3.3.

4.3 **Results**

4.3.1 *Microglial load distribution*

The distribution of microglial load across the cortical layers was analysed for each marker in the QSBB cohort using Friedman ANOVA, this test is inappropriate for sample size less than 8 therefore was not conducted in the mutation sub-groups, however trends will be discussed. Representative images of microglial load in each case can be seen for Iba1 in Figure 4-1, CD68 in Figure 4-2 and CR3/43 in Figure 4-3.

<u>Iba1</u>

In the QSBB cohort and mutation sub-groups, observed Iba1 load was highest in upper layers and lowest in the lower layers. When comparing between cortical layers, there were statistically significant differences in the QSBB cohort ($p<0.0001$, Friendman ANOVA). Specifically, layer 1 had significantly higher load compared to layers 4-6 ($p=0.0004$, $p=0.002$, $p=0.005$, Dunn's test), and layer 2 had higher load compared to layers 4-6 ($p=0.002$, $p=0.009$, $p=0.02$). Within all the mutation sub-groups, a similar pattern of higher load in the upper compared to the lower layers could be observed (Figure 4-4 A).

<u>CD68</u>

In the QSBB cohort and mutation sub-groups, the cortical distribution of CD68 appears to differ across the layers. CD68 load appears highest in layer 2 across all groups, while lowest load varies across the layers. Although no consistent pattern was observed, there was a trend for low load in cortical layer 1 across all groups. In the QSBB cohort, there were significant differences across the cortical layers in CD68 load distribution ($p<0.0001$, Friendman ANOVA) with significantly lower load in layer 1 than layers 2-4 ($p<.0001$, $p=0.003$, $p=0.007$, Dunn's test). While the *PSEN1* pre-codon 200 and *APP* groups reflect the whole QSBB cohort results, the *PSEN1* post codon 200 group differs slightly from this pattern (Figure 4-4 B). Specifically, the *PSEN1* post-codon 200 group had an unusually low CD68 load in layer 3 while lower layers had higher loads.

CR3/43

In the QSBB cohort and mutation groups, highest load was observed within upper layers 1-3 while the cortical layer with the lowest load differed between groups. Interestingly there appears to be a greater load of CR3/43 in the *APP* group, however as mentioned previously, average load did not significantly differ between groups. There were no statistically significant differences across the layers in the QSBB cohort ($p=0.14$, Friedman ANOVA) (Figure 4-4 C).

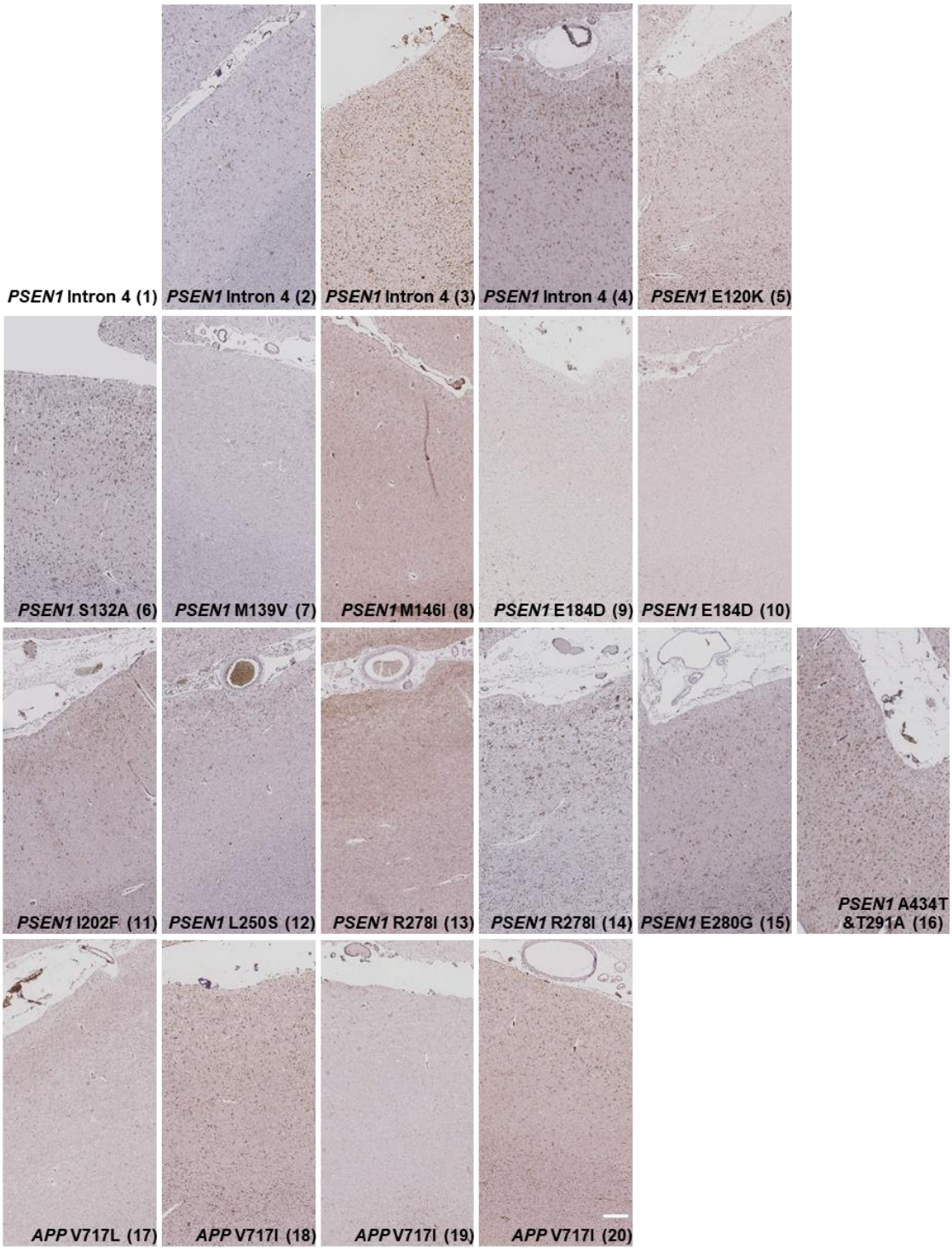

Figure 4-1 Representative images of frontal cortex serial sections immunohistochemically stained with Iba1 antibody.

Case number in bracket refers to those in Table 3-1 . White Scale bar represents 300µm. No image available for case 1.

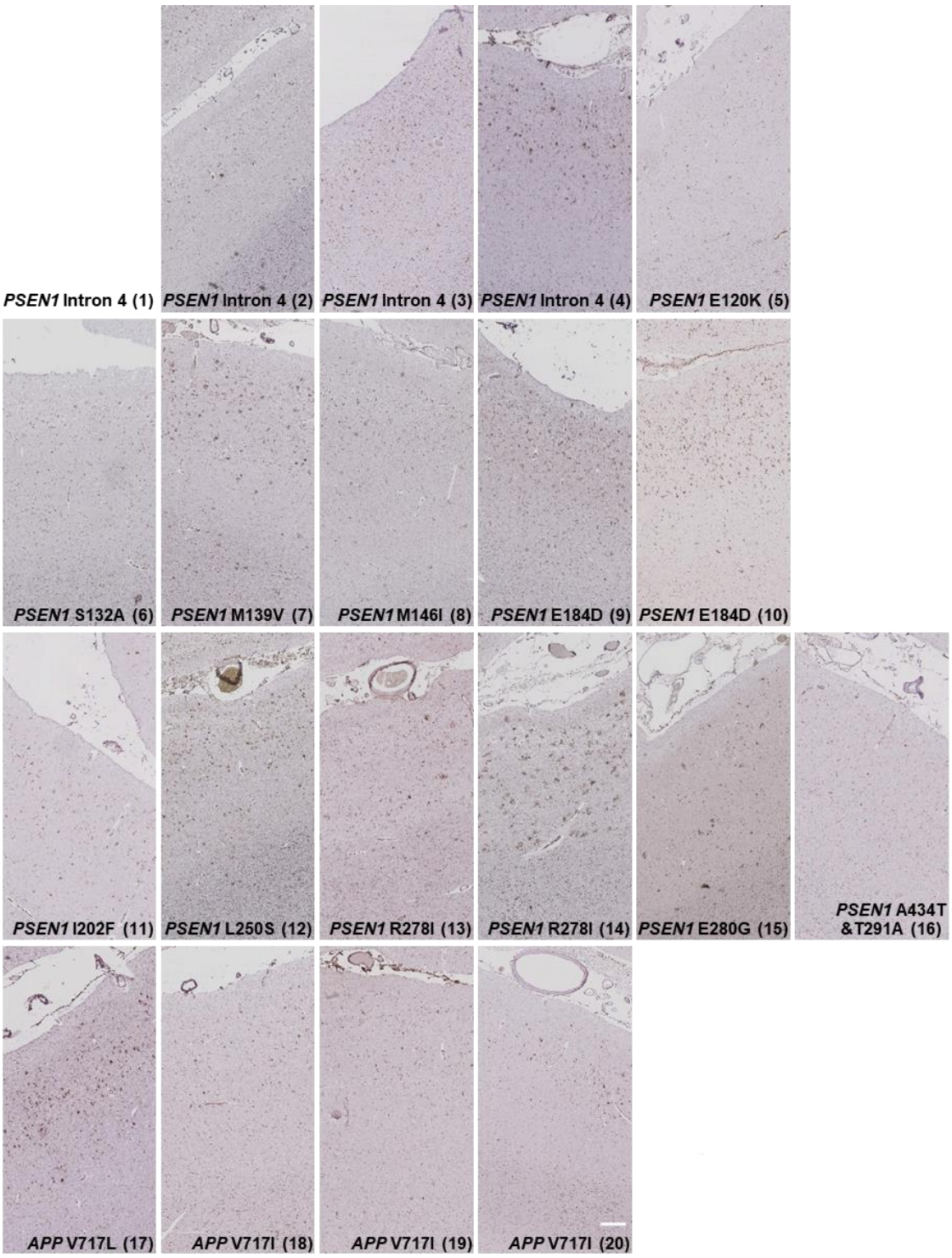

Figure 4-2 Representative images of frontal cortex serial sections immunohistochemically stained with CD68 antibody.

Case number in bracket refers to those in Table 3-1 . White Scale bar represents 300µm. No image available for case 1.

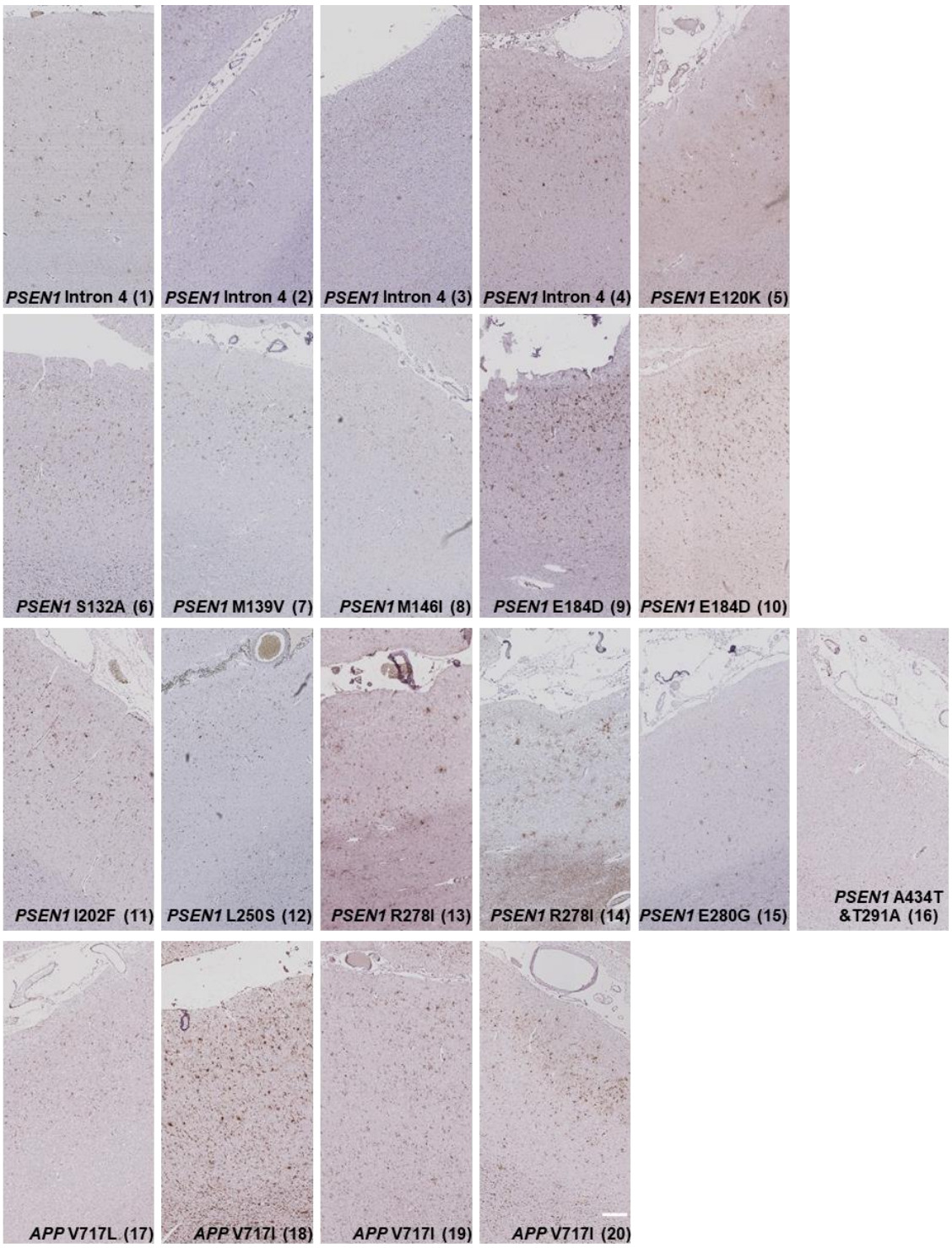

Figure 4-3 Representative images of frontal cortex serial sections immunohistochemically stained with CR3/43 antibody.

Case number in bracket refers to those in Table 3-1 . White Scale bar represents 300µm.

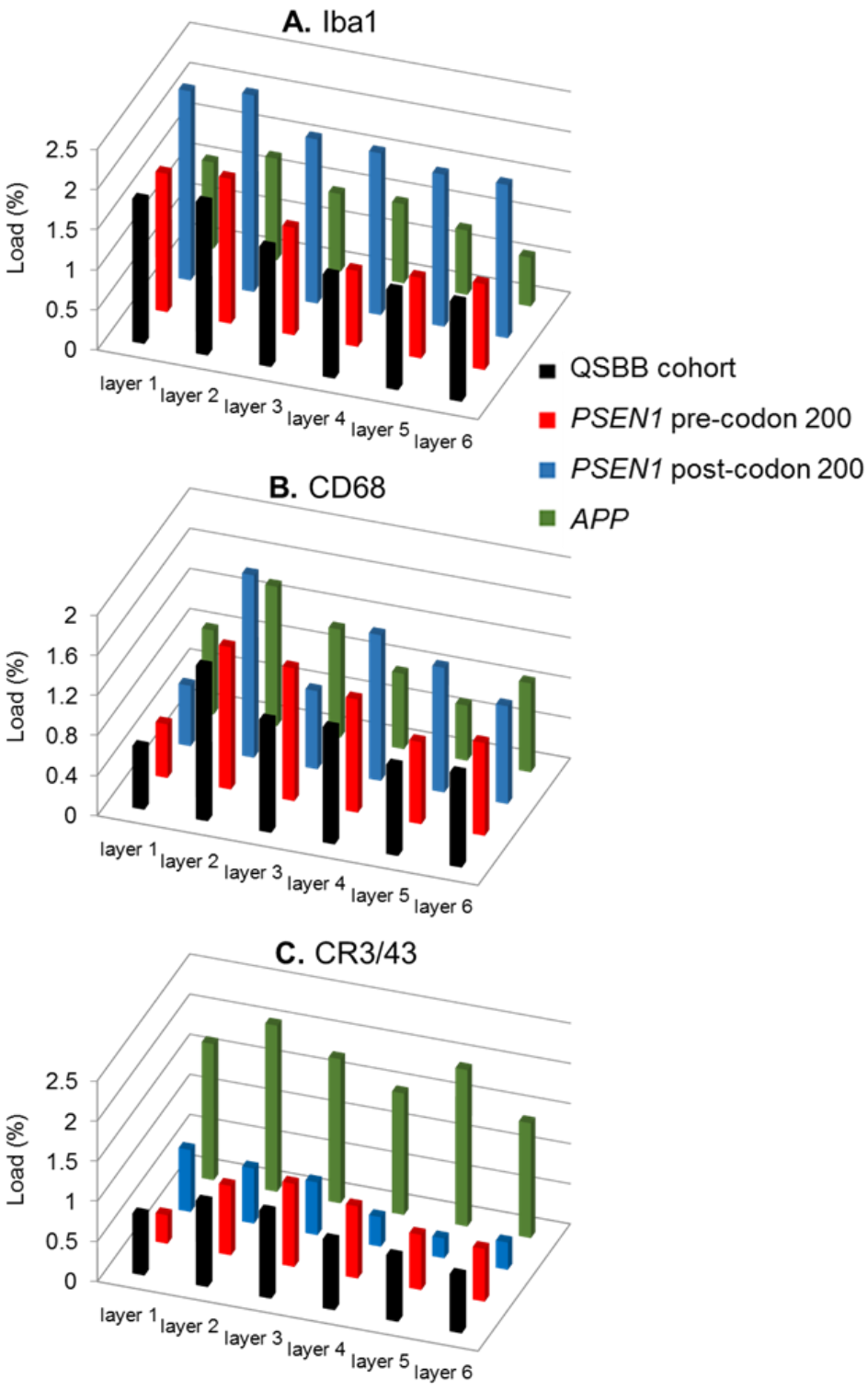

Figure 4-4 Microglial load by layer in the QSBB cohort and mutation sub-groups.

A: Iba1. B: CD68. C: CR3/43. Bars represent mean load (%).

4.3.2 *Microglial load and clinical data*

The relationship between average microglial load and clinical data (age at onset and disease duration) was assessed by correlation analysis using Kendall's tau-b, in the whole QSBB cohort and mutation sub-groups (see

Figure 4-5 A,B).

In the QSBB cohort and mutation sub-groups, there were no statistically significant correlations between Iba1 load and clinical data, additionally, the associations were weak associations (except in the small *APP* group), with no consistent direction of correlation.

CD68 generally showed positive correlations with both age at onset and disease duration in the whole QSBB cohort, as well as in the *PSEN1* pre and post-codon 200 groups but not in the *APP* group, however these did not reach statistical significance.

In the QSBB cohort CR3/43 was significantly positively correlated with age at onset ($p=0.04$), and a positive trend could also be seen in the *PSEN1* pre and post-codon 200 groups, with moderate strength of correlation. CR3/43 was also consistently positively correlated with disease duration and while the strength of correlations were moderate, they did not reach statistical significance.

Next, potential associations between the layer specific microglial marker load and age at onset were investigated (see Figure 4-6). Generally across the layers, correlation between Iba1 and the QSBB cohort was negligible, while in the mutation sub-groups Iba1 was weakly, negatively correlated with age at onset,. CD68 was generally weakly, positively correlated with age at onset in the whole QSBB cohort and *PSEN1* groups, but negatively in the *APP* group, no correlations reached statistical significance. In the QSBB cohort, layer 2 CR3/43 was significantly positively correlated with age at onset ($p=0.02$), with a similar pattern seen in the mutation sub-groups for layer 2 and layers 1, 3-5, however, the strengths of correlation were often low.

Layer specific microglial marker correlations with disease duration were also investigated (Figure 4-6 D-F). Results indicate Iba1 was not associated with

disease duration, although in the *APP* group strong but non-significant positive correlations were observed.

There was no clear trend for associations between CD68 and disease duration, with generally weak positive and negative correlations in the *PSEN1* pre-codon 200 group, some strong, non-significant positive correlations in the *PSEN1* post-codon 200 group and a mixture of strong positive and negative correlations in the *APP* group and. However, in the QSBB cohort as a whole, layer 6 CD68 was significantly positively correlated with disease duration (p=0.02) and this trend was consistent across all groups.

There was a general positive correlation between CR3/43 and disease duration seen in the QSBB cohort and sub-groups across the layers, although the strength of correlation ranged from weak to moderate. However, the correlation between layer 2 CR3/43 load and disease duration did reach statistical significance in the *PSEN1* pre-codon 200 group (p=0.04).

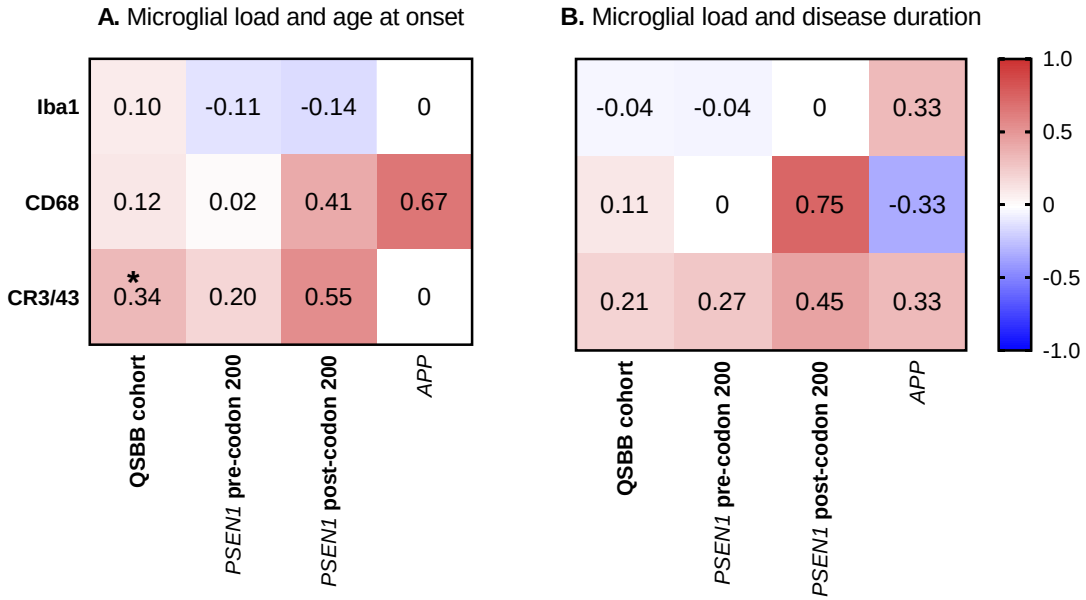

Figure 4-5 Correlation between clinical data and microglial load in the QSBB cohort.

CR3/43 was significantly correlated with age at onset in the QSBB cohort and this patter was observed across sub-groups. Data shown in heatmaps are τb correlation coefficients, Kendall's tau-b, * p<0.05.

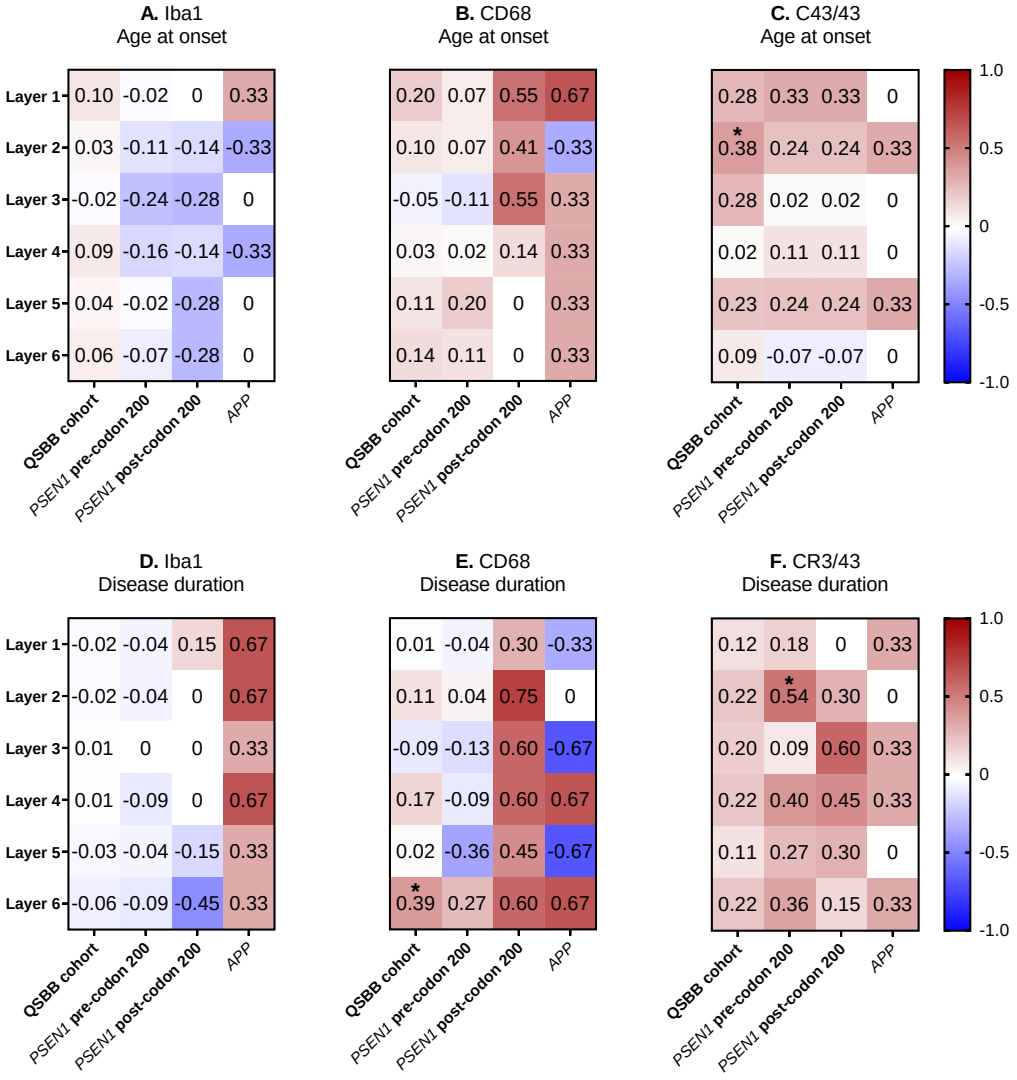

Figure 4-6 Correlation between microglial load by cortical layer and clinical data. Correlations for the QSBB cohort as a whole and mutation sub-groups are shown. A: Iba1 and age at onset. B: CD68 and age at onset. C: CR3/43 and age at onset, significant positive correlation in the QSBB cohort between layer 2 load and age at onset (p=0.02). D: Iba1 and disease duration. E: CD68 and disease duration, positive correlation in the QSBB cohort and layer 6 load with disease duration (p=0.02). F: CR3/43 and disease duration, positive correlation between layer 2 load and disease duration in the *PSEN1* pre-codon 200 group (p=0.04). Data shown in heatmaps are τ_b correlation coefficients, Kendall's tau-b, * p<0.05

4.3.3 *Comparison of microglial load by APOE status and sex*

Microglial load was compared between *APOE*4 carriers and non-carriers and between females and males, with no statistically significant differences found. However Iba1 load reached near statistical significance (p=0.07), with males

having a higher load than females (2.21 ± 1.65 vs 0.99 ± 1.37) although there was large variance within groups (Figure 4-7).

	Iba1		CD68		CR3/43	
	mean (SD)	p	mean (SD)	p	mean (SD)	p
APOE						
APOE4 non-carrier (n=12)	1.7 (1.9)	0.84	1.15 (0.69)	0.34	0.82 (1.2)	0.84
APOE4 carrier (n=7)	1.32 (0.87)		0.77 (0.39)		0.65 (0.5)	
Sex						
Male (n=8)	2.21 (1.65)	0.07	1.06 (0.59)	0.85	1.14 (1.43)	0.43
Female (n=12)	0.99 (1.37)		1.02 (0.64)		0.7 (0.79)	

Figure 4-7 Comparison of microglial load by *APOE4* status and sex.

Data shown as mean and standard deviation (SD). Ranksumex, p= p-value.

4.3.4 *Comparison of microglial load between FAD mutation sub-groups*

The average microglial load for each marker was compared between mutation sub-groups. Average Iba1 and CD68 load was highest in the *PSEN1* post-codon 200 group and lowest in the *APP* group, although there were no statistically significant differences between groups (Iba1: p=0.33, CD68: p=0.92, Kruskal-Wallis). Average CR3/43 load was highest in the *APP* group and lowest in the *PSEN1* post-codon 200 group, but did not statistically differ between groups (p=0.24) (Figure 4-8 A).

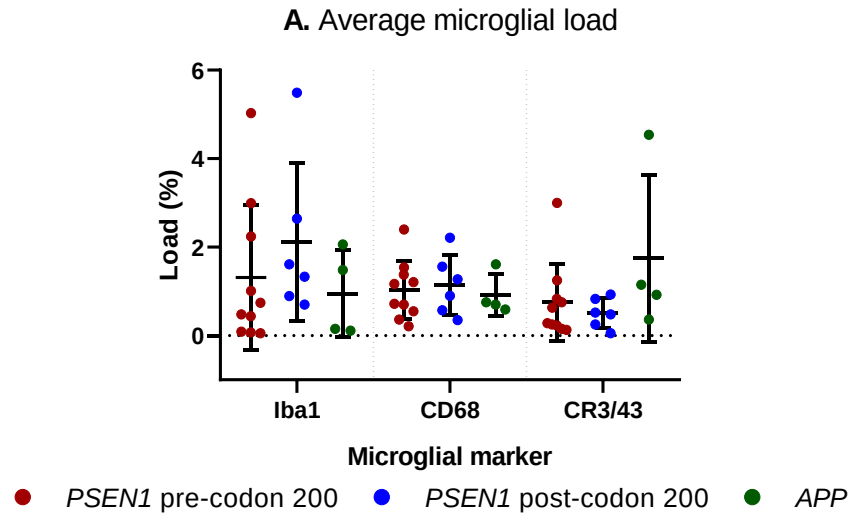

Figure 4-8 Comparison of microglial load by mutation sub-group.

There were no statistically significant differences in microglial load between mutation sub-groups. Kruskal-Wallis. Error bars represent mean and SD.

4.3.5 *Relationship between the microglial markers*

Investigating correlations between the microglial markers highlighted no significant correlations, however trends were observed. There was a negative trend between Iba1 and CD68, except in the *PSEN1* post-codon 200 group where a very weak positive correlation was observed. Relationships between the other microglial markers showed no clear trends, with opposite directions of correlation seen in the smaller *PSEN1* post-codon 200 and *APP* sub-groups, with no statistically significant correlations (Figure 4-9 A).

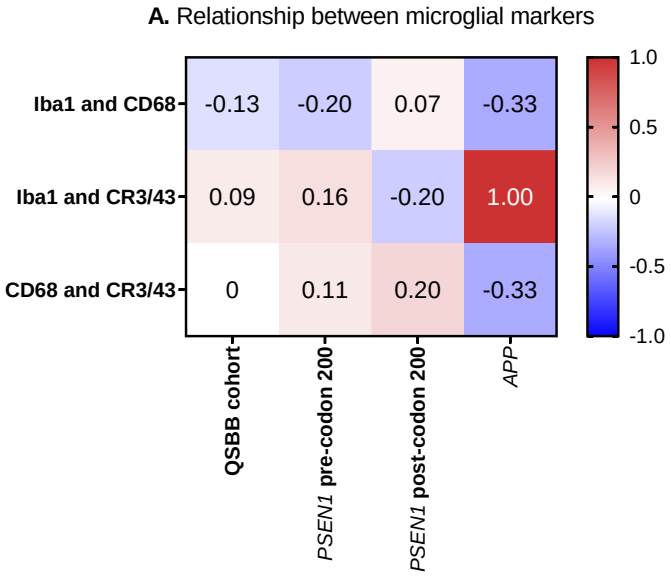

Figure 4-9 Relationship between microglial markers.

There were no significant correlations between the microglial markers, however Iba1 and CD68 show a negative trend. Data shown in heatmaps are τb correlation coefficients, Kendall's tau-b.

4.3.6 *Microglial load and amyloid-beta*

4.3.6.1 *Microglial load and CERAD scores*

Relationship between average microglial load and Aβ plaque types was investigated (Figure 4-10 A-C). Plaque type scores are from the total CERAD scores described in chapter: 3.3.3.

<u>Iba1</u>

There was a general trend for negative association between Iba1 and cortical and leptomeningeal CAA and subpial pathology, although the *PSEN1* post-codon 200 group was positively correlated. Iba1, a marker of surveying microglia, was consistently negatively associated with the frequency of cored plaques, and this was significant in the QSBB cohort (p=0.01). The strength of correlation coefficients for diffuse and total pathology were weak, indicating there may be no association. CWPs had varied directions of correlation between mutation sub-groups. The *PSEN1* pre-codon 200 group had a negative correlation while the *PSEN1* pre-codon 200 and *APP* groups had strong positive correlations. The difference in correlation between the *PSEN1* pre-codon 200 and *APP* group is despite them having the same average CWP score (2 ± 1.3 and 2 ± 1.0).

CD68

Although non-significant, CD68 load was generally positively correlated with cortical and leptomeningeal CAA and subpial pathology, except in the *PSEN1* post-codon 200 group, which had negative correlations. In contrast to Iba1, CD68 load was positively correlated with cored plaques, although the strength of correlation was low-moderate and non-significant.

CD68 was generally negatively associated with diffuse pathology, and this trend was also seen for total pathology, where there was a significant correlation in the QSBB cohort as a whole (p=0.01). A significant positive correlation between CD68 load and total CWP score was found in the *PSEN1* pre-codon 200 group (p=0.03), however the remaining sub-groups had negative correlations. This is despite the *PSEN1* pre-codon 200 and *APP* groups having the same average CWP score (2 ± 1.3 and 2 ± 1.0).

CR3/43

Generally, there was a mild negative correlation between CR3/43 with most types of pathology measured by CERAD. Interestingly, CWPs were positively correlated with CR3/43 and this was consistent in the QSBB cohort as a whole and mutation sub-groups, however none of the correlations reached statistical significance.

As noted, sub-groups sometimes had differing directions of correlation between some of the markers and types of pathology. As group sizes are small and there was large variance in microglial load, caution must be taken when interpreting these results.

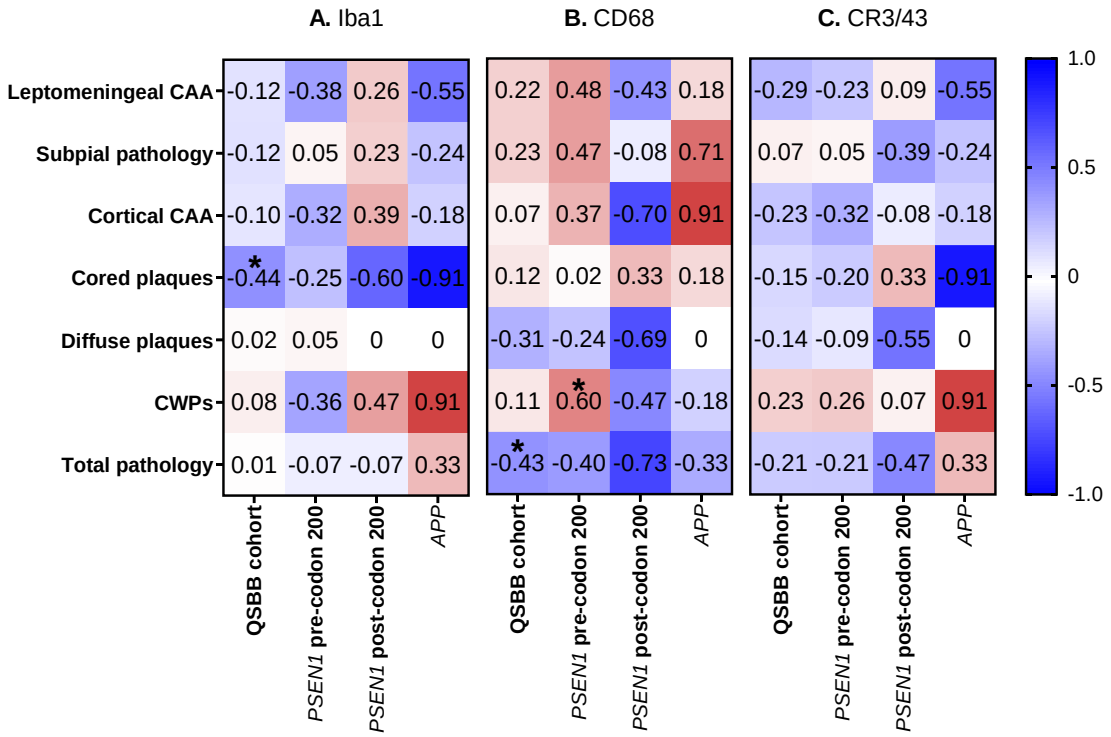

Figure 4-10 Correlation between microglial markers and total CERAD scores.
A: In the QSBB cohort, average Iba1 load significantly negatively correlates with total cored plaque score (p=0.01). B: In the QSBB cohort, CD68 load significantly negatively correlates with total plaque pathology (p=0.01) and in the PSEN1 pre-codon 200 group CD68 positively correlates with CWP score (p=0.03). C: No significant correlations between CR3/43 and pathology scores. Data shown in heatmaps are τb correlation coefficients, Kendall's tau-b, *p<0.05.

4.3.6.2 *Microglial load and Aβ load*

In addition to assessing the relationship between microglia and Aβ pathology as measured by CERAD scores, associations between microglial load and Aβ load were investigated (Figure 4-11 A). Specific patterns could be seen for the different microglial markers within the QSBB cohort and mutation sub-groups. Generally, there was a positive, but weak, correlation between Iba1 and Aβ load. In contrast, CD68 was consistently mildly, negatively correlated with Aβ load. CR3/43 also displayed negative trends but the strength of correlations were weak and in the

small *APP* group the direction of correlation was positive. Despite observed trends, no significant correlations were found. Of note, the direction of correlation for CD68 and CR3/43 with Aβ load was the same as that seen for the total pathology as measured by CERAD scores.

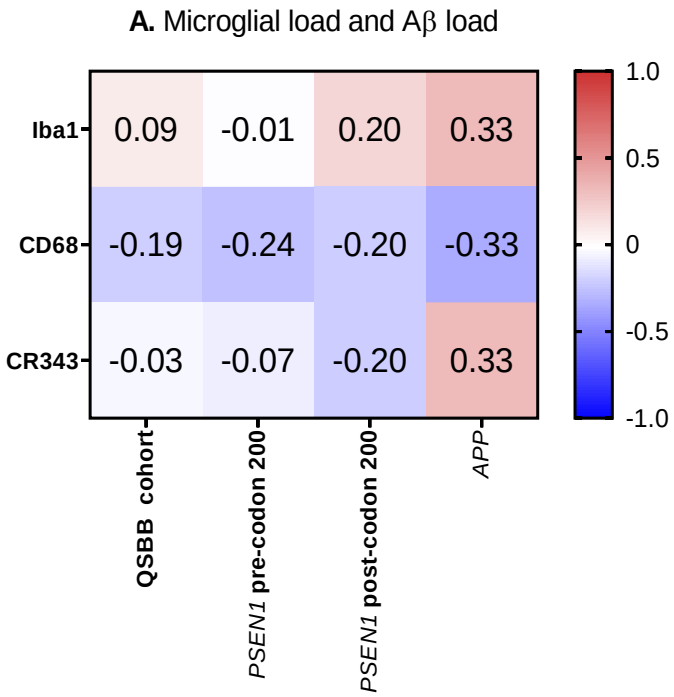

Figure 4-11 Correlation between microglial load and Aβ load.

Correlations shown for the QSBB cohort as a whole and mutation sub-groups. Data shown in heatmaps are τ_b correlation coefficients, Kendall's tau-b.

4.3.6.3 *Microglial load and Aβ load across cortical layers*

Because of the uneven distribution of both microglial and Aβ load across the cortical layers, the relationships for each cortical layer was analysed (i.e. correlating layer 1 with layer 1, layer 2 with layer 2 etc.) (See Figure 4-12 A-C).

<u>Iba1</u>

In the QSBB cohort, *PSEN1* post-codon 200 and *APP* groups, Iba1 was generally positively correlated with Aβ load across the cortical layers, although the strength of correlation was mainly low to moderate and there were no significant correlations. In contrast, in the upper layers, the *PSEN1* pre-codon 200 group had a non-significant negative trend between Iba1 and Aβ.

<u>CD68</u>

Generally, CD68 load had moderate, negative patterns of correlation with Aβ load in the upper layers (1-3) in all groups, with a significant association in layer 3 in the QSBB cohort as a whole (p=0.005). Interestingly layer 3 displays the highest Aβ load (Chapter 3.3.3.4). Although CD68 load only significantly differed in layer 1, results from chapter x indicated Aβ load was significantly higher in these upper layers. Contrastingly, CD68 was generally positively correlated with Aβ load in the lower layers (5-6), with a significant association in layer 6 in the QSBB cohort (p=0.02) and in the *PSEN1* pre-codon 200 groups (p=0.01). There were no significant correlations for the remaining subgroups.

CR3/43

In the QSBB cohort as a whole and the mutation sub-groups there were no significant associations, but CR3/43 was generally negatively correlated with Aβ load, except in layer 1 and 6 where generally, very weak positive correlations were observed. Interestingly, layer 1 and 6 are where lower Aβ load was observed.

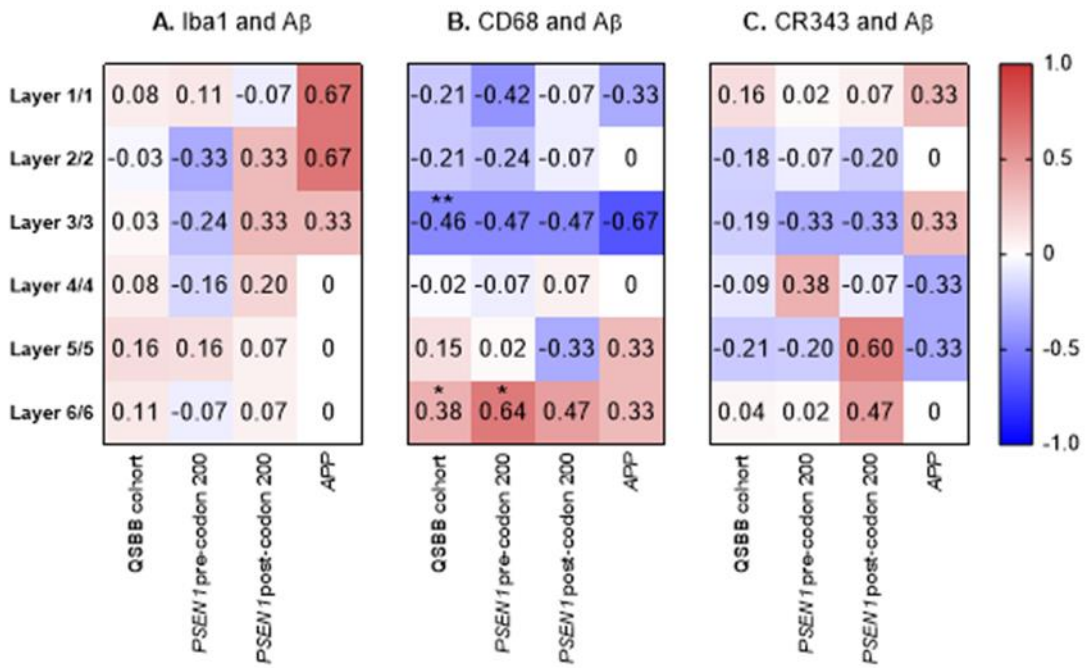

Figure 4-12 Correlation between microglial marker and Aβ by cortical layer.

Correlations shown for the QSBB cohort as a whole and mutation sub-groups. A: Iba1 and Aβ. B: In the QSBB cohort, layer 3 CD68 and Aβ load negatively correlate (p=0.005) and layer 6 CD68 and Aβ load positively correlate (p=0.02). In the *PSEN1* pre-codon 200 group, layer 6 CD68 and Aβ load positively correlate (p=0.01). C: CR343 and Aβ. Data shown in heatmaps are τb correlation coefficients, Kendall's tau-b, *p<0.05, **p<.01.

4.3.7 *Microglial load and tau load*

Average microglial load for each marker was correlated with the average tau load in the small subset of cases described in chapter: 3.3.5. No significant correlations were found. Iba1: τ_b=-0.2 p=0.57. CD68: τ_b=0.07 p=0.85. CR3/43: τ_b>0.00 p>0.99, Kendall's tau-b.

4.4 **Chapter Discussion**

	Main findings
Microglial load distribution	All markers had a trend for higher distribution in upper layers. IBA1 and CD68 load was observed to be greater in lower layers of the *PSEN1* post-codon 200 group.
Microglial load and clinical data	Trend for positive correlations for CD68 and CR3/43 with age at onset and disease duration.
Comparing microglial load between genetic and demographic groups	No significant differences between genetic and demographic groups was observed.
Correlation between markers	Weak trend for negative correlation between IBA1 and CD68
Microglial load and CERAD scores	Trend for a negative correlation between IBA1 and cored plaques (except in the *PSEN1* post codon 200 group), cortical and leptomeningeal CAA and Subpial pathology. CD68 positively correlated with leptomeningeal and cortical CAA, subpial pathology and cored plaques and negatively correlated with diffuse and total pathology. General negative correlations between CR3/43 and CERAD scores.
Microglial load and Aβ *load*	Trend for a weak positive correlation between Iba1 and Aβ,

	General negative correlation between CD68 and Aβ except in lower cortical layers where correlation is positive Trend for negative correlation between CR3/43 and Aβ

In this study we investigated associations between genotype, clinical data and microglial pathology in a small FAD cohort. The distribution of microglial pathology tended to reflect that of Aβ, implicating an association between the two pathologies. Further to this, distinct associations between specific microglial markers and Aβ plaque types were observed, suggesting there may be complex relationship between microglial phenotypes and Aβ pathology.

Distribution of microglial load

Microglial pathology was analysed in the QSBB cohort. Initially, the laminar distribution was assessed and microglial load across the cortical layers revealed a general trend for higher load in upper layers (2&3) compared to lower layers (5&6), reminiscent of the Aβ findings (4.3.1). In particular, Iba1 was significantly higher in upper layers except in the *PSEN1* post-codon 200 group, which may reflect the Aβ distribution pattern in this group, as Aβ load was also more evenly distributed across the layers. This suggests microglia are present in areas of Aβ pathology and may have been involved in underlying pathogenic processes occurring where Aβ deposition is highest. In support of this, Iba1 positive microglia are considered to be evenly distributed across cortical layers in health in rodent and human (Kongsui *et al.*, 2014; Torres-Platas *et al.*, 2014), therefore increased Iba1 load in upper layers indicates microglia may have moved towards and remained in the site of Aβ. CD68 and CR3/43 do not appear to be as significantly different between layers except in the *PSEN1* pre-codon 200 group. Small sub-group sizes may hinder identification of differences, and in the whole QSBB cohort, differences between mutations may mask trends. Between the groups however there were no significant differences in microglial load, although the *PSEN1* post-codon 200 and *APP* groups had opposite microglial phenotypes, with highest Iba1 and CD68 in the *PSEN1* post-codon 200 group and lowest in the *APP* group (Chapter: 4.3.4). The opposite was found for CR3/43. Despite this observation, we do not see significant correlations between average load of any microglial marker, indicating that a range of phenotypes can be present, rather

than just pro or anti-inflammatory. Additionally, microglia in areas of pathology may not be actively upregulating markers we have stained for, and other microglial specific antibodies may reveal more information.

Comparison of microglial load between groups

Iba1 and CD68 did not statistically differ between mutation groups (Chapter: 4.3.4). CR3/43 did not significantly differ between cases either although average load was notably higher in the *APP* group. In the small *APP* group, there was one case with high CR3/43 pathology. The effect of this can be large in such small numbers and may be artificially inflating some of the associations seen in this group. We did not investigate comorbidities in these cases so we cannot guarantee that the observed phenotype is due to FAD rather than some other factor. This may explain why there are frequent *APP* group differences in CR3/43 associations in the *APP* group. Based on this, it would be necessary to use a larger *APP* cohort to investigate the microglial role in these mutation carriers. There are also possible outliers in the *PSEN1* pre-codon 200 group for CR3/43 and Iba1 and in the post-codon 200 group for Iba1, but greater numbers in these groups may buffer the effect.

While the correlation analysis revealed some associations, looking at the data it becomes clear that in some cases, there is a lack of positivity for some of the microglial markers. This suggests that in some instances there may be a reduced microglial response. It would be interesting to see if those with decreased positivity for one marker has similar reduced expression in the other markers.

Clinical associations

Generally, we found no consistent association between Iba1 and age at onset or disease duration (Chapter: 4.3.2). This suggests that on pathological analysis, the overall load of Iba1 positive microglia does not associate with clinical course, at least at the end stage of disease. While overall in the whole QSBB cohort the association between Iba1 and age at onset was very weakly positive, within groups its association tended to be negative, particularly in layers 3 and 4. These results may not be applicable to different stages of disease however. It can also be concluded that research may need to focus on microglial phenotype rather

than overall presence. This view has been suggested by others who found that the method of analysis used lead to different findings (Hopperton *et al.*, 2017).

The analysis of CD68+ve phagocytic microglia revealed CD68 was generally positively associated with age at onset although this was not significant (Chapter: 4.3.2). Importantly, CD68 load did not differ between these groups, even though age at onset did. In contrast the association of CD68 with disease duration suggested group differences, with no correlation in *PSEN1* pre-codon 200 cases, positive correlation in *PSEN1* post-codon 200 cases and a negative correlation in *APP* cases, although again the associations were not significant. As the groups did not differ in CD68 load or disease duration, these differences may be related to the mutation groups. They may however be artefacts of small group sizes, as the greatest differences were observed in the smaller groups.

CR3/43 was significantly positively associated with age at onset, and was positively correlated with disease duration and this trend was seen throughout most of the cortical layers and mutation subgroups (Chapter: 4.3.2). CR3/43+ve microglia would typically be considered pro-inflammatory and associated with a detrimental response which contrasts with these findings (Boche *et al.*, 2013). Why this positive association is seen is uncertain, it may, however, suggest that a pro-inflammatory response may have certain beneficial effects in FAD. Alternatively, it may simply reflect changes in microglial phenotype over time, with microglia progressing to a CR3/43+ve phenotype in later disease stages.

As these analyses are correlations we cannot rule out other factors influencing results, including specific FAD mutation or *APOE*4 status. We have also not accounted for any differences between time between post-mortem and fixation, or the presence of additional comorbidities which may have impact immunological responses in these cases. Some of our results do not align with previous findings, such as negative associations of CR3/43 microglia with scores on clinical outcomes (Minett *et al.*, 2016). This could be due to age effects, as microglia may differ throughout age (Taipa *et al.*, 2018).

In AD, an increased inflammatory response has been associated with the *APOE*4 allele (Minett *et al.*, 2016; Rodriguez *et al.*, 2014). In our QSBB cohort, there was no difference in microglial load between *APOE*4 carriers and non-carriers

suggesting that in this cohort *APOE* may not significantly mediate microglial response in end stage FAD (Chapter: 4.3.3). Additionally, when comparing between sexes, we found no significant differences, although there was a near significant greater increase in Iba1 load in males compared to females. As there was no association with Iba1 and age at onset or disease duration however, it seems unlikely that this difference impacts upon clinical course.

Microglia and Aβ

As microglia are involved in the response to Aβ we investigated potential relationships between microglial load and Aβ load and types of Aβ pathology, however very few significant associations were found (Chapter: 4.3.6). Iba1 did not significantly associate with measures of overall Aβ in this study. Increased Iba1 has often been associated with Aβ in comparison to non-Aβ positive controls (see Hopperton *et al.* (2017)). The Iba1 response may therefore be to Aβ in general, but not increased with increasing Aβ. It is also suggested that microglia change and may lose ability to react efficiently over time (Sankowski *et al.*, 2019), with reduced motility (Minett et al., 2016) and reduced ability to react to pathology in AD (Hickman *et al.*, 2008). Interestingly, we found that Iba1 negatively correlated with cored plaques (Chapter: 4.3.6.1). This negative association of Iba1 with dense cored plaques was not found in a recent study on post mortem AD brain tissue, where instead they observed CR3/43 positive microglia to be associated with dense core plaques, something we also saw (Hendrickx *et al.*, 2017). However, this was within the hippocampus and like Aβ pathology, it is suggested that microglia pathology can differ over anatomical regions (Taipa *et al.*, 2017), and thus may be the cause of conflicting results. As Aβ pathology affects different anatomical regions over time, these differences may reflect temporal changes in microglial response over time. Additionally, in that study only four AD cases were assessed, leaving the results open to further investigation. In a separate study, Iba1 positive microglia were found to be in close proximity to dense core plaques (A. Serrano-Pozo *et al.*, 2013), which would seem inconsistent with our results, however theirs was a measurement of proximity rather than overall load of Iba1. It would be interesting to investigate this further in our FAD cohort.

As observed in immunized AD patient brain tissue, CD68 was reduced after immunization as was Aβ (Zotova *et al.*, 2013b), and CD68 was reduced in immunized cases compared to controls in areas of Aβ clearance (Zotova et al., 2011). This supports the hypothesis that CD68+ve microglia are involved in Aβ clearance mechanisms. Interestingly however, in our cases, the association differed across the cortical layers (Chapter: 4.3.6.3). CD68 was generally negatively correlated with Aβ in the upper layers, yet positively correlated in the lower layers across all mutation subgroups. In context, we showed that Aβ was greater in the upper layers, and lower in lower layers. It is possible that CD68 and Aβ negatively correlated in layer 3 due to microglial driven clearance, as in cases with high CD68 presence Aβ was negatively correlated. This is in concordance with data suggesting that Aβ levels are decreased in areas with increased CD68 after Aβ immunization (Nicolll *et al.*, 2003) and it is speculated that in these scenarios, CD68+ve microglia may be responsible for phagocytic Aβ clearance (Zotova *et al.*, 2011). This may be why in later studies, immunized dementia cases had lower CD68 levels compared to controls, in concordance with Aβ plaque removal and a subsequent downregulation of phagocytic activity (Zotova *et al.*, 2013b). In contrast, in our cases, positive correlations between CD68 load and Aβ in layer 6 may be in response to the speculated later Aβ deposition in this layer. Increased CD68 expression in parallel to Aβ deposition has been shown in a mouse model of FAD (Hoeijmakers *et al.*, 2018). This is particularly possible in the pre-codon 200 group, where both Aβ pathology and CD68 load in layer 6 were positively associated with longer disease duration. This suggests that although overall, Aβ is higher in upper layers, a greater CD68+ve microglial load in theses upper layers associates with lower Aβ. In comparison, cases with lower CD68+ve microglia would likely have higher Aβ load. Alternatively, the layer differences could be interpreted to suggest that at a certain level of high Aβ deposition, microglial phenotypes differ and there is a reduction in their phagocytic capabilities.

Interestingly, CD68 associations with other pathologies differed between mutation sub-groups (Chapter: 4.3.6.1). The *PSEN1* post-codon 200 group had negative associations between CD68 and CERAD measures of CAA, while the remaining groups displayed positive associations. In those with a positive association, it is plausible that CD68 positive microglia enhance Aβ clearance via

the perivascular clearance pathway. Neuropathological CD68+ve immunoreactivity aiding plaque burden reduction, likely via perivascular clearance, has been shown in Aβ-related angiitis cases (Bogner *et al.*, 2013). Interestingly this association was not found in the 'CAA only' cases which were used for comparison in the study. *PSEN1* post codon 200 cases have been linked to greater CAA, so the negative association between CD68 and CAA in these cases is interesting as a positive correlation may have been expected. However, this is end stage disease and if these cases do have a saturation of CAA, the association may be lost.

Models which can look into multifactor associations involving microglia, Aβ and clinical factors may shed light on associations between these combined features of disease. These types of associations have previously been shown, with CD68 positive microglia around dense core plaques positively associating with disease duration in a study of temporal cortex of sAD patients (Serrano-Pozo *et al.*, 2016). This was not observed with Iba1, highlighting microglial phenotype specific associations.

Aβ load and CR3/43 were generally negatively correlated, especially in those layers where CR3/43 was higher (Chapter: 4.3.6.2 and 4.3.6.3). As CR3/43 was also associated with age at onset and disease duration, this may suggest a beneficial response with CR3/43+ve microglia in FAD. This interesting finding may be important for consideration of immunomodulatory treatments. However opposite trends were seen in the *APP* group, although analysis in this group suffers from previously described issues such as small numbers and large outlier effects. If the results seen for the whole QSBB cohort and *PSEN1* pre and post-codon 200 cases could be replicated in larger cohorts and in *APP* mutation carriers, this may suggest that certain microglial phenotypes can benefit reduction of certain pathologies. Although not significant, CR3/43 was positively associated with CWPs although the correlation coefficient was least strong in the mutation group with the non-significant, but numerically highest CWP frequency (Chapter: 3.3.3.2). Within CWPs, microglial reactivity is not observed. The positive association we observe has not been shown before, but CWPs are associated with CAA, while CR3/43 was non-significantly negatively associated with CAA. This complex relationship could be due to numerous factors we have

not been able to apply to our analysis, but a more detailed future analysis of the proximity of microglia to CWPs and areas of CAA help to disentangle it.

Conclusion

In summary, although not consistently statistically significant, trends in microglia phenotype appear relevant to clinical aspects of FAD as well as plaque pathology and CAA. This has highlighted the importance of assessing these pathologies in relation to one another, as their underlying molecular mechanism may enhance or converge on pathways leading to degeneration. As immune-regulatory drugs are being explored it is important to recognise the importance of specific microglial phenotypes in FAD which, as we have shown, may be associated with disease duration. As more microglial associated genetic risk factors are found in AD, understanding pathological changes in microglia in FAD may enhance understanding of the interplay between microglial alterations and other associated risk factors.

Chapter 5

Involvement of cerebral amyloid angiopathy in FAD

5 Involvement of cerebral amyloid angiopathy in FAD

5.1 Abstract

Introduction: Considerable phenotypic and pathological heterogeneity is observed in FAD, including variability in the presence and severity of CAA. Causative gene, mutation location and *APOE* status may drive CAA and Aβ pathology and microglial reactivity may also associate with CAA. Here, the severity of CAA in the frontal cortex of FAD cases is investigated, followed by investigation of CAA in the occipital cortex, where this pathology is known to predominate.

Methods: Sections from the frontal cortex and occipital cortex of 41 FAD cases with mutations in *APP* (n=10) or *PSEN1* (31, 20 located pre-codon 200 and 11 post-codon 200) were stained immunohistochemically for Aβ, with the proportion and severity of CAA determined by vessel counts. Neuropathological correlates of Aβ and microglial pathology in relation to CAA severity in the frontal cortex were investigated in the 20 cases from the QSBB. All results were analysed in relation to age at onset and disease duration and potential associations with genetic mutation and *APOE* status were investigated.

Results: In the QSBB cohort, there were associations between the proportion and severity of CAA and specific pathologies. CAA was positively associated with CWPs, while there was a trend for a negative association between CAA and cored plaques. CAA severity also tended to be positively associated with Aβ load. CAA did not display many significant associations with microglial load, although general trends emerged with negative associations between CAA and Iba1 (except in the *PSEN1* post-codon 200 group), positive associations between CAA and CD68 (except in the *PSEN1* post codon 200 group) and negative associations between CAA and CR3/43 in all mutation subgroups. In the extended cohort, CAA did not significantly associate with age at onset or disease duration. CAA did however display significant differences between mutation subgroups and *APOE* genotypes, therefore may associate with both genetic mutation and *APOE* status.

Conclusions: Investigating CAA pathology in carriers of a variety of different FAD mutations and *APOE* genotypes may provide insights into its role in the

disease process. As CAA has emerged as an important factor in amyloid-modifying therapy, understanding its heterogeneous occurrence in FAD may have relevance for the development and evaluation of clinical trials.

5.2 **Introduction**

5.2.1 *Cerebral amyloid angiopathy in FAD*

As discussed in chapter: 1.10 - 1.11, particular FAD mutations have been associated with more severe CAA, particularly *APP* mutations within the Aβ coding domain as discussed above and reviewed in Ryan and Rossor (2010). Differences may also exist between *PSEN1* mutation carriers, with mutations post-codon 200 reported to cause more severe CAA pathology than pre-codon 200 mutations, more severe white matter hyperintensities on MRI and more frequent associations with spastic paraparesis (Karlstrom *et al.*, 2008; Ryan *et al.*, 2015a; Ryan *et al.*, 2016; Ryan & Rossor, 2010). CAA segregating with mutation location is however not always consistent, with the *PSEN1* 405S mutation appearing to have limited CAA (M. Yasuda *et al.*, 2000). Conversely mutations pre-codon 200 can have prominent CAA, e.g. M84T, L174M and E184D (Bertoli Avella *et al.*, 2002; Lanoiselée *et al.*, 2017; Minoru Yasuda *et al.*, 1997). CAA was also noted in our E148D cases (see Figure 3-2). These case reports show that there is large variation in CAA presence between individuals so other factors may also play a role.

Pathologically, CAA can be subtyped (Dietmar Rudolf Thal *et al.*, 2002), with type 1 CAA displaying Aβ in the cortical and leptomeningeal vessels, including capillaries, while type 2 has cortical and leptomeningeal vessel but no capillary CAA. *APOE4* is associated with type1 CAA while *APOE2* is associated with type 2 CAA. Having type 1 non-capillary CAA was also associated with *APOE*4 status in AD patients, as well as with the severity of CAA, dementia and severe AD type pathology (Mäkelä *et al.*, 2015). Distinction between a type 1 and type 2 pathology for both CAA and Aβ cortical pathology has also been suggested in FAD, with type 1 pathology displaying reduced Aβ40 deposits and reduced CAA while type 2 pathology is characterised by more severe Aβ40 deposition and CAA (David M. A. Mann *et al.*, 2001). Greater severity of this type 2 histology has been suggested to be associated with a less aggressive clinical phenotype with

later onset and longer disease duration. This type of pathology was more common in the *PSEN1* post-codon 200 mutation cases although whether this is due solely to mutation location or to CAA is unclear.

5.2.2 *Cerebral amyloid angiopathy and Aβ plaque types*

In aged cases with AD pathology, CAA severity has been shown to be significantly correlated to the number of plaques, and NFTs (Yamada *et al.*, 1987). This association between the presence of the two pathologies could indicate a mechanistic link. Considering Aβ load in general, it has been observed in sAD that cases with more severe CAA had lower parenchymal Aβ (Chalmers *et al.*, 2003). This can be interpreted to indicate a preference for vascular CAA over parenchymal CAA in some cases or reduced parenchymal and consequential increased vascular CAA in other cases. Although in the study mentioned, *APOE*4 also influenced CAA pathology. Combining data from across multiple brain regions in sAD cases, CAA and senile plaque deposition was negatively correlated (Tian *et al.*, 2003). However, higher CAA incidence with greater AD pathology has been shown in sAD cases (J. Attems *et al.*, 2007). As Aβ pathology in FAD is driven by mutation rather than clearance deficits, there may or may not be an association with total Aβ load and CAA in FAD.

CAA has also been associated with patterns of histological Aβ pathology. Four distinct types are classified which includes variations in the levels or severity of CAA and senile plaques (Allen *et al.*, 2014). However, as plaques are present in different forms, the relationship between CAA and plaques may be more specific and complex. This may even account for some discrepancies observed in direction of correlation between CAA and Aβ pathology in previously mentioned studies. Using the CERAD scoring system to rate frequency of plaque pathology, CAA has previously shown to have low correlation with CERAD scores in sAD cases (J. Attems & Jellinger, 2004), although capillary CAA, where Aβ deposits in the capillaries, did significantly correlate to CERAD scores. Interestingly, CAA with capillary CAA has been associated with CERAD in another study, amongst other features such as the severity of CAA and Braak stage (Mäkelä *et al.*, 2015). As this method of CERAD analysis did not differentiate plaques types as is in our study, there may still be associations not yet revealed. As mentioned previously, in FAD CAA and CWPs have often been observed

together and this deserves further investigation (Niwa *et al.*, 2013; Ryan *et al.*, 2015a). In *APP* A692G mutation carriers, dense-cored plaques have been shown to associate in proximity with CAA, while diffuse plaques did not (Kumar-Singh *et al.*, 2002) and in general, these cases notably have very high dense-core plaque pathology, as well as having CAA (Cras et al., 1998; Kumar-Singh et al., 2002). Conversely in an *APP* T714I mutation pedigree, the inverse was observed, with minimal dense-cored plaques and low CAA observed (Kumar-Singh et al., 2000). Similar findings of dene-core plaques proximity to vessels has also been observed in mouse models of AD (Kumar-Singh *et al.*, 2005). This highlights specific plaques may be associated to CAA and in particular, this may be a feature in FAD. As findings suggest associations, but minimal investigations involve specific types of pathology, it will be beneficial to see if there is a link between CAA, and severity therein with plaque specific pathology.

5.2.3 *Cerebral amyloid angiopathy and microglia*

The link between neuroinflammation, microglia and Aβ is well known, therefore it is fair to suggest microglia may be involved in CAA, or microglial dysfunction could contribute to CAA. One of the greatest indicators of an association between microglia and CAA is the observed increase in CAA in AD patients treated with immunomodulatory agents. In these studies, evidence of changes in microglial activity upon histological examination suggests that microglia promote vascular clearance (Boche *et al.*, 2008; Nicolll *et al.*, 2003; Sakai *et al.*, 2014). This is also recapitulated in mice models (D. M. Wilcock & Colton, 2009). With this in mind, as microglia are hypothesised to differentially impact plaque pathology, specific microglial phenotypes may differentially impact CAA pathology. While research into CAA in AD is continuing to expand, there is a significant lack of investigations in CAA and neuroinflammation in FAD. In a study with a *PSEN1* L282V mutation case, intense CAA was speculated to be related to an inflammatory phenotype, with gliosis and complement upregulation found (Dermaut *et al.*, 2001). Factors involved in complement have been shown in sAD cases with CAA (Zabel *et al.*, 2013), suggesting that there may be some similarities and shared mechanisms in sporadic and familial AD.

Neuroinflammatory response is observed in capillary CAA cases with no other AD pathology (Carrano *et al.*, 2012) which suggests there can be an Aβ+ve CAA

association with microglia that is specific to CAA pathology, without a link to cortical Aβ pathology. However, as these observations were specifically in capillary CAA cases, there may be some differences in aetiology and mechanisms may not be applicable to the situation in FAD or sAD. This has been suggested in a study where capillary CAA was associated with microglial activation, however CAA in larger vessels was not associated with microglial activation (Richard *et al.*, 2010). Nevertheless, there is still a need for further study due to the lack of understanding in the relationship between CAA and microglia. Additionally, capillary CAA is also observed in some FAD cases so may have an influence in disease (D. M. A. Mann *et al.*, 2018; Niwa *et al.*, 2013).

5.2.4 *Cerebral amyloid angiopathy and clinical data*

As mentioned, Aβ pathology has been linked to clinical features of sAD and FAD, therefore it has been speculated that CAA may also contribute to these features, particularly as CAA prominent forms of FAD develop dementia as do non-CAA prominent cases. CAA pathology has been associated with older onset of dementia in sAD cases (Ellis *et al.*, 1996). This may seem counter-intuitive but it may represent a greater removal of Aβ in earlier stages, which could be protective. In contrast, post-mortem CAA and Aβ pathology were the greatest risks associated with an earlier conversion to very mild and moderate-stage dementia (Vidoni *et al.*, 2016). In a separate study which included sAD cases and neurologically normal controls, of which some displayed CAA pathology, it was observed in the sAD cases, that the CAA severity did not correlate with age at onset or disease duration, suggesting the CAA did not positively or negatively affect disease course or outcome (Chalmers *et al.*, 2003). Similar findings which considered regional differences have also been observed, with the degree of CAA in the frontal or occipital cortex not significantly correlating with age at onset or duration of illness in AD post-mortem cases (Tian *et al.*, 2006). The study did however find associations between CAA and *APOE* genotype, thus more complex analysis which can include possible influential factors such as *APOE* genotype would help investigate associations. Allen *et al.* (2014) looked at associations between clinical features of disease and the CAA histology type that different AD cases were categorized into. They observed no significant differences between CAA histology type groups with regard to age of onset,

disease duration or disease presentation. However, women were over-represented in the type 1 phenotype group and men in the type 2 group. Whether this was due to sex specific associations or a results of over representation would need to be further investigated but it highlights how various factors may be involved. Specifically in FAD, it has been noted that *PSEN1* post-codon 200 cases had greater CAA compared to *PSEN1* pre-codon 200 cases, and post-codon 200 cases also had later age at onset than the pre-codon 200 cases (Ryan *et al.*, 2015a). Therefore in FAD CAA may not negatively impact disease course. As therapies against Aβ can lead to increased CAA it will be important to understand the relationship between CAA pathology and disease in both sAD and FAD.

In addition to age at onset and disease duration, the contribution of CAA pathology on cognitive aspects of AD have been explored. In AD, the presence of CAA was associated with cognitive decline, suggesting its influence exists in conjunction with other processes in AD (Boyle *et al.*, 2015). The cortical spreading of CAA was also related to clinical dementia rating scores in AD pathology positive cases (D. R. Thal *et al.*, 2003) although analysis involving Aβ pathology and NFT pathology was suggestive that these factors could also influence clinical dementia rating scores. These types of findings support the need for greater understanding of this pathology, however cognitive associations are beyond the scope of this study.

As previously discussed, *APOE* genotype has frequently been associated with CAA in SAD (Chapter: 1.16). The *APOE*4 allele has frequently been associated with a greater presence and severity of CAA (D. M. A. Mann *et al.*, 2018; Peuralinna *et al.*, 2011). A previously mentioned study found APOE to associate with CAA (Chalmers *et al.*, 2003). Specifically, in sAD cases they found that the number of *APOE*4 alleles was strongly associated with CAA, but not parenchymal Aβ load, suggesting *APOE*4 is more strongly associated with vascular deposition compared to parenchymal deposition. In our FAD cohort, it will be interesting to see if *APOE* genotype associates with CAA despite mutation driven FAD. Possession of the *APOE* ε4 allele has also been associated with capillary CAA (Allen *et al.*, 2014).

Similar to sAD, in FAD the involvement of *APOE* genotype in CAA has also received some study. With *APOE*4 likely leading to increased CAA via APOE4 isoform specific activities such as its interaction with Aβ and its interaction with other proteins involved in clearance pathways (D. M. Holtzman, 2001). In an imaging study assessing a cohort consisting of sAD, FAD and DS with AD cases, neuroimaging features of CAA were associated with APOE4 in the sAD group but not in the FAD or DS group (Carmona-Iragui *et al.*, 2017). While this suggests there is no evidence for an involvement in FAD, features associated with CAA on neuroimaging are not a direct marker of CAA so may not fully represent CAA.

To complicate matters, CAA and vascular pathologies in AD have been shown to also be associated with an interaction between sex and *APOE* (Cacciottolo *et al.*, 2016; Shinohara *et al.*, 2016). This highlights the complexity of genetic factors in pathology and the need for studies where methodologies beyond correlation can be incorporated, although this is often difficult in histological studies due to tissue availability and time required for tissue analysis.

5.2.5 *Aims*

In FAD, CAA pathology composed of Aβ is observed, and this may be related to multiple facets of disease. Investigating the proportion and severity of CAA in relation to Aβ pathology and microglial load can help unravel connections between these pathologies, while associations with clinical and genetic data can help highlight modulators of clinical course or pathology. To achieve these investigations, chapter 5 is separated into 3 sections with a range of aims:

<u>Section 1</u>

1. To determine if the proportion or severity of CAA associates with Aβ plaque type in the frontal cortex in genetic causes of FAD in the QSBB cohort.

<u>Section 2</u>

2. To determine if the proportion or severity of CAA associates with microglial load in the frontal cortex in genetic causes of FAD in the QSBB cohort.

Section 3

3. To assess in the extended cohort associations between sex, mutation or *APOE* genotype with clinical aspects of FAD (age at onset and disease duration).

4. To determine if the proportion or severity of CAA associates with clinical aspects of FAD (age at onset and disease duration) and if this exists in specific genetic causes of FAD in the frontal and occipital cortex.

5. To determine if the proportion or severity of CAA differs by genetic causes of FAD, or by *APOE* genotype in the frontal and occipital cortex.

5.2.6 *Materials and Methods*

Throughout this chapter, the CAA results refer to the proportion and severity of CAA pathology which was measured as a proportion, with up to 100 vessel being counted in the cortex and leptomeninges, and the severity of the CAA noted and calculated as a proportion (see chapter: 2.5.2) and other methods use are discussed in chapters: 2.3 and 2.3.3. In brief, the Aβ stained section previously described in chapter: 3.3 were used to investigate and the proportion and severity of CAA in the frontal cortex of the QSBB cohort. This was then analysed with the Aβ pathology data generated in chapter: 3.3. To investigate the association between CAA and microglia, the proportion and severity of CAA was assessed in relation to the microglial data generated in chapter: 4.3.

As the larger extended cohort was available, frontal cortex tissue of the remaining extended cohort and occipital cortex tissue for the full extended cohort was stained using an anti-Aβ antibody. The proportion and severity of CAA was calculated. Initially, clinical and demographic data in this extended cohort was assessed. Finally, the proportion and severity of CAA was assessed relation to clinical data and compared between mutation subgroups and by *APOE* genotype.

5.3 **Results**

QSBB cohort

The proportion and severity of CAA in the QSBB cohort was analysed using the immunohistochemically stained slides from chapter: 3 Aβ pathology in FAD. As

described in the methods (Chapter: 2.5.2), up to 100 vessels were counted and assessed for the presence of CAA. Presence of Aβ positive CAA pathology in vessels was graded on a scale from none-severe (0-3). The proportion of vessels with CAA and the proportion of vessels at each grade of severity were calculated.

5.3.1 *Proportion and severity of CAA and clinical data*

Relationships between CAA and clinical data were investigated in the QSBB cohort. As required assumptions for regression analysis were not met for all CAA severity measures, a correlation method has been used for all measures. However, as assumptions were met for the overall proportion of CAA, the regression analysis was conducted for the overall proportion of CAA only, and is presented.

Age at onset

Regression analysis was used to test whether the overall proportion of cortical CAA was associated with age at onset or disease duration, adjusted for mutation-subgroup, *APOE4* status and sex (n=19). There was no evidence to suggest that CAA was associated with age at onset, with a 0.008 increase in age at onset for every percentage point increase in CAA (p=0.92, 95% CI:-0.17 - 0.18). Similarly, there was no evidence to suggest that the proportion of leptomeningeal CAA associated with age at onset with -0.05 years decrease in age at onset for every percentage point increase in leptomeningeal CAA (p=0.39, 95% CI:-0.17 - 0.07).

Correlation analysis between the overall proportion and severity of cortical CAA and age at onset revealed weak correlations in the QSBB cohort and varying directions and strengths of correlation within the mutation subgroups, indicating there was no clear association and age at onset. The overall proportion and severity of leptomeningeal CAA was generally negatively correlated with age at onset, however, in contrast to this trend, in the *PSEN1* post-codon 200 group there was a significant positive correlation between mild leptomeningeal CAA and age at onset (p=0.04) (Figure 5-1 A,B).

Disease duration

Regression analysis was used to test whether CAA was associated with disease duration, adjusted for mutation sub-group and *APOE* status (n=19). There was

no evidence to suggest that the proportion of cortical CAA was associated with disease duration, with a -0.04 years decrease in disease duration for every percentage point increase in CAA (p=0.26, 95% CI: -0.13 - 0.04). Similarly there was no evidence to suggest that the overall proportion of leptomeningeal CAA was associated with disease duration, with -0.02 years decrease for every year percentage point increase in leptomeningeal CAA (p=0.52, 95% CI: -0.08 - 0.04).

In the cortex, correlation analysis revealed weak correlations in the QSBB cohort. Mutation sub-groups did not follow similar patterns and showed differences in strength and direction of correlation within and between groups. Leptomeningeal CAA was generally positively correlated with disease duration except in the *PSEN1* post-codon 200 group (Figure 5-1 C,D).

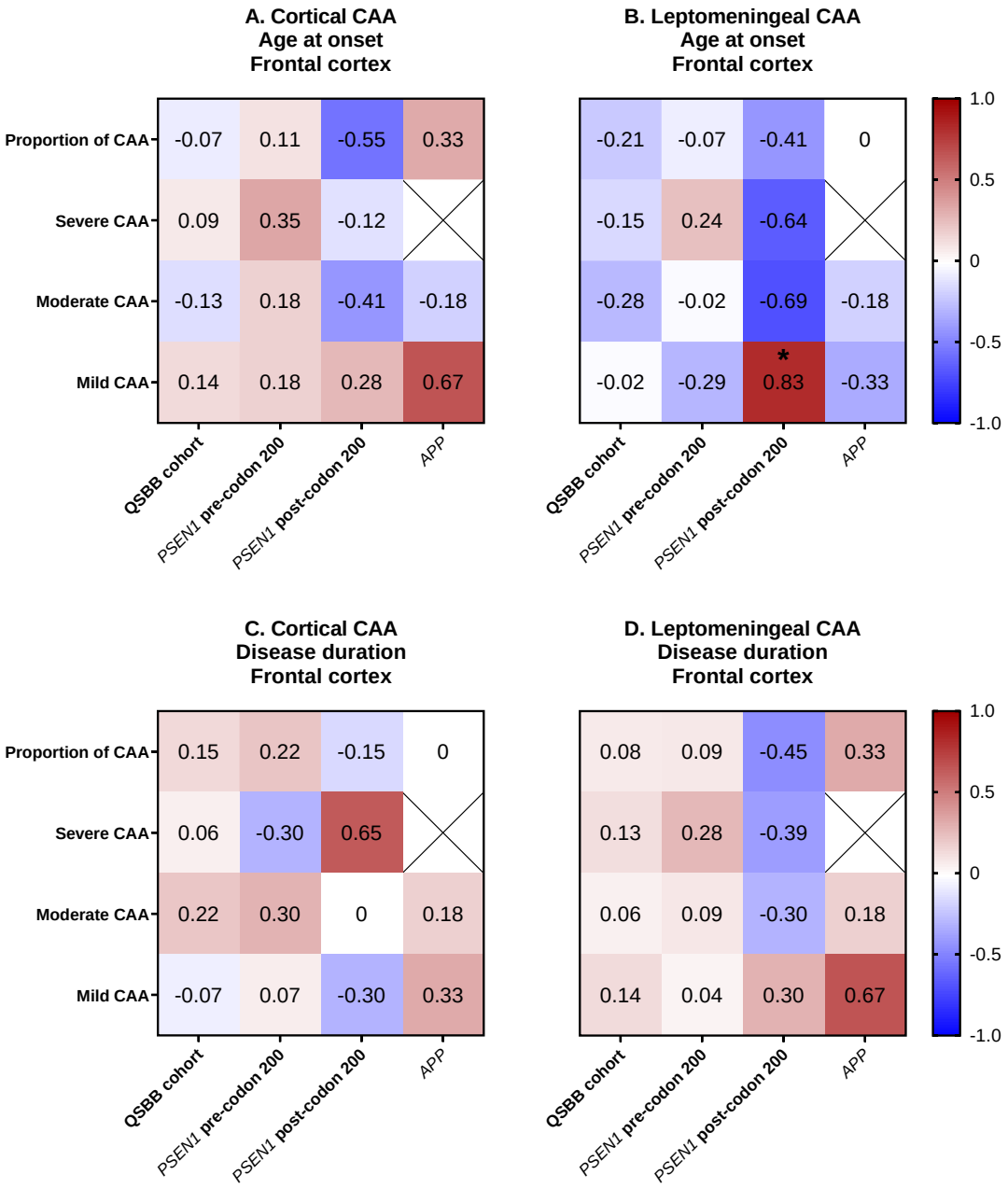

Figure 5-1 Correlation between proportion and severity of CAA and clinical data.

A: Cortical CAA and age at onset. B: significant positive correlation between mild leptomeningeal CAA and age at onset in the PSEN1 post-codon 200 group (p=0.04). C: Cortical CAA and disease duration. D: leptomeningeal CAA and disease duration. Crossed squares represent no data due to no severe CAA in the APP mutation group. Data shown in heatmaps are τb correlation coefficients, Kendall's tau-b, *p<0.05.

5.3.2 *Proportion of CAA and CERAD pathology*

The proportions of cortical and leptomeningeal CAA were significantly, positively correlated with total CERAD scores for cortical and leptomeningeal CAA

suggesting good coherence between these measures of CAA (cortical CAA: r_T=0.80, p<.0001, leptomeningeal CAA τ_b=0.74, p<.0001).

The overall proportion and severity of cortical and leptomeningeal CAA was correlated with CERAD pathology scores (Figure 5-2). In the QSBB cohort and mutation sub-groups, the overall proportion of CAA, severe CAA and moderate CAA in both the cortex and leptomeninges were positively correlated with subpial pathology, although the correlations were weak and non-significant.

In the QSBB cohort, the overall proportion of cortical CAA and moderate CAA was positively correlated with CWP score (p=0.003, p=0.007). Severe and mild cortical CAA were also positively correlated although they did not reach statistical significance. A similar pattern to the whole QSBB cohort was seen in the sub-groups, with the *PSEN1* post-codon 200 group having a significant positive correlation between the overall proportion of cortical CAA and CWP score (p=0.02) while both the *PSEN1* pre and post-codon 200 groups had a near significant positive correlation between moderate cortical CAA and CWP score (p=0.07, p=0.06).

The overall proportion of leptomeningeal CAA in the QSBB cohort was also positively correlated with CWPs although this did not reach significance (p=0.09), however severe and moderate leptomeningeal CAA were significantly positively correlated with CWPs (p=0.02, p=0.03). This trend was seen within sub-groups, reaching near statistical significance between the overall proportion of CAA and moderate CAA in the leptomeninges and CWPs in the *PSEN1* post-codon 200 group (p=0.06, p=0.06). Contrastingly, mild leptomeningeal CAA was generally negatively correlated with CWPs although there were no other significant correlations.

In cortex diffuse plaques did not significantly correlate with the overall proportion or severity of CAA and the strengths and direction of correlations were varied. Specifically, the proportion of CAA and moderate CAA positively correlated with diffuse plaques in the QSBB cohort and mutation sub-groups, however severe CAA was negatively correlated with diffuse plaques, and there was no correlation with mild CAA. In the leptomeninges there was also a positive correlation between diffuse plaques and the overall proportion of CAA and severe and

moderate CAA, while the relationship with mild CAA was varied across sub-groups, although again these correlations were all non-significant.

In contrast to the positive associations seen for other plaques, there was a specific trend for negative correlations between cored plaques and the overall proportion of CAA, the moderate cortical and leptomeningeal CAA and the mild cortical CAA in the QSBB cohort and mutation sub-groups. Specifically, the *PSEN1* post-codon 200 group had a near significant negative correlation between proportion of cortical CAA and total cored plaque score ($p=0.06$) and a significant negative correlation between moderate leptomeningeal CAA and total cored plaque score ($p=0.02$). There were no other significant correlations.

There were no significant differences between the overall proportion and severity of cortical and leptomeningeal CAA with total CERAD pathology (total CERAD pathology reflects the semi-quantitative assessment of overall Aβ deposition). Between the mutation subgroups, the direction of correlation was not consistent with only weak to mild strengths of correlation observed.

.

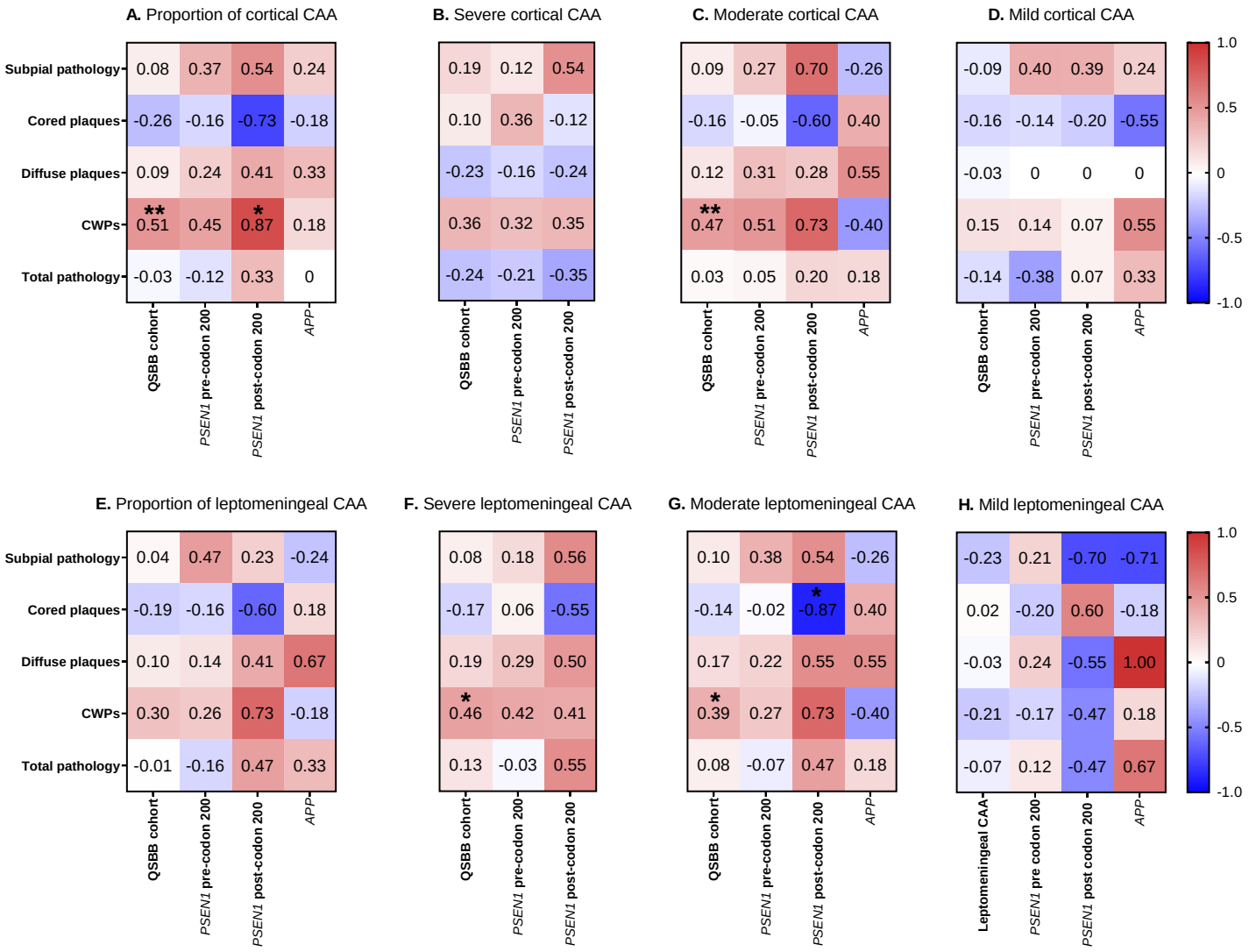
A. Proportion of cortical CAA
B. Severe cortical CAA
C. Moderate cortical CAA
D. Mild cortical CAA
E. Proportion of leptomeningeal CAA
F. Severe leptomeningeal CAA
G. Moderate leptomeningeal CAA
H. Mild leptomeningeal CAA
Subpial pathology
Cored plaques
Diffuse plaques
CWPs
Total pathology
QSBB cohort
PSEN1 pre-codon 200
PSEN1 post-codon 200
APP
Leptomeningeal CAA
PSEN1 pre codon 200
PSEN1 post codon 200
1.0
0.5
0
-0.5
-1.0

Figure 5-2 Correlation between CAA and CERAD scores.

In the QSBB cohort, the proportion of cortical CAA and moderate CAA was significantly positively correlated with CWP score (A: p=0.003. C: p=0.007). In the *PSEN1* post-codon 200 group there was a significant positive correlation between proportion of cortical CAA and CWP score (A: p=0.02). Severe and moderate leptomeningeal CAA were significantly positively correlated with CWP score (F: p=0.02. G: p=0.03). In the *PSEN1* post-codon 200 group, moderate leptomeningeal CAA was negatively correlated with cored plaque score (G: p=0.02). Date presented in heatmaps are τ_b correlation coefficients, Kendall's tau-b, *p<.05, **p<.01. No severe cortical or leptomeningeal CAA was present in the *APP* group.

5.3.3 *The proportion and severity of CAA and Aβ load*

In the QSBB cohort and mutation sub-groups there was a trend in both the cortex and leptomeninges for positive correlation between the overall proportion of CAA and severe and moderate CAA with Aβ load, while mild CAA was negatively correlated, except in the small *APP* group (see Figure 5-3). While results are not significant, the trend suggests that Aβ load was associated with a greater proportion and severity of CAA.

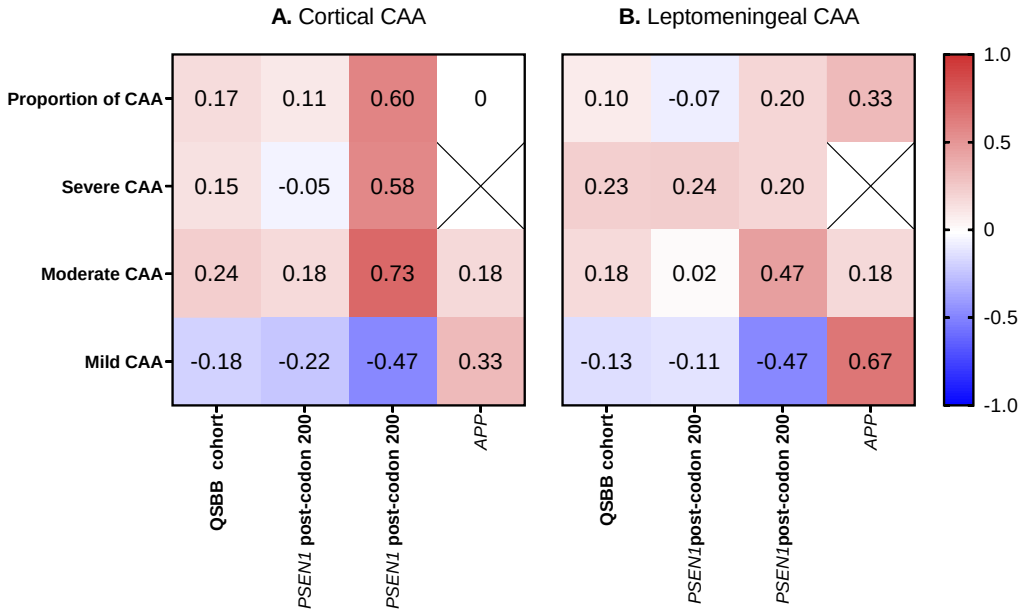

Figure 5-3 Correlation between the proportion and severity of CAA and Aβ load.

A: Cortical CAA and Aβ load. B: Leptomeningeal CAA and Aβ load. Crossed squares represent no data due to on severe CAA in the APP mutation group. Date presented in heatmaps are τb correlation coefficients, Kendall's tau-b.

5.4 The proportion and severity of cortical and leptomeningeal CAA and microglial load

The relationship between the proportion and severity of CAA and microglial load described in chapter: 4 Microglial response in FAD, was then investigated (see Figure 5-4 A-F). Generally, Iba1 was non-significantly negatively correlated with a greater proportion and higher severity of CAA in both the cortex and leptomeninges, except in the *PSEN1* post-codon 200 group. In concordance with this, Iba1 was non-significantly positively correlated with mild cortical CAA in the cortex, although this association was not consistent for all mutation sub-groups in the leptomeninges.

CD68 load was mildly to moderately positively correlated with the proportion and severity of cortical and leptomeningeal CAA except in the *PSEN1* post-codon 200 group. Specifically, In the *PSEN1* pre-codon 200 group the correlation reached near significance with the overall proportion of cortical CAA and mild cortical CAA ($p=0.07$ & $p=0.06$). In the leptomeninges the correlation was statistically significant between CD68 and the overall proportion of CAA ($p=0.03$). However, in the *PSEN1* post-codon group the overall proportion of CAA and CD68 was negatively correlated, reaching near significance ($p=0.06$).

Except from a few instances in the small *PSEN1* post-codon 200 and *APP* groups, CR3/43 was consistently negatively correlated with the overall proportion of CAA and severity of cortical and leptomeningeal CAA and in the QSBB cohort this reached borderline significance for moderate leptomeningeal CAA ($p=0.06$). These patterns of direction of correlation generally match those observed in the investigation of microglial load and CERAD scores of CAA.

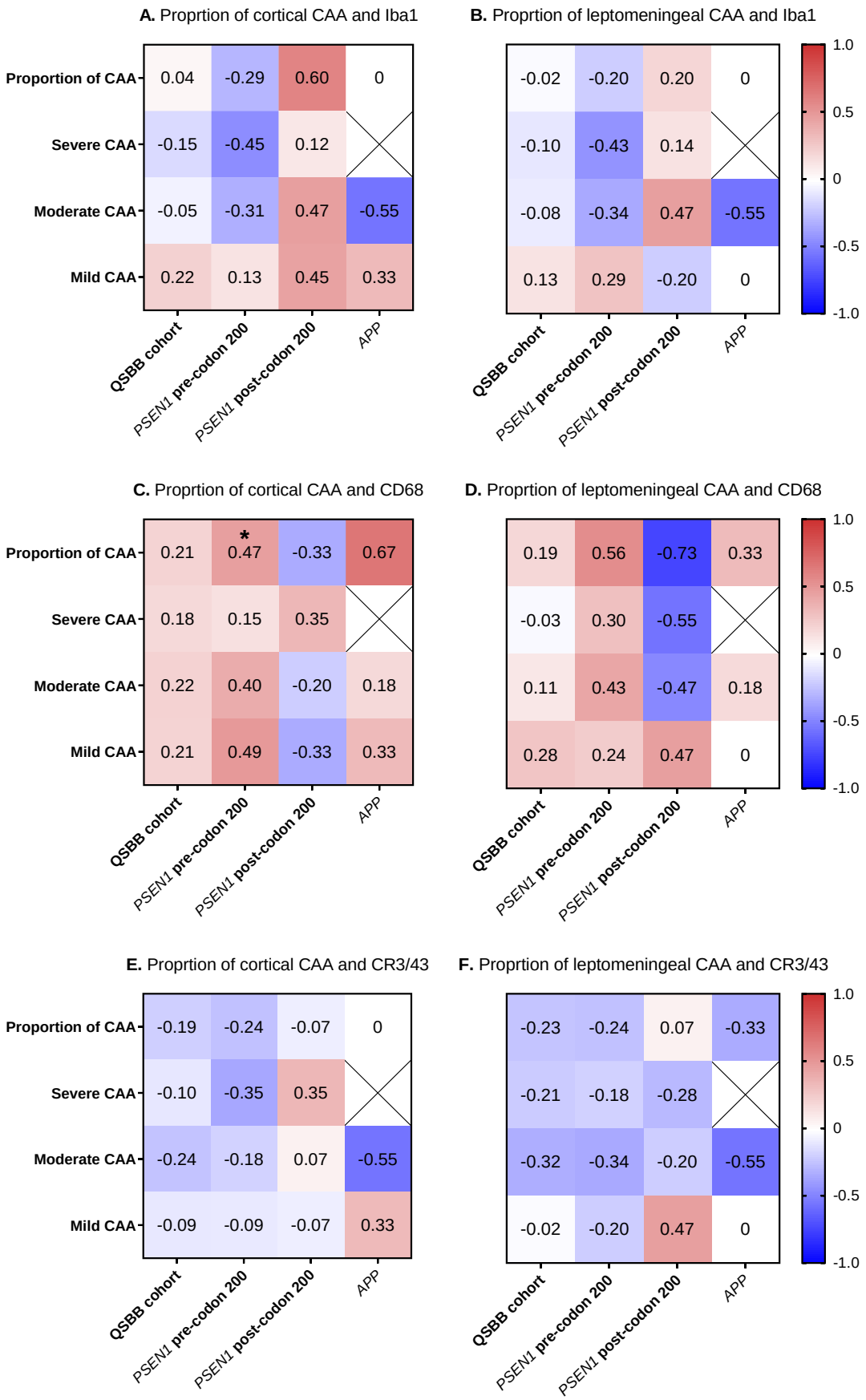
A. Proprtion of cortical CAA and Iba1
Proportion of CAA
Severe CAA
Moderate CAA
Mild CAA
0.04 -0.29 0.60 0
-0.15 -0.45 0.12
-0.05 -0.31 0.47 -0.55
0.22 0.13 0.45 0.33
QSBB cohort
PSEN1 pre-codon 200
PSEN1 post-codon 200
APP
B. Proprtion of leptomeningeal CAA and Iba1
-0.02 -0.20 0.20 0
-0.10 -0.43 0.14
-0.08 -0.34 0.47 -0.55
0.13 0.29 -0.20 0
1.0
0.5
0
-0.5
-1.0
C. Proprtion of cortical CAA and CD68
0.21 * 0.47 -0.33 0.67
0.18 0.15 0.35
0.22 0.40 -0.20 0.18
0.21 0.49 -0.33 0.33
D. Proprtion of leptomeningeal CAA and CD68
0.19 0.56 -0.73 0.33
-0.03 0.30 -0.55
0.11 0.43 -0.47 0.18
0.28 0.24 0.47 0
E. Proprtion of cortical CAA and CR3/43
-0.19 -0.24 -0.07 0
-0.10 -0.35 0.35
-0.24 -0.18 0.07 -0.55
-0.09 -0.09 -0.07 0.33
F. Proprtion of leptomeningeal CAA and CR3/43
-0.23 -0.24 0.07 -0.33
-0.21 -0.18 -0.28
-0.32 -0.34 -0.20 -0.55
-0.02 -0.20 0.47 0

Figure 5-4 Relationship between microglial load and the proportion and severity of CAA.

A, B: Iba1 was generally negatively correlated with the proportion of and higher severity CAA in the cortex and leptomeninges. C, D: The correlation between CD68 and CAA differs by mutation group and in the cortex/leptomeninges. In the *PSEN1* pre-codon 200 group, CD68 and the overall proportion of leptomeningeal CAA was significantly correlated ($p=0.03$). E, F: CR3/43 was generally negatively correlated with CAA. Crossed squares represent no data due to no severe CAA in the *APP* mutation group. Data shown in heatmaps are τ_b correlation coefficients, Kendall's tau-b, $^*p<0.05$.

5.5 **Proportion and severity of CAA in the extended cohort**

Further investigations into the involvement of CAA in FAD were carried out in the extended cohort, which comprised 41 cases. The additional 21 cases were from the IOPPN brain bank. *APOE* status was available for 38 of these cases. 41 cases are included in the analysis except when analysis includes *APOE* status/genotype, where only 38 cases could be included. Clinical data for these cases is summarised in Table 5-1.

	Number of cases	Age at onset	Disease duration
Extended cohort	41	44.20 (7.33)	10.25 (4.02)
Mutation subgroups			
PSEN1 pre-codon 200	20	40.00 (6.88)	8.98 (3.44)
PSEN1 post-codon 200	11	46.27 (3.72)	11.57 (4.75)
APP	10	50.30 (6.11)	11.35 (3.86)
APOE genotyped cases	38	44.61 (7.31)	10.21 (4.09)
APOE4 status			
non-carrier	24	44.50 (7.38)	8.65 (3.59)
Carrier	14	44.79 (7.74)	12.89 (3.70)
APOE allele genotype			
2/3	2	51.00 (4.24)	9.00 (4.24)
3/3	22	43.91 (7.38)	8.61 (3.64)
3/4	9	44.56 (8.75)	12.62 (3.97)
4/4	5	45.20 (6.42)	13.38 (3.55)

Table 5-1 Extended cohort clinical data by mutation group and *APOE* status/allele genotype.

Data are presented as mean and SD.

5.5.1 *Clinical analysis*

Between the mutation sub-groups there were no significant differences in the frequency of males and females (p=0.28, Fisher's exact), *APOE4* carriers and non-carriers (p=0.62) or *APOE* allele genotypes (p=0.88). Additionally, between males and females there was no significant differences in frequency of *APOE4* non-carriers/carriers (p=0.51) or *APOE* allele genotypes (p=0.21).

5.5.1.1 *Age at onset*

In the extended cohort, relationships between age at onset and mutation sub-group, *APOE4* status and sex were investigated. Linear regression indicated there was a significant association between mutation sub-group and age at onset (n=38, F test p=0.002). *PSEN1* post-codon 200 cases had a significantly later

age at onset of 5.41yrs compared to *PSEN1* pre-codon 200 cases (p=0.03, 95% CI: 0.53 - 10.28). *APP* mutation carriers had a significant later onset of 11.33yrs than *PSEN1* pre-codon 200 cases (p>.0001, 95% CI: 6.21 - 16.45) and a significant later onset of 5.92yrs than *PSEN1* post-codon 200 cases (p=0.05, 95% CI: 0.08 - 11.77). There was no significant effect of *APOE4* status on age at onset. Contrary to results for the QSBB cohort, there was also no influence of sex on age at onset (p=0.36, CI: -6.18 – 2.30).

5.5.1.2 *Disease duration*

For the extended cohort, relationships between disease duration and mutation sub-group, *APOE4* status and sex were investigated. Linear regression indicated that there was a significant association (n=38, F test p=0.002). *APP* mutation carriers had on average a 3.57yrs longer disease duration compared to *PSEN1* pre-codon 200 mutation carriers (p=0.02, 95% CI: 0.70 - 6.43). *PSEN1* post-codon 200 carriers had a disease duration on average 2.56yrs longer than *PSEN1* pre-codon 200 carriers although this did not reach significance (p=0.07, 95% CI: -0.17 - 5.30). *APOE*4 carriers had a significantly longer disease duration than non-carriers, typically 4.5yrs longer (p=0.001, 95% CI: 2.09 - 6.91). There was no effect of sex on disease duration (p=0.99, 95% CI: -2.39 – 2.39).

Due to a larger cohort, a linear regression model with *APOE* categorised by allele genotype (ε2/3, 3/3, 3/4, 4/4) was tested. Linear regression indicated that there was a significant association (n=38, F test p=0.01). *APP* mutation carriers had an average 3.60yrs longer disease duration compared to *PSEN1* pre-codon 200 mutation carriers (p=0.02, 95% CI: 0.61 - 6.6). *PSEN1* post-codon 200 carriers had a disease duration on average 2.55yrs longer than *PSEN1* pre-codon 200 carriers, although this did not reach significance (p=0.08, 95% CI: -0.28 - 5.37). Compared to the *APOE* 3/3 genotype, carriers of the 3/4 genotype had an average 4.45yrs longer disease duration (p=0.005, 95% CI: 1.47 - 7.43) and carriers of the *APOE* 4/4 genotype had an average 4.77yrs longer disease duration than 3/3 carriers (p=0.01, 95% CI: 1.18 - 8.37). Again, sex was not associated with disease duration (p=0.91, CI: -2.43 - 2.73).

Because the effect of using *APOE* allele genotype did not improve the model, the *APOE4* carrier/non-carrier will be used for any additional regression analysis with disease duration.

5.5.1.3 *Age at onset and disease duration*

To investigate whether there was an association between age at onset and disease duration, linear regression adjusted for *APOE4* status and mutation sub-group was conducted, with no evidence for an association found (p=0.98, coefficient: 0.002, 95% CI:-0.19 - 0.20).

5.5.2 *Proportion and severity of CAA and clinical data in the frontal cortex*

In the frontal cortex, associations between the proportion and severity of CAA and clinical data were investigated. Exploratory analysis of the CAA data highlighted that some of the severity results did not meet the required assumptions for regression analysis. Therefore, while regression could be presented for the proportion of CAA, to maintain consistency in analysis, a correlation method has been used and reported for all measures of CAA.

5.5.2.1 *Age at onset*

Regression analysis adjusted for mutation sub-group and *APOE* status revealed no evidence for an association between the overall proportion of cortical CAA and age at onset, with 0.02 years increase age at onset for each percentage point increase cortical CAA (p=0.73, 95% CI: -0.11 – 0.16). Similarly, there was no evidence for an association between the overall proportion of leptomeningeal CAA and age at onset, with -0.03 years decrease in age at onset for each percentage point increase in leptomeningeal CAA (p=0.41, 95% CI: -0.10 - 0.05).

In the extended cohort and *PSEN1* pre-codon 200 and *APP* groups, there was a general positive correlation between age at onset and the overall proportion of CAA and severity of CAA although the strength of correlations are generally weak and non-significant. However, in contrast, the *PSEN1* post-codon 200 group has non-significant negative correlations between the overall proportion of CAA and severity of CAA which suggests the relationship may be different in cases with mutations post-codon 200 (Figure 5-5 A,B) although these small group sizes and lack of significance restricts interpretations.

5.5.2.2 *Disease duration*

Regression analysis adjusted for mutation sub-group and *APOE4* status revealed no evidence for an association between the overall proportion of cortical CAA and

disease duration, with -0.05 years decrease in disease duration for each percentage point increase in cortical CAA (p=0.19, 95% CI: -0.12 - 0.02). Similarly, there was no evidence for an association between the overall proportion of leptomeningeal CAA and disease duration, with -0.02 years decrease in disease duration for each percentage point increase leptomeningeal CAA (p=0.43, 95% CI: -0.06 - 0.03).

In agreement, the extended cohort had no significant correlations between the overall proportion of cortical and leptomeningeal CAA and disease duration. However, in the mutation sub-groups significant correlations were observed for the different severities of CAA. In the *PSEN1* post-codon 200 group, severe cortical CAA was positively correlated with disease duration and mild CAA was nearly significantly negatively correlated with disease duration (p=0.03, p=0.06). In the *APP* group, the overall proportion of CAA, and mild cortical CAA, were significantly negatively correlated with disease duration (p=0.02, p=0.05). Observation of the direction of correlations between CAA and disease duration suggests there are group differences, with the *PSEN1* pre-codon 200 group having positive correlations while the *PSEN1* post-codon 200 and *APP* groups display some negative but often weak correlations (Figure 5-5 C,D).

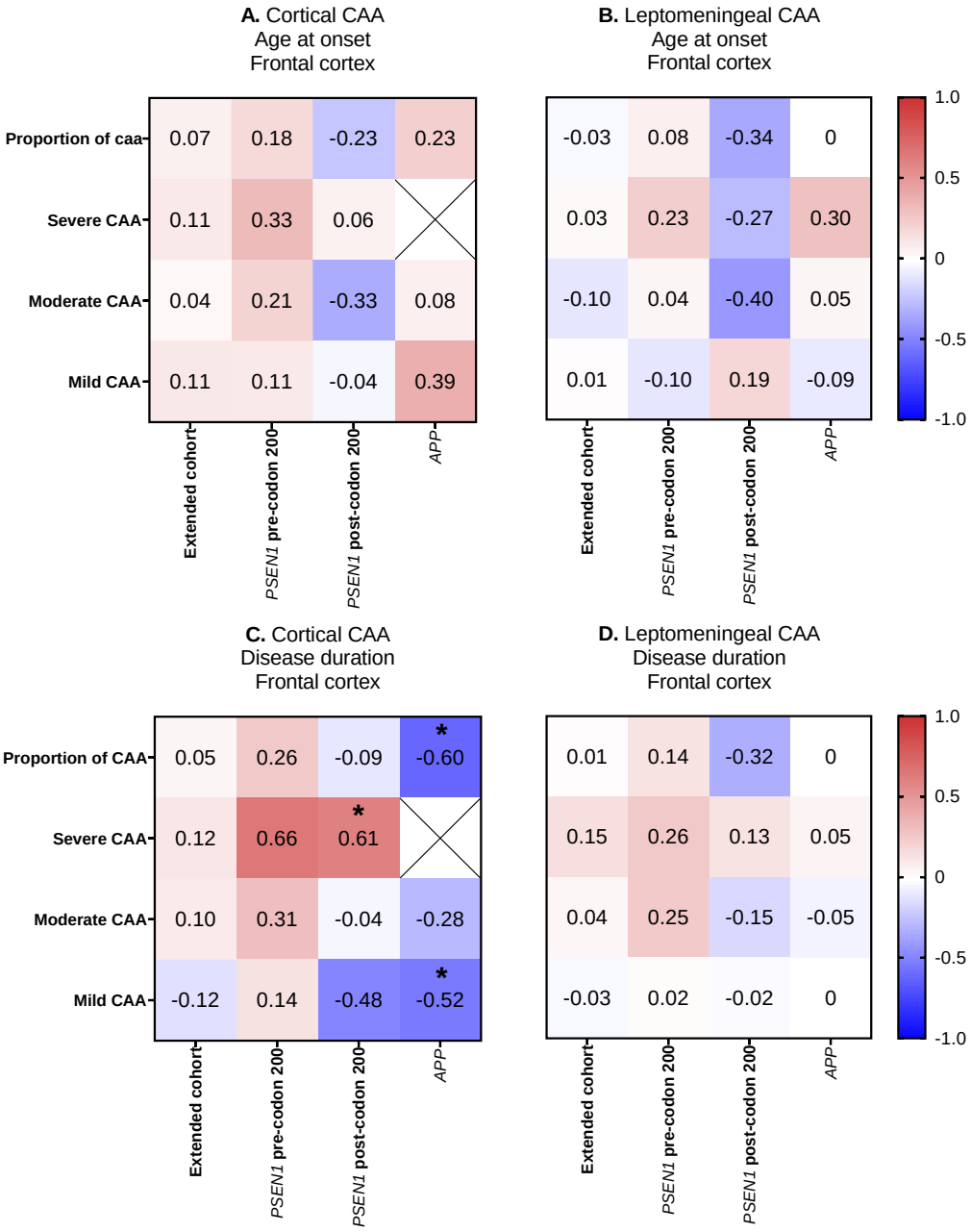

Figure 5-5 Correlation between CAA and clinical data.

A, B: No significant correlations between cortical and leptomeningeal CAA and age at onset in the frontal cortex. C. Significant correlation between disease duration and severe cortical CAA in the *PSEN1* post-codon 200 group (p=0.03) and between disease duration and the overall proportion of CAA and of mild CAA in the *APP* group (p=0.02, p=0.05). D. No significant correlations between leptomeningeal CAA and disease duration in the frontal cortex. Crossed squares represent no data due to no severe cortical CAA in the *APP* mutation group. Data presented in heat maps are τ_b correlation coefficients, Kendall's tau-b, *p<.05.

5.5.3 *Comparing the proportion and severity of CAA between mutation sub-groups in the frontal cortex*

Differences in CAA due to mutation location were assessed by comparing mutation sub-groups. There was a general trend for higher CAA in the *PSEN1* post-codon 200 group and lower CAA in the *APP* group, although large variance can be observed. Within the cortex there were significant differences in the overall proportion of CAA (p=0.02, Kruskal-Wallis) with higher CAA in the *PSEN1* post-codon 200 group compared to the *PSEN1* pre-codon 200 and *APP* groups (p=0.04, p=0.02, Dunn's test). Moderate cortical CAA was significantly different across groups (p=0.01) with higher CAA in the *PSEN1* post-codon 200 group compared to the *PSEN1* pre-codon 200 and *APP* groups (p=0.05, p=0.007). There were no significant differences in the leptomeninges. The average overall proportion and severity of CAA was consistently higher in the leptomeninges compared to the cortex (Figure 5-6).

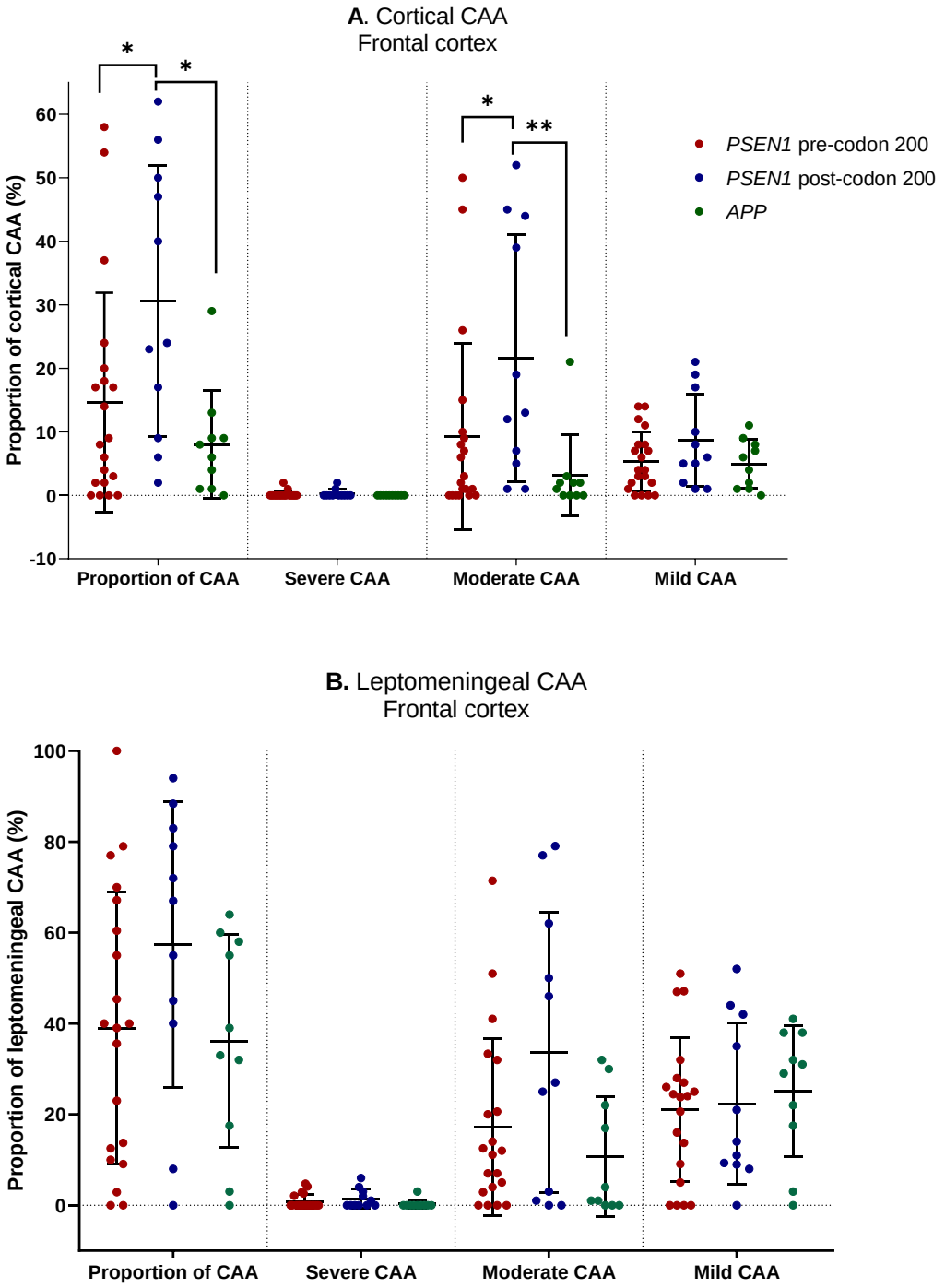

Figure 5-6 Comparison of the proportion and severity of CAA by mutation sub-group.

A: The proportion of cortical CAA was significantly different across groups (p=0.02; *PSEN1* post-codon 200 vs *PSEN1* pre-codon 200 and vs *APP*, p=0.04, p=0.02). Severe cortical CAA was significantly different between groups (p=0.01, *PSEN1* post-codon 200 vs *PSEN1* pre-codon 200 and vs *APP*, p=0.05, p=0.007). B: There were no significant differences in leptomeningeal CAA. Error bars represent mean and SD, Kruskal-Wallis with Dunn's test, *p<.05, **p<.01.

5.5.4 *Comparing the proportion and severity of CAA by APOE genotype in the frontal cortex*

In the extended pathology cohort of 41 cases, 38 cases had an *APOE* genotype available and these were used to investigate the relationship between *APOE* and CAA in FAD. When comparing CAA by *APOE*4 status (carriers and non-carriers), there were no significant differences except that severe leptomeningeal CAA was significantly higher in *APOE*4 carriers compared to non-carriers (p=0.004) (Figure 5-7).

CAA was then compared between specific *APOE* allele genotypes (2/3, 3/3, 3/4, 4/4). In general, there was a pattern for less CAA and lower severity of CAA in *APOE* 3/3 carriers compared to the other genotypes, although large variance could be observed. Specifically, there were significant differences in severe cortical CAA (p=0.05), with near significant higher CAA in the 2/3 compared to the 3/3 genotype (p=0.07). However, the very small 2/3 genotype group size (n=2) necessitates extreme caution. Severe leptomeningeal CAA also significantly differed (p=0.02), with higher CAA in the *APOE* 3/4 genotype compared to the 3/3 genotype (p=0.008) (Figure 5-8).

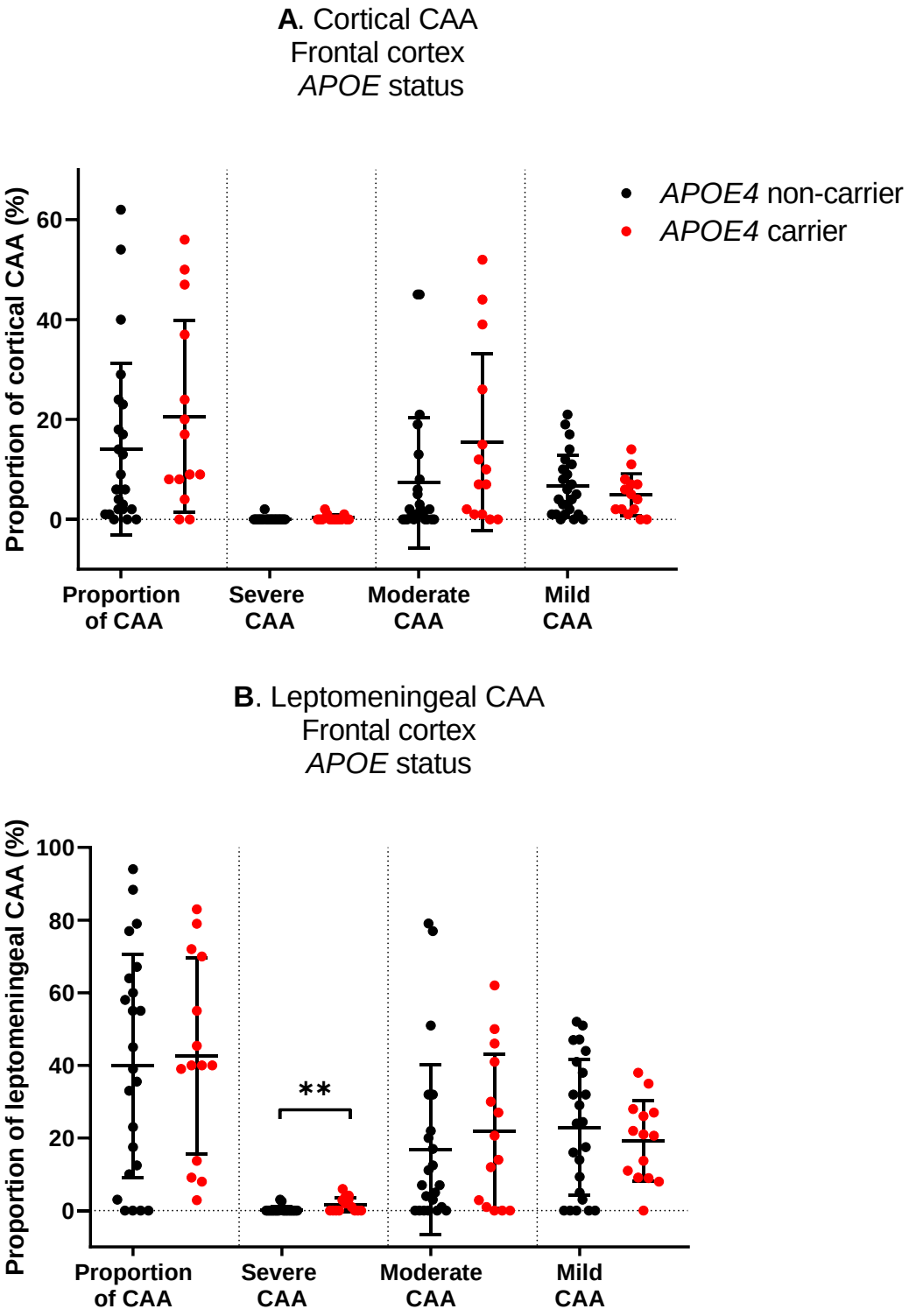

Figure 5-7 Comparison of the proportion and severity of CAA by *APOE4* status.

A: Cortical CAA was not significantly different between *APOE*4 carriers and non-carriers. B: Severe leptomeningeal CAA was significantly higher in *APOE*4 carriers compared to non-carriers (p=0.004, Ranksum), **p<0.01. Error bars represent mean and SD.

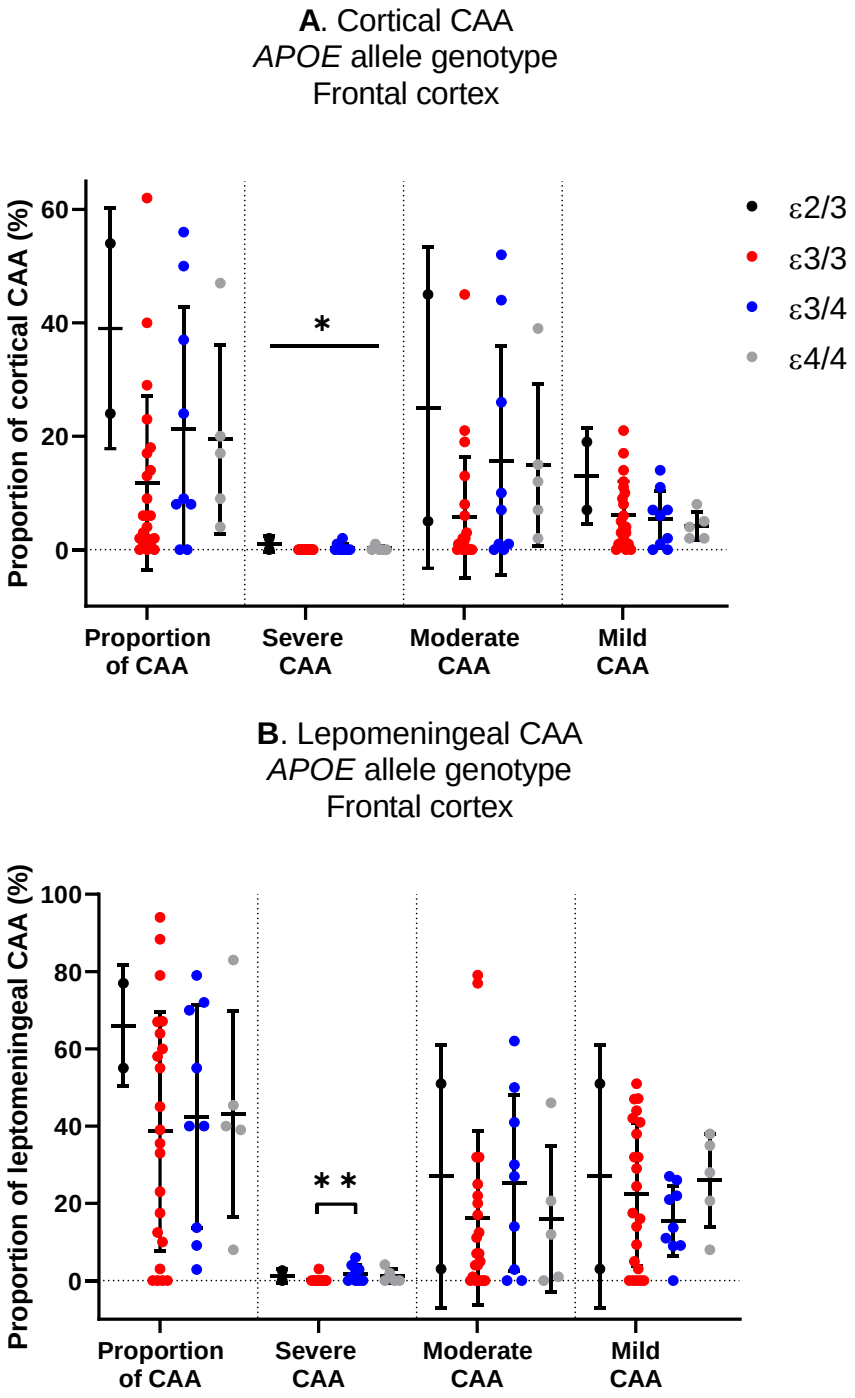

Figure 5-8 Comparison of the proportion and severity of CAA by *APOE* allele genotype.

A: Severe cortical CAA was significantly different across groups (p=0.05, Kruskal-Wallis). B: Severe leptomeningeal CAA was significantly different across groups (p=0.02) with greater severe CAA in *APOE*3/4 carriers compared to *APOE*3/3 carriers (p=0.008, Dunn's test). Error bars represent mean and SD, *p<0.05, **p<0.01.

5.5.5 *Proportion and severity of CAA and clinical data in the occipital cortex*

It has been shown that CAA predominately affects the occipital cortex, therefore this region was also assessed in the extended cohort. Associations between age at onset and proportion and severity of CAA were investigated. Again, exploratory analysis of the data highlighted that some of the severity measures did not meet the required assumptions for regression analysis. Therefore, while regression could be presented for the proportion of CAA, to maintain consistency in analysis, a correlation method has been used and presented for all measures of CAA.

5.5.5.1 *Age at onset*

In the extended cohort regression analysis was conducted to test whether the proportion of CAA was associated with age at onset, adjusted for mutation sub-group and *APOE* status (n=38). There was no evidence for an association, with 0.006 years increase in age at onset for each percentage point increase in the overall proportion of cortical CAA (p=0.90, 95% CI: -0.08 – 0.09). Similarly, there was no evidence for an association between the overall proportion of leptomeningeal CAA and age at onset, with -0.07 years decrease in age at onset for each percentage point increase in the overall proportion of leptomeningeal CAA (p=0.06, 95% CI: -0.15 -0.003).

In the extended cohort, the overall proportion and severity of cortical CAA did not correlate with age at onset. Within the mutation sub-groups, severe cortical CAA significantly correlated with age at onset in the *PSEN1* post-codon 200 group (p=0.04), although this was likely driven by a few cases, and not representative of the whole group (Appendix, Figure 9-5 E). Additionally, the overall proportion and severity of leptomeningeal CAA did not correlate with age at onset. Within the mutation groups, there was a significant negative correlation between mild leptomeningeal CAA and age at onset in the *APP* group (p=0.04) with a negative correlation seen across all groups. Generally, the strength of correlations were weak, indicating that CAA was not associated with age at onset in this cohort (Figure 5-9 A,B).

5.5.5.2 *Disease duration*

In the extended cohort, regression analysis was also conducted to test whether the proportion of CAA was associated with disease duration, adjusted for

mutation sub-group and *APOE* status (n=38). There was no evidence for an association, with a 0.006 years increase in disease duration for each percentage point increase in the overall proportion of cortical CAA (p=0.81, 95% CI: -0.04 – 0.06). Similarly, there was no evidence for an association between the overall proportion of leptomeningeal CAA and disease duration, with 0.006 years increase in disease duration for each percentage point increase in the overall proportion of leptomeningeal CAA (p=0.80, 95% CI: -0.04 - 0.05).

The overall proportion and severity of cortical CAA pathology was also analysed by correlation. In the extended cohort, the overall proportion of cortical CAA and severe cortical CAA positively correlated with disease duration (p=0.04, p=0.04) and moderate cortical CAA showed a trend towards positive correlation (p=0.07). Analysis by individual mutation subgroup showed the *PSEN1* pre-codon 200 group had a positive correlation between the overall proportion of cortical CAA and severe cortical CAA with disease duration (p=0.04, p=0.05), moderate CAA followed this trend (p=0.08) (Figure 5-9 C). While these correlations contrast with the regression analyses, they are only of moderate strength and do not take into account *APOE4* status, which could affect the associations

The overall proportion and severity of leptomeningeal CAA did not correlate with disease duration in the extended cohort, while mutation sub-group analysis showed the *PSEN1* post-codon 200 group had a near significant negative correlation between mild leptomeningeal CAA and disease duration (p=0.06) and oppositely, the *APP* group had a significant positive correlation between mild leptomeningeal CAA and disease duration (p=0.04) (Figure 5-9 D).

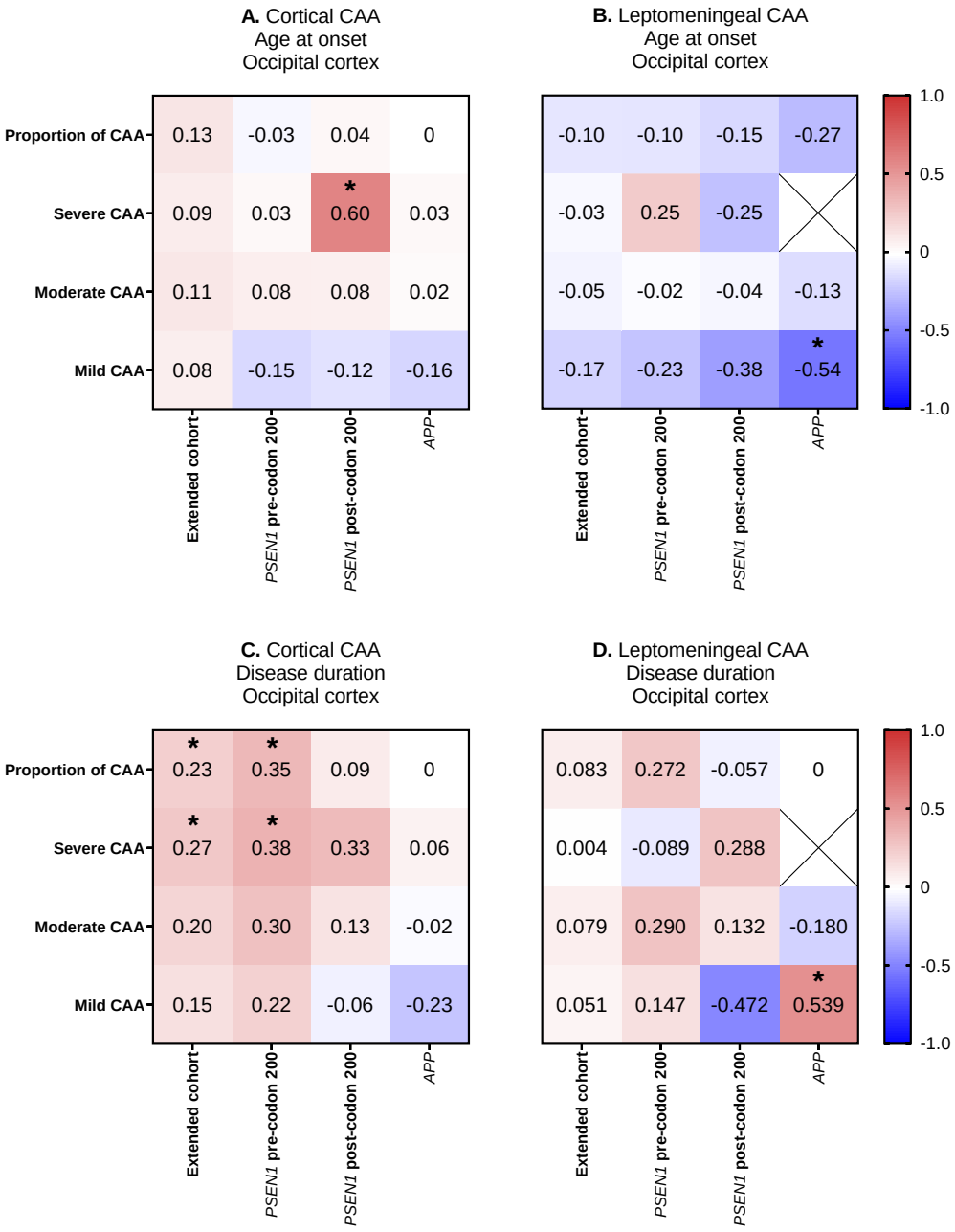

Figure 5-9 CAA and clinical data in the occipital cortex.

A: Severe CAA correlates with age at onset in the extended cohort in the *PSEN1* post-codon 200 group (p=0.04). B: Mild leptomeningeal CAA negatively correlates with age at onset in the *APP* group (p=0.04). C: The overall proportion of cortical CAA and severe cortical CAA positively correlated with disease duration in the extended cohort (p=0.04, p=0.04). The overall proportion of cortical CAA and severe cortical CAA positively correlated with disease duration in the *PSEN1* pre-codon 200 group (p=0.04, p=0.05). D: In the *APP* group mild leptomeningeal CAA significantly positively correlated with disease duration (p=0.04). Crossed squares represent no data due to no severe leptomeningeal CAA in the *APP* mutation group. Data presented in heat maps are τ_b correlation coefficients, Kendall's tau-b, *p<0.05.

5.5.6 *Comparing the proportion of CAA between mutation sub-groups in the occipital cortex*

In the extended cohort, 95% of cases had some degree of cortical CAA and 100% of cases had some degree of leptomeningeal CAA in occipital cortex. Regression analysis on CAA and the effect of mutation subgroup was not possible as assumptions were not met. In view of this, Kruskal-Wallis test with Dunn's test where appropriate has been used to compare between mutation groups.

Cortical CAA

The proportion and severity of cortical CAA was compared between mutation groups. There was a significant difference in the overall proportion of CAA (p=0.05) with *PSEN1* pre-codon 200 group having a significantly lower proportion compared to the *PSEN1* post-codon 200 group (p=0.02). Moderate CAA significantly differed between groups (p=0.04), with pairwise comparisons showing significantly higher moderate CAA in the *PSEN1* post-codon 200 group compared to the *PSEN1* pre-codon 200 group and a near significant higher proportion than the *APP* group (p=0.02 & p=0.07). Mild CAA was significantly different across the groups (p=0.05), with the *PSEN1* pre codon-200 group having significantly lower mild CAA than the *APP* group (p=0.05) (Figure 5-10 A).

Leptomeningeal CAA

There were no significant differences in the overall proportion of leptomeningeal CAA between groups. There was a near significant difference in severe leptomeningeal CAA (p=0.06), however this appears to be driven by one case. The observed average proportion and severity of CAA was consistently higher in the leptomeninges compared to the cortex (Figure 5-10 B).

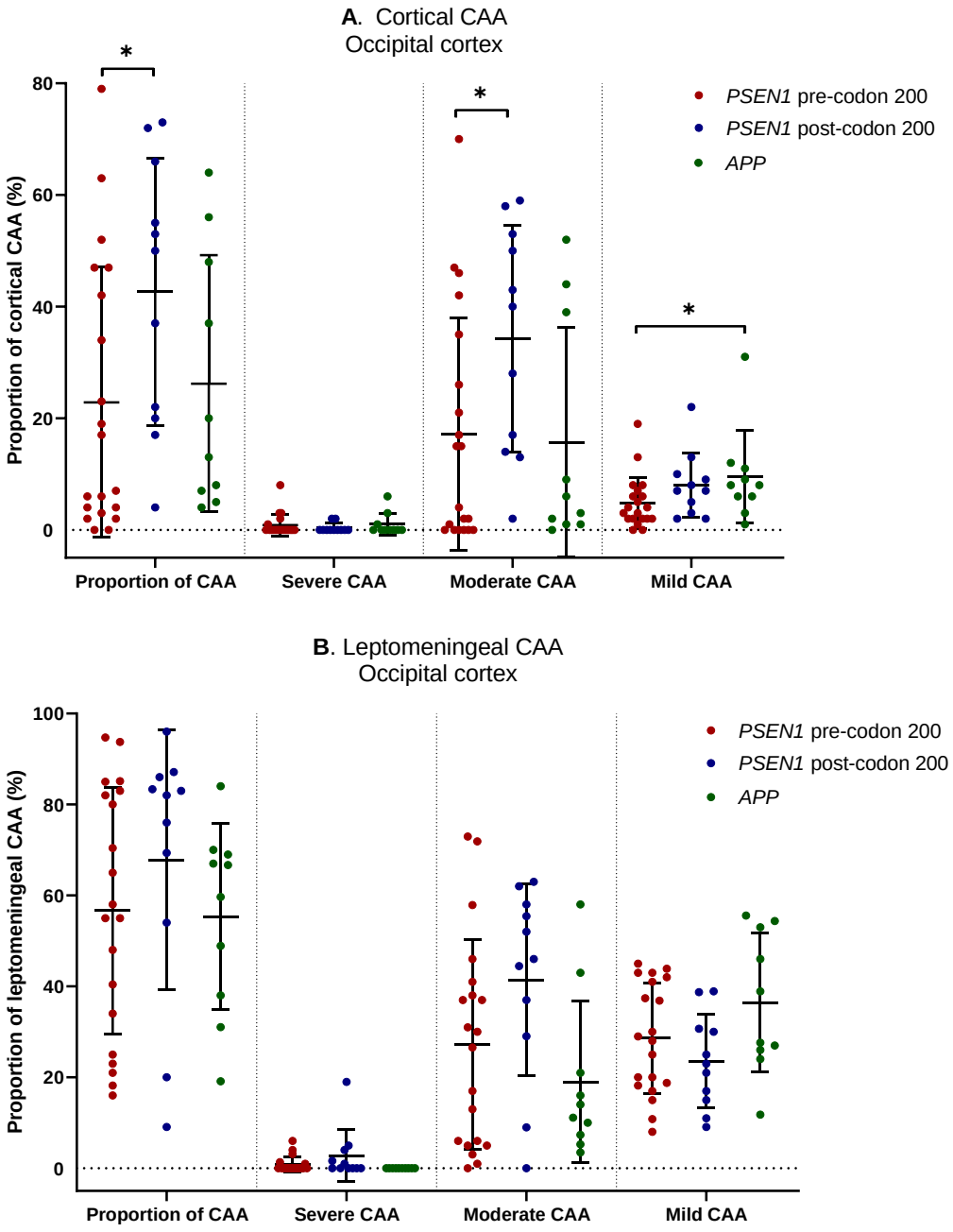

Figure 5-10 Comparison of the overall proportion and severity of CAA between mutation subgroups.

A: Cortical CAA in the Occipital cortex by mutation groups. There was a significant difference in the overall proportion of CAA (p=0.05; *PSEN1* pre-codon 200 vs *PSEN1* post-codon 200 p=0.02). Moderate CAA significantly differed between groups (p=0.04; *PSEN1* post-codon 200 vs *PSEN1* pre-codon 200 p=0.02). Mild CAA was significantly different across the groups (p=0.05; *PSEN1* pre codon-200 vs *APP* p=0.05). B: Leptomeningeal CAA in the occipital cortex by mutation groups. Error bars represent mean and SD. Kruskal-Wallis with Dunn's test, *p<0.05.

5.5.7 *Comparing the proportion of CAA by APOE genotype in the occipital cortex*

From the extended pathology cohort of 41 cases, 38 cases had an *APOE* genotype available and these were used to investigate the effect of *APOE* status on CAA in FAD.

We compared the overall proportion and severity of CAA between *APOE4* status groups (ε4 carriers and non-carriers). The overall proportion of CAA and severe and moderate CAA was consistently higher in APOE4 carriers in the cortex and leptomeninges, however there was no statistically significant difference (Figure 5-11 A,B).

Due to higher numbers in the extended cohort, differences between specific *APOE* allele genotypes were then investigated (e.g *APOE* 2/3, 3/3, 3/4 and 4/4). Between *APOE* allele genotypes, we found a significant difference in the overall proportion of cortical CAA (p=0.02) with higher CAA in 2/3 carriers compared to 3/3 carriers (p=0.03). Significant differences were also observed for severe cortical CAA (p=0.01) with higher CAA in 2/3 carriers compared to 3/3 carriers (p=0.02), there was a suggestion of differences in severe cortical CAA between other *APOE* allele genotypes with higher CAA in 2/3 compared to 3/4 carriers (p=0.08) and 4/4 compared to 3/3 carriers (p=0.08). Moderate cortical CAA also significantly differed between groups (p=0.02) with higher CAA in 2/3 compared to 3/3 carriers (p=0.03). No other significant differences were observed for cortical or leptomeningeal CAA. As there are only 2 cases with a 2/3 allele these results should be interpreted with extreme caution and require replication in larger cohorts. Interestingly, it was observed that the overall proportion of CAA and severe and moderate CAA in the cortex and leptomeninges increases with increasing ε4 allele (APOE genotype 3/3 through to 4/4) although there were no statistically significant difference (Figure 5-12 A,B).

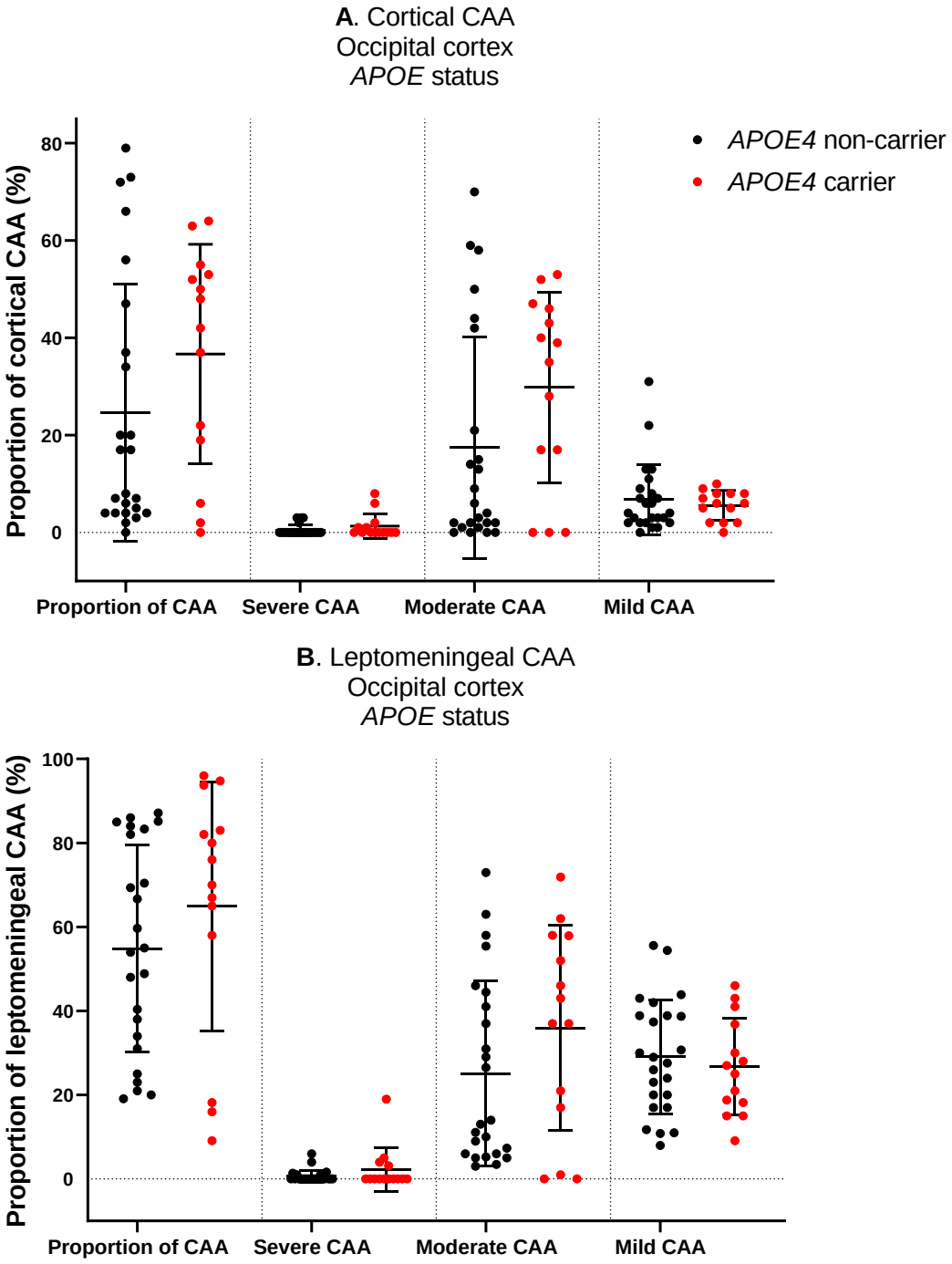

Figure 5-11 Comparison of the overall proportion and severity of CAA between *APOE*4 allele carriers and non-carriers in the occipital cortex.

There were no significant differences in the overall proportion and severity of cortical (A) or leptomeningeal (B) CAA between *APOE*4 carriers and non-carriers (ranksum).Error bars represent mean and SD.

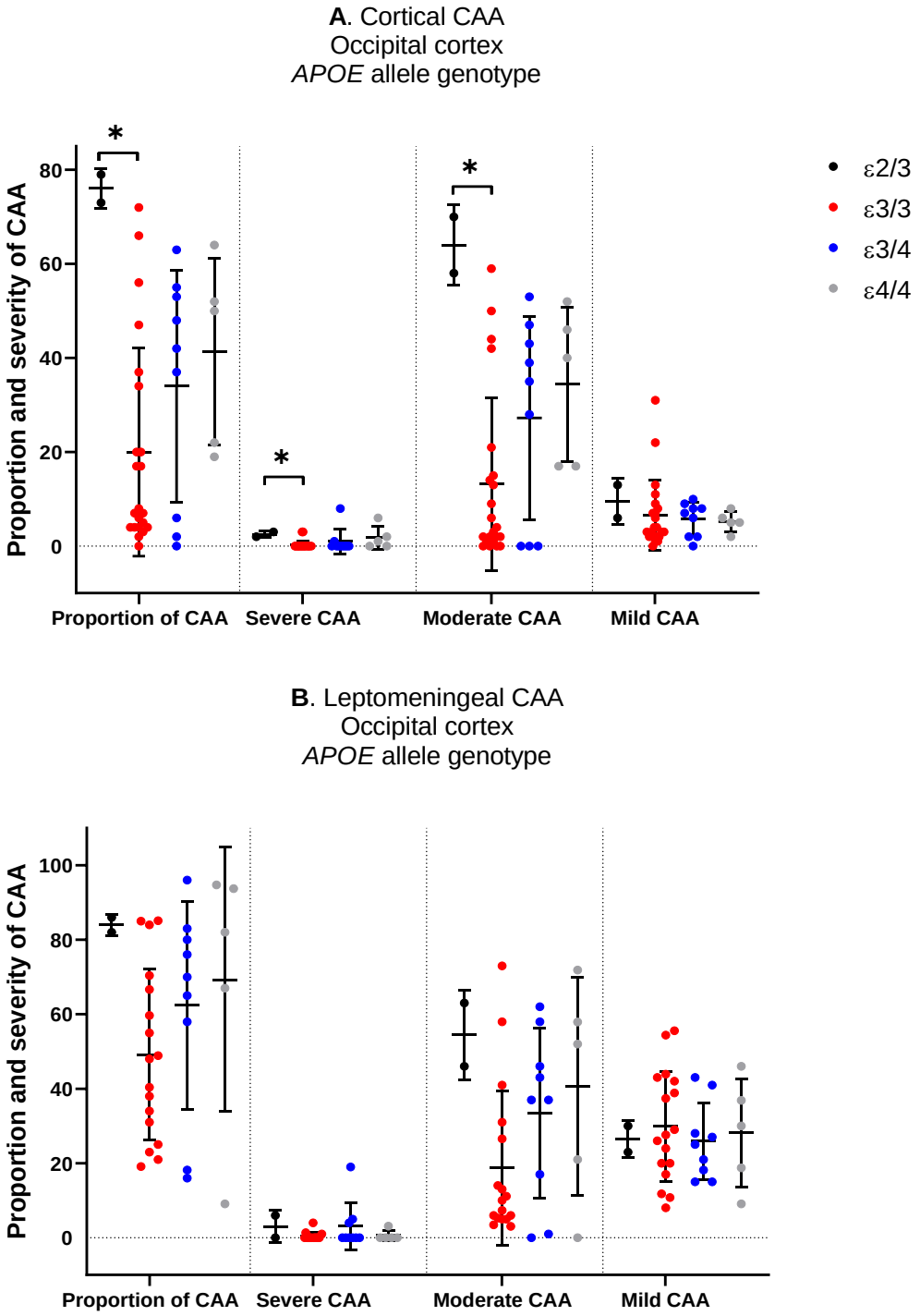

Figure 5-12 Comparison of the overall proportion and severity of CAA between *APOE* allele genotype in the occipital cortex.

A: The overall proportion of CAA significantly differs between groups (p=0.02; 2/3 vs 3/3 p=0.03). Severe cortical CAA was significantly different between groups (p=.01; 2/3 v 3/3 p=0.02) as was moderate CAA (p=0.02; 2/3 v 3/3 p=0.03). B: There were no significant differences between *APOE* genotype in leptomeningeal CAA. Error bars represent mean and SD. Kruskal-Wallis with Dunn's test, *p<0.05.

5.5.8 *Comparing the proportion of CAA in the frontal and occipital cortices*

As expected, the overall proportion of cortical CAA was numerically higher in the occipital cortex compared to the frontal cortex (28.99 ± 24.78 vs 17.29 ± 18.55) and this remained true for the different severities of CAA (Severe: 0.76 ± 1.71 vs 0.15 ± 0.48 Moderate: 21.39 ± 21.61 vs 11.05 ± 15.94. Mild: 6.83 ± 6.16 vs 6.10 ± 5.42).

The overall proportion of leptomeningeal CAA was also numerically higher in the occipital lobe compared to the frontal cortex (59.31 ± 25.98 vs 43.23 ± 29.55) and this was true for the different severities of CAA (Severe: 1.12 ± 3.23 vs 0.86 ± 1.61. Moderate: 29.03 ± 22.46 vs 20.05 ± 23.11. Mild: 29.16 ± 13.09 vs 22.36 ± 15.74).

5.6 **Chapter discussion**

	Main findings
Overall proportion and severity of CAA and CERAD scores	Trends for a negative correlation between the overall proportion and severity of cortical and leptomeningeal CAA with cored plaques, and a positive correlation with CWPs.
Overall proportion and severity CAA and Aβ load	Trends for a positive correlation between the overall proportion of CAA, severe CAA and moderate CAA, in both the cortex and leptomeninges, with Aβ load.
Overall proportion and severity of CAA and Microglial load	The overall proportion and severity of cortical and leptomeningeal CAA was generally; 1) Negatively correlated with IBA1 and positively correlated with CD68 except in the *PSEN1* post-codon 200 group. 2) Negatively correlated with CR3/43
Clinical overview	FAD mutation associated with both age at onset and disease duration, although sex did not. *APOE* genotype was significantly associated with disease duration only.
Overall proportion and severity of CAA by mutation groups	Significant trends for greater overall proportion and severity of cortical and leptomeningeal in the *PSEN1* post-codon 200 group.

Overall proportion and severity of CAA by APOE genotypes	Non-significant trend for greater overall proportion and severity of cortical and leptomeningeal CAA in *APOE*4 carriers, and in *APOE*2 carriers.

In this study we investigated associations between CAA and pathological, clinical and genetic aspects of FAD. In the frontal cortex, the association between both the overall proportion and severity of CAA and Aβ plaque pathology and load was investigated in the QSBB cohort as a whole and by mutation subgroups. Additionally, in the frontal cortex, the association between both the overall proportion and severity of CAA and the load of three microglial phenotypes were investigated in the QSBB cohort as a whole and by mutation subgroups. Finally, in both the frontal and occipital cortices of the larger extended cohort the overall proportion and severity of CAA was further investigated in relation to clinical and genetic aspects of FAD.

Frontal cortex CAA and Aβ pathology

CAA was measured by vessel counts and this was analysed in relation to the Aβ and microglial pathology discussed in chapter 3: Aβ pathology in FAD and chapter 4: Microglial response in FAD. While the previously assessed CERAD scoring included a frequency score of cortical and leptomeningeal CAA, the vessel count measure enabled a more detailed investigation and may reveal further possible associations.

In the QSBB cohort, the overall proportion of CAA was not significantly associated with the amount of Aβ, however there was a trend for increasing proportion and severity of CAA with increasing Aβ load/pathology (Chapter: 5.3.3). This suggests that with greater Aβ levels, CAA is exacerbated, likely as a result of deposition in the vasculature due to clearance attempts. As a consequence, clearance may be reduced due to pathway disruption, leading to increased cortical deposition. Associations between greater CAA and Aβ deposition has been previously shown (Brenowitz *et al.*, 2015; Pfeifer *et al.*, 2002). The negative association between Aβ load and mild CAA also supports that worse CAA is associated with greater Aβ pathology as it implies a shift from mild to more severe CAA. Interestingly, the negative association between mild CAA was not seen in the *APP* group, suggestive of group differences, although small group numbers affect

interpretations. It may also be due to the *APP* group having the lowest average proportion and severity of CAA, in which case, association with mild CAA in this group may be reflective of worse CAA in a less CAA prone group.

To further understand the association between CAA and Aβ, correlations between the proportion and severity of CAA and CERAD scores were assessed in the QSBB cohort (Chapter: 5.3.2). Previously in chapter 3: Aβ pathology in FAD, CERAD measures of CAA positively correlated with CWPs and this was replicated using vessel counts. CWP's have been frequently observed to co-occur with CAA (Crook *et al.*, 1998; Niwa *et al.*, 2013; Ryan *et al.*, 2015a) and these repeated statistically significant associations and trends strengthen the plausibility of the association, particularly as the vessel counts provide greater detail on the severity of CAA. While an association has been demonstrated, the molecular connection between these pathologies is unclear, particularly as the different pathologies are primarily composed of different Aβ isoforms. As mentioned, CAA is primarily composed of Aβ40, while CWPs are primarily composed of Aβ42. However, Aβ42 is observed in both vessels and CWPs, which may link the pathologies. Further analysis investigating the precise make up of CAA in CWP positive cases would help to understand the association. Although not statistically significant, it was noted that CAA was generally negatively associated with cored plaques. This could raise the possibility of a negative association between these two types of Aβ pathology, however, it was also seen in chapter 3 that CWPs and cored plaques were negatively correlated, therefore the association with CAA could be a consequence of multicollinearity. Increased CAA has however been associated with plaque clearance in immunized AD cases. In particular, Aβ40 was noted to be higher in the cerebrovasculature in these cases, along with a decreased Aβ load in the parenchyma. Evidence suggests cored plaques are composed of both Aβ40 and Aβ42, therefore there may indeed be a negative association between these pathologies in high CAA cases (Boche *et al.*, 2008).

<u>CAA and microglia</u>

Assessing microglial load with the proportion and severity of CAA enabled a more detailed investigation of the associations (Chapter: 5.4). In the QSBB cohort as a whole and in the individual mutation subgroups, Iba1 was negatively associated

with more severe CAA although this was not significant. Associations were positive for mild CAA, which may indicate a change in interaction, although it is not possible to infer whether microglia would influence CAA or CAA would influence microglia.

Similar to findings in chapter: 4.3.6, CD68 and CAA were generally positively correlated, potentially indicating that a phagocytic phenotype may benefit the removal of Aβ via clearance mechanisms. Ultimately this increased Aβ in the vasculature may lead to further deposition and increased CAA severity. Increased CAA upon plaque removal has been observed in human and mouse models (Donna M. Wilcock *et al.*, 2004; Zotova *et al.*, 2013b).

For both Iba1 and CD68 in the *PSEN1* post-codon 200 group we see opposite correlations between Iba1 and CD68 with CAA. This group did not differ in microglial load or have differing correlations between Iba1 and CD68 compared to the remaining groups (see chapter: 4.3.4 and 4.3.5). This suggests the differences may be due to associations with CAA, which was highest in this group. This again could indicate a difference in microglial phenotype in relation to severity of CAA. These associations are non-significant however so assumptions should not be made. Indeed, a lack of association with microglial markers and CAA has previously been observed (Zotova *et al.*, 2013b).

As observed in chapter: 4.3.6.1, CR3/43 was negatively associated with CAA, although this was not significant. It does however suggest proinflammatory response may not increase CAA. Interestingly, CR3/43 was also weakly but non-significantly, negatively correlated with Aβ load (see chapter: 4.3.6.2 and 4.3.6.3). Therefore in cases with a CR3/43+ve microglial phenotype, both cortical and vessel Aβ may be reduced. This could be due to CR3/43+ve microglia promoting mechanisms which cause reduced Aβ load, such as Aβ degrading enzymes. This way, clearance via vascular routes may be reduced or the degraded Aβ in a non-aggregation prone state, therefore cleared efficiently.

Interestingly CR3/43 was positively associated with CWPs. However CWPs were positively associated with CAA. As CAA and CWPs are composed of different Aβ isoforms, the association of these with CR3/43+ve microglia and CAA may be Aβ isoform dependent. Differences in immune cell responses to Aβ40/42 isoforms

has been previously seen in immune cell lines (Morelli *et al.*, 1999) although associations are not always found (Garção *et al.*, 2006). In human tissue, analysis has revealed a preference of microglia for plaques containing Aβ40 (Fukumoto *et al.*, 1996a; D. M. A. Mann *et al.*, 1995). These studies suggest there are microglial specific responses to Aβ isoforms which could influence Aβ and CAA pathology in our cohort.

The different direction of associations depending on marker indicates that differences in microglial phenotype or activity may associate with CAA. Alternatively, the method of analysis may influence results due to effects of morphology. As mentioned, phagocytic microglia are associated with a rounded and condensed morphology. Therefore decreased Iba1 may be related to a decrease in cell surface coverage due to morphological change. To counteract this problem, the measurement of microglial circularity could be employed, where the microglia are measured by their morphology. This may produce results more reflective of microglial activity. However, the majority of correlations were not significant, and the discussion is based trends in the data which must be considered with caution. The results may however be helpful for guiding future research.

Clinical analysis

As CAA is predominant in the occipital cortex, we extended our CAA analysis into this region in a larger cohort (Chapter: 5.5.1). With this larger cohort, clinical analysis could be conducted to see if previous findings remained in a larger cohort. After adjustment for *APOE* status and sex, age at onset was again confirmed to be associated with mutation, and more mutation-specific associations with age at onset were found. This confirms and expands the earlier findings in chapter 3, and what has previously been noted by others, highlighting the importance of genetic mutation on influencing the manifestation of disease. In our data, some of the cases are from the same family, and it has been shown that family membership also accounts for some of the variance in age at onset in FAD, in addition to mutation (Ryan *et al.*, 2016; Ryman *et al.*, 2014). In the current study, there were only a few related cases so numbers were too small to investigate influence of family membership on the results, although the

contribution was likely to be minimal. In larger cohorts it will be necessary to consider the effects of family membership and specific mutation.

In this larger cohort we also found mutation associated differences in disease duration, after adjustment sex and *APOE* status (Chapter: 5.5.1). These results suggest that specific mutations are linked to a less aggressive disease course. Longest duration was observed in the group with the latest onset, implying those with later onset also may have a less aggressive disease progression. This differs to that observed in a separate study where longer duration was associated with earlier onset in a sAD/FAD mixed cohort (Armstrong, 2014). However, linear regression showed that there was no association between age at onset and disease duration in our cohort (5.5.1.3). Previous studies have also failed to show associations, although Ryman *et al.* (2014) found an inverted U shape association in a large sample of FAD cases, whereby individuals with the earliest and latest ages at onset had the shortest disease durations. It would be useful to investigate this relationship in this cohort and other non-linear relationships between the two, with adjustment for known modifiers such as *APOE*.

After adjustment for sex and mutation*, APOE* genotype was not associated with age at onset (Chapter: 5.5.1), which has been shown previously in FAD (Ryman *et al.*, 2014). However, there are studies which have found evidence to suggest *APOE*4 is associated with a younger age at onset in a *PSEN1* intron4 cohort (Janssen *et al.*, 2000). *APOE*4 and age at onset has been discussed in chapter: 1.14.

The role of *APOE* genotype as a modifier of disease duration in FAD was confirmed in this larger cohort. While the result is surprising, as discussed in chapter: 3.4, it has previously been alluded to in sAD (Basun *et al.*, 1995). While we showed that one *APOE*4 allele lead to significantly longer disease duration compared to no *APOE*4 allele, the increase in duration was not significantly different between hetero or homozygous *APOE*4 carriers, although this may be due to small numbers of *APOE*4 homozygotes. The mechanism by which *APOE4* could be associated with longer disease duration is unclear, although as our results imply, it is not a consequence of earlier age at onset. Meta-analysis in sAD suggest *APOE*4 does not influence disease duration (Allan & Ebmeier, 2011). There is little literature specifically on *APOE* effects on disease duration,

with a greater focus on age at onset or disease progression. In some instances age at death is considered. However, this measure is only indicative of duration if the age at onset is taken in to account. It may be beneficial for future studies to consider disease duration, mutation and *APOE*4 genotype in FAD studies. A potential further analysis could be to include age at onset in the regression and see if the association between *APOE*4 and disease duration remains. This is particularly important as APOE directed therapies are likely to be investigated due to the recent report of a protective effect of the *APOE* christchurch mutation, which was found in a *PSEN1* E280A mutation carrier, with a homozygous christchurch *APOE*3/3 genotype, who did not develop cognitive impairment until several decades later than the typical age at onset for her family (Arboleda-Velasquez *et al.*, 2019).

Why *APOE*4 status would give rise to longer duration is unclear. As seen in multiple studies, *APOE4* associates with increased Aβ deposition. Possibly, this may reduce toxic soluble Aβ and its downstream consequences. It is also important to note the age difference in our cohort compared to sAD cases. *APOE*4 status has been shown to have differing effects depending on factors including age, therefore the benefit of *APOE*4 may only be relevant in FAD and potentially early onset non-familial AD (J. Kim *et al.*, 2018). This may be despite earlier Aβ deposition in FAD *APOE*4 carriers (Bussy *et al.*, 2019). APOE is involved in immune/inflammatory mechanisms and microglia are known to differ over age and disease (Sankowski *et al.*, 2019), in FAD the microglia may be at a stage where response can be more beneficial rather than reduced. *APOE*4 is also associated with CAA-related inflammation and may link to benefits due to clearance. It is possible that these factors may have some beneficial effects in FAD regarding the response to Aβ.

The sex effect on age at onset observed in chapter: 3.3.2 was not confirmed in the extended cohort (Chapter: 5.5.1). The difference may be due to case numbers, as larger studies have also shown no association between age at onset and sex in FAD (Ryman *et al.*, 2014). One potential confounder in age at onset assessment is that there may be differences in clinical assessment due to variation in presentation (Koedam *et al.*, 2010) and/or sex (Liesinger *et al.*, 2018). These factors will be hard to prevent as they are dependent on the individual patient. Overall, we found that sex is likely not a strong contributor to age at onset

in this FAD cohort. With this in mind it is promising to see the retention of the remaining associations we found, for example with genetic mutation and *APOE* genotype.

CAA and clinical data

CAA is a frequent pathological feature of AD but its relationship to the clinical manifestation of disease is unclear. We were able to investigate the hypothesis that CAA severity may be related to age at onset and/or disease duration in the QSBB cohort and in the extended cohort, considering difference between regions due to their specific associations with CAA (Chapter: 5.5.2 and 5.5.5).

Overall, our results revealed that CAA was not clearly associated with age at onset or disease duration and this was observed in the QSBB and extended cohort (Chapters: 5.3.1, 5.5.2 and 5.5.5. Differences in direction of association were noted between groups, however were often non-significant and do not confirm any mutation group differences. Interestingly, the directional differences were noted in the *PSEN1* post-codon 200 group, with negative associations between severe cortical CAA, the overall proportion of leptomeningeal CAA, severe and moderate leptomeningeal CAA with age at onset. Additionally, severe cortical CAA and disease duration were positively correlated while the proportion of leptomeningeal CAA overall, severe and moderate leptomeningeal CAA were negatively associated with disease duration. This group had the highest average CAA, and may hint towards stronger associations when CAA is more severe.

The extended cohort analysis within the frontal cortex also indicated that there were few strong, significant or consistent associations between CAA and clinical data. Similar trends were observed to the QSBB analysis but decreased strength of correlation was noted. There were however some significant correlations. In the frontal cortex, severe cortical CAA was significantly positively correlated with disease duration in the *PSEN1* post-codon 200 group, while the overall proportion of CAA and mild CAA were significantly negatively correlated with disease duration in the *APP* group. In the occipital cortex, severe cortical CAA was significantly positively correlated with age at onset in the *PSEN1* post-codon 200 group, while mild CAA was significantly negatively correlated with age at onset in the *APP* group. In the occipital cortex, disease duration was significantly

positively correlated with the overall proportion of cortical CAA and severe CAA in the extended cohort as a whole and in the *PSEN1* pre-codon 200 group, while mild leptomeningeal CAA in the *APP* group was positively correlated with disease duration. The regression analysis in the occipital cortex revealed there was a near significant negative association between the overall proportion of leptomeningeal CAA and age at onset. While not significant this could potentially imply that leptomeningeal CAA could either 1) negatively affect disease progression and hasten onset or 2) be due to a longer occurring pre-symptomatic pathological deposition of leptomeningeal CAA. Regression analysis in the occipital cortex for CAA and disease duration revealed no significant associations, despite the significant correlations observed and this is likely due to the differences between the statistical tests. As group numbers were small, most findings non-significant and correlations not adjusted for known associates of clinical data, the data and assumptions should be interpreted with caution. Particularly as the regression results were generally suggestive of there being no association, and this model included adjustment for mutation and *APOE* status. However, the effect of the processes involved in CAA development may by complex and not linearly associated with disease. As mentioned before there may be early beneficial stages followed by detrimental effects. As amyloid-modifying therapies can lead to increased CAA, it needs to be understood how CAA may impact upon disease duration, warranting further investigation.

Comparisons between mutation and *APOE* genotype groups

Significant differences between mutation groups in the overall proportion and severity of CAA were found in the extended cohort, supporting the consensus that CAA differs by mutation location (Chapter: 5.5.3 and 5.5.6). The *PSEN1* post-codon 200 group consistently had a greater proportion of and greater severity of CAA, with more severe CAA previously noted in post-codon 200 mutation carriers by others (David M. A. Mann *et al.*, 2001; Ringman *et al.*, 2016). *APP* mutations had the least proportion and severity of CAA and this may be due to the cohort not containing *APP* mutations located within the Aβ coding domain, which are associated with particularly severe CAA (Ryan & Rossor, 2010). Compared to mutations within the Aβ coding domain of *APP* and *PSEN1* mutations, the *APP* mutations represented in our cohort which are all located distal to the γ-secretase cleavage site, may be associated with less severe CAA. We have shown that

APP V717I mutations alter γ-secretase cleavage site preference to favour the Aβ48>45>42>38 pathway (Charles Arber *et al.*, 2019a), which may be relevant given that Aβ40 is the predominant isoform seen in CAA. This highlights site specific mutations within and between causative genes which may influence the disease process.

The observed mutation group differences may potentially be related to other PSEN1 substrates, of which some are likely to be particularly relevant to the vasculature. *PSEN1* mutations, in particular those located post-codon 200, may affect processing of other substrates, which could impact upon vascular health. In fact, in mice PSEN1 has been shown to be important for vascular as well as cortical development (Nakajima *et al.*, 2006; Wen *et al.*, 2005). Altered PSEN1 processivity may therefore affect vasculature development/maintenance and lead to additional dysfunction. As APP is expressed in endothelial cells (Forloni *et al.*, 1992; Ye Zhang *et al.*, 2014), and our *APP* mutation carriers show the least Aβ+ve CAA, it supports the suggestion the *PSEN1* mutations may lead to worse CAA due to additive mechanisms on top of Aβ. Another possibility is that certain *PSEN1* post-codon 200 mutations produce increased Aβ40 levels and/or ratios, which is a large component of CAA, thereby increasing CAA pathology.

The differences between mutation groups were notable in both the frontal and occipital cortex. It is interesting that the differences are observed in both cortical regions even though the occipital cortex is particularly predisposed to CAA (J. Attems, 2005; Johannes Attems *et al.*, 2005; Vinters & Gilbert, 1983). This does highlight how CAA is a global pathology in FAD and is likely important to the overall disease process. While differences were consistent in the cortex and leptomeninges, differences were non-significant in the leptomeninges. This could be due to longer deposition in the leptomeninges masking group differences, as at least in mice, leptomeningeal CAA appears to occur prior to cortical vessel deposition (Robbins *et al.*, 2006; Schelle *et al.*, 2019).

Despite consistent group trends, there was large variability within groups. This could be due to a number of factors such as specific mutation, *APOE* genotype, or other unknown factors. The statistical approach used did not allow for these possibilities to be factored in and would require larger numbers for this type of assessment to occur. We did however separately assess for differences between

APOE genotypes. Generally, differences were not significant but trended towards increased CAA in *APOE*4 carriers, in an *APOE*4 allele dose dependant manner, particularly in the occipital cortex (Chapter: 5.5.4 and 5.5.7). *APOE*4 could therefore be a contributor to the heterogeneity observed in the mutation groups.

An additive effect of ε4 alleles on CAA has previously been shown (P. T. Nelson *et al.*, 2013). *APOE*4 carriers are likely to have gene dose dependant increases in CAA due to APOE4 specific binding properties with Aβ and to APOE4 specific interactions with Aβ receptors at the BBB. For example, APOE4 bound Aβ is transported more slowly across the BBB by the LRP1 receptor (Deane *et al.*, 2008). We also found that there was higher CAA in *APOE* 2/3 carriers, which corroborates literature suggesting that the *APOE* ε2 allele is associated with CAA (P. T. Nelson *et al.*, 2013). Although interesting, this result should be interpreted with caution due to the low number of cases. Overall, *APOE* genotype may influence CAA pathology in FAD with allele specific relationships, and our results reflect similar effects of *APOE* genotype on CAA severity that have been seen in clinical trials of amyloid-modifying therapy in AD patients (Sakai *et al.*, 2014).

Conclusions

This study has confirmed our previous finding of an association between the *APOE*4 allele and longer disease duration (Chapter 3.3.2) specifically in FAD. Future clinical analyses in larger FAD cohorts will need to take *APOE*4 genotype into account and further investigate the relationship between disease duration and APOE genotype in a range of mutations to confirm our findings. If the association is maintained, the molecular basis for this association should be further investigated. Importantly, therapies affected by *APOE* status could have particular effects in FAD cohorts where, from our data, it appears that possessing an *APOE4* allele does not necessarily negatively affect disease outcomes.

The associations between microglial phenotypes and CAA also merit further investigation, especially as there were observed mutation differences in the direction of associations. This is particularly true as there are alterations in microglia that can occur in response to treatments, which can also lead to CAA.

Both mutation type and *APOE* genotype associated with CAA in this study, although the results indicated that FAD mutation type had the greater association

with CAA. These aspects are important as drug treatments may lead to an increase in amyloid imaging related abnormalities (ARIA) in AD, which are thought to represent an immune response to vascular amyloid, with *APOE4* status influencing outcomes (Arrighi *et al.*, 2016; Coric *et al.*, 2012; Ostrowitzki *et al.*, 2012; R. Sperling *et al.*, 2012). Despite the heterogeneity we have shown in CAA, understanding its role will be important as it may modulate clinical outcomes, including cognitive features, with the impact differing between mutations.

Chapter 6

Aβ isoform specific pathology in FAD

6 Aβ isoform specific pathology in FAD

6.1 Abstract

Introduction: FAD mutations in *PSEN1* and *APP* are linked to alterations in the amyloidogenic processing of *APP,* leading to alterations in the ratios of Aβ isoforms. The altered Aβ isoform profile can differ between different mutations, and in some cases mutations cause an overall increase Aβ production (Citron *et al.*, 1992; Kwart *et al.*, 2019; Sun *et al.*, 2017). Certain isoforms may be more toxic than others and contribute to plaque pathology in distinct ways due to their aggregation profiles. Knowing which mutations are linked to what type of Aβ isoform and plaque pathology has the potential to further help our understanding of disease causing mechanisms and their relationships to phenotypic heterogeneity.

Methods: IHC with Aβ42, 40 and 43 isoform specific antibodies was conducted on the temporal and occipital cortex of 20 FAD cases from the QSBB. Positive staining was visually analysed and described.

Results: Visual inspection confirms that Aβ isoform specific plaque pathology is maintained in a range of *PSEN1* and *APP* mutations, with Aβ42 present in all pathologies, Aβ40 more prominent in CAA and cored plaque pathology and Aβ43 present in cored plaques, but generally minimally present in other plaque types and CAA. Aβ42 was abundant across all cases, however Aβ40 and Aβ43 were not prominent in all cases. The *PSEN1* post-codon 200 mutation cases with R278I, E280G and A434T & T291I mutations harboured Aβ43 pathology in both the temporal and occipital cortex. These mutations also expressed Aβ40. *APOE*4/4 may be associated with greater Aβ40 pathology in FAD mutation cases, but not Aβ43 pathology. The single *APOE*2/3 case also displayed strong immunoreactivity for Aβ40 IHC.

Conclusions: Isoform specific pathology is observed in FAD brain tissue. Consistency is generally observed between same mutation carriers, however *APOE*4 status may exert effects on Aβ pathology in same mutation carriers. Confirming mutation and *APOE* specific effects on pathology highlights the importance of considering these genetic factors when developing and delivering treatments which may interact differently with the Aβ isoforms.

6.2 **Introduction**

6.2.1 *Isoforms and plaque types*

Using Aβ isoform specific antibodies, immunohistochemical analysis of post-mortem human brain tissue has highlighted differences in the presence and distribution of specific isoforms. One study on a small number of sAD cases using an antibody against both Aβ42 and 43 indicated that positive deposits were only present in cortical plaques and not in blood vessels in the form of CAA, while Aβ40 was frequently deposited in vessels, but greatly reduced in senile plaques compared to Aβ42(43) (Iizuka *et al.*, 1995). However, in another study, antibodies against Aβ42 revealed it was present in vessels as well as a range of plaque types, with Aβ40 only present in cored plaques and vessels, or perivascular (Savage *et al.*, 1995). Using alternative methods of peptide identification, mass spectrometry (MS) analysis of plaques from *PSEN1* I143T mutation cases revealed high levels of Aβ42/43 in plaques cores (Keller *et al.*, 2010).

Recently, 12 sAD cases with a range of CAA severities studied with immunoprecipitation coupled with mass spec analysis of cortical tissue were found to express different Aβ compositions in relation to CAA (Gkanatsiou *et al.*, 2019). Another study, which included 5 AD cases with CAA pathology, utilised matrix-assisted laser desorption/ionization (MALD)-MS to investigate the deposition of Aβ isoforms and complemented this with IHC (Kakuda *et al.*, 2017). MALDI-MS of occipital cortex tissue confirmed that Aβ1-42 and Aβ1-43 were deposited in senile plaques, while Aβ1-36 through to Aβ1-41 were preferentially deposited in leptomeningeal blood vessels. Subpial deposition composed of Aβ1-42 was also noted. IHC confirmed MALDI-MS findings but both methods confirmed Aβ42 can be seen on vessels and Aβ40 can be seen in plaques although the proportions of the peptides differ between the pathologies. A further interesting observation from this study was that the N-terminal truncations were more important for plaque localisation compared to C-terminal truncations which depict the Aβ isoform (eg.40/42/43). Using synthetic peptides, *in vitro* analysis of aggregation kinetics showed that there was a faster aggregation ability in Aβ42 compared to Aβ40 and 41, which was suggested as the cause of greater Aβ42 senile plaque deposition.

Even in DS with AD pathology, Aβ40 is similarly present in the dense core, in addition to observed subpial pathology in the cerebellum (D. M. A. Mann & Iwatsubo, 1996). The similarities in isoform specific plaques and plaque types across AD with a range of causes highlights the importance of isoforms and their potential to influence disease.

The hypothesis for these specific patterns of deposition are related to the aggregation potential of the isoforms and the removal of Aβ40 though clearance mechanisms. The ratio of isoforms in general may also be involved in pathological Aβ distribution. By looking at the pathology in transgenic mice, it was found that overexpression of APP protein with the E693Q mutation lead to vascular pathology and greater Aβ40/42 ratio while overexpression of wild type human APP lead to predominant parenchymal Aβ and lower Aβ40/42 ratio. By crossing the *App* E693Q mice with mutated *Psen1* G348A mice they were able to show redistribution of Aβ to the parenchyma along with a reduction in the Aβ40/42 ratio (Herzig *et al.*, 2004). This highlights how isoforms can greatly impact pathology and possibly effect disease course. However, as different isoforms can aggregate into multi species aggregates, the interplay between them may also affect deposition. Even the ratio of the different isoforms has been shown to affect aggregation potentials and toxicity of aggregates applied to cell cultures (Jan *et al.*, 2008).

6.2.2 *Isoforms and cortical regions*

As previously mentioned, the occipital cortex is more severely affected by CAA compared to other regions and CAA has been shown to possess a different Aβ composition compared to cortical plaques. Differences in peptide concentrations have been shown to differ between regions in FAD, with highest peptide concentrations of Aβ42 and 43 observed in the occipital cortex (Keller *et al.*, 2010). Comparison between different FAD mutations has highlighted mutation differences across cortical regions. Lower levels of soluble Aβ40 were found in the frontal cortex and lower levels of insoluble Aβ40 were found in the frontal and occipital cortex of *PSEN1* M146V mutation carriers compared to *APPswe* mutation carriers. Soluble Aβ42 was also reduced in the occipital cortex in the *PSEN1* mutation carriers. Across the four brain regions analysed, different patterns in the order of average soluble and insoluble Aβ40 and Aβ42 levels were

also observed (Hellstrom-Lindahl *et al.*, 2009). Our previous analysis of CAA revealed the mean % of CAA was consistently higher in the occipital cortices compared to frontal cortex (Chapter: 5.5.8), and on average, higher in *PSEN1* post-codon 200 cases (Chapter: 5.5.3 and 5.5.6). It would be of interest to investigate whether isoform specific differences are observable between regions in a larger number of FAD mutation cases.

6.2.3 *Isoforms and mutations*

Previous work suggests that mutation specific pathologies and clinical presentations can occur in FAD. For example, spastic paraparesis and CWP pathology are frequently seen in patients with *PSEN1* exon 9 deletions (Crook *et al.*, 1998; D. M. A. Mann *et al.*, 2001b). As Aβ isoforms may be linked to different pathologies, it is important to know whether mutations are associated with specific isoform pathology in brain tissue.

Inspection of IHC with isoform specific antibodies in multiple regions of human brain tissue from two family members with the *PSEN1* I143T mutation revealed a specific Aβ isoform presentation. Aβ40 was absent from the cortex and any Aβ40 that was observed was confined to vessels while in contrast, antibodies specific to Aβ42 and Aβ43 highlighted abundant plaque pathology and presence in both the cortical tissue and vessels (Keller *et al.*, 2010). A neuropathological report of one case with the alternative *PSEN1* I143V mutation was also shown to display minimal Aβ40 plaques, and had no CAA pathology (C. Xue *et al.*, 2019). This case also showed a particular banding pattern with Aβ42 staining in the insula tissue section (Gallo *et al.*, 2011). High Aβ43 pathology plaque deposition was also shown in sibling patient brains with the I435F mutation, with Aβ43 deposition not observed in a separate FAD case with a different mutation (Kretner *et al.*, 2016).

Concerning *APP* mutations, mutations at *APP* 7I7 (those with substitutions Val > Ile and Val > Gly) have been reported to display reduced Aβ40 pathology, and predominant Aβ42(43) pathology, while mutations at *APP* 670/671 display predominant Aβ42(43) but also have Aβ40. In both the *APP* 717 and *APP* 670/671 mutations, CAA was predominantly composed of Aβ40 (D. M. Mann *et al.*, 1996). In a small cohort study which compared between causative genes,

PSEN1 mutation carriers were found to have significantly greater Aβ42 plaque size compared to *APP* mutation carriers (Ishii *et al.*, 2001). However, the precise location of the *PSEN1* mutation was not found to have an effect on the relationship between Aβ isoform and plaque morphology. These small studies show the heterogeneity present within FAD and different between mutations, which warrants better understanding.

As one method of Aβ clearance from the brain involves the removal via the CSF, Aβ isoforms present in CSF can potentially reflect isoform differences in the brain. CSF analysis of Aβ peptides in a range of FAD mutation carriers has shown differences between mutations (Thordardottir *et al.*, 2017). The CSF differences may reflect differences in plaque pathology which would be interesting to confirm at post mortem. If post mortem pathology is in agreement with CSF analysis, then knowing associations between isoforms and plaques, deposition and other genetic factors would increase our understanding of AD pathogenesis. In addition to human tissue observations, cellular models from FAD patients also support and highlight isoform differences by mutation (Charles Arber *et al.*, 2019a). In this previous work, Aβ ratios were investigated in an *APP* V717I mutation case for which iPSC derived cortical neurons, CSF and brain tissue was available. The study revealed consistencies in the Aβ38:40 ratio across samples. Aβ42:40 did slightly differ across samples with greater Aβ42 in conditioned media and brain sample. This however was likely due to the effects of increased Aβ42 in brain sample due to deposition in plaques, and Aβ42 build up in conditioned media as it is not cleared. Collectively the data support these multiple modelling systems enabling understanding of Aβ isoform pathology.

6.2.4 *Isoforms and APOE genotypes*

It has been shown that the *APOE4* allele can be associated with greater Aβ deposition, and this has been noted in multiple studies of sAD. APOE can also be associated with Aβ isoform specific plaque pathology. In sAD, it has been shown via IHC techniques on human cortical tissue that *APOE*4 carriers display differences in AD plaque pathology, with *APOE4* being linked to greater Aβ40 (Gearing *et al.*, 1996; P. M. Smith *et al.*, 1997). In sAD and FAD brain tissue, *APOE4* status was associated with a greater area of Aβ1-40 plaques, but not for Aβ42 plaques (Ishii *et al.*, 2001) and there was also observable variation in Aβ

pathology between cases. Furthermore, in a large cohort of cases, which consisted solely of *PSEN1* FAD mutation carriers, *APOE* status was shown to be associated with Aβ isoform pathology. In the frontal cortex, it was observed that *APOE4* carriers had greater Aβ40 deposition compared to non-carriers (David M. A. Mann *et al.*, 2001). It was proposed that APOE4 had this effect through decreasing the fibrilisation threshold of Aβ40, enabling greater deposition of Aβ40 on plaques. Because *APOE4* status is linked to CAA-related inflammation and to the amyloid related imaging abnormalities (ARIA) observed in some trials of amyloid-modifying therapy trials, it is necessary to understand the contribution of *APOE* to Aβ specific isoform pathology, especially as distinct isoforms may have different effects on the clinical manifestations associated with CAA. An association between ARIA, *APOE*4 genotype and CAA related inflammation has been noted in a single case FAD case study (Ryan *et al.*, 2015b).

6.2.5 *Aims*

As discussed, Aβ isoforms can contribute to pathology in different ways and different FAD mutations can lead to differing Aβ isoform ratios. In order to investigate possible FAD mutation specific effects on Aβ pathology, Aβ isoform specific plaque and CAA pathology in the temporal and occipital cortices of the QSBB cohort was assessed. The aims for chapter 6 were:

1. To qualitatively assess if the observed contribution of specific Aβ peptides differs between plaque types (Cored, CWP, diffuse) and CAA in the temporal and occipital cortices.

2. To qualitatively assess if the observed contribution of specific Aβ peptides to pathological deposits differs by genetic cause of FAD in the temporal and occipital cortices.

3. To qualitatively assess if the observed contribution of specific Aβ peptides to pathological deposits differs by *APOE* genotype in the temporal and occipital cortices.

6.2.6 *Material and methods*

Sections from the temporal and occipital cortex of the 20 QSBB cases were cut and underwent IHC with antibodies specific to Aβ40, 42 and 43 (see chapter:

2.3). Sections were qualitatively assessed microscopically. The type and distribution of Aβ+ve pathology for each Aβ isoform specific antibody was visually inspected. Patterns and differences in staining were noted and are described. Descriptive comparisons between mutation subgroups and *APOE* genotype were conducted. No statistical analyses were used within this chapter.

6.3 **Results**

Pathological analysis in the previous chapters has used the Aβ antibody M0872 (DAKO) (Table 2-3, Chapter 3: Aβ pathology in FAD). This antibody is raised to a synthetic peptide containing residues 8-17 of the Aβ peptide, therefore it will bind to the majority of Aβ peptides, including Aβ40, 42 and 43. To investigate the contribution of specific Aβ isoforms to pathology in FAD cases and investigate potential differences between FAD mutations in the QSBB cohort, tissue sections from the temporal and occipital cortex were immunohistochemically stained with isoform specific antibodies to Aβ40, Aβ42 and Aβ43 (Table 2-3). While the pattern and distribution of pathology is discussed in terms of distribution over the cortical layers, cortical layers were not defined in these tissue sections using Nissl staining. Presence of distinct plaque types is discussed (cored, diffuse, CWP), as is cortical and leptomeningeal CAA, however, these were not semi-quantitatively analysed for this descriptive study.

6.3.1 *Aβ42 IHC*

6.3.1.1 *Temporal cortex*

Intense Aβ42 positive staining was seen in all cases with staining present across the depth of the cortical layers (Figure 6-1). The intensity and abundance of staining mirrored that of the M0872 DAKO antibody (Figure 3-2). Intense Aβ deposition was observed across all layers except with paucity in layer 1 for most cases (e.g. *PSEN1* cases 7: M139V, 14: R278I, and *APP* case 17: V717L). Despite intense deposition, distinct patterns can be observed in a few cases. For example, case 3 (*PSEN1* intron4) has a particular band of large diffuse plaque pathology in lower layers (layers 4/5), with contrasting sparse distribution of small dense diffuse plaques in the lowest region likely corresponding to cortical layer 6. Case 13 (*PSEN1* R278I) also displays distinct pathology with large, less intensely stained deposits in layer 3 compared to the other cortical layers.

Diffuse plaque pathology can be seen in all cases, cored plaques are less frequent but still observed (e.g. case 14: *PSEN1* R278I) and CWPs are also less frequent but present in some cases (e.g. case 16: *PSEN1* A434T & T291A). Presence of all types of plaques and CAA indicates that Aβ42 is present in all types of Aβ pathologies in this cohort. *APOE4* genotype did not appear to influence amount or type of Aβ42 pathology, even within same mutation carriers. For example, there appears to be greater deposition in the *APOE*4 positive *PSEN1* R278I (case 13) compared to the *APOE*4 negative *PSEN1* R278I (case 14), however, the *APOE*4 positive *APP* V717I (case 20) does not appear to have greater deposition than the *APOE*4 negative *APP* V717I (case 19).

Similar to results obtain using the DAKO antibody in the frontal cortex (Figure 3-2), cortical and leptomeningeal vessels showed positive staining for Aβ42 in a range of cases (eg. *PSEN1* cases 2: Intron4, 5: E120K, 8: M146I, 9-10: E184D, 11: I202F, 13-14: R278I, 15: E280G, 16: A434T & T291A, *APP* V717I cases 19-20, Figure 6-2). The severity ranges from mild to severe with severe leptomeningeal CAA observable in case 13 (*PSEN1* R278I), moderate leptomeningeal CAA in case 14 (*PSEN1* R278I) and mild observable in case 19 (*APP* V717I), although there are cases with no observable CAA (e.g. case 11: *PSEN1* I202F). This range of CAA pathology is comparable to that observed with the DAKO antibody. Diffuse subpial pathology can also be seen in a number of cases in the *PSEN1* pre-codon 200, post-codon 200 and *APP* groups (*PSEN1* cases 4: Intron4, 8: M146I, 13-14: R278I, and *APP* V717I cases 18-19).

6.3.1.2 *Occipital cortex Aβ42 IHC*

As in the temporal cortex, there was Aβ42 positive staining in all cases with plaque deposition present across the depth of the occipital cortex (Figure 6-3). In contrast to the temporal cortex, the frequency of Aβ42 deposition appears reduced, suggesting regional differences (e.g. *PSEN1* cases 8: M146I, 9: E184D, 12: L250S, 14: R278I, 16: A434T & T291A and *APP* V717I case 19). From the stained sections used in chapter 3.3 and 5.3, a decrease in DAKO positive staining in the occipital cortex compared to frontal cortex was also noted.

The Aβ42 antibody stains frequent plaque deposits in cases in all mutation groups, with plaques present across the depth of the cortex. While deposition is seen across all cortical layers, in some cases there are appears to be layer

specific patterns. For example, in *PSEN1* cases 1-4 (Intron4) 5 (E120K) 8 (M146I) 9-10 (E184D) and 12 (L250S), layers 4/5 present a particular type of plaque pathology, with abundant, large and poorly defined diffuse plaques, compared to the other cortical layers. There are notable differences between some cases in the frequency of plaque deposits, for instance *PSEN1* cases 1-4 (Intron4) 5 (E120K), 7 (M139V), 9-10 (E184D) 11 (I202F) 12 (L250S) and 15 (E280G) have frequent deposition in comparison to *PSEN1* cases such as 6 (S132A), 13-14 (R278I) 16 (A434T & T291A) and *APP* cases 17 (V717L) and 18-19 (V717I). These differences span the mutation groups with no obvious group specific patterns.

There is a range of plaque types present. Cored plaques are observable and particularly evident in case 8 and 13. Diffuse pathology is seen in all cases, with a noticeable banding pattern in some cases as previously mentioned. CWPs are seen in a few cases, with a noticeable presence in the *PSEN1* R278I cases (13-14). Interestingly, *PSEN1* case 16 (A434T & T291A) does not have any CWPs in the occipital cortex, even though CWPs were abundant in the temporal cortex with the Aβ42 antibody. There are no obvious differences between cases with or without an *APOE4* allele.

There was Aβ42 deposition observed in both the cortical and leptomeningeal vessels. Severe leptomeningeal CAA can be seen (case 2: *PSEN1* Intron4), as can moderate CAA (8: *PSEN1* M146I) and mild CAA (4: *PSEN1* Intron4), although there are cases with no CAA observable (e.g. 12: *PSEN1* L250S, 19: *APP* V717I). A range of severity levels of CAA are also observable in the cortex, with CAA present extensively in some cases (e.g. *PSEN1* cases 8:M146I, 9:E184D, 13:R278I, and *APP* V717I case 20, Figure 6-4). This pattern was similar in the DAKO antibody staining from previous chapters. Localised diffuse staining around cortical vessels which have CAA is more apparent than in the temporal cortex (e.g. *PSEN1* cases 8: M146I, 9&10: E184D, and *APP* case 17: V717L). Subpial pathology composed of diffuse plaques was present in a number of cases, in the *PSEN1* pre-codon 200 (cases 2-4: Intron4, 5: E120K, 6: S132A), post-codon 200 (cases 12: L250S, 13: R278I) and *APP* groups (cases 17: V717L, 18-19: V717I).

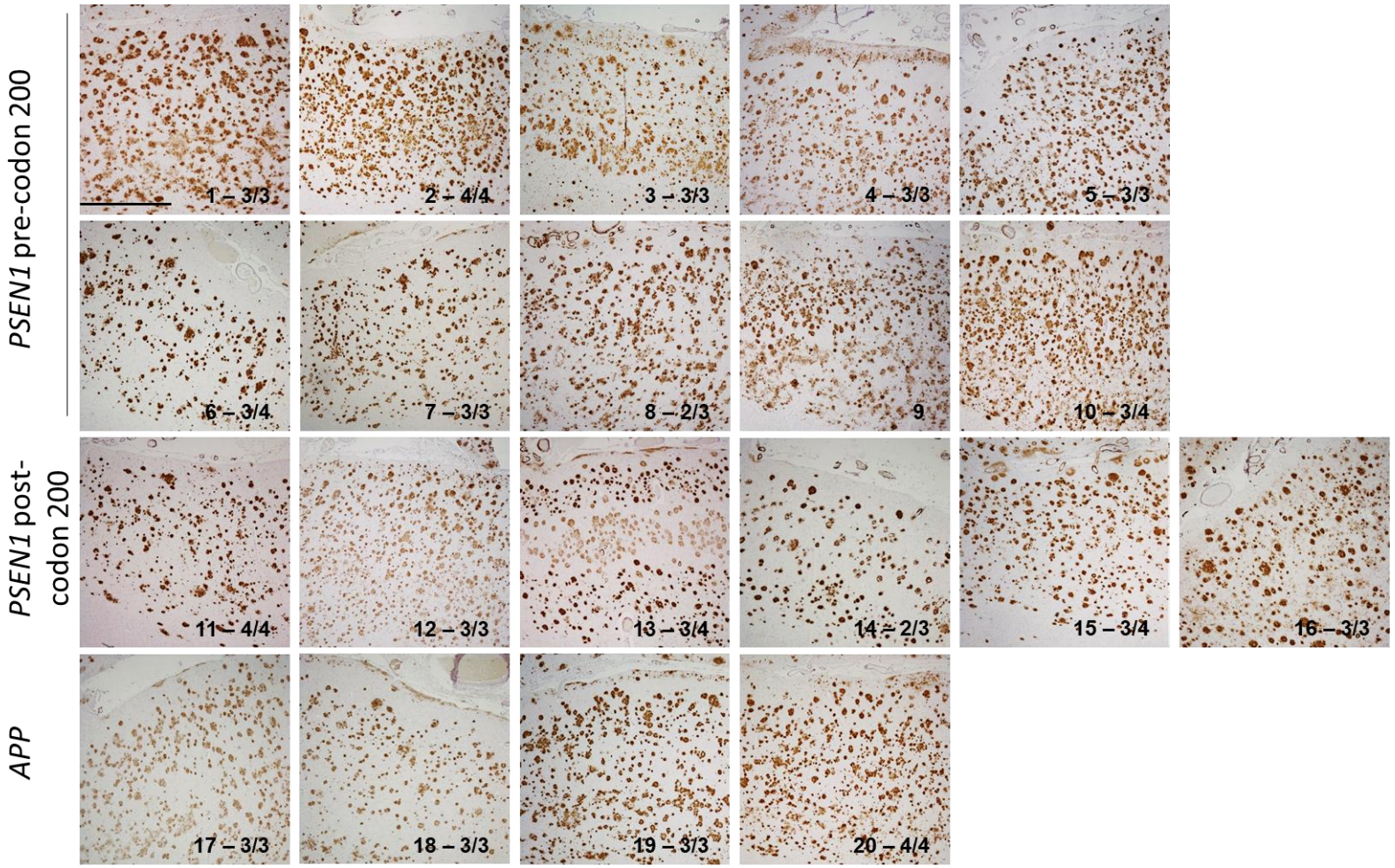

Figure 6-1 Representative images showing Aβ42 specific IHC in the temporal cortex.

Text on individual images represent QSBB cohort case number – *APOE* genotype. No *APOE* genotype available for case 9 Scale bar represents 100µm, 4x objective magnification.

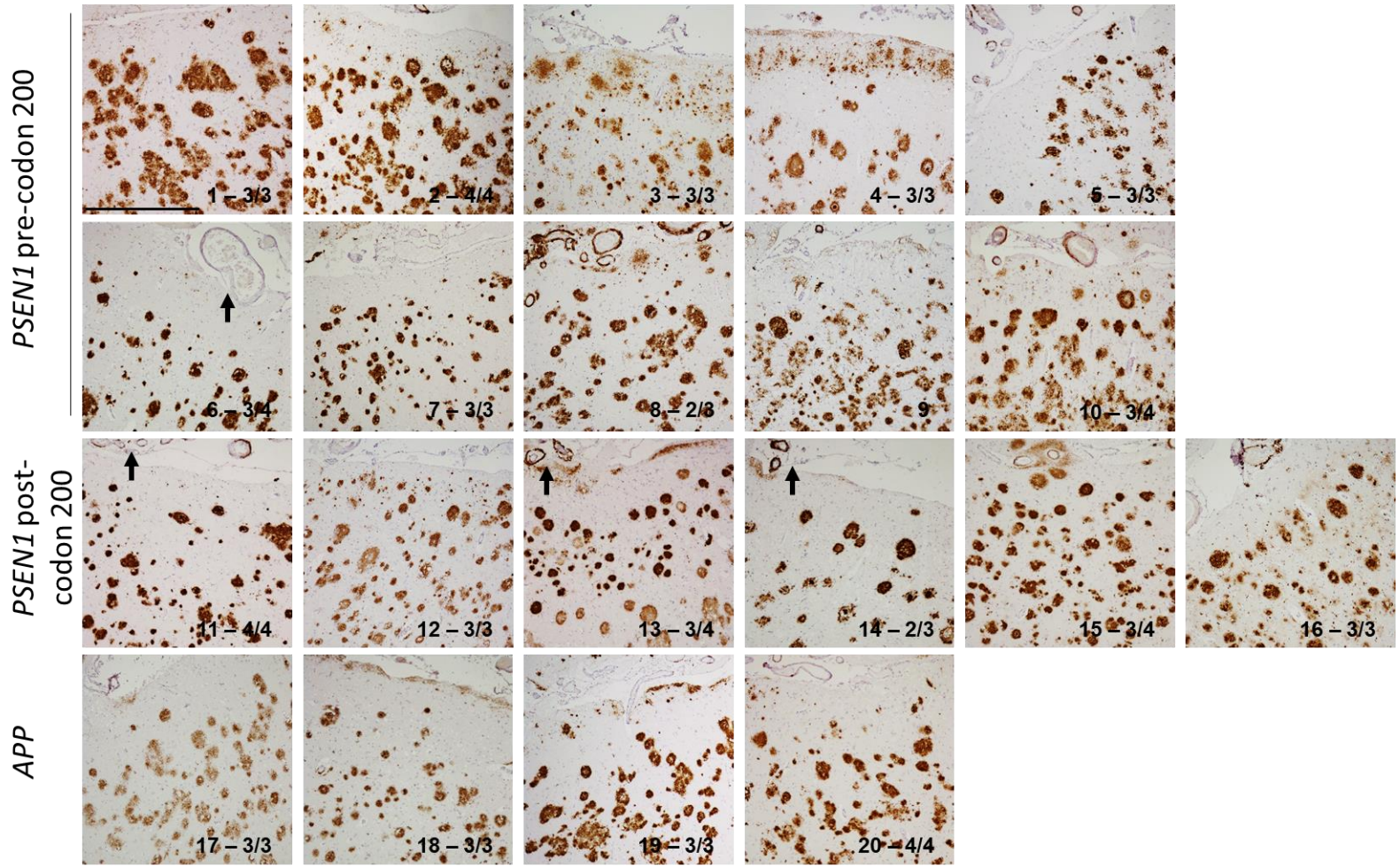

Figure 6-2 Representative images showing Aβ42 specific IHC in the temporal cortex.

Text on individual images represent QSBB cohort case number – *APOE* genotype. No *APOE* genotype available for case 9. Arrows indicate CAA severity, 6=none, 11=mild, 14=moderate, 13=severe. Scale bar represents 50µm, 10x objective magnification of images shown in Figure 6-1.

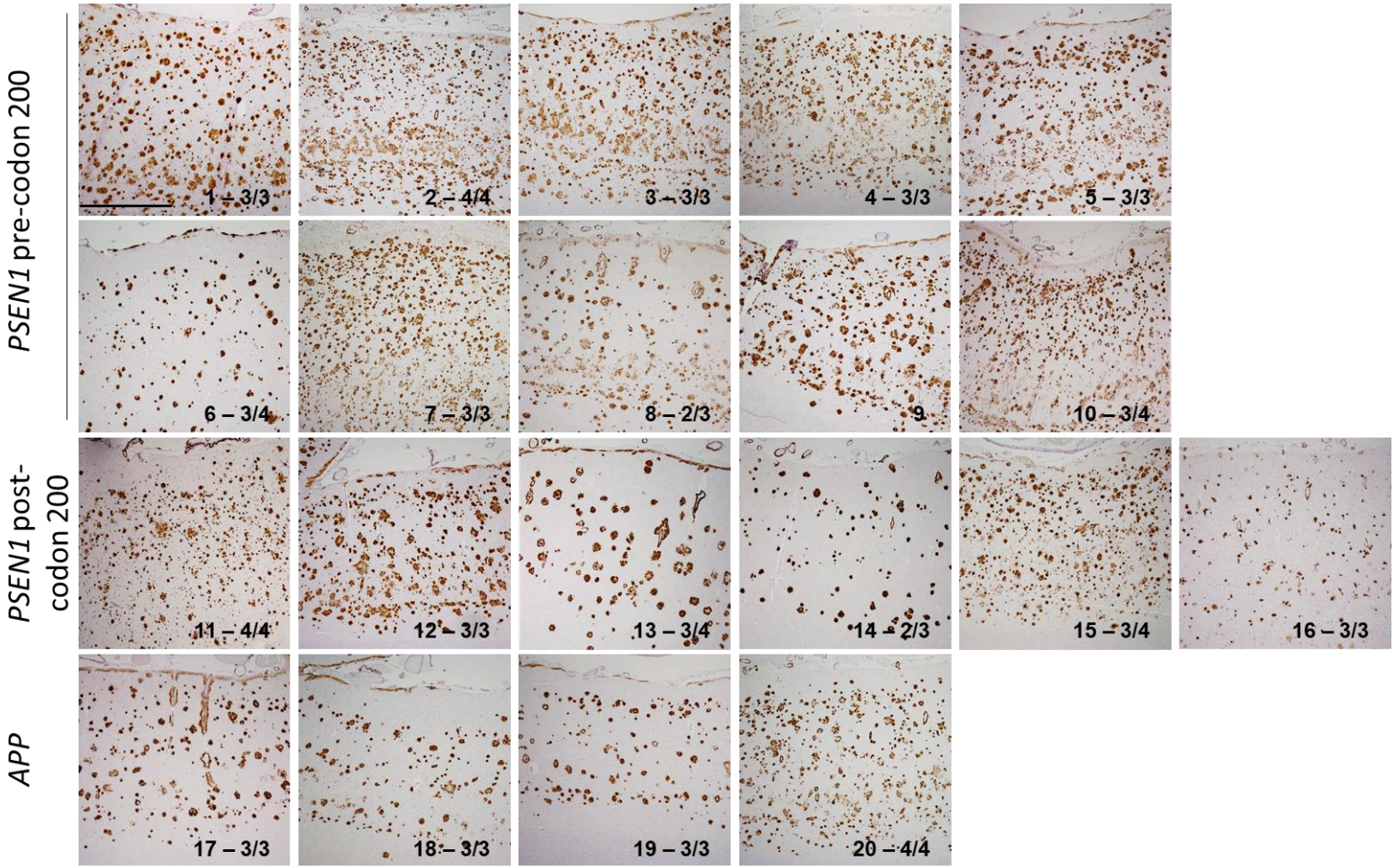

Figure 6-3 Representative images showing Aβ42 specific IHC in the occipital cortex, calcarine region.

Text on individual images represent QSBB cohort case number – *APOE* genotype. No *APOE* genotype available for case 9 Scale bar represents 100µm, 4x objective magnification.

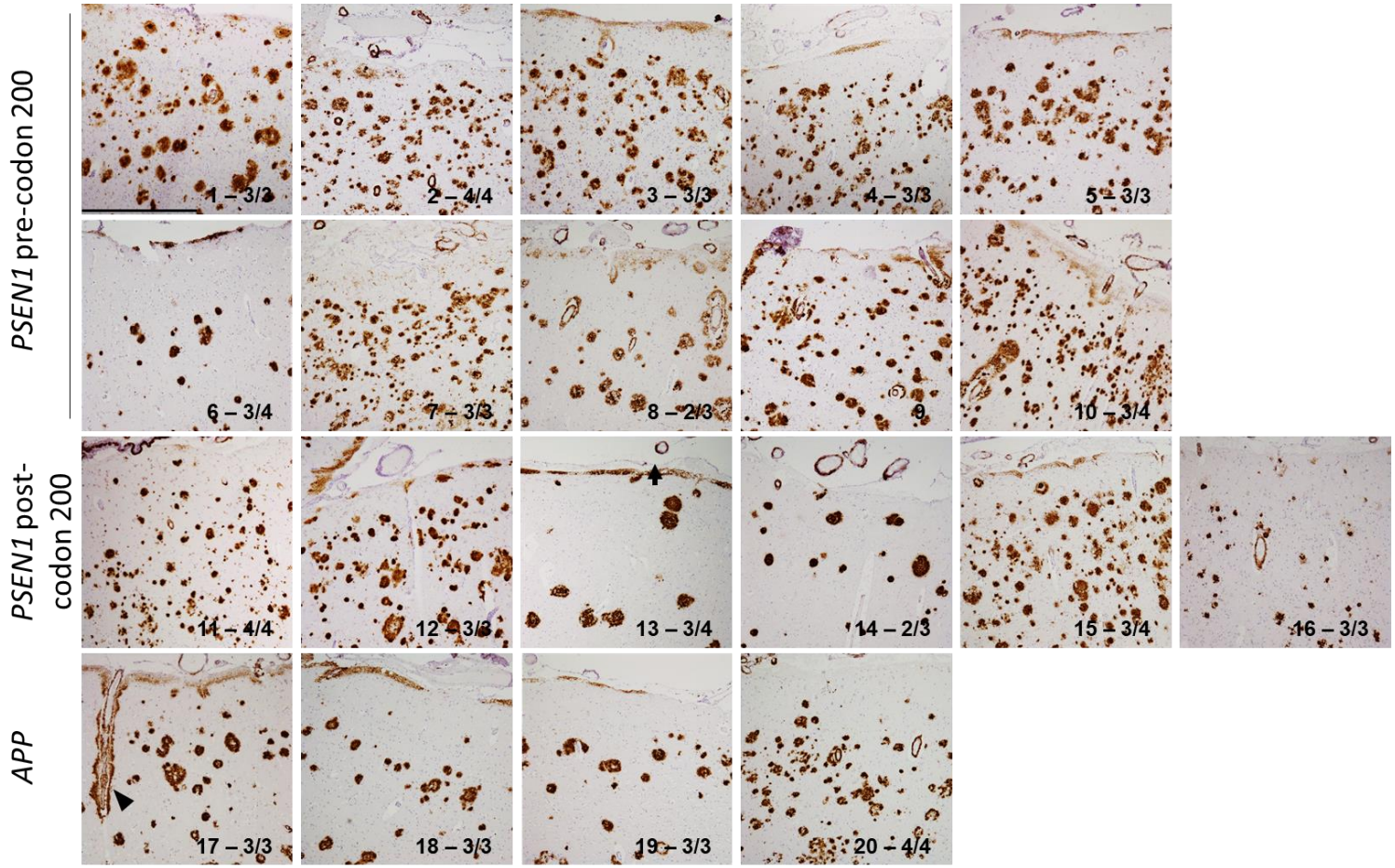

Figure 6-4 Representative images showing Aβ42 specific IHC in the occipital cortex, calcarine region.

Text on individual images represent QSBB cohort case number – *APOE* genotype. No *APOE* genotype available for case 9. Arrow indicates leptomeningeal CAA (13). Arrow head indicates cortical CAA (17). Scale bar represents 50µm, 10x objective magnification of images shown in Figure 6-3.

6.3.2 *Aβ40 IHC*

6.3.2.1 *Temporal cortex*

Compared to the Aβ42 IHC, there was noticeably less positive staining with the Aβ40 antibody in the QSBB cohort, and this is particularly evident within the parenchyma Figure 6-5. For a comparison of specific cases see Figure 6-13.

In the cortex, there were differences between cases in the frequency of Aβ40 plaque deposition. For example, case 2 (*PSEN1* intron4) had frequent Aβ40 positive plaque pathology across the cortex, while the other *PSEN1* intron4 cases had less frequent deposition (*PSEN1* Intron4 cases 1, 3-4). Of note, case 2 was *APOE*4 homozygous, while the other intron4 cases were all *APOE*3 homozygous. Within cases where there were moderately frequent plaques, the plaques were seen across all layers with no consistent layer specific patterning.

Plaque staining for Aβ40 varied in intensity, with only faint staining in some cases (e.g. *PSEN1* pre-codon 200 cases 6: S132A, 7:M139V, and *APP* V717I case 18), intense staining in others (*PSEN1* pre-codon 200 cases 2: Intron4, 5: E120K, 10:E184D) and mixed intensity also seen (e.g. in *PSEN1* pre-codon 200 case 8: M146I, *PSEN1* post-codon 200 cases 11:I202F, 14: R278I and *APP* V717I case 20). These patterns are not specific to any one mutation sub-group. Despite differences in staining intensity, multiple plaque types can be observed. Diffuse plaque staining can be seen, particularly in case 2 (*PSEN1* Intron4, *APOE*4 homozygous). CWPs are also apparent although these were generally faintly stained (example cases *PSEN1* 14: R278I and 16: A434T & T291A). There was evidence of intense Aβ40 staining of the central core of cored plaques, with the halo being only faintly positive (*PSEN1* example cases 6: S132A, 7: M139V and *APP* V717I case 17) although the halo staining can be strong in some cases (*PSEN1* case 8: M146I and 9: E184D). Differences in the intensity of Aβ40 deposition between the *APOE4/4 PSEN1* intron4 case 2 compared to *APOE3/3* Intron4 cases 1,3-4 were quite striking, with frequent plaques observed in the *APOE*4/4 case only. This same pattern was also seen in the *APOE*4/4 A*PP* V717I case 13 comp*ared to APOE*3/3 *APP V717I cases 18-19.* There were no other obvious differences between cases with or without an *APOE*4 allele. *APOE*2 positive case 8 and 14 *(PSEN1* M146I and R278I) both exhibit intense

leptomeningeal CAA. While there was no available image of the temporal cortex for the other R278I case (13) which is *APOE3/4*, in the occipital region, this case also displayed prominent Aβ40 deposition in the leptomeninges. For a comparison of *APOE*4 positive cases with frequent Aβ40 pathology compared to those with minimal pathology, see Figure 6-14.

Aβ40 positive staining was visible in the cortical and leptomeningeal vessels, with CAA evident in cases which also displayed Aβ42 positive vessels in the temporal cortex (*PSEN1* cases 2-3: Intron4, 5: E120K, 8: M146I, 9&10: E184D, 11: I202F, 14: R278I 15: E280G 16: A434T & T291A and *APP* cases 17: V717L and 19-20: V717I, Figure 6-6). In the majority of instances, the vessel staining was more intense than the plaque staining (*PSEN1* cases 8: M146I, 11:L250S, 14: R278I, 15: E280G, 16: A434T & T291A and *APP* V171L case 17). Subpial pathology was seen in some cases although less intensely in some of the cases which displayed strong Aβ42 positive subpial pathology (*PSEN1* Intron4 case 4 and *APP* V717I cases 18 & 19). These types of pathology were seen across mutation-subgroups.

For a comparison of Aβ40 positive cases with frequent pathology compared to those with minimal pathology, see Figure 6-13.

6.3.2.2 *Occipital cortex*

Aβ40 positive staining in the occipital cortex was comparable to that observed in the temporal cortex, with some cases displaying low frequency of Aβ40 positive plaques and others displaying frequent Aβ40 plaques (Figure 6-7). Again, Aβ40 positive staining was noticeably distinct from Aβ42 IHC.

Generally, Aβ40 positive plaque deposition was much less frequent compared to Aβ42, with comparable levels only seen in *PSEN1* post-codon 200 cases 13&14 (R278I) and 16 (A434T & T291A). While the *PSEN1* E280G case 15 also had high Aβ40 levels, this was not higher than that observed with Aβ42 as this case had high Aβ42 positivity in the occipital cortex. A few cases showed frequent plaques (*PSEN1* cases 2: Intron4, 8: M146I, 13-14: R278I, 15: E280G and 16: A434T & T291A) while some cases show mild frequency (*PSEN1* cases 1: Intron4, 9-10: E184D, 11: I202F and 12: L250S) however these differences did not appear to be mutation sub-group specific. Plaque pathology had no obvious

layer specific plaque deposition. Faint diffuse plaques were observed (for example in *PSEN1* cases 8: M146I, 12: L250S, 15: E280G and *APP* V717I case 19). Similar to the temporal cortex, the central core of cored plaques were visibly present in the Aβ40 staining at low magnification (5: E120K, 6: S132A, 7: M139V, 10: E184D, 12: L250S, 15: E280G and *APP* V717I cases 17 and 19) while the outer halo was less intensely stained. However, the core halo was intensely stained in the *PSEN1* R278I case 13 and also noticeable to a lesser extent in the *PSEN1* R278I case 14. Similar to the temporal cortex, the *APOE*4/4 *PSEN1* intron4 case 2 showed frequent Aβ40 positive plaques in the occipital cortex, which was in contrast to the remaining *APOE*3/3 *PSEN1* intron4 cases (1,3-4), and this same pattern was also seen in the *APOE*4/4 A*PP* V717I case 13 compared t*o* the *APOE3*/3 A*PP* V717I cases 18-19. Again, the *APOE*2 positive cases 8 and 14 *(PSEN1* M146I and *PSEN1* R278I) both exhibited intense leptomeningeal CAA, but *APOE*3/4 *PSEN1* R278I case 13 also had leptomeningeal CAA, so it is unclear if this is linked to FAD mutation or *APOE* status.

In some cases, the majority of Aβ40 staining was predominantly within the vessels in both the cortex and leptomeninges (e.g. *PSEN1* cases 3: Intron4 and 7: M139V). Observed cortical and leptomeningeal CAA could be intensely stained by Aβ40 compared to Aβ42, and CAA was more apparent in the occipital cortex compared to the temporal cortex (PSEN1 cases 1 & 3: Intron4, 7: M139V and 11: I202F). There was also intense subpial pathology present in a subset of cases (*PSEN1* pre-codon 200 cases 8: M146I and 10: E184D and *PSEN1* post-codon 200 case 13: R278I), although leptomeningeal CAA was present without subpial pathology in cases from all mutation sub-groups (e.g. *PSEN1* cases 1 & 3: Intron4, 7: M139V, 9: E184D, 14: R278I, and *APP* V717L case 17). Of note was the intense diffuse pathology in the cortex seen around vessels with intense CAA (e.g. *PSEN1* cases 8: M146I, 10: E184D, 13: R278I, & *APP* V717I case 17). See Figure 6-8.

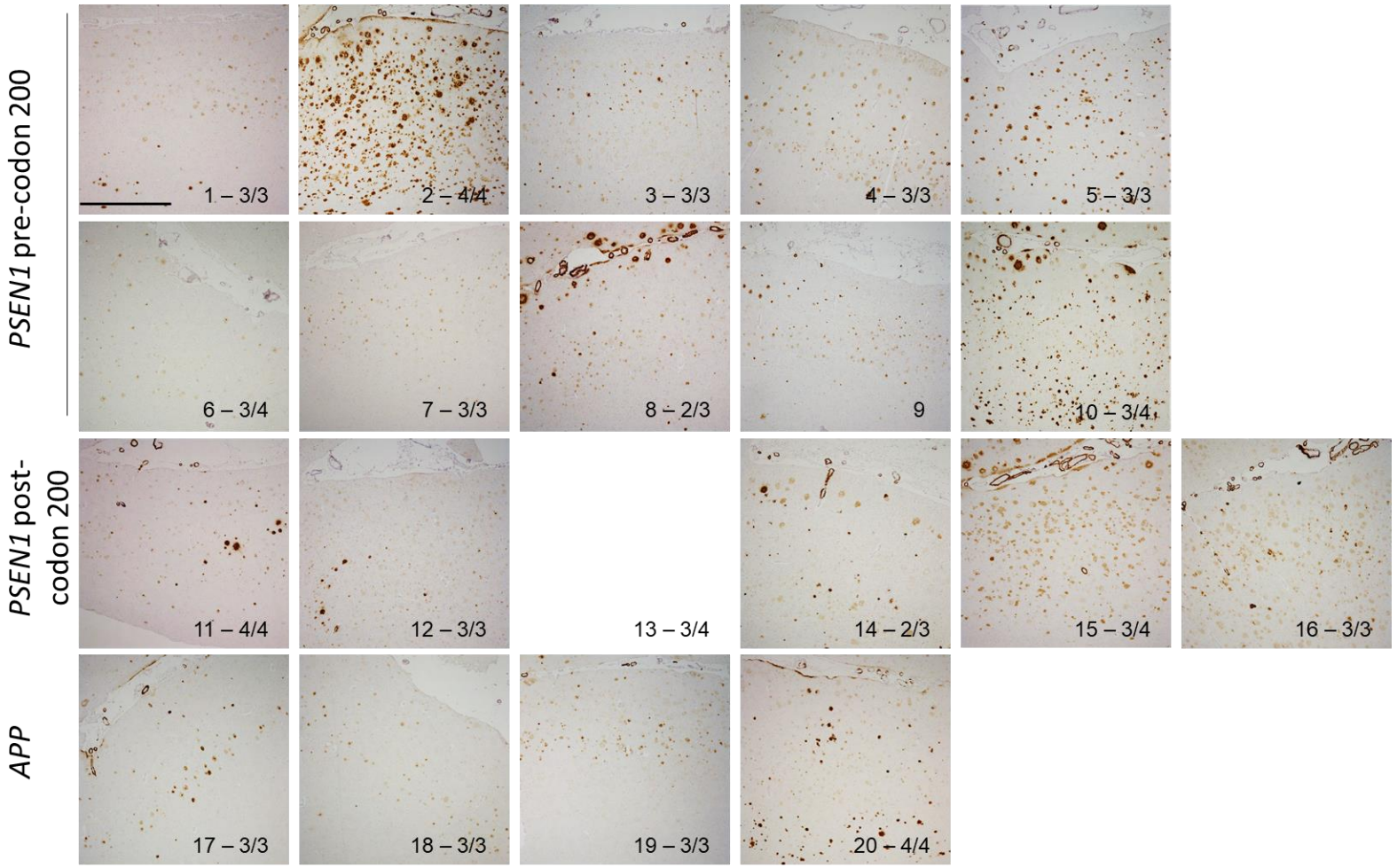

Figure 6-5 Representative images showing Aβ40 specific IHC in the temporal cortex.

Text on individual images represent QSBB cohort case number – *APOE* genotype. No *APOE* genotype available for case 9. No image for case 13 due to tissue damage during IHC. Scale bar represents 100µm, 4x objective magnification.

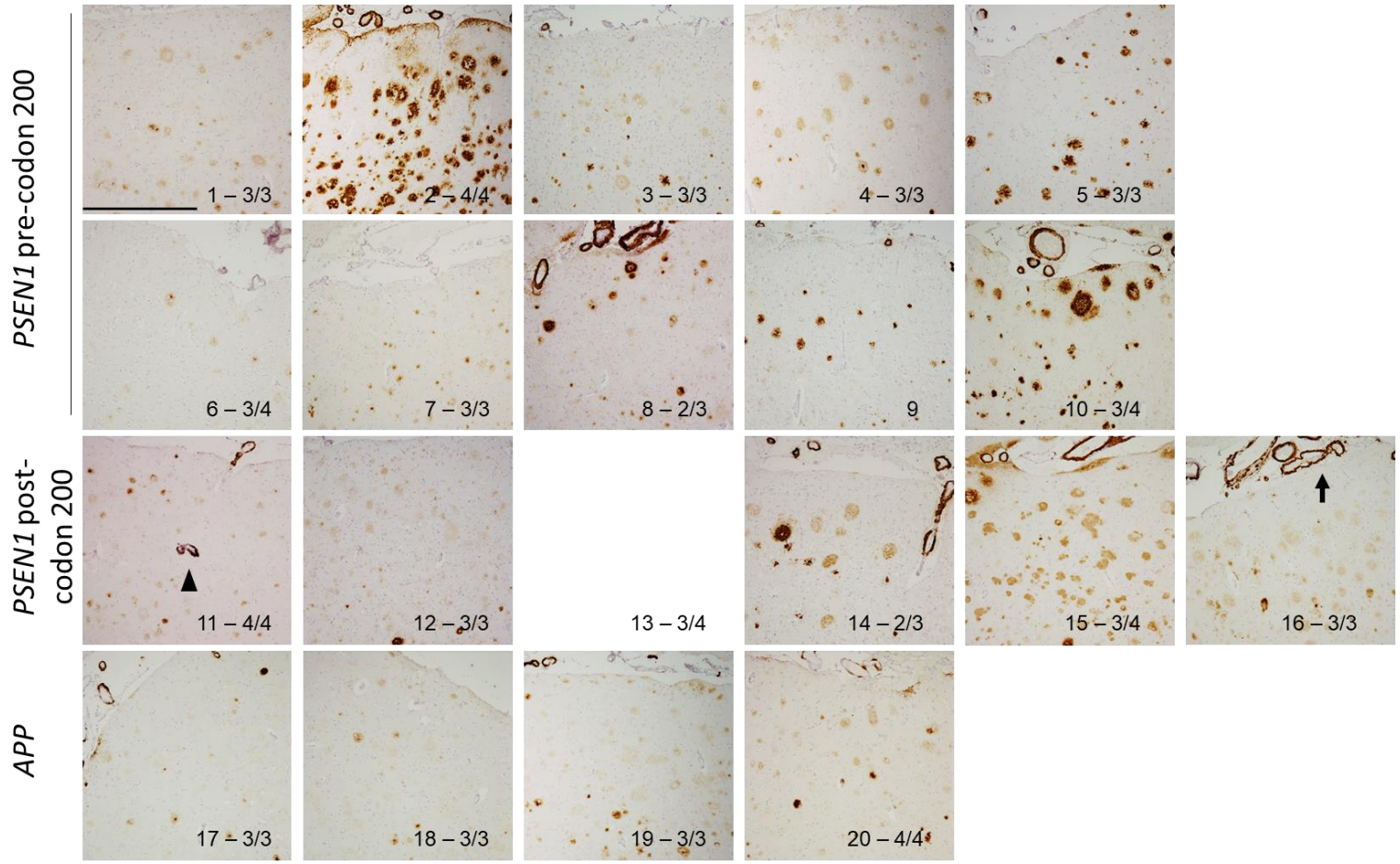

Figure 6-6 Representative images showing Aβ40 specific IHC in the temporal cortex.

Text on individual images represent QSBB cohort case number – *APOE* genotype. No *APOE* genotype available for case 9. No image for case 13 due to tissue damage during IHC. Arrow indicates leptomeningeal CAA (16). Arrowhead indicates cortical CAA (11). Scale bar represents 50µm, 10x objective magnification of images shown in Figure 6-5.

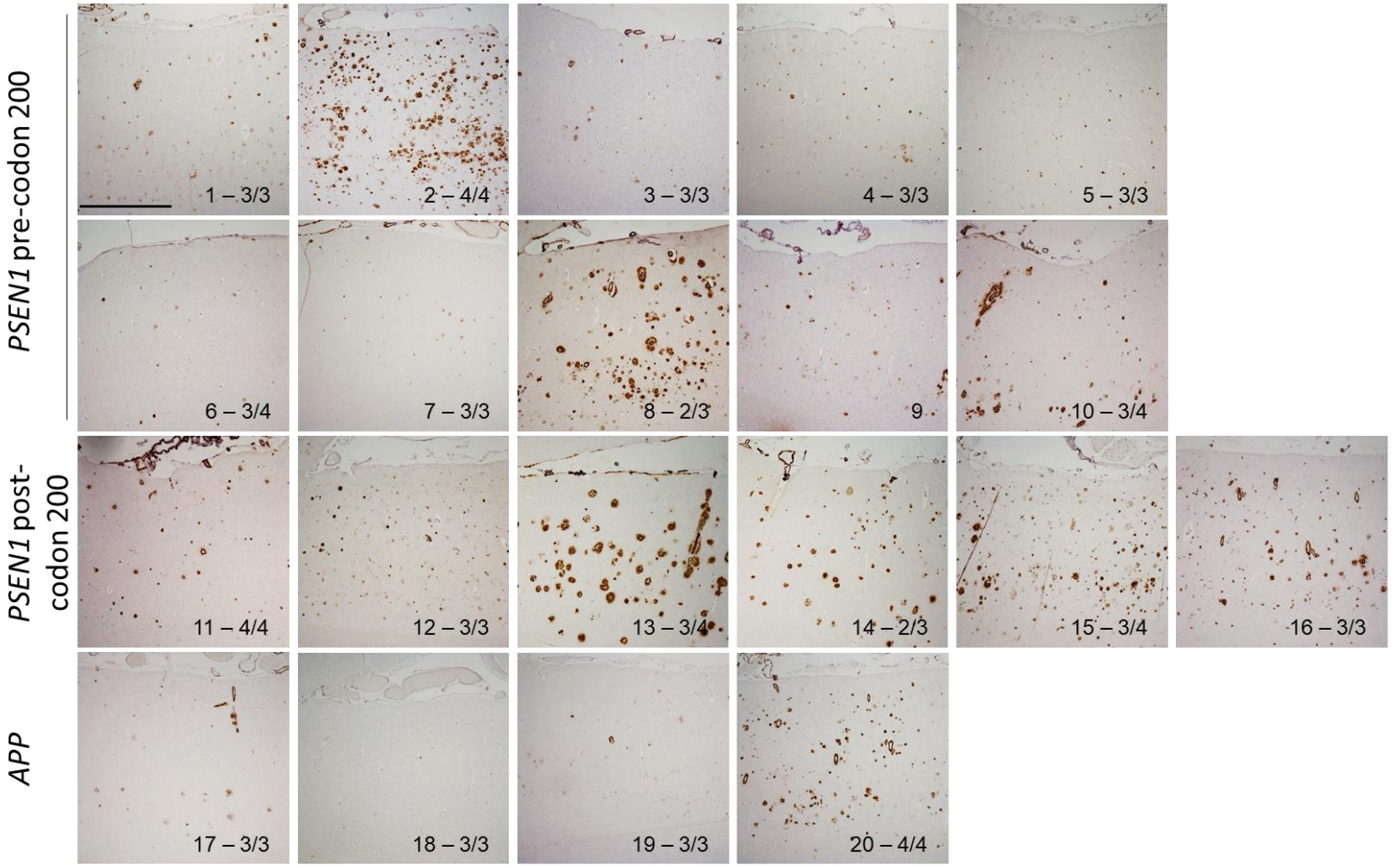

Figure 6-7 Representative images showing Aβ40 specific IHC in the occipital cortex, calcarine region.

Text on individual images represent QSBB cohort case number – *APOE* genotype. No *APOE* genotype available for case 9 Scale bar represents 100µm, 4x objective magnification.

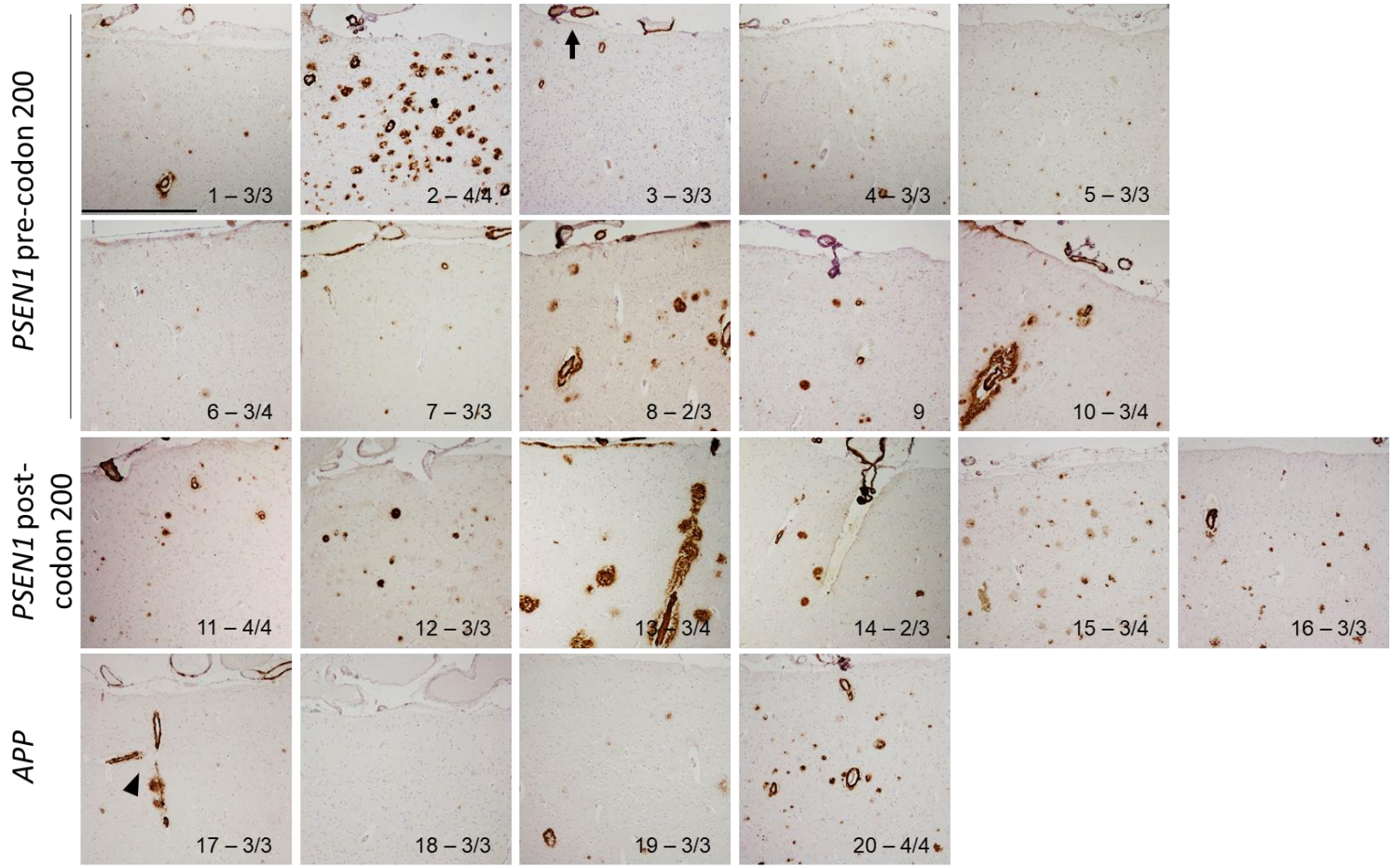

Figure 6-8 Representative images showing Aβ40 specific IHC in the occipital cortex, calcarine region.

Text on individual images represent QSBB cohort case number – *APOE* genotype. No *APOE* genotype available for case 9. Arrow indicates leptomeningeal CAA (3). Arrow head indicates cortical CAA (17). Scale bar represents 50µm, 10x objective magnification of images shown in Figure 6-7.

6.3.3 *Aβ43 IHC*

6.3.3.1 *Temporal cortex*

In contrast to Aβ42, but similar to Aβ40, Aβ43 positive staining was not present in all cases. For a comparison of specific cases see Figure 6-13. There was even a lack of Aβ43 in some cases where there was abundant Aβ40 staining e.g. *PSEN1* Intron4 case 2 and *APP* V717I case 20.

In the cases that have Aβ43 positive staining, there was evidence of plaques across the cortical layers although distinct patterns could be observed (Figure 1.9). For example, in *PSEN1* R278I cases 13 and 14, there were frequent plaques in all layers but staining intensity was faint in layer 3 compared to the staining in the remaining layers. In contrast, in *PSEN1* E280G case 15 there was frequent plaque deposition but staining intensity was faint in all layers. *PSEN1* pre-codon 200 E184D mutation cases 9 and 10 show further differences, with frequent plaque deposition in layer 3 and reduced plaque frequency in lower layers. *PSEN1* post-codon 200 cases 13-16 (*PSEN*1 R278I, R278I, E280G and A434T&T291A respectively) are distinct from the other cases with frequent plaques compared to all other cases, however the intensity is slightly less than that observed with Aβ42 staining. Moderately frequent plaque deposition was present in a few *PSEN1* pre-codon 200 cases (5: E120K 6: S132A, 9-10: E184D) and some weak staining in cases 3-4, 7 and 8 (*PSEN1* Intron4, Intron4, M139V and M146I, respectively). *APP* cases (17-20) has little to no Aβ43 positive staining, although the *APP* V717L case (17) had slightly more deposition compared to the *APP* V717I cases (18-20). Similar to Aβ40, there was intense staining of cores in cored plaques and Aβ43 positive cored plaques were frequently observed in all mutation sub-groups (*PSEN1* cases 3-4: Intron4, 5: E120K, 6: S132A, 7: M139V, 8: M146I, 9-10: E184D, 14: R278I, and *APP* V717I case 17). Diffuse pathology was seen in other cases (e.g. 13: R278I 15: E280G and 16: A434T&T291A) and CWP's were also present and this was particularly noticeable in case 16. There were no obvious differences in Aβ43 deposition between cases with or without an *APOE4* allele.

Aβ43 deposition was seen in cortical and leptomeningeal vessels in a select number of cases (2: Intron4, 5: E120K, 8: M146I, 9-10: E184D, 13-14: R278I, 15:

E280G and 16: A434T&T291A). These cases have both *PSEN1* pre and post-codon 200 mutations: Intron4, E120K, two E184D, two R278I, E280G and the double mutation A434T & T291I (Figure 6-9 and Figure 6-10). However, in some of these cases the intensity of staining was low compared to that of Aβ42 or Aβ40 (e.g *PSEN1* cases 8: M146I, 15: E280G) and there was an apparent lack of Aβ43 in the vessels in cases which had CAA in their vessels with Aβ42 or Aβ40 IHC (e.g *APP* V717I cases 19 and 20). Subpial Aβ43 deposition was absent in all cases except some very mild deposition in *PSEN1* post-codon 200 cases 13 (R278I) and 15 (E280G).

For a comparison of Aβ43 positive cases with frequent pathology compared to those with minimal pathology, see Figure 6-13.

6.3.3.2 *Occipital cortex*

Similar to the temporal cortex, Aβ43 was only noticeable in a few cases, and positive staining was much less frequent compared to the other antibodies (Figure 6-11 and Figure 6-12).

Aβ43 positive pathology was uncommon in *PSEN1* pre-codon 200 cases and in the *PSEN1* post-codon 200 cases 11 (I202F) and 12 (L250S). Interestingly, *PSEN1* post-codon 200 mutations R278I, E280G and A434T & T291A (cases 13-16) had a visually distinctive abundance of plaque deposition compared to all other cases. Noticeably, there was a lack of Aβ43 in the *APP* mutation cases. In cases with staining, there was evidence of central cores staining intensely. In the *PSEN1* post-codon 200 cases, which displayed the greatest pathology, plaques were intensely stained, including central cores (for example in R278I case 13) and there was intense staining of small dense deposits (e.g. A434T & T291A case 16). There were no obvious difference between cases with or without an *APOE4* allele.

As seen in the temporal cortex, Aβ43 deposition as occipital CAA in the cortex and leptomeninges was present in some cases (2: Intron4, 8: M146I, 10: E184D, 13-14: R278I, 15: E280G, 16: A434T & T291A) although not always to the extent of intensity seen in the Aβ40/42 IHC (Figure 1.12). Some cases which had CAA detectable with the other antibodies did not display CAA with Aβ43 e.g. cases 7 (*PSEN1* M139V), 17 (*APP* V717L) and 20 (*APP* V717I). Diffuse subpial Aβ43

pathology was present only in the R278I case 13 and very mildly in case 14, despite subpial pathology having been present in other cases when stained with the Aβ40/42 antibodies.

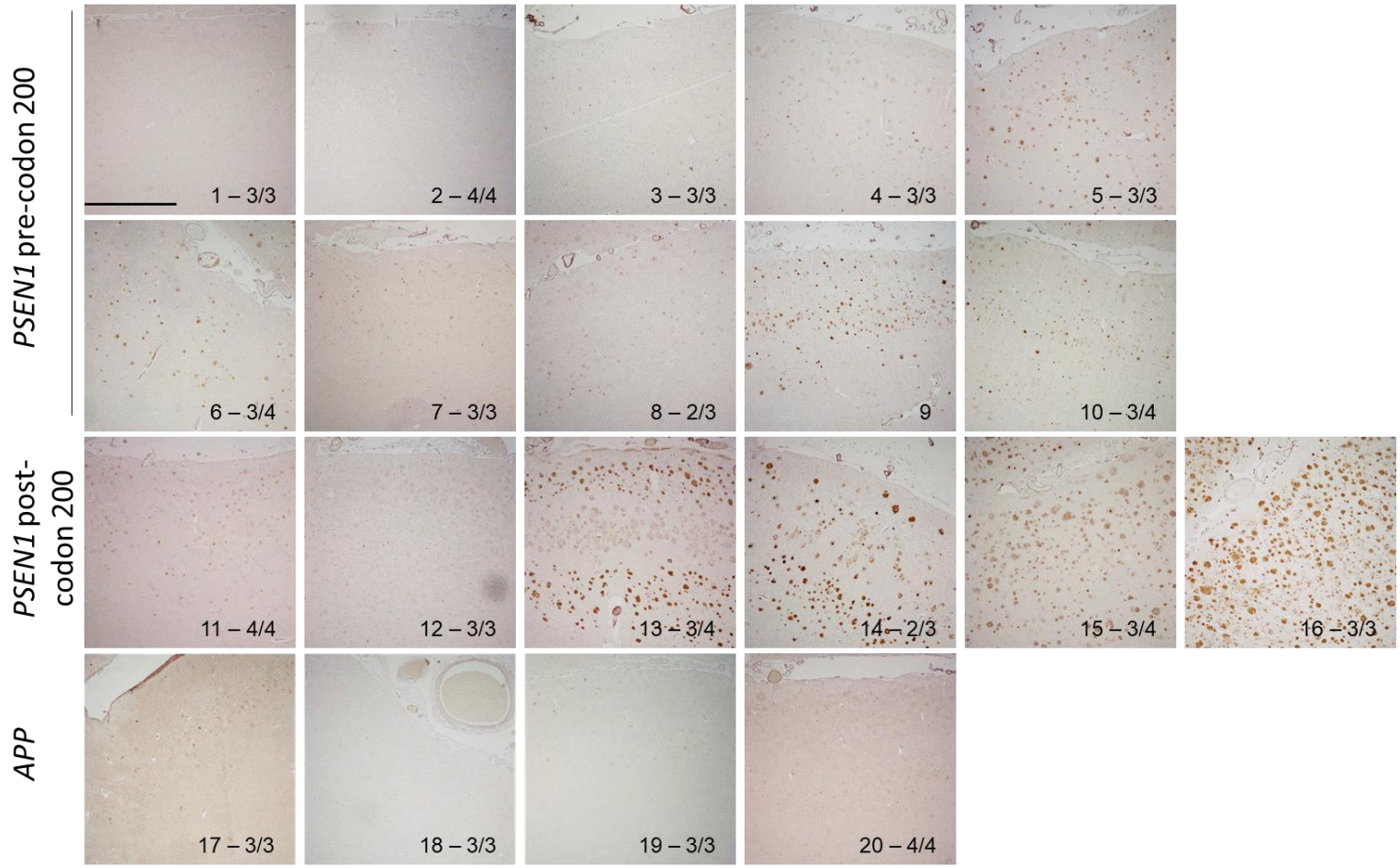

Figure 6-9 Representative images showing Aβ43 specific IHC in the temporal cortex.

Text on individual images represent QSBB cohort case number – *APOE* genotype. No *APOE* genotype available for case 9 Scale bar represents 100µm, 4x objective magnification.

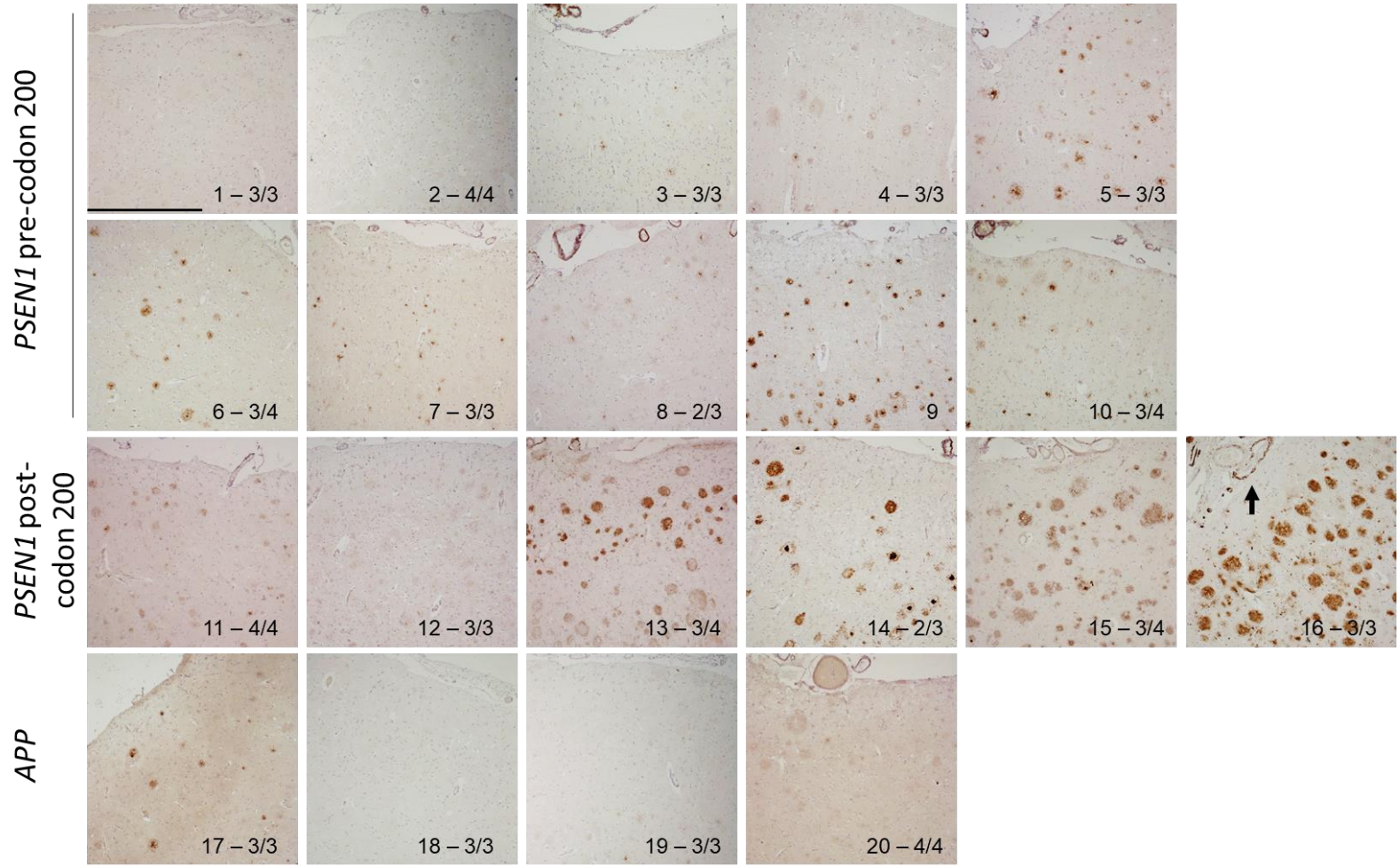

Figure 6-10 Representative images showing Aβ43 specific IHC in the temporal cortex.

Text on individual images represent QSBB cohort case number – *APOE* genotype. No *APOE* genotype available for case 9. Arrow indicates leptomeningeal CAA (16). Scale bar represents 50µm, 10x objective magnification of images shown in Figure 6-9.

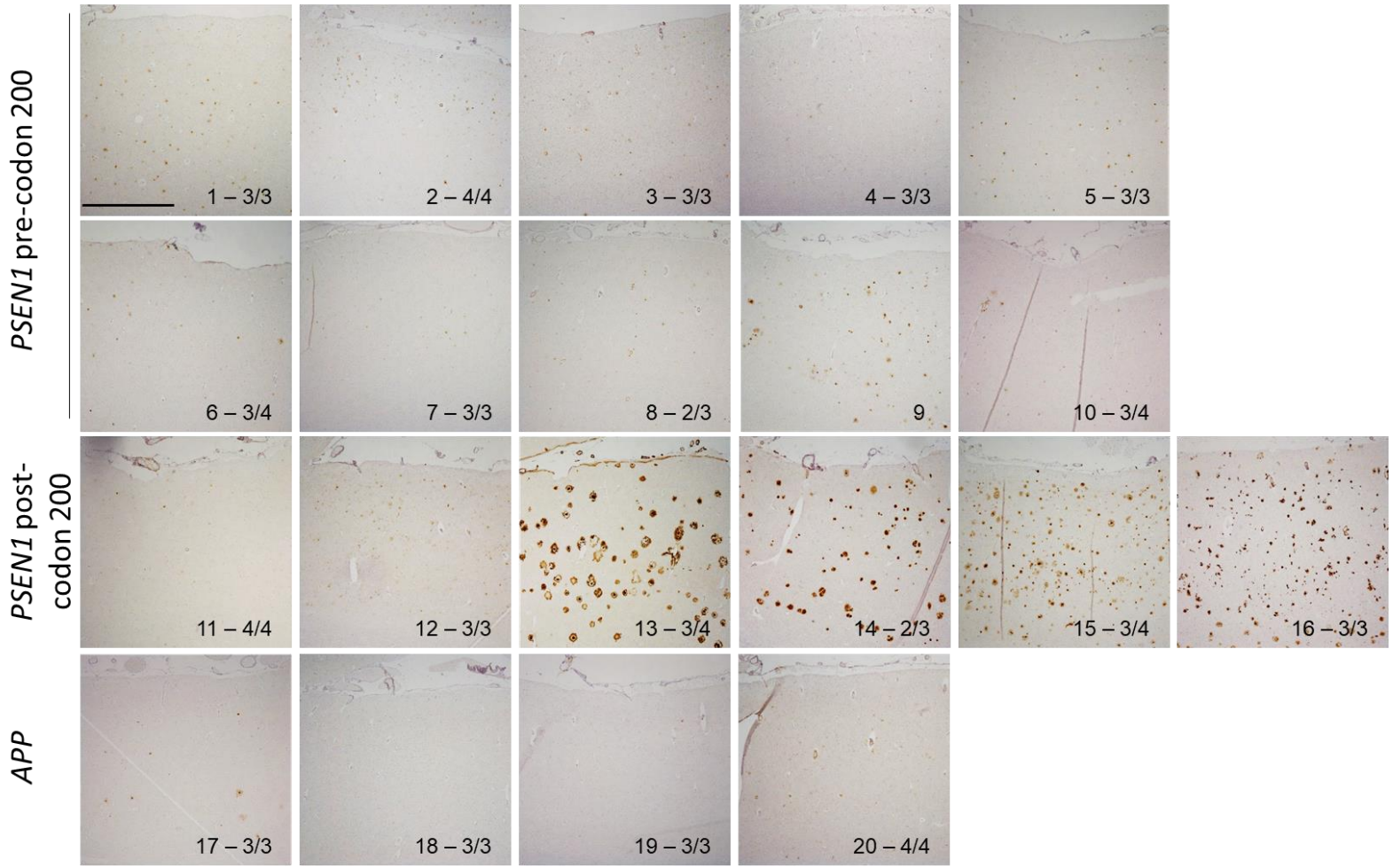

Figure 6-11 Representative images showing Aβ43 specific IHC in the occipital cortex, calcarine region.

Text on individual images represent QSBB cohort case number – *APOE* genotype. No *APOE* genotype available for case 9. Scale bar represents 100µm, 4x objective magnification.

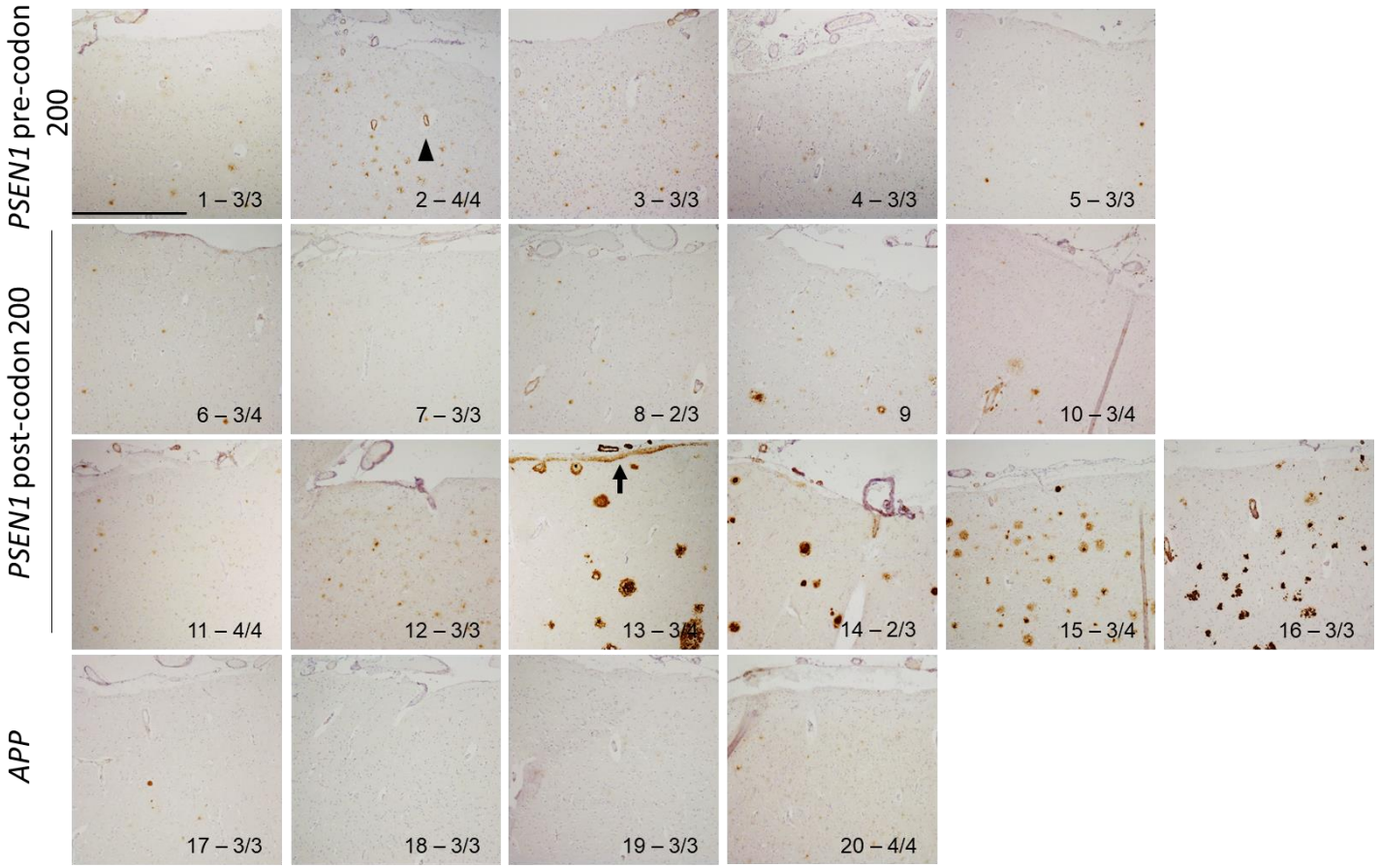

Figure 6-12 Representative images showing Aβ43 specific IHC in the occipital cortex, calcarine region.

Text on individual images represent QSBB cohort case number – *APOE* genotype. No *APOE* genotype available for case 9. Arrow indicates leptomeningeal CAA (13). Arrow head indicates cortical CAA (2). Scale bar represents 50µm, 10x objective magnification of images shown in Figure 6-11.

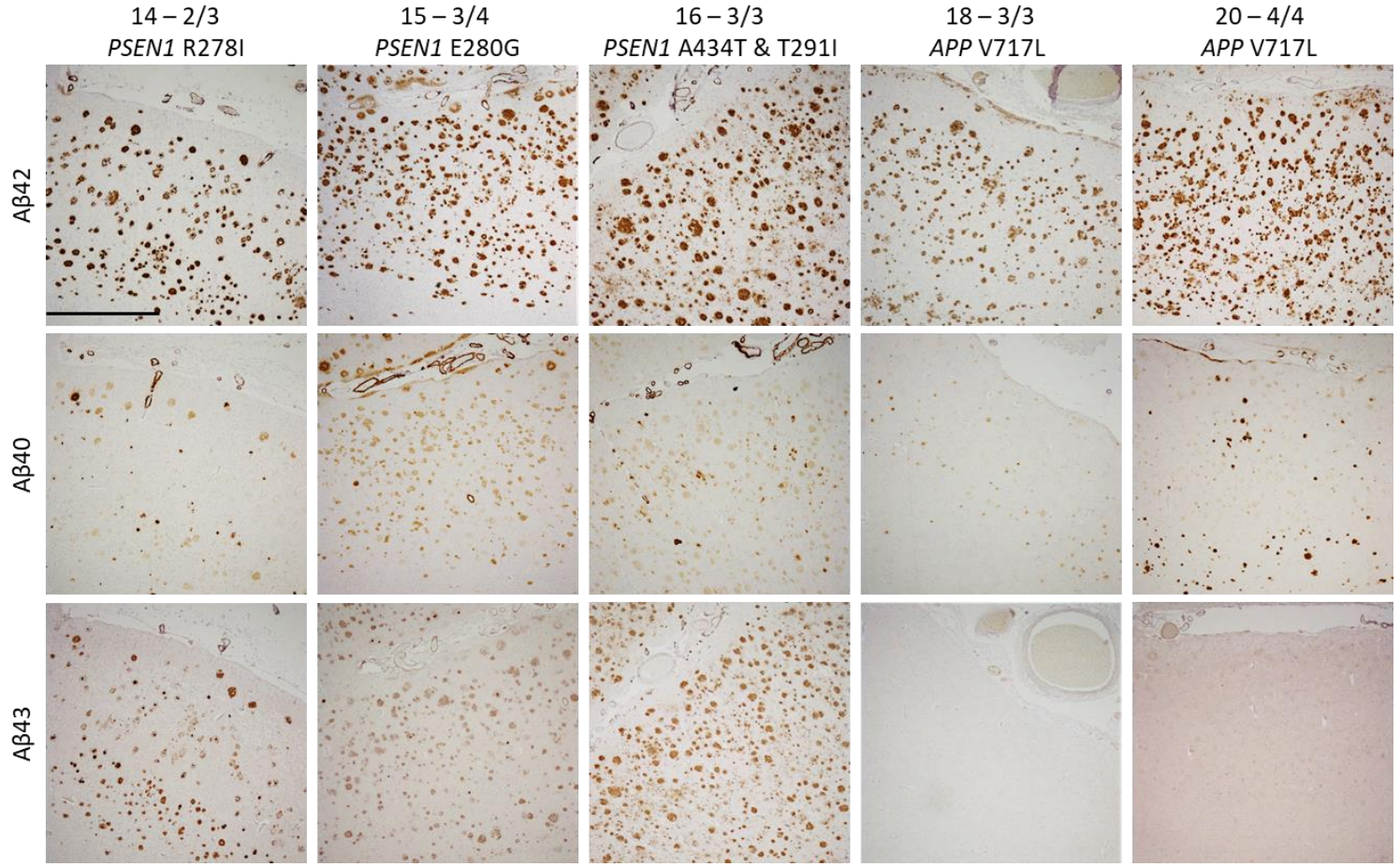

Figure 6-13 Comparison of Aβ42, 40 and 43 IHC between cases with varying Aβ profiles in the temporal cortex.

PSEN1 post-codon 200 cases 14-16 were all strongly positive for Aβ42, 40 and 43. Case 18 was representative of cases with Aβ42 positivity but little to no positivity for Aβ40 and 43. Case 20 with APOE4/4 was positive for Aβ42 and 40 but not Aβ43. Scale bar represents 100µm, 4x objective magnification.

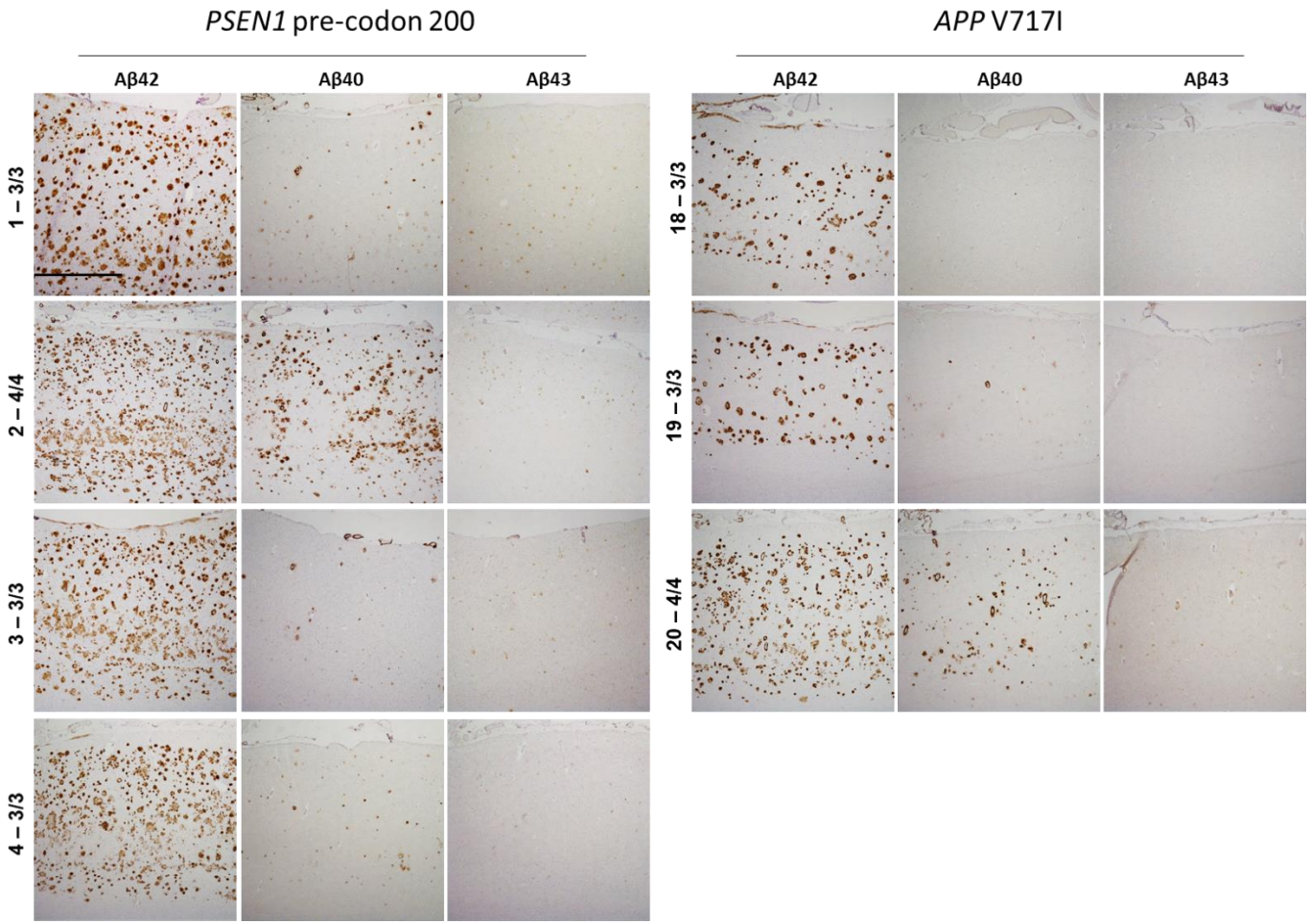

Figure 6-14 Effect of *APOE*4 genotype on Aβ isoform pathology.

PSEN1 pre-codon 200 Intron4 cases, column A = Aβ42 in, B = Aβ40, C = Aβ43. *APP* V717I cases, column D = Aβ42, E = Aβ40, F = Aβ43. Labels on the left side of images refer to case number and *APOE* genotype. Occipital cortex, scale bar represents 100µm, 4x objective magnification.

6.4 **Discussion**

	Main findings
Aβ *isoform contribution to plaques*	Aβ42 was present in all plaque types and CAA. Aβ40 was notable in the central cored of cored plaques and in CAA. Aβ43 was notable in the central cored of cored plaques, but also evident in other plaque types. It had reduced CAA contribution.
Aβ *isoform differences between FAD mutation sub-groups*	*PSEN1* post-codon 200 group had greater Aβ43 deposition, particularly in the *PSEN1* R278I, E280G and A434T & T291A mutation cases.
Aβ *isoform differences between APOE4 genotypes*	Greater Aβ40 was observed in *APOE*4 carriers, including when compared to same mutation A*POE*4 negative cases.

This study aimed to assess Aβ specific isoforms in the QSBB FAD cohort. The regional and cortical layer distribution was observed, as were mutation group and *APOE4* status differences. Differences in plaque composition was also noted. All assessments within this chapter were purely descriptive with no statistical tests applied. However observational analysis enabled trends and associations to be observed. While isoform patterns have been studied before, this research expanded the depth and breadth of analysis and has revealed important genetic implications.

Regional differences

Regional differences in Aβ pathology have been previously described (Martikainen *et al.*, 2010; Pearson *et al.*, 1985; Rogers & Morrison, 1985). In our cohort using isoform specific IHC, Aβ40 and Aβ43 pathology displayed no clear differences between the temporal and occipital cortices with similar frequency in both regions (Chapter: 6.3.2 and 6.3.3). It could have been expected to see greater Aβ40 in the occipital cortex due to its greater propensity for CAA, however this was not readily observed. Aβ43 is not necessarily produced in large quantities by all FAD mutations so regional differences were not expected. Aβ42

was frequent in all cases and generally consistent across regions although it was noted there was potentially less deposition in the occipital cortex in the *APP* cases only (Chapter: 6.3.1). Although associated with later age at onset, *APP* cases in the QSBB cohort were not associated with a shorter duration so it may not be due to reduced time for the aggregates to form. *APP* V717I mutations, have been shown to alter Aβ42:40 ratios by increasing Aβ42 (Charles Arber *et al.*, 2019a; De Jonghe *et al.*, 2001). This does not explain the observed decreased Aβ42 plaque deposition. A more detailed level of assessment would be required, as visual inspection at low magnification is not powerful enough to analyse discrete differences. In general, the regional observations are similar and the Aβ42 staining was similar to that observed in the frontal cortex in chapter 3: Figure 3-2, with the same types of amyloid pathology observed.

Isoform differences

As expected, we saw differences in the amount of staining between the isoform specific antibodies. Aβ42 positive staining was frequently present in all cases, while Aβ40 and Aβ43 positive staining differed between cases and may be linked to mutation and *APOE* status (See Figure 6-13 and Figure 6-14). Aβ42 stained all plaque types including CWPs, was largely responsible for diffuse pathology, was present in cortical and leptomeningeal vessels, and looked similar to staining with the DAKO Aβ antibody, which binds to all Aβ isoforms which contain residues 8-17. Aβ40 varied between cases, but displayed preferences in most cases for the central core of cored plaques and CAA. This is similar to observations reported by others (Fukumoto *et al.*, 1996b; Hirayama *et al.*, 2003; Iwatsubo *et al.*, 1994; Kumar-Singh *et al.*, 2002; Nakamura *et al.*, 1995; Uchihara *et al.*, 2003; Yamaguchi *et al.*, 1995). Aβ40 is known to be the least aggregation prone isoform and is found at high levels in CSF indicating its clearance (Portelius *et al.*, 2006; Vigo-Pelfrey *et al.*, 1993), which may be why lower plaque but greater vessel pathology is observed with this isoform.

Aβ43 was also seen predominantly in plaque cores but was the least frequently observed isoform, with noticeable expression in select cases, including *PSEN1* mutation cases R278I, E280G and A434T & T291A. In these cases, presence of Aβ43 in CWPs could be observed, particularly in the temporal cortex. Slight Aβ43 deposition in the blood vessels was present in cases with high plaque pathology

as well as a *PSEN1* Intron4 mutation case which also had high Aβ40 pathology and CAA (case 2). Aβ43 deposition in vessels agrees with some and contrasts with other research findings (Iizuka *et al.*, 1995; Kakuda *et al.*, 2017; Keller *et al.*, 2010). In some of the cases with Aβ43 in the vessels, it has been shown that these mutations are linked to high ratios of Aβ43, including R278I and A434T (Charles Arber *et al.*, 2019a; Nakaya *et al.*, 2005; Veugelen *et al.*, 2016). Therefore, in cases with greater Aβ43 levels or ratios, presence along clearance pathways may be expected. Some studies may have lacked Aβ43 generating mutation cases, therefore failed to detect this type of pathology. It is unlikely that lack of Aβ43 pathology in other cases is related to better clearance of this isoform (as is the case for Aβ40) due to Aβ43's aggregation propensity (Conicella & Fawzi, 2014). Using additional methods to analyse Aβ isoforms may shed more light on the contribution of different isoforms to pathology, particularly with ELISA and mass spec methods. Lack of observation of certain isoforms by IHC does not guarantee lack of expression in the tissue as low level production of toxic species may prevent visible plaques due to fibrilisation thresholds not being met. Additionally, mass spec will enable analysis of post translational modifications such as the previously mentioned pyroglutamate and others including isoaspartate, which may also be important in pathogenesis (Barykin *et al.*, 2017; Wildburger *et al.*, 2017; Zakharova *et al.*, 2018).

Mutation differences

When comparing between mutation groups, there did not appear to be any obvious differences in the deposition of Aβ42 between the groups (Chapter: 6.3.1). When considering Aβ40, there were varied levels between cases, however there was Aβ40 cases present in all mutation groups (Chapter: 6.3.2). Distinct alterations in Aβ pathway selection have been noted in specific mutations and may explain these mutation specific differences. For instance mutations which lead to greater selection of the Aβ49 pathway, which can lead to the generation of Aβ40 may result in greater cortical Aβ40 deposition. Mutations which result in increased selection of the Aβ49 pathway include *PSEN1* R278I and A434T (Charles Arber *et al.*, 2019a; Sun *et al.*, 2017). It would be interesting to investigate if the Aβ40 positive cases are those which have shown higher levels of CAA as that may account for some of the differences in vessel staining. Indeed, some cases (2, 8, 13, 14, 16 and 20) had notable high CAA positive vessels in

the occipital cortex, with Aβ40 positivity seen in the occipital cortex Aβ40 specific IHC.

Aβ43 was not observed in all cases (6.3.3). There was little to none present in the *APP* cases, suggesting that *APP* V717I and V717L mutations favour the processing of Aβ via the Aβ48 pathway, as has been previously suggested (Charles Arber *et al.*, 2019a). This matches with the idea that *APP* mutations lead to altered Aβ42:40 ratios due to amino acid changes altering APP structure, hindering processivity (Dimitrov *et al.*, 2013). In the *PSEN1* post-codon 200 cases there was frequent Aβ43 in the *PSEN1* R278I, E280G and A434T & T291A cases. As mentioned, multiple studies have shown the R278I mutation is associated with increases in Aβ43 ratios (Charles Arber *et al.*, 2019a; Nakaya *et al.*, 2005; Veugelen *et al.*, 2016). The findings from our R278I case support this, highlighting how this work is complementary in that it shows Aβ43 deposition in human brain tissue, which was not used in the previously mentioned studies (Saito *et al.*, 2011b; Veugelen *et al.*, 2016). Aβ40 deposition is also apparent, which would be expected given that both Aβ40 and 43 are on the same Aβ pathway. Similar findings have been found in an A434T mutation model and in other mutations near this locus (Kretner *et al.*, 2016; Nakaya *et al.*, 2005; Sun *et al.*, 2017), with these similar results replicated in our T291I & A434T double mutation case. Additionally, high levels of Aβ40 production in a cell model of the alternative T291P mutation have been found, matching our pathological observation of Aβ40 in the tissue of the T291I & A434T double mutation carrier (Dumanchin *et al.*, 2006). The E280G mutation has been shown to have an increased Aβ42:40 ratio compared to controls, but this was not as significant as other mutations (Dumanchin *et al.*, 2006), which may imply Aβ40 levels are still high in these mutations. This would correspond to the high Aβ40 seen in our case with this mutation. Despite the reduced Aβ40 ratio, pathology may be high in these cases with Aβ43 as it has the ability to aggregate Aβ40 (Burnouf *et al.*, 2015). The link between these observations and reported Aβ ratios highlights mutation specific differences in Aβ isoform pathology. This may have effects on disease course due to varying toxicity of the different isoforms. Interestingly, some cases without Aβ43 had Aβ40 pathology, suggesting better cleavage of Aβ43 to Aβ40 in those mutation cases.

<u>Differences between *APOE* genotypes</u>

As discussed, Aβ deposition is frequently shown to be higher in *APOE*4 carriers. By microscopic observation in our cohort, the frequency of Aβ42 or Aβ43 did not appear to differ by *APOE* genotype (Chapter: 6.3.1 and 6.3.3 and Figure 6-14). In chapter: 3.3.4, there was a non-significant trend for increased average Aβ load in our *APOE*4 carriers. The increase in *APOE*4 carriers may therefore be due to increased Aβ40. In this cohort, the Aβ40 IHC revealed an increase in cortical Aβ40 pathology in *APOE*4 carriers (Chapter: 6.3.2 and Figure 6-14). Aβ40 deposition was also particularly strong in blood vessels, however this was also observed in *APOE*4 non-carriers. As previously discussed, *APOE*4 is associated with greater Aβ40 deposition in sAD cases and has been suggested in FAD cases (Gearing *et al.*, 1996; David M. A. Mann *et al.*, 2001; P. M. Smith *et al.*, 1997) and *APOE*4 has previously shown no effect on Aβ42 pathology in sAD and FAD (Ishii *et al.*, 2001). Our results show this same effect of *APOE*4 in FAD. In particular we show that this effect appears to be consistent across the same mutation, in different mutation carriers, namely the *PSEN1* Intron4 and *APP* V717L mutation cases.

Pathologically, Intron4 cases have been shown to express high Aβ42 pathology, but generally low Aβ40 pathology, although presence as CAA can be seen and distinct patterns of cortical layer pathology have been noted, with diffuse pathology in upper layers which became more compact in the lower layers (Janssen *et al.*, 2000; Singleton *et al.*, 2000). Analysis of *PSEN1* intron4 mutation cell lines also confirms significantly increased Aβ42:40 ratios compared to controls (Charles Arber *et al.*, 2019b). Aβ42 production by PSEN1 was also shown to be increased in extracts containing PSEN1 from *PSEN1* Intron4 mutation brain tissue, and this was notable in comparison to control and other *PSEN1* mutations (Szaruga *et al.*, 2015). In our cases, Aβ40 is relatively low except in the *APOE*4 positive case, which supports the suggestion that Aβ40 deposition is influenced by the *APOE*4 genotype.

Frequently, in *APP* V717I lines Aβ40 ratios or levels have been shown to be low in comparison to other mutations (De Jonghe *et al.*, 2001; Muratore *et al.*, 2014; Tamaoka *et al.*, 1994). Using patient iPSC-derived neuronal cell lines, we have also shown this mutation produces greater Aβ42 and Aβ42:43 ratios compared to controls, with no significant difference in Aβ43:40 compared to controls (Charles Arber *et al.*, 2019b). These results indicate that this mutation

significantly affects the Aβ48 pathway, increasing Aβ42 production and not Aβ40 production. Again this supports the suggestion that Aβ40 deposition is enhanced by the *APOE*4 genotype in these cases. As APOE4 has been shown to increase the Aβ40 fibrilisation potential, this may explain the mechanism for this increased deposition. This highlights that even in FAD, *APOE*4 genotype can affect pathological outcome.

Interestingly, in the two R278I mutation cases, Aβ40 pathology was frequent in both cases despite one being an *APOE4* carrier and the other a non-carrier (Chapter: 6.3.2). The non-carrier did however have an ε2 allele which has also been linked to CAA, which is highly composed of Aβ40. However, as there are only two cases with this mutation, it cannot be confirmed how much the pathology is influenced by the *APOE* genotypes. It is possible that FAD cases which lead to selection of the Aβ49 pathway, as has been shown in R278I mutations, also lead to high Aβ40 pathology, regardless of APOE4 influences. FAD mutations driving Aβ40 pathology were seen in other *APOE*4 negative cases, although there were no additional matched mutation cases for comparison. A larger number of same mutation cases with different *APOE* genotypes would be needed to explore these differences further and decipher the influence of *APOE*4 genotype.

Conclusion

The results from this small subset confirm previous findings regarding isoform specific pathology but extended this into a range of *PSEN1* and *APP* mutation cases, with matched mutations and differing *APOE* genotypes for comparison. The results highlight the importance of *APOE* genotypes in FAD and that these should be considered in FAD patients, particularly in relation to amyloid-modifying therapy trials. CAA is increased in some patients after amyloid modifying treatment, and is noted particularly in *APOE*4 carriers. The release of the pool of Aβ40 present in the parenchyma at higher levels in *APOE*4/4 carriers may contribute to the greater risk of immune responses to vascular amyloid that may be seen following these therapies. It may therefore be important in future clinical trials of these therapies to take into account both FAD mutation and *APOE* genotype and consider stratifying treatment accordingly.

Chapter 7

Cellular model of FAD

7 Cellular model of FAD

7.1 Abstract

Introduction: Mutations in FAD alter the cleavage of APP, affecting APP processing, leading to generation of Aβ. In particular, alterations in the ratios of Aβ isoforms may be particularly influential in disease pathogenicity and heterogeneity.

Methods: Using two control and four iPSC cells lines from *PSEN1* FAD mutation carriers (One M146I, one R278I and two E280G), two of which were generated for this study, the Aβ profiles of FAD mutation lines were analysed and PSEN1 protein maturity assessed.

Results: Aβ ratios significantly differed between FAD lines and controls, and between FAD lines. Aβ ratios were significantly altered in a mutation specific way. Aβ42:40 was increased in the M146I and E280G lines compared to controls but was not significantly different in R278I neurons. The Aβ43:40 ratio was increased in R278I and E280G lines compared to controls while M146I was not. Differences were not related to changes in *PSEN1* expression. PSEN1 maturity may also differ in association with mutation.

Conclusions: These results, in concert with other similar findings, highlight the role of mutation location in the pathological phenotype, due to alterations in PSEN1 activity. By using iPSC, it is possible to analyse alterations in molecular mechanisms in FAD and further study will enable greater understanding of pathogenic mechanisms in AD.

7.2 Introduction

As discussed in Chapter: 1.7 Aβ peptides of varying length are generated via the initial epsilon cleavage of the C99 fragment producing Aβ49 and Aβ48. These fragments are further cleaved in a carboxypeptidase manner, generating the small Aβ fragments (Figure 7-1). As discussed previously (Chapter: 6) Aβ isoforms have different pathological presentation, and Aβ ratios are linked to disease progression. Additionally, ratios are altered in mutation specific ways. Studies in cell lines with FAD mutations have complemented these findings (Charles Arber *et al.*, 2019a; Suárez-Calvet *et al.*, 2014; Sun *et al.*, 2017;

Veugelen *et al.*, 2016). Importantly the analysis of ratios in cell models is likely reflective of the early perturbations in Aβ processing, a benefit compared to FAD brain tissue which is end stage.

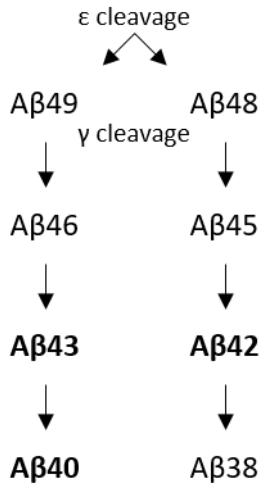

Figure 7-1 Aβ generation.

The initial epsilon cleavage by γ-secretase of the C99 fragment leads to the generation of an Aβ49 or Aβ48 peptide which undergoes sequential cleavage.

Evidence from cell assays suggests that the majority of *PSEN1* mutations are believed to cause an increase in the ratio of Aβ42 to total Aβ, compared with wild type *PSEN1* (Murayama *et al.*, 1999). However, it is known that the mechanism by which ratios are altered can differ by mutation. In transfected SH-SY5Y cells, *PSEN1* I249L and *PSEN1* P433S mutations were shown to have differing effects on Aβ production. Both lines generated increase Aβ42/40 ratios, but only the P433S mutation inhibited PSEN1 endoprotease activity and had enhanced Aβ43 production (Shen *et al.*, 2019). Mouse embryonic fibroblasts with the PSEN1 I213T mutation showed altered Aβ ratios, which was driven by a decrease in Aβ40 production, caused by reduced γ-secretase activity. This was confirmed in mouse brain homogenate with the same mutation. Even though there were ratio alterations, there was an additional overall decrease in Aβ production, highlighting a mutation effect on PSEN1 activity (Shimojo *et al.*, 2008). In cells stably expressed a range of FAD mutations, authors found the method of Aβ42/40 ratio alteration occurred via mutation specific mechanisms (N. Li *et al.*, 2016). Six mutations mainly increase the generation of Aβ42 by decreasing the cleavage of Aβ42-Aβ38 and Aβ43-Aβ40 implicating γ-secretase disruption, while epsilon cleavage alteration was implicated in six mutations which increased selection of

the Aβ48 line, and one case lead to a decrease in the selection of the Aβ49 pathway. An important study randomly generated FAD mutations and expressed them in cell lines to analyse mutation characteristics, including PSEN1 maturity. Initially, PSEN1 exists as a full length immature form which undergoes proteolytic autocleavage to generate mature PSEN1 composed of an N-terminal and C-terminal unit. Western blot analysis reveal multiple mutations results in an increase in immature PSEN1, including the A434T, L435H, and R278I mutations. The R278I, L435H and A434T lines showed increased Aβ43 production compared to Aβ40 production via ELISA. Further investigation of the L435H, and R278I mutations showed this alteration in Aβ profile was not a consequence of altered PSEN1 cellular location, and through additional mutagenesis at these residues they found that the effect on PSEN1 was caused by mutations and this was specific to distinct SNP which caused specific amino acid alterations (Nakaya *et al.*, 2005). Although these studies were not conducted in human iPSC derived neurons, they show how mutations can differ in their contribution to disease.

In a study using some of the iPSC generated in this chapter, 7 iPSC FAD lines were differentiated in to neurons and Aβ ratios analysed. Compared to controls, all FAD lines had increased Aβ42:40 ratios. However, ratios for Aβ43, Aβ38 and other shorter fragments showed variation compared to controls. For example i) the *APP* V717I mutation lead to a preference for the Aβ48 pathway ii) the M146I mutation lead to increased Aβ42 ratios, possibly via reduced PSEN1 processivity and iii) the R278I mutation lead to greater Aβ43 ratios, possibly via selection of the Aβ49 pathway and reduced PSEN1 processivity. Between individual mutation lines differences were also observed, although they were not compared statistically (Charles Arber *et al.*, 2019a). Another recent study from the author showed that Aβ ratios were altered in a CRISPR edited *PSEN1* intron4 deletion mutation cell line series. This alteration was in a gene dosage specific manner with greater differences in the homozygous mutant cell line (Charles Arber *et al.*, 2019b). These findings show that PSEN1 γ-secretase processivity can be modelled in iPSC derived neurons with FAD mutations, which may be more relevant to disease than other non-neuronal models.

There are fewer studies which involve numerous *APP* mutations, however from those that exist, they tend to show an increase in Aβ42 production, and this was also observed in a DSAD line which had *APP* trisomy (Dashinimaev *et al.*, 2017).

However, there are different expression patterns between different *APP* mutations, with overall decreased extracellular Aβ40 and Aβ42 in the *APP*E693Δ mutation line while an *APP* V717L mutation line had increased extracellular Aβ42 (Kondo *et al.*, 2013).

Comparison between *PSEN1* and *APP* mutation in iPSC derived neurons also highlights mutation differences between causative genes, with *PSEN1* mutations showing reduced percentage of Aβ40 and reduced ratio of Aβ38/Aβ42 compared to *APP* V7171I neurons (Moore *et al.*, 2015). Using ELISA to analyse conditioned media, a patient fibroblast cell line with the PSEN1 I143T mutation showed an increased Aβ42:40 ratio compared to controls and an *APP* KM670/671NL mutation line (Keller *et al.*, 2010).

Additionally, findings in FAD iPSC have been observed in FAD and sAD tissue, with increased ratios of the Aβ peptides, implying γ-secretase alterations can occur in sAD (Sandebring *et al.*, 2013). These universal findings highlight how these models are essential to developing basic molecular understanding, necessary for drug design and advancement.

Precise mechanisms by which mutations alter Aβ ratios are still being explored. However, in some specific mutations an increase in Aβ43 ratio has been linked to an increase in the immature form of PSEN1. The *PSEN1* R278I mutation is one that has previously been shown by our group (Charles Arber *et al.*, 2019a), but also by other groups in different models (Nakaya *et al.*, 2005; Saito *et al.*, 2011b; Veugelen *et al.*, 2016). Importantly, alterations in PSEN1 maturity was not caused by differences in *PSEN1* expression, and *APP* expression did not differ either (Charles Arber *et al.*, 2019a) implying the mutation affects disease by alterations in the structure of the encoded protein. Along with R278I, other mutations with high Aβ43 ratios tend to lie around the intracellular loop implicating the lack of PSEN1 endoproteolysis as a driver of this phenotype.

Overall there is evidence to suggest that mutations lead to specific alteration in Aβ processing and in *PSEN1* mutation cases this is due to alterations in PSEN1 processivity. However, the E280G mutation has not previously been investigated in iPSC. Although compared to controls, HEK lines expressing this mutation showed significantly increased Aβ42 concentration, non-significantly increased Aβ40 concentration and an overall significantly increased Aβ42:40 ratio in

conditioned media (Dumanchin *et al.*, 2006). However, as discussed by the authors, these results suffer from the caveat that only mutated PSEN1 is expressed in these lines compared to heterozygous mutation carriers where wild type PSEN1 is also expressed. Pathologically, a biopsy from a PSEN1 E280G carrier showed numerous Aβ deposition, including CWPs and CAA (O'Riordan *et al.*, 2002). E280Q mutations also show similar pathology (Rogaeva *et al.*, 2003). With a patient derived E280G fibroblast cell line available, Aβ will be investigated in this line, with the hypothesis that the mutation will lead to an increase in Aβ43:40 ratio compared to controls due to its proximity to the R278I mutation.

7.2.1 *Aims*

Cellular models with FAD mutations can be used to investigate the molecular effects of the precise mutations. In this chapter, the aim was to generate FAD IPSC, explore molecular effects of mutations in induced cortical neurons and to extend the resource of FAD mutation IPSC available for future research. The main aims were:

1. To generate a range of FAD mutation containing stem lines by reprogramming patient derived fibroblasts, including the E280G mutation.

2. To induce a range of FAD mutation containing iPSC in to neuronal like cultures.

3. To determine the secreted Aβ peptide profiles of a range of FAD mutations from induced cortical neuronal like cultures.

4. To determine PSEN1 maturity from a range of FAD mutations in lysate derived from induced cortical neuronal like cultures.

7.2.2 *Material and methods*

Methods used for this project are described in chapter: 2.6-2.8. In brief, fibroblasts were reprogrammed into iPSC using the Shi *et al.* (2012b) method. Cells were transfected with episomal vectors to convert fibroblasts into a stem cell phenotype. iPSC were then pushed towards a neuronal fate using dual SMAD inhibition. Aβ in conditioned media from day 100 media was analysed by ELISA, PSEN1 protein was analysed by western blot and qPCR, neuronal phenotype

was assessed by ICC and qPCR, with statistical analysis conducted where appropriate.

7.3 **Results**

7.3.1 *Data analysis methods*

ELISA Data within this chapter were assessed for normality using QQ plots (see chapter: 9

Appendix, Figure 9-8) and qPCR data for PSEN1 was assessed for normality (Figure 7-15). QQ plots show results are reasonably normally distributed and so parametric statistical analysis have been applied throughout.

7.3.2 *Reprogramming and characterisation*

In total, five separate stem cell lines were generated from patient fibroblasts: four *PSEN1* mutations (R278I, Y115H and two E280G) and one *APP* V717I. Demographic details of each participant are shown in Table 7-1.

Mutation	Line name	Sex	D.O.B.	Biopsy date	Age at onset	Status at biopsy	*APOE* status	*TREM2 R62H*
-	A1	F	-	20-24	-	-	3/4	n/a
-	RB101	M	-	45-49	-	-	3/3	n/a
APP V717I *		F	1970	15.12.14	-	A-symptomatic	3/3	n/a
PSEN1 Y115H *		M	1971	22.11.10	34	Affected	3/3	n/a
PSEN1 M146I	M146I	M	1974		33	Affected	3/3	n/a
PSEN1 R278I *	R278I	M	1950	15.11.10	58	Affected	2/4	n/a
PSEN1 E280G *	E280G.A	M	1966	15.09.15	38	Affected	3/4	G/A
PSEN1 E280G *	E280G.B	M	1968	10.03.14	41	Affected	3/3	G/G

Table 7-1 Stem cell line clinical data.

D.O.B.: Date of birth. n/a: *TREM2* genotype not confirmed in these cases. Asterisk (*) indicates mutation lines reprogrammed for this study.

Fibroblasts were reprogrammed as described in 2.6.1. Stem cell identity was confirmed via ICC to markers of pluripotency: SSEA4 and Oct4 (Figure 7-2 and Figure 7-3). SSEA4 is a glycosphingolipid cell surface antigen expressed in early embryonic development and in pluripotent stem cells. It's expression expected in puncta throughout the cell (Breimer *et al.*, 2017; Kannagi *et al.*, 1983). Oct4 is a transcription factor involved in pluripotency maintenance and its expression is expected within the cell nucleus (Nichols *et al.*, 1998; Pan *et al.*, 2002). Both markers are restricted to this stem cell stage and should not be expressed upon differentiation. ICC confirming stem cell identity in the *APP* V717, *PSEN1* Y115H,

R278I, E280G.A and E280G.B cell lines is shown in Figure 7-2 and the A1, RB101 and M146I cell lines is shown in Figure 7-3.

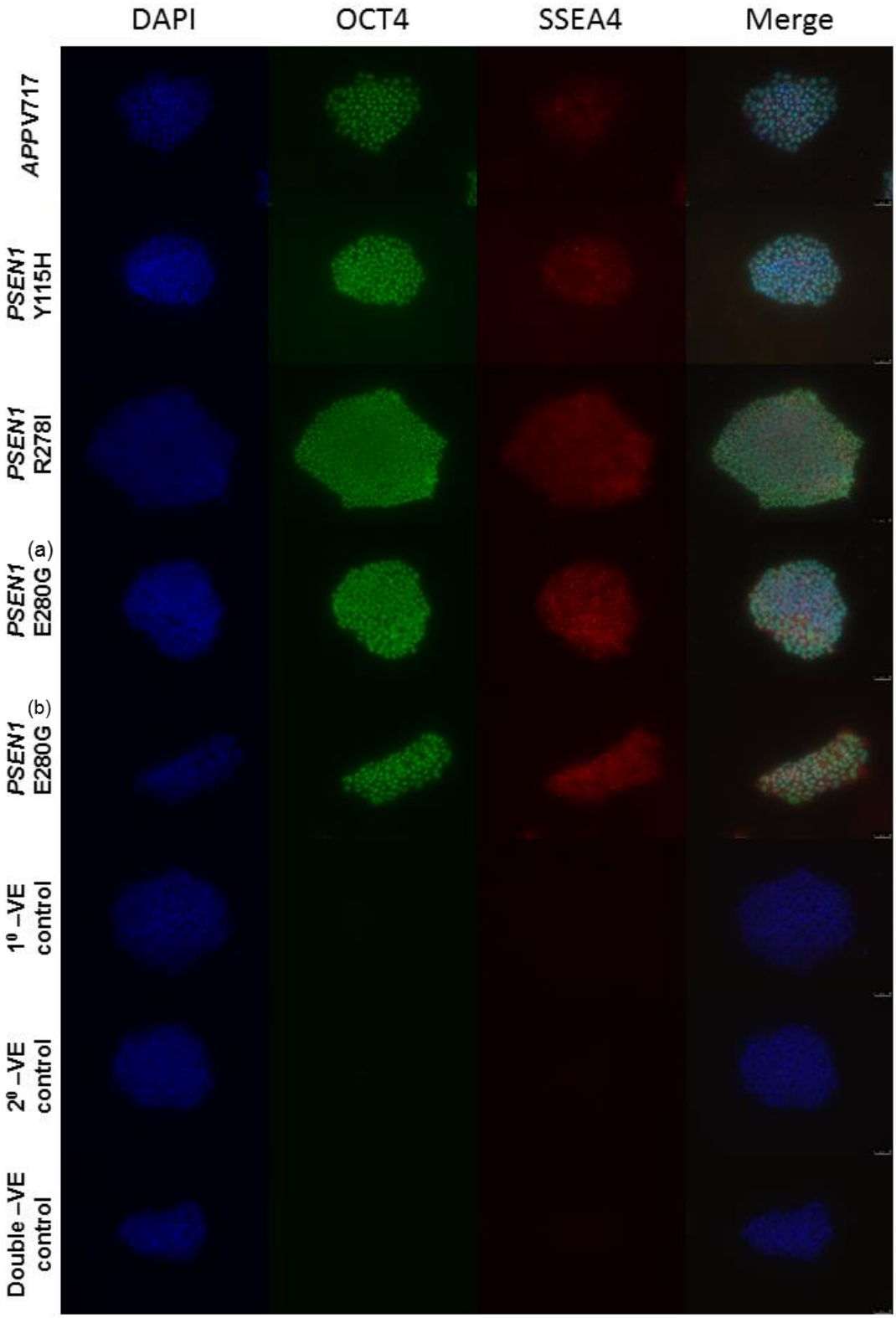

Figure 7-2 ICC confirming stem cell phenotype.

Representative images of each FAD iPSC line showing endogenous pluripotency markers. DAPI: blue, Oct4: green, SSEA4: red. Representative images from *APP* V717I, *PSEN1* Y115H, R278I, E280G.A and E280G.B are shown. Scale bar represents 50µm.

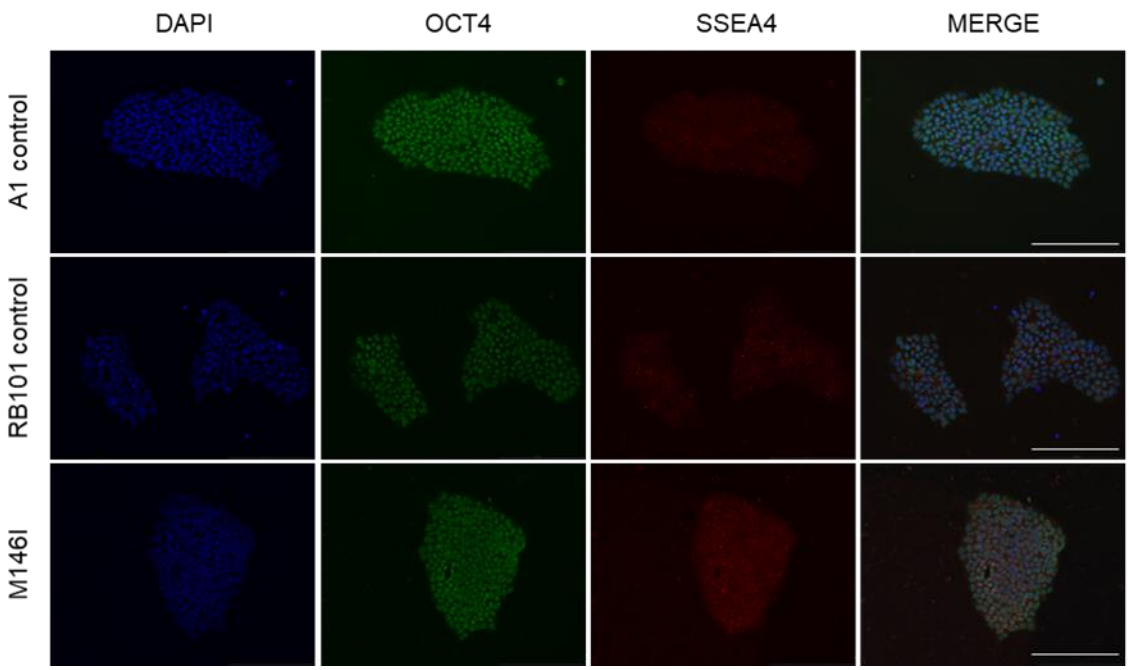

Figure 7-3 ICC confirming stem cell phenotype in additional cell lines.
Representative images of each additional FAD iPSC line (A1 and RB101 controls and M146I) showing endogenous pluripotency markers. DAPI: blue, Oct4: green, SSEA4: red. Scale bar represents 200µm

7.3.3 *Karyotype analysis*

DNA from the E280G.B and E280G.A lines were analysed for chromosomal abnormalities using the hPSC Genetic Analysis Kit. Results from the qPCR were analysed on the StemCell genetic analysis app (Figure 7-4). Results indicate an amplification in a minimal critical region of chromosome 17 of the E280G.B line, with a calculated copy number of 3.36. There were no significant amplifications in the E280G.A line.

The *PSEN1* Y115H, R278I and *APP* V717I lines developed jointly by myself and Christopher Lovejoy were sent for karyotypic analysis (TDL genetics, London), the preparation of this was conducted by Christopher Lovejoy and Dr Charlie Arber. All lines were deemed karyotypically normal (chromosome images are shown in Appendix, Figure 9-7, and with details shown in Charles Arber *et al.* (2019a)).

Control cell lines A1 and RB101 (RBi001-A at EBISC cell bank) were obtained from the EBISC cell bank (https://ebisc.org/) and have been previously characterised before distribution, including karyotype analysis. They have been studied extensively within the Wray lab and did not undergo karyotype analysis for this project.

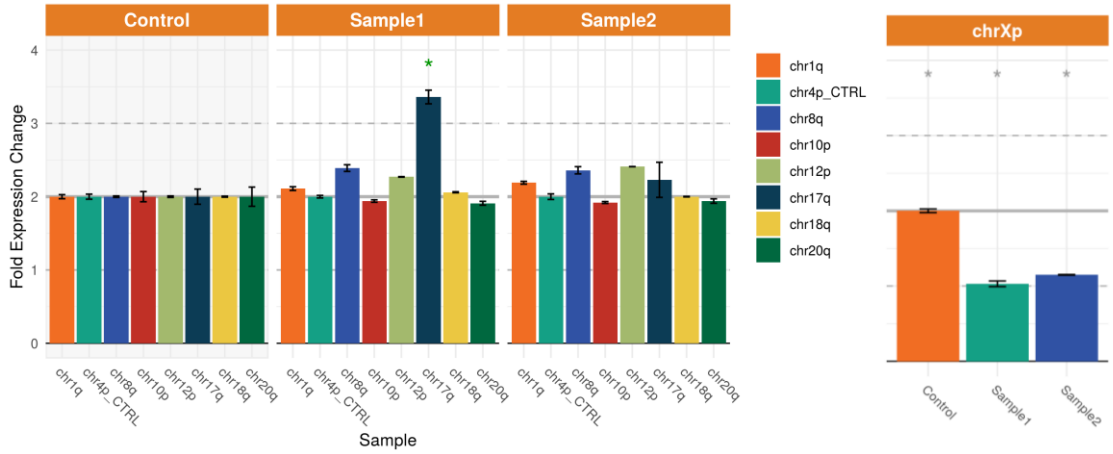

Figure 7-4 Karyotype analysis of E280G lines.

A: Significant amplification indicated (asterisk *) by primer pair chr17q in sample 1. B: Graph showing results for primer pair chrXp, control is female, confirming male sex in both E280G lines. Sample1 = E280G.B, sample 2= E280G.A. Data based on technical repeat n=2 and normalised to control.

7.3.4 *Genotyping*

APOE genotyping was conducted on *PSEN1* Y115H, M146I, R278I, E280G and *APP* V717I stem cell lines. Genotype was given by comparing PCR bands to control DNA with confirmed *APOE* identity. The genotype results are presented in an agarose gel image (Figure 7-5) and described in Table 7-1.

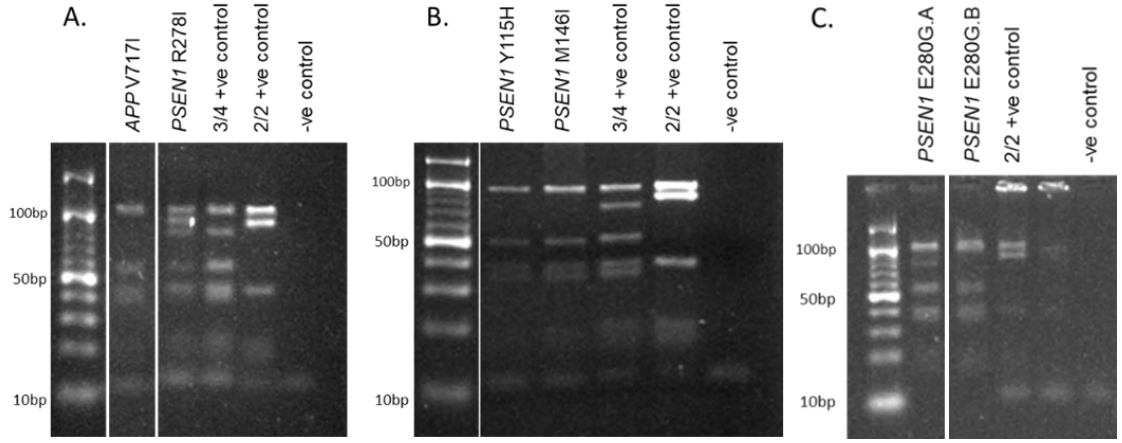

Figure 7-5 PCR amplification and restriction enzyme digestion of *APOE* DNA in the FAD stem cell lines.

Gel A: *APP* V717L *APOE* 3/3, *PSEN1* R278I *APOE* 2/4. Gel B: *PSEN1* Y115H *APOE* 3/3, *PSEN1* M146I *APOE* 3/3. Gel C: *PSEN1* E280G.A 3/4, *PSEN1* E280G.B 3/3. *APOE* alleles are indicated by presence of bands with following base pair length: ε2= 91, 83, ε3= 91, 48, 35, ε4= 72, 48, 35, 19. *APOE* 3/4 and A*POE* 2/2 genotypes are used as controls to highlight each possible allele (ε2, ε3, ε4). Gaps in gel images represent excised lanes from samples irrelevant to these results.

PSEN1 E280G

DNA from the E280G lines was amplified by PCR, followed by PCR clean up, after which DNA was sequenced by Source BioScience sequencing. Sequences were analysed and *PSEN1* E280G mutation was confirmed in both lines (Figure 7-6).

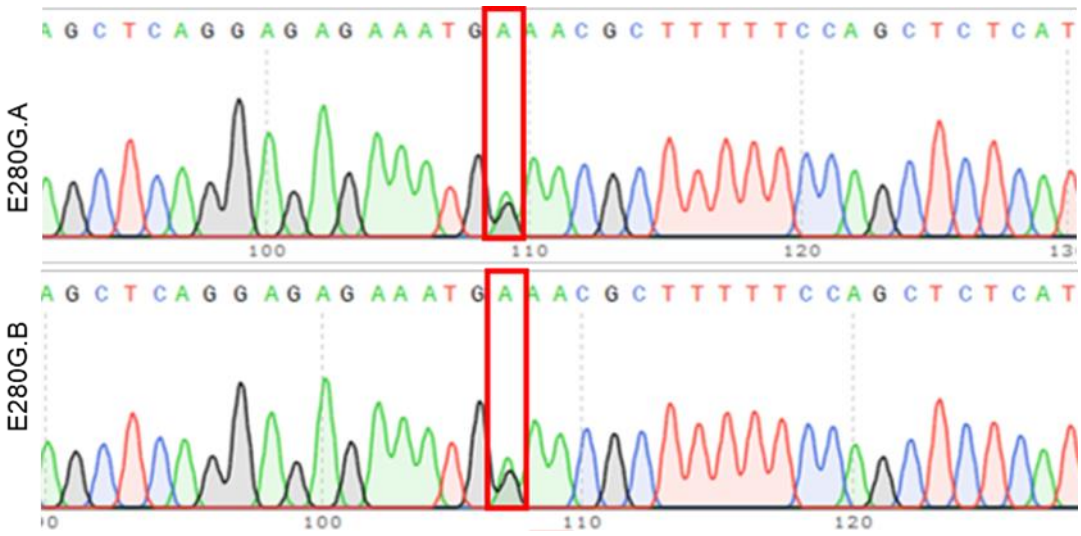

Figure 7-6 *PSEN1* sequencing.

Sequencing reads confirm *PSEN1* exon 8 E280G SNP (A>G) in one allele, confirming heterozygous mutation in both cell lines. Red box outlines E280G SNP location.

TREM2

DNA from the E280G lines was amplified by PCR, followed by PCR clean up, after which DNA was sequeunced by Source BioScience sequencing. Sequences were analysed and R62H mutation was confirmed in the E280G.A line (Figure 7-7).

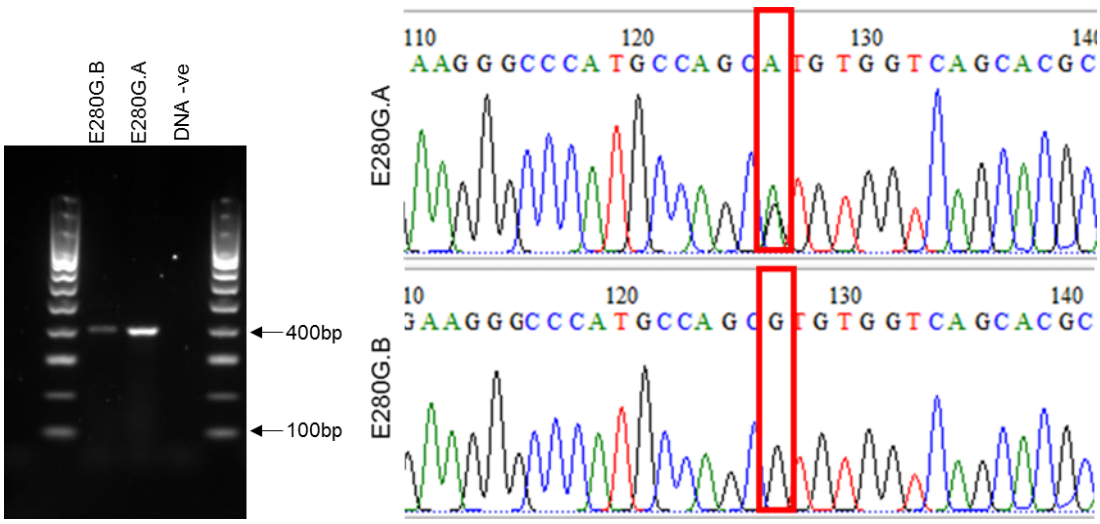

Figure 7-7 *TREM2* sequencing.

1% agarose gel showing PCR amplified DNA from E280G cell lines using TREM2 primers. Band observed is at the expected 385bp. Sequencing reads confirm TREM2 R62H SNP (G>A) in one allele in the E280G.A cell line. Red box outlines R62H SNP location.

7.3.5 *Characterisation of FAD neurons.*

7.3.5.1 *ICC*

Neural Rosettes

As described in the methods, stem cells were differentiated into cortical neurons (Chapter: 2.6.5). On day ~20 cells were split and replated. During this process a small fraction was replated on to coverslips. On day 25 the coverslips were fixed. ICC was conducted on these coverslips using antibodies which bind proteins indicative of an early neural progenitor population (Figure 7-8).

TUJ1 is a neuronal specific marker, highlighting post mitotic neurons throughout all stages of development. It is a component of microtubules, present throughout the cytoplasm of the neuron (M. K. Lee *et al.*, 1990; Menezes & Luskin, 1994). FOXG1 is a neuron specific transcription factor, acting as a transcriptional repressor, preventing neurogenesis of the initial layer 1 neurons. In the developing brain it is expressed in proliferate cells, acting to control the rate of neurogenesis (Hanashima *et al.*, 2004; Tao & Lai, 1992). In Figure 7-8, FOXG1 expression can be seen within nuclei of cells within the rosettes, while some of the neuronal TUJ1 expressing cells separate from the rosettes do not express FOXG1.

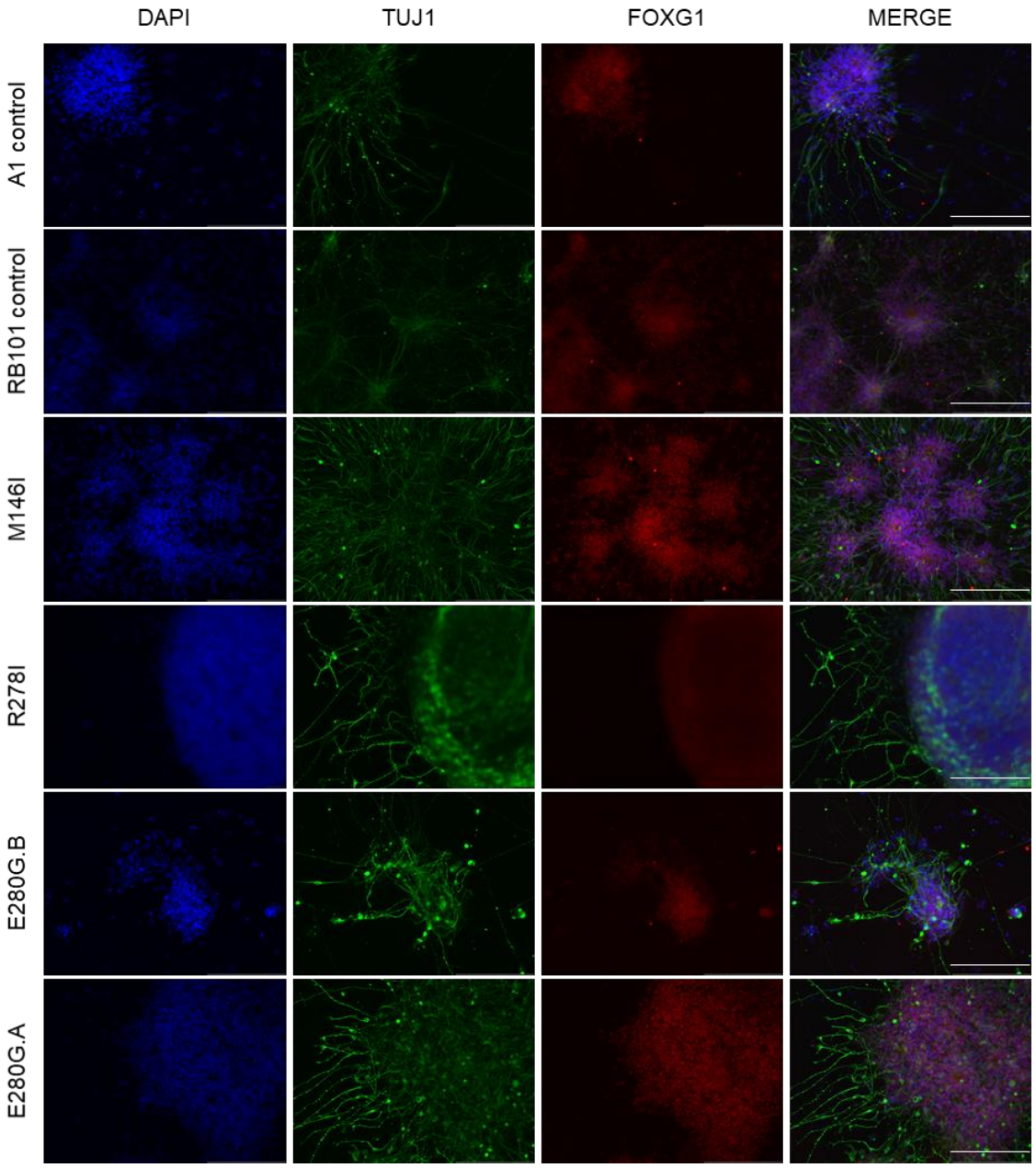

Figure 7-8 Confirmation of cortical neurogenesis in D25 cortical neurons.
Representative images shown. DAPI: blue, TUJ1: green, FOXG1: red. White scale bar represent 200µm and is the scale for all images

Cortical neurons

T-box Brain Transcription Factor 1 (TBR1) is a nuclear transcription factor expressed in early glutamatergic cortical neurons and is involved in regulation of differentiation of lower layer neurons (Hevner *et al.*, 2001). BRN2 is a neural specific marker representative of upper layer neurons. It is a nuclear, temporally expressed transcription factor expressed in post mitotic neurons, involved in regulation of layer migration, and continues to be expressed in mature neurons

(Dominguez *et al.*, 2013; M. K. Lee *et al.*, 1990). Collectively, along with TUJ1, expression of these markers indicate neural differentiation of neurons representative of all stages of cortical development. For TBR1 staining see Figure 7-9, for BRN2 staining see Figure 7-10.

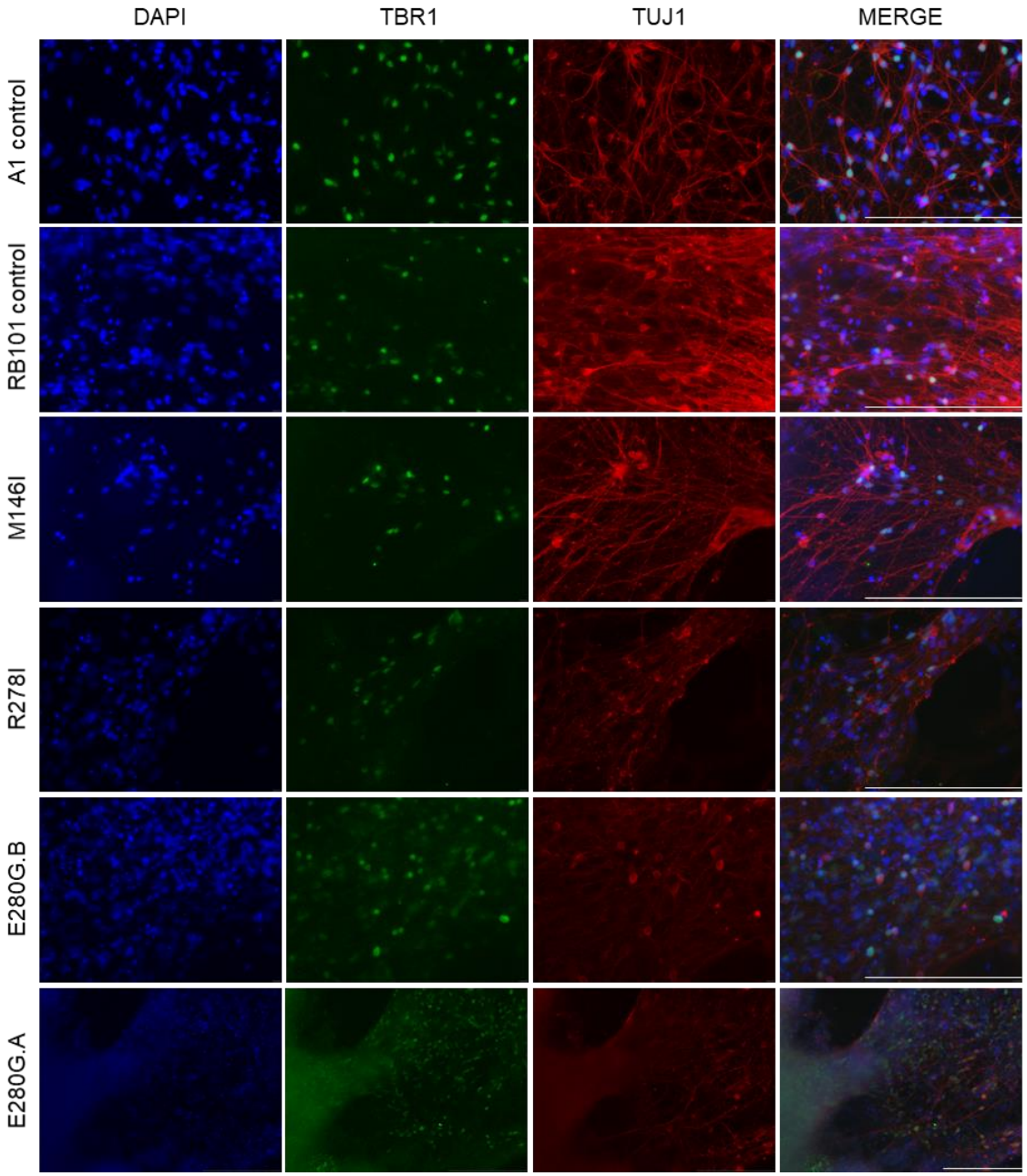

Figure 7-9 Images of ICC using TBR1 and TUJ1.

DAPI: blue, TBR1: green, TUJ1: red. White scale bar represent 200µm and is the scale for all images. Image shown for E280G.A is at 20x magnification rather than 40x magnification, unable to retake at 40x due to COVID19 governmental guidelines. ~D100 neurons.

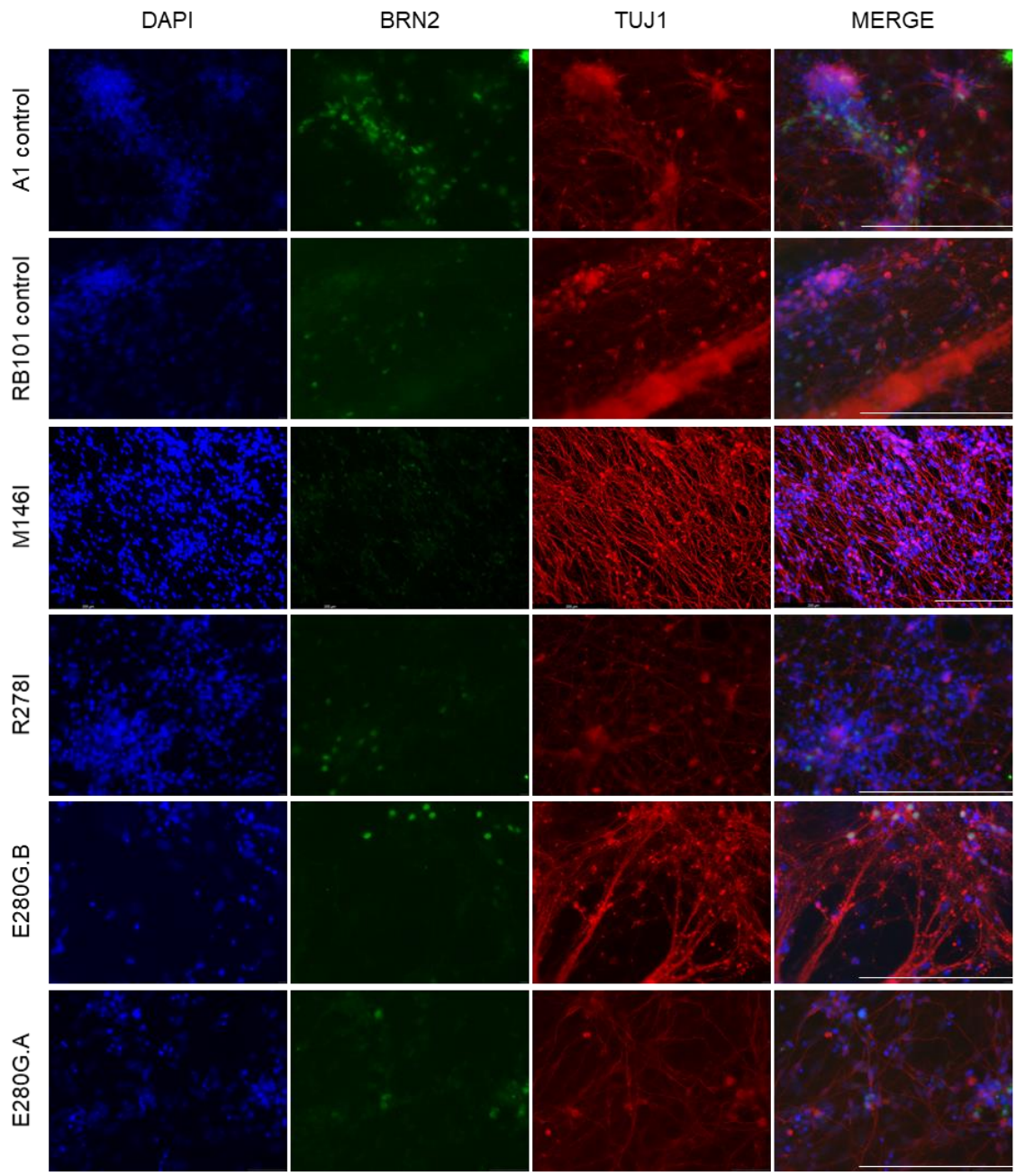

Figure 7-10 Images of ICC using BRN2 and TUJ1.

DAPI: blue, BRN2: green, TUJ1: red. White scale bar represent 200µm and is the scale for all images. Image shown for M146I is at 20x magnification rather than 40x magnification, unable to retake at 40x due to COVID19 governmental guidelines. ~D100 neurons.

7.3.5.2 *Quantification of Aβ isoform production by ELISA*

It has previously been suggested that different FAD mutations may differentially influence the production of Aβ isoforms (Charles Arber *et al.*, 2019a; Thordardottir *et al.*, 2017; Veugelen *et al.*, 2016). To investigate how the E280G mutation affects Aβ production in human neurons, ELISA analysis of Aβ 40, 42 and 43 was

conducted on the cell line conditioned media to measure the Aβ isoforms. To compare between lines, isoform ratios rather than absolute levels were used. This is because using ratios might not be affected by differences in cell numbers in the separate cultures, and have been shown to remain consistent over time (Charles Arber *et al.*, 2019a). Additionally, in CSF, ratios have been shown to be more highly correlated with measures of AD than absolute values (Jan *et al.*, 2008).

Aβ42/38 (Figure 7-11 A)

The ratio of Aβ42/38 was significantly different across the cell lines ($p<0.0001$, ANOVA). Compared to controls, M146I, E280G.B and E380G.A had a significantly increased ratio ($p=0.04$, $p=0.0009$, $p<0.0001$, Dunn's test). Compared to R278I, E280G.A an E280G.B had a significantly increased ratio ($p=0.03$, $p<0.0001$). The E280G.A also had a significantly increased ratio compared to M146I and E280G.B ($p<0.0001$, $p=0.0005$).

Aβ43/40 (Figure 7-11 B)

Aβ43:40 is significantly different between cell lines ($p<0.0001$). Compared to controls, there was a significantly higher ratio in the R278I, E280G.B and E280G.A lines ($p=0.0001$, $p<0.0001$, $p=0.001$). The ratio in the R278I, E280G.B and E280G.A lines was also significantly higher compared to M146I ($p=0.0003$, $p=0.0002$, $p=0.003$).

Aβ42/43 (Figure 7-11 C)

The ratio of Aβ42/43 is significantly different across cell lines ($p=0.002$). Compared to controls, there was a significantly decreased ratio in the R278I, E280G.B and E280G.A lines ($p=0.04$, $p=0.05$, $p=0.05$). Additionally, compared to M146I, there was a significantly decreased ratio in the R278I, E280G.B and E280G.A lines ($p=0.01$, $p=0.01$, $p=0.01$).

Aβ42/40 (Figure 7-11 D)

There was a significant difference in the Aβ42/40 ratio across the cell lines ($p<0.0001$). Compared to controls, there was a significantly increased ratio in the M146I, E280G.B and E280G.A lines ($p<0.0001$, $p<0.0001$, $p=0.006$). M146I and

E280G.B also had significantly increased ratios compared to R278I (p=0.0003, p=0.003). The M146I line also had a significantly increased ratio compared to E280G.A (p=0.01).

Aβ38/40 (Figure 7-11 E)

There was a significant difference across the lines in the ratio of 38/40 (p<0.0001). Controls had a significantly increased ratio compared to R278I, E280G.B and E280G.A lines (p=0.01, p<0.0001, p<0.0001). The M146I line had a significantly increased ratio compared to the E280G lines (B: p=0.0003 A: p<0.0001). R278I also had a significantly increased ratio compared to the E280G lines (B: p=0.03 A: p<0.0001). The ratio was also significantly increased in the E280G.B compared to E280G.A (p=0.0002).

Representative images of Aβ isoform specific IHC on matched mutation human cortical tissue, but not matched patient, are shown in Figure 7-12. These images display intense Aβ42 deposition in all cases. Aβ40 is also present in all cases but present mainly as CAA in M146I while present as CAA and cortical deposition in the remaining cases. Aβ43 IHC specifically shows the difference in Aβ43 deposition, with low deposition in the M146I line but abundant deposition in the R278I and E280G lines, which matches the ELISA results for high Aβ43 levels in those lines.

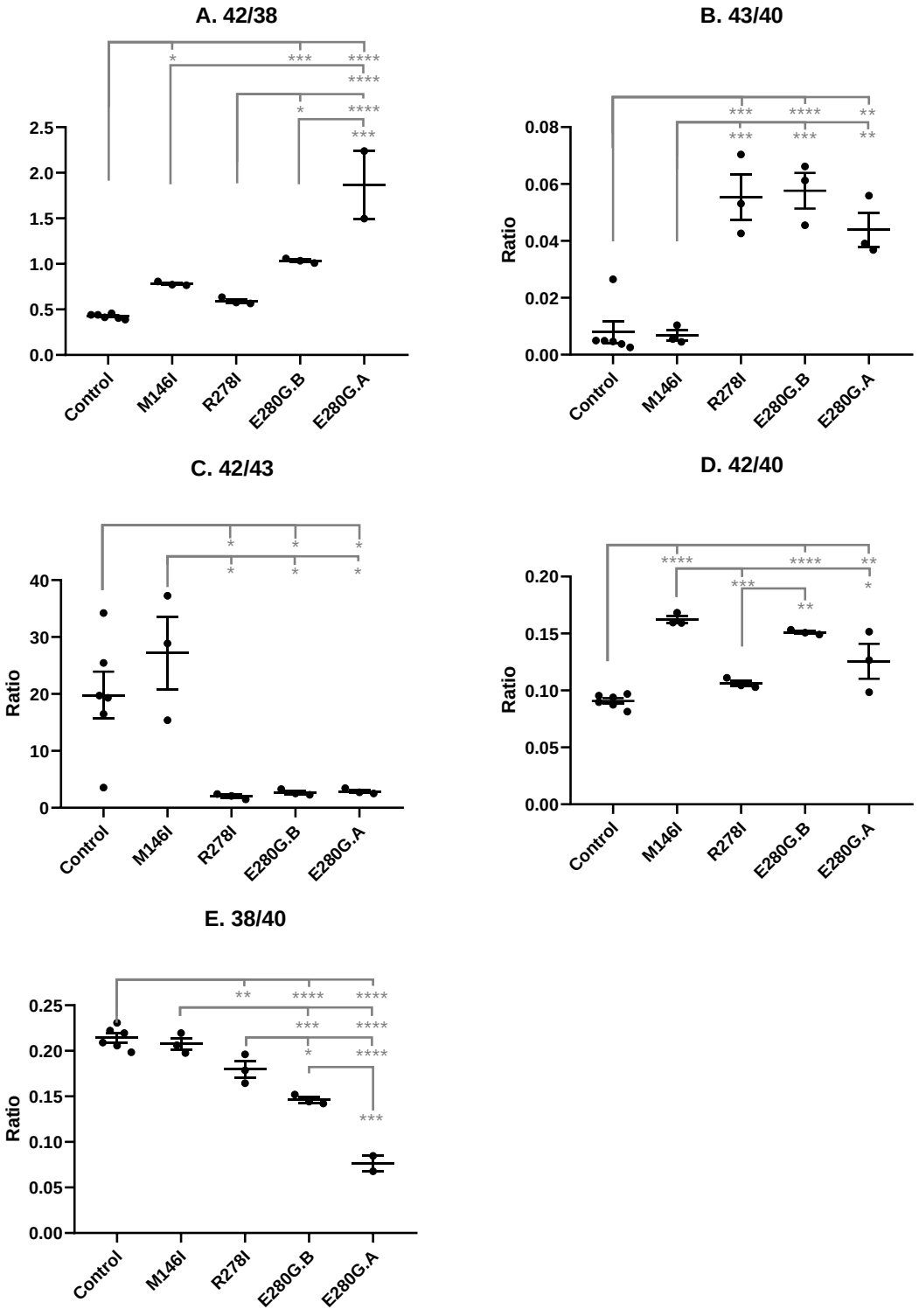

Figure 7-11 Aβ ratios in the cell lines.

A. Aβ42/38 B. Aβ42/40 C. Aβ42/43 D. Aβ43/40 E. Aβ38/40. Controls n=6, *PSEN1* mutation lines n=3. N=2 for Aβ38 in E280G.A as levels were undetectable in 1 induction. Error bars represent mean and standard error of the mean (SEM), one-way ANOVA with Tukey's test, *p<0.05, **p<0.01, ***p<0.001, ****p<0.0001. *PSEN1* E280G.A line has the *TREM2* R62H AD risk associated variant.

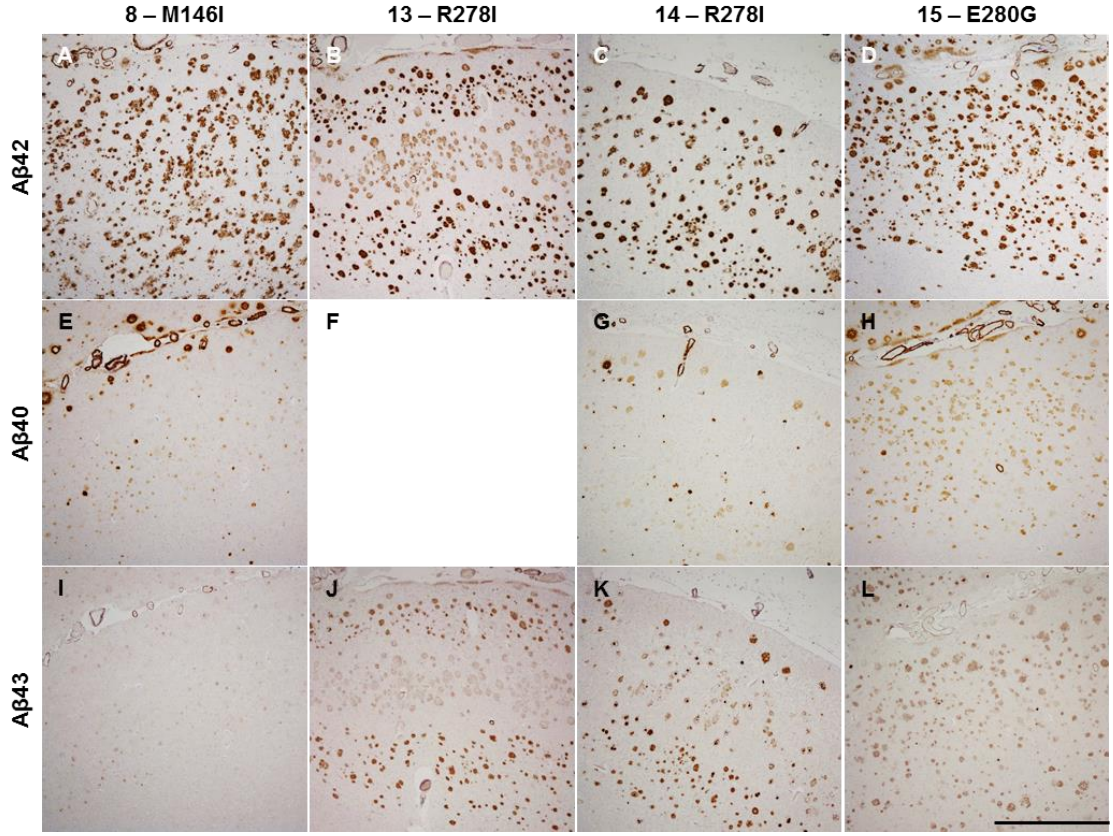

Figure 7-12 Aβ pathology in mutation matched cortical tissue.

Representative images of IHC performed on temporal cortex using antibodies specific to Aβ42 (A-D), Aβ40 (E-H) and Aβ43 (I-L) (See chapter: 6.3). Images and ELISA results cannot be directly compared as ELISA is expressed as ratio and IHC images are not quantified. There is abundant Aβ42 in all cases. Aβ40 is present in all cases however, by observation E280G displays the greatest Aβ40 deposition. Aβ43 is absent in M146I, however is present in R278I and E280G cases. No figure available for image F due to tissue damage during IHC. Scale bar represents 100µm, 4x objective magnification applicable to all images.

7.3.5.3 *Quantification of PSEN1 protein by western blot*

As has been previously shown, the R278I and E280G lines have been seen to have PSEN1 in both the mature cleaved formation as well as the immature un-cleaved PSEN1. By using western blots to probe for the PSEN1 NTF the presence of mature and immature PSEN1 were assessed in the cell lines (see Figure 7-14 A-C). In each induction mature PSEN1 was present in all cell lines. The full length immature PSEN1 showed variability between lines and inductions. Actin used as a protein loading control is presented below each western blot.

The presence of other bands on western blots was also observed, likely reflecting non-specific binding of the antibody or degradation products in the lysates. To

ensure the correct bands were analysed, we loaded previously confirmed positive loading control sample (R278I.CA, Figure 7-14 B). The composition of the other bands is currently unclear and has not been investigated further.

To quantify western blots, immature and mature PSEN1 relative to actin were compared between cell lines, relative to control line RB101. Additionally, immature PSEN1 relative to mature PSEN1 was compared between cell lines, relative to control line RB101. Positive control sample was not included in the analysis.

Immature PSEN1

Firstly the amount of immature PSEN1, relative to actin and normalised to the RB101 control cell line was compared between cell lines. There was no statistically significant difference across the lines ($p=0.09$, one-way ANOVA) however a trend for increasing levels in the R278I, E280G.B and E280G.A lines can be observed (Figure 7-13 A).

Mature PSEN1

Secondly, the amount of mature PSEN1, relative to actin and normalised to the RB101 control line was compared between cell lines. Mature PSEN1 levels significantly differed across lines ($p=0.0007$). Compared to the A1 control line, mature PSEN1 was significantly higher in the E280G.B and E280G.A lines ($p=0.008$ and $p=0.004$ respectively, Tukey's multiple comparison test). Compared to the R278I line, mature PSEN1 was also significantly higher in the E280G.B and E280G.A lines ($p=0.005$ and $p=0.002$ respectively), see Figure 7-13 B.

Immature PSEN1 relative to Mature PSEN1

Finally, the levels of immature PSEN1 relative to mature PSEN1, normalised to the RB101 control line was compared between cell lines. Immature PSEN1 relative to mature PSEN1 was significantly different across lines ($p=0.0008$) with higher immature PSEN1 levels in the R278I line compared to all other lines (R278I compared to A1: $p=0.002$, RB101: 0.001, M146I: $P=0.002$, E280G.B: $P=0.005$, E280G.A: $P=0.005$), see Figure 7-13 C. This indicates a mutation specific effect in the R278I line on the processing of immature to mature PSEN1.

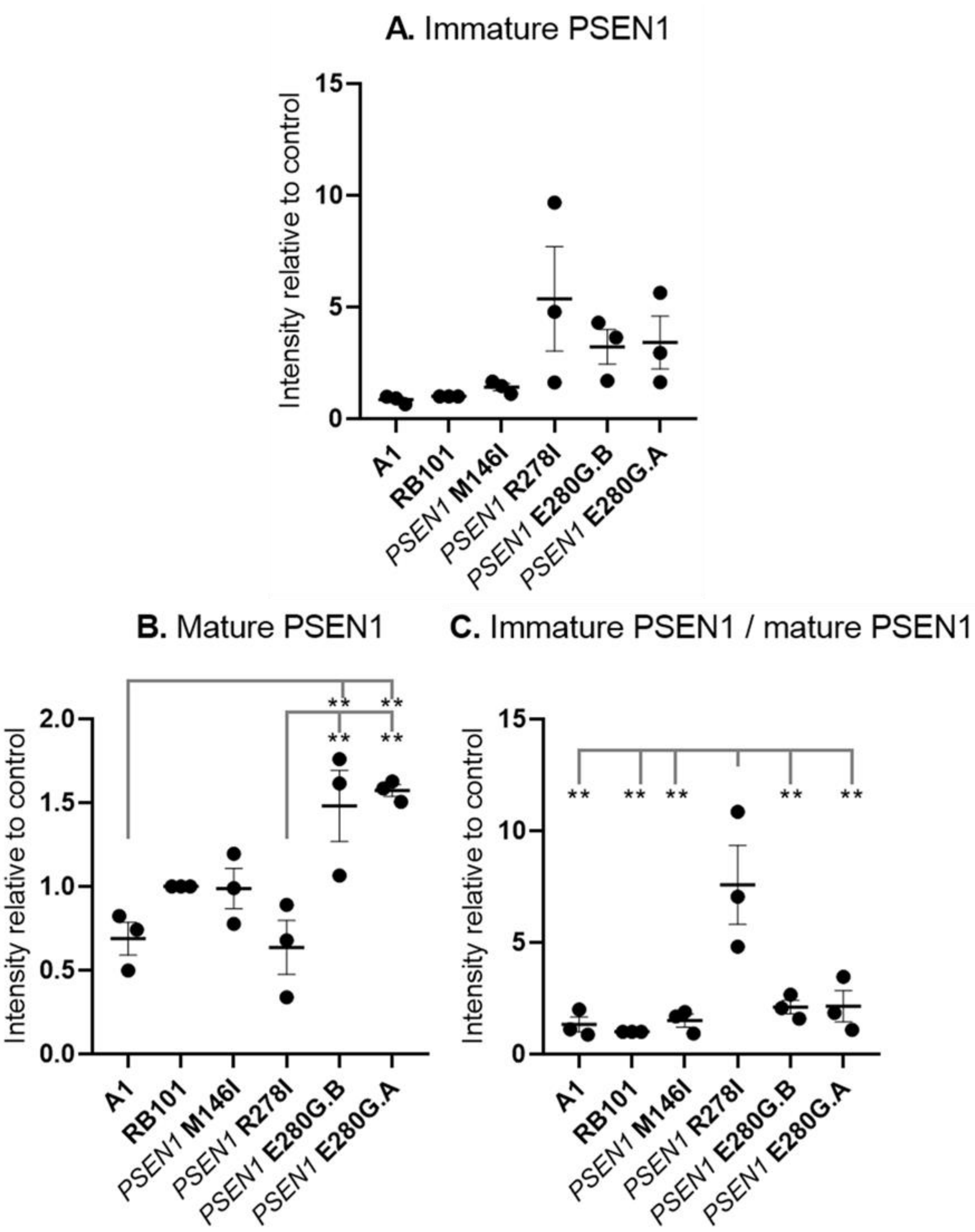

Figure 7-13 Western blot analysis of PSEN1 in the cell lines.

A: Immature PSEN1 did not statistically differ across cells lines. B: Mature PSEN1 was significantly higher in the E280G.B and E280G.B lines compared to the A1 control and *PSEN1* R278I lines. C: Immature PSEN1 relative to mature PSEN1 was significantly higher in the *PSEN1* R278I line compared to all other lines. One-way ANOVA with Tukey's multiple comparison, error bars represent mean and SEM, *p<0.05, **p<0.01.

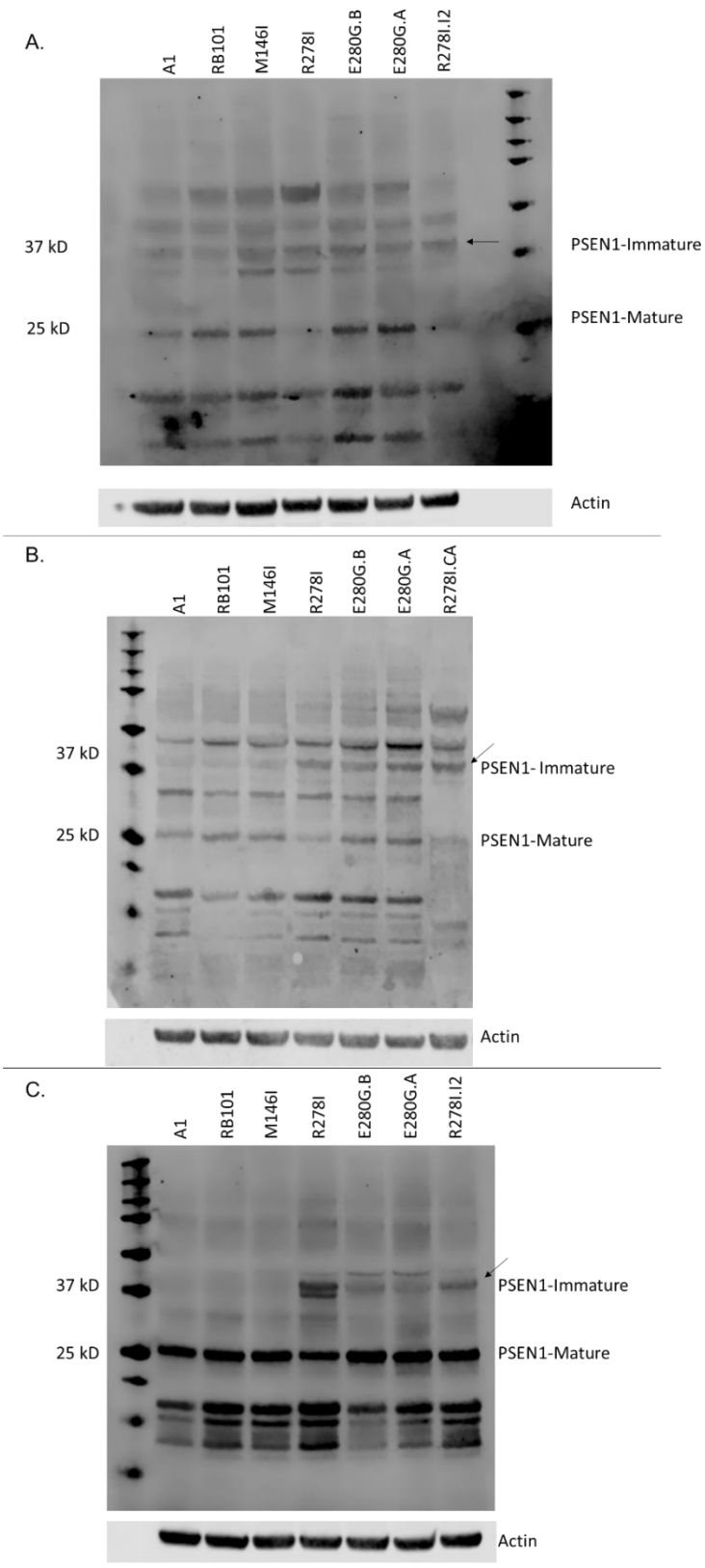

Figure 7-14 Western blot of PSEN1.

A: induction 1. B: Induction 2. C: Induction 3. Arrows indicate the full length PSEN1 (immature) in the loading control. Loading control in B is R278I.CA (sample from ARBER ET AL). Loading control in A and C is R278I.I2, which is the R278I sample from Induction 2 (see B).

7.3.5.4 *Quantitative PCR*

Differences in PSEN1 protein are hypothesised to be due to mutation effects on protein structure, rather than differences in *PSEN1* expression. To determine *PSEN1* expression in the different mutations, qPCR was conducted. This was to assess for any differences in gene expression which may influence protein expression. *RPL18* gene which encodes for the 60S Ribosomal protein L18 protein, was used as a house keeping gene, and has previously been published as a housekeeping gene in neurons with FAD mutations (Charles Arber *et al.*, 2019b). The control line RB101 was used as the normalisation cell line. For each line in one induction, raw CT values used for analysis were calculated from duplicate rather than triplicate as inspection of the dissociation curve indicated a separate peak for one row of repeats in that qPCR. As the anomaly was present in each line for only 1 repeat from the triplicate, this indicates that there was an issue in the wells for that row, rather than a qPCR wide issue. Based on this, values from that row were omitted. Unfortunately as time was limiting, the PCR was not repeated to rectify this issue although this would be possible as cDNA is preserved at -80^0c. Dissociation curves and amplification plots can be seen in chapter: 9, Figure 9-9, Figure 9-10 and Figure 9-11.

The average fold change from the qPCR results were compared between the different cell lines, normalised to controls. Normality was assessed by QQ plot, with an acceptable result. There were no statistically significant difference between the cell lines ($p=0.44$, One-Way ANOVA), indicating that there was no significant differences in gene expression between the cell lines.

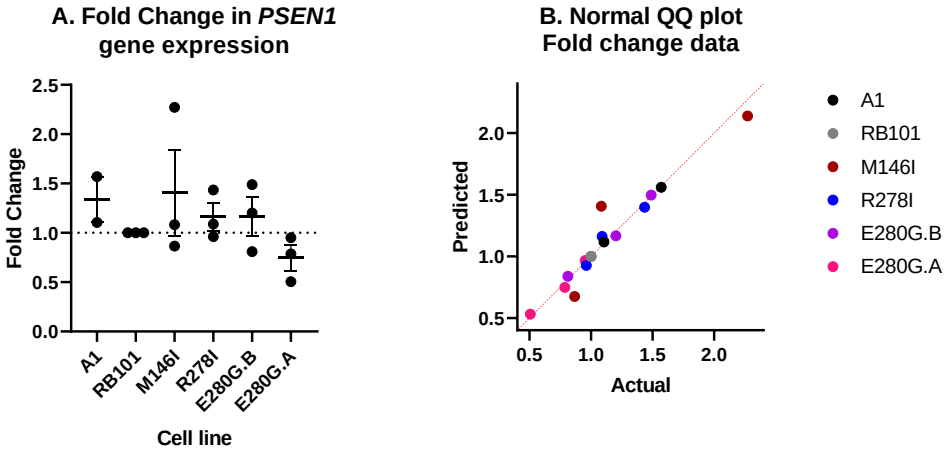

Figure 7-15 *PSEN1* qPCR.

A: Fold change in PSEN1 expression (2^delat delta CT), normalised to RB101 control line. No significant differences between lines. N=3 per cell line with each individual dot representing qPCR data from triplicate technical repeats, except in the A1 line where n=2. Additionally, in each cell line, one dot represents qPCR data from duplicate technical repeats. Error bars represent mean and SEM. B: QQ plot of the fold change data. Each dot represents the same data shown in graph A.

Due to some weak staining in the ICC images, qPCR was conducted to assess the transcriptional level of TUJ1 (encoded by *Tubulin Beta Class III* (*TUBB3*)), TBR1 and Special AT-rich sequence-binding protein 2 (SATB2). SATB2 is a DNA binding protein which is expressed in later born cortical neurons (Saito *et al.*, 2011a) and was used in replacement for BRN2 as there were no BRN2 primers readily available in the lab for qPCR. For all qPCRs the control line RB101 was used as the normalisation cell line. This is because cDNA from one of the A1 inductions did not work (induction 1). Dissociation curves and amplification plots can be seen in chapter: 9, Figure 9-12, Figure 9-13 and Figure 9-14.

Expression of TBR1 (lower layer cortical neurons) was compared across cell lines, relative to the RB101 control cell line. There was a significant difference across cell lines ($p=0.05$, one-way ANOVA with Tukey's multiple comparison test) however multiple comparisons revealed there was no significant difference between individual mutation groups. A trend for decreased TBR1 expression in the FAD lines can be seen, especially in the E280G.A cell lines.

Expression of SATB2 (upper layer neurons) was compared across cell lines, relative to the RB101 control cell line. There was no statistically significant differences in SATB2 expression between cell lines (p=0.4).

Expression of TUJ1 was compared across cell lines, relative to the RB101 control cell line. Expression of TUJ1 was significantly different across all cell lines (p=0.04) however multiple comparison revealed no significant difference when comparing directly between individual cell lines.

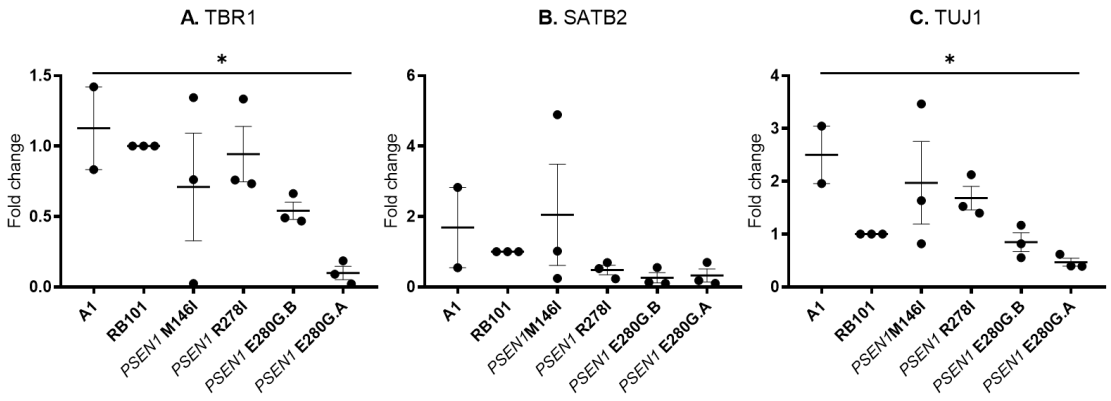

Figure 7-16 qPCR of neuronal markers.

A: TBR1 expression significantly differed across cell lines. B: SATB2 expression did not significantly differ across cell lines. C: TUJ1 expression significantly differed across cell lines. n=3 per cell line with each individual dot representing qPCR data from triplicate technical repeats, except in the A1 line where n=2. Error bars represent mean and SEM. One-Way ANOVA with Tukey's multiple comparison, *p<.05.

7.4 **Discussion**

	Main findings
Generation of FAD mutation iPSC from patient derived fibroblasts	5 FAD mutation iPSC lines were generated (3 in collaboration with Christopher Lovejoy, 2 independently) including the first E280G mutation line.
Neuronal characterisation	Reduced expression of neuronal markers were observed in some of the FAD mutation lines, especially the E280G lines.
Aβ *peptide profiles*	FAD mutation lines produce distinct Aβ peptide profiles.

	Significant differences in ratios exist when comparing between both controls and other FAD mutation lines.
PSEN1 protein maturity	FAD mutations lines have significant differences in PSEN1 protein maturity when comparing between both controls and other FAD mutation cell lines.

In this study we generated FAD stem cell lines from five individuals, permitting the study of mutation-specific disease mechanisms. Some of the lines generated have had their potential to generate neurons confirmed in published reports, with analysis of Aβ profiles indicating mutation-specific differences on Aβ ratios (Charles Arber *et al.*, 2019a). The work within this study confirms observations of altered Aβ peptide levels and ratios in FAD cell lines, reviewed in C. Arber *et al.* (2017); J. Yang *et al.* (2016) but also extends the analysis into mutation specific effects revealing a specific effect of the E280G and R278I mutations on increasing Aβ43 production.

Genetic analysis

APOE genotyping was conducted in all cell lines to provide more detailed information but also to confirm the identity of the E280G lines which had distinct *APOE* genotypes (Figure 7-5). Although we have not been able to investigate differences by *APOE* genotype, future work with greater cell line numbers should attempt to investigate the effects of *APOE* in FAD lines. This will be important as *APOE* genotype has been shown to influence neuronal cells in culture, leading to altered transcriptional profiles, early differentiation, increased and impaired Aβ clearance compared to controls (Y.-T. Lin *et al.*, 2018). It was also shown in earlier chapters that *APOE* genotype can influence multiple aspects of FAD, such as disease duration (chapters: 3.3.2 and 5.5.1) and CAA pathology (chapters: 5.5.4, 5.5.7). Although the molecular mechanism of all associations are not yet understood, it could affect cells in culture.

Karyotypic analysis of the newly generated lines detected a chromosomal alteration on chromosome 17 in the E280G.B line, while no significant alterations were observed in the E280G.A line (Figure 7-4). The exact primer probe binding sequence is not disclosed by the StemCell technologies thus the exact region of amplification cannot be confirmed. However, analysis of the literature on

chromosome 17 amplifications can be used to consider the potential effects of this abnormality. Amplifications in 17q are commonly found in hPSC cultures indicating a pro-survival benefit to stem cells (Draper *et al.*, 2004). They are also associated with neuroblastoma, with multiple candidate oncogenic genes within the 17q region, such as *BIRC5* which encodes survivin and *NME* which encodes NME/NM23 nucleoside diphosphate Kinase 1 (Bown *et al.*, 1999). A lack of differentiation potential would suggest an overriding pluripotent phenotype due to the amplification. The presence of this abnormality did not impact on the initial neuronal differentiation and therefore the line was included in experimentation and analysis.

The 17q region also contains the *MAPT* gene. *MAPT* encodes for tau, which forms pathological deposits in multiple dementia's including FAD where it occurs downstream of Aβ pathology. A *MAPT* mutation which leads to chromosomal instability and copy number variations in mutation carrier lymphocytes and fibroblasts exist (Rossi *et al.*, 2012), and so further analysis of tau in our lines could be warranted.

There is no indication that PSEN1 physically interacts with tau or that *PSEN1* mutations would influence tau protein expression. It has been shown that FAD mutations are not associated with increased tau in human cortical neurons (Moore *et al.*, 2015). In contrast, Aβ may interact with tau, and increased aggregation prone Aβ peptide ratios in our FAD lines, as well as a potential increase in tau if the *MAPT* gene is amplified, could lead to increased interaction between the two proteins which could exacerbate pathology. The E280G.A line has no amplification in this region and the results from this line are generally comparable to the E280G.B line indicating there is no obvious effect of the 17q amplification on Aβ peptides. However, future work would aim to use other iPSC clones of this mutation with normal karyotypes.

Characterisation

In this study we have generated five FAD patient derived cell lines, two of which contain the *PSEN1* E280G mutation which had not previously been developed from patient fibroblasts. This has expanded the repertoire of available FAD iPSC which were confirmed to be iPSC using ICC and morphological analysis, showing

cells expressing pluripotent factors and morphologically accurate cell type. Their ability to differentiate was also confirmed by ICC, showing that these lines are able to generate early and late born neurons, making them a physiologically relevant tool for investigating the neuronal based mechanisms in FAD. While ICC is useful for confirming expression of specific markers, issues can be encountered with this method.

During ICC characterisation, a particular issue was encountered when too many cells have been plated on coverslips. This leads to dense packing of the cells making imaging of nuclear markers difficult, as nuclear bodies can be masked and under cellular processes. This problem may be more severe for later born neurons as restriction of space due to earlier born neurons will lead to clumping of these cells. Indeed cells positive for later markers can be seen in clumped structures. This issue was encountered on coverslips for different lines, indicating it was not a mutation specific issue, rather a technical issue. In situations such as this, further quantification of expression of relevant markers can be confirmed by qPCR.

The qPCR analysis of markers for neuronal identity highlighted a trend for decreased expression of neuronal markers in some of the mutation cell lines (Chapter: 7.3.5.4). Further steps to investigate the phenotype of the cells in more detail would involve looking at astrocytic markers and also stem cell markers. Astrocytic markers would assess if a greater proportion of cells had become astrocytic while stem cell markers would investigate if a reduced conversion from stem cells to neurons has occurred. While differences between controls and mutations line can be of concern, it has also been suggested that a reduced neuronal phenotype and increased astrocytic phenotype may exist in FAD mutation cell populations, by deconvolution analysis of transcriptomic data from human brain samples (Z. Li *et al.*, 2018) therefore assessing the astrocytic phenotype may be an important next step. Additionally the *APOE*4 genotype also displayed this phenotype and could compound the affect. Alternations in neuronal differentiation in FAD mutation cell lines has also been noted, with premature differentiation and decreased proliferation (J. Yang *et al.*, 2017). Differences we observe may be related to these interesting observations. Additionally, observations within the R278I line match those previously described (Charles

Arber *et al.*, 2019a) highlighting the results do recapitulate mutation specific effects.

If the mutation lines are less neuronal, this may not be negatively impact on the validity of findings as the use of ratios helps to normalise the data. Additionally, analysis of PSEN1 mutations has been studied in non-neuronal populations, including fibroblasts (Braggin *et al.*, 2019; Gray & Quinn, 2015) where mutation effects on readouts such as Aβ levels are still observed, implying non-neuronal phenotypes are able to recapitulate phenotypes. Mutations expressed in mouse embryonic fibroblasts also reveal mutation specific effects that are applicable to human brain samples (Szaruga *et al.*, 2015; Veugelen *et al.*, 2016). Other types of cell lines have also been used for studying FAD mutations (Suárez-Calvet *et al.*, 2014). This suggests that the results observed may still be valid in relation to mutation effects. That the PSEN1 transcriptional levels do not change cross cell lines also supports that differences observed are related to effect of mutation on PSEN1 processivity.

Aβ ratios

Our ELISA analysis confirms that FAD PSEN1 mutations can lead to quantitative differences in Aβ ratios compared to controls (Chapter: 7.3.5.2). We also show mutation specific differences, highlighting heterogeneity in FAD. Results from the M146I line confirm previous findings showing increased Aβ42 ratios (Charles Arber *et al.*, 2019a). The R278I line results do not always reach statistical significance compared to controls as was previously found, however the same trends are observed. The discrepancies are possibly related to technical differences between the studies, including greater *n* number in the former, and different statistical tests employed to answer slightly different questions. With this in mind the current results should be considered to show similar findings to those previously found. Both the M146I and R278I lines had significantly different ratios highlighting the different effect of these mutations on PSEN1 processivity.

As expected, the E280G line ratios significantly differed compared to controls. Importantly, they also differed from the other FAD lines, highlighting mutation linked heterogeneity in FAD. It also highlights differences exist within mutations classified into the *PSEN1* post-codon 200 group. The alterations in ratios in the

E280G lines can be interpreted to show an endopeptidase and a carboxypeptidase alteration in both the Aβ48 and 49 pathways. This carboxypeptidase alteration is particularly notable due to the low, and in one E280G.A induction undetectable, levels of Aβ38. Interestingly, we found there to be differences between the two E280G lines in terms of the extent of the changes with more extreme ratios in the E280G.A line, although the pattern for increase/decrease was the same. A number of factors could contribute to this, such as the different *APOE* genotypes. As previously mentioned, *APOE*4 genotypes have been shown to lead to differences in cells compared to *APOE*3 genotypes, including alterations in synaptic number, early endosomes, increased Aβ42 and an altered transcriptome profile (Y.-T. Lin *et al.*, 2018). The patient from which the E280G.A line is derived has also been diagnosed neuropathologically as having both FAD and multiple sclerosis (MS). The cause of the MS in this case is currently uncertain and its effects in cell culture are unknown. Inflammation is a major feature of MS and the combination of *TREM2* and *APOE*4 genotype may influence inflammatory responses in this case. However, the *TREM2* mutation may not contribute to differences observed in our neuronal culture as TREM2 is not expressed in neurons. Despite this the unknown effects of these factors have to be considered in relation to this line.

Knowing that mutations have specific effects on γ-secretase processivity will be important for therapies. In particular, those which modulate PSEN1 processivity. As reviewed by (Golde *et al.*, 2013) This would be in addition to the negative consequences caused by PSEN1 inhibitors which effect processing of substrates other than APP, such as notch (Chávez-Gutiérrez *et al.*, 2012). Kukar *et al.* (2008) discuss γ-secretase modulators, and differences in PSEN1 processivity may to some extant explain why PSEN1 modulating therapies so far have not always been successful. A variety of modulators which tackle the range specific alteration caused by the FAD mutation will need to be developed and correctly administered to match the mutation driven alteration. To do this, mutation-specific effects need to be known. iPSC are a practical and feasible tool for this analysis.

The use of therapies is only relevant if they produce significant clinical effects. One issue within this study is that for the majority of cell lines, fibroblast biopsies were taken prior to symptom onset, therefore clinical correlations could not be conducted. In the future it may be possible to include these data to asses if

different ratio patterns differentially affect phenotypic heterogeneity such disease onset, duration or clinical features. Aβ43 is thought to be particularly toxic therefore it may be expected that this is form could associate with more severe outcomes.

An interesting aspect of our results was the observation of Aβ specific IHC in matched mutation human cortical tissue, which confirmed ELISA findings (Figure 7-12). While matched cases would be a gold standard, this method has enabled some confirmation of cell line results to human pathological tissue, highlighting the validity of the models to recapitulate FAD mechanisms and their appropriateness to investigate clinical and pathological associations.

Western blot analysis revealed a trend for increased immature PSEN1 in the *PSEN1* R278I and E280G mutation cell lines (Chapter: 7.3.5.3). This has previously been shown for the R278I line, with a significant increase in immature PSEN1 observed, and has been linked to Aβ43 production (Charles Arber *et al.*, 2019a; Nakaya *et al.*, 2005; Saito *et al.*, 2011b; Veugelen *et al.*, 2016). The findings by western blot corroborate with the results from the ELISA analysis, where high levels of Aβ43 were observed in the *PSEN1* R278I and E280G mutation lines. It is likely that the mutation location hinders processivity of immature in to mature PSEN1.

The levels of mature PSEN1 were also observed to be higher, and significantly so in the E280G mutation lines (Chapter: 7.3.5.3). As PSEN1 expression measured by qPCR was not higher in these lines, it suggests that in the E280G lines there is an accumulation of mature PSEN1 levels, and possibly this may also be why there are higher levels of immature PSEN1 in these mutation lines, possibly in addition to the proposed mutation effect on the processing of immature PSEN1 to its mature form. This increase in mature PSEN1 may explain the high levels of Aβ42 observed in these lines, in addition to the high Aβ43. This again is replicated in the human post mortem tissue where intense Aβ42 deposition is observed.

Finally, the level of immature relative to mature PSEN1 was significantly higher in the R278I line, which reflects the increase in products of the Aβ49 pathway only in this line (Chapter: 7.3.5.3). This measure also highlights that the R278I

mutation specifically effects the processing of immature to mature PSEN1, compared to other lines.

Conclusions

Our results show significant differences in *PSEN1* γ-secretase processivity between FAD mutations in a physiologically relevant model. This highlights the variable routes by which FAD mutations can lead to ab pathology, albeit centered on Aβ. The FAD lines will enable future research into mutation specific mechanism in pathogenesis with these lines. Of particular interest are the *PSEN1* E280G lines where Aβ production and PSEN1 processivity can be analysed between same mutation carriers from non-related patients which may help further understanding of heterogeneity between same mutation carriers, and the potential influence of other genetic factors.

Chapter 8

Discussion

8 Discussion

The field of AD research is complex, and the exact role of Aβ in disease remains unclear. While Aβ pathology has long been observed in sAD, the finding of genetic mutations which cause AD via disruption in the Aβ pathway confirmed its causal role in neurodegeneration. The mechanisms by which altered Aβ processing leads to downstream consequences have not been fully ascertained. There is ongoing research into many possible routes to degeneration, as studies using various FAD models have highlighted disturbances in multiple processes including metabolic pathways (Mosconi *et al.*, 2006; Schöll *et al.*, 2011; Yau *et al.*, 2015), lysosomes (Piras *et al.*, 2016), calcium pathway abnormalities (Cheung *et al.*, 2008; Tu *et al.*, 2006), mitochondria (Martín-Maestro *et al.*, 2017; Trushina *et al.*, 2012) and astrocytes (Jones *et al.*, 2017; M. Oksanen *et al.*, 2017).

Histologically, Aβ is seen as aggregates but the role of soluble Aβ present as toxic oligomers is another field of research and has been reviewed elsewhere (S. Li *et al.*, 2018; D. J. Selkoe & Hardy, 2016; Shankar *et al.*, 2008). Understanding the activity of these soluble forms on the above mentioned pathways will help explain how the Aβ molecule can cause such widespread dysfunction and cellular death. Nevertheless, investigations into the histological aggregates can reveal insights into molecular underpinnings and effects on clinical course.

This study has focused on *PSEN1* and *APP* mutations, which cause FAD. Due to the shared pathology with sAD, it is hoped that findings from the study of FAD may be applicable to increasing our understanding of sAD. In FAD research there are many individual case reports but as greater numbers of cases come to post-mortem, larger studies with multiple cases has enabled more detailed analysis of the disease. Currently, the location of mutation has been shown to play a role in the pathological and clinical heterogeneity that has been observed (David M. A. Mann *et al.*, 2001; Ryan *et al.*, 2015a; Shea *et al.*, 2016). The aim of this thesis was to further elucidate the differences considering a wide range of pathologies in addition to genetic and clinical factors (Age at onset and disease duration). Using multiple techniques, associations and contributions of these features have been investigated.

As mentioned, all cases in the study had been classified pathologically as end stage Alzheimer's. However, upon inspection it can be observed that despite this end stage AD pathology classification, the FAD cases in the QSBB have marked variability in the type and laminar distribution of Aβ pathology.

By looking into to the pathology in detail using semi-quantitative and quantitative methods, it was found that there were mutation specific effects. For instance, CWP presence was higher in layer 5 in the post-codon 200 cases (chapter: 3.3.3.4). This is interesting as CWP pathology has been associated with motor features, which was present in some of our cases (Not described within this thesis). As layer 5 neurons can project to regions associated with motor functions (Gerfen *et al.*, 2016), this suggests a mechanistic linked between pathology and phenotype. An association between CWP and CAA was also found (chapter: 3.3.3.3 and 5.3.2), which has been noted in CWP cases previously (Niwa *et al.*, 2013; Ryan *et al.*, 2015a) and indicates a molecular link.

Further to Aβ pathology, it was investigated whether microglial load differed over cortical layers (chapter: 4.3.1), varied by FAD mutation (chapter: 4.3.4), or differentially associated with Aβ plaque type and laminar distribution (chapter: 4.3.6 - 4.3.6.3). The findings highlighted that microglial deposition tended to follow Aβ deposition, and that specific microglial markers were differentially associated with Aβ pathologies, suggesting an active role of microglia in pathology.

Given the interesting results found regarding CAA and its associations with mutation position, this was further investigated in more detail in a larger extended cohort. Within this extended cohort, it was observed that mutation type had some association with CAA (chapter: 3.3.3.2, 5.3.2, 5.5.3, 5.5.6) and results for *APOE* genotypes were also suggestive of an influence (chapter: 5.5.4 and 5.5.7). Briefly, *PSEN1* post-codon 200 mutation and *APOE*4 carriers have a greater proportion or more severe CAA, respectively.

As pathologies are known to be composed of different Aβ isoform, it was sought to investigate if these differences may relate to differential isoform production by different mutations. By using IHC antibodies specific for Aβ isoforms, it was observed that mutation was indeed associated with differential isoform pathology (chapter: 6.3), as was the *APOE*4 genotype (chapter: 6.3). Notably for the

mutation associations, it was observed that Aβ43 was predominantly present in *PSEN1* post-codon 200 mutation carriers with the R278I, E280G and A434T & T291A mutations. Interestingly, these mutations have also been associated with prominent CWP, CAA and atypical clinical phenotypes.

As fibroblasts had been donated by *PSEN1* R278I and E280G carriers, there was an opportunity to study the molecular mechanisms of these mutations further in iPSC derived neurons. Analysis of Aβ production revealed that there were mutations specific differences in Aβ production (chapter: 7.3.5.2), and this matched what was observed in isoform specific IHC on tissue from matched mutation carriers (see Figure 7-12). Interestingly, protein maturity for PSEN1, the catalytic component of γ-secretase responsible for APP cleavage, differed between mutations (chapter: 7.3.5.3) and may explain mutation differences in Aβ production.

Overview of findings

By confirming differences in clinical course due to mutation (chapter: 3.3.2 and 5.5.1) we highlight how differences as small as a point mutation can cause such heterogeneity in the same disease and that understanding the initial molecular mechanisms in AD are essential to developing effective treatments and prevention. This study provided important insights into the influence of *APOE* genotype in FAD, with a longer disease duration observed in *APOE*4 carriers. While this may initially seem counter-intuitive given that *APOE*4 is such a strong risk factor for sAD, there are potential explanations. Antagonistic pleiotrophy of *APOE*4 in younger adults, such as those with FAD, may be involved, as better cognitive capabilities in young *APOE*4 carriers have been observed (Moreau *et al.*, 2013; Rusted *et al.*, 2013; Zink *et al.*, 2019). While this is not the same as disease duration, it shows positive benefits of *APOE*4 genotype at younger ages can occur. In a recent review on *APOE* by Belloy *et al.* (2019), it was highlighted that while a genome wide association study (GWAS) has indicated *APOE*4 to be negatively associated with longevity and *APOE*2 positively associated, there was a study conducted in younger people which did not find this association. This could indicate that age effects are important. As mutations have been shown by others, and confirmed here, to affect onset and duration this may provide valuable knowledge to clinicians and those with FAD linked mutations. While currently

there are no disease-modifying treatments available, understanding more about the likely progression of disease may be helpful for prognostication and for future research into factors that may modify disease progression. These findings also highlight that other pathways affected by FAD need to be investigated, as some of these may also be contributing to sAD. The effects of APOE may also be mediated via microglia. In particular, microglia states are believed to differ over ageing (Olah *et al.*, 2018). The effect of both microglia and APOE could therefore be relevant to age, especially in this FAD cohort.

Changes in Aβ are one of the initial alterations in AD. With disease progression, Aβ can deposit as multiple distinct pathologies. These have been shown to vary between cases and may link to specific clinical features (for a review of the literature, see chapter: 3.2.4 and 3.2.5). In our clinically well-characterised cohort, associations were investigated and although trends were observed, significant associations were infrequent. This was a small sample study with few matched mutation cases, therefore reducing ability to find associations. To address this, analysis was also conducted in a larger extended cohort, although only CAA was investigated in this larger group (Chapter: 5.5). From this we observed CAA to be associated with mutation sub-group and possible evidence for increased severity of CAA in an *APOE*4 dependant manner, as well as support for clinical associations found in the smaller cohort, such as the previously mentioned effects of mutation and *APOE* on age at onset and disease duration (chapter: 5.3.1). However, associations between different pathological features highlighted potential shared mechanism between these different pathologies, such as the strong association between CAA and CWPs (Chapter: 5.3.2). Deciphering the molecular connection between these will be the next step, and may involve Aβ isoform specific pathways or microglia associated mechanisms.

The previously discussed differences in layer pathology observed in sAD (Chapter: 3.2.2) were also found in our FAD cohort (Chapter: 3.3.4.3) and suggests vulnerability or higher risk in specific cortical layers which is not currently understood. One notable finding was not only higher load in lower layers in the *PSEN1* post-codon 200 group compared to other subgroups, but higher CWP frequency in layer 5 in some of these cases (Chapter: 3.3.3.4). CWPs were found to associate with CAA and high CAA pathology was noted in the *PSEN1* post-codon 200 cases: I202F, one R278I, E280G and A434T/T291A. Some of

the *PSEN1* mutation cases were then observed to have greater Aβ43 pathology, and Aβ43 present as CWP pathology (Chapter: 6.3.3). The Aβ43 expression was then shown in cellular models of these specific mutation cases (P*SEN1* R278I, E280G, chapter: 7.3.5.2). Interestingly, the E280G mutation has been linked to atypical clinical phenotype, including prominent spastic paraparesis (O'Riordan *et al.*, 2002), suggestive of a connection between these disease aspects.

Another finding was high Aβ plaque frequency and Aβ load in layer 3 (Chapter: 3.3.3 and 3.3.4.3), and using isoform specific antibodies, we were able to show that this layer specificity was particularly notable with the Aβ42 antibody (Chapter: 6.3.1). Aβ42 showing this pattern may be a result of it being the most abundantly observed isoform in these cases, with Aβ40 and Aβ43 deposition not reaching high enough levels for such patterns to be noted. Although in cases where prominent Aβ40 and Aβ43 was observed, no consistent trend in laminar specific pathological deposition was observed.

Microglia are involved in AD although whether the dysfunction observed is a cause or consequence is unclear. Microglia have been shown to be initially reactive, but they may also reach a level of senescence, hindering any further beneficial activities (Tang & Le, 2016). In our cohort we showed that microglial load did not differ between mutation groups (Chapter: 4.3.4), implying reactivity to Aβ pathology overall is the same despite differences between the mutation groups. As has been observed in AD previously, specific associations were observed between specific microglia phenotypes and distinct Aβ pathologies, (D'Andrea *et al.*, 2004; Nagele *et al.*, 2004; Sheng *et al.*, 1995; Styren *et al.*, 1990), indicating they are directly involved in certain pathological phenotypes. For instance, in chapter: 4.3.6, we showed that Iba1 was negatively correlated with cored plaques, and had no association to diffuse plaques. CD68 was generally positively associated with CAA, except in the *PSEN1* post-codon 200 group, while CD68 was negatively correlated with total Aβ pathology and load. In general, CR3/43 had negative associations with Aβ pathologies and load. As our analysis was on post-mortem tissue, the cause and direction of association cannot be determined but supports research into microglia in AD as they can influence disease mechanisms.

CAA is a frequent pathology seen in sAD and in FAD, although it's role disease is not yet fully understood. In our cohort, CAA did not strongly associate with age at onset or duration although trends were observed (Chapters: 5.5.2 and 5.5.5). In both the frontal and occipital cortex in the extended cohort, the overall proportion and severity of cortical CAA tended to positively associate with age at onset and disease duration, although many associations were weak and variability in direction could be observed between disease groups and levels of CAA severity. The association between the overall proportion and severity of leptomeningeal CAA was particularly mixed, and did not show associations as consistent as the cortical CAA. Study of larger cohorts would be needed to clarify any associations. FAD mutations are associated with CAA and in sAD *APOE* genotypes are associated with CAA, with the *APOE*4 allele conferring greater risk and severity (Ryan *et al.*, 2015a; Shinohara *et al.*, 2016). The combined effect of these two genetic influences in FAD is not clarified, and while *APOE* may play a role, it appeared that mutation may be a greater driving force in our study. Regression analysis adjusted for both FAD mutation and *APOE* genotype would allow greater investigation of the potential influence of these genotypes. While FAD shares many similarities with sAD, the role of CAA in sAD merits further investigation and the findings from FAD may not fully generalise to sAD, as impaired Aβ clearance may more strongly associate with sAD (for reviews, see Baranello *et al.* (2015); Wildsmith *et al.* (2013)).

The range of pathological deposits of Aβ are known to be unevenly contributed to by different Aβ isoforms, as previously discussed (Chapter: 6). For example results from chapter 6.3 show that the central core of cored plaques was composed of Aβ40/43 while the outer ring was Aβ42, CWPs were primarily composed of Aβ42 and generally lacked Aβ40, although Aβ43+ve CWPs were present in some cases, CAA was primarily composed of Aβ40, but may also contain Aβ42 and while Aβ43+ve CAA was less common. As FAD mutations are being shown to differentially influence generation of Aβ isoform ratios, this may impact on plaque pathology in FAD. Few studies have assessed multiple mutations with a range of isoform specific antibodies, but based on the findings shown in the thesis it appears the processivity of PSEN1 does to some extent, affect the development of specific plaque pathologies and observed heterogeneity. We have shown that *PSEN1* post-codon 200 mutations R278I,

E280G and A434T & T291A have intense Aβ43 and Aβ40 deposition compared to many other cases and these mutation cases also displayed intense CAA (Chapter: 6.3.2 and 6.3.3). This could be related to the immature PSEN1 within these mutation carriers (Chapter: 7.3.5.3).

Recently, here has been increasing research into the effect of FAD mutations on processivity of PSEN1, leading to qualitative changes in Aβ isoform profiles (Charles Arber *et al.*, 2019a; Charles Arber *et al.*, 2019b; Szaruga *et al.*, 2017; Szaruga *et al.*, 2015). The mode of action for these differences is under investigation but it appears that there may be a range of ways that processivity is affected, such as reduced processivity, reduced substrate retention and decreased PSEN1 maturity. While there is some debate over whether certain mutations lead to a loss of PSEN1 function (Xia *et al.*, 2015), it is generally accepted that alterations in function occur. The consequences of these changes are investigated in different models as it has been shown toxicity differs between generated isoforms. How these qualitative changes in Aβ relate to clinical course and pathology in a post-mortem cohort in unclear, however we have shown here matched findings in cell lines and post-mortem tissue indicating the changes may be reflected in pathological heterogeneity. Relation to clinical aspects could be further investigated, not only including age at onset and disease duration, but also behavioural, cognitive and motor phenotypes.

Overarching theme

Piecing results from all chapters together, a link emerges between mutation, Aβ peptide production and pathology. As recounted above, in the *PSEN1* post-codon 200 group, increased lower layer pathology was observed. In the Aβ isoform specific IHC, Aβ43 pathology was greater in this groups, with distribution over the cortical layers, in contrast to the greater Aβ42 deposition in the upper compared to lower layers. This suggests that in the *PSEN1* post-codon 200 group, greater lower layer deposition may be a result of the increased Aβ43 deposition. The FAD cell line work corroborates the Aβ43 pathology, with increased Aβ43 ratios produced specifically in the *PSEN1* post-codon 200 lines. As Aβ43 is aggregation prone (Conicella & Fawzi, 2014), it may aid deposition of other isoforms (Burnouf *et al.*, 2015), and lead to the greater deposition in this group. This may also result in greater CAA, which was observed in this group, as Aβ43 was seen in the

vasculature showing it can reach the IPAD pathway, although it may promote deposition and thus disruption of this mechanism. Consequent of Aβ43 deposition in the vasculature could also be greater Aβ42 and Aβ40 deposition, further increasing the proportion and severity of CAA. This Aβ43 may also underline differences in microglial associations with CAA in the *PSEN1* post-codon 200 group. Aβ43 may undergo phagocytosis less readily than the more physiological forms (such as Aβ40/Aβ42), leading to clearance via alternative routes, such as the IPAD pathway. Differences in Aβ peptide specific cellular uptake have been reported (Wesén *et al.*, 2017). Therefore, mutation may relate not only to clinical factors and Aβ production, but the clearance and pathological deposition of Aβ.

There was also evidence in this cohort that microglia were linked to the Aβ pathology, with CD68 correlating with reduced plaque load (Chapter: 4.3.6). CD68 microglia are phagocytic therefore can contribute to plaque reduction via internalisation and degradation of Aβ. CD68 was also positively correlated with greater CAA, in addition to reduced plaque burden. This may indicate that in situations of reduced IPAD clearance efficiency (with vascular Aβ build up), microglia may contribute to the clearance of Aβ via the phagocytic pathway (shown by CD68 +ve microglia), as an alternate method of removal. CR3/43 was also negatively associated with Aβ load (chapter: 4.3.6), however in contrast to CD68+ve microglia, the association with CAA was negative (Chapter: 5.4, indicating microglial phenotype differentially associates with Aβ pathology type, likely via consequences of the different downstream effects of their reactivity status.

Conclusion

Collectively, this thesis has confirmed that FAD mutations are associated with clinical and pathological heterogeneity. Diverse pathological features of FAD have been shown to have differing associations with mutation subgroups, and with distinct pathologies. Other factors beyond Aβ may also be influencing disease as Aβ did not fully account for all observations. This may include microglia, as we have shown, but could also include astrocytes. As astrocytes express APOE (Ye Zhang et al., 2014), they may be particularly important due to the influence of *APOE* genotype on certain features of FAD. Imaging of

astrocytosis in an FAD mutation cohort revealed increased astrocytosis in pre-symptomatic carriers compared to controls, as well as increased PIB retention, suggesting a link between Aβ and astrocyte reactivity (Scholl et al., 2015). Histologically it has been shown astrocytes can accumulate Aβ (Nagele et al., 2003), likely via phagocytic mechanisms. Importantly, it has also been shown that degradation of Aβ plaques by astrocytes may heavily depend on the presence of APOE (Koistinaho et al., 2004), thus effects of isoform differences in function may affect plaque interactions. Alterations in astrocytes has been observed in premature stages of CAA pathology in the transgenic arctic β-amyloid mouse expressing humanised APP protein (Merlini et al., 2011) and as discussed *APOE* genotype may influence CAA in FAD. The varied function and role of astrocytes provide routes for influence on pathology. However the study of astrocytes was beyond the scope of this study. For instance, astrocytes may influence plaque pathology, CAA or neuronal health

As FAD mutations influence clinical (Ryman *et al.*, 2014; Shea *et al.*, 2016) and pathological (D. M. A. Mann *et al.*, 2018; David M. A. Mann *et al.*, 2001; Ryan *et al.*, 2015a) heterogeneity, there is a need for mutation specific investigations. Work in cell models highlights specific mutation differences on Aβ isoform production (Charles Arber *et al.*, 2019a; Keller *et al.*, 2010; N. Li *et al.*, 2016; Moore *et al.*, 2015; Nakaya *et al.*, 2005). As Aβ isoforms can influence pathological Aβ deposits, the altered production of ratios may link to specific pathologies and their association with mutation sub-groups. For instance, histological analysis of Aβ isoforms in the E280G mutation carrier revealed distinct pathology compared to other mutations (Chapter: 6.3), and a distinct PSEN1 phenotype was also observed in the iPSC model compared to other mutations, such as the M146I line (Chapter: 7.3.5.3). This was also true for the R278I mutation line. This highlights the benefit of using multiple models to investigate disease mechanisms. Deciphering the mechanism which lead to these behind pathology may enable new and more focused approaches to treatment in the future.

While this study was limited by case numbers due to the rarity of FAD mutations, it has shown the importance of using FAD cases as a model for AD, as different routes to pathology are uncovered, which may provide insights into different disease pathways that may be involved in sAD. All studies on human post-

mortem tissue are restricted in the assumptions which can be made based on associations found. This is because end-stage pathology cannot determine the temporal sequence events. However, they do help direct areas of investigation. Importantly, the cell model results from Chapter 7.3 complement the Aβ neuropathological data observed throughout the thesis. This highlights that the underlying effects from the FAD mutations on Aβ production occur at early stages and likely lead to the development of heterogeneous Aβ pathology observed in different FAD mutation cases. With the isoform specific contribution to plaque type and the isoform/plaque type specific interaction of microglia and clearance systems combining to generate the overall pathological phenotype. To conclude, the results here have shown that heterogeneity in FAD may be linked to mutation, genetics, Aβ pathology and microglial phenotype which can be explored further in future work.

8.1.1 *Future directions*

This study has highlighted multiple associations between pathological, clinical and genetic features of FAD. Future work will need to focus on exploring these associations further. Investigations which could be conducted include:

1. A future aim onwards from this thesis, is to incorporate the histological data generated with clinical features observed in the patients. Available data on features such as myoclonus, seizures, pyramidal, extrapyramidal and cerebellar signs from clinical notes will be used. The frequency data could be analysed using chi square methods to decipher if certain features are more frequent in association with the different pathological features. For example, we may observe and association between specific motor features (such as spastic paraparesis) and lower layer Aβ pathology or CWP pathology. This would extend upon previous observations that have been made between clinical features and mutation location by (Ryan *et al.*, 2016), deepening understanding of the patho-clinical associations.

2. Another continuation from this thesis would involve investigating the relationship between the Aβ isoform specific peptide IHC with both the overall proportion and severity of CAA and microglial markers. This would enable the hypothesised link between these pathological components to

be interrogated. The Aβ isoform specific could be evaluated via % area stained or with a grading scale, and the values form this would be correlated to the values that exist for the other mentioned targets of interest.

3. Mice models with FAD mutations that produce distinct Aβ peptide profiles could be used to compare clearance of Aβ peptides. Mutations that produce high Aβ42, high Aβ40 and high Aβ43 would be used, and the patterns of Aβ pathology in terms of plaque frequency, type and distribution, and CAA would be investigated. Analysis of microglia via IHC/ imaging mass cytometry (IMC) in relation to these features would indicate if the microglial response differs in association with Aβ peptides. Aside from using IHC/IMC to phenotype the microglia, RNA sequence analysis could indicate if there is greater expression of proteins related to the clearance pathways in the different model. For instance, compare differences in the levels of transcripts for gene involved in enzymatic degradation and phagocytosis. Using this approach would help reduce heterogeneity inherent in human based studies.

4. Proximity of microglial subtype to distinct Aβ pathologies could be assessed in human post-mortem tissue to investigate if observed associations are due to potential interaction between these pathologies. IF using antibodies against microglia and Aβ, or a fluorescent dye for Aβ could be conducted. Using image analysis on software such as ImageJ, proximity could be calculated, with spatial association indicating if specific relationships between the microglial phenotypes and Aβ pathologies exist.

   A novel approach to expand on this would be to use IMC. This would allow the expansion of staining to include multiple microglial markers for deeper phenotyping, and Aβ peptide specific markers to assess relationship between specific peptides and microglia. Using this method, other cellular types could be investigated, such as astrocytes; this would allow a more global analysis of the mechanisms, and allow investigation of APOE location in relation to the histological features.

5. Generate control FAD mutation lines, where only the FAD mutation is altered to WT, allowing precise dissection of FAD mutation specific influence. This would initially focus on Aβ peptide ratios, and PSEN1 maturity to confirm the mutation associated differences observed in these assessments.

   Data would be analysed using a two-sample t-test. Based on the data for Aβ peptide ratios from the cell data (Chapter: 7.3.5.2), using the values from the ratios with highest SD and no observed significant difference between control line and a FAD mutation line, to reach a power of >0.8, at the significance alpha level set to 0.05, a sample size of would be required repeat n=20. However, for comparison of ratios where a significant difference between the control data and an FAD mutation line data were observed, power calculations reveal repeat n=3 provides a power of >0.9.

   A modelling approach similar to this could be conducted in mice, enabling *in vivo* validation of results. However, generating multiple strains of mice would be costly in terms of both money and time, therefore unfeasible as an approach in the first instance.

6. Cell line studies involving multiple lines with the same mutation to investigate consistency and heterogeneity in same mutation carriers. This could also be used to help understand the effect of *APOE* genotype in FAD. The use of CRISPR models would be an alternative to generate mutation lines without the influence of patient heterogeneity. This could be employed for multiple aims with an example being:

   Generation of multiple FAD mutation lines with a range of *APOE* genotypes. By investigating measures of cellular differentiation, health and survival, comparison of health between *APOE* genotypes could help investigate if the *APOE*4 genotype associates with any beneficial effects in FAD cell lines which may suggest routes for the *APOE*4 genotype benefit observed. RNA sequence analysis would highlight molecular pathways that are altered between *APOE* genotypes and may contribute to the *APOE* genotype affects observed. Using Nanostring technology,

transcripts relating to specific panels, such as cellular survival could be compared between groups.

7. As APOE is largely produced in astrocytes, astrocyte/neuronal co-cultures could investigate the mechanistic role of APOE in FAD lines in an attempt to investigate the effects of the APOE4 isoform on neuronal health/survival. Humanised mouse models with FAD mutations expressing the range of human APOE isoforms could be generated, with FACS coupled single cell RNA sequencing allowing cell specific changes related to *Apoe*4 genotype investigated. Transcripts of particular interest would be those related to cell survival.

8. Conduct regression analysis on a larger cohort of FAD cases consisting of a wide range of mutations and un-related individuals to investigate *APOE* effects on FAD onset and disease duration. Both linear and non-linear methods should be investigated, with the relationship between age at onset and disease duration included as an interaction. Power calculations based on figures obtained from linear regression in the thesis (Chapter: 5.5.1.2, disease duration adjusted for mutation group and *APOE* status) indicate that with the 38 cases we have in the current cohort, the power of detection is 0.99 with significance alpha set to 0.05, therefore greater numbers would provide powered results and enable the inclusion of more prediction variables in the model, such as family membership.

Appendix

9 Appendix

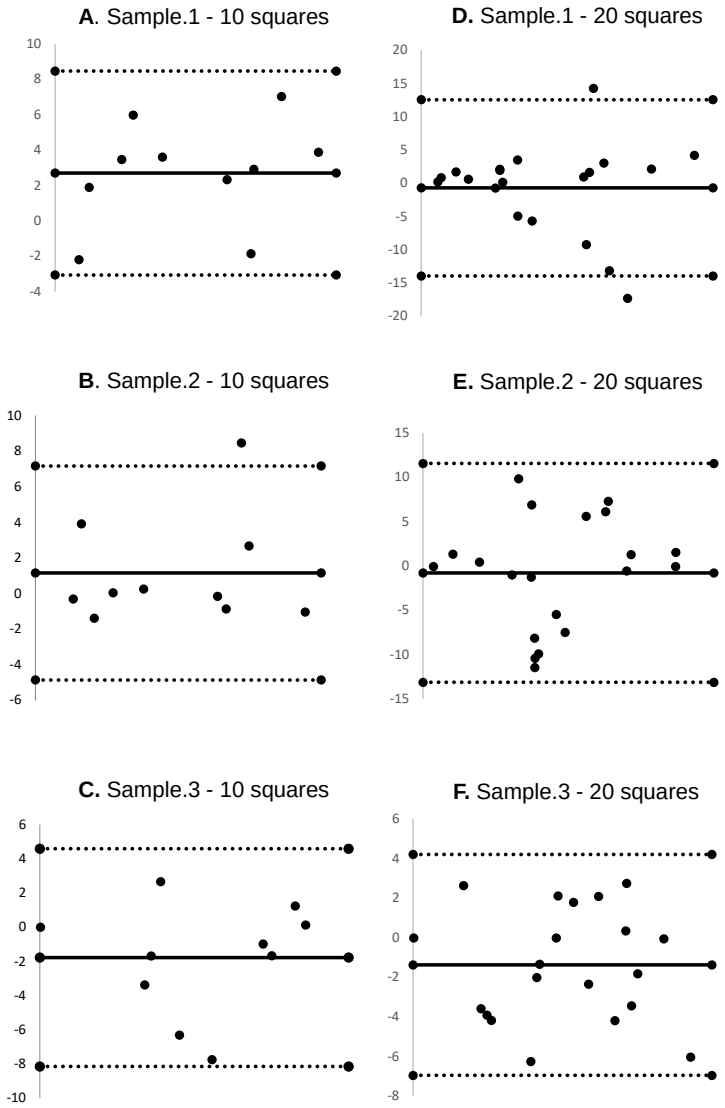

Figure 9-1. Bland Altman plots for determining number of squares (ROIs) to be analysed.

A, B, C: Plot for 10 squares for the 3 separate samples (1,2,3 respectively). D,E,F: Plot for 20 squares for the 3 separate samples (1,2,3 respectively).

	10 squares		20 squares	
	R^2	P	R^2	P
Sample.1	0.08	0.43	0.02	0.60
Sample.2	0.02	0.68	0.02	0.52
Sample.3	0.006	0.83	0.002	0.86

Table 9-1 linear regression results for determining number of squares (ROIs) to be analysed.

Lower R squared (R^2) values and higher p values signify a more reliable method. 20 squares had better consistency compared to 10 squares however, it was not feasible to measure 20 squares so 15 squares were chosen as a compromise. Regression analysis preformed on GraphPad Prism version 8.00 for Windows.

A	B	A	B	A	B	A	B	A	B	A	B
0	0	1	1	2	2	2	2	3	3	0	0
0	0	0	0	3	3	2	2	2	2	2	2
1	1	0	0	2	2	2	2	2	2	0	0
0	0	1	1	3	3	0	0	3	3	3	3
1	2	0	0	2	2	2	2	2	2	0	0
1	1	0	1	1	1	3	3	2	2	0	0
0	0	1	1	3	3	3	3	2	2	0	0
0	0	1	0	2	2	2	2	3	3	0	0
1	1	0	0	3	3	2	2	0	0	0	0
0	0	1	1	3	3	3	3	1	1	0	0
1	1	0	0	2	2	2	2	3	3	0	0
0	0	1	1	2	2	3	3	3	3	0	0
0	0	1	1	2	2	2	2	0	0	1	1
0	0	1	1	2	2	1	1	0	0	0	0
0	0	1	1	2	2	3	3	3	3	3	3
1	1	0	0	1	2	3	3	0	0	0	0
1	1	2	2	1	1	3	3	3	3	0	0
2	2	1	1	2	2	3	3	0	0	0	0
0	1	1	1	1	1	3	2	0	0	0	0
1	1	0	0	3	3	3	3	0	0	0	0
1	1	2	2	2	2	3	3	3	3	0	0
0	0	3	3	2	2	3	3	3	3	0	0
2	2	2	2	3	3	2	2	3	3	0	0
0	0	2	2	2	2	3	3	0	0	0	0
1	1	2	2	2	2	2	2	3	3	0	0
2	2	2	2	2	2	3	3	0	0	3	3
2	2	2	2	2	1	3	3	3	3	0	0
2	2	2	2	2	2	2	2	0	0	0	0
2	2	2	2	3	2	2	2	2	2	0	0
2	2	0	0	1	1	2	2	0	0	3	3
0	0	2	2	3	3	2	2	0	0	2	2
1	1	3	2	1	1	3	2	3	3	2	2
0	0	3	3	1	1	2	2	3	3	0	0
1	1	2	2	3	3	3	3	1	1	1	1
0	0	2	2	2	2	2	2	0	0	3	3
0	0	2	2	2	2	2	2	3	3	3	3
0	1	3	2	2	2	3	3	0	0	3	2
0	0	2	2	3	3	2	2	3	3	0	0
2	2	1	0	2	2	2	2	0	0		
1	1	3	2	3	3	1	2	0	0		
1	0	2	2	2	2	2	2	0	0		

Table 9-2 Grading scores from grading repeats for intra-rater reliability testing.

A high degree of consistency was found. The average measure intraclass correlation coefficient was 0.97 (95% CI: 0.97 - 0.98) ($F(242,242)= 73.23$, approximate $p<0.0000$). Intraclass correlation coefficient for consistency. Grading by myself, A = repeat 1, B = repeat 2.

Rater 1	Rater 2	Rater1	Rater 2	Rater1	Rater 2	Rater1	Rater 2
0	0	1	1	2	2	0	0
1	1	2	2	1	2	0	0
0	0	3	2	1	2		
2	1	3	3	2	2		
2	1	2	1	2	2		
0	0	2	2	2	2		
0	1	2	2	1	2		
2	2	3	2	2	2		
2	2	2	2	0	0		
2	2	2	1	3	3		
1	2	2	1	0	0		
1	1	2	2	0	0		
2	2	2	2	0	0		
1	1	2	2	3	3		
1	1	2	1	0	0		
0	0	0	0	0	0		
1	1	2	2	0	0		
2	1	2	2	3	3		
1	1	2	2	0	0		
1	1	1	1	0	0		
1	1	2	2	0	0		
1	1	3	3	3	3		
2	2	3	3	0	0		
0	0	1	2	0	0		
3	2	2	3	0	0		
2	2	3	3	3	3		
1	1	3	3	0	0		
2	2	2	2	0	0		
3	3	2	2	0	0		
3	3	2	2	3	3		

Table 9-3 *Grading* scores from rater 1 and rater 2 for inter-rater reliability testing.
A high degree of agreement was found between the two raters. The average measure intraclass correlation coefficient was 0.96 (95% CI: 0.94 - 0.97) ($F(91,91)= 23.02$, $p<0.0000$). Intraclass correlation coefficient for absolute agreement. Rater 1= QSBB PhD student, rater 2 = Nanet Willumsen.

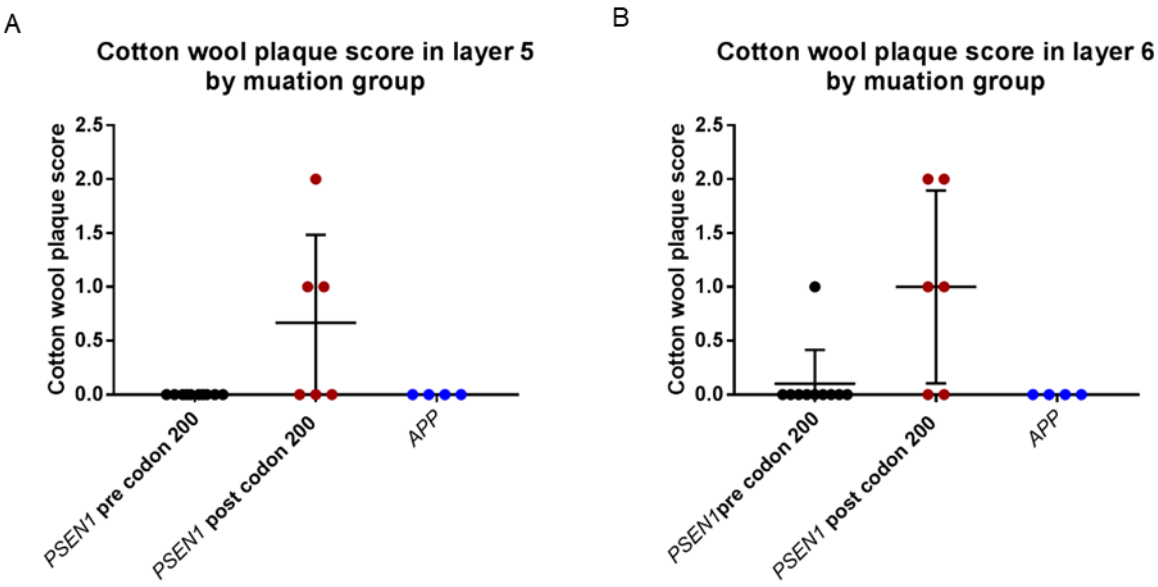

Figure 9-2 CWP frequency by layer.

CWP frequency varied in the *PSEN1* post-codon 200 group in layer 5 (A) and layer 6 (B).

A.

Iba1	Iba1 load			
	QSBB cohort	*PSEN1* pre-codon 200	*PSEN1 post-codon 200*	*APP*
Average	1.48 (1.57)	1.31 (1.63)	2.11 (1.79)	0.95 (0.98)
1	1.78 (1.37)	1.72 (1.71)	2.36 (0.82)	1.07 (0.78)
2	1.89 (1.78)	1.8 (2.05)	2.45 (1.64)	1.26 (1.33)
3	1.48 (1.51)	1.34 (1.53)	2.04 (1.77)	0.97)1.11)
4	1.27 (1.84)	0.95 (1.76)	2.02 (2.38)	0.99 (1.1)
5	1.23 (1.4)	1 (1.29)	1.89 (2.41)	0.8 (1.02)
6	1.23 (1.77)	1.07 (1.82)	1.91 (2.18)	0.61 (0.78)

B.

CD68	CD68 load			
	QSBB cohort	*PSEN1* pre-codon 200	*PSEN1 post-codon 200*	*APP*
Average		1.02 (0.66)	1.14 (0.69)	0.91 (0.47)
1	0.61 (0.54)	0.53 (0.47)	0.60 (0.37)	0.84 (0.93)
2	1.53 (1.29)	1.42 (1.06)	1.82 (1.83)	1.39 (1.16)
3	1.11 (0.83)	1.32 (1.03)	0.78 (0.45)	1.08 (0.69)
4	1.15 (0.85)	1.13 (0.81)	1.45 (1.16)	0.75 (0.17)
5	0.89 (0.55)	0.82 (0.5)	1.24 (0.6)	0.55 (0.35)
6	0.93 (.53)	0.92 (0.62)	0.97 (0.6)	0.89 (0.22)

C.

CR343	CR343 load			
	QSBB cohort	*PSEN1* pre-codon 200	*PSEN1 post-codon 200*	*APP*
Average	0.88 (1.08)	0.75 (0.87)	0.51 (0.34)	1.74 (1.9)
1	0.75 (1.1)	0.35 (0.4)	0.77 (1.16)	1.7 (1.79)
2	1.05 (1.34)	0.86 (1.33)	0.68 (0.53)	2.07 (1.93)
3	1.07 (1.22)	1.03 (1.47)	0.66 (0.51)	1.8 (1.25)
4	0.86 (1.13)	0.9 (0.89)	0.37 (0.36)	1.51 (2.12)
5	0.81 (1.37)	0.68 (0.66)	0.25 (0.19)	1.95 (2.85)
6	0.72 (0.98)	0.66 (0.86)	0.34 (0.33)	1.43 (1.66)

Figure 9-3 Average microglial load in the QSBB cohort and in mutation groups.

A: Iba1. B: CD68. C: CR343. Data presented as mean and standard deviation.

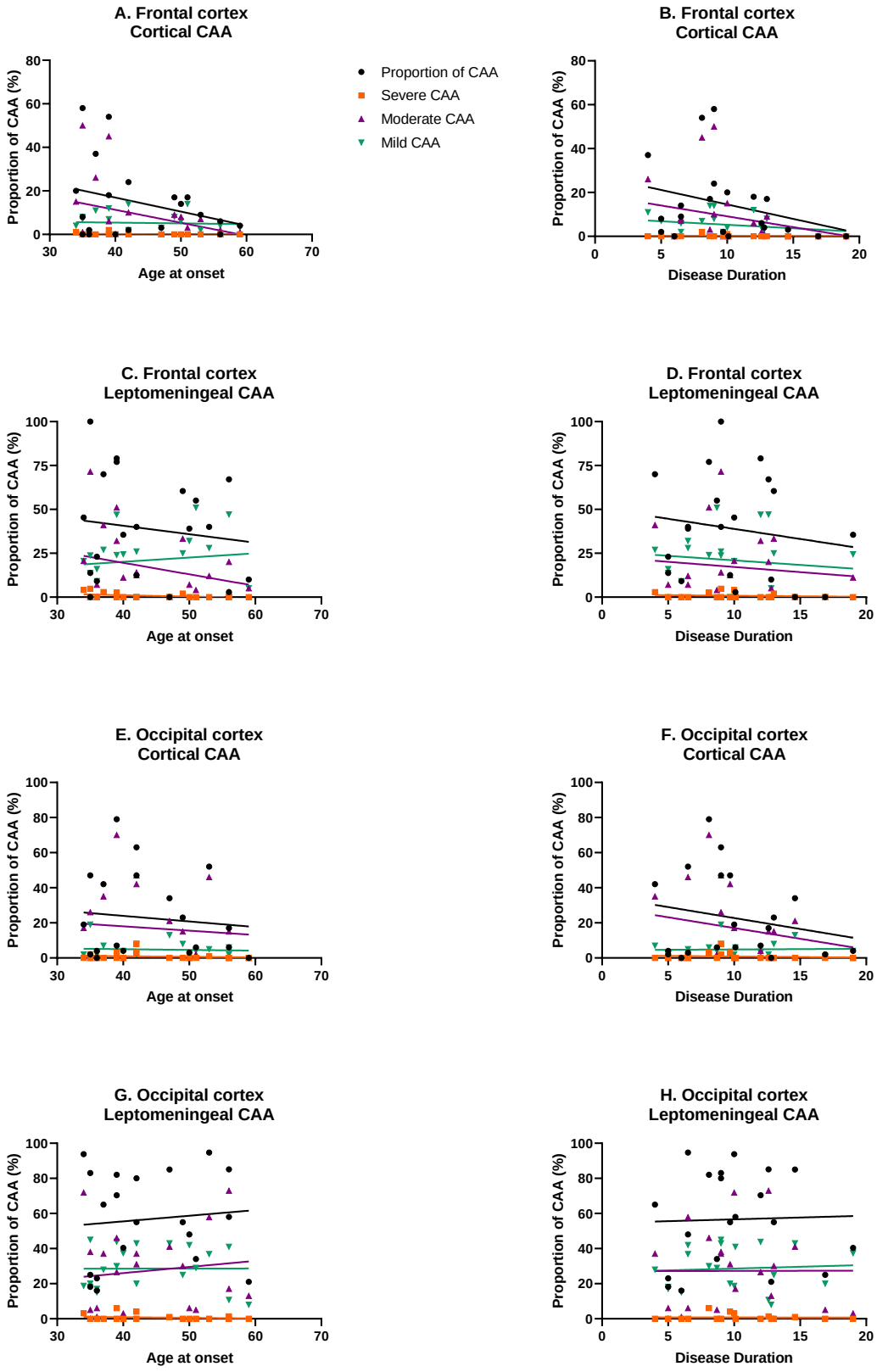

Figure 9-4 CAA severity and demographic data in the *PSEN1* pre-codon 200 group.

Correlation between the proportion and severity of CAA and age at onset (A,C,E,G) or disease duration (B,D,F,H) in the frontal (A-D) and occipital cortex (E-F).

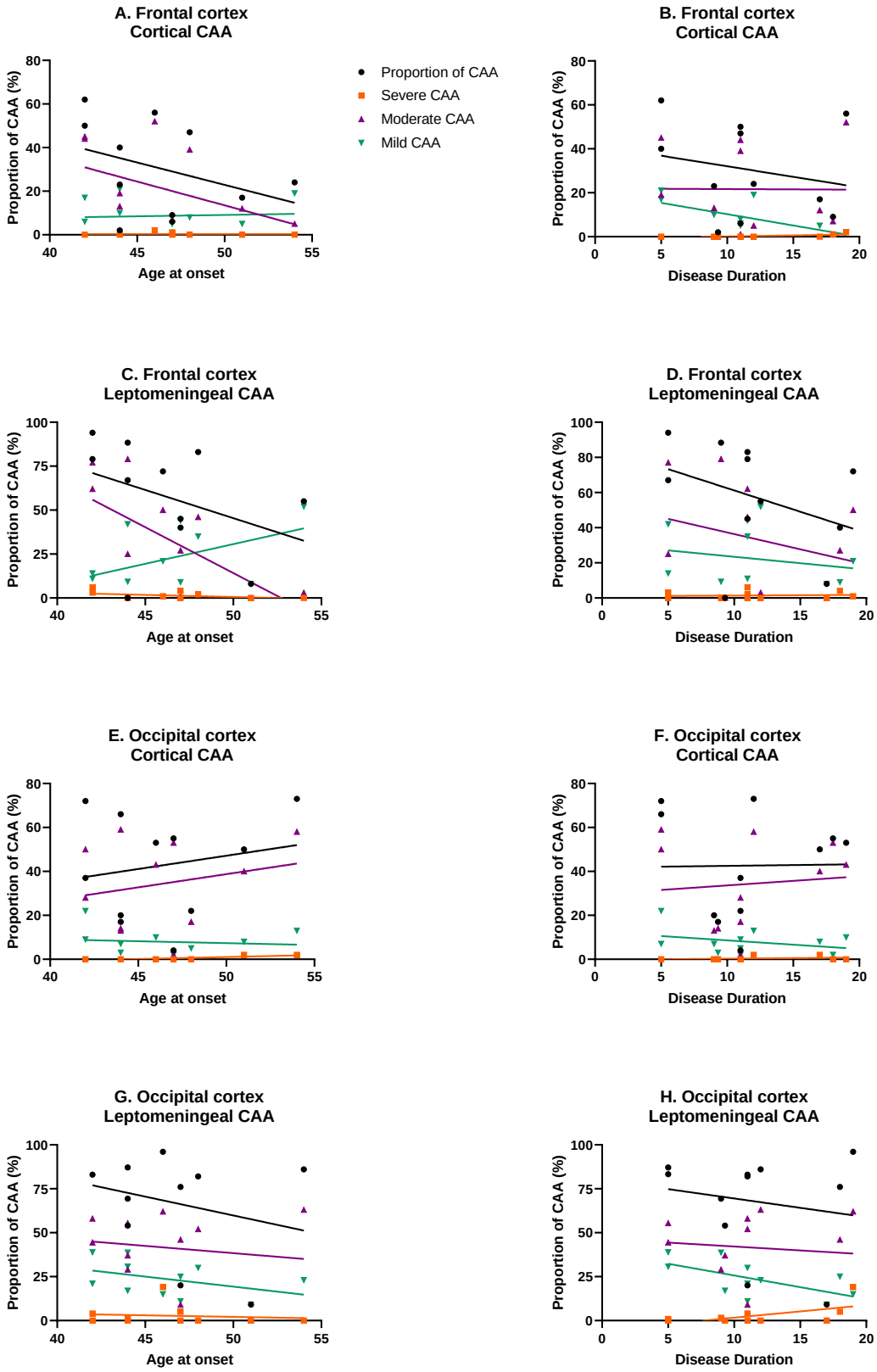

Figure 9-5 CAA severity and demographic data in the *PSEN1* post-codon 200 group.

Correlation between the proportion and severity of CAA and age at onset (A,C,E,G) or disease duration (B,D,F,H) in the frontal (A-D) and occipital cortex (E-F).

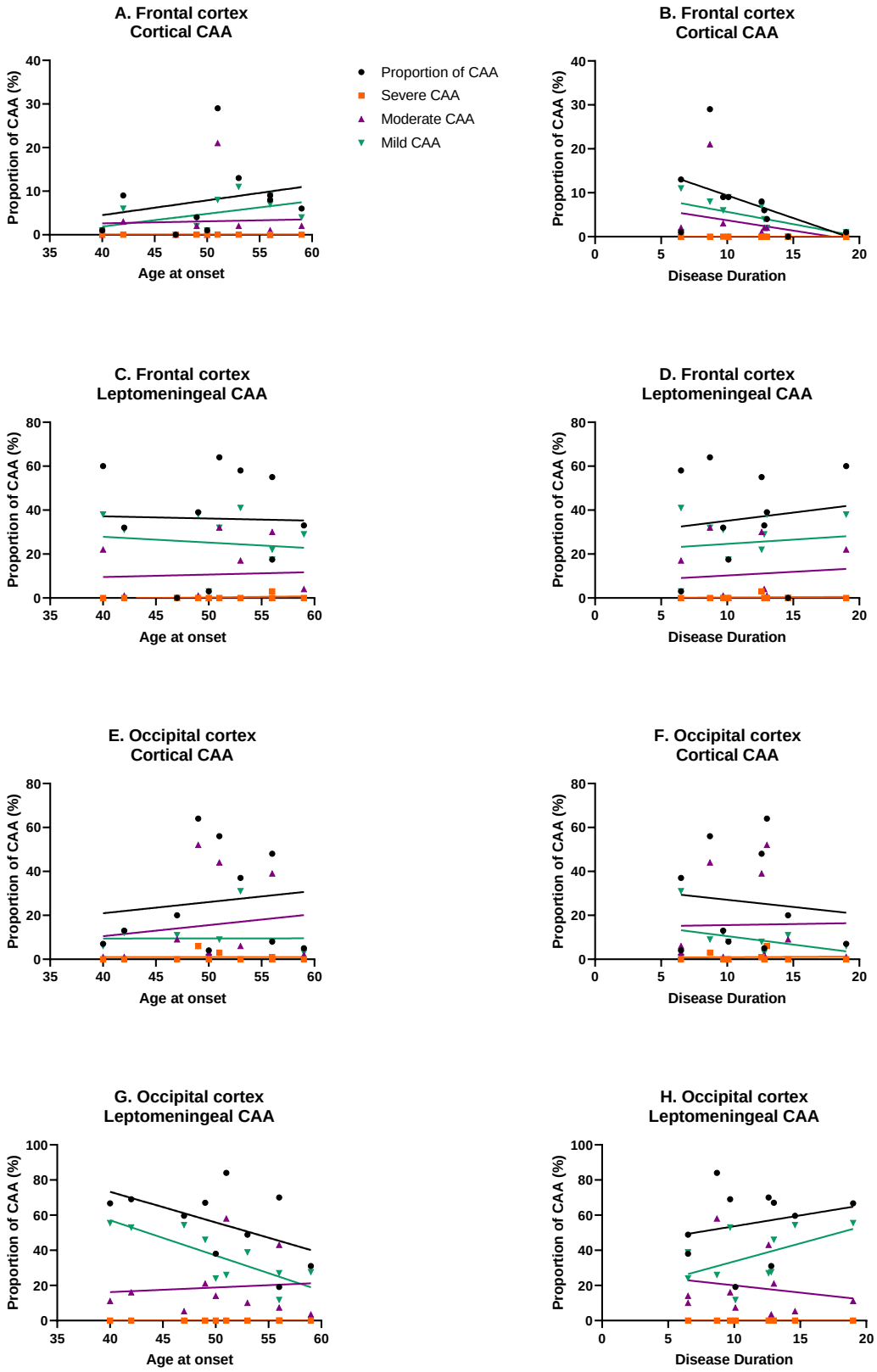

Figure 9-6 CAA severity and demographic data in the *APP* group.

Correlation between the proportion and severity of CAA and age at onset (A,C,E,G) or disease duration (B,D,F,H) in the frontal (A-D) and occipital cortex (E-F).

Cell induction	Cell line	Concentration (ng/ul)	260/280	260/230
Induction 1	A1	51.05	2.34	0.22
	RB101	203.2	1.8	1.93
	M146I	157.71	1.77	1.99
	R278I	19.31	1.69	0.76
	E280G.B	241.99	1.78	1.69
	E280G.A	233.92	1.84	1.92
Induction 2	A1	31.44	1.61	0.83
	RB101	109.71	1.71	1.45
	M146I	117.02	1.76	1.56
	R278I	13.13	1.41	0.36
	E280G.B	205.2	1.86	2.18
	E280G.A	325.01	1.87	2.03
Induction 3	A1	17.68	1.59	0.37
	RB101	102.93	1.77	1.98
	M146I	48.73	1.7	0.7
	R278I *	14.8	1.51	0.4
	E280G.B *	62.23	1.73	1.62
	E280G.A	170.36	1.85	2.12

Table 9-4 RNA concentration and purity.

RNA measured from 1:10 dilution of the 20ul stock RNA. *=Diluted 1:5.

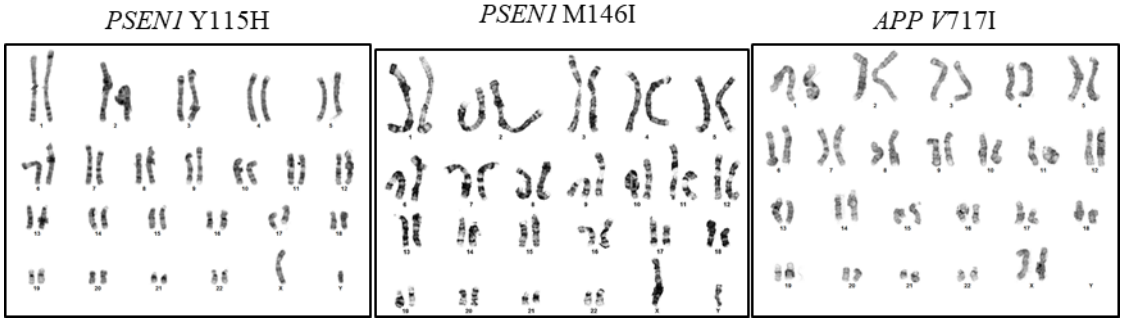

Figure 9-7 Karyotype images for *PSEN1* R278I, *PSEN1* M146I and *APP* V717I lines.

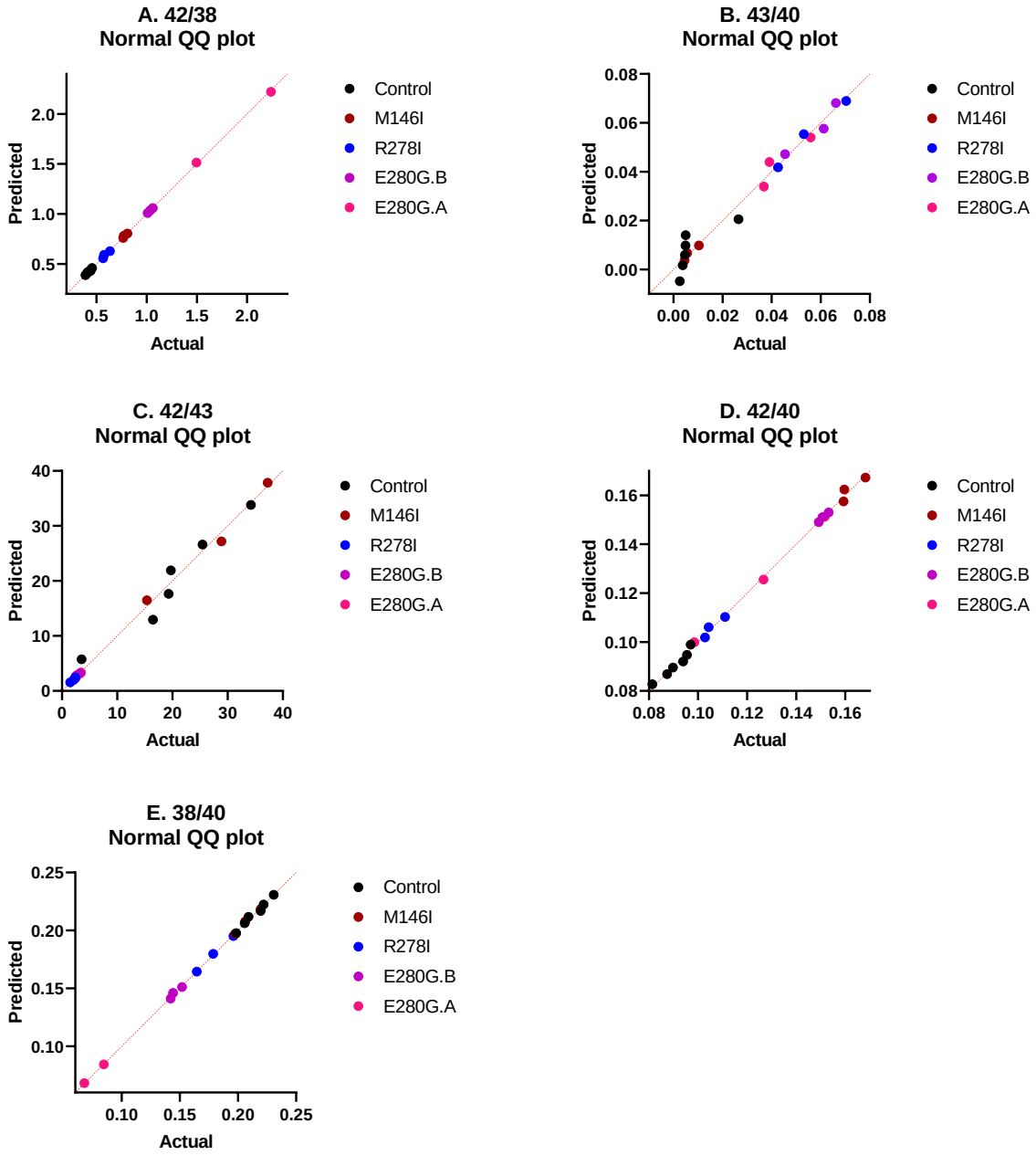

Figure 9-8 QQ plots showing data normality for ratio values from ELISA analysis. Each dot represents one induction. Control n= 6, M146I n= 3, R278I n= 3, E280G.B n= 3, E20G.A n=3.

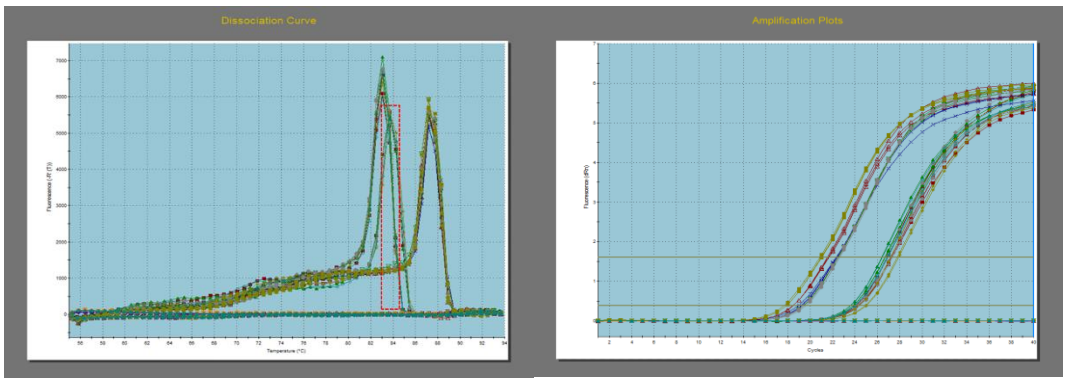

Figure 9-9 Induction 1 PSEN1 dissociation curve and amplification plot.

Dissociation curve y axis = Fluorenscence (-R' (T)), x axis = temperature. Amplification plot y axis = Flourescence (dRn), x axis = cycles. Red box indicates the anomaly relating to a separate peak, all samples within the peak were from the first row of samples. Graphs produced on software.

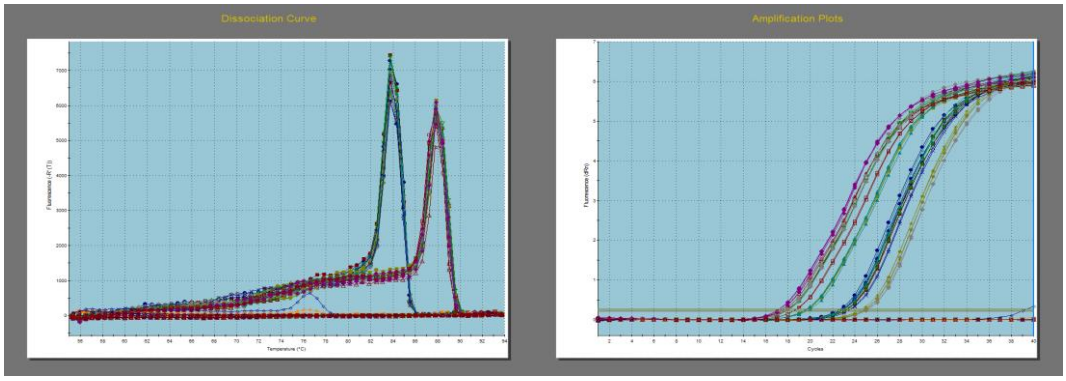

Figure 9-10 Induction 2 PSEN1 dissociation curve and amplification plot.

Dissociation curve y axis = Fluorenscence (-R' (T)), x axis = temperature. Amplification plot y axis = Flourescence (dRn), x axis = cycles. Graphs produced on software.

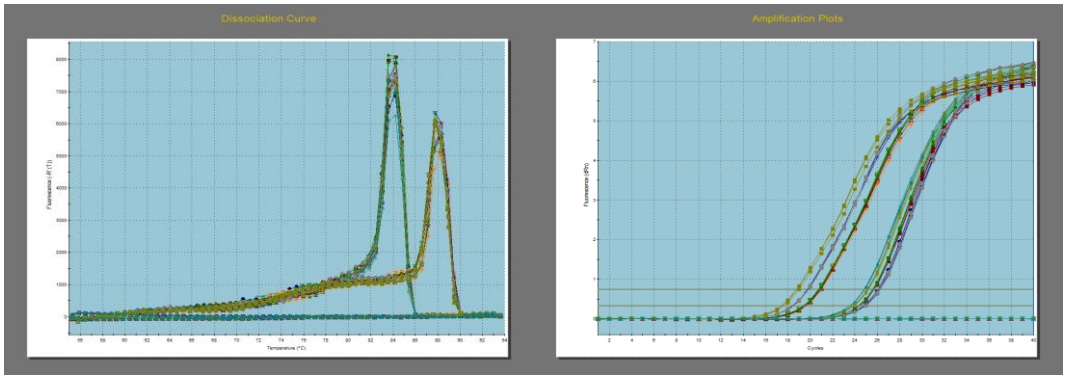

Figure 9-11 Induction 3 PSEN1 dissociation curve and amplification plot.

Dissociation curve y axis = Fluorenscence (-R' (T)), x axis = temperature. Amplification plot y axis = Flourescence (dRn), x axis = cycles. Graphs produced on software.

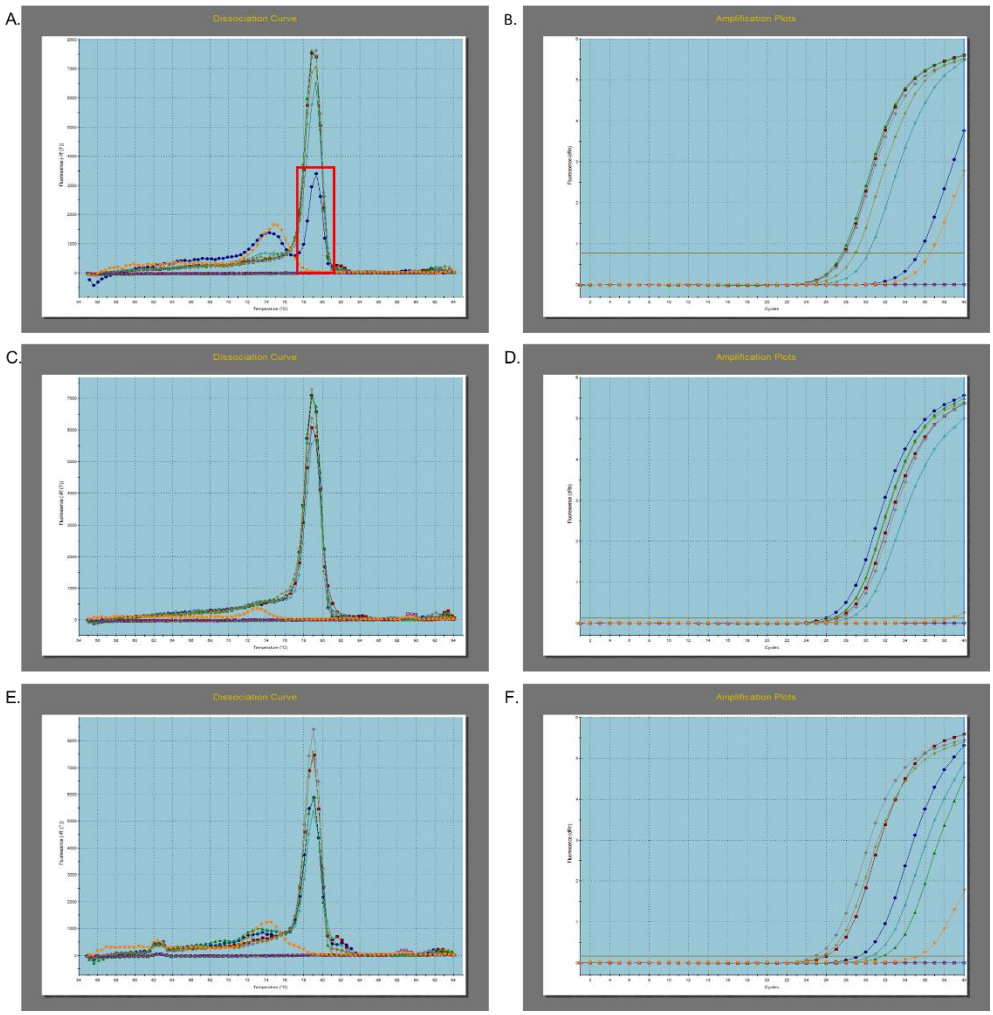

Figure 9-12 TBRI dissociation curve and amplification plots.

Dissociation curves for TBRI gene expression qPCR (A: induction 1, C: Induction 2,E: induction3). Corresponding amplification curves for TBRI gene expression (B: induction 1, D: Induction 2, F: induction3). Dissociation curve y axis = Fluorenscence (-R' (T)), x axis = temperature. Amplification plot y axis = Flourescence (dRn), x axis = cycles. Red box indicates poor amplification of induction 1, sample A1, which was omitted from analysis. Graphs produced on software.

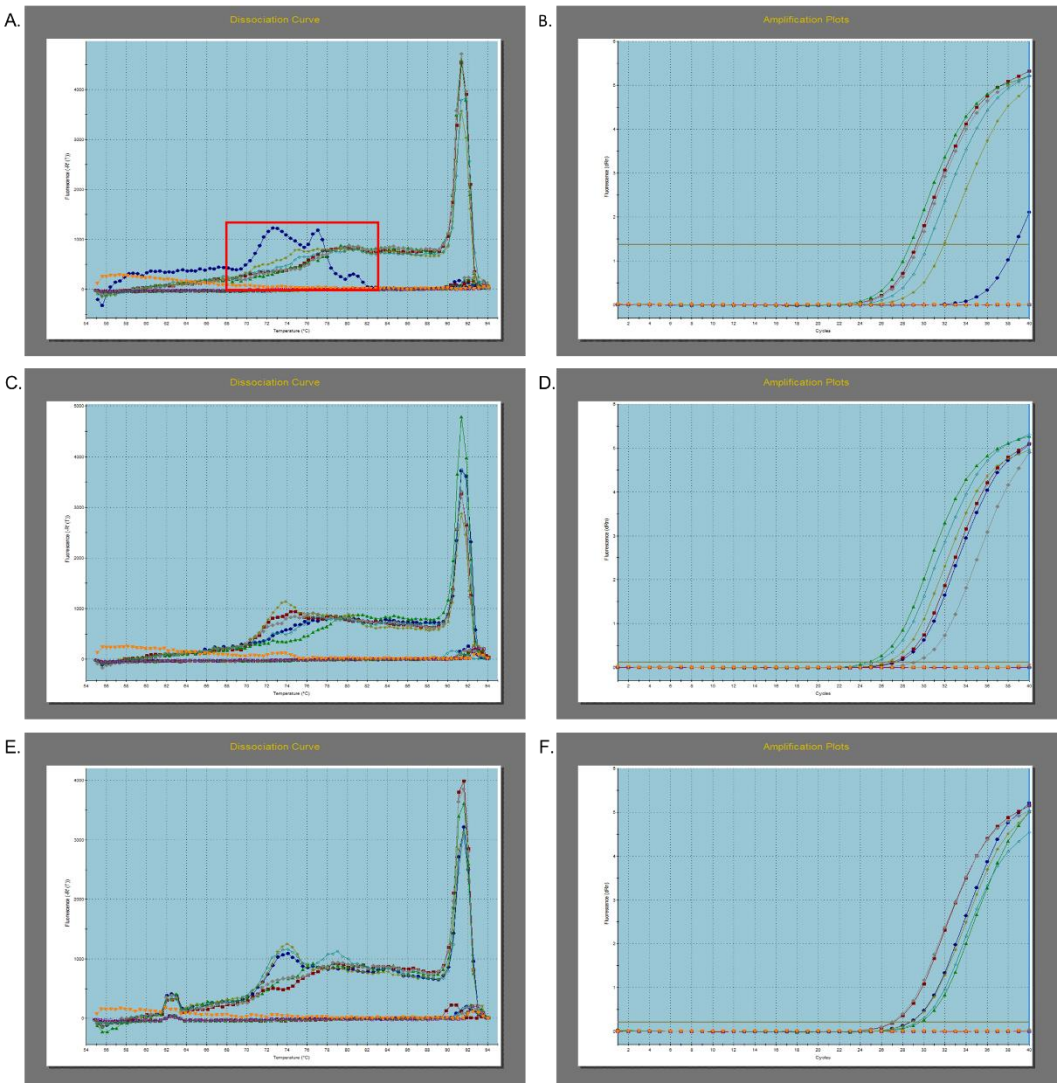

Figure 9-13 SATB2 dissociation curve and amplification plots.

Dissociation curves for SATB2 gene expression qPCR (A: induction 1, C: Induction 2, E: induction3). Corresponding amplification curves for SATB2 gene expression (B: induction 1, D: Induction 2, F: induction3). Dissociation curve y axis = Fluorenscence (-R' (T)), x axis = temperature. Amplification plot y axis = Flourescence (dRn), x axis = cycles. Red box indicates poor amplification of induction 1, sample A1, which was omitted from analysis. Graphs produced on software.

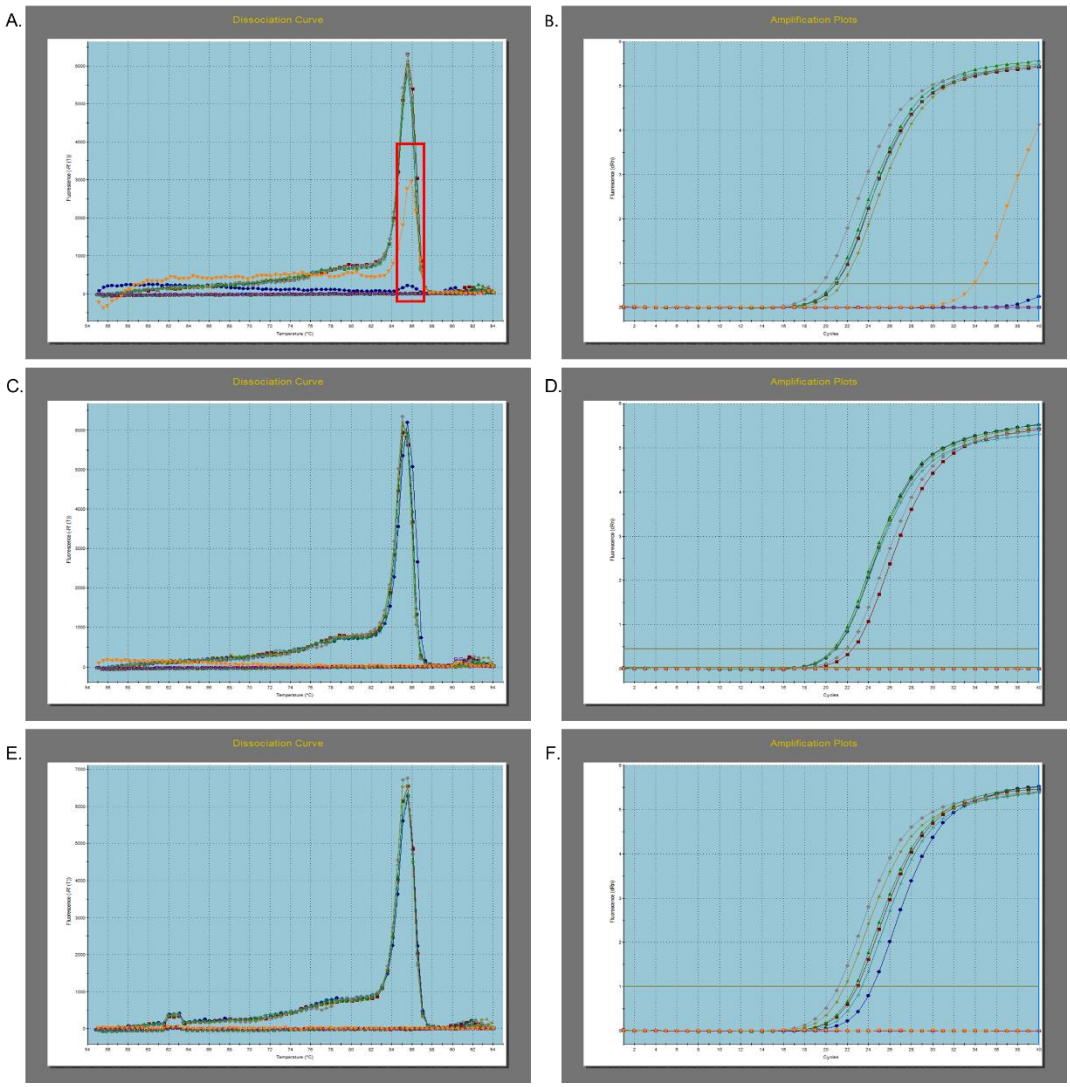

Figure 9-14 TUJ1 dissociation curve and amplification plots.

Dissociation curves for TUJ1 gene expression qPCR (A: induction 1, C: Induction 2, E: induction3). Corresponding amplification curves for TUJ1 gene expression (B: induction 1, D: Induction 2, F: induction3). Dissociation curve y axis = Fluorenscence (-R' (T)), x axis = temperature. Amplification plot y axis = Flourescence (dRn), x axis = cycles. Red box indicates poor amplification of induction 1, sample A1, which was omitted from analysis. Graphs produced on software.

10 References

Abdala, B. B., dos Santos, J. M., Gonçalves, A. P., da Motta, L. B., Laks, J., de Borges, M. B., . . . Santos-Rebouças, C. B. (2017). Influence of low frequency PSEN1 variants on familial Alzheimer's disease risk in Brazil. *Neuroscience Letters, 653*, 341-345. doi:10.1016/j.neulet.2017.05.053

Abner, E. L., Neltner, J. H., Jicha, G. A., Patel, E., Anderson, S. L., Wilcock, D. M., . . . Nelson, P. T. (2018). Diffuse Amyloid- β Plaques, Neurofibrillary Tangles, and the Impact of APOE in Elderly Persons' Brains Lacking Neuritic Amyloid Plaques. *Journal of Alzheimer's Disease, 64*(4), 1307-1324. doi:10.3233/JAD-180514

Adlard, P. A., & Vickers, J. C. (2002). Morphologically distinct plaque types differentially affect dendritic structure and organisation in the early and late states of Alzheimer's disease. *Acta Neuropathologica, 103*(4), 377-383. doi:10.1007/s00401-001-0476-6

Ahmed, R., Akcan, M., Khondker, A., Rheinstädter, M. C., Bozelli, J. C., Epand, R. M., . . . Melacini, G. (2019). Atomic resolution map of the soluble amyloid beta assembly toxic surfaces. *Chemical Science, 10*(24), 6072-6082. doi:10.1039/C9SC01331H

Alafuzoff, I., Overmyer, M., Helisalmi, S., Sr, P. R., & Soininen, H. (1999). β-amyloid load, astroglia and microglia in Alzheimer's disease: Association with apoE genotype. *Alzheimer's Reports, 2*(5), 283-289.

Aldea, R., Weller, R. O., Wilcock, D. M., Carare, R. O., & Richardson, G. (2019). Cerebrovascular smooth muscle cells as the drivers of intramural periarterial drainage of the brain. *Frontiers in Aging Neuroscience, 11*(JAN). doi:10.3389/fnagi.2019.00001

Allan, C. L., & Ebmeier, K. P. (2011). The influence of ApoE4 on clinical progression of dementia: A meta-analysis. *International Journal of Geriatric Psychiatry, 26*(5), 520-526. doi:10.1002/gps.2559

Allen D. Roses, M. D. (1996). APOLIPOPROTEIN E ALLELES AS RISK FACTORS IN ALZHEIMER'S DISEASE. *Annual Review of Medicine, 47*(1), 387-400. doi:10.1146/annurev.med.47.1.387

Allen, N., Robinson, A. C., Snowden, J., Davidson, Y. S., & Mann, D. M. A. (2014). Patterns of cerebral amyloid angiopathy define histopathological phenotypes in Alzheimer's disease. *Neuropathology and Applied Neurobiology, 40*(2), 136-148. doi:10.1111/nan.12070

Altmann, A., Tian, L., Henderson, V. W., & Greicius, M. D. (2014). Sex modifies the APOE-related risk of developing Alzheimer disease. *Annals of Neurology, 75*(4), 563-573. doi:10.1002/ana.24135

Andreadis, A., Brown, W. M., & Kosik, K. S. (1992). Structure and Novel Exons of the Human τ Gene. *Biochemistry, 31*(43), 10626-10633. doi:10.1021/bi00158a027

Anholt, R. R. H., Pedersen, P. L., De Souza, E. B., & Snyder, S. H. (1986). The peripheral-type benzodiazepine receptor. Localization to the mitochondrial outer membrane. *Journal of Biological Chemistry, 261*(2), 576-583.

Annaert, W. G., Esselens, C., Baert, V., Boeve, C., Snellings, G., Cupers, P., . . . De Strooper, B. (2001). Interaction with telencephalin and the amyloid precursor protein predicts a ring structure for presenilins. *Neuron, 32*(4), 579-589. doi:10.1016/S0896-6273(01)00512-8

Arber, C., Lovejoy, C., & Wray, S. (2017). Stem cell models of Alzheimer's disease: Progress and challenges. *Alzheimer's Research and Therapy, 9*(1). doi:10.1186/s13195-017-0268-4

Arber, C., Toombs, J., Lovejoy, C., Ryan, N. S., Paterson, R. W., Willumsen, N., . . . Wray, S. (2019a). Familial Alzheimer's disease patient-derived neurons reveal distinct mutation-specific effects on amyloid beta. *Molecular Psychiatry*. doi:10.1038/s41380-019-0410-8

Arber, C., Villegas-Llerena, C., Toombs, J., Pocock, J. M., Ryan, N. S., Fox, N. C., . . . Wray, S. (2019b). Amyloid precursor protein processing in human neurons with an allelic series of the PSEN1 intron 4 deletion mutation and total presenilin-1 knockout. *Brain Communications*. doi:10.1093/braincomms/fcz024

Arboleda-Velasquez, J. F., Lopera, F., O'Hare, M., Delgado-Tirado, S., Marino, C., Chmielewska, N., . . . Quiroz, Y. T. (2019). Resistance to autosomal dominant Alzheimer's disease in an APOE3 Christchurch homozygote: a case report. *Nature Medicine, 25*(11), 1680-1683. doi:10.1038/s41591-019-0611-3

Armijo, E., Gonzalez, C., Shahnawaz, M., Flores, A., Davis, B., & Soto, C. (2017). Increased susceptibility to Aβ toxicity in neuronal cultures derived from familial Alzheimer's disease (PSEN1-A246E) induced pluripotent stem cells. *Neuroscience Letters, 639*, 74-81. doi:https://doi.org/10.1016/j.neulet.2016.12.060

Armstrong, R. A. (2012). The visual cortex in alzheimer's disease: Laminar distribution of the pathological changes in visual areas V1 and V2. In *Visual Cortex: Anatomy, Functions and Injuries* (pp. 99-128).

Armstrong, R. A. (2014). Factors Determining Disease Duration in Alzheimer's Disease: A Postmortem Study of 103 Cases Using the Kaplan-Meier Estimator and Cox Regression. *BioMed Research International, 2014*, 623487. doi:10.1155/2014/623487

Armstrong, R. A. (2015). Laminar distribution of β-amyloid (Aβ) peptide deposits in the frontal lobe in familial and sporadic Alzheimer's disease. *Folia Neuropathologica, 53*(1), 15-23. doi:10.5114/fn.2015.49970

Arrighi, H. M., Barakos, J., Barkhof, F., Tampieri, D., Jack, C., Jr., Melançon, D., . . . Brashear, H. R. (2016). Amyloid-related imaging abnormalities-haemosiderin (ARIA-H) in patients with Alzheimer's disease treated with bapineuzumab: A historical, prospective secondary analysis. *Journal of Neurology, Neurosurgery and Psychiatry, 87*(1), 106-112. doi:10.1136/jnnp-2014-309493

Asami-Odaka, A., Ishibashi, Y., Kikuchi, T., Kitada, C., & Suzuki, N. (1995). Long Amyloid .beta.-Protein Secreted from Wild-Type Human Neuroblastoma IMR-32 Cells. *Biochemistry, 34*(32), 10272-10278. doi:10.1021/bi00032a022

Attems, J. (2005). Sporadic cerebral amyloid angiopathy: Pathology, clinical implications, and possible pathomechanisms. *Acta Neuropathologica, 110*(4), 345-359. doi:10.1007/s00401-005-1074-9

Attems, J., & Jellinger, K. A. (2004). Only cerebral capillary amyloid angiopathy correlates with Alzheimer pathology - A pilot study. *Acta Neuropathologica, 107*(2), 83-90. doi:10.1007/s00401-003-0796-9

Attems, J., Jellinger, K. A., & Lintner, F. (2005). Alzheimer's disease pathology influences severity and topographical distribution of cerebral amyloid angiopathy. *Acta Neuropathologica, 110*(3), 222-231. doi:10.1007/s00401-005-1064-y

Attems, J., Quass, M., Jellinger, K. A., & Lintner, F. (2007). Topographical distribution of cerebral amyloid angiopathy and its effect on cognitive decline are influenced by Alzheimer disease pathology. *Journal of the Neurological Sciences, 257*(1-2), 49-55. doi:10.1016/j.jns.2007.01.013

Bachstetter, A. D., Van Eldik, L. J., Schmitt, F. A., Neltner, J. H., Ighodaro, E. T., Webster, S. J., . . . Nelson, P. T. (2015). Disease-related microglia heterogeneity in the hippocampus of Alzheimer's disease, dementia with Lewy bodies, and hippocampal sclerosis of aging. *Acta Neuropathologica Communications, 3*, 32. doi:10.1186/s40478-015-0209-z

Bai, X.-C., Yan, C., Yang, G., Lu, P., Ma, D., Sun, L., . . . Shi, Y. (2015). An atomic structure of human γ-secretase. *Nature, 525*(7568), 212-217. doi:10.1038/nature14892

Balbach, J. J., Ishii, Y., Antzutkin, O. N., Leapman, R. D., Rizzo, N. W., Dyda, F., . . . Tycko, R. (2000). Amyloid Fibril Formation by Aβ16-22, a Seven-Residue Fragment of the Alzheimer's β-Amyloid Peptide, and Structural Characterization by Solid State NMR. *Biochemistry, 39*(45), 13748-13759. doi:10.1021/bi0011330

Bales, K. R., Liu, F., Wu, S., Lin, S., Koger, D., DeLong, C., . . . Paul, S. M. (2009). Human APOE Isoform-Dependent Effects on Brain β-Amyloid Levels in PDAPP Transgenic Mice. *The Journal of Neuroscience, 29*(21), 6771-6779. doi:10.1523/jneurosci.0887-09.2009

Balez, R., Steiner, N., Engel, M., Muñoz, S. S., Lum, J. S., Wu, Y., . . . Ooi, L. (2016). Neuroprotective effects of apigenin against inflammation, neuronal excitability and apoptosis in an induced pluripotent stem cell model of Alzheimer's disease. *Scientific Reports, 6*. doi:10.1038/srep31450

Bamberger, M. E., Harris, M. E., McDonald, D. R., Husemann, J., & Landreth, G. E. (2003). A cell surface receptor complex for fibrillar β-amyloid mediates microglial activation. *Journal of Neuroscience, 23*(7), 2665-2674.

Baranello, R. J., Bharani, K. L., Padmaraju, V., Chopra, N., Lahiri, D. K., Greig, N. H., . . . Sambamurti, K. (2015). Amyloid-beta protein clearance and degradation (ABCD) pathways and their role in Alzheimer's disease. *Current Alzheimer Research, 12*(1), 32-46. doi:10.2174/1567205012666141218140953

Barykin, E. P., Mitkevich, V. A., Kozin, S. A., & Makarov, A. A. (2017). Amyloid β Modification: A Key to the Sporadic Alzheimer's Disease? *Frontiers in genetics, 8*, 58-58. doi:10.3389/fgene.2017.00058

Basun, H., Grut, M., Winblad, B., & Lannfelt, L. (1995). Apolipoprotein ε{lunate}4 allele and disease progression in patients with late-onset Alzheimer's disease. *Neuroscience Letters, 183*(1-2), 32-34. doi:10.1016/0304-3940(94)11107-T

Bateman, R. J., Aisen, P. S., De Strooper, B., Fox, N. C., Lemere, C. A., Ringman, J. M., . . . Xiong, C. (2011). Autosomal-dominant Alzheimer's disease: a review and proposal for the prevention of Alzheimer's disease. *Alzheimer's Research & Therapy, 3*(1), 1-1. doi:10.1186/alzrt59

Bayraktar, O. A., Bartels, T., Polioudakis, D., Holmqvist, S., Haim, L. B., Young, A. M. H., . . . Rowitch, D. H. (2018). Single-cell in situ transcriptomic map of astrocyte cortical layer diversity. 432104. doi:10.1101/432104 %J bioRxiv

Bell, R. D., & Zlokovic, B. V. (2009). Neurovascular mechanisms and blood-brain barrier disorder in Alzheimer's disease. *Acta Neuropathologica, 118*(1), 103-113. doi:10.1007/s00401-009-0522-3

Belloy, M. E., Napolioni, V., & Greicius, M. D. (2019). A Quarter Century of APOE and Alzheimer's Disease: Progress to Date and the Path Forward. *Neuron, 101*(5), 820-838. doi:10.1016/j.neuron.2019.01.056

Benitez, B. A., Karch, C. M., Cai, Y., Jin, S. C., Cooper, B., Carrell, D., . . . Cruchaga, C. (2013). The PSEN1, p.E318G variant increases the risk of Alzheimer's disease in APOE-ε4 carriers. *PLoS genetics, 9*(8), e1003685-e1003685. doi:10.1371/journal.pgen.1003685

Bentahir, M., Nyabi, O., Verhamme, J., Tolia, A., Horré, K., Wiltfang, J., . . . De Strooper, B. (2006). Presenilin clinical mutations can affect γ-secretase activity by different mechanisms. *Journal of Neurochemistry, 96*(3), 732-742. doi:10.1111/j.1471-4159.2005.03578.x

Benzinger, T. L., Gregory, D. M., Burkoth, T. S., Miller-Auer, H., Lynn, D. G., Botto, R. E., & Meredith, S. C. (1998). Propagating structure of Alzheimer's beta-amyloid(10-35) is parallel beta-sheet with residues in exact register. *Proceedings of the National Academy of Sciences of the United States of America, 95*(23), 13407-13412. doi:10.1073/pnas.95.23.13407

Bertoli Avella, A., Marcheco Teruel, B., Llibre Rodriguez, J., Gomez Viera, N., Borrajero Martinez, I., Severijnen, E., . . . Heutink, P. (2002). A novel presenilin 1 mutation (L174 M) in a large Cuban family with early onset Alzheimer disease. *Neurogenetics, 4*(2), 97-104. doi:10.1007/s10048-002-0136-6

Birnbaum, J. H., Wanner, D., Gietl, A. F., Saake, A., Kündig, T. M., Hock, C., . . . Tackenberg, C. (2018). Oxidative stress and altered mitochondrial protein expression in the absence of amyloid-β and tau pathology in iPSC-derived neurons from sporadic Alzheimer's disease patients. *Stem Cell Research, 27*, 121-130. doi:10.1016/j.scr.2018.01.019

Blennow, K., Hampel, H., Weiner, M., & Zetterberg, H. (2010). Cerebrospinal fluid and plasma biomarkers in Alzheimer disease. *Nature Reviews Neurology, 6*(3), 131-144. doi:10.1038/nrneurol.2010.4

Blume, T., Focke, C., Peters, F., Deussing, M., Albert, N. L., Lindner, S., . . . Brendel, M. (2018). Microglial response to increasing amyloid load saturates with aging: A longitudinal dual tracer in vivo μpET-study 11

Medical and Health Sciences 1109 Neurosciences. *Journal of Neuroinflammation, 15*(1). doi:10.1186/s12974-018-1347-6

Boche, D., Denham, N., Holmes, C., & Nicoll, J. A. R. (2010). Neuropathology after active Aβ42 immunotherapy: Implications for Alzheimer's disease pathogenesis. *Acta Neuropathologica, 120*(3), 369-384. doi:10.1007/s00401-010-0719-5

Boche, D., Perry, V. H., & Nicoll, J. A. R. (2013). Review: Activation patterns of microglia and their identification in the human brain. *Neuropathology and Applied Neurobiology, 39*(1), 3-18. doi:10.1111/nan.12011

Boche, D., Zotova, E., Weller, R. O., Love, S., Neal, J. W., Pickering, R. M., . . . Nicoll, J. A. R. (2008). Consequence of Aβ immunization on the vasculature of human Alzheimer's disease brain. *Brain, 131*(12), 3299-3310. doi:10.1093/brain/awn261

Bogner, S., Bernreuther, C., Matschke, J., Barrera-Ocampo, A., Sepulveda-Falla, D., Leypoldt, F., . . . Glatzel, M. (2013). Immune activation in amyloid-β-related angiitis correlates with decreased parenchymal amyloid-β plaque load. *Neurodegenerative Diseases, 13*(1), 38-44. doi:10.1159/000352020

Boon, B. D. C., Hoozemans, J. J. M., Lopuhaä, B., Eigenhuis, K. N., Scheltens, P., Kamphorst, W., . . . Bouwman, F. H. (2018). Neuroinflammation is increased in the parietal cortex of atypical Alzheimer's disease. *Journal of Neuroinflammation, 15*(1), 170-170. doi:10.1186/s12974-018-1180-y

Bown, N., Cotterill, S., Łastowska, M., O'Neill, S., Pearson, A. D. J., Plantaz, D., . . . Van Roy, N. (1999). Gain of chromosome arm 17q and adverse outcome in patients with neuroblastoma. *New England Journal of Medicine, 340*(25), 1954-1961. doi:10.1056/NEJM199906243402504

Boyle, P. A., Yu, L., Nag, S., Leurgans, S., Wilson, R. S., Bennett, D. A., & Schneider, J. A. (2015). Cerebral amyloid angiopathy and cognitive outcomes in community-based older persons. *Neurology, 85*(22), 1930-1936. doi:10.1212/WNL.0000000000002175

Braak, H., Alafuzoff, I., Arzberger, T., Kretzschmar, H., & Del Tredici, K. (2006). Staging of Alzheimer disease-associated neurofibrillary pathology using paraffin sections and immunocytochemistry. *Acta Neuropathologica, 112*(4), 389-404. doi:10.1007/s00401-006-0127-z

Braak, H., & Braak, E. (1991). Neuropathological stageing of Alzheimer-related changes. *Acta Neuropathologica, 82*(4), 239-259. doi:10.1007/bf00308809

Braggin, J. E., Bucks, S. A., Course, M. M., Smith, C. L., Sopher, B., Osnis, L., . . . Jayadev, S. (2019). Alternative splicing in a presenilin 2 variant associated with Alzheimer disease. *Annals of Clinical and Translational Neurology, 6*(4), 762-777. doi:10.1002/acn3.755

Breimer, M. E., Säljö, K., Barone, A., & Teneberg, S. (2017). Glycosphingolipids of human embryonic stem cells. *Glycoconjugate Journal, 34*(6), 713-723. doi:10.1007/s10719-016-9706-y

Breitner, J. C. S., Wyse, B. W., Anthony, J. C., Welsh-Bohmer, K. A., Steffens, D. C., Norton, M. C., . . . Khachaturian, A. (1999). APOE-ε4 count predicts age when prevalence of AD increases, then declines: The cache county study. *Neurology, 53*(2), 321-331.

Brenowitz, W. D., Nelson, P. T., Besser, L. M., Heller, K. B., & Kukull, W. A. (2015). Cerebral amyloid angiopathy and its co-occurrence with Alzheimer's disease and other cerebrovascular neuropathologic changes. *Neurobiology of Aging, 36*(10), 2702-2708. doi:10.1016/j.neurobiolaging.2015.06.028

Brooks, W. S., Kwok, J. B. J., Kril, J. J., Broe, G. A., Blumbergs, P. C., Tannenberg, A. E., . . . Schofield, P. R. (2003). Alzheimer's disease with spastic paraparesis and 'cotton wool' plaques: Two pedigrees with PS-1 exon 9 deletions. *Brain, 126*(4), 783-791. doi:10.1093/brain/awg084

Brouwers, N., Sleegers, K., Engelborghs, S., Bogaerts, V., Serneels, S., Kamali, K., . . . Theuns, J. (2006). Genetic risk and transcriptional variability of amyloid precursor protein in Alzheimer's disease. *Brain, 129*(11), 2984-2991. doi:10.1093/brain/awl212

Brunkan, A. L., & Goate, A. M. (2005). Presenilin function and γ-secretase activity. *Journal of Neurochemistry, 93*(4), 769-792. doi:10.1111/j.1471-4159.2005.03099.x

Bugiani, O., Giaccone, G., Rossi, G., Mangieri, M., Capobianco, R., Morbin, M., . . . Tagliavini, F. (2010). Hereditary cerebral hemorrhage with amyloidosis associated with the E693K mutation of APP. *Archives of Neurology, 67*(8), 987-995. doi:10.1001/archneurol.2010.178

Bukhari, H., Glotzbach, A., Kolbe, K., Leonhardt, G., Loosse, C., & Müller, T. (2017). Small things matter: Implications of APP intracellular domain AICD nuclear signaling in the progression and pathogenesis of Alzheimer's disease. *Progress in Neurobiology, 156*, 189-213. doi:10.1016/j.pneurobio.2017.05.005

Burnouf, S., Gorsky, M. K., Dols, J., Grönke, S., & Partridge, L. (2015). Aβ43 is neurotoxic and primes aggregation of Aβ40 in vivo. *Acta Neuropathologica, 130*(1), 35-47. doi:10.1007/s00401-015-1419-y

Bussy, A., Snider, B. J., Coble, D., Xiong, C., Fagan, A. M., Cruchaga, C., . . . Morris, J. C. (2019). Effect of apolipoprotein E4 on clinical, neuroimaging, and biomarker measures in noncarrier participants in the Dominantly Inherited Alzheimer Network. *Neurobiology of Aging, 75*, 42-50. doi:10.1016/j.neurobiolaging.2018.10.011

Cabrejo, L., Guyant-Maréchal, L., Laquerrière, A., Vercelletto, M., De La Fournière, F., Thomas-Antérion, C., . . . Hannequin, D. (2006). Phenotype associated with APP duplication in five families. *Brain, 129*(11), 2966-2976. doi:10.1093/brain/awl237

Cacciottolo, M., Christensen, A., Moser, A., Liu, J., Pike, C. J., Smith, C., . . . Finch, C. E. (2016). The APOE4 allele shows opposite sex bias in microbleeds and Alzheimer's disease of humans and mice. *Neurobiology of Aging, 37*, 47-57. doi:10.1016/j.neurobiolaging.2015.10.010

Cairns, N. J., Perrin, R. J., Franklin, E. E., Carter, D., Vincent, B., Xie, M., . . . Morris, J. C. (2015). Neuropathologic assessment of participants in two multi-center longitudinal observational studies: The Alzheimer Disease Neuroimaging Initiative (ADNI) and the Dominantly Inherited Alzheimer Network (DIAN). *Neuropathology, 35*(4), 390-400. doi:10.1111/neup.12205

Capell, A., Steiner, H., Romig, H., Keck, S., Baader, M., Grim, M. G., . . . Haass, C. (2000). Presenilin-1 differentially facilitates endoproteolysis of the β-amyloid precursor protein and Notch. *Nature Cell Biology, 2*(4), 205-211. doi:10.1038/35008626

Capetillo-Zarate, E., Staufenbiel, M., Abramowski, D., Haass, C., Escher, A., Stadelmann, C., . . . Thal, D. R. (2006). Selective vulnerability of different types of commissural neurons for amyloid β-protein-induced neurodegeneration in APP23 mice correlates with dendritic tree morphology. *Brain, 129*(11), 2992-3005. doi:10.1093/brain/awl176

Carare, R. O., Bernardes-Silva, M., Newman, T. A., Page, A. M., Nicoll, J. A. R., Perry, V. H., & Weller, R. O. (2008). Solutes, but not cells, drain from the brain parenchyma along basement membranes of capillaries and arteries: Significance for cerebral amyloid angiopathy and neuroimmunology. *Neuropathology and Applied Neurobiology, 34*(2), 131-144. doi:10.1111/j.1365-2990.2007.00926.x

Carare, R. O., Hawkes, C. A., Jeffrey, M., Kalaria, R. N., & Weller, R. O. (2013). Review: Cerebral amyloid angiopathy, prion angiopathy, CADASIL and the spectrum of protein elimination failure angiopathies (PEFA) in neurodegenerative disease with a focus on therapy. *Neuropathology and Applied Neurobiology, 39*(6), 593-611. doi:10.1111/nan.12042

Carmona-Iragui, M., Balasa, M., Benejam, B., Alcolea, D., Fernández, S., Videla, L., . . . Fortea, J. (2017). Cerebral amyloid angiopathy in Down syndrome and sporadic and autosomal-dominant Alzheimer's disease. *Alzheimer's and Dementia, 13*(11), 1251-1260. doi:10.1016/j.jalz.2017.03.007

Carpenter, A. F., Carpenter, P. W., & Markesbery, W. R. (1993). Morphometric analysis of microglia in alzheimer's disease. *Journal of Neuropathology and Experimental Neurology, 52*(6), 601-608. doi:10.1097/00005072-199311000-00007

Carrano, A., Hoozemans, J. J. M., Van Der Vies, S. M., Van Horssen, J., De Vries, H. E., & Rozemuller, A. J. M. (2012). Neuroinflammation and blood-brain barrier changes in capillary amyloid angiopathy. *Neurodegenerative Diseases, 10*(1-4), 329-331. doi:10.1159/000334916

Casey, D. A., Antimisiaris, D., & O'Brien, J. (2010). Drugs for Alzheimer's Disease: Are They Effective? *Pharmacy and Therapeutics, 35*(4), 208-211.

Castellano, J. M., Kim, J., Stewart, F. R., Jiang, H., DeMattos, R. B., Patterson, B. W., . . . Holtzman, D. M. (2011). Human apoE isoforms differentially regulate brain amyloid-β peptide clearance. *Science Translational Medicine, 3*(89), 89ra57-89ra57. doi:10.1126/scitranslmed.3002156

Cervantes, S., Gonzàlez-Duarte, R., & Marfany, G. (2001). Homodimerization of presenilin N-terminal fragments is affected by mutations linked to Alzheimer's disease. *FEBS Letters, 505*(1), 81-86. doi:10.1016/S0014-5793(01)02785-5

Cervantes, S., Saura, C. A., Pomares, E., Gonzàlez-Duarte, R., & Marfany, G. (2004). Functional implications of the presenilin dimerization: Reconstitution of γ-secretase activity by assembly of a catalytic site at the dimer interface of two catalytically inactive presenilins. *Journal of*

Biological Chemistry, 279(35), 36519-36529. doi:10.1074/jbc.M404832200

Chalmers, K., Wilcock, G. K., & Love, S. (2003). APOE ε4 influences the pathological phenotype of Alzheimer's disease by favouring cerebrovascular over parenchymal accumulation of Aβ protein. *Neuropathology and Applied Neurobiology, 29*(3), 231-238. doi:10.1046/j.1365-2990.2003.00457.x

Chambers, S. M., Fasano, C. A., Papapetrou, E. P., Tomishima, M., Sadelain, M., & Studer, L. (2009). Highly efficient neural conversion of human ES and iPS cells by dual inhibition of SMAD signaling. *Nature biotechnology, 27*(3), 275-280. doi:10.1038/nbt.1529

Chartier-Hariln, M.-C., Parfitt, M., Legrain, S., Pérez-Tur, J., Brousseau, T., Evans, A., . . . Amouyel, P. (1994). Apolipoprotein E, ε4 allele as a major risk factor for sporadic early and late-onset forms of Alzheimer's disease: analysis of the 19q13.2 chromosomal region. *Human Molecular Genetics, 3*(4), 569-574. doi:10.1093/hmg/3.4.569

Chávez-Gutiérrez, L., Bammens, L., Benilova, I., Vandersteen, A., Benurwar, M., Borgers, M., . . . De Strooper, B. (2012). The mechanism of γ-Secretase dysfunction in familial Alzheimer disease. *The EMBO Journal, 31*(10), 2261-2274. doi:10.1038/emboj.2012.79

Cheung, K. H., Shineman, D., Müller, M., Cárdenas, C., Mei, L., Yang, J., . . . Foskett, J. K. (2008). Mechanism of Ca2+ Disruption in Alzheimer's Disease by Presenilin Regulation of InsP3 Receptor Channel Gating. *Neuron, 58*(6), 871-883. doi:10.1016/j.neuron.2008.04.015

Christensen, D. Z., Schneider-Axmann, T., Lucassen, P. J., Bayer, T. A., & Wirths, O. (2010). Accumulation of intraneuronal Aβ correlates with ApoE4 genotype. *Acta Neuropathologica, 119*(5), 555-566. doi:10.1007/s00401-010-0666-1

Cipolla, M. (2009). The Cerebral Circulation: Chapter 2, Anatomy and Ultrastructure. *San Rafael (CA): Morgan & Claypool Life Sciences*.

Citron, M., Oltersdorf, T., Haass, C., McConlogue, L., Hung, A. Y., Seubert, P., . . . Selkoe, D. J. (1992). Mutation of the β-amyloid precursor protein in familial Alzheimer's disease increases β-protein production. *Nature, 360*(6405), 672-674. doi:10.1038/360672a0

Cleveland, D. W., Hwo, S. Y., & Kirschner, M. W. (1977a). Physical and chemical properties of purified tau factor and the role of tau in microtubule assembly. *Journal of molecular biology, 116*(2), 227-247. doi:10.1016/0022-2836(77)90214-5

Cleveland, D. W., Hwo, S. Y., & Kirschner, M. W. (1977b). Purification of tau, a microtubule-associated protein that induces assembly of microtubules from purified tubulin. *Journal of molecular biology, 116*(2), 207-225. doi:10.1016/0022-2836(77)90213-3

Colle, M. A., Duyckaerts, C., Laquerrière, A., Pradier, L., Czech, C., Checler, F., & Hauw, J. J. (2000). Laminar specific loss of isocortical presenilin 1 immunoreactivity in Alzheimer's disease. Correlations with the amyloid load and the density of tau-positive neurofibrillary tangles. *Neuropathology*

and Applied Neurobiology, 26(2), 117-123. doi:10.1046/j.1365-2990.2000.026002117.x

Colton, C. A. (2009). Heterogeneity of microglial activation in the innate immune response in the brain. *Journal of Neuroimmune Pharmacology, 4*(4), 399-418. doi:10.1007/s11481-009-9164-4

Combs, C. K., Colleen Karlo, J., Kao, S. C., & Landreth, G. E. (2001). β-amyloid stimulation of microglia anti monocytes results in TNFα-dependent expression of inducible nitric oxide synthase and neuronal apoptosis. *Journal of Neuroscience, 21*(4), 1179-1188.

Conicella, A. E., & Fawzi, N. L. (2014). The C-terminal threonine of Aβ43 nucleates toxic aggregation via structural and dynamical changes in monomers and protofibrils. *Biochemistry, 53*(19), 3095-3105. doi:10.1021/bi500131a

Corder, E. H., Saunders, A. M., Strittmatter, W. J., Schmechel, D. E., Gaskell, P. C., Small, G. W., . . . Pericak-Vance, M. A. (1993). Gene dose of apolipoprotein E type 4 allele and the risk of Alzheimer's disease in late onset families. *Science, 261*(5123), 921-923. doi:10.1126/science.8346443

Coric, V., Van Dyck, C. H., Salloway, S., Andreasen, N., Brody, M., Richter, R. W., . . . Berman, R. M. (2012). Safety and tolerability of the γ-secretase inhibitor avagacestat in a phase 2 study of mild to moderate Alzheimer disease. *Archives of Neurology, 69*(11), 1430-1440. doi:10.1001/archneurol.2012.2194

Cras, P., van Harskamp, F., Hendriks, L., Ceuterick, C., van Duijn, C. M., Stefanko, S. Z., . . . van Harskamp, F. (1998). Presenile Alzheimer dementia characterized by amyloid angiopathy and large amyloid core type senile plaques in the APP 692Ala→Gly mutation. *Acta Neuropathologica, 96*(3), 253-260. doi:10.1007/s004010050892

Crook, R., Verkkoniemi, A., Perez-Tur, J., Mehta, N., Baker, M., Houlden, H., . . . Haltia, M. (1998). A variant of Alzheimer's disease with spastic paraparesis and unusual plaques due to deletion of exon 9 of presenilin 1. *Nature Medicine, 4*(4), 452-455. doi:10.1038/nm0498-452

Cugola, F. R., Fernandes, I. R., Russo, F. B., Freitas, B. C., Dias, J. L. M., Guimarães, K. P., . . . Beltrao-Braga, P. C. B. B. (2016). The Brazilian Zika virus strain causes birth defects in experimental models. *Nature, 534*(7606), 267-271. doi:10.1038/nature18296

Cupidi, C., Capobianco, R., Goffredo, D., Marcon, G., Ghetti, B., Bugiani, O., . . . Giaccone, G. (2010). Neocortical variation of Aβ load in fully expressed, pure Alzheimer's disease. *Journal of Alzheimer's Disease, 19*(1), 57-68. doi:10.3233/JAD-2010-1205

D'Andrea, M. R., Cole, G. M., & Ard, M. D. (2004). The microglial phagocytic role with specific plaque types in the Alzheimer disease brain. *Neurobiology of Aging, 25*(5), 675-683. doi:10.1016/j.neurobiolaging.2003.12.026

D'Andrea, M. R., & Nagele, R. G. (2010). Morphologically distinct types of amyloid plaques point the way to a better understanding of Alzheimer's disease pathogenesis. *Biotechnic and Histochemistry, 85*(2), 133-147. doi:10.3109/10520290903389445

D'Andrea, M. R., Reiser, P. A., Gumula, N. A., Hertzog, B. M., & Andrade-Gordon, P. (2001). Application of triple immunohistochemistry to characterize amyloid plaque-associated inflammation in brains with Alzheimer's disease. *Biotechnic and Histochemistry, 76*(2), 97-106. doi:10.1080/bih.76.2.97.106

Dá Mesquita, S., Ferreira, A. C., Sousa, J. C., Correia-Neves, M., Sousa, N., & Marques, F. (2016). Insights on the pathophysiology of Alzheimer's disease: The crosstalk between amyloid pathology, neuroinflammation and the peripheral immune system. *Neuroscience and Biobehavioral Reviews, 68*, 547-562. doi:10.1016/j.neubiorev.2016.06.014

Dal Forno, G., Carson, K. A., Brookmeyer, R., Troncoso, J., Kawas, C. H., & Brandt, J. (2002). APOE genotype and survival in men and women with Alzheimer's disease. *Neurology, 58*(7), 1045-1050. doi:10.1212/WNL.58.7.1045

Dashinimaev, E. B., Artyuhov, A. S., Bolshakov, A. P., Vorotelyak, E. A., & Vasiliev, A. V. (2017). Neurons Derived from Induced Pluripotent Stem Cells of Patients with Down Syndrome Reproduce Early Stages of Alzheimer's Disease Type Pathology in vitro. *Journal of Alzheimer's Disease, 56*(2), 835-847. doi:10.3233/JAD-160945

De Groot, C. J. A., Hulshof, S., Hoozemans, J. J. M., & Veerhuis, R. (2001). Establishment of microglial cell cultures derived from postmortem human adult brain tissue: Immunophenotypical and functional characterization. *Microscopy Research and Technique, 54*(1), 34-39. doi:10.1002/jemt.1118

De Jonghe, C., Esselens, C., Kumar-Singh, S., Craessaerts, K., Serneels, S., Checler, F., . . . De Strooper, B. (2001). Pathogenic APP mutations near the γ-secretase cleavage site differentially affect Aβ secretion and APP C-terminal fragment stability. *Human Molecular Genetics, 10*(16), 1665-1671.

De Luca, V., Orfei, M. D., Gaudenzi, S., Caltagirone, C., & Spalletta, G. (2016). Inverse effect of the APOE epsilon4 allele in late- and early-onset Alzheimer's disease. *European Archives of Psychiatry and Clinical Neuroscience, 266*(7), 599-606. doi:10.1007/s00406-015-0663-4

De Strooper, B. (2003). Aph-1, Pen-2, and Nicastrin with Presenilin generate an active γ-Secretase complex. *Neuron, 38*(1), 9-12. doi:10.1016/S0896-6273(03)00205-8

De Strooper, B., Iwatsubo, T., & Wolfe, M. S. (2012). Presenilins and γ-Secretase: Structure, Function, and Role in Alzheimer Disease. *Cold Spring Harbor Perspectives in Medicine, 2*(1), a006304. doi:10.1101/cshperspect.a006304

De Strooper, B., Saftig, P., Craessaerts, K., Vanderstichele, H., Guhde, G., Annaert, W., . . . Van Leuven, F. (1998). Deficiency of presenilin-1 inhibits the normal cleavage of amyloid precursor protein. *Nature, 391*(6665), 387-390. doi:10.1038/34910

De Strooper, B., Van Leuven, F., & Van Den Berghe, H. (1991). The amyloid β protein precursor or proteinase nexin II from mouse is closer related to its human homolog than previously reported. *BBA - Gene Structure and Expression, 1129*(1), 141-143. doi:10.1016/0167-4781(91)90231-A

Deane, R., Sagare, A., Hamm, K., Parisi, M., Lane, S., Finn, M. B., . . . Zlokovic, B. V. (2008). apoE isoform-specific disruption of amyloid β peptide clearance from mouse brain. *Journal of Clinical Investigation, 118*(12), 4002-4013. doi:10.1172/JCI36663

Deane, R., Wu, Z., Sagare, A., Davis, J., Du Yan, S., Hamm, K., . . . Zlokovic, B. V. (2004). LRP/amyloid β-peptide interaction mediates differential brain efflux of Aβ isoforms. *Neuron, 43*(3), 333-344. doi:10.1016/j.neuron.2004.07.017

Dèlaere, P., Duyckaerts, C., Brion, J. P., Poulain, V., & Hauw, J. J. (1989). Tau, paired helical filaments and amyloid in the neocortex: a morphometric study of 15 cases with graded intellectual status in aging and senile dementia of Alzheimer type. *Acta Neuropathologica, 77*(6), 645-653. doi:10.1007/BF00687893

Delaère, P., Duyckaerts, C., He, Y., Piette, F., & Hauw, J. J. (1991). Subtypes and differential laminar distributions of βA4 deposits in Alzheimer's disease: relationship with the intellectual status of 26 cases. *Acta Neuropathologica, 81*(3), 328-335. doi:10.1007/BF00305876

Delatour, B., Blanchard, V., Pradier, L., & Duyckaerts, C. (2004). Alzheimer pathology disorganizes cortico-cortical circuitry: direct evidence from a transgenic animal model. *Neurobiology of Disease, 16*(1), 41-47. doi:https://doi.org/10.1016/j.nbd.2004.01.008

Demars, M., Hu, Y. S., Gadadhar, A., & Lazarov, O. (2010). Impaired neurogenesis is an early event in the etiology of familial Alzheimer's disease in transgenic mice. *Journal of Neuroscience Research, 88*(10), 2103-2117. doi:10.1002/jnr.22387

Demars, M. P., Bartholomew, A., Strakova, Z., & Lazarov, O. (2011). Soluble amyloid precursor protein: A novel proliferation factor of adult progenitor cells of ectodermal and mesodermal origin. *Stem Cell Research and Therapy, 2*(4). doi:10.1186/scrt77

Dermaut, B., Kumar-Singh, S., De Jonghe, C., Cruts, M., Löfgren, A., Lübke, U., . . . Van Broeckhoven, C. (2001). Cerebral amyloid angiopathy is a pathogenic lesion in Alzheimer's disease due to a novel presenilin 1 mutation. *Brain, 124*(12), 2383-2392.

Deshpande, A., Mina, E., Glabe, C., & Busciglio, J. (2006). Different conformations of amyloid β induce neurotoxicity by distinct mechanisms in human cortical neurons. *Journal of Neuroscience, 26*(22), 6011-6018. doi:10.1523/JNEUROSCI.1189-06.2006

Di Fede, G., Catania, M., Morbin, M., Rossi, G., Suardi, S., Mazzoleni, G., . . . Tagliavini, F. (2009). A recessive mutation in the APP gene with dominant-negative effect on amyloidogenesis. *Science, 323*(5920), 1473-1477. doi:10.1126/science.1168979

Dickson, D. W., Ahmed, Z., Algom, A. A., Tsuboi, Y., & Josephs, K. A. (2010). Neuropathology of variants of progressive supranuclear palsy. *Current Opinion in Neurology, 23*(4), 394-400. doi:10.1097/WCO.0b013e32833be924

Dickson, D. W., Lee, S. C., Mattiace, L. A., Yen, S. C., & Brosnan, C. (1993). Microglia and cytokines in neurological disease, with special reference to

AIDS and Alzheimer's disease. *GLIA, 7*(1), 75-83. doi:10.1002/glia.440070113

Dickson, T. C., & Vickers, J. C. (2001). The morphological phenotype of β-amyloid plaques and associated neuritic changes in Alzheimer's disease. *Neuroscience, 105*(1), 99-107. doi:10.1016/S0306-4522(01)00169-5

Diem, A. K., Sharp, M. M., Gatherer, M., Bressloff, N. W., Carare, R. O., & Richardson, G. (2017). Arterial pulsations cannot drive intramural periarterial drainage: Significance for Aβ drainage. *Frontiers in Neuroscience, 11*(AUG). doi:10.3389/fnins.2017.00475

Dimitrov, M., Alattia, J. R., Lemmin, T., Lehal, R., Fligier, A., Houacine, J., . . . Fraering, P. C. (2013). Alzheimer's disease mutations in APP but not γ-secretase modulators affect epsilon-cleavage-dependent AICD production. *Nature Communications, 4*. doi:10.1038/ncomms

Dintchov Traykov, L., Mehrabian, S., Van Den Broeck, M., Radoslavova Raycheva, M., Cruts, M., Kirilova Jordanova, A., & Van Broeckhoven, C. (2009). Novel PSEN1 Mutation in a Bulgarian Patient with Very Early-Onset Alzheimer's Disease, Spastic Paraparesis, and Extrapyramidal Signs. *American Journal of Alzheimer's Disease and other Dementias, 24*(5), 404-407. doi:10.1177/1533317509341464

Doens, D., & Fernández, P. L. (2014). Microglia receptors and their implications in the response to amyloid β for Alzheimer's disease pathogenesis. *Journal of Neuroinflammation, 11*, 48-48. doi:10.1186/1742-2094-11-48

Dominguez, M. H., Ayoub, A. E., & Rakic, P. (2013). POU-III transcription factors (Brn1, Brn2, and Oct6) influence neurogenesis, molecular identity, and migratory destination of upper-layer cells of the cerebral cortex. *Cerebral Cortex, 23*(11), 2632-2643. doi:10.1093/cercor/bhs252

Dong, L. M., & Weisgraber, K. H. (1996). Human apolipoprotein E4 domain interaction. Arginine 61 and glutamic acid 255 interact to direct the preference for very low density lipoproteins. *Journal of Biological Chemistry, 271*(32), 19053-19057. doi:10.1074/jbc.271.32.19053

Doody, R. S., Raman, R., Farlow, M., Iwatsubo, T., Vellas, B., Joffe, S., . . . Mohs, R. (2013). A Phase 3 Trial of Semagacestat for Treatment of Alzheimer's Disease. *New England Journal of Medicine, 369*(4), 341-350. doi:10.1056/NEJMoa1210951

Draper, J. S., Smith, K., Gokhale, P., Moore, H. D., Maltby, E., Johnson, J., . . . Andrews, P. W. (2004). Recurrent gain of chromosomes 17q and 12 in cultured human embryonic stem cells. *Nature biotechnology, 22*(1), 53-54. doi:10.1038/nbt922

Drummond, E., & Wisniewski, T. (2017). Alzheimer's disease: experimental models and reality. *Acta Neuropathologica, 133*(2), 155-175. doi:10.1007/s00401-016-1662-x

Duan, L., Bhattacharyya, B. J., Belmadani, A., Pan, L., Miller, R. J., & Kessler, J. A. (2014). Stem cell derived basal forebrain cholinergic neurons from Alzheimer's disease patients are more susceptible to cell death. *Molecular Neurodegeneration, 9*(1), 3. doi:10.1186/1750-1326-9-3

Dulubova, I., Ho, A., Huryeva, I., Südhof, T. C., & Rizo, J. (2004). Three-Dimensional Structure of an Independently Folded Extracellular Domain

of Human Amyloid-β Precursor Protein. *Biochemistry, 43*(30), 9583-9588. doi:10.1021/bi049041o

Dumanchin, C., Tournier, I., Martin, C., Didic, M., Belliard, S., Carlander, B., . . . Campion, D. (2006). Biological effects of four PSEN1 gene mutations causing Alzheimer disease with spastic paraparesis and cotton wool plaques. *Human Mutation, 27*(10), 1063. doi:10.1002/humu.9458

Duyckaerts, C., Hauw, J.-J., Bastenaire, F., Piette, F., Poulain, C., Rainsard, V., . . . Berthaux, P. (1986). Laminar distribution of neocortical senile plaques in senile dementia of the alzheimer type. *Acta Neuropathologica, 70*(3), 249-256. doi:10.1007/bf00686079

Egan, M. F., Kost, J., Tariot, P. N., Aisen, P. S., Cummings, J. L., Vellas, B., . . . Michelson, D. (2018). Randomized Trial of Verubecestat for Mild-to-Moderate Alzheimer's Disease. *New England Journal of Medicine, 378*(18), 1691-1703. doi:10.1056/NEJMoa1706441

Egensperger, R., Kösel, S., Von Eitzen, U., & Graeber, M. B. (1998). Microglial activation in Alzheimer disease: Association with APOE genotype. *Brain Pathology, 8*(3), 439-447.

Elali, A., & Rivest, S. (2013). The role of ABCB1 and ABCA1 in beta-amyloid clearance at the neurovascular unit in Alzheimer's disease. *Frontiers in Physiology, 4 MAR*. doi:10.3389/fphys.2013.00045

Ellis, R. J., Olichney, J. M., Thal, L. J., Mirra, S. S., Morris, J. C., Beekly, D., & Heyman, A. (1996). Cerebral amyloid angiopathy in the brains of patients with Alzheimer's disease: The CERAD experience, part XV. *Neurology, 46*(6), 1592-1596. doi:10.1212/WNL.46.6.1592

Emi, M., Wu, L. L., Robertson, M. A., Myers, R. L., Hegele, R. A., Williams, R. R., . . . Lalouel, J. M. (1988). Genotyping and sequence analysis of apolipoprotein E isoforms. *Genomics, 3*(4), 373-379. doi:10.1016/0888-7543(88)90130-9

Esch, F. S., Keim, P. S., Beattie, E. C., Blacher, R. W., Culwell, A. R., Oltersdorf, T., . . . Ward, P. J. (1990). Cleavage of amyloid β peptide during constitutive processing of its precursor. *Science, 248*(4959), 1122-1124. doi:10.1126/science.2111583

Fagan, A. M., Xiong, C., Jasielec, M. S., Bateman, R. J., Goate, A. M., Benzinger, T. L. S., . . . Holtzman, D. M. (2014). Longitudinal change in CSF biomarkers in autosomal-dominant Alzheimer's disease. *Science Translational Medicine, 6*(226). doi:10.1126/scitranslmed.3007901

Fan, Q. W., Iosbe, I., Asou, H., Yanagisawa, K., & Michikawa, M. (2001). Expression and regulation of apolipoprotein E receptors in the cells of the central nervous system in culture: A review. *Journal of the American Aging Association, 24*(1), 1-10. doi:10.1007/s11357-001-0001-9

Fan, Z., Brooks, D. J., Okello, A., & Edison, P. (2017). An early and late peak in microglial activation in Alzheimer's disease trajectory. *Brain, 140*(3), 792-803. doi:10.1093/brain/aww349

Farris, W., Mansourian, S., Chang, Y., Lindsley, L., Eckman, E. A., Frosch, M. P., . . . Guénette, S. (2003). Insulin-degrading enzyme regulates the levels of insulin, amyloid β-protein, and the β-amyloid precursor protein intracellular domain in vivo. *Proceedings of the National Academy of Sciences of the*

United States of America, 100(7), 4162-4167. doi:10.1073/pnas.0230450100

Farris, W., Schütz, S. G., Cirrito, J. R., Shankar, G. M., Sun, X., George, A., . . . Selkoe, D. J. (2007). Loss of neprilysin function promotes amyloid plaque formation and causes cerebral amyloid angiopathy. *American Journal of Pathology, 171*(1), 241-251. doi:10.2353/ajpath.2007.070105

Felsky, D., Roostaei, T., Nho, K., Risacher, S. L., Bradshaw, E. M., Petyuk, V., . . . De Jager, P. L. (2019). Neuropathological correlates and genetic architecture of microglial activation in elderly human brain. *Nature Communications, 10*(1), 409-409. doi:10.1038/s41467-018-08279-3

Fernandez-Madrid, I., Levy, E., Marder, K., & Frangione, B. (1991). Codon 618 variant of alzheimer amyloid gene associated with inherited cerebral hemorrhage. *Annals of Neurology, 30*(5), 730-733. doi:10.1002/ana.410300516

Ferrer, I., Boada Rovira, M., Sánchez Guerra, M. L., Rey, M. J., & Costa-Jussá, F. (2004). Neuropathology and Pathogenesis of Encephalitis Following Amyloid-β Immunization in Alzheimer's Disease. *Brain Pathology, 14*(1), 11-20.

Ferretti, M. T., Iulita, M. F., Cavedo, E., Chiesa, P. A., Schumacher Dimech, A., Santuccione Chadha, A., . . . the Alzheimer Precision Medicine, I. (2018). Sex differences in Alzheimer disease - the gateway to precision medicine. *Nature reviews. Neurology, 14*(8), 457-469. doi:10.1038/s41582-018-0032-9

Fisher, R. S., Buchwald, N. A., Hull, C. D., & Levine, M. S. (1988). GABAergic basal forebrain neurons project to the neocortex: The localization of glutamic acid decarboxylase and choline acetyltransferase in feline corticopetal neurons. *Journal of Comparative Neurology, 272*(4), 489-502. doi:10.1002/cne.902720404

Fitz, N. F., Cronican, A. A., Saleem, M., Fauq, A. H., Chapman, R., Lefterov, I., & Koldamova, R. (2012). Abca1 deficiency affects Alzheimer's disease-like phenotype in human ApoE4 but not in ApoE3-targeted replacement mice. *The Journal of neuroscience : the official journal of the Society for Neuroscience, 32*(38), 13125-13136. doi:10.1523/JNEUROSCI.1937-12.2012

Forleo, P., Nacmias, B., Tedde, A., Latorraca, S., Piacentini, S., Marcon, C., . . . Sorbi, S. (1997). Presenilin genes analysis in italian families with early-onset alzheimer's disease. *Italian Journal of Neurological Sciences, 18*(4), 27.

Forloni, G., Demicheli, F., Giorgi, S., Bendotti, C., & Angeretti, N. (1992). Expression of amyloid precursor protein mRNAs in endothelial, neuronal and glial cells: modulation by interleukin-1. *Molecular Brain Research, 16*(1-2), 128-134. doi:10.1016/0169-328X(92)90202-M

Fu, L., Sun, Y., Guo, Y., Chen, Y., Yu, B., Zhang, H., . . . Wu, H. (2017). Comparison of neurotoxicity of different aggregated forms of Aβ40, Aβ42 and Aβ43 in cell cultures. *Journal of Peptide Science, 23*(3), 245-251. doi:10.1002/psc.2975

Fukumoto, H., Asami-Odaka, A., Suzuki, N., & Iwatsubo, T. (1996a). Association of Aβ40-positive senile plaques with microglial cells in the brains of patients with Alzheimer's disease and in non-demented aged individuals. *Neurodegeneration, 5*(1), 13-17. doi:10.1006/neur.1996.0002

Fukumoto, H., Asami-Odaka, A., Suzuki, N., Shimada, H., Ihara, Y., & Iwatsubo, T. (1996b). Amyloid beta protein deposition in normal aging has the same characteristics as that in Alzheimer's disease. Predominance of A beta 42(43) and association of A beta 40 with cored plaques. *The American Journal of Pathology, 148*(1), 259-265.

Fukuyama, R., Mizuno, T., Mizuno, T., Mori, S., Nakajima, K., Fushiki, S., & Yanagisawa, K. (2000). Age-Dependent Change in the Levels of Aβ40 and Aβ42 in Cerebrospinal Fluid from Control Subjects, and a Decrease in the Ratio of Aβ42 to Aβ40 Level in Cerebrospinal Fluid from Alzheimer's Disease Patients. *European Neurology, 43*(3), 155-160. doi:10.1159/000008156

Fullerton, S. M., Clark, A. G., Weiss, K. M., Nickerson, D. A., Taylor, S. L., Stengård, J. H., . . . Sing, C. F. (2000). Apolipoprotein E variation at the sequence haplotype level: Implications for the origin and maintenance of a major human polymorphism. *American Journal of Human Genetics, 67*(4), 881-900. doi:10.1086/303070

Gallo, M., Marcello, N., Curcio, S. A. M., Colao, R., Geracitano, S., Bernardi, L., . . . Bruni, A. C. (2011). A novel pathogenic PSEN1 mutation in a family with Alzheimer's disease: Phenotypical and neuropathological features. *Journal of Alzheimer's Disease, 25*(3), 425-431. doi:10.3233/JAD-2011-110185

Garai, K., Verghese, P. B., Baban, B., Holtzman, D. M., & Frieden, C. (2014). The binding of apolipoprotein E to oligomers and fibrils of amyloid-β alters the kinetics of amyloid aggregation. *Biochemistry, 53*(40), 6323-6331. doi:10.1021/bi5008172

Garção, P., Oliveira, C. R., & Agostinho, P. (2006). Comparative study of microglia activation induced by amyloid-beta and prion peptides: Role in neurodegeneration. *Journal of Neuroscience Research, 84*(1), 182-193. doi:10.1002/jnr.20870

Gearing, M., Mori, H., & Mirra, S. S. (1996). Aβ-peptide length aid apolipoprotein E genotype in Alzheimer's disease. *Annals of Neurology, 39*(3), 395-399. doi:10.1002/ana.410390320

Geling, A., Steiner, H., Willem, M., Bally-Cuif, L., & Haass, C. (2002). A γ-secretase inhibitor blocks Notch signaling in vivo and causes a severe neurogenic phenotype in zebrafish. *EMBO Reports, 3*(7), 688-694. doi:10.1093/embo-reports/kvf124

Gerfen, C. R., Economo, M. N., & Chandrashekar, J. (2016). Long distance projections of cortical pyramidal neurons. *Journal of Neuroscience Research*. doi:10.1002/jnr.23978

Ghosh, S., Sil, T. B., Dolai, S., & Garai, K. (2018). Apolipoprotein E interacts with amyloid-β oligomers via positively cooperative multivalent binding. *bioRxiv*, 473892. doi:10.1101/473892

Giau, V. V., Wang, M. J., Bagyinszky, E., Youn, Y. C., An, S. S. A., & Kim, S. (2018). Novel PSEN1 p.Gly417Ala mutation in a Korean patient with early-onset Alzheimer's disease with parkinsonism. *Neurobiology of Aging, 72*, 188.e113-188.e117. doi:10.1016/j.neurobiolaging.2018.08.003

Gkanatsiou, E., Portelius, E., Toomey, C. E., Blennow, K., Zetterberg, H., Lashley, T., & Brinkmalm, G. (2019). A distinct brain beta amyloid signature in cerebral amyloid angiopathy compared to Alzheimer's disease. *Neuroscience Letters, 701*, 125-131. doi:10.1016/j.neulet.2019.02.033

Goate, A., Chartier-Harlin, M. C., Mullan, M., Brown, J., Crawford, F., Fidani, L., . . . Hardy, J. (1991). Segregation of a missense mutation in the amyloid precursor protein gene with familial Alzheimer's disease. *Nature, 349*(6311), 704-706. doi:10.1038/349704a0

Godbolt, A. K., Cipolotti, L., Watt, H., Fox, N. C., Janssen, J. C., & Rossor, M. N. (2004). The natural history of alzheimer disease: A longitudinal presymptomatic and symptomatic study of a familial cohort. *Archives of Neurology, 61*(11), 1743-1748. doi:10.1001/archneur.61.11.1743

Golde, T. E., Koo, E. H., Felsenstein, K. M., Osborne, B. A., & Miele, L. (2013). γ-Secretase inhibitors and modulators. *Biochimica et biophysica acta, 1828*(12), 2898-2907. doi:10.1016/j.bbamem.2013.06.005

Gómez-Tortosa, E., Barquero, S., Barón, M., Gil-Neciga, E., Castellanos, F., Zurdo, M., . . . Jiménez-Escrig, A. (2010). Clinical-genetic correlations in familial Alzheimer's disease caused by presenilin 1 mutations. *Journal of Alzheimer's Disease, 19*(3), 873-884. doi:10.3233/JAD-2010-1292

Gonzalez, C., Armijo, E., Bravo-Alegria, J., Becerra-Calixto, A., Mays, C. E., & Soto, C. (2018). Modeling amyloid beta and tau pathology in human cerebral organoids. *Molecular Psychiatry, 23*(12), 2363-2374. doi:10.1038/s41380-018-0229-8

Gordon, B. A., Blazey, T. M., Christensen, J., Dincer, A., Flores, S., Keefe, S., . . . Benzinger, T. L. S. (2019). Tau PET in autosomal dominant Alzheimer's disease: relationship with cognition, dementia and other biomarkers. *Brain, 142*(4), 1063-1076. doi:10.1093/brain/awz019

Grabowski, T. J., Cho, H. S., Vonsattel, J. P. G., William Rebeck, G., & Greenberg, S. M. (2001). Novel amyloid precursor protein mutation in an Iowa family with dementia and severe cerebral amyloid angiopathy. *Annals of Neurology, 49*(6), 697-705. doi:10.1002/ana.1009

Gralle, M., Botelho, M. M., de Oliveira, C. L. P., Torriani, I., & Ferreira, S. T. (2002). Solution studies and structural model of the extracellular domain of the human amyloid precursor protein. *Biophysical journal, 83*(6), 3513-3524. doi:10.1016/S0006-3495(02)75351-4

Grathwohl, S. A., Kälin, R. E., Bolmont, T., Prokop, S., Winkelmann, G., Kaeser, S. A., . . . Jucker, M. (2009). Formation and maintenance of Alzheimer's disease β-amyloid plaques in the absence of microglia. *Nature neuroscience, 12*(11), 1361-1363. doi:10.1038/nn.2432

Gray, N. E., & Quinn, J. F. (2015). Alterations in mitochondrial number and function in Alzheimer's disease fibroblasts. *Metabolic Brain Disease, 30*(5), 1275-1278. doi:10.1007/s11011-015-9667-z

Gridley, T. (2007). Notch signaling in vascular development and physiology. *Development, 134*(15), 2709-2718. doi:10.1242/dev.004184

Grimm, M., Mett, J., Stahlmann, C., Haupenthal, V., Zimmer, V., & Hartmann, T. (2013). Neprilysin and Aβ Clearance: Impact of the APP Intracellular Domain in NEP Regulation and Implications in Alzheimer's Disease. *Frontiers in Aging Neuroscience, 5*(98). doi:10.3389/fnagi.2013.00098

Grimmer, T., Goldhardt, O., Yakushev, I., Ortner, M., Sorg, C., Diehl-Schmid, J., . . . Miners, S. (2019). Associations of Neprilysin Activity in CSF with Biomarkers for Alzheimer's Disease. *Neurodegenerative Diseases, 19*(1), 43-50. doi:10.1159/000500811

Groot, C., Sudre, C. H., Barkhof, F., Teunissen, C. E., Van Berckel, B. N. M., Seo, S. W., . . . Ossenkoppele, R. (2018). ARTICLE Clinical phenotype, atrophy, and small vessel disease in APOE2 carriers with Alzheimer disease. *Neurology, 91*(20), E1851-E1859. doi:10.1212/WNL.0000000000006503

Grundke-Iqbal, I., Iqbal, K., Tung, Y. C., Quinlan, M., Wisniewski, H. M., & Binder, L. I. (1986). Abnormal phosphorylation of the microtubule-associated protein tau (tau) in Alzheimer cytoskeletal pathology. *Proceedings of the National Academy of Sciences of the United States of America, 83*(13), 4913-4917. doi:10.1073/pnas.83.13.4913

Guerreiro, R., Wojtas, A., Bras, J., Carrasquillo, M., Rogaeva, E., Majounie, E., . . . Hardy, J. (2013). TREM2 variants in Alzheimer's disease. *New England Journal of Medicine, 368*(2), 117-127. doi:10.1056/NEJMoa1211851

Guillemot, F., Molnár, Z., Tarabykin, V., & Stoykova, A. (2006). Molecular mechanisms of cortical differentiation. *European Journal of Neuroscience, 23*(4), 857-868. doi:10.1111/j.1460-9568.2006.04626.x

Guven, G., Erginel-Unaltuna, N., Samanci, B., Gulec, C., Hanagasi, H., & Bilgic, B. (2019). A patient with early-onset Alzheimer's disease with a novel PSEN1 p.Leu424Pro mutation. *Neurobiology of Aging*. doi:10.1016/j.neurobiolaging.2019.05.014

Guyant-Marechal, I., Berger, E., Laquerrière, A., Rovelet-Lecrux, A., Viennet, G., Frebourg, T., . . . Hannequin, D. (2008). Intrafamilial diversity of phenotype associated with app duplication. *Neurology, 71*(23), 1925-1926. doi:10.1212/01.wnl.0000339400.64213.56

Hama, E., Shirotani, K., Masumoto, H., Sekine-Aizawa, Y., Aizawa, H., & Saido, T. C. (2001). Clearance of extracellular and cell-associated amyloid β peptide through viral expression of neprilysin in primary neurons. *Journal of Biochemistry, 130*(6), 721-726. doi:10.1093/oxfordjournals.jbchem.a003040

Hamming, I., Timens, W., Bulthuis, M. L. C., Lely, A. T., Navis, G. J., & van Goor, H. (2004). Tissue distribution of ACE2 protein, the functional receptor for SARS coronavirus. A first step in understanding SARS pathogenesis. *Journal of Pathology, 203*(2), 631-637. doi:10.1002/path.1570

Hanashima, C., Li, S. C., Shen, L., Lai, E., & Fishell, G. (2004). Foxg1 Suppresses Early Cortical Cell Fate. *Science, 303*(5654), 56-59. doi:10.1126/science.1090674

Hansen, D. V., Hanson, J. E., & Sheng, M. (2018). Microglia in Alzheimer's disease. *J Cell Biol, 217*(2), 459-472. doi:10.1083/jcb.201709069

Hansson, O., Lehmann, S., Otto, M., Zetterberg, H., & Lewczuk, P. (2019). Advantages and disadvantages of the use of the CSF Amyloid β (Aβ) 42/40 ratio in the diagnosis of Alzheimer's Disease. *Alzheimer's Research & Therapy, 11*(1), 34. doi:10.1186/s13195-019-0485-0

Hardy, J., & Allsop, D. (1991). Amyloid deposition as the central event in the aetiology of Alzheimer's disease. *Trends in Pharmacological Sciences, 12*(C), 383-388. doi:10.1016/0165-6147(91)90609-V

Hardy, J., & Higgins, G. (1992). Alzheimer's disease: the amyloid cascade hypothesis. *Science, 256*(5054), 184-185. doi:10.1126/science.1566067

Harigaya, Y., Saido, T. C., Eckman, C. B., Prada, C. M., Shoji, M., & Younkin, S. G. (2000). Amyloid β protein starting pyroglutamate at position 3 is a major component of the amyloid deposits in the Alzheimer's disease brain. *Biochemical and Biophysical Research Communications, 276*(2), 422-427. doi:10.1006/bbrc.2000.3490

Hashimoto, T., Serrano-Pozo, A., Hori, Y., Adams, K. W., Takeda, S., Banerji, A. O., . . . Hyman, B. T. (2012). Apolipoprotein e, especially apolipoprotein E4, increases the oligomerization of amyloid β peptide. *Journal of Neuroscience, 32*(43), 15181-15192. doi:10.1523/JNEUROSCI.1542-12.2012

Hayashi, S.-i., Sato, N., Yamamoto, A., Ikegame, Y., Nakashima, S., Ogihara, T., & Morishita, R. (2009). Alzheimer Disease–Associated Peptide, Amyloid β40, Inhibits Vascular Regeneration With Induction of Endothelial Autophagy. *Arteriosclerosis, Thrombosis, and Vascular Biology, 29*(11), 1909-1915. doi:doi:10.1161/ATVBAHA.109.188516

Hebert, L. E., Weuve, J., Scherr, P. A., & Evans, D. A. (2013). Alzheimer disease in the United States (2010–2050) estimated using the 2010 census. *Neurology, 80*(19), 1778-1783. doi:10.1212/WNL.0b013e31828726f5

Heilig, E. A., Xia, W., Shen, J., & Kelleher Iii, R. J. (2010). A presenilin-1 mutation identified in familial Alzheimer disease with cotton wool plaques causes a nearly complete loss of γ-secretase activity. *Journal of Biological Chemistry, 285*(29), 22350-22359. doi:10.1074/jbc.M110.116962

Hellstrom-Lindahl, E., Viitanen, M., & Marutle, A. (2009). Comparison of Aβ levels in the brain of Swedish APP(670, 671) and PS1(M146V) mutation carriers and patients with sporadic Alzheimer's disease. *Neurochemistry international, 55*(4), 243-252. doi:10.1016/j.neuint.2009.03.007

Helman, A. M., Siever, M., McCarty, K. L., Lott, I. T., Doran, E., Abner, E. L., . . . Head, E. (2019). Microbleeds and Cerebral Amyloid Angiopathy in the Brains of People with Down Syndrome with Alzheimer's Disease. *Journal of Alzheimer's Disease, 67*(1), 103-112. doi:10.3233/JAD-180589

Hendrickx, D. A. E., van Eden, C. G., Schuurman, K. G., Hamann, J., & Huitinga, I. (2017). Staining of HLA-DR, Iba1 and CD68 in human microglia reveals partially overlapping expression depending on cellular morphology and pathology. *Journal of Neuroimmunology, 309*, 12-22. doi:10.1016/j.jneuroim.2017.04.007

Herl, L., Thomas, A. V., Lill, C. M., Banks, M., Deng, A., Jones, P. B., . . . Berezovska, O. (2009). Mutations in amyloid precursor protein affect its

interactions with presenilin/γ-secretase. *Molecular and Cellular Neuroscience, 41*(2), 166-174. doi:10.1016/j.mcn.2009.02.008

Herzig, M. C., Winkler, D. T., Burgermeister, P., Pfeifer, M., Kohler, E., Schmidt, S. D., . . . Jucker, M. (2004). Aβ is targeted to the vasculature in a mouse model of hereditary cerebral hemorrhage with amyloidosis. *Nature neuroscience, 7*(9), 954-960. doi:10.1038/nn1302

Hevner, R. F., Shi, L., Justice, N., Hsueh, Y. P., Sheng, M., Smiga, S., . . . Rubenstein, J. L. R. (2001). Tbr1 regulates differentiation of the preplate and layer 6. *Neuron, 29*(2), 353-366. doi:10.1016/S0896-6273(01)00211-2

Hibaoui, Y., Grad, I., Letourneau, A., Sailani, M. R., Dahoun, S., Santoni, F. A., . . . Feki, A. (2014). Modelling and rescuing neurodevelopmental defect of Down syndrome using induced pluripotent stem cells from monozygotic twins discordant for trisomy 21. *EMBO Molecular Medicine, 6*(2), 259-277. doi:10.1002/emmm.201302848

Hickman, S. E., Allison, E. K., & El Khoury, J. (2008). Microglial dysfunction and defective β-amyloid clearance pathways in aging alzheimer's disease mice. *Journal of Neuroscience, 28*(33), 8354-8360. doi:10.1523/JNEUROSCI.0616-08.2008

Hirayama, A., Horikoshi, Y., Maeda, M., Ito, M., & Takashima, S. (2003). Characteristic developmental expression of amyloid β40, 42 and 43 in patients with Down syndrome. *Brain and Development, 25*(3), 180-185. doi:10.1016/S0387-7604(02)00209-7

Hixson, J. E., & Vernier, D. T. (1990). Restriction isotyping of human apolipoprotein E by gene amplification and cleavage with HhaI. *J Lipid Res, 31*.

Hoeijmakers, L., Meerhoff, G. F., de Vries, J. W., Ruigrok, S. R., van Dam, A. M., van Leuven, F., . . . Lucassen, P. J. (2018). The age-related slow increase in amyloid pathology in APP.V717I mice activates microglia, but does not alter hippocampal neurogenesis. *Neurobiology of Aging, 61*, 112-123. doi:10.1016/j.neurobiolaging.2017.09.013

Hof, P. R., & Morrison, J. H. (1991). Neocortical neuronal subpopulations labeled by a monoclonal antibody to calbindin exhibit differential vulnerability in Alzheimer's disease. *Experimental Neurology, 111*(3), 293-301. doi:10.1016/0014-4886(91)90096-U

Hof, P. R., Morrison, J. H., & Cox, K. (1990). Quantitative analysis of a vulnerable subset of pyramidal neurons in Alzheimer's disease: I. Superior frontal and inferior temporal cortex. *Journal of Comparative Neurology, 301*(1), 44-54. doi:10.1002/cne.903010105

Holness, C. L., & Simmons, D. L. (1993). Molecular cloning of CD68, a human macrophage marker related to lysosomal glycoproteins. *Blood, 81*(6), 1607-1613.

Holtzman, D. M. (2001). Role of apoE/Aβ interactions in the pathogenesis of Alzheimer's disease and cerebral amyloid angiopathy. *Journal of Molecular Neuroscience, 17*(2), 147-155. doi:10.1385/JMN:17:2:147

Holtzman, D. M., Herz, J., & Bu, G. (2012). Apolipoprotein E and apolipoprotein E receptors: normal biology and roles in Alzheimer disease. *Cold Spring*

Harbor Perspectives in Medicine, 2(3), a006312-a006312. doi:10.1101/cshperspect.a006312

Honda, M., Minami, I., Tooi, N., Morone, N., Nishioka, H., Uemura, K., . . . Aiba, K. (2016). The modeling of Alzheimer's disease by the overexpression of mutant Presenilin 1 in human embryonic stem cells. *Biochemical and Biophysical Research Communications, 469*(3), 587-592. doi:https://doi.org/10.1016/j.bbrc.2015.12.025

Hong, S., Beja-Glasser, V. F., Nfonoyim, B. M., Frouin, A., Li, S., Ramakrishnan, S., . . . Stevens, B. (2016). Complement and microglia mediate early synapse loss in Alzheimer mouse models. *Science, 352*(6286), 712-716. doi:10.1126/science.aad8373

Hopperton, K. E., Mohammad, D., Trépanier, M. O., Giuliano, V., & Bazinet, R. P. (2017). Markers of microglia in post-mortem brain samples from patients with Alzheimer's disease: a systematic review. *Molecular Psychiatry, 23*, 177. doi:10.1038/mp.2017.246

Houlden, H., Baker, M., McGowan, E., Lewis, P., Hutton, M., Crook, R., . . . Revesz, T. (2000). Variant Alzheimer's disease with spastic paraparesis and cotton wool plaques is caused by PS-1 mutations that lead to exceptionally high amyloid-β concentrations. *Annals of Neurology, 48*(5), 806-808. doi:10.1002/1531-8249(200011)48:5<806::AID-ANA18>3.0.CO;2-F

Hu, J., Igarashi, A., Kamata, M., & Nakagawa, H. (2001). Angiotensin-converting Enzyme Degrades Alzheimer Amyloid β-Peptide (Aβ); Retards Aβ Aggregation, Deposition, Fibril Formation; and Inhibits Cytotoxicity. *Journal of Biological Chemistry, 276*(51), 47863-47868. doi:10.1074/jbc.M104068200

Huynh, T. P. V., Davis, A. A., Ulrich, J. D., & Holtzman, D. M. (2017). Apolipoprotein E and Alzheimer's disease: The influence of apolipoprotein E on amyloid-β and other amyloidogenic proteins. *Journal of Lipid Research, 58*(5), 824-836. doi:10.1194/jlr.R075481

Hyman, B. T., Phelps, C. H., Beach, T. G., Bigio, E. H., Cairns, N. J., Carrillo, M. C., . . . Montine, T. J. (2012). National Institute on Aging–Alzheimer's Association guidelines for the neuropathologic assessment of Alzheimer's disease. *Alzheimer's & dementia : the journal of the Alzheimer's Association, 8*(1), 1-13. doi:10.1016/j.jalz.2011.10.007

Iizuka, T., Shoji, M., Harigaya, Y., Kawarabayashi, T., Watanabe, M., Kanai, M., & Hirai, S. (1995). Amyloid β-protein ending at Thr43 is a minor component of some diffuse plaques in the Alzheimer's disease brain, but is not found in cerebrovascular amyloid. *Brain Research, 702*(1-2), 275-278. doi:10.1016/0006-8993(95)01163-2

Imai, Y., Ibata, I., Ito, D., Ohsawa, K., & Kohsaka, S. (1996). A Novel Geneiba1in the Major Histocompatibility Complex Class III Region Encoding an EF Hand Protein Expressed in a Monocytic Lineage. *Biochemical and Biophysical Research Communications, 224*(3), 855-862. doi:https://doi.org/10.1006/bbrc.1996.1112

Ishii, K., Lippa, C., Tomiyama, T., Miyatake, F., Ozawa, K., Tamaoka, A., . . . Mori, H. (2001). Distinguishable effects of Presenilin-1 and APP717

mutations on amyloid plaque deposition. *Neurobiology of Aging, 22*(3), 367-376. doi:https://doi.org/10.1016/S0197-4580(01)00216-0

Israel, M. A., Yuan, S. H., Bardy, C., Reyna, S. M., Mu, Y., Herrera, C., . . . Goldstein, L. S. B. (2012). Probing sporadic and familial Alzheimer's disease using induced pluripotent stem cells. *Nature, 482*(7384), 216-220. doi:10.1038/nature10821

Itagaki, S., McGeer, P. L., Akiyama, H., Zhu, S., & Selkoe, D. (1989). Relationship of microglia and astrocytes to amyloid deposits of Alzheimer disease. *Journal of Neuroimmunology, 24*(3), 173-182. doi:10.1016/0165-5728(89)90115-X

Ito, D., Imai, Y., Ohsawa, K., Nakajima, K., Fukuuchi, Y., & Kohsaka, S. (1998). Microglia-specific localisation of a novel calcium binding protein, Iba1. *Molecular Brain Research, 57*(1), 1-9. doi:https://doi.org/10.1016/S0169-328X(98)00040-0

Iwata, N., Tsubuki, S., Takaki, Y., Watanabe, K., Sekiguchi, M., Hosoki, E., . . . Saido, T. C. (2000). Identification of the major Aβ1-42-degrading catabolic pathway in brain parenchyma: Suppression leads to biochemical and pathological deposition. *Nature Medicine, 6*(2), 143-150. doi:10.1038/72237

Iwatsubo, T., Odaka, A., Suzuki, N., Mizusawa, H., Nukina, N., & Ihara, Y. (1994). Visualization of Aβ42(43) and Aβ40 in senile plaques with end-specific Aβ monoclonals: Evidence that an initially deposited species is Aβ42(43). *Neuron, 13*(1), 45-53. doi:https://doi.org/10.1016/0896-6273(94)90458-8

Jack Jr, C. R., Knopman, D. S., Jagust, W. J., Shaw, L. M., Aisen, P. S., Weiner, M. W., . . . Trojanowski, J. Q. (2010). Hypothetical model of dynamic biomarkers of the Alzheimer's pathological cascade. *The Lancet Neurology, 9*(1), 119-128. doi:10.1016/S1474-4422(09)70299-6

Jäkel, L., Boche, D., Nicoll, J. A. R., & Verbeek, M. M. (2019). Aβ43 in human Alzheimer's disease: effects of active Aβ42 immunization. *Acta Neuropathologica Communications, 7*(1), 141. doi:10.1186/s40478-019-0791-6

Jan, A., Gokce, O., Luthi-Carter, R., & Lashuel, H. A. (2008). The ratio of monomeric to aggregated forms of Aβ40 and Aβ42 is an important determinant of amyloid-β aggregation, fibrillogenesis, and toxicity. *Journal of Biological Chemistry, 283*(42), 28176-28189. doi:10.1074/jbc.M803159200

Jana, M. K., Cappai, R., Pham, C. L. L., & Ciccotosto, G. D. (2016). Membrane-bound tetramer and trimer Aβ oligomeric species correlate with toxicity towards cultured neurons. *Journal of Neurochemistry, 136*(3), 594-608. doi:10.1111/jnc.13443

Jankowsky, J. L., & Zheng, H. (2017). Practical considerations for choosing a mouse model of Alzheimer's disease. *Molecular Neurodegeneration, 12*(1). doi:10.1186/s13024-017-0231-7

Jansen, I. E., Savage, J. E., Watanabe, K., Bryois, J., Williams, D. M., Steinberg, S., . . . Posthuma, D. (2019). Genome-wide meta-analysis identifies new loci and functional pathways influencing Alzheimer's disease risk. *Nature Genetics, 51*(3), 404-413. doi:10.1038/s41588-018-0311-9

Janssen, J. C., Hall, M., Fox, N. C., Harvey, R. J., Beck, J., Dickinson, A., . . . Rossor, M. N. (2000). Alzheimer's disease due to an intronic presenilin-1 (PSEN1 intron 4) mutation. A clinicopathological study. *Brain, 123*(5), 894-907. doi:10.1093/brain/123.5.894

Jarrett, J. T., Berger, E. P., & Lansbury, P. T., Jr. (1993). The Carboxy Terminus of the β Amyloid Protein Is Critical for the Seeding of Amyloid Formation: Implications for the Pathogenesis of Alzheimer's Disease. *Biochemistry, 32*(18), 4693-4697. doi:10.1021/bi00069a001

Jiang, Q., Lee, C. Y. D., Mandrekar, S., Wilkinson, B., Cramer, P., Zelcer, N., . . . Landreth, G. E. (2008). ApoE Promotes the Proteolytic Degradation of Aβ. *Neuron, 58*(5), 681-693. doi:10.1016/j.neuron.2008.04.010

Jones, V. C., Atkinson-Dell, R., Verkhratsky, A., & Mohamet, L. (2017). Aberrant iPSC-derived human astrocytes in Alzheimer's disease. *Cell Death and Disease, 8*(3). doi:10.1038/cddis.2017.89

Jonsson, T., Atwal, J. K., Steinberg, S., Snaedal, J., Jonsson, P. V., Bjornsson, S., . . . Stefansson, K. (2012). A mutation in APP protects against Alzheimer‘s disease and age-related cognitive decline. *Nature, 488*(7409), 96. doi:10.1038/nature11283

Jonsson, T., Stefansson, H., Steinberg, S., Jonsdottir, I., Jonsson, P. V., Snaedal, J., . . . Stefansson, K. (2013). Variant of TREM2 associated with the risk of Alzheimer's disease. *The New England journal of medicine, 368*(2), 107-116. doi:10.1056/NEJMoa1211103

Joshi, A., Ringman, J. M., Lee, A. S., Juarez, K. O., & Mendez, M. F. (2012). Comparison of clinical characteristics between familial and non-familial early onset Alzheimer's disease. *Journal of Neurology, 259*(10), 2182-2188. doi:10.1007/s00415-012-6481-y

Kadir, A., Marutle, A., Gonzalez, D., Schöll, M., Almkvist, O., Mousavi, M., . . . Nordberg, A. (2011). Positron emission tomography imaging and clinical progression in relation to molecular pathology in the first Pittsburgh Compound B positron emission tomography patient with Alzheimer's disease. *Brain, 134*(1), 301-317. doi:10.1093/brain/awq349

Kaether, C., Lammich, S., Edbauer, D., Ertl, M., Rietdorf, J., Capell, A., . . . Haass, C. (2002). Presenilin-1 affects trafficking and processing of βAPP and is targeted in a complex with nicastrin to the plasma membrane. *Journal of Cell Biology, 158*(3), 551-561. doi:10.1083/jcb.200201123

Kakuda, N., Funamoto, S., Yagishita, S., Takami, M., Osawa, S., Dohmae, N., & Ihara, Y. (2006). Equimolar production of amyloid β-protein and amyloid precursor protein intracellular domain from β-carboxyl-terminal fragment by γ-secretase. *Journal of Biological Chemistry, 281*(21), 14776-14786. doi:10.1074/jbc.M513453200

Kakuda, N., Miyasaka, T., Iwasaki, N., Nirasawa, T., Wada-Kakuda, S., Takahashi-Fujigasaki, J., . . . Ikegawa, M. (2017). Distinct deposition of amyloid-β species in brains with Alzheimer's disease pathology visualized with MALDI imaging mass spectrometry. *Acta Neuropathologica Communications, 5*(1), 73. doi:10.1186/s40478-017-0477-x

Kalimo, H., Lalowski, M., Bogdanovic, N., Philipson, O., Bird, T. D., Nochlin, D., . . . Ingelsson, M. (2013). The Arctic AβPP mutation leads to Alzheimer’s

disease pathology with highly variable topographic deposition of differentially truncated Aβ. *Acta Neuropathologica Communications, 1*(1), 60. doi:10.1186/2051-5960-1-60

Kamino, K., Orr, H. T., Payami, H., Wijsman, E. M., Alonso, M. E., Pulst, S. M., . . . White, J. A. (1992). Linkage and mutational analysis of familial Alzheimer disease kindreds for the APP gene region. *American Journal of Human Genetics, 51*(5), 998-1014.

Kanekiyo, T., Liu, C. C., Shinohara, M., Li, J., & Bu, G. (2012). Lrp1 in brain vascular smooth muscle cells mediates local clearance of Alzheimer's amyloid-β. *Journal of Neuroscience, 32*(46), 16458-16465. doi:10.1523/JNEUROSCI.3987-12.2012

Kannagi, R., Cochran, N. A., Ishigami, F., Hakomori, S., Andrews, P. W., Knowles, B. B., & Solter, D. (1983). Stage-specific embryonic antigens (SSEA-3 and -4) are epitopes of a unique globo-series ganglioside isolated from human teratocarcinoma cells. *EMBO Journal, 2*(12), 2355-2361.

Karch, C. M., Hernández, D., Wang, J.-C., Marsh, J., Hewitt, A. W., Hsu, S., . . . Goate, A. M. (2018). Human fibroblast and stem cell resource from the Dominantly Inherited Alzheimer Network. *Alzheimer's Research & Therapy, 10*(1), 69-69. doi:10.1186/s13195-018-0400-0

Karlstrom, H., Brooks, W. S., Kwok, J. B. J., Broe, G. A., Kril, J. J., McCann, H., . . . Schofield, P. R. (2008). Variable phenotype of Alzheimer's disease with spastic paraparesis. *Journal of Neurochemistry, 104*(3), 573-583. doi:10.1111/j.1471-4159.2007.05038.x

Kasuga, K., Shimohata, T., Nishimura, A., Shiga, A., Mizuguchi, T., Tokunaga, J., . . . Ikeuchi, T. (2009). Identification of independent APP locus duplication in Japanese patients with early-onset Alzheimer disease. *Journal of Neurology, Neurosurgery and Psychiatry, 80*(9), 1050-1052. doi:10.1136/jnnp.2008.161703

Keable, A., Fenna, K., Yuen, H. M., Johnston, D. A., Smyth, N. R., Smith, C., . . . Carare, R. O. (2016). Deposition of amyloid β in the walls of human leptomeningeal arteries in relation to perivascular drainage pathways in cerebral amyloid angiopathy. *Biochimica et Biophysica Acta - Molecular Basis of Disease, 1862*(5), 1037-1046. doi:10.1016/j.bbadis.2015.08.024

Kehoe, P. G., Wong, S., Al Mulhim, N., Palmer, L. E., & Miners, J. S. (2016). Angiotensin-converting enzyme 2 is reduced in Alzheimer's disease in association with increasing amyloid-β and tau pathology. *Alzheimer's Research and Therapy, 8*(1). doi:10.1186/s13195-016-0217-7

Keller, L., Welander, H., Chiang, H. H., Tjernberg, L. O., Nennesmo, I., Wallin, A. K., & Graff, C. (2010). The PSEN1 I143T mutation in a Swedish family with Alzheimer's disease: Clinical report and quantification of AB in different brain regions. *European Journal of Human Genetics, 18*(11), 1202-1208. doi:10.1038/ejhg.2010.107

Keren-Shaul, H., Spinrad, A., Weiner, A., Matcovitch-Natan, O., Dvir-Szternfeld, R., Ulland, T. K., . . . Amit, I. (2017). A Unique Microglia Type Associated with Restricting Development of Alzheimer's Disease. *Cell, 169*(7), 1276-1290.e1217. doi:10.1016/j.cell.2017.05.018

Kim, D. S., Lee, J. S., Leem, J. W., Huh, Y. J., Kim, J. Y., Kim, H. S., . . . Kim, D. W. (2010). Robust enhancement of neural differentiation from human ES and iPS cells regardless of their innate difference in differentiation propensity. *Stem Cell Reviews and Reports, 6*(2), 270-281. doi:10.1007/s12015-010-9138-1

Kim, J., Park, S., Yoo, H., Jang, H., Kim, Y., Kim, K. W., . . . Kim, H. J. (2018). The impact of APOE ϵ4 in Alzheimer's disease differs according to age. *Journal of Alzheimer's Disease, 61*(4), 1377-1385. doi:10.3233/JAD-170556

Kim, Y. J., Seo, S. W., Park, S. B., Yang, J. J., Lee, J. S., Lee, J., . . . Kim, H. J. (2017). Protective effects of APOE e2 against disease progression in subcortical vascular mild cognitive impairment patients: A three-year longitudinal study. *Scientific Reports, 7*(1). doi:10.1038/s41598-017-02046-y

Knezevic, D., Verhoeff, N. P. L., Hafizi, S., Strafella, A. P., Graff-Guerrero, A., Rajji, T., . . . Mizrahi, R. (2018). Imaging microglial activation and amyloid burden in amnestic mild cognitive impairment. *Journal of cerebral blood flow and metabolism : official journal of the International Society of Cerebral Blood Flow and Metabolism, 38*(11), 1885-1895. doi:10.1177/0271678X17741395

Knopman, D. S., Parisi, J. E., Salviati, A., Floriach-Robert, M., Boeve, B. F., Ivnik, R. J., . . . Petersen, R. C. (2003). Neuropathology of Cognitively Normal Elderly. *Journal of Neuropathology & Experimental Neurology, 62*(11), 1087-1095. doi:10.1093/jnen/62.11.1087

Koedam, E. L. G. E., Lauffer, V., Van Der Vlies, A. E., Van Der Flier, W. M., Scheltens, P., & Pijnenburg, Y. A. L. (2010). Early-versus late-onset Alzheimer's disease: More than age alone. *Journal of Alzheimer's Disease, 19*(4), 1401-1408. doi:10.3233/JAD-2010-1337

Koenigsknecht, J., & Landreth, G. (2004). Microglial phagocytosis of fibrillar β-amyloid through a β1 integrin-dependent mechanism. *Journal of Neuroscience, 24*(44), 9838-9846. doi:10.1523/JNEUROSCI.2557-04.2004

Koistinaho, M., Lin, S., Wu, X., Esterman, M., Koger, D., Hanson, J., . . . Paul, S. M. (2004). Apolipoprotein E promotes astrocyte colocalization and degradation of deposited amyloid-β peptides. *Nature Medicine, 10*(7), 719-726. doi:10.1038/nm1058

Kolb, H., Fernandez, E., & Nelson, R. (2007). *Webvision: The Organization of the Retina and Visual System*: National Library of Medicine (US).

Kollmer, M., Close, W., Funk, L., Rasmussen, J., Bsoul, A., Schierhorn, A., . . . Fändrich, M. (2019). Cryo-EM structure and polymorphism of Aβ amyloid fibrils purified from Alzheimer's brain tissue. *Nature Communications, 10*(1), 4760. doi:10.1038/s41467-019-12683-8

Kondo, T., Asai, M., Tsukita, K., Kutoku, Y., Ohsawa, Y., Sunada, Y., . . . Inoue, H. (2013). Modeling Alzheimer's disease with iPSCs reveals stress phenotypes associated with intracellular Aβ and differential drug responsiveness. *Cell Stem Cell, 12*(4), 487-496. doi:10.1016/j.stem.2013.01.009

Kongsui, R., Beynon, S. B., Johnson, S. J., & Walker, F. R. (2014). Quantitative assessment of microglial morphology and density reveals remarkable consistency in the distribution and morphology of cells within the healthy prefrontal cortex of the rat. *Journal of Neuroinflammation, 11*(1). doi:10.1186/s12974-014-0182-7

Koriath, C., Lashley, T., Taylor, W., Druyeh, R., Dimitriadis, A., Denning, N., . . . Mead, S. (2019). ApoE4 lowers age at onset in patients with frontotemporal dementia and tauopathy independent of amyloid-β copathology. *Alzheimer's and Dementia: Diagnosis, Assessment and Disease Monitoring, 11*, 277-280. doi:10.1016/j.dadm.2019.01.010

Kouri, N., Whitwell, J. L., Josephs, K. A., Rademakers, R., & Dickson, D. W. (2011). Corticobasal degeneration: A pathologically distinct 4R tauopathy. *Nature Reviews Neurology, 7*(5), 263-272. doi:10.1038/nrneurol.2011.43

Kretner, B., Trambauer, J., Fukumori, A., Mielke, J., Kuhn, P. H., Kremmer, E., . . . Steiner, H. (2016). Generation and deposition of Aβ43 by the virtually inactive presenilin-1 L435F mutant contradicts the presenilin loss-of-function hypothesis of Alzheimer's disease. *EMBO Molecular Medicine, 8*(5), 458-465. doi:10.15252/emmm.201505952

Kubo, K. I., & Nakajima, K. (2003). Cell and molecular mechanisms that control cortical layer formation in the brain. *Keio Journal of Medicine, 52*(1), 8-20. doi:10.2302/kjm.52.8

Kukar, T. L., Ladd, T. B., Bann, M. A., Fraering, P. C., Narlawar, R., Maharvi, G. M., . . . Golde, T. E. (2008). Substrate-targeting γ-secretase modulators. *Nature, 453*(7197), 925-929. doi:10.1038/nature07055

Kumar-Singh, S., Cras, P., Wang, R., Kros, J. M., Van Swieten, J., Lübke, U., . . . Van Broeckhoven, C. (2002). Dense-core senile plaques in the Flemish variant of Alzheimer's disease are vasocentric. *American Journal of Pathology, 161*(2), 507-520. doi:10.1016/S0002-9440(10)64207-1

Kumar-Singh, S., De Jonghe, C., Cruts, M., Kleinert, R., Wang, R., Mercken, M., . . . Van Broeckhoven, C. (2000). Nonfibrillar diffuse amyloid deposition due to a γ 42-secretase site mutation points to an essential role for N-truncated Aβ 42 in Alzheimer's disease. *Human Molecular Genetics, 9*(18), 2589-2598.

Kumar-Singh, S., Pirici, D., McGowan, E., Serneels, S., Ceuterick, C., Hardy, J., . . . Van Broeckhoven, C. (2005). Dense-core plaques in Tg2576 and PSAPP mouse models of Alzheimer's disease are centered on vessel walls. *American Journal of Pathology, 167*(2), 527-543. doi:10.1016/S0002-9440(10)62995-1

Kumar, N. T., Liestøl, K., Løberg, E. M., Reims, H. M., & Mæhlen, J. (2015). Apolipoprotein E allelotype is associated with neuropathological findings in Alzheimer's disease. *Virchows Archiv, 467*(2), 225-235. doi:10.1007/s00428-015-1772-1

Kutoku, Y., Ohsawa, Y., Kuwano, R., Ikeuchi, T., Inoue, H., Ataka, S., . . . Sunada, Y. (2015). A Second Pedigree with Amyloid-less Familial Alzheimer's Disease Harboring an Identical Mutation in the Amyloid Precursor Protein Gene (E693delta). *Internal Medicine, 54*(2), 205-208. doi:10.2169/internalmedicine.54.3021

Kwart, D., Gregg, A., Scheckel, C., Murphy, E., Paquet, D., Duffield, M., . . . Tessier-Lavigne, M. (2019). A Large Panel of Isogenic APP and PSEN1 Mutant Human iPSC Neurons Reveals Shared Endosomal Abnormalities Mediated by APP β-CTFs, Not Aβ. *Neuron, 104*(2), 256-270.e255. doi:10.1016/j.neuron.2019.07.010

Kyttälä, A., Moraghebi, R., Valensisi, C., Kettunen, J., Andrus, C., Pasumarthy, K. K., . . . Trokovic, R. (2016). Genetic Variability Overrides the Impact of Parental Cell Type and Determines iPSC Differentiation Potential. *Stem cell reports, 6*(2), 200-212. doi:10.1016/j.stemcr.2015.12.009

Lai, A. Y., & McLaurin, J. (2012). Clearance of amyloid-β peptides by microglia and macrophages: The issue of what, when and where. *Future Neurology, 7*(2), 165-176. doi:10.2217/fnl.12.6

Lammich, S., Kojro, E., Postina, R., Gilbert, S., Pfeiffer, R., Jasionowski, M., . . . Fahrenholz, F. (1999). Constitutive and regulated α-secretase cleavage of Alzheimer's amyloid precursor protein by a disintegrin metalloprotease. *Proceedings of the National Academy of Sciences of the United States of America, 96*(7), 3922-3927. doi:10.1073/pnas.96.7.3922

Lancaster, M. A., & Knoblich, J. A. (2014). Generation of cerebral organoids from human pluripotent stem cells. *Nature Protocols, 9*(10), 2329-2340. doi:10.1038/nprot.2014.158

Lancaster, M. A., Renner, M., Martin, C. A., Wenzel, D., Bicknell, L. S., Hurles, M. E., . . . Knoblich, J. A. (2013). Cerebral organoids model human brain development and microcephaly. *Nature, 501*(7467), 373-379. doi:10.1038/nature12517

Lanoiselée, H.-M., Nicolas, G., Wallon, D., Rovelet-Lecrux, A., Lacour, M., Rousseau, S., . . . collaborators of the, C. N. R. M. A. J. p. (2017). APP, PSEN1, and PSEN2 mutations in early-onset Alzheimer disease: A genetic screening study of familial and sporadic cases. *PLoS medicine, 14*(3), e1002270-e1002270. doi:10.1371/journal.pmed.1002270

Le, T. V., Crook, R., Hardy, J., & Dickson, D. W. (2001). Cotton wool plaques in non-familial late-onset Alzheimer disease. *Journal of Neuropathology and Experimental Neurology, 60*(11), 1051-1061. doi:10.1093/jnen/60.11.1051

Lee, C. Y. D., & Landreth, G. E. (2010). The role of microglia in amyloid clearance from the AD brain. *Journal of Neural Transmission, 117*(8), 949-960. doi:10.1007/s00702-010-0433-4

Lee, C. Y. D., Tse, W., Smith, J. D., & Landreth, G. E. (2012). Apolipoprotein E promotes β-amyloid trafficking and degradation by modulating microglial cholesterol levels. *Journal of Biological Chemistry, 287*(3), 2032-2044. doi:10.1074/jbc.M111.295451

Lee, G., Neve, R. L., & Kosik, K. S. (1989). The microtubule binding domain of tau protein. *Neuron, 2*(6), 1615-1624. doi:10.1016/0896-6273(89)90050-0

Lee, M. K., Tuttle, J. B., Rebhun, L. I., Cleveland, D. W., & Frankfurter, A. (1990). The expression and posttranslational modification of a neuron-specific β-tubulin isotype during chick embryogenesis. *Cell Motility and the Cytoskeleton, 17*(2), 118-132. doi:10.1002/cm.970170207

Leissring, M. A., Farris, W., Chang, A. Y., Walsh, D. M., Wu, X., Sun, X., . . . Selkoe, D. J. (2003). Enhanced proteolysis of β-amyloid in APP transgenic

mice prevents plaque formation, secondary pathology, and premature death. *Neuron, 40*(6), 1087-1093. doi:10.1016/S0896-6273(03)00787-6

Lemere, C. A., Lopera, F., Kosik, K. S., Lendon, C. L., Ossa, J., Saido, T. C., . . . Arango V, J. C. (1996). The E280A presenilin 1 Alzheimer mutation produces increased Aβ42 deposition and severe cerebellar pathology. *Nature Medicine, 2*(10), 1146-1150. doi:10.1038/nm1096-1146

Levy, E., Prelli, F., & Frangione, B. (2006). Studies on the first described Alzheimer's disease amyloid β mutant, the Dutch variant. *Journal of Alzheimer's Disease, 9*(SUPPL. 3), 329-339.

Leyssen, M., Ayaz, D., Hébert, S. S., Reeve, S., De Strooper, B., & Hassan, B. A. (2005). Amyloid precursor protein promotes post-developmental neurite arborization in the Drosophila brain. *EMBO Journal, 24*(16), 2944-2955. doi:10.1038/sj.emboj.7600757

Li, L., Roh, J. H., Chang, E. H., Lee, Y., Lee, S., Kim, M., . . . Song, J. (2018). iPSC modeling of presenilin1 mutation in Alzheimer's disease with cerebellar ataxia. *Experimental Neurobiology, 27*(5), 350-364. doi:10.5607/en.2018.27.5.350

Li, L., Roh, J. H., Kim, H. J., Park, H. J., Kim, M., Koh, W., . . . Song, J. (2019). The first generation of iPSC line from a Korean Alzheimer's disease patient carrying APP-V715M mutation exhibits a distinct mitochondrial dysfunction. *Experimental Neurobiology, 28*(3), 329-336. doi:10.5607/en.2019.28.3.329

Li, N., Liu, K., Qiu, Y., Ren, Z., Dai, R., Deng, Y., & Qing, H. (2016). Effect of presenilin mutations on APP cleavage; Insights into the pathogenesis of FAD. *Frontiers in Aging Neuroscience, 8*(MAR). doi:10.3389/fnagi.2016.00051

Li, S., Jin, M., Liu, L., Dang, Y., Ostaszewski, B. L., & Selkoe, D. J. (2018). Decoding the synaptic dysfunction of bioactive human AD brain soluble Aβ to inspire novel therapeutic avenues for Alzheimer's disease. *Acta Neuropathologica Communications, 6*(1), 121. doi:10.1186/s40478-018-0626-x

Li, Y. M., Xu, M., Lai, M. T., Huang, Q., Castro, J. L., DiMuzlo-Mower, J., . . . Gardell, S. J. (2000). Photoactivated γ-secretase inhibitors directed to the active site covalently label presenilin 1. *Nature, 405*(6787), 689-694. doi:10.1038/35015085

Li, Z., Del-Aguila, J. L., Dube, U., Budde, J., Martinez, R., Black, K., . . . Harari, O. (2018). Genetic variants associated with Alzheimer's disease confer different cerebral cortex cell-type population structure. *Genome Medicine, 10*(1). doi:10.1186/s13073-018-0551-4

Liao, F., Zhang, T. J., Jiang, H., Lefton, K. B., Robinson, G. O., Vassar, R., . . . Holtzman, D. M. (2015). Murine versus human apolipoprotein E4: differential facilitation of and co-localization in cerebral amyloid angiopathy and amyloid plaques in APP transgenic mouse models. *Acta Neuropathologica Communications, 3*(1), 70. doi:10.1186/s40478-015-0250-y

Liesinger, A. M., Graff-Radford, N. R., Duara, R., Carter, R. E., Hanna Al-Shaikh, F. S., Koga, S., . . . Murray, M. E. (2018). Sex and age interact to determine

clinicopathologic differences in Alzheimer's disease. *Acta Neuropathologica, 136*(6), 873-885. doi:10.1007/s00401-018-1908-x

Lill, C. M., Rengmark, A., Pihlstrøm, L., Fogh, I., Shatunov, A., Sleiman, P. M., . . . Bertram, L. (2015). The role of TREM2 R47H as a risk factor for Alzheimer's disease, frontotemporal lobar degeneration, amyotrophic lateral sclerosis, and Parkinson's disease. *Alzheimer's & dementia : the journal of the Alzheimer's Association, 11*(12), 1407-1416. doi:10.1016/j.jalz.2014.12.009

Lin, M. T., & Beal, M. F. (2006). Mitochondrial dysfunction and oxidative stress in neurodegenerative diseases. *Nature, 443*(7113), 787-795. doi:10.1038/nature05292

Lin, Y.-T., Seo, J., Gao, F., Feldman, H. M., Wen, H.-L., Penney, J., . . . Tsai, L.-H. (2018). APOE4 Causes Widespread Molecular and Cellular Alterations Associated with Alzheimer's Disease Phenotypes in Human iPSC-Derived Brain Cell Types. *Neuron, 98*(6), 1141-1154.e1147. doi:https://doi.org/10.1016/j.neuron.2018.05.008

Lippa, C. F., Swearer, J. M., Kane, K. J., Nochlin, D., Bird, T. D., Ghetti, B., . . . Drachman, D. A. (2000). Familial Alzheimer's disease: Site of mutation influences clinical phenotype. *Annals of Neurology, 48*(3), 376-379. doi:10.1002/1531-8249(200009)48:3<376::AID-ANA13>3.0.CO;2-U

Liu, G., Yao, L., Liu, J., Jiang, Y., Ma, G., Chen, Z., . . . Li, K. (2014). Cardiovascular disease contributes to Alzheimer's disease: Evidence from large-scale genome-wide association studies. *Neurobiology of Aging, 35*(4), 786-792. doi:10.1016/j.neurobiolaging.2013.10.084

Liu, Q., Waltz, S., Woodruff, G., Ouyang, J., Israel, M. A., Herrera, C., . . . Yuan, S. H. (2014). Effect of potent γ-secretase modulator in human neurons derived from multiple presenilin 1-induced pluripotent stem cell mutant carriers. *JAMA neurology, 71*(12), 1481-1489. doi:10.1001/jamaneurol.2014.2482

Liu, S., Liu, J., Miura, Y., Tanabe, C., Maeda, T., Terayama, Y., . . . Komano, H. (2014). Conversion of Aβ43 to Aβ40 by the successive action of angiotensin-converting enzyme 2 and angiotensin-converting enzyme. *Journal of Neuroscience Research, 92*(9), 1178-1186. doi:10.1002/jnr.23404

Lopez, O. L., & Claassen, D. (1991). Cerebral amyloid angiopathy in Alzheimer's disease: Clinicopathological correlations. *Dementia, 2*(6), 285-290.

Ma, T., Wang, C., Wang, L., Zhou, X., Tian, M., Zhang, Q., . . . Yang, Z. (2013). Subcortical origins of human and monkey neocortical interneurons. *Nature neuroscience, 16*(11), 1588-1597. doi:10.1038/nn.3536

Maarouf, C. L., Daugs, I. D., Spina, S., Vidal, R., Kokjohn, T. A., Patton, R. L., . . . Roher, A. E. (2008). Histopathological and molecular heterogeneity among individuals with dementia associated with Presenilin mutations. *Molecular Neurodegeneration, 3*(1), 20. doi:10.1186/1750-1326-3-20

Maat-Schieman, M. L. C., Yamaguchi, H., Van Duinen, S. G., Natté, R., & Roos, R. A. C. (2000). Age-related plaque morphology and C-terminal heterogeneity of amyloid β in Dutch-type hereditary cerebral hemorrhage

with amyloidosis. *Acta Neuropathologica, 99*(4), 409-419. doi:10.1007/s004010051143

Mahairaki, V., Ryu, J., Peters, A., Chang, Q., Li, T., Park, T. S., . . . Koliatsos, V. E. (2014). Induced pluripotent stem cells from familial alzheimer's disease patients differentiate into mature neurons with amyloidogenic properties. *Stem Cells and Development, 23*(24), 2996-3010. doi:10.1089/scd.2013.0511

Mahley, R. (1988). Apolipoprotein E: cholesterol transport protein with expanding role in cell biology. *Science, 240*(4852), 622-630. doi:10.1126/science.3283935

Mahley, R. W., Innerarity, T. L., Rall Jr, S. C., & Weisgraber, K. H. (1984). Plasma lipoproteins: Apolipoprotein structure and function. *Journal of Lipid Research, 25*(12), 1277-1294.

Mäkelä, M., Paetau, A., Polvikoski, T., Myllykangas, L., & Tanskanen, M. (2015). Capillary Amyloid-β Protein Deposition in a Population-Based Study (Vantaa 85). *Journal of Alzheimer's Disease, 49*(1), 149-157. doi:10.3233/JAD-150241

Malek-Ahmadi, M., Perez, S. E., Chen, K., & Mufson, E. J. (2016). Neuritic and Diffuse Plaque Associations with Memory in Non-Cognitively Impaired Elderly. *Journal of Alzheimer's Disease, 53*(4), 1641-1652. doi:10.3233/JAD-160365

Mallon, B. S., Hamilton, R. S., Kozhich, O. A., Johnson, K. R., Fann, Y. C., Rao, M. S., & Robey, P. G. (2014). Comparison of the molecular profiles of human embryonic and induced pluripotent stem cells of isogenic origin. *Stem Cell Research, 12*(2), 376-386. doi:10.1016/j.scr.2013.11.010

Mandrekar, S., Jiang, Q., Lee, C. Y. D., Koenigsknecht-Talboo, J., Holtzman, D. M., & Landreth, G. E. (2009). Microglia mediate the clearance of soluble aβ through fluid phase macropinocytosis. *Journal of Neuroscience, 29*(13), 4252-4262. doi:10.1523/JNEUROSCI.5572-08.2009

Mann, D. M., Iwatsubo, T., Ihara, Y., Cairns, N. J., Lantos, P. L., Bogdanovic, N., . . . Rossor, M. N. (1996). Predominant deposition of amyloid-beta 42(43) in plaques in cases of Alzheimer's disease and hereditary cerebral hemorrhage associated with mutations in the amyloid precursor protein gene. *The American Journal of Pathology, 148*(4), 1257-1266.

Mann, D. M. A., Davidson, Y. S., Robinson, A. C., Allen, N., Hashimoto, T., Richardson, A., . . . Strydom, A. (2018). Patterns and severity of vascular amyloid in Alzheimer’s disease associated with duplications and missense mutations in APP gene, Down syndrome and sporadic Alzheimer’s disease. *Acta Neuropathologica, 136*(4), 569-587. doi:10.1007/s00401-018-1866-3

Mann, D. M. A., & Iwatsubo, T. (1996). Diffuse plaques in the cerebellum and corpus striatum in Down's syndrome contain amyloid β protein (Aβ) only in the form of Aβ(42(43)). *Neurodegeneration, 5*(2), 115-120. doi:10.1006/neur.1996.0017

Mann, D. M. A., Iwatsubo, T., Fukumoto, H., Ihara, Y., Odaka, A., & Suzuki, N. (1995). Microglial cells and amyloid β protein (Aβ) deposition: association

with Aβ<inf>40</inf>-plaques. *Acta Neuropathologica, 90*(5), 472-477. doi:10.1007/BF00294808

Mann, D. M. A., Pickering-Brown, S. M., Takeuchi, A., & Iwatsubo, T. (2001). Amyloid Angiopathy and Variability in Amyloid β Deposition Is Determined by Mutation Position in Presenilin-1-Linked Alzheimer's Disease. *The American Journal of Pathology, 158*(6), 2165-2175. doi:10.1016/s0002-9440(10)64688-3

Mann, D. M. A., Pickering-Brown, S. M., Takeuchi, A., Iwatsubo, T., Arango, J., Bird, T., . . . Tabira, T. (2001a). Amyloid angiopathy and variability in amyloid β deposition is determined by mutation position in presenilin-1-linked Alzheimer's disease. *American Journal of Pathology, 158*(6), 2165-2175. doi:10.1016/S0002-9440(10)64688-3

Mann, D. M. A., Takeuchi, A., Sato, S., Cairns, N. J., Lantos, P. L., Rossor, M. N., . . . Iwatsubo, T. (2001b). Cases of Alzheimer's disease due to deletion of exon 9 of the presenilin-1 gene show an unusual but characteristic β-amyloid pathology known as 'cotton wool' plaques. *Neuropathology and Applied Neurobiology, 27*(3), 189-196. doi:10.1046/j.1365-2990.2001.00316.x

Marchani, E. E., Bird, T. D., Steinbart, E. J., Rosenthal, E., Yu, C. E., Schellenberg, G. D., & Wijsman, E. M. (2010). Evidence for three loci modifying age-at-onset of Alzheimer's disease in early-onset PSEN2 families. *American Journal of Medical Genetics, Part B: Neuropsychiatric Genetics, 153*(5), 1031-1041. doi:10.1002/ajmg.b.31072

Marín-Muñoz, J., Noguera-Perea, M. F., Gómez-Tortosa, E., López-Motos, D., Antequera-Torres, M., Martínez-Herrada, B., . . . Antúnez-Almagro, C. (2016). Novel Mutation (Gly212Val) in the PS2 Gene Associated with Early-Onset Familial Alzheimer's Disease. *Journal of Alzheimer's Disease, 53*(1), 73-78. doi:10.3233/JAD-160050

Marr, R. A., Rockenstein, E., Mukherjee, A., Kindy, M. S., Hersh, L. B., Gage, F. H., . . . Masliah, E. (2003). Neprilysin gene transfer reduces human amyloid pathology in transgenic mice. *Journal of Neuroscience, 23*(6), 1992-1996.

Martikainen, P., Pikkarainen, M., Pöntynen, K., Hiltunen, M., Lehtovirta, M., Tuisku, S., . . . Alafuzoff, I. (2010). Brain pathology in three subjects from the same pedigree with presenilin-1 (PSEN1) P264L mutation. *Neuropathology and Applied Neurobiology, 36*(1), 41-54. doi:10.1111/j.1365-2990.2009.01046.x

Martín-Maestro, P., Gargini, R., Sproul, A. A., García, E., Antón, L. C., Noggle, S., . . . García-Escudero, V. (2017). Mitophagy failure in fibroblasts and iPSC-derived neurons of alzheimer's disease-associated presenilin 1 mutation. *Frontiers in Molecular Neuroscience, 10*. doi:10.3389/fnmol.2017.00291

Martinez, B., & Peplow, P. V. (2019). Amelioration of Alzheimer's disease pathology and cognitive deficits by immunomodulatory agents in animal models of Alzheimer's disease. *Neural Regeneration Research, 14*(7), 1158-1176. doi:10.4103/1673-5374.251192

Masullo, C., Daniele, A., Seripa, D., Filippini, V., Gravina, C., Carbone, G., . . . Fazio, V. M. (1998). Apolipoprotein E genotype in sporadic early- and late-

onset Alzheimer's disease. *Dementia and Geriatric Cognitive Disorders, 9*(3), 121-125. doi:10.1159/000017034

Mathews, P. M., Cataldo, A. M., Kao, B. H., Rudnicki, A. G., Qin, X., Yang, J. L., . . . Nixon, R. A. (2000). Brain expression of presenilins in sporadic and early-onset, familial Alzheimer's disease. *Molecular medicine (Cambridge, Mass.), 6*(10), 878-891.

Matsumoto, H., Kumon, Y., Watanabe, H., Ohnishi, T., Shudou, M., Ii, C., . . . Tanaka, J. (2007). Antibodies to CD11b, CD68, and lectin label neutrophils rather than microglia in traumatic and ischemic brain lesions. *Journal of Neuroscience Research, 85*(5), 994-1009. doi:10.1002/jnr.21198

Mattiace, L. A., Davies, P., Yen, S. H., & Dickson, D. W. (1990). Microglia in cerebellar plaques in Alzheimer's disease. *Acta Neuropathologica, 80*(5), 493-498. doi:10.1007/BF00294609

McConnell, S. K. (1995). Constructing the cerebral cortex: Neurogenesis and fate determination. *Neuron, 15*(4), 761-768. doi:10.1016/0896-6273(95)90168-X

McGeer, P. L., Itagaki, S., & McGeer, E. G. (1988). Expression of the histocompatibility glycoprotein HLA-DR in neurological disease. *Acta Neuropathologica, 76*(6), 550-557. doi:10.1007/BF00689592

McGeer, P. L., Kawamata, T., Walker, D. G., Akiyama, H., Tooyama, I., & McGeer, E. G. (1993). Microglia in degenerative neurological disease. *GLIA, 7*(1), 84-92. doi:10.1002/glia.440070114

McNaughton, D., Knight, W., Guerreiro, R., Ryan, N., Lowe, J., Poulter, M., . . . Mead, S. (2012). Duplication of amyloid precursor protein (APP), but not prion protein (PRNP) gene is a significant cause of early onset dementia in a large UK series. *Neurobiology of Aging, 33*(2), 426.e413-426.e424.426E421. doi:10.1016/j.neurobiolaging.2010.10.010

Mehta, P. D., Pirttilä, T., Mehta, S. P., Sersen, E. A., Aisen, P. S., & Wisniewski, H. M. (2000). Plasma and Cerebrospinal Fluid Levels of Amyloid β Proteins 1-40 and 1-42 in Alzheimer Disease. *Archives of Neurology, 57*(1), 100-105. doi:10.1001/archneur.57.1.100

Menezes, J. R. L., & Luskin, M. B. (1994). Expression of neuron-specific tubulin defines a novel population in the proliferative layers of the developing telencephalon. *Journal of Neuroscience, 14*(9), 5399-5416.

Merlini, M., Meyer, E. P., Ulmann-Schuler, A., & Nitsch, R. M. (2011). Vascular β-amyloid and early astrocyte alterations impair cerebrovascular function and cerebral metabolism in transgenic arcAβ mice. *Acta Neuropathologica, 122*(3), 293-311. doi:10.1007/s00401-011-0834-y

Michelucci, A., Heurtaux, T., Grandbarbe, L., Morga, E., & Heuschling, P. (2009). Characterization of the microglial phenotype under specific pro-inflammatory and anti-inflammatory conditions: Effects of oligomeric and fibrillar amyloid-β. *Journal of Neuroimmunology, 210*(1-2), 3-12. doi:10.1016/j.jneuroim.2009.02.003

Michno, W., Nyström, S., Wehrli, P., Lashley, T., Brinkmalm, G., Guerard, L., . . . Hanrieder, J. (2019). Pyroglutamation of amyloid-βx-42 (Aβx-42) followed by Aβ1-40 deposition underlies plaque polymorphism in progressing

Alzheimer's disease pathology. *Journal of Biological Chemistry, 294*(17), 6719-6732. doi:10.1074/jbc.RA118.006604

Miners, J. S., Barua, N., Kehoe, P. G., Gill, S., & Love, S. (2011). Aβ-Degrading Enzymes: Potential for Treatment of Alzheimer Disease. *Journal of Neuropathology & Experimental Neurology, 70*(11), 944-959. doi:10.1097/NEN.0b013e3182345e46

Minett, T., Classey, J., Matthews, F. E., Fahrenhold, M., Taga, M., Brayne, C., . . . Mrc, C. (2016). Microglial immunophenotype in dementia with Alzheimer's pathology. *Journal of Neuroinflammation, 13*, 135. doi:10.1186/s12974-016-0601-z

Miravalle, L., Calero, M., Takao, M., Roher, A. E., Ghetti, B., & Vidal, R. (2005). Amino-terminally truncated Aβ peptide species are the main component of cotton wool plaques. *Biochemistry, 44*(32), 10810-10821. doi:10.1021/bi0508237

Mirra, S. S., Heyman, A., McKeel, D., Sumi, S. M., Crain, B. J., Brownlee, L. M., . . . Berg, L. (1991). The Consortium to Establish a Registry for Alzheimer's Disease (CERAD). *Part II. Standardization of the neuropathologic assessment of Alzheimer's disease, 41*(4), 479-479. doi:10.1212/wnl.41.4.479

Montine, T. J., Phelps, C. H., Beach, T. G., Bigio, E. H., Cairns, N. J., Dickson, D. W., . . . Hyman, B. T. (2012). National institute on aging-Alzheimer's association guidelines for the neuropathologic assessment of Alzheimer's disease: A practical approach. *Acta Neuropathologica, 123*(1), 1-11. doi:10.1007/s00401-011-0910-3

Moore, S., Evans, Lewis D., Andersson, T., Portelius, E., Smith, J., Dias, Tatyana B., . . . Livesey, Frederick J. (2015). APP Metabolism Regulates Tau Proteostasis in Human Cerebral Cortex Neurons. *Cell Reports, 11*(5), 689-696. doi:10.1016/j.celrep.2015.03.068

Moreau, P. H., Bott, J. B., Zerbinatti, C., Renger, J. J., Kelche, C., Cassel, J. C., & Mathis, C. (2013). ApoE4 confers better spatial memory than apoE3 in young adult hAPP-Yac/apoE-TR mice. *Behavioural Brain Research, 243*(1), 1-5. doi:10.1016/j.bbr.2012.12.043

Morelli, L., Castaño, E. M., & Prat, M. I. (1999). Differential accumulation of soluble amyloid β peptides 1-40 and 1-42 in human monocytic and neuroblastoma cell lines. Implications for cerebral amyloidogenesis. *Cell and Tissue Research, 298*(2), 225-232. doi:10.1007/s004419900109

Morris, C. S., & Esiri, M. M. (1998). The expression of cytokines and their receptors in normal and mildly reactive human brain. *Journal of Neuroimmunology, 92*(1-2), 85-97. doi:10.1016/S0165-5728(98)00181-7

Morrow, J. A., Segall, M. L., Lund-Katz, S., Phillips, M. C., Knapp, M., Rupp, B., & Weisgraber, K. H. (2000). Differences in stability among the human apolipoprotein E isoforms determined by the amino-terminal domain. *Biochemistry, 39*(38), 11657-11666. doi:10.1021/bi000099m

Mosconi, L., Sorbi, S., De Leon, M. J., Li, Y., Nacmias, B., Myoung, P. S., . . . Pupi, A. (2006). Hypometabolism exceeds atrophy in presymptomatic early-onset familial Alzheimer's disease. *Journal of Nuclear Medicine, 47*(11), 1778-1786.

Mou, X., Wu, Y., Cao, H., Meng, Q., Wang, Q., Sun, C., . . . Zhang, H. (2012). Generation of disease-specific induced pluripotent stem cells from patients with different karyotypes of Down syndrome. *Stem cell research & therapy, 3*(2). doi:10.1186/scrt105

Mouchard, A., Boutonnet, M.-C., Mazzocco, C., Biendon, N., Macrez, N., & Neuro, C. E. B. N. N. (2019). ApoE-fragment/Aβ heteromers in the brain of patients with Alzheimer's disease. *Scientific Reports, 9*(1), 3989. doi:10.1038/s41598-019-40438-4

Mucke, L., Masliah, E., Johnson, W. B., Ruppe, M. D., Alford, M., Rockenstein, E. M., . . . Abraham, C. R. (1994). Synaptotrophic effects of human amyloid β protein precursors in the cortex of transgenic mice. *Brain Research, 666*(2), 151-167. doi:https://doi.org/10.1016/0006-8993(94)90767-6

Muratore, C. R., Rice, H. C., Srikanth, P., Callahan, D. G., Shin, T., Benjamin, L. N. P., . . . Young-Pearse, T. L. (2014). The familial alzheimer's disease APPV717I mutation alters APP processing and Tau expression in iPSC-derived neurons. *Human Molecular Genetics, 23*(13), 3523-3536. doi:10.1093/hmg/ddu064

Murayama, O., Tomita, T., Nihonmatsu, N., Murayama, M., Sun, X., Honda, T., . . . Takashima, A. (1999). Enhancement of amyloid β 42 secretion by 28 different presenilin 1 mutations of familial Alzheimer's disease. *Neuroscience Letters, 265*(1), 61-63. doi:10.1016/S0304-3940(99)00187-1

Nagayach, A., Patro, N., & Patro, I. (2016). Microglia in the Physiology and Pathology of Brain. *Proceedings of the National Academy of Sciences India Section B - Biological Sciences, 86*(4), 781-794. doi:10.1007/s40011-015-0585-y

Nagele, R. G., D'Andrea, M. R., Lee, H., Venkataraman, V., & Wang, H. Y. (2003). Astrocytes accumulate Aβ42 and give rise to astrocytic amyloid plaques in Alzheimer disease brains. *Brain Research, 971*(2), 197-209. doi:10.1016/S0006-8993(03)02361-8

Nagele, R. G., Wegiel, J., Venkataraman, V., Imaki, H., Wang, K. C., & Wegiel, J. (2004). Contribution of glial cells to the development of amyloid plaques in Alzheimer's disease. *Neurobiology of Aging, 25*(5), 663-674. doi:10.1016/j.neurobiolaging.2004.01.007

Nagy, Z., Yilmazer-Hanke, D. M., Braak, H., Braak, E., Schultz, C., & Hanke, J. (1998). Assessment of the Pathological Stages of Alzheimer's Disease in Thin Paraffin Sections: A Comparative Study. *Dementia and Geriatric Cognitive Disorders, 9*(3), 140-144.

Nakajima, M., Ogawa, M., Shimoda, Y., Hiraoka, S., Iida, M., Koseki, H., . . . Furukawa, K. (2006). Presenilin-1 controls the growth and differentiation of endothelial progenitor cells through its β-catenin-binding region. *Cell Biology International, 30*(3), 239-243. doi:10.1016/j.cellbi.2005.11.003

Nakamura, S. i., Tamaoka, A., Sawamura, N., Shoji, S. i., Nakayama, H., Ono, F., . . . Doi, K. (1995). Carboxyl end-specific monoclonal antibodies to amyloid β protein (Aβ) subtypes (Aβ40 and Aβ42(43)) differentiate Aβ in senile plaques and amyloid angiopathy in brains of aged cynomolgus monkeys. *Neuroscience Letters, 201*(2), 151-154. doi:https://doi.org/10.1016/0304-3940(95)12160-9

Nakaya, Y., Yamane, T., Shiraishi, H., Wang, H. Q., Matsubara, E., Sato, T., . . . Nishimura, M. (2005). Random mutagenesis of presenilin-1 identifies novel mutants exclusively generating long amyloid β-peptides. *Journal of Biological Chemistry, 280*(19), 19070-19077. doi:10.1074/jbc.M501130200

Nelson, O., Supnet, C., Liu, H., & Bezprozvanny, I. (2010). Familial Alzheimer's disease mutations in presenilins: Effects on endoplasmic reticulum calcium homeostasis and correlation with clinical phenotypes. *Journal of Alzheimer's Disease, 21*(3), 781-793. doi:10.3233/JAD-2010-100159

Nelson, P. T., Pious, N. M., Jicha, G. A., Wilcock, D. M., Fardo, D. W., Estus, S., & William Rebeck, G. (2013). APOE-ε2 and APOE ε4 correlate with increased amyloid accumulation in cerebral vasculature. *Journal of Neuropathology and Experimental Neurology, 72*(7), 708-715. doi:10.1097/NEN.0b013e31829a25b9

Nhan, H. S., Chiang, K., & Koo, E. H. (2015). The multifaceted nature of amyloid precursor protein and its proteolytic fragments: friends and foes. *Acta Neuropathologica, 129*(1), 1-19. doi:10.1007/s00401-014-1347-2

Nichols, J., Zevnik, B., Anastassiadis, K., Niwa, H., Klewe-Nebenius, D., Chambers, I., . . . Smith, A. (1998). Formation of pluripotent stem cells in the mammalian embryo depends on the POU transcription factor Oct4. *Cell, 95*(3), 379-391. doi:10.1016/S0092-8674(00)81769-9

Nicoll, J. A. R., Barton, E., Boche, D., Neal, J. W., Ferrer, I., Thompson, P., . . . Holmes, C. (2006). Aβ species removal after Aβ42 immunization. *Journal of Neuropathology and Experimental Neurology, 65*(11), 1040-1048. doi:10.1097/01.jnen.0000240466.10758.ce

Nicolll, J. A. R., Wilkinson, D., Holmes, C., Steart, P., Markham, H., & Weller, R. O. (2003). Neuropathology of human Alzheimer disease after immunization with amyloid-β peptide: A case report. *Nature Medicine, 9*(4), 448-452. doi:10.1038/nm840

Nilsberth, C., Westlind-Danielsson, A., Eckman, C. B., Condron, M. M., Axelman, K., Forsell, C., . . . Lannfelt, L. (2001). The 'Arctic' APP mutation (E693G) causes Alzheimer's disease by enhanced Aβ protofibril formation. *Nature neuroscience, 4*(9), 887-893. doi:10.1038/nn0901-887

Nimmerjahn, A., Kirchhoff, F., & Helmchen, F. (2005). Resting Microglial Cells Are Highly Dynamic Surveillants of Brain Parenchyma in Vivo. *Science, 308*(5726), 1314-1318. doi:10.1126/science.1110647

Niwa, A., Matsuo, K., Shindo, A., Yata, K., Shiraishi, T., & Tomimoto, H. (2013). Clinical and neuropathological findings in a patient with familial Alzheimer disease showing a mutation in the PSEN1 gene. *Neuropathology, 33*(2), 199-203. doi:doi:10.1111/j.1440-1789.2012.01340.x

Noctor, S. C., Martinez-Cerdeño, V., Ivic, L., & Kriegstein, A. R. (2004). Cortical neurons arise in symmetric and asymmetric division zones and migrate through specific phases. *Nature neuroscience, 7*(2), 136-144. doi:10.1038/nn1172

Norton, J. B., Cairns, N. J., Chakraverty, S., Wang, J., Levitch, D., Galvin, J. E., & Goate, A. (2009). Presenilin1 G217R mutation linked to Alzheimer

disease with cotton wool plaques. *Neurology, 73*(6), 480-482. doi:10.1212/WNL.0b013e3181b163ba

O'Riordan, S., McMonagle, P., Janssen, J. C., Fox, N. C., Farrell, M., Collinge, J., . . . Hutchinson, M. (2002). Presenilin-1 mutation (E280G), spastic paraparesis, and cranial MRI white-matter abnormalities. *Neurology, 59*(7), 1108-1110. doi:10.1212/WNL.59.7.1108

Oakley, H., Cole, S. L., Logan, S., Maus, E., Shao, P., Craft, J., . . . Vassar, R. (2006). Intraneuronal β-amyloid aggregates, neurodegeneration, and neuron loss in transgenic mice with five familial Alzheimer's disease mutations: Potential factors in amyloid plaque formation. *Journal of Neuroscience, 26*(40), 10129-10140. doi:10.1523/JNEUROSCI.1202-06.2006

Obici, L., Demarchi, A., de Rosa, G., Bellotti, V., Marciano, S., Donadei, S., . . . Merlini, G. (2005). A novel AβPP mutation exclusively associated with cerebral amyloid angiopathy. *Annals of Neurology, 58*(4), 639-644. doi:10.1002/ana.20571

Ochalek, A., Mihalik, B., Avci, H. X., Chandrasekaran, A., Téglási, A., Bock, I., . . . Dinnyés, A. (2017). Neurons derived from sporadic Alzheimer's disease iPSCs reveal elevated TAU hyperphosphorylation, increased amyloid levels, and GSK3B activation. *Alzheimer's Research and Therapy, 9*(1). doi:10.1186/s13195-017-0317-z

Ohsawa, K., Imai, Y., Kanazawa, H., Sasaki, Y., & Kohsaka, S. (2000). Involvement of Iba1 in membrane ruffling and phagocytosis of macrophages/microglia. *Journal of Cell Science, 113*(17), 3073-3084.

Oksanen, M., Hyötyläinen, I., Voutilainen, J., Puttonen, K. A., Hämäläinen, R. H., Graff, C., . . . Koistinaho, J. (2018). Generation of a human induced pluripotent stem cell line (LL008 1.4) from a familial Alzheimer's disease patient carrying a double KM670/671NL (Swedish) mutation in APP gene. *Stem Cell Research, 31*, 181-185. doi:https://doi.org/10.1016/j.scr.2018.07.024

Oksanen, M., Petersen, A. J., Naumenko, N., Puttonen, K., Lehtonen, Š., Gubert Olivé, M., . . . Koistinaho, J. (2017). PSEN1 Mutant iPSC-Derived Model Reveals Severe Astrocyte Pathology in Alzheimer's Disease. *Stem cell reports, 9*(6), 1885-1897. doi:10.1016/j.stemcr.2017.10.016

Olah, M., Patrick, E., Villani, A.-C., Xu, J., White, C. C., Ryan, K. J., . . . Bradshaw, E. M. (2018). A transcriptomic atlas of aged human microglia. *Nature Communications, 9*(1), 539. doi:10.1038/s41467-018-02926-5

Ossenkoppele, R., Schonhaut, D. R., Schöll, M., Lockhart, S. N., Ayakta, N., Baker, S. L., . . . Rabinovici, G. D. (2016). Tau PET patterns mirror clinical and neuroanatomical variability in Alzheimer's disease. *Brain, 139*(5), 1551-1567. doi:10.1093/brain/aww027

Ostrowitzki, S., Deptula, D., Thurfjell, L., Barkhof, F., Bohrmann, B., Brooks, D. J., . . . Santarelli, L. (2012). Mechanism of amyloid removal in patients with Alzheimer disease treated with gantenerumab. *Archives of Neurology, 69*(2), 198-207. doi:10.1001/archneurol.2011.1538

Ovchinnikov, D. A., Korn, O., Virshup, I., Wells, C. A., & Wolvetang, E. J. (2018). The Impact of APP on Alzheimer-like Pathogenesis and Gene Expression

in Down Syndrome iPSC-Derived Neurons. *Stem cell reports, 11*(1), 32-42. doi:10.1016/j.stemcr.2018.05.004

Pan, G. J., Chang, Z. Y. I., Schöler, H. R., & Pei, D. (2002). Stem cell pluripotency and transcription factor Oct4. *Cell Research, 12*(5-6), 321-329. doi:10.1038/sj.cr.7290134

Parbo, P., Ismail, R., Hansen, K. V., Amidi, A., Mårup, F. H., Gottrup, H., . . . Brooks, D. J. (2017). Brain inflammation accompanies amyloid in the majority of mild cognitive impairment cases due to Alzheimer's disease. *Brain, 140*(7), 2002-2011. doi:10.1093/brain/awx120

Paresce, D. M., Chung, H., & Maxfield, F. R. (1997). Slow degradation of aggregates of the Alzheimer's disease amyloid β- protein by microglial cells. *Journal of Biological Chemistry, 272*(46), 29390-29397. doi:10.1074/jbc.272.46.29390

Paresce, D. M., Ghosh, R. N., & Maxfield, F. R. (1996). Microglial cells internalize aggregates of the Alzheimer's disease amyloid β-protein via a scavenger receptor. *Neuron, 17*(3), 553-565. doi:10.1016/S0896-6273(00)80187-7

Parker, J., Mozaffar, T., Messmore, A., Deignan, J. L., Kimonis, V. E., & Ringman, J. M. (2019). Homozygosity for the A431E mutation in PSEN1 presenting with a relatively aggressive phenotype. *Neuroscience Letters, 699*, 195-198. doi:10.1016/j.neulet.2019.01.047

Pașca, S. P. (2018). The rise of three-dimensional human brain cultures. *Nature, 553*, 437. doi:10.1038/nature25032

Pastor, P., Roe, C. M., Villegas, A., Bedoya, G., Chakraverty, S., García, G., . . . Goate, A. M. (2003). Apolipoprotein Eε4 modifies Alzheimer's disease onset in an E280A PS1 kindred. *Annals of Neurology, 54*(2), 163-169. doi:10.1002/ana.10636

Pearson, R. C., Esiri, M. M., Hiorns, R. W., Wilcock, G. K., & Powell, T. P. (1985). Anatomical correlates of the distribution of the pathological changes in the neocortex in Alzheimer disease. *Proceedings of the National Academy of Sciences of the United States of America, 82*(13), 4531-4534.

Penney, J., Ralvenius, W. T., & Tsai, L.-H. (2019). Modeling Alzheimer's disease with iPSC-derived brain cells. *Molecular Psychiatry*. doi:10.1038/s41380-019-0468-3

Peuralinna, T., Tanskanen, M., Mäkelä, M., Polvikoski, T., Paetau, A., Kalimo, H., . . . Myllykangas, L. (2011). APOE and AβPP gene variation in cortical and cerebrovascular amyloid-β pathology and alzheimer's disease: A population-based analysis. *Journal of Alzheimer's Disease, 26*(2), 377-385. doi:10.3233/JAD-2011-102049

Pfeifer, L. A., White, L. R., Ross, G. W., Petrovitch, H., & Launer, L. J. (2002). Cerebral amyloid angiopathy and cognitive function. *The HAAS autopsy study, 58*(11), 1629-1634. doi:10.1212/wnl.58.11.1629

Piras, A., Collin, L., Grüninger, F., Graff, C., & Rönnbäck, A. (2016). Autophagic and lysosomal defects in human tauopathies: analysis of post-mortem brain from patients with familial Alzheimer disease, corticobasal degeneration and progressive supranuclear palsy. *Acta Neuropathologica Communications, 4*, 22. doi:10.1186/s40478-016-0292-9

Poirier, J., Bertrand, P., Poirier, J., Kogan, S., Gauthier, S., Poirier, J., . . . Davignon, J. (1993). Apolipoprotein E polymorphism and Alzheimer's disease. *The Lancet, 342*(8873), 697-699. doi:https://doi.org/10.1016/0140-6736(93)91705-Q

Polo, J. M., Liu, S., Figueroa, M. E., Kulalert, W., Eminli, S., Tan, K. Y., . . . Hochedlinger, K. (2010). Cell type of origin influences the molecular and functional properties of mouse induced pluripotent stem cells. *Nature biotechnology, 28*(8), 848-855. doi:10.1038/nbt.1667

Portelius, E., Lashley, T., Westerlund, A., Persson, R., Fox, N. C., Blennow, K., . . . Zetterberg, H. (2015). Brain amyloid-beta fragment signatures in pathological ageing and Alzheimer's disease by hybrid immunoprecipitation mass spectrometry. *Neurodegener Dis, 15*(1), 50-57. doi:10.1159/000369465

Portelius, E., Westman-Brinkmalm, A., Zetterberg, H., & Blennow, K. (2006). Determination of β-amyloid peptide signatures in cerebrospinal fluid using immunoprecipitation-mass spectrometry. *Journal of Proteome Research, 5*(4), 1010-1016. doi:10.1021/pr050475v

Prasher, V. P., Sajith, S. G., Rees, S. D., Patel, A., Tewari, S., Schupf, N., & Zigman, W. B. (2008). Significant effect of APOE epsilon 4 genotype on the risk of dementia in Alzheimer's disease and mortality in persons with Down syndrome. *International Journal of Geriatric Psychiatry, 23*(11), 1134-1140. doi:10.1002/gps.2039

Preston, S. D., Steart, P. V., Wilkinson, A., Nicoll, J. A. R., & Weller, R. O. (2003). Capillary and arterial cerebral amyloid angiopathy in Alzheimer's disease: Defining the perivascular route for the elimination of amyloid β from the human brain. *Neuropathology and Applied Neurobiology, 29*(2), 106-117. doi:10.1046/j.1365-2990.2003.00424.x

Priller, C., Bauer, T., Mitteregger, G., Krebs, B., Kretzschmar, H. A., & Herms, J. (2006). Synapse formation and function is modulated by the amyloid precursor protein. *The Journal of neuroscience : the official journal of the Society for Neuroscience, 26*(27), 7212-7221. doi:10.1523/JNEUROSCI.1450-06.2006

Prince, J. A., Feuk, L., Gu, H. F., Johansson, B., Gatz, M., Blennow, K., & Brookes, A. J. (2003). Genetic Variation in a Haplotype Block Spanning IDE Influences Alzheimer Disease. *Human Mutation, 22*(5), 363-371. doi:10.1002/humu.10282

Prince, M., Bryce, R., Albanese, E., Wimo, A., Ribeiro, W., & Ferri, C. P. (2013). The global prevalence of dementia: A systematic review and metaanalysis. *Alzheimer's & Dementia, 9*(1), 63-75.e62. doi:http://dx.doi.org/10.1016/j.jalz.2012.11.007

Pulford, K. A., Rigney, E. M., Micklem, K. J., Jones, M., Stross, W. P., Gatter, K. C., & Mason, D. Y. (1989). KP1: a new monoclonal antibody that detects a monocyte/macrophage associated antigen in routinely processed tissue sections. *Journal of clinical pathology, 42*(4), 414-421. doi:10.1136/jcp.42.4.414

Qi-Takahara, Y., Morishima-Kawashima, M., Tanimura, Y., Dolios, G., Hirotani, N., Horikoshi, Y., . . . Ihara, Y. (2005). Longer forms of amyloid β protein: Implications for the mechanism of intramembrane cleavage by γ-

secretase. *Journal of Neuroscience, 25*(2), 436-445. doi:10.1523/JNEUROSCI.1575-04.2005

Qi, Y., Zhang, X.-J., Renier, N., Wu, Z., Atkin, T., Sun, Z., . . . Studer, L. (2017). Combined small-molecule inhibition accelerates the derivation of functional cortical neurons from human pluripotent stem cells. *Nature biotechnology, 35*(2), 154-163. doi:10.1038/nbt.3777

Qiu, W. Q., Walsh, D. M., Ye, Z., Vekrellis, K., Zhang, J., Podlisny, M. B., . . . Selkoe, D. J. (1998). Insulin-degrading enzyme regulates extracellular levels of amyloid β- protein by degradation. *Journal of Biological Chemistry, 273*(49), 32730-32738. doi:10.1074/jbc.273.49.32730

Quintero-Monzon, O., Martin, M. M., Fernandez, M. A., Cappello, C. A., Krzysiak, A. J., Osenkowski, P., & Wolfe, M. S. (2011). Dissociation between the processivity and total activity of γ-secretase: Implications for the mechanism of Alzheimer's disease-causing presenilin mutations. *Biochemistry, 50*(42), 9023-9035. doi:10.1021/bi2007146

Quiroz, Y. T., Schultz, A. P., Chen, K., Protas, H. D., Brickhouse, M., Fleisher, A. S., . . . Reiman, E. M. (2015). Brain imaging and blood biomarker abnormalities in children with autosomal dominant Alzheimer disease a cross-sectional study. *JAMA neurology, 72*(8), 912-919. doi:10.1001/jamaneurol.2015.1099

Raffaï, R. L., Dong, L.-M., Farese, R. V., & Weisgraber, K. H. (2001). Introduction of human apolipoprotein E4 “domain interaction” into mouse apolipoprotein E. *Proceedings of the National Academy of Sciences, 98*(20), 11587. doi:10.1073/pnas.201279298

Raja, W. K., Mungenast, A. E., Lin, Y. T., Ko, T., Abdurrob, F., Seo, J., & Tsai, L. H. (2016). Self-organizing 3D human neural tissue derived from induced pluripotent stem cells recapitulate Alzheimer's disease phenotypes. *PLoS ONE, 11*(9). doi:10.1371/journal.pone.0161969

Rall Jr, S. C., Weisgraber, K. H., & Mahley, R. W. (1982). Human apolipoprotein E. The complete amino acid sequence. *Journal of Biological Chemistry, 257*(8), 4171-4178.

Raman, A., Lin, X., Suri, M., Hewitt, M., Constantinescu, C. S., & Phillips, M. F. (2007). A presenilin 1 mutation (Arg278Ser) associated with early onset Alzheimer's disease and spastic paraparesis. *Journal of the Neurological Sciences, 260*(1-2), 78-82. doi:10.1016/j.jns.2007.04.013

Rannikmäe, K., Kalaria, R. N., Greenberg, S. M., Chui, H. C., Schmitt, F. A., Samarasekera, N., . . . Sudlow, C. L. M. (2014). APOE associations with severe CAA-associated vasculopathic changes: Collaborative meta-analysis. *Journal of Neurology, Neurosurgery and Psychiatry, 85*(3), 300-305. doi:10.1136/jnnp-2013-306485

Rannikmäe, K., Samarasekera, N., Martînez-Gonzâlez, N. A., Salman, R. A. S., & Sudlow, C. L. M. (2013). Genetics of cerebral amyloid angiopathy: Systematic review and meta-analysis. *Journal of Neurology, Neurosurgery and Psychiatry, 84*(8), 901-908. doi:10.1136/jnnp-2012-303898

Rasmussen, J., Mahler, J., Beschorner, N., Kaeser, S. A., Häsler, L. M., Baumann, F., . . . Jucker, M. (2017). Amyloid polymorphisms constitute distinct clouds of conformational variants in different etiological subtypes

of Alzheimer's disease. *Proceedings of the National Academy of Sciences of the United States of America, 114*(49), 13018-13023. doi:10.1073/pnas.1713215114

Rasmussen, M. K., Mestre, H., & Nedergaard, M. (2018). The glymphatic pathway in neurological disorders. *The Lancet Neurology, 17*(11), 1016-1024. doi:10.1016/S1474-4422(18)30318-1

Reiman, E. M., Quiroz, Y. T., Fleisher, A. S., Chen, K., Velez-Pardo, C., Jimenez-Del-Rio, M., . . . Lopera, F. (2012). Brain imaging and fluid biomarker analysis in young adults at genetic risk for autosomal dominant Alzheimer's disease in the presenilin 1 E280A kindred: A case-control study. *The Lancet Neurology, 11*(12), 1048-1056. doi:10.1016/S1474-4422(12)70228-4

Revesz, T., Ghiso, J., Lashley, T., Plant, G., Rostagno, A., Frangione, B., & Holton, J. L. (2003). Cerebral amyloid angiopathies: A pathologic, biochemical, and genetic view. *Journal of Neuropathology and Experimental Neurology, 62*(9), 885-898. doi:10.1093/jnen/62.9.885

Rezaie, P., & Male, D. (2002). Differentiation, ramification and distribution of microglia within the central nervous system examined. *Neuroembryology, 1*(1), 29-43. doi:10.1159/000051020

Richard, E., Carrano, A., Hoozemans, J. J., Van Horssen, J., Van Haastert, E. S., Eurelings, L. S., . . . Rozemuller, A. J. M. (2010). Characteristics of dyshoric capillary cerebral amyloid angiopathy. *Journal of Neuropathology and Experimental Neurology, 69*(11), 1158-1167. doi:10.1097/NEN.0b013e3181fab558

Ries, M., & Sastre, M. (2016). Mechanisms of Aβ Clearance and Degradation by Glial Cells. *Frontiers in Aging Neuroscience, 8*(160). doi:10.3389/fnagi.2016.00160

Ringman, J. M., Monsell, S., Ng, D. W., Zhou, Y., Nguyen, A., Coppola, G., . . . Vinters, H. V. (2016). Neuropathology of autosomal dominant Alzheimer disease in the national Alzheimer coordinating center database. *Journal of Neuropathology and Experimental Neurology, 75*(3), 284-290. doi:10.1093/jnen/nlv028

Rizzu, P., Van Swieten, J. C., Joosse, M., Hasegawa, M., Stevens, M., Tibben, A., . . . Heutink, P. (1999). High prevalence of mutations in the microtubule-associated protein tau in a population study of frontotemporal dementia in the Netherlands. *American Journal of Human Genetics, 64*(2), 414-421. doi:10.1086/302256

Robbins, E. M., Betensky, R. A., Domnitz, S. B., Purcell, S. M., Garcia-Alloza, M., Greenberg, C., . . . Bacskai, B. J. (2006). Kinetics of cerebral amyloid angiopathy progression in a transgenic mouse model of Alzheimer disease. *Journal of Neuroscience, 26*(2), 365-371. doi:10.1523/JNEUROSCI.3854-05.2006

Rodriguez, G. A., Tai, L. M., LaDu, M. J., & Rebeck, G. W. (2014). Human APOE4 increases microglia reactivity at Aβ plaques in a mouse model of Aβ deposition. *Journal of Neuroinflammation, 11*. doi:10.1186/1742-2094-11-111

Roe, M. T., Dawson, D. V., Hulette, C. M., Einstein, G., & Grain, B. J. (1996). Microglia are not exclusively associated with plaque-rich regions of the dentate gyrus in Alzheimer's disease. *Journal of Neuropathology and Experimental Neurology, 55*(3), 366-371. doi:10.1097/00005072-199603000-00012

Rogaeva, E., Bergeron, C., Sato, C., Moliaka, I., Kawarai, T., Toulina, A., . . . St. George-Hyslop, P. H. (2003). PS1 Alzheimer's disease family with spastic paraplegia: The search for a gene modifier. *Neurology, 61*(7), 1005-1007. doi:10.1212/WNL.61.7.1005

Rogers, J., & Morrison, J. H. (1985). Quantitative morphology and regional and laminar distributions of senile plaques in Alzheimer's disease. *The Journal of Neuroscience, 5*(10), 2801-2808. doi:10.1523/jneurosci.05-10-02801.1985

Romito-DiGiacomo, R. R., Menegay, H., Cicero, S. A., & Herrup, K. (2007). Effects of Alzheimer's Disease on Different Cortical Layers: The Role of Intrinsic Differences in Aβ Susceptibility. *The Journal of Neuroscience, 27*(32), 8496-8504. doi:10.1523/jneurosci.1008-07.2007

Rossi, G., Bastone, A., Piccoli, E., Mazzoleni, G., Morbin, M., Uggetti, A., . . . Tagliavini, F. (2012). New mutations in MAPT gene causing frontotemporal lobar degeneration: biochemical and structural characterization. *Neurobiology of Aging, 33*(4), 834.e831-834.e836. doi:https://doi.org/10.1016/j.neurobiolaging.2011.08.008

Rossjohn, J., Cappai, R., Feil, S. C., Henry, A., McKinstry, W. J., Galatis, D., . . . Parker, M. W. (1999). Crystal structure of the N-terminal, growth factor-like domain of Alzheimer amyloid precursor protein. *Nature Structural Biology, 6*(4), 327-331. doi:10.1038/7562

Rosso, S. M., Kaat, L. D., Baks, T., Joosse, M., De Koning, I., Pijnenburg, Y., . . . Van Swieten, J. C. (2003). Frontotemporal dementia in The Netherlands: Patient characteristics and prevalence estimates from a population-based study. *Brain, 126*(9), 2016-2022. doi:10.1093/brain/awg204

Rosso, S. M., Kamphorst, W., De Graaf, B., Willemsen, R., Ravid, R., Niermeijer, M. F., . . . Van Swieten, J. C. (2001). Familial frontotemporal dementia with ubiquitin-positive inclusions is linked to chromosome 17q21-22. *Brain, 124*(10), 1948-1957.

Rovelet-Lecrux, A., Hannequin, D., Raux, G., Le Meur, N., Laquerrière, A., Vital, A., . . . Campion, D. (2006). APP locus duplication causes autosomal dominant early-onset Alzheimer disease with cerebral amyloid angiopathy. *Nature Genetics, 38*(1), 24-26. doi:10.1038/ng1718

Russo, C., Violani, E., Salis, S., Venezia, V., Dolcini, V., Damonte, G., . . . Schettini, G. (2002). Pyroglutamate-modified amyloid β-peptides - AβN3(pE) - strongly affect cultured neuron and astrocyte survival. *Journal of Neurochemistry, 82*(6), 1480-1489. doi:10.1046/j.1471-4159.2002.01107.x

Rusted, J. M., Evans, S. L., King, S. L., Dowell, N., Tabet, N., & Tofts, P. S. (2013). APOE e4 polymorphism in young adults is associated with improved attention and indexed by distinct neural signatures. *NeuroImage, 65*, 364-373. doi:https://doi.org/10.1016/j.neuroimage.2012.10.010

Ryan, N. S., Bastos-Leite, A. J., Rohrer, J. D., Werring, D. J., Fox, N. C., Rossor, M. N., & Schott, J. M. (2012). Cerebral microbleeds in familial Alzheimer's disease. *Brain : a journal of neurology, 135*(Pt 1), e201-e202. doi:10.1093/brain/awr126

Ryan, N. S., Biessels, G. J., Kim, L., Nicholas, J. M., Barber, P. A., Walsh, P., . . . Fox, N. C. (2015a). Genetic determinants of white matter hyperintensities and amyloid angiopathy in familial Alzheimer's disease. *Neurobiol Aging, 36*(12), 3140-3151. doi:10.1016/j.neurobiolaging.2015.08.026

Ryan, N. S., Lashley, T., Revesz, T., Dantu, K., Fox, N. C., & Morris, H. R. (2015b). Spontaneous ARIA (Amyloid-related imaging abnormalities) and cerebral amyloid angiopathy related inflammation in presenilin 1-associated familial Alzheimer's disease. *Journal of Alzheimer's Disease, 44*(4), 1069-1074. doi:10.3233/JAD-142325

Ryan, N. S., Nicholas, J. M., Weston, P. S. J., Liang, Y., Lashley, T., Guerreiro, R., . . . Fox, N. C. (2016). Clinical phenotype and genetic associations in autosomal dominant familial Alzheimer's disease: a case series. *The Lancet Neurology, 15*(13), 1326-1335. doi:10.1016/S1474-4422(16)30193-4

Ryan, N. S., & Rossor, M. N. (2010). Correlating familial Alzheimer's disease gene mutations with clinical phenotype. *Biomarkers in medicine, 4*(1), 99-112.

Ryman, D. C., Acosta-Baena, N., Aisen, P. S., Bird, T., Danek, A., Fox, N. C., . . . Bateman, R. J. (2014). Symptom onset in autosomal dominant Alzheimer disease: A systematic review and meta-analysis. *Neurology, 83*(3), 253-260. doi:10.1212/WNL.0000000000000596

Saido, T. C., Iwatsubo, T., Mann, D. M. A., Shimada, H., Ihara, Y., & Kawashima, S. (1995). Dominant and differential deposition of distinct β-amyloid peptide species, AβN3(pE), in senile plaques. *Neuron, 14*(2), 457-466. doi:10.1016/0896-6273(95)90301-1

Saito, T., Hanai, S., Takashima, S., Nakagawa, E., Okazaki, S., Inoue, T., . . . Itoh, M. (2011a). Neocortical layer formation of human developing brains and lissencephalies: Consideration of layer-specific marker expression. *Cerebral Cortex, 21*(3), 588-596. doi:10.1093/cercor/bhq125

Saito, T., Suemoto, T., Brouwers, N., Sleegers, K., Funamoto, S., Mihira, N., . . . Saido, T. C. (2011b). Potent amyloidogenicity and pathogenicity of Aβ 243. *Nature neuroscience, 14*(8), 1023-1032. doi:10.1038/nn.2858

Sakae, N., Heckman, M. G., Vargas, E. R., Carrasquillo, M. M., Murray, M. E., Kasanuki, K., . . . Dickson, D. W. (2019). Evaluation of Associations of Alzheimer's Disease Risk Variants that Are Highly Expressed in Microglia with Neuropathological Outcome Measures. *Journal of Alzheimer's Disease, 70*(3), 659-666. doi:10.3233/JAD-190451

Sakae, N., Roemer, S. F., Bieniek, K. F., Murray, M. E., Baker, M. C., Kasanuki, K., . . . Dickson, D. W. (2019). Microglia in frontotemporal lobar degeneration with progranulin or C9ORF72 mutations. *Annals of Clinical and Translational Neurology, 6*(9), 1782-1796. doi:10.1002/acn3.50875

Sakai, K., Boche, D., Carare, R., Johnston, D., Holmes, C., Love, S., & Nicoll, J. A. R. (2014). Aβ immunotherapy for Alzheimer’s disease: effects on apoE

and cerebral vasculopathy. *Acta Neuropathologica, 128*(6), 777-789. doi:10.1007/s00401-014-1340-9

Sandebring, A., Welander, H., Winblad, B., Graff, C., & Tjernberg, L. O. (2013). The pathogenic aβ43 is enriched in familial and sporadic Alzheimer disease. *PLoS ONE, 8*(2), e55847-e55847. doi:10.1371/journal.pone.0055847

Sankowski, R., Böttcher, C., Masuda, T., Geirsdottir, L., Sagar, Sindram, E., . . . Prinz, M. (2019). Mapping microglia states in the human brain through the integration of high-dimensional techniques. *Nature neuroscience, 22*(12), 2098-2110. doi:10.1038/s41593-019-0532-y

Sarkar, B., Mithu, V. S., Chandra, B., Mandal, A., Chandrakesan, M., Bhowmik, D., . . . Maiti, S. (2014). Significant Structural Differences between Transient Amyloid-β Oligomers and Less-Toxic Fibrils in Regions Known To Harbor Familial Alzheimer′s Mutations. *Angewandte Chemie International Edition, 53*(27), 6888-6892. doi:10.1002/anie.201402636

Sasaki, A., Yamaguchi, H., Ogawa, A., Sugihara, S., & Nakazato, Y. (1997). Microglial activation in early stages of amyloid β protein deposition. *Acta Neuropathologica, 94*(4), 316-322. doi:10.1007/s004010050713

Sasaki, Y., Ohsawa, K., Kanazawa, H., Kohsaka, S., & Imai, Y. (2001). Iba1 Is an Actin-Cross-Linking Protein in Macrophages/Microglia. *Biochemical and Biophysical Research Communications, 286*(2), 292-297. doi:https://doi.org/10.1006/bbrc.2001.5388

Saunders, A. M., Strittmatter, W. J., Schmechel, D., St. George-Hyslop, P. H., Pericak-Vance, M. A., Joo, S. H., . . . Roses, A. D. (1993). Association of apolipoprotein E allele ϵ4 with late-onset familial and sporadic Alzheimer's disease. *Neurology, 43*(8), 1467-1467. doi:10.1212/wnl.43.8.1467

Savage, M. J., Kawooya, J. K., Pinsker, L. R., Emmons, T. L., Mistretta, S., Siman, R., & Greenberg, B. D. (1995). Elevated aβ levels in Alzheimer's disease brain are associated with selective accumulation of aβ42 in parenchymal amyloid plaques and both aβ40 and aβ42 in cerebrovascular deposits. *Amyloid, 2*(4), 234-240. doi:10.3109/13506129508999005

Schelle, J., Wegenast-Braun, B. M., Fritschi, S. K., Kaeser, S. A., Jährling, N., Eicke, D., . . . Jucker, M. (2019). Early Aβ reduction prevents progression of cerebral amyloid angiopathy. *Annals of Neurology, 86*(4), 561-571. doi:10.1002/ana.25562

Schetters, S. T. T., Gomez-Nicola, D., Garcia-Vallejo, J. J., & Van Kooyk, Y. (2018). Neuroinflammation: Microglia and T cells get ready to tango. *Frontiers in Immunology, 8*(JAN). doi:10.3389/fimmu.2017.01905

Scheuner, D., Eckman, C., Jensen, M., Song, X., Citron, M., Suzuki, N., . . . Younkin, S. (1996). Secreted amyloid beta-protein similar to that in the senile plaques of Alzheimer's disease is increased in vivo by the presenilin 1 and 2 and APP mutations linked to familial Alzheimer's disease. *Nat Med, 2*. doi:10.1038/nm0896-864

Schilling, S., DeStefano, A. L., Sachdev, P. S., Choi, S. H., Mather, K. A., DeCarli, C. D., . . . Debette, S. (2013). APOE genotype and MRI markers of cerebrovascular disease: systematic review and meta-analysis. *Neurology, 81*(3), 292-300. doi:10.1212/WNL.0b013e31829bfda4

Schmechel, D. E., Saunders, A. M., Strittmatter, W. J., Crain, B. J., Hulette, C. M., Joo, S. H., . . . Roses, A. D. (1993). Increased amyloid β-peptide deposition in cerebral cortex as a consequence of apolipoprotein E genotype in late-onset Alzheimer disease. *Proceedings of the National Academy of Sciences of the United States of America, 90*(20), 9649-9653. doi:10.1073/pnas.90.20.9649

Schneider, C. A., Rasband, W. S., & Eliceiri, K. W. (2012). NIH Image to ImageJ: 25 years of image analysis. *Nat Meth, 9*(7), 671-675.

Schöll, M., Almkvist, O., Axelman, K., Stefanova, E., Wall, A., Westman, E., . . . Nordberg, A. (2011). Glucose metabolism and PIB binding in carriers of a His163Tyr presenilin 1 mutation. *Neurobiology of Aging, 32*(8), 1388-1399. doi:10.1016/j.neurobiolaging.2009.08.016

Scholl, M., Carter, S. F., Westman, E., Rodriguez-Vieitez, E., Almkvist, O., Thordardottir, S., . . . Nordberg, A. (2015). Early astrocytosis in autosomal dominant Alzheimer's disease measured in vivo by multi-tracer positron emission tomography. *Scientific Reports, 5*. doi:10.1038/srep16404

Selkoe, D. J. (1997). Alzheimer's Disease--Genotypes, Phenotype, and Treatments. *Science, 275*(5300), 630-631. doi:10.1126/science.275.5300.630

Selkoe, D. J., & Hardy, J. (2016). The amyloid hypothesis of Alzheimer's disease at 25 years. *EMBO Molecular Medicine, 8*(6), 595-608. doi:10.15252/emmm.201606210

Serrano-Pozo, A., Betensky, R. A., Frosch, M. P., & Hyman, B. T. (2016). Plaque-Associated Local Toxicity Increases over the Clinical Course of Alzheimer Disease. *The American Journal of Pathology, 186*(2), 375-384. doi:10.1016/j.ajpath.2015.10.010

Serrano-Pozo, A., Mielke, M. L., Muzitansky, A., Gómez-Isla, T., Growdon, J. H., Bacskai, B. J., . . . Hyman, B. T. (2012). Stable size distribution of amyloid plaques over the course of Alzheimer disease. *Journal of Neuropathology and Experimental Neurology, 71*(8), 694-701. doi:10.1097/NEN.0b013e31825e77de

Serrano-Pozo, A., Muzikansky, A., Gómez-Isla, T., Growdon, J. H., Betensky, R. A., Frosch, M. P., & Hyman, B. T. (2013). Differential relationships of reactive astrocytes and microglia to fibrillar amyloid deposits in alzheimer disease. *Journal of Neuropathology and Experimental Neurology, 72*(6), 462-471. doi:10.1097/NEN.0b013e3182933788

Serrano-Pozo, A., Qian, J., Monsell, S. E., Frosch, M. P., Betensky, R. A., & Hyman, B. T. (2013). Examination of the clinicopathologic continuum of Alzheimer disease in the autopsy cohort of the National Alzheimer Coordinating Center. *Journal of Neuropathology and Experimental Neurology, 72*(12), 1182-1192. doi:10.1097/NEN.0000000000000016

Sevigny, J., Chiao, P., Bussière, T., Weinreb, P. H., Williams, L., Maier, M., . . . Sandrock, A. (2016). The antibody aducanumab reduces Aβ plaques in Alzheimer's disease. *Nature, 537*(7618), 50-56. doi:10.1038/nature19323

Shankar, G. M., Li, S., Mehta, T. H., Garcia-Munoz, A., Shepardson, N. E., Smith, I., . . . Selkoe, D. J. (2008). Amyloid-β protein dimers isolated directly from

Alzheimer's brains impair synaptic plasticity and memory. *Nature Medicine, 14*(8), 837-842. doi:10.1038/nm1782

Shea, Y. F., Chu, L. W., Chan, A. O., Ha, J., Li, Y., & Song, Y. Q. (2016). A systematic review of familial Alzheimer's disease: Differences in presentation of clinical features among three mutated genes and potential ethnic differences. *J Formos Med Assoc, 115*(2), 67-75. doi:10.1016/j.jfma.2015.08.004

Shen, L., Qin, W., Wu, L., Zhou, A., Tang, Y., Wang, Q., . . . Jia, J. (2019). Two novel presenilin-1 mutations (I249L and P433S) in early onset Chinese Alzheimer's pedigrees and their functional characterization. *Biochemical and Biophysical Research Communications, 516*(1), 264-269. doi:10.1016/j.bbrc.2019.05.185

Sheng, J. G., Griffin, W. S. T., Royston, M. C., & Mrak, R. E. (1998). Distribution of interleukin-1-immunoreactive microglia in cerebral cortical layers: Implications for neuritic plaque formation in Alzheimer's disease. *Neuropathology and Applied Neurobiology, 24*(4), 278-283. doi:10.1046/j.1365-2990.1998.00122.x

Sheng, J. G., Mrak, R. E., & Griffin, W. S. T. (1995). Microglial inter leukin-1α expression in brain regions in Alzheimer's disease: correlation with neuritic plaque distribution. *Neuropathology and Applied Neurobiology, 21*(4), 290-301. doi:10.1111/j.1365-2990.1995.tb01063.x

Shepherd, C. E., Gregory, G. C., Vickers, J. C., & Halliday, G. M. (2005). Novel 'inflammatory plaque' pathology in presenilin-1 Alzheimer's disease. *Neuropathology and Applied Neurobiology, 31*(5), 503-511. doi:10.1111/j.1365-2990.2005.00667.x

Sherrington, R., Froelich, S., Sorbi, S., Campion, D., Chi, H., Rogaeva, E. A., . . . St George-Hyslop, P. H. (1996). Alzheimer's disease associated with mutations in presenilin 2 is rare and variably penetrant. *Human Molecular Genetics, 5*(7), 985-988. doi:10.1093/hmg/5.7.985

Shi, Y., Kirwan, P., Smith, J., MacLean, G., Orkin, S. H., & Livesey, F. J. (2012a). A human stem cell model of early Alzheimer's disease pathology in Down syndrome. *Science Translational Medicine, 4*(124), 124ra129-124ra129. doi:10.1126/scitranslmed.3003771

Shi, Y., Kirwan, P., Smith, J., Robinson, H. P. C., & Livesey, F. J. (2012b). Human cerebral cortex development from pluripotent stem cells to functional excitatory synapses. *Nature neuroscience, 15*(3), 477-S471. doi:10.1038/nn.3041

Shibata, M., Yamada, S., Ram Kumar, S., Calero, M., Bading, J., Frangione, B., . . . Zlokovic, B. V. (2000). Clearance of Alzheimer's amyloid-β1-40 peptide from brain by LDL receptor-related protein-1 at the blood-brain barrier. *Journal of Clinical Investigation, 106*(12), 1489-1499. doi:10.1172/JCI10498

Shimojo, M., Sahara, N., Mizoroki, T., Funamoto, S., Morishima-Kawashima, M., Kudo, T., . . . Takashima, A. (2008). Enzymatic characteristics of I213T mutant presenilin-1/γ-secretase in cell models and knock-in mouse brains: Familial Alzheimer disease-linked mutation impairs γ-site cleavage of amyloid precursor protein C-terminal fragment β. *Journal of Biological Chemistry, 283*(24), 16488-16496. doi:10.1074/jbc.M801279200

Shinohara, M., Murray, M. E., Frank, R. D., Shinohara, M., DeTure, M., Yamazaki, Y., . . . Kanekiyo, T. (2016). Impact of sex and APOE4 on cerebral amyloid angiopathy in Alzheimer's disease. *Acta Neuropathologica, 132*(2), 225-234. doi:10.1007/s00401-016-1580-y

Shrimpton, A. E., Schelper, R. L., Linke, R. P., Hardy, J., Crook, R., Dickson, D. W., . . . Davis, R. L. (2007). A presenilin 1 mutation (L420R) in a family with early onset Alzheimer disease, seizures and cotton wool plaques, but not spastic paraparesis. *Neuropathology, 27*(3), 228-232. doi:10.1111/j.1440-1789.2007.00766.x

Silvin, A., & Ginhoux, F. (2018). Microglia heterogeneity along a spatio–temporal axis: More questions than answers. *GLIA, 66*(10), 2045-2057. doi:10.1002/glia.23458

Siman, R., & Salidas, S. (2004). Gamma-secretase subunit composition and distribution in the presenilin wild-type and mutant mouse brain. *Neuroscience, 129*(3), 615-628. doi:10.1016/j.neuroscience.2004.08.028

Singleton, A. B., Hall, R., Ballard, C. G., Perry, R. H., Xuereb, J. H., Rubinsztein, D. C., . . . Morris, C. M. (2000). Pathology of early-onset Alzheimer's disease cases bearing the Thr113-114ins presenilin-1 mutation. *Brain, 123*(12), 2467-2474.

Sleegers, K., Brouwers, N., Gijselinck, I., Theuns, J., Goossens, D., Wauters, J., . . . Van Broeckhoven, C. (2006). APP duplication is sufficient to cause early onset Alzheimer's dementia with cerebral amyloid angiopathy. *Brain, 129*(11), 2977-2983. doi:10.1093/brain/awl203

Smith, M. J., Kwok, J. B. J., McLean, C. A., Kril, J. J., Anthony Broe, G., Nicholson, G. A., . . . Brooks, W. S. (2001). Variable phenotype of Alzheimer's disease with spastic paraparesis. *Annals of Neurology, 49*(1), 125-129. doi:10.1002/1531-8249(200101)49:1<125::AID-ANA21>3.0.CO;2-1

Smith, P. M., Bains, J. S., & Ferguson, A. V. (1997). Preferential deposition of amyloid β protein (Aβ) in the form Aβ40 in Alzheimer's disease is associated with a gene dosage effect of the apolipoprotein E E4 allele. *Neuroscience Letters, 221*(2-3), 81-84. doi:10.1016/S0304-3940(96)13294-8

Somavarapu, A. K., & Kepp, K. P. (2016). Loss of stability and hydrophobicity of presenilin 1 mutations causing Alzheimer's disease. *Journal of Neurochemistry, 137*(1), 101-111. doi:10.1111/jnc.13535

Somavarapu, A. K., & Kepp, K. P. (2017). Membrane Dynamics of γ-Secretase Provides a Molecular Basis for β-Amyloid Binding and Processing. *ACS Chemical Neuroscience, 8*(11), 2424-2436. doi:10.1021/acschemneuro.7b00208

Sorbi, S., Nacmias, B., Forleo, P., Piacentini, S., Latorraca, S., & Amaducci, L. (1995). Epistatic effect of APP717 mutation and apolipoprotein E genotype in familial Alzheimer's disease. *Annals of Neurology, 38*(1), 124-127. doi:10.1002/ana.410380120

Spalice, A., Parisi, P., Nicita, F., Pizzardi, G., Del Balzo, F., & Iannetti, P. (2009). Neuronal migration disorders: Clinical, neuroradiologic and genetics

aspects. *Acta Paediatrica, International Journal of Paediatrics, 98*(3), 421-433. doi:10.1111/j.1651-2227.2008.01160.x

Sperling, R., Salloway, S., Brooks, D. J., Tampieri, D., Barakos, J., Fox, N. C., . . . Grundman, M. (2012). Amyloid-related imaging abnormalities in patients with Alzheimer's disease treated with bapineuzumab: A retrospective analysis. *The Lancet Neurology, 11*(3), 241-249. doi:10.1016/S1474-4422(12)70015-7

Sperling, R. A., Jack, C. R., Black, S. E., Frosch, M. P., Greenberg, S. M., Hyman, B. T., . . . Schindler, R. J. (2011). Amyloid Related Imaging Abnormalities (ARIA) in Amyloid Modifying Therapeutic Trials: Recommendations from the Alzheimer's Association Research Roundtable Workgroup. *Alzheimer's & dementia : the journal of the Alzheimer's Association, 7*(4), 367-385. doi:10.1016/j.jalz.2011.05.2351

Sproul, A. A., Jacob, S., Pre, D., Kim, S. H., Nestor, M. W., Navarro-Sobrino, M., . . . Noggle, S. A. (2014). Characterization and molecular profiling of PSEN1 familial alzheimer's disease iPSC-Derived neural progenitors. *PLoS ONE, 9*(1). doi:10.1371/journal.pone.0084547

St George-Hyslop, P., & Fraser, P. E. (2012). Assembly of the presenilin γ-/ε-secretase complex. *Journal of Neurochemistry, 120*(s1), 84-88. doi:10.1111/j.1471-4159.2011.07505.x

Steiner, H., Revesz, T., Neumann, M., Helmut, R., Grim, M. G., Pesold, B., . . . Haass, C. (2001). A Pathogenic Presenilin-1 Deletion Causes Abberrant Aβ42 Production in the Absence of Congophilic Amyloid Plaques. *Journal of Biological Chemistry, 276*(10), 7233-7239. doi:10.1074/jbc.M007183200

Steiner, H., Romig, H., Pesold, B., Philipp, U., Baader, M., Citron, M., . . . Haass, C. (1999). Amyloidogenic function of the Alzheimer's disease-associated presenilin 1 in the absence of endoproteolysis. *Biochemistry, 38*(44), 14600-14605. doi:10.1021/bi9914210

Storandt, M., Balota, D. A., Aschenbrenner, A. J., & Morris, J. C. (2014). Clinical and Psychological Characteristics of Initial Cohort of the Dominantly Inherited Alzheimer Network (DIAN). *Neuropsychology, 28*(1), 10.1037/neu0000030. doi:10.1037/neu0000030

Stout, R. D., Jiang, C., Matta, B., Tietzel, I., Watkins, S. K., & Suttles, J. (2005). Macrophages sequentially change their functional phenotype in response to changes in microenvironmental influences. *Journal of Immunology, 175*(1), 342-349. doi:10.4049/jimmunol.175.1.342

Styren, S. D., Civin, W. H., & Rogers, J. (1990). Molecular, cellular, and pathologic characterization of HLA-DR immunoreactivity in normal elderly and Alzheimer's disease brain. *Experimental Neurology, 110*(1), 93-104. doi:10.1016/0014-4886(90)90054-V

Suárez-Calvet, M., Belbin, O., Pera, M., Badiola, N., Magrané, J., Guardia-Laguarta, C., . . . Lleõ, A. (2014). Autosomal-dominant Alzheimer's disease mutations at the same codon of amyloid precursor protein differentially alter Aβ production. *Journal of Neurochemistry, 128*(2), 330-339. doi:10.1111/jnc.12466

Sun, L., Zhao, L., Yang, G., Yan, C., Zhou, R., Zhou, X., . . . Shi, Y. (2015). Structural basis of human γ-secretase assembly. *Proceedings of the National Academy of Sciences of the United States of America, 112*(19), 6003-6008. doi:10.1073/pnas.1506242112

Sun, L., Zhou, R., Yang, G., & Shi, Y. (2017). Analysis of 138 pathogenic mutations in presenilin-1 on the in vitro production of Aβ42 and Aβ40 peptides by γ-secretase. *Proceedings of the National Academy of Sciences, 114*(4), E476-E485. doi:10.1073/pnas.1618657114

Sutovsky, S., Smolek, T., Turcani, P., Petrovic, R., Brandoburova, P., Jadhav, S., . . . Zilka, N. (2018). Neuropathology and biochemistry of early onset familial Alzheimer's disease caused by presenilin-1 missense mutation Thr116Asn. *Journal of Neural Transmission, 125*(6), 965-976. doi:10.1007/s00702-018-1850-z

Szaruga, M., Munteanu, B., Lismont, S., Veugelen, S., Horré, K., Mercken, M., . . . Chávez-Gutiérrez, L. (2017). Alzheimer's-Causing Mutations Shift Aβ Length by Destabilizing γ-Secretase-Aβn Interactions. *Cell, 170*(3), 443-456.e414. doi:10.1016/j.cell.2017.07.004

Szaruga, M., Veugelen, S., Benurwar, M., Lismont, S., Sepulveda-Falla, D., Lleo, A., . . . Chavez-Gutierrez, L. (2015). Qualitative changes in human gamma-secretase underlie familial Alzheimer's disease. *J Exp Med, 212*(12), 2003-2013. doi:10.1084/jem.20150892

Taipa, R., Brochado, P., Robinson, A., Reis, I., Costa, P., Mann, D. M., . . . Sousa, N. (2017). Patterns of Microglial Cell Activation in Alzheimer Disease and Frontotemporal Lobar Degeneration. *Neurodegenerative Diseases, 17*(4-5), 145-154. doi:10.1159/000457127

Taipa, R., Ferreira, V., Brochado, P., Robinson, A., Reis, I., Marques, F., . . . Sousa, N. (2018). Inflammatory pathology markers (activated microglia and reactive astrocytes) in early and late onset Alzheimer disease: a post mortem study. *Neuropathology and Applied Neurobiology, 44*(3), 298-313. doi:10.1111/nan.12445

Takahashi, K., Tanabe, K., Ohnuki, M., Narita, M., Ichisaka, T., Tomoda, K., & Yamanaka, S. (2007). Induction of Pluripotent Stem Cells from Adult Human Fibroblasts by Defined Factors. *Cell, 131*(5), 861-872. doi:https://doi.org/10.1016/j.cell.2007.11.019

Takami, M., Nagashima, Y., Sano, Y., Ishihara, S., Morishima-Kawashima, M., Funamoto, S., & Ihara, Y. (2009). γ-Secretase: Successive tripeptide and tetrapeptide release from the transmembrane domain of β-carboxyl terminal fragment. *Journal of Neuroscience, 29*(41), 13042-13052. doi:10.1523/JNEUROSCI.2362-09.2009

Takeo, K., Watanabe, N., Tomita, T., & Iwatsubo, T. (2012). Contribution of the γ-secretase subunits to the formation of catalytic pore of presenilin 1 protein. *Journal of Biological Chemistry, 287*(31), 25834-25843. doi:10.1074/jbc.M111.336347

Tamaoka, A., Odaka, A., Ishibashi, Y., Usami, M., Sahara, N., Suzuki, N., . . . Kanazawa, I. (1994). APP717 missense mutation affects the ratio of amyloid beta protein species (A beta 1-42/43 and a beta 1-40) in familial Alzheimer's disease brain. *Journal of Biological Chemistry, 269*(52), 32721-32724.

Tang, Y., & Le, W. (2016). Differential Roles of M1 and M2 Microglia in Neurodegenerative Diseases. *Molecular Neurobiology, 53*(2), 1181-1194. doi:10.1007/s12035-014-9070-5

Tao, W., & Lai, E. (1992). Telencephalon-restricted expression of BF-1, a new member of the HNF-3/fork head gene family, in the developing rat brain. *Neuron, 8*(5), 957-966. doi:https://doi.org/10.1016/0896-6273(92)90210-5

Tarasoff-Conway, J. M., Carare, R. O., Osorio, R. S., Glodzik, L., Butler, T., Fieremans, E., . . . De Leon, M. J. (2015). Clearance systems in the brain - Implications for Alzheimer disease. *Nature Reviews Neurology, 11*(8), 457-470. doi:10.1038/nrneurol.2015.119

Thal, D. R., Ghebremedhin, E., Orantes, M., & Wiestler, O. D. (2003). Vascular Pathology in Alzheimer Disease: Correlation of Cerebral Amyloid Angiopathy and Arteriosclerosis/Lipohyalinosis with Cognitive Decline. *Journal of Neuropathology and Experimental Neurology, 62*(12), 1287-1301. doi:10.1093/jnen/62.12.1287

Thal, D. R., Ghebremedhin, E., Rüb, U., Yamaguchi, H., Del Tredici, K., & Braak, H. (2002). Two Types of Sporadic Cerebral Amyloid Angiopathy. *Journal of Neuropathology & Experimental Neurology, 61*(3), 282-293. doi:10.1093/jnen/61.3.282

Thal, D. R., Griffin, W. S. T., de Vos, R. A. I., & Ghebremedhin, E. (2008). Cerebral amyloid angiopathy and its relationship to Alzheimer's disease. *Acta Neuropathologica, 115*(6), 599-609. doi:10.1007/s00401-008-0366-2

Thal, D. R., Rüb, U., Orantes, M., & Braak, H. (2002). Phases of Aβ-deposition in the human brain and its relevance for the development of AD. *Neurology, 58*(12), 1791-1800. doi:10.1212/wnl.58.12.1791

Thinakaran, G., Borchelt, D. R., Lee, M. K., Slunt, H. H., Spitzer, L., Kim, G., . . . Sisodia, S. S. (1996). Endoproteolysis of Presenilin 1 and Accumulation of Processed Derivatives In Vivo. *Neuron, 17*(1), 181-190. doi:https://doi.org/10.1016/S0896-6273(00)80291-3

Thordardottir, S., Kinhult Ståhlbom, A., Almkvist, O., Thonberg, H., Eriksdotter, M., Zetterberg, H., . . . Graff, C. (2017). The effects of different familial Alzheimer's disease mutations on APP processing in vivo. *Alzheimer's Research and Therapy, 9*(1). doi:10.1186/s13195-017-0234-1

Thordardottir, S., Rodriguez-Vieitez, E., Almkvist, O., Ferreira, D., Saint-Aubert, L., Kinhult-Ståhlbom, A., . . . Graff, C. (2018). Reduced penetrance of the PSEN1 H163Y autosomal dominant Alzheimer mutation: A 22-year follow-up study. *Alzheimer's Research and Therapy, 10*(1). doi:10.1186/s13195-018-0374-y

Thornton, E., Vink, R., Blumbergs, P. C., & Van Den Heuvel, C. (2006). Soluble amyloid precursor protein α reduces neuronal injury and improves functional outcome following diffuse traumatic brain injury in rats. *Brain Research, 1094*(1), 38-46. doi:10.1016/j.brainres.2006.03.107

Tian, J., Shi, J., Bailey, K., & Mann, D. M. A. (2003). Negative association between amyloid plaques and cerebral amyloid angiopathy in Alzheimer's disease. *Neuroscience Letters, 352*(2), 137-140. doi:10.1016/j.neulet.2003.08.048

Tian, J., Shi, J., & Mann, D. M. A. (2004). Cerebral amyloid angiopathy and dementia. *Panminerva Medica, 46*(4), 253-264.

Tian, J., Shi, J., Smallman, R., Iwatsubo, T., & Mann, D. M. A. (2006). Relationships in Alzheimer's disease between the extent of Aβ deposition in cerebral blood vessel walls, as cerebral amyloid angiopathy, and the amount of cerebrovascular smooth muscle cells and collagen. *Neuropathology and Applied Neurobiology, 32*(3), 332-340. doi:10.1111/j.1365-2990.2006.00732.x

Timmers, W. F., Tagliavini, F., Haan, J., & Frangione, B. (1990). Parenchymal preamyloid and amyloid deposits in the brains of patients with hereditary cerebral hemorrhage with amyloidosis—Dutch type. *Neuroscience Letters, 118*(2), 223-226. doi:https://doi.org/10.1016/0304-3940(90)90632-J

Tominaga, A., Cai, T., Takagi-Niidome, S., Iwatsubo, T., & Tomita, T. (2016). Conformational changes in transmembrane domain 4 of presenilin 1 are associated with altered amyloid-β 42 production. *Journal of Neuroscience, 36*(4), 1362-1372. doi:10.1523/JNEUROSCI.5090-14.2016

Tomiyama, T., Matsuyama, S., Iso, H., Umeda, T., Takuma, H., Ohnishi, K., . . . Mori, H. (2010). A Mouse Model of Amyloid β Oligomers: Their Contribution to Synaptic Alteration, Abnormal Tau Phosphorylation, Glial Activation, and Neuronal Loss In Vivo</em&gt. *The Journal of Neuroscience, 30*(14), 4845. doi:10.1523/JNEUROSCI.5825-09.2010

Tomiyama, T., Nagata, T., Shimada, H., Teraoka, R., Fukushima, A., Kanemitsu, H., . . . Mori, H. (2008). A new amyloid β variant favoring oligomerization in Alzheimer's-type dementia. *Annals of Neurology, 63*(3), 377-387. doi:10.1002/ana.21321

Torres-Platas, S. G., Comeau, S., Rachalski, A., Bo, G. D., Cruceanu, C., Turecki, G., . . . Mechawar, N. (2014). Morphometric characterization of microglial phenotypes in human cerebral cortex. *Journal of Neuroinflammation, 11*(1), 12. doi:10.1186/1742-2094-11-12

Treusch, S., Cyr, D. M., & Lindquist, S. (2009). Amyloid deposits: Protection against toxic protein species? *Cell Cycle, 8*(11), 1668-1674. doi:10.4161/cc.8.11.8503

Triarhou, L. C. (2013). The Cytoarchitectonic Map of Constantin von Economo and Georg N. Koskinas. In S. Geyer & R. Turner (Eds.), *Microstructural Parcellation of the Human Cerebral Cortex: From Brodmann's Post-Mortem Map to in Vivo Mapping with High-Field Magnetic Resonance Imaging* (pp. 33-53). Berlin, Heidelberg: Springer Berlin Heidelberg.

Trushina, E., Nemutlu, E., Zhang, S., Christensen, T., Camp, J., Mesa, J., . . . Poduslo, J. F. (2012). Defects in mitochondrial dynamics and metabolomic signatures of evolving energetic stress in mouse models of familial alzheimer's disease. *PLoS ONE, 7*(2). doi:10.1371/journal.pone.0032737

Tu, H., Nelson, O., Bezprozvanny, A., Wang, Z., Lee, S. F., Hao, Y. H., . . . Bezprozvanny, I. (2006). Presenilins Form ER Ca2+ Leak Channels, a Function Disrupted by Familial Alzheimer's Disease-Linked Mutations. *Cell, 126*(5), 981-993. doi:10.1016/j.cell.2006.06.059

Turner, R. S., Suzuki, N., Chyung, A. S. C., Younkin, S. G., & Lee, V. M.-Y. (1996). Amyloids and Are Generated Intracellularly in Cultured Human Neurons and Their Secretion Increases with Maturation. *Journal of Biological Chemistry, 271*(15), 8966-8970. doi:10.1074/jbc.271.15.8966

Uchihara, T., Nakamura, A., Nakayama, H., Arima, K., Ishizuka, N., Mori, H., & Mizushima, S. (2003). Triple Immunofluorolabeling with Two Rabbit Polyclonal Antibodies and a Mouse Monoclonal Antibody Allowing Three-dimensional Analysis of Cotton Wool Plaques in Alzheimer Disease. *Journal of Histochemistry & Cytochemistry, 51*(9), 1201-1206. doi:10.1177/002215540305100910

Ulvestad, E., Williams, K., Bjerkvig, R., Tiekotter, K., Antel, J., & Matre, R. (1994). Human microglial cells have phenotypic and functional characteristics in common with both macrophages and dendritic antigen-presenting cells. *Journal of Leukocyte Biology, 56*(6), 732-740.

Vallejo-Diez, S., Fleischer, A., Martín-Fernández, J. M., Sánchez-Gilabert, A., Castresana, M., Aguillón, D., . . . Bachiller, D. (2019). Generation of one iPSC line (IMEDEAi006-A) from an early-onset familial Alzheimer's Disease (fAD) patient carrying the E280A mutation in the PSEN1 gene. *Stem Cell Research, 37*, 101440. doi:https://doi.org/10.1016/j.scr.2019.101440

Van Broeckhoven, C., Haan, J., Bakker, E., Hardy, J., Van Hul, W., Wehnert, A., . . . Roos, R. (1990). Amyloid beta protein precursor gene and hereditary cerebral hemorrhage with amyloidosis (Dutch). *Science, 248*(4959), 1120-1122. doi:10.1126/science.1971458

van der Kant, R., Langness, V. F., Herrera, C. M., Williams, D. A., Fong, L. K., Leestemaker, Y., . . . Goldstein, L. S. B. (2019). Cholesterol Metabolism Is a Druggable Axis that Independently Regulates Tau and Amyloid-β in iPSC-Derived Alzheimer's Disease Neurons. *Cell Stem Cell, 24*(3), 363-375.e369. doi:10.1016/j.stem.2018.12.013

Vandenberghe, R., Rinne, J. O., Boada, M., Katayama, S., Scheltens, P., Vellas, B., . . . Clinical Study, I. (2016). Bapineuzumab for mild to moderate Alzheimer’s disease in two global, randomized, phase 3 trials. *Alzheimer's Research & Therapy, 8*, 18. doi:10.1186/s13195-016-0189-7

Vassar, R., Bennett, B. D., Babu-Khan, S., Kahn, S., Mendiaz, E. A., Denis, P., . . . Citron, M. (1999). β-Secretase cleavage of Alzheimer's amyloid precursor protein by the transmembrane aspartic protease BACE. *Science, 286*(5440), 735-741. doi:10.1126/science.286.5440.735

Vehmas, A. K., Kawas, C. H., Stewart, W. F., & Troncoso, J. C. (2003). Immune reactive cells in senile plaques and cognitive decline in Alzheimer’s disease. *Neurobiology of Aging, 24*(2), 321-331. doi:https://doi.org/10.1016/S0197-4580(02)00090-8

Veiga, S., Carrero, P., Pernia, O., Azcoitia, I., & Garcia-Segura, L. M. (2007). Translocator protein (18 kDa) is involved in the regulation of reactive gliosis. *GLIA, 55*(14), 1426-1436. doi:10.1002/glia.20558

Vélez, J. I., Lopera, F., Sepulveda-Falla, D., Patel, H. R., Johar, A. S., Chuah, A., . . . Arcos-Burgos, M. (2016). APOE∗E2 allele delays age of onset in PSEN1 E280A Alzheimer's disease. *Molecular Psychiatry, 21*(7), 916-924. doi:10.1038/mp.2015.177

Verkkoniemi, A., Kalimo, H., Paetau, A., Somer, M., Iwatsubo, T., Hardy, J., & Haltia, M. (2001). Variant Alzheimer disease with spastic paraparesis: Neuropathological phenotype. *Journal of Neuropathology and Experimental Neurology, 60*(5), 483-492. doi:10.1093/jnen/60.5.483

Verkkoniemi, A., Somer, M., Rinne, J. O., Myllykangas, L., Crook, R., Hardy, J., . . . Haltia, M. (2000). Variant Alzheimer's disease with spastic paraparesis: Clinical characterization. *Neurology, 54*(5), 1103-1109. doi:10.1212/WNL.54.5.1103

Veugelen, S., Saito, T., Saido, T. C., Chávez-Gutiérrez, L., & De Strooper, B. (2016). Familial Alzheimer's Disease Mutations in Presenilin Generate Amyloidogenic Aβ Peptide Seeds. *Neuron, 90*(2), 410-416. doi:10.1016/j.neuron.2016.03.010

Vidoni, E. D., Yeh, H. W., Morris, J. K., Newell, K. L., Alqahtani, A., Burns, N. C., . . . Billinger, S. A. (2016). Cerebral β-amyloid angiopathy is associated with earlier dementia onset in Alzheimer's disease. *Neurodegenerative Diseases, 16*(3-4), 218-224. doi:10.1159/000441919

Vigo-Pelfrey, C., Lee, D., Keim, P., Lieberburg, I., & Schenk, D. B. (1993). Rapid Communication: Characterization of β-Amyloid Peptide from Human Cerebrospinal Fluid. *Journal of Neurochemistry, 61*(5), 1965-1968. doi:10.1111/j.1471-4159.1993.tb09841.x

Villegas-Llerena, C., Phillips, A., Reitboeck, P. G., Hardy, J., & Pocock, J. M. (2016). Microglial genes regulating neuroinflammation in the progression of Alzheimer's disease. *Current Opinion in Neurobiology, 36*, 74-81. doi:10.1016/j.conb.2015.10.004

Vinters, H. V., & Gilbert, J. J. (1983). Cerebral amyloid angiopathy: Incidence and complications in the aging brain. II. The distribution of amyloid vascular changes. *Stroke, 14*(6), 924-928. doi:10.1161/01.STR.14.6.924

Vöglein, J., Paumier, K., Jucker, M., Preische, O., McDade, E., Hassenstab, J., . . . Levin, J. (2019). Clinical, pathophysiological and genetic features of motor symptoms in autosomal dominant Alzheimer's disease. *Brain, 142*(5), 1429-1440. doi:10.1093/brain/awz050

Vonsattel, J. P. G., Myers, R. H., Tessa Hedley-Whyte, E., Ropper, A. H., Bird, E. D., & Richardson, E. P., Jr. (1991). Cerebral amyloid angiopathy without and with cerebral hemorrhages: A comparative histological study. *Annals of Neurology, 30*(5), 637-649. doi:10.1002/ana.410300503

Wang, G., Coble, D., McDade, E. M., Hassenstab, J., Fagan, A. M., Benzinger, T. L. S., . . . Xiong, C. (2019). Staging biomarkers in preclinical autosomal dominant Alzheimer's disease by estimated years to symptom onset. *Alzheimer's and Dementia, 15*(4), 506-514. doi:10.1016/j.jalz.2018.12.008

Wang, S., Wang, R., Chen, L., Bennett, D. A., Dickson, D. W., & Wang, D. S. (2010). Expression and functional profiling of neprilysin, insulin-degrading enzyme, and endothelin-converting enzyme in prospectively studied elderly and Alzheimer's brain. *Journal of Neurochemistry, 115*(1), 47-57. doi:10.1111/j.1471-4159.2010.06899.x

Wang, Y., & Ha, Y. (2004). The X-ray structure of an antiparallel dimer of the human amyloid precursor protein E2 domain. *Molecular Cell, 15*(3), 343-353. doi:10.1016/j.molcel.2004.06.037

Wang, Z., Wang, B., Yang, L., Guo, Q., Aithmitti, N., Songyang, Z., & Zheng, H. (2009). Presynaptic and postsynaptic interaction of the amyloid precursor protein promotes peripheral and central synaptogenesis. *Journal of Neuroscience, 29*(35), 10788-10801. doi:10.1523/JNEUROSCI.2132-09.2009

Wei, L. K., Au, A., Menon, S., Griffiths, L. R., Kooi, C. W., Irene, L., . . . Aziz, Z. A. (2017). Polymorphisms of MTHFR, eNOS, ACE, AGT, ApoE, PON1, PDE4D, and Ischemic Stroke: Meta-Analysis. *Journal of Stroke and Cerebrovascular Diseases, 26*(11), 2482-2493. doi:https://doi.org/10.1016/j.jstrokecerebrovasdis.2017.05.048

Weisgraber, K. H., Rall Jr, S. C., & Mahley, R. W. (1981). Human E apoprotein heterogeneity. Cysteine-arginine interchanges in the amino acid sequence of the apo-E isoforms. *Journal of Biological Chemistry, 256*(17), 9077-9083.

Weller, R. O., Massey, A., Newman, T. A., Hutchings, M., Kuo, Y.-M., & Roher, A. E. (1998). Cerebral Amyloid Angiopathy: Amyloid β Accumulates in Putative Interstitial Fluid Drainage Pathways in Alzheimer's Disease. *The American Journal of Pathology, 153*(3), 725-733. doi:https://doi.org/10.1016/S0002-9440(10)65616-7

Wells, J. (1983). Human neuroanatomy, 8th edition. Edited by W. B. Carpenter, J. Sutin, 872 pp, Williams & Wilkins, Baltimore, MD, 1983. $44.00. *Muscle & Nerve, 6*(6), 462-462. doi:10.1002/mus.880060612

Wen, P. H., De Gasperi, R., Gama Sosa, M. A., Rocher, A. B., Friedrich Jr, V. L., Hof, P. R., & Elder, G. A. (2005). Selective expression of presenilin 1 in neural progenitor cells rescues the cerebral hemorrhages and cortical lamination defects in presenilin 1-null mutant mice. *Development, 132*(17), 3873-3883. doi:10.1242/dev.01946

Wesén, E., Jeffries, G. D. M., Matson Dzebo, M., & Esbjörner, E. K. (2017). Endocytic uptake of monomeric amyloid-β peptides is clathrin- and dynamin-independent and results in selective accumulation of Aβ(1-42) compared to Aβ(1-40). *Scientific Reports, 7*(1), 2021-2021. doi:10.1038/s41598-017-02227-9

Wijsman, E. M., Daw, E. W., Yu, X., Steinbart, E. J., Nochlin, D., Bird, T. B., & Schellenberg, G. D. (2005). APOE and other loci affect age-at-onset in Alzheimer's disease families with PS2 mutation. *American Journal of Medical Genetics - Neuropsychiatric Genetics, 132 B*(1), 14-20. doi:10.1002/ajmg.b.30087

Wilcock, D. M., & Colton, C. A. (2009). Immunotherapy, vascular pathology, and microhemorrhages in transgenic mice. *CNS and Neurological Disorders - Drug Targets, 8*(1), 50-64. doi:10.2174/187152709787601858

Wilcock, D. M., Munireddy, S. K., Rosenthal, A., Ugen, K. E., Gordon, M. N., & Morgan, D. (2004). Microglial activation facilitates Aβ plaque removal following intracranial anti-Aβ antibody administration. *Neurobiology of Disease, 15*(1), 11-20. doi:https://doi.org/10.1016/j.nbd.2003.09.015

Wildburger, N. C., Esparza, T. J., LeDuc, R. D., Fellers, R. T., Thomas, P. M., Cairns, N. J., . . . Brody, D. L. (2017). Diversity of Amyloid-beta Proteoforms in the Alzheimer's Disease Brain. *Scientific Reports, 7*(1), 9520-9520. doi:10.1038/s41598-017-10422-x

Wildsmith, K. R., Holley, M., Savage, J. C., Skerrett, R., & Landreth, G. E. (2013). Evidence for impaired amyloid β clearance in Alzheimer's disease. *Alzheimer's Research and Therapy, 5*(4). doi:10.1186/alzrt187

Willer, C. J., Sanna, S., Jackson, A. U., Scuteri, A., Bonnycastle, L. L., Clarke, R., . . . Abecasis, G. R. (2008). Newly identified loci that influence lipid concentrations and risk of coronary artery disease. *Nature Genetics, 40*(2), 161-169. doi:10.1038/ng.76

Wiseman, F. K., Pulford, L. J., Barkus, C., Liao, F., Portelius, E., Webb, R., . . . LonDown, S. C. (2018). Trisomy of human chromosome 21 enhances amyloid-β deposition independently of an extra copy of APP. *Brain : a journal of neurology, 141*(8), 2457-2474. doi:10.1093/brain/awy159

Wolf, D. S., Gearing, M., Snowdon, D. A., Mori, H., Markesbery, W. R., & Mirra, S. S. (1999). Progression of regional neuropathology in Alzheimer disease and normal elderly: Findings from the Nun Study. *Alzheimer Disease and Associated Disorders, 13*(4), 226-231. doi:10.1097/00002093-199910000-00009

Wolfe, M. S., Xia, W., Ostaszewski, B. L., Diehl, T. S., Kimberly, W. T., & Selkoe, D. J. (1999). Two transmembrane aspartates in presenilin-1 required for presenilin endoproteolysis and γ-secretase activity. *Nature, 398*(6727), 513-517. doi:10.1038/19077

World Health Organization. (2015). World report on ageing and health. *Geneva: World Health Organization*.

Wray, S., Self, M., Consortium, N. P. s. D. i., Consortium, N. H. s. D. i., Consortium, N. A. i., Lewis, P. A., . . . Hardy, J. (2012). Creation of an Open-Access, Mutation-Defined Fibroblast Resource for Neurological Disease Research. *PLoS ONE, 7*(8), e43099. doi:10.1371/journal.pone.0043099

Xia, D., Watanabe, H., Wu, B., Lee, S. H., Li, Y., Tsvetkov, E., . . . Kelleher, R. J. (2015). Presenilin-1 knockin mice reveal loss-of-function mechanism for familial alzheimer's disease. *Neuron, 85*(5), 967-981. doi:10.1016/j.neuron.2015.02.010

Xu, Q., Bernardo, A., Walker, D., Kanegawa, T., Mahley, R. W., & Huang, Y. (2006). Profile and Regulation of Apolipoprotein E (ApoE) Expression in the CNS in Mice with Targeting of Green Fluorescent Protein Gene to the ApoE Locus. *The Journal of Neuroscience, 26*(19), 4985-4994. doi:10.1523/jneurosci.5476-05.2006

Xue, C., Tran, J., Wang, H., Park, G., Hsu, F., & Guo, Z. (2019). Ab42 fibril formation from predominantly oligomeric samples suggests a link between oligomer heterogeneity and fibril polymorphism. *Royal Society Open Science, 6*(7). doi:10.1098/rsos.190179

Xue, Y., Zhan, X., Sun, S., Karuppagounder, S. S., Xia, S., Dawson, V. L., . . . Ying, M. (2019). Synthetic mRNAs Drive Highly Efficient iPS Cell Differentiation to Dopaminergic Neurons. *Stem cells translational medicine, 8*(2), 112-123. doi:10.1002/sctm.18-0036

Yagi, T., Ito, D., Okada, Y., Akamatsu, W., Nihei, Y., Yoshizaki, T., . . . Suzuki, N. (2011). Modeling familial Alzheimer's disease with induced pluripotent

stem cells. *Human Molecular Genetics, 20*(23), 4530-4539. doi:10.1093/hmg/ddr394

Yamada, M., Tsukagoshi, H., Otomo, E., & Hayakawa, M. (1987). Cerebral amyloid angiopathy in the aged. *Journal of Neurology, 234*(6), 371-376. doi:10.1007/BF00314080

Yamaguchi, H., Sugihara, S., Ishiguro, K., Takashima, A., & Hirai, S. (1995). Immunohistochemical analysis of COOH-termini of amyloid beta protein (aβ using end-specific antisera for aβ40 and aβ42 in Alzheimer's disease and normal aging. *Amyloid, 2*(1), 7-16. doi:10.3109/13506129509031882

Yang, J., Li, S., He, X. B., Cheng, C., & Le, W. (2016). Induced pluripotent stem cells in Alzheimer's disease: Applications for disease modeling and cell-replacement therapy. *Molecular Neurodegeneration, 11*(1). doi:10.1186/s13024-016-0106-3

Yang, J., Zhao, H., Ma, Y., Shi, G., Song, J., Tang, Y., . . . Le, W. (2017). Early pathogenic event of Alzheimer's disease documented in iPSCs from patients with PSEN1 mutations. *Oncotarget, 8*(5), 7900-7913. doi:10.18632/oncotarget.13776

Yang, M., & Teplow, D. B. (2008). Amyloid beta-protein monomer folding: free-energy surfaces reveal alloform-specific differences. *Journal of molecular biology, 384*(2), 450-464. doi:10.1016/j.jmb.2008.09.039

Yasuda, M., Maeda, K., Ikejiri, Y., Kawamata, T., Kuroda, S., & Tanaka, C. (1997). A novel missense mutation in the presenilin-1 gene in a familial Alzheimer's disease pedigree with abundant amyloid angiopathy. *Neuroscience Letters, 232*(1), 29-32. doi:https://doi.org/10.1016/S0304-3940(97)00569-7

Yasuda, M., Maeda, S., Kawamata, T., Tamaoka, A., Yamamoto, Y., Kuroda, S., . . . Tanaka, C. (2000). Novel presenilin-1 mutation with widespread cortical amyloid deposition but limited cerebral amyloid angiopathy. *Journal of neurology, neurosurgery, and psychiatry, 68*(2), 220-223. doi:10.1136/jnnp.68.2.220

Yau, W. Y. W., Tudorascu, D. L., McDade, E. M., Ikonomovic, S., James, J. A., Minhas, D., . . . Klunk, W. E. (2015). Longitudinal assessment of neuroimaging and clinical markers in autosomal dominant Alzheimer's disease: A prospective cohort study. *The Lancet Neurology, 14*(8), 804-813. doi:10.1016/S1474-4422(15)00135-0

Yokota, O., Tsuchiya, K., & Kuniaki, S. (2011). Early onset dementia with abundant non-neuritic aβ plaques and without significant neuronal loss: Report of two Japanese autopsy cases. In *Alzheimer's Disease Diagnosis and Treatments* (pp. 35-58).

Youmans, K. L., Tai, L. M., Nwabuisi-Heath, E., Jungbauer, L., Kanekiyo, T., Gan, M., . . . Ladu, M. J. (2012). APOE4-specific changes in Aβ accumulation in a new transgenic mouse model of Alzheimer disease. *The Journal of biological chemistry, 287*(50), 41774-41786. doi:10.1074/jbc.M112.407957

Yu, G., Nishimura, M., Arawaka, S., Levitan, D., Zhang, L., Tandon, A., . . . George-Hyslop, P. S. (2000). Nicastrin modulates presenilin-mediated

notch/glp-1 signal transduction and βAPP processing. *Nature, 407*(6800), 48-54. doi:10.1038/35024009

Zabel, M., Schrag, M., Crofton, A., Tung, S., Beaufond, P., Van Ornam, J., . . . Kirsch, W. M. (2013). A shift in microglial β-amyloid binding in Alzheimer's disease is associated with cerebral amyloid angiopathy. *Brain Pathology, 23*(4), 390-401. doi:10.1111/bpa.12005

Zakharova, N. V., Bugrova, A. E., Kononikhin, A. S., Indeykina, M. I., Popov, I. A., & Nikolaev, E. N. (2018). Mass spectrometry analysis of the diversity of Aβ peptides: difficulties and future perspectives for AD biomarker discovery. *Expert Review of Proteomics, 15*(10), 773-775. doi:10.1080/14789450.2018.1525296

Zarea, A., Charbonnier, C., Rovelet-Lecrux, A., Nicolas, G., Rousseau, S., Borden, A., . . . Wallon, D. (2016). Seizures in dominantly inherited Alzheimer disease. *Neurology, 87*(9), 912-919. doi:10.1212/WNL.0000000000003048

Zeenat, M., Vikram, G. P., & Mohammad, A. K. (2014). Protein Interactions Between the C-Terminus of Aβ-Peptide and Phospholipase A₂ - A Structure Biology Based Approach to Identify Novel Alzheimer's Therapeutics. *CNS & Neurological Disorders - Drug Targets, 13*(7), 1224-1231. doi:http://dx.doi.org/10.2174/18715273136661409171122 48

Zekonyte, J., Sakai, K., Nicoll, J. A. R., Weller, R. O., & Carare, R. O. (2016). Quantification of molecular interactions between ApoE, amyloid-beta (Aβ) and laminin: Relevance to accumulation of Aβ in Alzheimer's disease. *Biochimica et Biophysica Acta - Molecular Basis of Disease, 1862*(5), 1047-1053. doi:10.1016/j.bbadis.2015.08.025

Zhang, H., Liu, D., Huang, H., Zhao, Y., & Zhou, H. (2018). Characteristics of insulin-degrading enzyme in alzheimer's disease: A meta-analysis. *Current Alzheimer Research, 15*(7), 610-617. doi:10.2174/1567205015666180119105446

Zhang, S., Lei, C., Liu, P., Zhang, M., Tao, W., Liu, H., & Liu, M. (2015). Association between variant amyloid deposits and motor deficits in FAD-associated presenilin-1 mutations: A systematic review. *Neuroscience and Biobehavioral Reviews, 56*, 180-192. doi:10.1016/j.neubiorev.2015.07.003

Zhang, Y., Chen, K., Sloan, S. A., Bennett, M. L., Scholze, A. R., O'Keeffe, S., . . . Wu, J. Q. (2014). An RNA-sequencing transcriptome and splicing database of glia, neurons, and vascular cells of the cerebral cortex. *The Journal of neuroscience : the official journal of the Society for Neuroscience, 34*(36), 11929-11947. doi:10.1523/JNEUROSCI.1860-14.2014

Zhang, Y., Pak, C., Han, Y., Ahlenius, H., Zhang, Z., Chanda, S., . . . Südhof, T. C. (2013). Rapid single-step induction of functional neurons from human pluripotent stem cells. *Neuron, 78*(5), 785-798. doi:10.1016/j.neuron.2013.05.029

Zhao, Y., Wu, X., Li, X., Jiang, L.-L., Gui, X., Liu, Y., . . . Xu, H. (2018). TREM2 Is a Receptor for β-Amyloid that Mediates Microglial Function. *Neuron,*

97(5), 1023-1031.e1027. doi:https://doi.org/10.1016/j.neuron.2018.01.031

Zhong, N., & Weisgraber, K. H. (2009). Understanding the association of apolipoprotein E4 with Alzheimer disease: clues from its structure. *The Journal of biological chemistry, 284*(10), 6027-6031. doi:10.1074/jbc.R800009200

Zink, N., Bensmann, W., Arning, L., Beste, C., & Stock, A. K. (2019). Apolipoprotein ε4 is associated with better cognitive control allocation in healthy young adults. *NeuroImage, 185*, 274-285. doi:10.1016/j.neuroimage.2018.10.046

Zotova, E., Bharambe, V., Cheaveau, M., Morgan, W., Holmes, C., Harris, S., . . . Boche, D. (2013a). Inflammatory components in human Alzheimer's disease and after active amyloid-β42 immunization. *Brain, 136*(9), 2677-2696. doi:10.1093/brain/awt210

Zotova, E., Bharambe, V., Cheaveau, M., Morgan, W., Holmes, C., Harris, S., . . . Boche, D. (2013b). Inflammatory components in human Alzheimer's disease and after active amyloid-β<inf>42</inf> immunization. *Brain, 136*(9), 2677-2696. doi:10.1093/brain/awt210

Zotova, E., Holmes, C., Johnston, D., Neal, J. W., Nicoll, J. A. R., & Boche, D. (2011). Microglial alterations in human Alzheimer's disease following Aβ42 immunization. *Neuropathology and Applied Neurobiology, 37*(5), 513-524. doi:10.1111/j.1365-2990.2010.01156.x

Zuroff, L., Daley, D., Black, K. L., & Koronyo-Hamaoui, M. (2017). Clearance of cerebral Aβ in Alzheimer’s disease: reassessing the role of microglia and monocytes. *Cellular and Molecular Life Sciences, 74*(12), 2167-2201. doi:10.1007/s00018-017-2463-7